



Engineering and
Physical Sciences
Research Council



The University of
Nottingham

UNITED KINGDOM • CHINA • MALAYSIA

Novel Routes for Recycling of Polyethylene Terephthalate with Supercritical Carbon Dioxide and Microwaves

Bradley Ieuan Hopkins

Thesis submitted to the University of Nottingham
September 2024 for the degree of
Doctor of Philosophy

Supervisors: Dr Eleanor Binner, Dr Mohamed Adam, Dr Daniel Keddie,
Professor Derek Irvine, Professor Steve Howdle

Declaration

The work presented in this thesis is the original work of the author, except where references have been made in the text to external sources. This work has not been submitted for any other degree or qualification.

Bradley Ieuan Hopkins

28th September 2024

Contents

Acknowledgements	7
Abbreviations.....	8
Abstract.....	12
1 Introduction	13
1.1 The Plastic Waste Problem	13
1.1.1 Barriers to a Circular Economy.....	18
1.2 Polyethylene terephthalate	23
1.3 Transitioning to a Circular Economy.....	24
1.3.1 Deposit Return Schemes and Plastic Taxes.....	25
1.3.2 Recycling	26
1.4 Supercritical Carbon Dioxide.....	55
1.4.1 Supercritical Induced Plasticisation	56
1.5 Aims and Objectives	57
2 Materials and Methodology	60
2.1 Overview	60
2.2 Materials	60
2.2.1 Supercritical Impregnation of Polyethylene Terephthalate with Various Organic Microwave Susceptors	60
2.2.2 Microwave Pyrolysis of Polyethylene Terephthalate	61
2.2.3 Chemical Depolymerisations	61
2.3 Supercritical Experiments	61
2.3.1 Double-Ended High-Pressure View Cell.....	61
2.3.2 High Pressure Autoclaves	63
2.4 Dielectric Property Measurements	64
2.4.1 Heat and Hold Cavity Perturbation	64
2.4.2 Simultaneous Heating and Measurement.....	66
2.4.3 Coaxial Probe.....	67
2.5 Microwave Pyrolysis.....	68
2.6 Analytical Methods and Instrumentation.....	70
2.6.1 Thermogravimetric Analysis	70
2.6.2 Differential Scanning Calorimetry	70
2.6.3 Dynamic Mechanical Analysis.....	71

2.6.4 X-ray Scattering.....	71
2.6.5 Nuclear Magnetic Resonance.....	71
2.6.6 Atmospheric Pressure Chemical Ionisation (APCI)	72
2.6.7 Infrared Spectroscopy	72
2.6.8 Gel Permeation Chromatography	72
2.6.9 Matrix-assisted laser desorption ionization–time of flight mass spectrometry(MALDI-TOF).....	73
2.6.10 High Pressure Liquid Chromatography – Mass Spectrometry (HPLC-MS).....	73
2.6.11 Gas Chromatography Mass Spectrometry (GC-MS).....	73
3 Enhancement of Polyethylene Terephthalate’s Dielectric Properties via Supercritical Carbon Dioxide Impregnation	75
Overview	75
3.1 Introduction	75
3.1.1 Microwave Heating and Dielectric Properties.....	76
3.1.2 Measurement of Dielectric Properties	85
3.1.3 Microwave Heating of Polymers	87
3.1.4 Supercritical Carbon Dioxide Impregnation	89
3.1.5 Aims and Objectives.....	94
3.2 Experimental Procedures	95
3.2.1 Solubility testing of Organic Susceptor Candidates in Supercritical Carbon Dioxide.....	95
3.2.2 Supercritical Impregnation of Polyethylene Terephthalate with Organic Susceptor Candidates	95
3.2.3 Coaxial Probe Dielectric Measurements.....	95
3.2.4 Heat and Hold Cavity Perturbation Dielectric Measurements	96
3.2.5 Dynamic Cavity Perturbation Dielectric Measurements	96
3.2.6 Thermogravimetric Analysis (TGA)	96
3.2.7 Differential Scanning Calorimetry (DSC).....	96
3.2.8 Dynamic Mechanical Analysis	97
3.2.9 Small and Wide-Angle X-Ray Scattering (SAXS/WAXS).....	97
3.3 Results and Discussions	98
3.3.1 Identification of a Suitable Degradable Microwave Susceptor	98
3.3.2 Supercritical Impregnation of PET	105
3.3.3 Dielectric Analysis.....	111
3.3.4 Thermal Characterisation and X-ray Scattering	121

3.4 Conclusion.....	126
4 Microwave Pyrolysis of Polyethylene Terephthalate	127
Overview	127
4.1 Introduction	127
4.1.1 Current State of PET Microwave Pyrolysis	127
4.1.2 Drawbacks of Susceptor Use and Pushing the Boundaries of Product Analysis	133
4.1.3 Aims and Objectives	135
4.2 Experimental	137
4.2.1 Supercritical Impregnation of Polyethylene Terephthalate with Ethylene Glycol.....	137
4.2.2 Microwave Pyrolysis of Polyethylene Terephthalate	139
4.2.3 Microwave Pyrolysis of Polyethylene Terephthalate Impregnated with Ethylene Glycol.....	141
4.2.4 Nuclear Magnetic Resonance (^1H NMR, ^{13}C NMR, COSY, HSQC, HMBC) ...	143
4.2.5 Gas Chromatography-Mass Spectrometry (GC-MS)	143
4.2.6 Matrix-assisted laser desorption/ionization – Time of Flight Spectrometry (MALDI-ToF)	143
4.2.7 Atmospheric Pressure Chemical Ionisation (APCI)	144
4.2.8 Infrared Spectroscopy	144
4.3 Results and Discussion.....	145
4.3.1 Scale Up of PET Impregnation in Supercritical Carbon Dioxide with Ethylene Glycol.....	145
4.3.2 PET Performance During Microwave Pyrolysis	147
4.3.3 Analysis of the Products	161
4.4 Conclusions	174
5 Supercritical Depolymerisation of Polyethylene Terephthalate	175
Overview	175
5.1 Introduction	175
5.1.1 Solvolysis of Polyethylene Terephthalate	175
5.1.2 Is PET Solvolysis Sustainable from a Solvent Waste Point of View?	181
5.1.3 PET Solvolysis in Supercritical Carbon Dioxide	185
5.1.4 Supercritical Extraction as a Route Towards Monomer Purification	191
5.1.5 Aims and Objectives	193
5.2 Experimental.....	195

5.2.1 Solubility Testing of Supercritical Solvolytic Systems	195
5.2.2 Methanolysis of Polyethylene Terephthalate in Supercritical Carbon Dioxide	195
5.2.3 Transesterification of Crude Methanolysis Product to BHET	196
5.2.4 Solubility Testing of PET monomers in Supercritical Carbon Dioxide	196
5.2.5 Supercritical Extraction of Dimethyl Terephthalate and PET Oligomers	196
5.2.6 Nuclear Magnetic Resonance (¹ H NMR, ¹³ C NMR, COSY, HSQC, HMBC) ...	197
5.2.7 Gas Chromatography-Mass Spectrometry (GC-MS)	197
5.2.8 High Pressure Liquid Chromatography – Mass Spectrometry (HPLC-MS)...	197
5.2.9 Gel Permeation Chromatography (GPC)	198
5.3 Results and Discussion	199
5.3.1 Identification of an scCO ₂ Solvolytic System for PET.....	199
5.3.2 Supercritical Methanolysis of PET	201
5.3.3 Closing the Loop	221
5.3.4 One Pot Depolymerisation-Extraction.....	231
5.3.5 Expanding the Scope to Real World Materials	234
5.4 Conclusions.....	236
6 Conclusions and Future Work.....	237
Overview	237
6.1 Enhancement of Polyethylene Terephthalate's Dielectric Properties via Impregnation in Supercritical Carbon Dioxide	237
6.2 Microwave Pyrolysis of Polyethylene Terephthalate	239
6.3 Supercritical Depolymerisation of Polyethylene Terephthalate.....	240
7 References.....	241
Appendix	262
Chapter 3.....	262
Chapter 4.....	272
Chapter 5.....	348

Acknowledgements

I would like to thank my supervisors: Dr Eleanor Binner, Dr Mohamed Adam, Prof Derek Irvine, Dr Daniel Keddle and Prof Steve Howdle. You have all supported me with your individual talents and expertise – and I am incredibly grateful.

I would also like to thank the EPSRC Atoms to Products (A2P) CDT in Sustainable Chemistry for securing the funding for this PhD and their constant support, particularly Prof Pete Licence as well as Louise and Mandy.

The work in this project would not have been possible without the fantastic technical support in the School of Chemistry. I would like to extend a special thank you to Richard Wilson, Matthew McAdam, David Litchfield, Ben Pointer-Gleadhill and Mark Guyler, as well as the entire workshop team for the never-ending help and technical education.

One of the highlights from my PhD was the opportunity to spend time in Valencia and Tennessee. So, I would like to thank Professor Felipe Penaranda Foix, Dr Michelle Kidder, Dr Wim Bras and Dr Logan Kearney for helping to arrange my trips abroad, as well as hosting me after I arrived. Thank you again to Ellie, Derek and Steve for putting me in touch with them.

Thank you to all lab members, past and present, of B10, B10a, B9, A04 and B25 for their advice and friendship over the last four years. I would like to name Dr Mohamed Adam, Dr Vincenzo Taresco, Dr Daniel Keddle, Dr John Duncan and Dr Kris Kortszen for taking the time to integrate me into the laboratories and for training me in the correct use of so many instruments.

To my Mum, Nan and Grandad – thank you for raising me and imparting your values and work ethic that have been so valuable during my studies.

Abbreviations

1,2-dimethoxyethane	1,2-DME
1,5,7-Triazabicyclo(4.4.0)dec-5-ene	TBD
1,6-hexanediol	1,6-HD
1,8-Diazabicyclo(5.4.0)undec-7-ene	DBU
2-aminopyridine	2-AP
4-dimethylaminopyridine	DMAP
Aluminium Oxide	Al ₂ O ₃
Aluminium triisopropoxide	AIP
Bis(2-hydroxyethyl) terephthalamide	(BHETA)
Bis(2-hydroxyethyl) terephthalate	BHET
Bis(3-hydroxypropyl) terephthalamide	BHPTA
Boiling Point	b.p.
Bond Dissociation Energy	BDE
British Plastics Federation	BPF
Calcium Oxide	CaO
Carbon Dioxide	CO ₂
Carbon Monoxide	CO
Carbonised Coconut Husk	CHC
Chloroform	CHCl ₃
Cobalt Acetate	Co(OAc) ₂
Daltons	Da
Density Functional Theory	DFT
Deposit Return Scheme	DRS
Dichlorobenzene	DCB
Dichloromethane	DCM

Dielectric Constant	ϵ'
Dielectric Loss factor	ϵ''
Dielectric Loss tangent	$\tan \delta$
Dielectric Permittivity	ϵ
Differential Scanning Calorimetry	DSC
Diffuse Reflectance Infrared Fourier Transform Spectroscopy	DRIFT
Dimethyl carbonate	DMC
Dimethyl formamide	DMF
Dimethyl sulfoxide	DMSO
Dimethyl terephthalate	DMT
Dynamic Mechanical Analysis	DMA
Economically developed countries	EDC
Electromagnetic	EM
Electron Ionisation	EI
End of Life	EOL
Ethylene carbonate	EC
European Union	EU
Ferroferric Oxide	Fe_3O_4
Fourier Transform Infrared Spectroscopy	FT-IR
Gas Chromatography Mass Spectrometry	GC-MS
Gel Permeation Chromatography	GPC
Glass Transition Temperature	T_g
High Density Polyethylene	HDPE
Hydrochloric Acid	HCl
Hyperspectral Imaging Spectroscopy	HIS

Liquid Chromatography Mass Spectrometry	LC-MS
Lithium methoxide	LiOMe
Low Density Polyethylene	LDPE
Matrix Assisted Laser Desorption Ionisation	MALDI
Microalgae	MA
Million tonnes	Mt
Molecular Weight	M_w
National Renewable Energy Laboratory	NREL
near infrared	NIR
<i>N</i> -methylimidazole	NMI
Nuclear Magnetic Resonance	NMR
Partition Co-efficient	K
Penetration Depth	D_p
Polylactic acid	PLA
Polymethyl methacrylate	PMMA
Polybrominated diphenyl ethers	PBDE
Polyethylene Terephthalate	PET
Polypropylene	PP
Polystyrene	PS
Polyvinyl chloride	PVC
Potassium carbonate	K_2CO_3
Power Density	P_d
Rice Husk	RH
Ring-opening polymerisation	ROP
Silicon Carbide	SiC
Small Angle X-Ray Scattering	SAXS

Sophora Wood	SW
Supercritical carbon dioxide	scCO ₂
Surface Area to Volume Ratio	S:V
Sustainable Development Goals	SDGs
Terephthalic Acid	TPA
Terephthalonitrile	TPN
Thermogravimetric Analysis	TGA
Total Ion Content Chromatogram	TICC
United Nations	UN
United States Food and Drug Administration	FDA
Water	H ₂ O
Wide Angle X-Ray Scattering	WAXS
X-Ray Diffraction	XRD
Zinc acetate	Zn(OAc) ₂
Zinc Oxide	ZnO

Abstract

Reliance on plastic by society has resulted in large volumes of waste requiring treatment.

Often, this waste is disposed of in ways that harm the environment or prevent the re-use of the material, such as landfill or incineration. Therefore, the plastic value chain is often described as being linear because of the poor end-of-life strategies currently in place.

It is crucial to introduce some circularity into the plastic value chain, to increase the useful lifespan of plastic material and to minimise plastic pollution of the natural environment. One route to achieve this is to recycle plastic.

Chemical recycling, an umbrella term used to describe a plethora of recycling strategies, describes the deliberate breakdown of a plastic material by a controlled process to yield monomers, or other low-molecular weight products. These products can then be used to produce fresh, high-quality plastic, or other valuable materials.

However, many chemical recycling processes suffer from drawbacks such as poor product selectivity and purification steps requiring large volumes of solvents. Both issues have led to challenges surrounding the proper cleaning and disposal of solvents used in the synthetic and purification steps, meaning that chemical recycling processes often find themselves in violation of the first Principle of Green Chemistry - it is better to prevent waste than to treat or clean up waste after it has been created.

In this work, two novel projects are undertaken to develop routes to chemically recycle polyethylene terephthalate with little to no solvent waste. Supercritical carbon dioxide is employed as a key solvent in both projects, whilst microwave heating is also exploited as an energy source for plastic degradation.

1 Introduction

1.1 The Plastic Waste Problem

Plastics are ubiquitous in our daily life. Food packaging, medical equipment and clothing are just three examples of how plastics contribute to the normal running of society. As a class of materials, plastics exhibit an unparalleled range of useful properties, such as: flexibility, ductility, high tensile strength, and high thermal resistance – driving their suitability for a plethora of applications. The ability of plastics to meet a range of needs has fuelled a demand for the material, which is reflected in the 20-fold increase of consumption since 1950, reaching 311 million tonnes in 2014, with this figure expected to double by 2035 (Fig. 1.1).¹

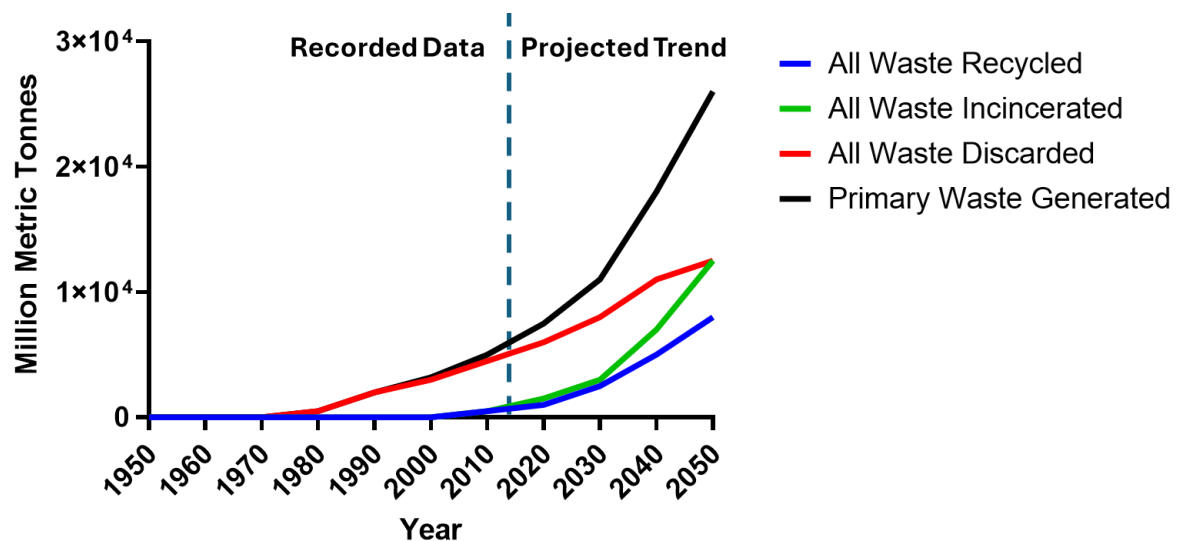


Figure 1.1- Plot showing the increase in the rate of plastic waste production since 1950 and projections of how this will increase in the future. The capacity of various waste treatments strategies is shown on the blue and green lines.¹

It is inarguable that plastics have helped increase the quality of life for people around the world, by enabling the cheap manufacture of everyday products. But the mass usage has led to several undesirable consequences on the natural environment and human health which largely arise from poor treatment of plastic waste.

These consequences are collectively referred to as the “Plastic Waste Problem”, which can be considered as four parts:

1. Many plastic products being intended for single use.
2. Improper disposal after a short period of use.
3. The impacts on the natural environment and human health which arise from poor plastic disposal.
4. Limitations of current recycling technologies.

The sheer volume of plastic produced exacerbates the issues which arise from the categories discussed above. Global Plastics Flow estimated, that in 2018 alone, 250 million tonnes (mt) of plastic waste material was generated worldwide.² Only 70% (175 mt) of this waste material has been formally accounted for, leaving the fate of 75 mt of waste material unknown. 20% (50 mt) was collected for recycling, an additional 20% (50 mt) was incinerated to recover the energy in the chemical bonds, 30% (75 mt) was disposed of via landfilling whilst a further 25% (62 mt) was classed as being improperly disposed. The final 5% (13 mt) was leaked into the environment.

The figures from 2018 demonstrate that the plastics value chain is still incredibly linear, as 50% of plastic waste was disposed of in a manner which prevents its reuse – this is known as the take-make-waste model (Fig. 1.2).³ The linearity arises from the fact that the majority of products consumed today only ever move in one direction along their value chain: from raw material to waste. The Ellen MacArthur Foundation, a charity leading the transition away from these linear models, identifies the root of the take-make-waste model in the industrial revolution. This marked the first time that goods could be mass produced and there appeared to be an infinite supply of the raw material needed. The practices and frameworks established during the industrial revolution became embedded across many economically developed

countries (EDC's) as the abundance of useful goods soared, allowing living standards to rise and population growth to increase.

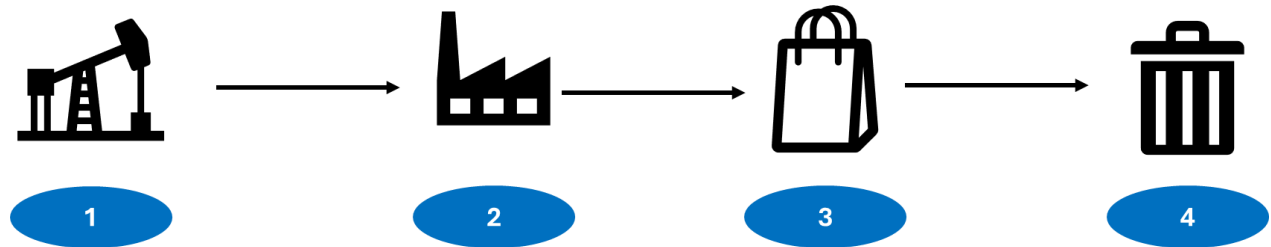


Figure 1. 2 – An illustration of the take-make-waste model of the plastic's value chain.

1: Extraction of crude oil from natural reserves.

2: Crude oil is refined into its various fractions, which provide platform chemicals for plastic manufacture.

3: Plastic products are consumed by society.

4: Plastics are disposed of in a manner that prevents their re-use (landfill, incineration).

At the time, many of the harmful environmental consequences due to this linear approach were not apparent. But with a rising awareness surrounding issues such as: microplastics, ocean pollution, and an unacceptable accumulation of plastic waste in landfills, time and resources are being directed towards more sustainable practices for the treatment, and re-use, of plastic that has reached the end of its useful lifespan.

The Ellen MacArthur Foundation advocates for a transition to a circular economy, an approach which aims to avoid ever wasting material whilst simultaneously regenerating the harm done to the natural environment (Fig. 1.3). According to the Ellen MacArthur Foundation, a circular economy consists of three key concepts: ⁴

- Eliminate waste and pollution.
- Circulate products and materials (at their highest value).
- Regenerate nature.

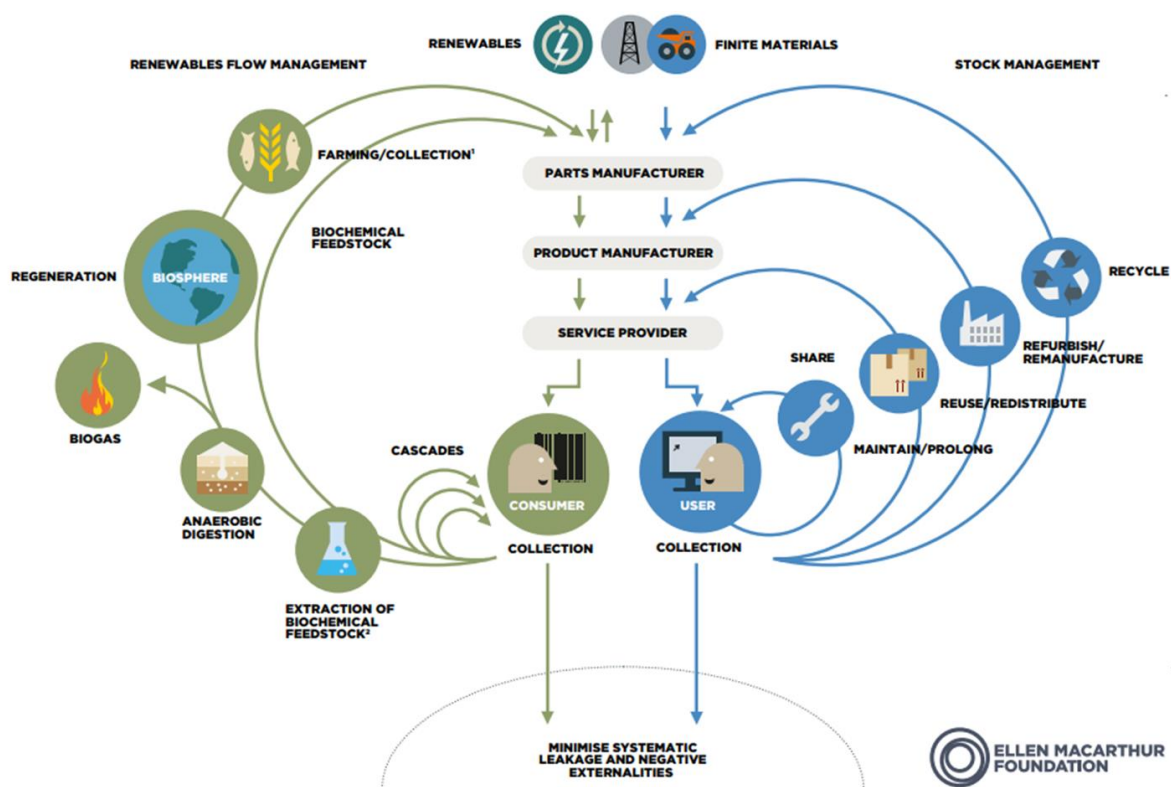


Figure 1. 3 – An illustration of the circular economy compiled by the Ellen MacArthur Foundation. ⁴

As a concept, the circular economy continues to gain momentum. In the academic space, the aims of a circular economy are well-aligned with the 12 Principles of Green Chemistry originally developed by Paul Anastas.⁵ Specific principles that relate well to the circular economy are:

- It is better to prevent waste than to treat or clean up waste after it has been created.
- A raw material or feedstock should be renewable rather than depleting whenever technically and economically practicable.
- Chemical products should be designed so that at the end of their function they break down into innocuous degradation products and do not persist in the environment.

International bodies have also been placing sustainable development at the centre of their objectives. In 1992 the United Nations (UN) hosted the Earth Summit Conference, where 178

member states adopted a strategy to build a global partnership for sustainable development to improve human lives and protect the environment titled Agenda 21.⁶

Agenda 21, alongside subsequent UN resolutions and meetings, laid the groundwork for the 2030 Agenda for Sustainable Development summarised in 17 Sustainable Development Goals (SDGs).⁷ These goals are designed to facilitate the movement towards a more sustainable world, and express values and objectives consistent with the goal of a circular economy, specifically:

- Goal 9: Industry, Innovation and Infrastructure - Build resilient infrastructure, promote inclusive and sustainable industrialization and foster innovation.
- Goal 11: Sustainable Cities and Communities - Make cities and human settlements inclusive, safe, resilient, and sustainable.
- Goal 12: Responsible Consumption and Production - Ensure sustainable consumption and production patterns.
- Goal 14: Life Below Water - Conserve and sustainably use the oceans, seas and marine resources for sustainable development.
- Goal 15: Life on Land - Protect, restore and promote sustainable use of terrestrial ecosystems, sustainably manage forests, combat desertification, and halt and reverse land degradation and halt biodiversity loss.

Whilst there is clear evidence of the recognition for a need to transition towards a more sustainable, circular approach for plastic waste in the academic and political space, the rate of change is very slow.

1.1.1 Barriers to a Circular Economy

Many of the embedded attitudes and behaviours found across developed countries worldwide inevitably lead to a linear plastics value chain, as the cost-effective, most convenient approach for the disposal of plastic waste is often prioritised.

1.1 1.1.1 International Shipment of Plastic Waste

Most plastic waste is challenging to recycle as it will consist of a blend of different materials and may also contain additives to further tune the material properties for a specific purpose. An easy solution many Western countries have adopted in recent years is to ship plastic waste to countries such as China and Turkey, where it is landfilled or incinerated *en masse*, as opposed to developing domestic infrastructure aimed at re-using and recycling plastic waste.

China became a major importer of Western countries plastic waste during the 1990s as many of its industries were able to manufacture cheap goods for export from the material. However, China gradually increased its regulations on the quality of imported plastic waste during the 2010s to prevent poor quality material effectively being “dumped” by other countries.⁸ One of the more famous acts undertaken by China to prevent import of sub-standard material was “Operation Green Fence” which was launched in February 2013. Intensive inspections of shipping containers entering the country began, to search for poor quality recycled material transported by legitimate means and smugglers.⁹ Companies found to be in breach of Chinese quality standards faced severe penalties, such as the loss of shipping licences and incurring additional expenditure when arranging the return of recyclate denied entry into China.¹⁰ Operation Green Fence, among other acts, such as doubling import fees⁹, was eventually followed by a comprehensive ban on the import of foreign recyclate into China from the beginning of 2018.⁸

Following this ban, many countries pivoted to shipping their plastic waste to Turkey as the annual amount of plastic waste imported increased from 261,864 tonnes to 772,831 tonnes by 2020. Although the waste is officially imported to be recycled or re-used, a large proportion is estimated to be landfilled or burned at the side of the road instead.¹¹ The combined volume of imported and domestic solid waste has overwhelmed the capacity of the Turkish recycling industry, resulting in leakage of the excess into the Mediterranean Sea. In 2021, the largest proportion of European waste plastic marine pollution (16.8 %) was believed to originate from Turkey's southern shore.¹²

Rising awareness of the problem has spurred the Turkish government to act, aimed at curbing the volume of waste plastic imported and improperly disposed. 152 waste facilities in the Adana province were audited in 2021, resulting in the closure of 29 and an additional 32 being fined after poor compliance with waste disposal was uncovered.¹³

Additionally, Turkey also introduced legislation mandating recycling companies to source at least 20% of their waste material from domestic sources at the end of 2019, with the minimum sourcing of domestic waste being increased to 50% from September 2020.¹⁴ Alongside this requirement to source recycle domestically, Turkey also banned the import of mixed plastic wastes (as these are difficult to separate and recycle, leading to low quality products) and introduced an outright ban on the import of waste polyethylene. After lobbying from the recycling industry, the ban on polyethylene import was overturned but a requirement for contamination totalling <1% was introduced.¹⁴

Supernational bodies, such as the United Nations Environment Programme, are attempting to minimise the transportation of hazardous wastes around the world purely for their disposal, alongside providing a regulatory framework to ensure that any harms to the environment or human health that may arise from the shipping of waste are mitigated. One such example was

the adoption of the Basel Convention on the Control of Transboundary Movements of Hazardous Wastes and their Disposal in 1989.¹⁵ Originally written in response to the discovery of toxic waste discovered in Africa which had been imported from other countries, the Basel Convention first aims to reduce waste generation by promoting sustainable practices, followed by restricting and regulating transboundary movement of hazardous wastes to ensure it is undertaken in a manner compliant with waste management best practice.

Although the practice of countries exporting hazardous waste, plastic or otherwise, to places in the world where it can be disposed of improperly with less scrutiny is clearly unacceptable, some organisations, such as the British Plastics Federation (BPF), argue that many countries currently have no choice as they lack sufficient capacity domestically to dispose of their plastic waste.¹⁶ The BPF have devised a recycling roadmap, which projects the progress the UK could reasonably make by 2030 if the correct drivers are put in place. These include technological advancements and legislative changes, which proposes a zero reliance on exporting low quality recycle as a key objective.¹⁷

1.1.1.2 Landfilling and Leakage to the Environment

The large volumes of plastic waste requiring treatment, as well as the complexity of many commercial plastic products (additives, blends of multiple polymers), has led to landfilling as the main legacy disposal method. This is demonstrated by approximately half of the 300 million tonnes of waste plastic generated in 2022 being disposed this way.¹⁸ Landfilling is where waste material is dumped, or buried, and left to decompose at a dedicated site. As plastics are very durable, decomposition can take hundreds of years. Clearly landfill is far from a viable long-term solution for managing plastic disposal – despite its convenience. Moreover, exposure to a variety of changing conditions at the landfill site (pH, temperature, moisture, evolving gases),

can aid the decomposition of plastic waste into microplastics and their release via leaching into the groundwater.

Microplastics are classified as plastics particles less than 5 mm in diameter, although particles as small as 1.6 μm have been identified, and have come to be associated with a range of environmental and health concerns.¹⁹ Leaching of these particles, alongside other additives found in waste plastic, through groundwater can release them into the natural environment. The durability of microplastics grants them plenty of opportunity to be ingested by fish²⁰ or land animals.²¹ Ingestion of these microplastics has been shown to form blockages in the digestive tract²² and a link to cancer has also been identified.²³ Should animals that ingest microplastics survive, the potential for microplastics to move further up the food chain through predation – including to humans - exists.

Besides microplastics, many additives included in commercial plastics leach from landfill and are released into water ways. Additives are a necessary addition to most plastic products, in order to impart specific properties (such as biocides, UV stabilisers , flame retardants or pigments), tuning the properties of the material to make it more suitable for its intended purpose.²⁴ However, these additional chemicals present a significant hazard to the environment and health once waste material is landfilled, as they gradually leach into waterways.

For example, a single study of a Japanese landfill identified over 190 additives found in plastics, largely consisting of organic phosphates and phthalates.²⁵ Health concerns have started to arise as additives have been detected in the tissues of fish²⁶, birds²⁷ and marine mammals.²⁸ The chemical diversity seen in such a broad number of additives has led to concerns that an equally broad number of negative health outcomes may be observed, as there is potential for many biological processes (metabolism, endocrine signalling etc.) to be effected.²⁹ Further to this, prolonged exposure to plastic additives has been linked to cases of cancer.^{20, 24}

These health concerns surrounding the leakage of microplastics, and additives, demonstrate the considerable flaws in a continued reliance on landfilling as a route to dispose of plastic waste. Even if these concerns were found to be unwarranted, the poor circularity of landfilling means that it is an unsuitable strategy to remove plastic waste moving forward, as the re-use of large volumes of material is prevented.

1.1.1.3 Incineration of Plastic Waste

Incineration can be carried out on waste plastics which are not possible to treat another way, in order to recover the energy held inside the chemical bonds and put it to another use, such as electricity generation.³⁰ Reasons that the plastic has become untreatable can include a high level of contamination, separation complications or serious degradation of the polymer chemical structure.³¹ Incineration is now an established practice for the treatment of plastic waste, shown by an increase globally at a rate of 0.7% p.a. since 1980.¹

Another benefit of incineration is the prevention of plastics being sent to landfill, but this value can be negated by the release of toxic gases and substances during the incineration process.³² However, by avoiding the need for landfill, the leakage of chemicals in the plastic waste to the environment can be mitigated.

This mitigation potential means that incineration could play a role in cleaning up the oceans. Currently large amounts of highly contaminated, difficult to sort plastic is circulating through the oceans and other waterways. Incineration, alongside burial and some recycling, has been identified as a possible strategy to reduce the plastic pollution in the oceans.³³ Incineration overcomes many complications seen in recycling, due to removing the need to sort and remove contaminants and does not require large-scale use of land needed for burial of waste.

Despite these pragmatic arguments that have been outlined in favour of incineration, the point remains that it ultimately leads to the destruction of valuable material, and it is preferable to either extend the useful lifespan of that material through its re-use or recycling.

1.2 Polyethylene terephthalate

Polyethylene terephthalate (PET) is a thermoplastic which is widely employed in commercial plastic products (Fig 1.4). It is suitable for a range of purposes due to its many useful properties, including chemical inertness, transparency and flexibility. Food packaging is a major use of PET, resulting in it being the third most commonly used plastic in the packaging sector. PET accounts for 16% of all plastic consumed in Europe, with one major use being in the production of drinking bottles.³⁴

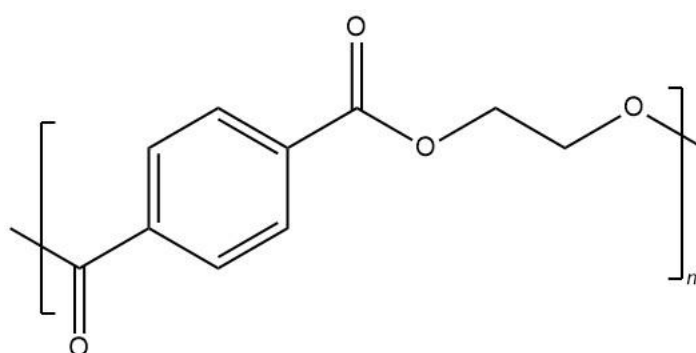


Figure 1.4 - Repeating unit of polyethylene terephthalate (PET).

PET has traditionally been synthesised in a two-step process. Initially either a direct esterification route involving terephthalic acid and ethylene glycol, or an ester interchange between dimethyl terephthalate and ethylene glycol (Fig. 1.5).

Both routes yield bis(2-Hydroxyethyl) terephthalate (BHET), which is polymerised in bulk to produce PET via a polycondensation reaction.³⁵⁻³⁷

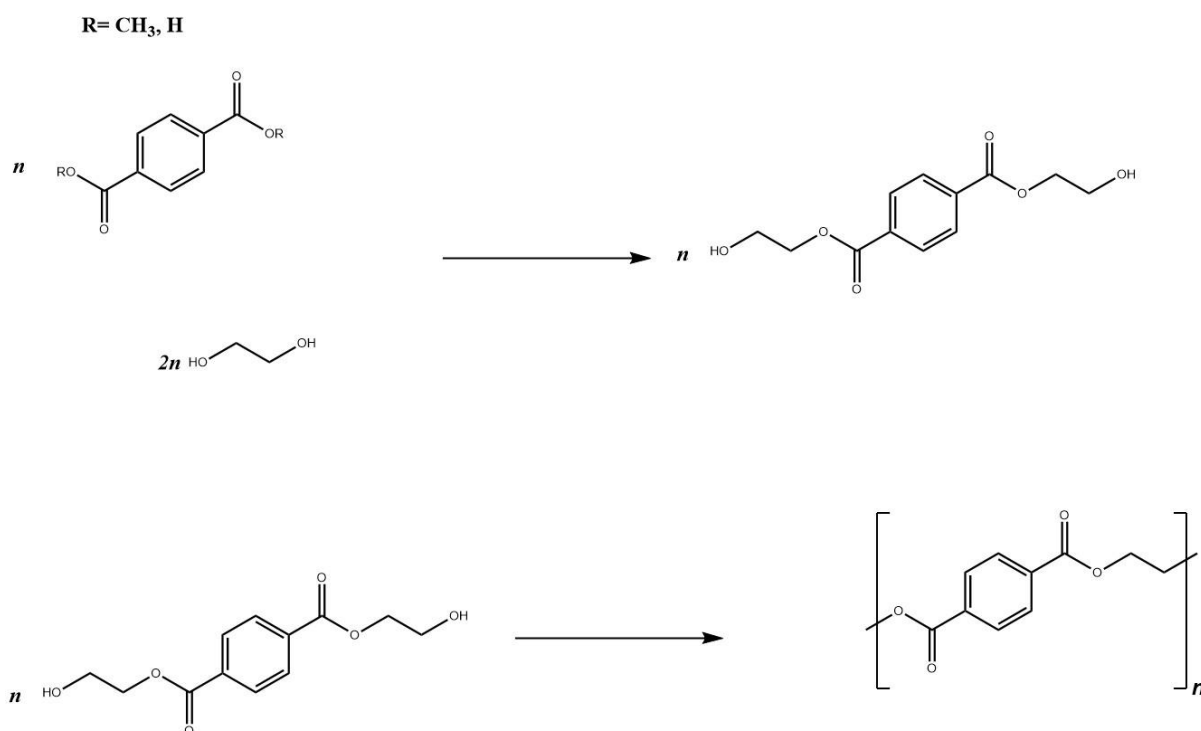


Figure 1.5-Synthesis of PET. Transesterification reaction to produce BHET from dimethyl terephthalate ($R=\text{CH}_3$) or terephthalic acid ($R=\text{H}$) (top). Bulk polycondensation of BHET to produce PET (bottom).

The desirable properties PET exhibits, which may be further tuned by the aforementioned additives, have fuelled a demand for the material. Five million tonnes of PET was sold in Europe in 2022, 97 % of which was used for packaging.³⁸ Therefore, this plastic is of great commercial interest and it is important to include it in the circular economy. For these reasons, PET will be the main focus of this thesis.

1.3 Transitioning to a Circular Economy

Much of the reasoning behind our reliance on the linear waste treatment strategies outlined above can be explained largely by convenience. Much of the infrastructure to facilitate landfilling and incineration already exist, and they can be carried out easily and cheaply. Although recycling's capacity is growing to meet the challenge, incentives are starting to

change at a governmental level in order to push stakeholders in the plastics value chain to adopt greener, more sustainable practices.

1.3.1 Deposit Return Schemes and Plastic Taxes

Consumers purchase 31 billion single-use drinks containers in the UK every year, and the UK government currently estimates collection rates at 75% with a significant amount ending up littered or in landfill.³⁹ In an attempt to boost recycling rates in the UK up to 90%, and reduce littering of drinks containers by 85% in three years, the UK government is aiming to implement a deposit return scheme (DRS) in 2025, where customers who purchase a drinks bottle will receive a small cash reward for returning it to a DRS vending machine once used. The scheme is intended to collect drinks containers ranging in volume from 150 mL to 3 L.⁴⁰ This policy has been inspired by the European Union's (EU) Plastic's strategy, part of which is intended to curb the usage of single use plastic bottles, many of which are manufactured from PET.⁴¹ Caution, however, is warranted as Germany saw an increase in the market share of single-use drinks bottles after a DRS was introduced in 2003, with a corresponding fall in the market share of multi-use drinks bottles (Fig. 1.6). This was attributed to the ease which customers could return single-use PET bottles via the DRS, along with the financial rewards of returning a single-use bottle (0.25 Euros per bottle).⁴²

DRS is a new scheme in the UK, and it is preceded by another government intervention, the Plastics Packaging Tax, which came into force 1st April 2022.⁴³ Under this new intervention, any business which imports, or manufactures, plastic packaging containing less than 30% recycled content is required to pay £200 per metric tonne of plastic used. The objectives of this tax are to encourage investment in recycling strategies and reduce reliance on virgin plastic freshly produced from non-sustainable sources like crude oil.

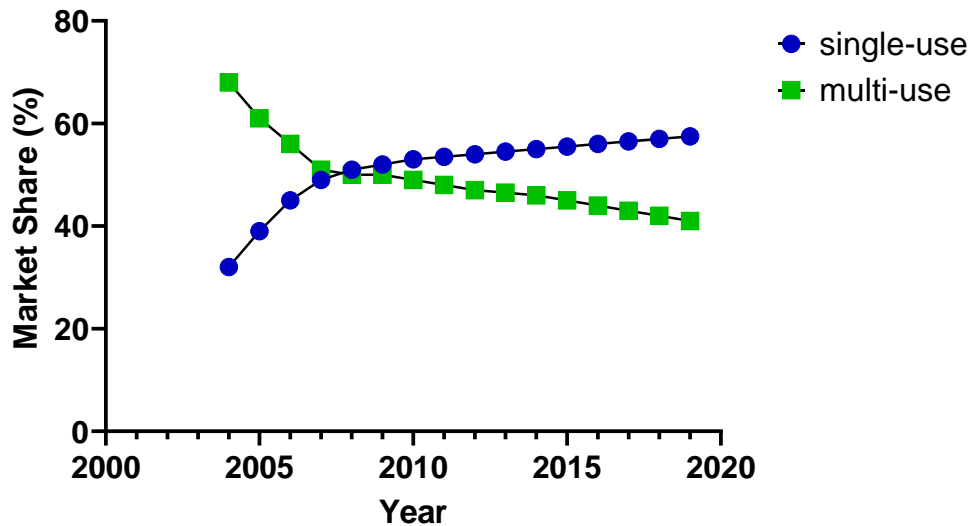


Figure 1.6 – Trend of increasing purchases of single-use bottles, with a concurrent drop in multi-use bottle usage, after DRS was introduced in Germany in 2003. ⁴²

The EU implemented a similar tax from 1st January 2021, known as the EU Plastics Contribution.⁴⁴ Estimated to raise € 7 billion per year, EU member states are obligated to pay € 0.80 per kilogram of non-recycled plastic packaging waste. This is in addition to any domestic plastic taxes countries implement and, much like the British version, is intended to incentivise the uptake of recycling and re-use strategies over the traditional linear waste treatment methods.

1.3.2 Recycling

1.3.2.1 Nomenclature

Discussing the plastic waste problem is complicated by several factors: the diversity of plastics in use, the variation in end of life (EOL) treatments, and the inconsistency in the nomenclature found in the recycling literature. For example, “chemical recycling” may be used to refer to both a protocol which breaks down plastic by pyrolysis, controlled thermal degradation, or via

solvolysis – where a polymer is depolymerised to monomers by a controlled chemical reaction in excess organic solvent.

In order to simplify the discussion around recycling in this work, the following hierarchy of recycling outlined in *Green Chemistry*⁴⁵ will be used to define different recycling strategies:

1. Closed-loop recycling describes when a plastic material may be used in the same product pre and post recycling, e.g. recycling PET bottles in a way to produce new PET bottles, such as degrading to monomers then re-polymerising.
2. Open-loop recycling describes when a plastic material may only be used for a different application post-recycling; this may also be referred to as downcycling.
3. Molecule recycling describes where a polymer is chemically converted to a valuable material other than the original monomers.
4. Energy recovery through incineration.

This hierarchy has been proposed as an effective framework for a simpler discussion around recycling approaches to plastics, as a processes place in the hierarchy is dictated by the end product and not the process itself. For example, a pyrolysis or solvolysis process able to degrade PET to its constituent monomers would be referred to as closed-loop recycling as they both produce material capable of being repolymerised to fresh PET. This is preferable to the interchangeable, and therefore confusing, terms of “thermal recycling”, “chemical recycling” and “solvolysis” which all may be used to describe these processes too.

1.3.2.2 Open Loop Recycling

As described above, open-loop recycling processes result in a material of lower quality than the virgin product, meaning it may not be possible for reuse in the exact same application. Often the

second application is considered to be of “lesser value” than the original, but the BPF have argued this can be offset by recycling the material into an application with a long lifespan such as high-density polyethylene (HDPE) bottles into plastic pipes used for construction.⁴⁶

Open-loop recycling is also commonly referred to as mechanical recycling, where waste plastics are processed into secondary raw material without significantly altering their chemical composition. This is achieved through a variety of sorting, grinding and washing steps, followed by re-extrusion. Currently, it is the most common route for recycling waste plastic, with AMI Plastics calculating that 36 million tonnes of recyclate was produced mechanically in 2022, which is projected to increase to 55 million tonnes by 2030.⁴⁷

A key strength of mechanical recycling is the tackling of heterogenous plastic waste streams collected kerbside from people’s homes, resulting in it becoming institutional in the recycling industry. The heterogeneous waste stream is collected at a variety of rates (41-76%) across Western Europe (UK, France, Germany, Spain and Italy), and consists of a variety of materials: polypropylene (PP), high-density polyethylene (HDPE), low-Density polyethylene (LDPE), poly(ethylene terephthalate) (PET) and polystyrene (PS).⁴⁸

The heterogenous nature of the waste collected at the kerbside mean that several separation steps are required before reprocessing to avoid contaminating the recyclate (Fig 1.7).⁴⁹ It is necessary to remove foreign materials, such as glass or ceramics, as well as separating out the individual polymers themselves. Simpler methods of doing this include manual sorting, but the greater mass of glass and ceramics when compared to plastics also means that they may be isolated by an air classifier or the float-sink method. The magnetism of metals also opens up routes for their removal from plastic waste streams through the use of magnets.⁵⁰

After the removal of these foreign materials, the polymers themselves can also be isolated from one another by exploiting their different densities in a float-sink separation. However, the most common method remains manual sorting on a conveyor belt, with the assistance of a near infrared red (NIR) detector. NIR makes it possible to identify many polymers by their unique absorbance spectrum, but there remains the limitations of discriminating between very similar plastic materials (HDPE and LDPE) and identifying a black plastic, as this will absorb all of the light. Hyperspectral imaging spectroscopy (HIS) or X-ray fluorescence may be used in combination with NIR to overcome these limitations.⁵¹

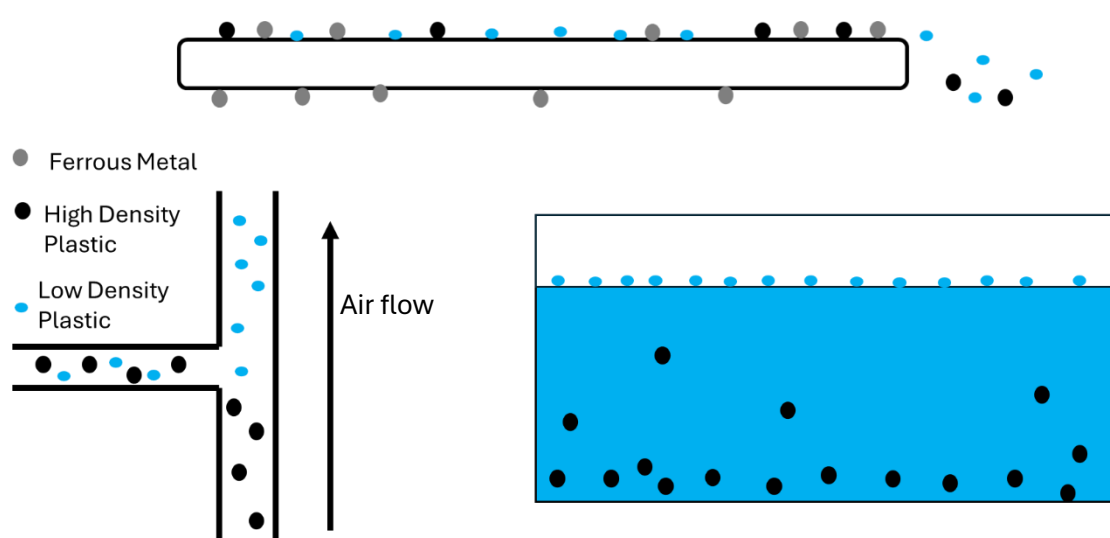


Figure 1.7 -Schematics of common sorting techniques in mechanical recycling. Removal of ferrous metals through use of a magnetic conveyor belt (top). Separating lighter plastics from heavier plastics by air classifier (bottom left) or float-sink separation (bottom right).

Much of the plastic waste will also be contaminated by substances it comes into contact with during its application. Food packaging may still contain residual amounts of food waste, and dirt may also be easily picked up too. Therefore, all plastic waste must also be washed to avoid contamination of the recycle. To streamline the recycling process, this cleaning may be integrated with the float-sink step mentioned previously, but some persistent materials may require removal with an organic solvent or detergent, which then needs to be cleaned or disposed of.^{52, 53}

After this pre-treatment, the plastic material undergoes melt extrusion. The plastic material is heated, and moved by rotating screws, in order to be softened.⁵⁴ The process is then completed by feeding the melt through a barrel of a specific size, to give extrudate of a desired size. This material can then be reformed into new plastic products.⁵⁵

Melt extrusion is relatively cheap, does not require organic solvents and can be used to process a wide range of polymers, hence its popularity.⁵⁶ However, the intense processing conditions inside the extruder (high temperature, mechanical shearing) cause polymer chains to undergo chemical degradation processes, such as: chain scission or oxidation.^{57, 58}

These modifications can result in a reduction of the molecular weight of the polymer, cross-linking of the material, or introduction of different functional groups.⁵⁹ Unfortunately, these changes on the molecular level on the polymer chain have an impact on the products reusability. Mechanical strength is weakened, discolouration takes place and thermal resistance is reduced.⁶⁰ The intense processing conditions employed in mechanical recycling can be simulated through repeated injection moulding. Virgin PET underwent several rounds of injection moulding, and a more brittle, less ductile material of lower molecular weight was produced (Fig. 1.8). These changes in mechanical properties were attributed to chain scission in the diethylene glycol region of the backbone to ethylene glycol units.⁶¹

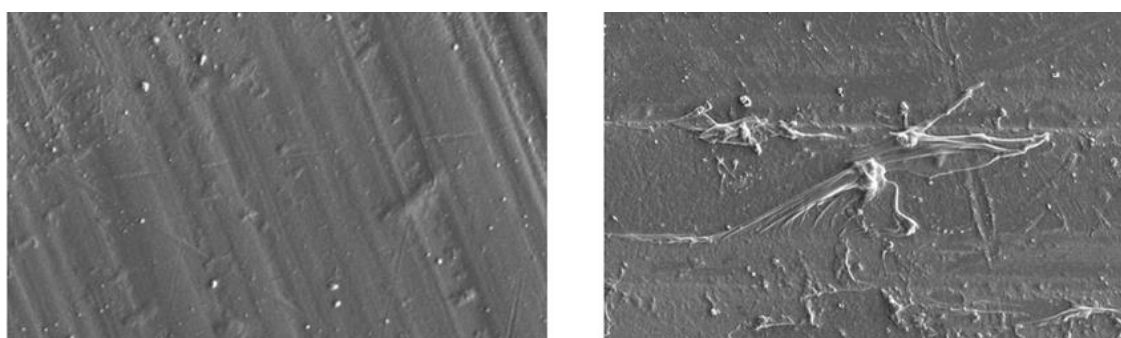


Figure 1.8- SEM images of virgin PET (left) and recycled PET (right), note the visible defects on PET's surface due to processing conditions of mechanical recycling.⁶¹

Mitigation strategies have been adopted to try and minimise the side effects seen during melt extrusion. Addition of new, virgin polymer “dilutes” the amount of damaged plastic in the extruded material. Additives known as compatibilisers may also be integrated into a recycled polymer that has been contaminated with a different polymer due to sorting limitations. For example, a short chain block polypropylene-PET copolymer (PP-PET) may be included in recycled PET which contains residual amounts of PP, to prevent phase separation of the two polymers leading to weak spots in the material.^{62, 63}

Despite these mitigations, the steady decline in a polymer’s properties continues with each cycle. It is considered technically feasible to recycle PP up to four times before the thermal degradation becomes pronounced enough to be detrimental. In practice however, most PP is downcycled once into playground equipment or clothing.⁶⁴ The same poor recyclability is seen for PET, as drinks bottles can only be recycled into lower value products such as textiles.⁶⁵ This is due to strict regulations on the quality and purity level of plastics that will come into contact with food, meaning it is currently challenging to mechanically recycle used food packaging into new food packaging.

It is clear that new recycling technologies are needed which will preserve the properties of polymers, enabling their perpetual reuse in similar applications across multiple lifetimes. Closed-loop recycling, where a polymer is degraded to monomers or oligomers which then may be re-polymerised to fresh polymer of equal quality to the virgin, is a popular route to improving the circularity of the plastics value chain.

Molecule recycling, however, is another viable route to prolong the life of waste plastic, by chemically converting it into a fuel or some other useful material or substance. Molecule recycling differs from closed-loop recycling as it does not produce the original monomer,

preventing repolymerisation, but it still avoids the damage inflicted on materials by open-loop methods and it is still a more circular approach than landfilling or incineration.

1.3.2.3 Molecule Recycling

Molecule recycling is an umbrella term in the hierarchy of recycling used to describe a host of routes used to convert plastic materials into valuable chemical commodities, such as fuels. As this is carried out by converting the plastic via a chemical process, molecule recycling is often used interchangeably with chemical recycling which complicates the discussion. In this work, molecule recycling will be used to describe a chemical process which converts a polymer into a product other than its monomers or oligomers.

Gasification, conventional pyrolysis, microwave pyrolysis and solvolysis are all examples of molecule recycling. Brief descriptions of gasification and conventional pyrolysis are included for purposes of breadth, but the main focus of this work is to develop novel recycling pathways based on microwave pyrolysis and solvolysis routes.

1.3.2.3.1 Gasification

Gasification describes the conversion of carbonaceous materials, including waste plastics, into syngas. This processing involves reacting the material in the presence of steam or carbon dioxide, at temperatures between 700 to 900°C, producing hydrogen and carbon monoxide mixtures which may also contain methane, nitrogen, carbon dioxide and water. These gaseous products may be burnt as a fuel directly or converted into a liquid fuel for use later.⁶⁶ The distribution of products for the two-stage gasification of PET is shown (Tab.1.1).⁶⁷

Product	Composition (volume %)
Hydrogen	50.19 ±0.06
Nitrogen	6.11 ±2.02
Carbon Monoxide	14.96 ±1.12
Carbon Dioxide	23.80 ±2.16
Methane	4.76 ±0.10
Ethane	<0.01
Ethene	0.01 ±0.00
C3+C4+C5	<0.01
Benzene	0.17 ±0.08
Toluene	<0.01

Table 1.1 – Composition of materials produced from the gasification of PET. ⁶⁷

Temperature = 800°C, time =60 minutes, steam: PET ratio=2:1

Gasification setups are relatively simple, and very tolerant to a wide variety of feedstocks, but the high temperatures associated with gasification means there are high energy costs, and waste residues consist of low-value tar and ash. ⁶⁸

1.3.2.3.2 Conventional Pyrolysis

Unlike gasification, pyrolysis is controlled thermal degradation in an oxygen-deficient environment, typically under an inert atmosphere or vacuum, preventing oxidation reactions. ⁶⁹

Pyrolysis of plastics has been reported to take place across a broad range of temperatures (200°C to 1300°C), depending on the nature of the feedstock and the pyrolysis method.

Conventional pyrolysis refers to protocols where a feedstock is heated through “normal” heating processes, and the energy is dissipated through conduction, convection and radiation.

Once in the reactor, there is scope to tune the decomposition of the polymers to particular products, by varying the retention time as well as the reaction temperature. A decomposition carried out at a lower temperature, over a longer retention time, is referred to as a slow pyrolysis. During slow pyrolysis, the feedstock is heated at a rate of 1-10 °C/min and the major product is char as solid residue formation is favoured by slower heating rates (Fig. 1.9).⁷⁰

Fast pyrolysis refers to procedures where a waste feedstock is heated to temperatures between 500-700 °C at a rate of 100 °C/min (Fig. 1.9).⁷¹ The majority product (≈75%) of fast pyrolysis are oils and yields of 90 wt% have been reached for pyrolyzed polyolefins.⁷²⁻⁷⁴ Flash pyrolysis is the third, and fastest, variant of conventional pyrolysis, where feedstock is heated to over 700 °C in a very short time and the major product is gases (Fig. 1.9).⁷⁰

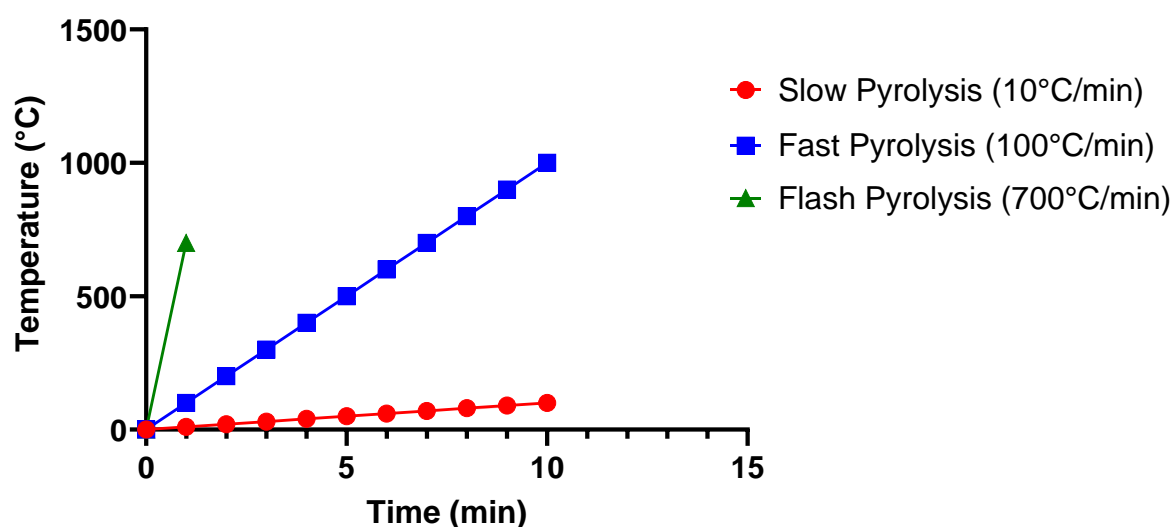


Figure 1.9 – Illustration of relative heating profiles of slow (red), fast (blue) and flash (green) pyrolysis in a 10-minute residence time.

Pyrolysis' contribution to the circular economy lies in the many applications that can be applied to the products. Metals found in soils can be extracted from the char of biomass which undergoes pyrolysis⁷⁵, and bio-oils have been successfully recovered from microwave-assisted pyrolysis of kitchen waste.⁷⁶

With PET feedstocks specifically, a challenge presented by conventional pyrolysis is the formation of char: a low-value product (\$100/ton) which can be difficult to isolate from additional solid products.⁷⁷ Char formation has been attributed to the loss of oxygen and hydrogen from the polymer backbone when exposed to high temperatures, as they may be released in a variety of gaseous products such as carbon dioxide (CO₂), carbon monoxide (CO) or ethylene.⁷⁸⁻⁸⁰ One route to prevent loss of these elements has been the inclusion of water in

the pyrolysis reactor, as this will promote hydrolysis reactions, forming terephthalic acid (TPA,) over char formation.⁷⁸ Upon the addition of water to the pyrolysis set-up, yields of TPA increased from 35.0 wt% to 85.5 wt%, and the formation of char was eliminated almost entirely. Solid impurities were identified using liquid chromatography-mass spectrometry (LC-MS) as benzoic acid, styrene, monovinyl terephthalate and diphenyl terephthalate.

Yuan *et al* also reported a procedure for generating nitrogen-doped microporous carbon for CO₂ capture via conventional pyrolysis of PET in the presence of potassium hydroxide and urea at 700 °C.⁷⁹ CO₂ released in the pyrolysis reacted with potassium hydroxide to produce potassium carbonate, which was then able to further react with carbon domains in the pyrolysing PET to release further gaseous products, thereby increasing the diameter of pores in the final char product. The microporous structure of the final char enabled the uptake of urea, which enhanced the uptake of CO₂ by the pyrolyzed products, due to the basicity of the nitrogen functionality aiding CO₂ binding. In this way, char, a typically low-value product of PET pyrolysis, was successfully modified towards a useful application.

Catalytic pyrolysis of PET in the presence of ammonia with an aluminium oxide (Al₂O₃) catalyst at 500 °C yielded terephthalonitrile (TPN) with a 90% selectivity in the products, opening up a route to a platform chemical valuable to the pharmaceutical and agricultural industries.⁸⁰ However, whilst the selectivity of TPN was 90% in the nitrile products, a nitrile yield of only 58% was observed and difficulties surrounding the separation of so many chemically similar products (TPN, benzonitrile, acetonitrile) remain, and the catalyst began to deactivate after five cycles.

Co-pyrolysis of mixed plastic wastes, as well as mixed waste streams of plastics and biomass, has been explored too. Difficulties in sorting plastic waste streams out from one another, as

discussed in section 1.3.2.1, has fuelled an interest in developing processes capable of treating heterogeneous waste streams.

Fast co-pyrolysis of PET with paulownia wood was studied, but large amounts of char were observed to form. The degree of char formation increased with the amount of PET included in the pyrolysis feedstock. It was hypothesised that the solid pyrolysis products from the PET fraction were cross-linking with those products from the paulownia wood pyrolysis, enabling greater char formation as alongside a corresponding reduction in gaseous products – primarily methane.⁸¹

Slow pyrolysis of PET was undertaken by Çepeliogullar *et al* as a mixed feedstock with several different types of biomass (hazelnut shells, sunflower residues, cotton stalks and *Euphorbia rigida*) up to 500 °C at heating rate of 10 °C/min.⁸² Pyrolysis oils were obtained when these biomass feedstocks were pyrolysed alone, analysed by gas chromatography-mass spectrometry (GC-MS) and Fourier transform infrared spectroscopy (FT-IR), and were shown to be mixtures rich in a variety of phenolic and benzene derivatives, in addition to polycyclic aromatic hydrocarbons, ketones and alkanes. The yield of pyrolysis oils increased marginally when these biomasses were co-pyrolysed with PET, and an enhanced selectivity for benzene derivatives over phenol derivatives occurred. This change in product nature is attributed to “synergistic effects” but no real attempt is made at elucidating what they may be, and no additional higher molecular weight analysis techniques, such as Gel Permeation Chromatography (GPC) or Matrix-Assisted Laser Desorption/Ionization (MALDI) to ensure a complete picture of the pyrolysis oil nature was obtained.

What these examples of non-catalytic, catalytic and co-pyrolysis of PET demonstrate is that, although valuable products may be obtained, the exact yield and composition of those products is highly variable and dependent on a number of factors: feedstock nature,

temperature, heating rate, inclusion of additional reagents or a catalyst. This complicated picture makes drawing a general conclusion about conventional pyrolysis of PET challenging, other than to say the commercial viability of a given process is highly dependent on the feedstock being economically obtainable, and a sufficient amount of valuable material must be produced to generate sufficient income.

One major drawback of conventional pyrolysis however is the long residence times required, in order to ensure uniform heating of the feedstock. Given the large volumes of waste plastic being produced, a degradation method with high turnover would be extremely valuable.

1.3.2.3.3 Microwave Pyrolysis

Microwaves are a non-ionising form of radiation found between frequencies of 300 MHz-300 GHz, and wavelengths 1 m – 1 mm, in the electromagnetic spectrum. Like all electromagnetic radiation, microwaves consist of two separate components, electric and magnetic, which are perpendicular to one another and in phase. Microwaves have found many industrial uses, pyrolysis being one of particular interest to this work. In order to avoid disrupting communications, international agreements have determined specific microwave frequencies for industrial, domestic and medical uses. These frequencies are 910 MHz or 2450 MHz, meaning that the material being processed must possess a sufficient dielectric response at these frequencies. In addition, consideration must be given to sample placement in a single-mode reactor if repeatable results are desired; this is less of an issue in a multi-mode set up with continuous stirring.⁸³

One unique property of microwave radiation that imparts it a distinct advantage over conventional pyrolysis is volumetric heating (Fig. 1.10). Provided a feedstock is susceptible to microwave heating, its core will be heated at the same rate as its surface, eliminating the need

for heat transfer through conduction or convection - enabling very rapid heating. These unique properties of microwave radiation will be discussed further in section 3.1.1, but one major advantage of the rapid heating seen with microwaves is excellent energy efficiency. Zhou *et al* calculated that microwave pyrolysis of HDPE at 400 °C with a zeolite catalyst boasted an energy efficiency of 89.6%.⁸⁴



Figure 1.10 - Temperature profile of volumetric heating (left) compared with conventional heating (right).

This creates the potential to develop novel recycling routes for materials with short residence times and high turnover, with a growing interest in microwave pyrolysis observed in the literature. When the search terms “Microwave Pyrolysis” and “Plastics” are entered into *Web of Science*, 20 results or less can be seen to be published pre-2020 per year. From 2020 onwards, this value more than triples – peaking at 64 publications in 2022 (Fig. 1.11).⁸⁵

One challenge concerning the microwave pyrolysis of plastics specifically is that many polymers are very high molecular weight, semi-crystalline and may not possess the polar regions necessary to interact with microwave radiation (see Chapter 3), all of which impede the ability of the polymer chains to dissipate energy as heat when exposed to a microwave field.⁸⁶

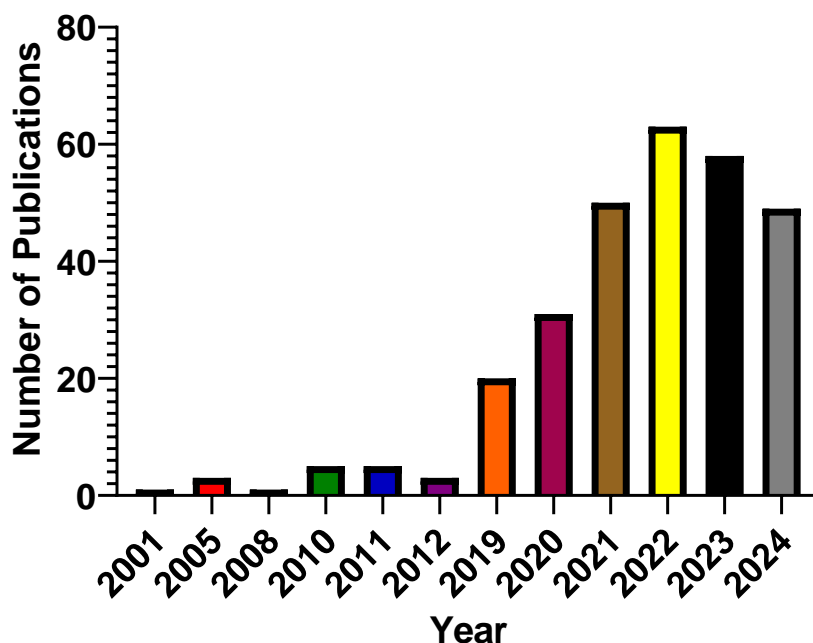


Figure 1.11 - Growth of literature published on microwave pyrolysis since 2001. Omitted years had zero contributions to the literature.

To overcome this, many polymers are commonly doped with a susceptor, a chemical species capable of strongly absorbing microwave radiation, or a catalyst is included in the pyrolysis reactor.⁸⁷⁻⁸⁹ In this way, heat energy from the microwave may be indirectly transferred to the polymer through contact with a susceptor or catalyst, facilitating their degradation. A susceptor is commonly mixed in mechanically with the material intended to be pyrolyzed.⁸⁹

Susceptors and catalysts play similar roles in microwave pyrolysis, and the terms may be used interchangeably. In this work, susceptor will refer to a species mixed with a plastic to allow indirect heating by microwaves, but plays no obvious role in the chemistry, whereas a catalyst will refer to a species which may allow indirect heating of the plastic but also influences the yield and selectivity of the products through the role it plays in the pyrolysis mechanism.

1.3.2.3.3.1 Applications of Microwave Pyrolysis towards Plastic Recycling

Despite the lack of abundance in the literature studying the microwave pyrolysis of plastic, a wide range of different materials have been explored. An early example was the successful pyrolysis of toothpaste tubes by Ludlow-Palafox and Chase.⁹⁰ A HDPE/Aluminium composite (toothpaste tube) was successfully degraded by microwave heating, with 500 – 700 °C being achieved by use of particulate carbon as a microwave susceptor. HDPE was shown to be converted to a range of aliphatic and aromatic compounds by GC-MS, whilst the aluminium remained intact and was easily recovered from the reactor.

HDPE has also been degraded to an oil by use of waste tires or char as a microwave susceptor.⁹¹ Oil yields of 37 wt% and 80.2 wt% were produced by switching between tire and char susceptors, demonstrating that product selectivity can be tuned through susceptor choice. Yields of valuable oil were enhanced by increasing input power for the same susceptor.

GC-MS and IR analysis determined that these liquids consisted of a complicated mixture of alkane, alkene and aromatic compounds, which were hypothesised to arise from a series of radical or Diels-Alder reactions as the polymer backbone underwent homolytic chain scission during pyrolysis (Fig. 1.12). The authors argued that pyrolysis of HDPE in the presence of the butadiene-styrene rubber material the tires consist of, illustrates that it is tolerant to industrial contaminants.

Polystyrene has also undergone microwave processing in the presence of coal. This co-pyrolysis was hypothesised to enhance the yield of oil, whilst reducing gaseous products, by synergistic interactions between the polystyrene and active species produced from the coal during pyrolysis. The work appeared to be successful as three liquid fractions (aqueous, oily and sticky) totalling 80.0 % of the yield were produced, whilst a gas yield of only 6.0 % was recorded.

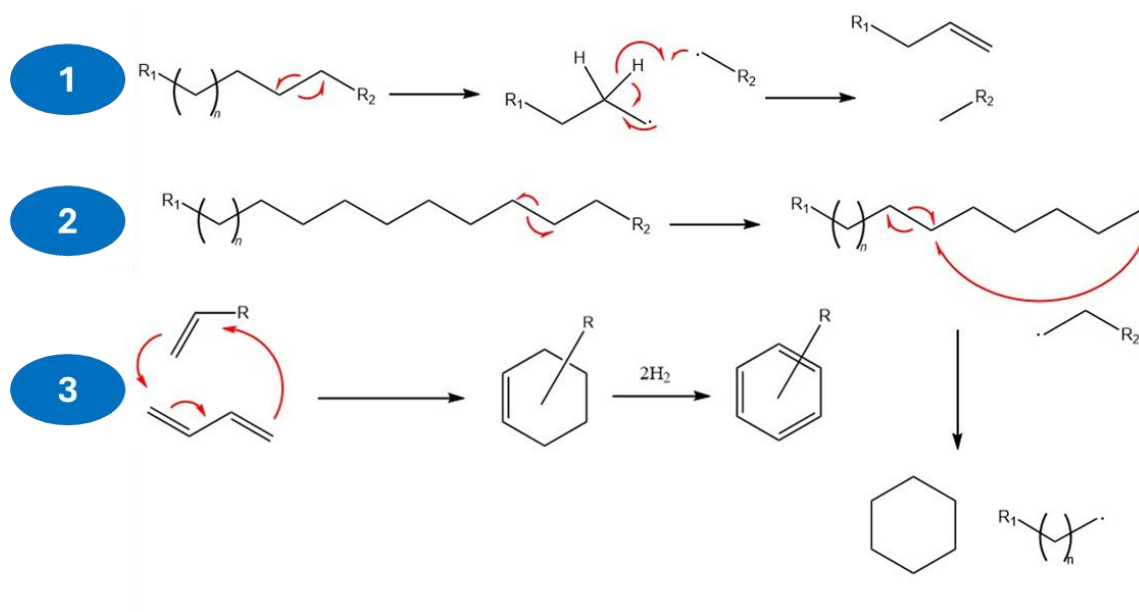


Figure 1.12 – Proposed radical mechanism HDPE undergoes during microwave pyrolysis.

1. Homolytic scission of the backbone to produce vinyl and alkane products.
2. Homolytic chain scission followed by chain backbiting to give cyclic products.
3. Diels-Alder reaction between vinyl pyrolysis products to give aromatic products

However, the authors give little detail about what the synergistic effects may be taking place in their system, but they do state that the high temperature employed in pyrolysis will generate various radical species capable of initiating cracking of the polymer backbone. The primary analytical technique was GC-MS, and it identified a narrow distribution of phenolic compounds in the oily liquid product (Fig. 1.13).

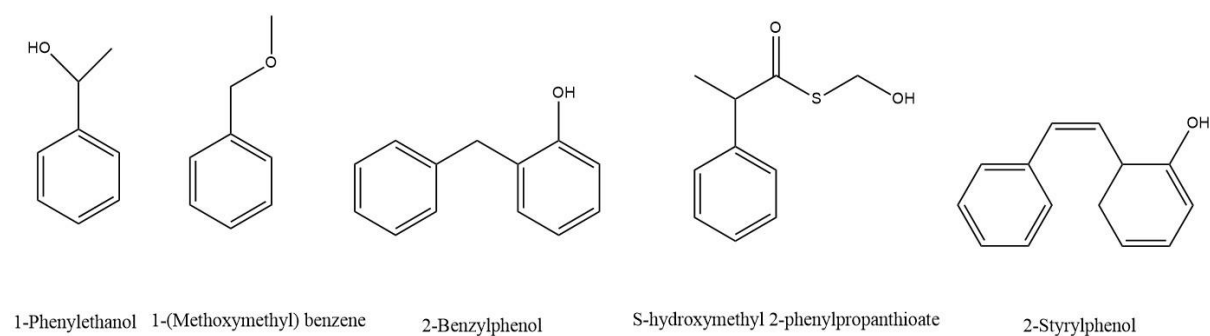


Figure 1.13 – Various aromatic products produced by microwave pyrolysis of polystyrene in the presence of coal.

Using metals as microwave susceptors for microwave pyrolysis of polystyrene has also produced promising results. *Hussain et al* showed that addition of an aluminium coil in a pyrolysis reactor enabled full conversion of polystyrene in 10 minutes, with a liquid yield of 88 wt%.⁹² The microwaves selectively heated the aluminium coil, which was then able to heat the polystyrene to high temperature by conduction, initiating its degradation. GC-MS analysis determined that the liquid yield consisted of eight different aromatic species. A key outcome of this study was the minimal amount of low-value char generated (≈ 2 wt%), but the input power, and resulting temperature, are not stated in the methodology, which makes meaningful comparisons with other publications difficult.

The same group also conducted pyrolysis of polystyrene where an iron mesh was included as a microwave absorber.⁹³ The mesh enabled temperatures of 1100 – 1200 °C to be reached, resulting in a pyrolysis oil and gas yields of 80 % and 15 % respectively. Different forms of iron (solid cylinder, chips, and mesh) were tested for their absorbing ability, with a solid block of iron resulting in the slowest heating (pyrolysis took 30 minutes to complete) and the mesh yielding the most efficient heating (pyrolysis took 10 minutes). This is ascribed to the higher surface area to volume ratio of the mesh, facilitating better reflection of absorbed microwave energy out as heat.

Polyvinyl chloride (PVC) is commonly co-pyrolysed with biomass, as the water inherent in the biomass acts as a strong microwave absorber.⁹⁴ As the biomass also forms part of the product, the need to isolate the susceptor from the pyrolysis products is avoided in this set-up. A final benefit appears to be that corrosive hydrochloric acid (HCl) generated by PVC degradation is removed from the final products by secondary dehydration reactions with carbohydrates in the biomass.⁹⁵

One example is the co-pyrolysis of PVC with microwaves alongside microalgae (MA).⁹⁴ Pyrolysis was carried out at 550 °C at input powers of 800 and 1000 W. As the proportion of MA in the initial feedstock increased, the distribution of the final products was seen to favour valuable pyrolysis oil over char, with both gas and oil yields improving at 1000 W input power as PVC backbone was cracked more thoroughly, preventing char formation. Similar to previous PS and HDPE examples, GC-MS of the liquid products revealed a complex mixture of alkane, alkene and aromatic products.

Co-pyrolysis of PVC with sophora wood (SW) has been reported as a route to suppress the chlorine-content of the pyrolysis products.⁹⁶ Inclusion of SW reduces the content of chlorine-containing compounds in the oil fraction to <1% for pyrolysis carried out below 550 °C. Furthermore, with increasing SW: PVC ratio, the concentration of chlorine in the gas phase decreased from 59.07% to 28.09%. A temperature range 450–550 °C was found to be the optimum for reducing HCl in gaseous products, minimising the content of chlorine-containing compounds in oil and retaining chlorine in the less-valuable char.

1.3.2.3.3.1 Current Limitations to Microwave Pyrolysis

Whilst the use of a susceptor or catalyst in microwave pyrolysis has brought inarguable benefits to the overall efficiency and selectivity of the processes, they are not without their limitations. As many susceptors are mixed mechanically with the feedstock, they are often not evenly distributed throughout the material. This results in uneven heating of the feedstock, and can result in incomplete pyrolysis or, more concerningly, the generation of unintentional “hot spots” which can damage the reactor or cause fires (Fig. 1.14).⁹⁷

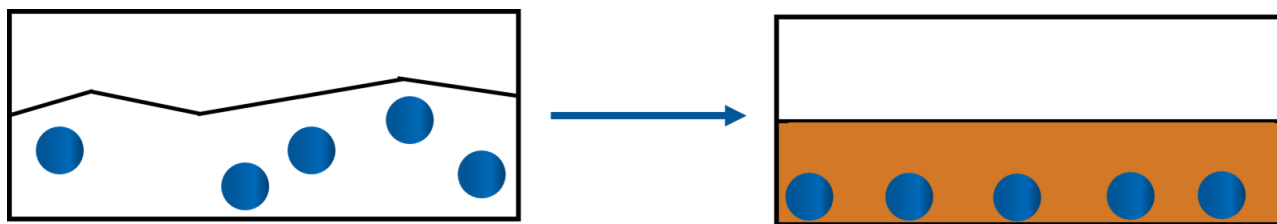


Figure 1.14 - Schematic showcasing issues with microwave susceptors. The susceptor material may not be evenly spread throughout the plastic (left) and it may be challenging to isolate a solid susceptor from the solid pyrolysis products seen with PET (right).

Another challenge of all pyrolysis techniques is the heterogeneity of the recovered products. For PET in particular, it is common to recover materials in the solid and gas phase with pyrolysis oils being less common. This necessitates an additional recovery step post-pyrolysis, and it can be challenging to isolate solid susceptors from the solid products, complicating their recovery and re-use. Furthermore, the fact that the glycolic portion of the PET repeating unit is typically converted into a gas during pyrolysis, rather than ethylene glycol, prevents the immediate repolymerisation of the products back to PET post-pyrolysis.

More controlled chemical degradations have gained significant traction in the literature, as they can be carried out in a single liquid phase and exhibit excellent control over products. These processes are collectively referred to as solvolysis.

1.3.2.3.4 Solvolysis

Solvolysis involves the degradation of a material in excess organic solvent, often with the presence of a catalyst to aid reaction time, temperature, and selectivity to a single desired product. The solvent serves a dual purpose: the dissolution of reagents/swelling of the polymer being degraded as well as playing the role of a nucleophile in the chemical reaction.

It is necessary for the polymer to contain a labile functional group in its backbone which can be degraded by a nucleophile (Fig. 1.15). Correspondingly, many examples of solvolysis can be found for polyesters⁹⁸, polyamides⁹⁹, polyurethanes¹⁰⁰ and polycarbonates¹⁰¹. As they typically

possess an unreactive C-C backbone, it is less common to see solvolysis performed on polyolefins.

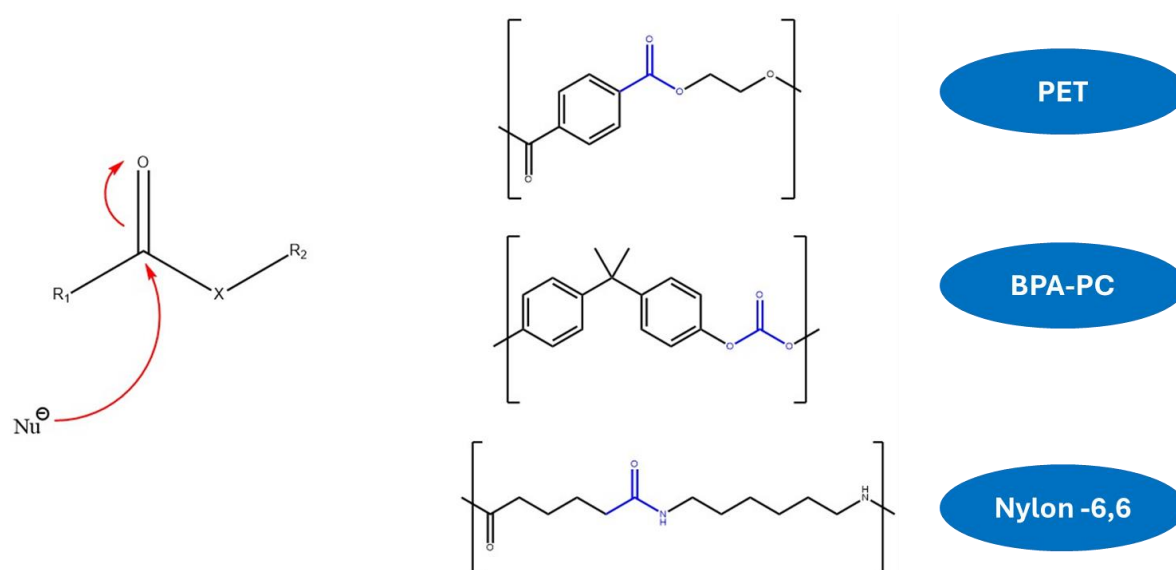


Figure 1.15 – Mechanism of nucleophilic attack on a carbonyl that many solvolysis mechanisms proceed by (left). Acid or base catalysis is usually necessary – see Chapter 5. Portions of the backbone where nucleophilic attack takes place in commercially available polymer are highlighted in blue (right).

Solvolysis tends to be well associated with closed-loop recycling routes for PET, but there are a few strategies that fall into the molecule recycling category too. PET may be depolymerised with the use of amines to chemically produce terephthalamides, referred to as aminolysis. The mechanism is presented as a classic nucleophilic attack of the polymer backbone, the ester linkage in the case of PET, and the exact structure of the terephthalamide may be tuned by varying the exact amine used (Fig 1.16).

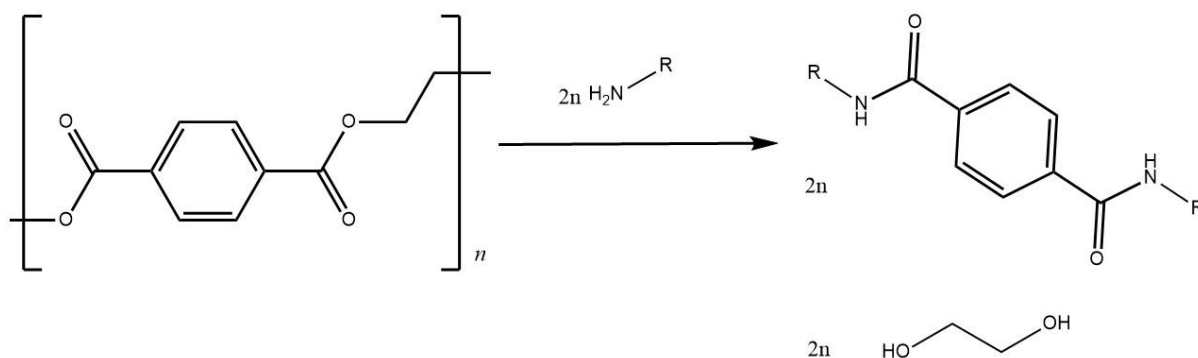


Figure 1.16- Generic representation of PET aminolysis to give the corresponding terephthalamide and ethylene glycol.

Shukla and Harad successfully degraded PET to bis(2-hydroxyethyl)terephthalamide (BHETA) by ethanolamine in 8 hrs under reflux, catalysed by glacial acetic acid, sodium acetate or potassium sulphite.¹⁰² This BHETA preparation from PET was then carried forward by Shamsi *et al*¹⁰³ and Aslzadeh *et al*¹⁰⁴ as they identified that BHETA could be employed as a pre-cursor for polyurethane synthesis.

After successful PET depolymerisation, BHETA has been successfully reacted with a variety of acids to generate plasticisers for polyvinyl chloride (PVC), such as decanoic acid¹⁰⁵, heptanoic acid¹⁰⁶ and butyric acid.¹⁰⁷

Microwave-assisted aminolysis has gained popularity in the literature, as the uniform heating ability of microwave radiation suppresses reaction times from hours to less than 5 minutes. BHETA has been produced in yields greater than 90% in these incredibly short reaction times when microwave heating is employed.^{108, 109}

Replacing ethanolamine with 3-amino-1-propanol produces bis-(3-hydroxypropyl)terephthalamide (BHPTA), which may undergo a cyclisation reaction with thionyl chloride to produce bisoxazolines -compounds which find uses as chain extenders or crosslinkers in polymer synthesis.^{110, 111}

Aminolysis has been shown as a viable route to multiple secondary useful life spans for waste PET. However, the use of an amine as the nucleophile prevents regenerating the original monomers that could be used to produce new PET, therefore this series of reactions falls into the molecule recycling category alongside many pyrolysis and gasification treatments of PET.

Many other solvolysis routes for PET waste treatment fall into the closed-loop recycling category as they generate monomers in high yields and have therefore gained significant attention.

1.3.2.4 Closed-Loop Recycling

Closed-loop recycling processes enable a plastic product to be re-used in its original application after re-processing. In order to do this, it is key that the polymers retain their physiochemical properties during the recycling process. The most common route is the controlled chemical degradation of the polymer to its constituent monomers or short chain oligomers. These products can then be repolymerised to produce a fresh polymer with identical properties to the virgin material, as the intense conditions seen in mechanical recycling (thermal degradation, shearing) are avoided.

The popularity of closed-loop routes for PET recycling is reflected in the range of review papers available on the subject.¹¹²⁻¹¹⁵

1.3.2.4.1 Common PET Closed-Loop Products

Much like the aminolysis protocols in the previous section, the exact chemical nature of the solvolysis products can be tuned by selection of the appropriate nucleophile. Ethylene glycol, methanol, and water produce compounds that can be re-polymerised back to PET (Fig. 1.17).

Glycolysis of PET provides a direct route to BHET, which can be re-polymerised back to PET with no pre-treatments. Methanolysis yields dimethyl terephthalate, alongside ethylene glycol, which can be converted into BHET by a simple transesterification reaction. Hydrolysis of PET with water will degrade PET into terephthalic acid and ethylene glycol, which may also be converted into BHET albeit with slightly harsher conditions than the dimethyl terephthalic analogues, due to the higher temperature needed to dissolve terephthalic acid in ethylene glycol.¹¹⁶

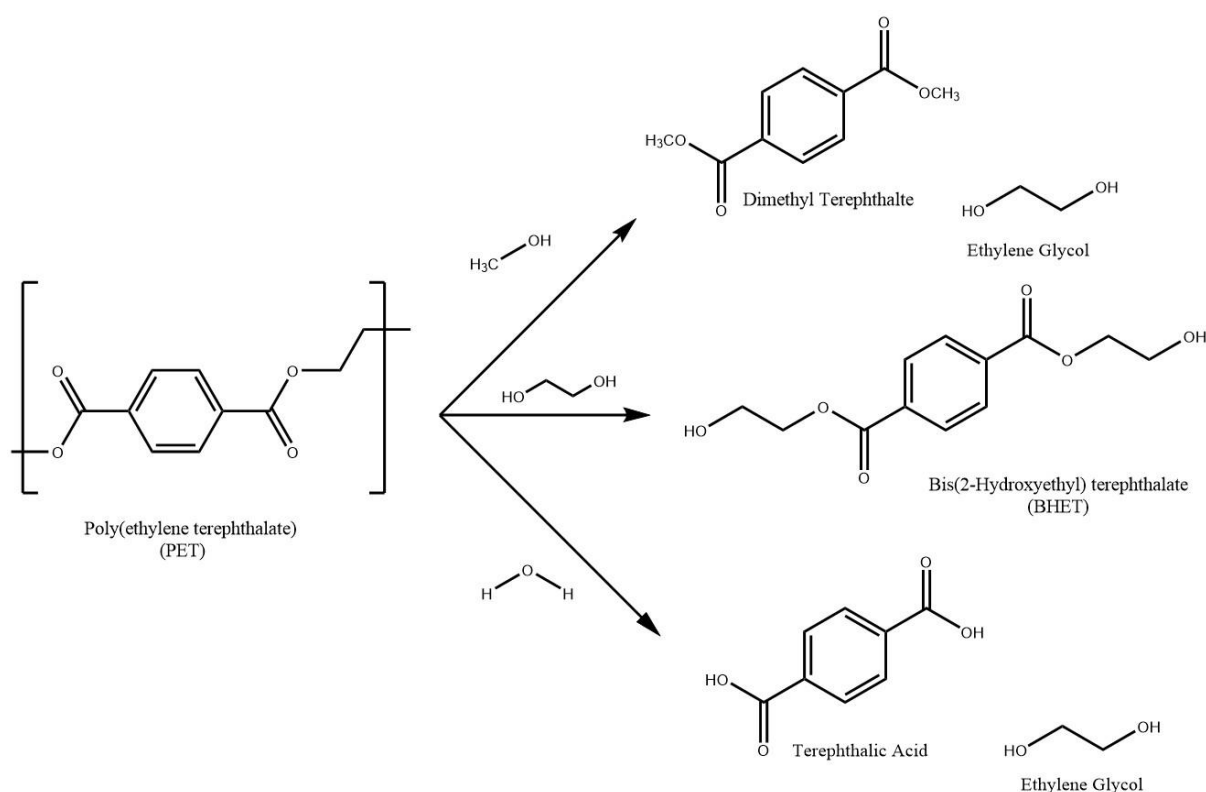


Figure 1.17- Schemes of common PET degradation pathways to monomers: methanol to dimethyl terephthalate and ethylene glycol (top), ethylene glycol to BHET (middle) and water to terephthalic acid and ethylene glycol (bottom).

1.3.2.4.2 Catalytic Systems

Whilst the choice of nucleophile for a closed-loop recycling system of PET is limited to one of ethylene glycol, methanol, ethanol or water, an eclectic range of catalytic systems have been studied.

Original systems in the literature employed various metal-based, Lewis acid catalysts, which are able to accept electrons from an oxygen atom in a carbonyl group, and thereby activate the carbonyl towards attack by the nucleophile (Fig. 1.18) ¹¹⁷. A range of yields have been obtained at a range of temperatures (Tab.1.2).

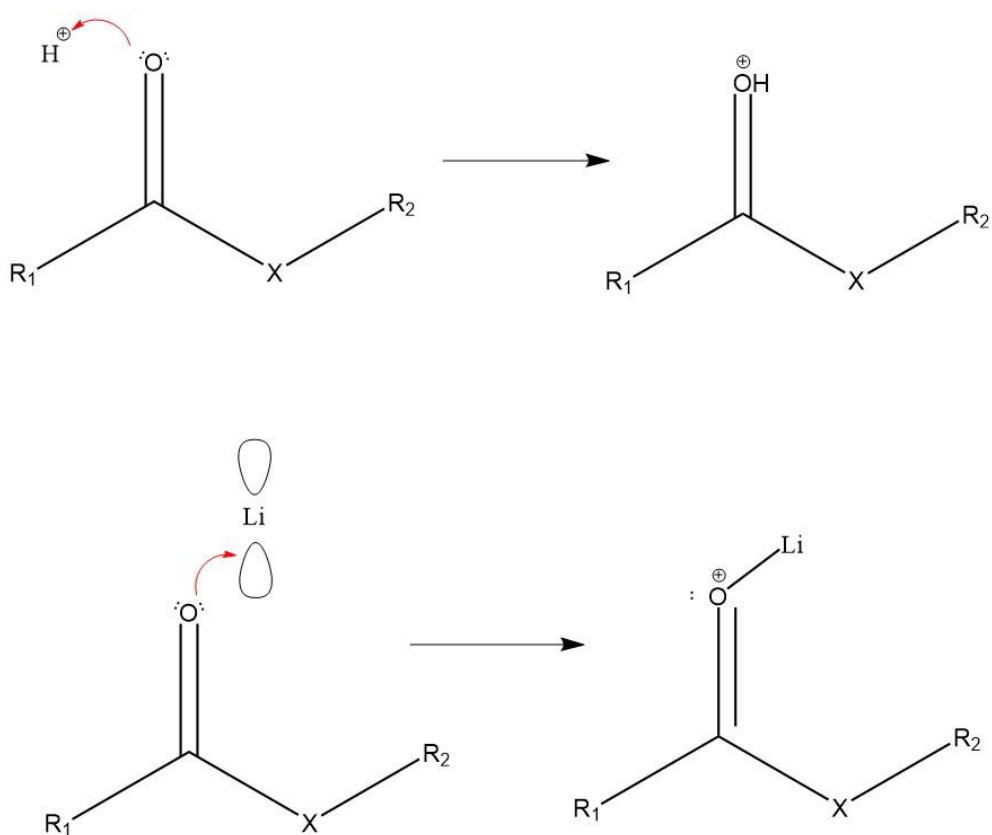


Figure 1.18 – Mechanism of a Bronsted acid protonating the oxygen in a carbonyl group (top).

Lewis acids undergo a similar interaction, except they accept the electrons from the oxygen rather than donating a proton (bottom).

As in aminolysis, microwave-irradiated systems have also been explored. PET has been successfully glycolysed with a range of glycolytic solvents (diethylene glycol, propylene glycol, polyethylene glycol, 1,4-butanediol), with 100% conversion being achieved in under 10 minutes. In most cases, zinc acetate is the most popular catalyst of choice, but potassium carbonate, calcium oxide or sodium methoxide can also be employed. ^{118, 119}

Table 1.2- Examples of metal catalysed PET degradation protocols, producing a range of closed-loop products.

Nucleophile	Catalyst	Products	Yield	Temperature	Time	Ref
Methanol	Aluminium Triisopropoxide	Dimethyl Terephthalate	64%	200 °C	120 mins	120
		Ethylene Glycol/	63%			
Methanol	Lead Acetate/Zinc Acetate	Dimethyl Terephthalate	100 %	120 °C	60-150 mins	121
Ethylene Glycol	Cobalt Acetate	Ethylene Glycol/	100%	190 °C	90 mins	122
		BHET	100%			
Diethylene Glycol/ Dipropylene Glycol	Titanium (IV) Butoxide	Assorted Polyols	N/A	200-240 °C	N/A	123

Zinc acetate catalysed systems have been utilised to degrade mixed plastics systems as well. Refluxing a mixed PLA-PET feedstock in methanol or ethanol yielded the corresponding alkyl lactate of the PLA, whilst PET was unaltered. This unreacted PET can be separated from the crude PLA depolymerisation products through filtration, then refluxed in ethylene glycol at a higher temperature with zinc acetate to yield BHET. ¹²⁴

Selective degradation of mixed PLA-PET is possible as depolymerisation of aliphatic polyesters is known to be more facile than their aromatic analogues. This is attributed to the reduced steric hindrance seen in aliphatic examples, due to the absence of the aromatic ring, and in the case of PLA-PET systems specifically the greater abundance of amorphous regions seen in PLA enables an easier initiation of the depolymerisation. ¹²⁵⁻¹²⁷

Organobases have been identified as alternative catalysts for the degradation of polymers. Examples include the guanidine and amidine bases 1,5,7-triazabicyclo[4.4.0]dec-5-ene (TBD) and 1,8-diazabicyclo(5.4.0)undec-7-ene (DBU) due to their basic nature – TBD $pK_a = 26$ in acetonitrile ¹²⁸, DBU $pK_a = 24.3$ in acetonitrile (Fig.1.19). ¹²⁹ In polymer science, they were originally used to catalyse the ring-opening polymerisation (ROP) of cyclic monomers ^{130, 131},

these catalysts have also been successfully deployed in the degradation of a range of polymers such as polyesters^{132, 133} and polycarbonates.^{134, 135}

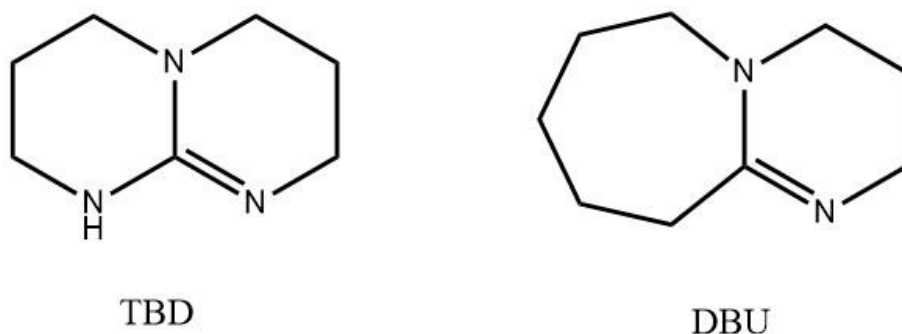


Figure 1.19 – Structures of organobases TBD and DBU.

Two pathways by which organobases catalyse both ROP and depolymerisations have been proposed in the literature (Fig. 1.20):

1. Nucleophilic Mechanism – the organobase deprotonates the nucleophilic species (methanol, ethylene glycol etc.) which is transformed into its more reactive alkoxide state and goes on to attack the polymer at its labile functional moiety.
2. Hydrogen Bonding Mechanism – rather than actively deprotonating the attacking nucleophile, the organobase hydrogen bonds to both reagents simultaneously and brings them into close proximity/favourable orientation to undergo reaction. This example is TBD specific, as it contains both hydrogen bond donor and acceptor groups.

Computational studies have been conducted to determine which mechanism is likely to dominate over the other for ROP. Unless there is considerable strain in the cyclic monomers, the hydrogen bonding mechanism has been calculated to be energetically favourable, with this

conclusion being further evidenced by the reduction of the reaction rate for ROP of L-lactide by a factor of 90 when methyl TBD is used in the place of TBD removing TBD's dual hydrogen bond donor/acceptor functionality.¹³⁶⁻¹³⁸

However Horn *et al*'s calculations found that where the depolymerisation of PET with an alcoholic nucleophile was concerned, a more energetically favourable transition state could be observed where TBD deprotonated the alcohol to form its more reactive alkoxide suggesting the chemistry proceeds by a nucleophilic mechanism.¹³⁹

Regardless of the debates surrounding the mechanism, the power of these organobases catalyse the degradation of polymers has been demonstrated with a plethora of examples. Precise examples of PET degradation with these catalysts in supercritical carbon dioxide (scCO₂) will be presented in Chapter 5 but for now one more set of uncatalysed routes warrant discussion.

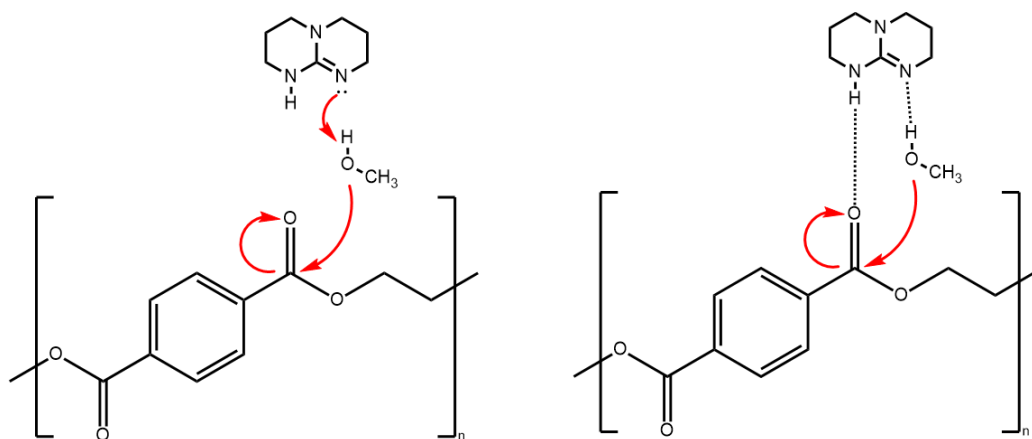


Figure 1.20 – Proposed nucleophilic mechanism for TBD-catalysed PET depolymerisation (left), against proposed hydrogen-bonding mechanism (right). The key difference being that TBD's structure remains unaltered in the latter mechanism.

1.3.2.4.3 Supercritical Degradation

PET degradation has been well documented in supercritical fluids of water (scH₂O) and methanol (scMeOH). The intense conditions required to achieve the supercritical states of these solvents, alongside the high diffusivity and excellent mass transport properties of supercritical fluids, provides a catalyst-free route to monomers in incredibly short reaction times (Tab. 1.3).^{140, 141}

Table 1.3- Critical temperatures and pressures for common supercritical fluids. Note that the temperature required to reach the critical point of carbon dioxide is far lower than water or methanol.

Supercritical Fluid	Critical Temperature (°C)	Critical Pressure (bar)	Reference
Carbon Dioxide	31.1	73.8	142
Water	372.9	221.0	143
Methanol	238.9	80.9	144

Yang *et al* demonstrated that PET could be degraded to dimethyl terephthalate and ethylene glycol in as little as 20 minutes when an 8:1 weight excess of methanol was used with respect to PET at 260 °C and 110 bar.¹⁴⁵ Genta *et al* determined that the mechanism of PET degradation in scMeOH proceeded by a transesterification mechanism at random ester linkages along the PET backbone to produce oligomeric species and monomers, and that side products, such as 2-methoxyethanol, arose when secondary reactions occurred between the monomers and the supercritical fluid.¹⁴⁰

Hydrolysis of PET in scH₂O is a route to terephthalic acid in reaction times as low as 30 minutes (100 % yield, 97 % purity) at 400 °C and 400 bar, but ethylene glycol was observed to undergo secondary degradation reactions at these conditions.¹⁴⁶ Yamamoto *et al* were able to recover ethylene glycol from supercritical hydrolysis of PET by limiting temperature to 300 °C, preventing its conversion into acetaldehyde.¹⁴⁷

In all of the above cases, temperature was seen as an important variable for controlling the degradation of PET, but increasing pressure resulted in no observable effect once the supercritical state had been achieved.

1.3.2.4.4 Current Drawbacks with Closed-Loop Methods

A plethora of closed-loop methods have been developed for PET recycling that are able to yield all of the monomers of interest (dimethyl terephthalate, ethylene glycol, BHET) in high yields, with reasonable reaction times.¹¹²

Whilst PET is typically not soluble in the organic solvents used in solvolysis, the product monomers are. This necessitates an additional purification step after the depolymerisation has been completed in order to isolate the monomers from the reaction mixture. Typically, this is achieved by decanting a large excess of water into the crude reaction mixture in order to precipitate the monomers which may then be collected by filtration.

Common procedures will utilise up to 100 mL of water to extract monomers which have been produced from less than 1 g of PET, these solvents must then be disposed of or purified before re-use. The requirement for such large volumes of solvent in the purification of these monomers means that many of these closed-loop recycling methods conflict with the Principles of Green Chemistry outlined in section 1.1 specifically:

- It is better to prevent waste than to treat or clean up waste after it has been created.
- Use of auxiliary substances (e.g., solvents, separation agents, etc.) should be made unnecessary wherever possible.

These challenges surrounding the isolation of monomers in closed-loop recycling methods have created scope to explore solvents which may be easily removed from reaction mixtures.

1.4 Supercritical Carbon Dioxide

When a compound is exposed to conditions above its critical point, it simultaneously exhibits the properties of a gas and a liquid. The high diffusivity of a gas imparts excellent mass transfer properties to the supercritical fluid, whilst it also possesses a density sufficient to dissolve solutes.^{148, 149}

In contrast to other common supercritical fluids, supercritical carbon dioxide's (scCO₂) critical point is achieved at very mild conditions (31.1 °C, 73.8 bar). Additional benefits of scCO₂ include its non-toxicity, non-flammability, tuneable density and the simple isolation of products which may be achieved by reducing the pressure and converting CO₂ back to a gas.¹⁵⁰ In this way, the energy-demanding solvent removal step seen for many chemical processes can be avoided.

With the exception of fluorinated and siloxane-based polymers, scCO₂ is a poor solvent for polymers as it is a small non-polar molecule. However, infrared studies on the supercritical fluid have demonstrated that CO₂ is capable of undergoing Lewis acid–Lewis base interactions with the oxygen of carbonyl groups.¹⁵¹ The ability of scCO₂ to undergo limited molecular interactions with polymers, and the enhanced pressure of the supercritical state, enables the swelling of polymers in an scCO₂ medium. This ability to permeate into a polymer's internal morphology, and increase the free volume between the individual chains, has created a raft of opportunities to modify polymer properties at mild temperatures – avoiding any unintended damage to the polymer's molecular structure.^{152, 153}

The unique ability of scCO₂ to swell polymers at mild temperatures has been exploited in a range of studies aiming to either impregnate or extract additives from a polymer bulk.¹⁵⁴⁻¹⁵⁸ Combined with the excellent mass transport properties of scCO₂, swelling of polymers allows for rapid

diffusion of scCO_2 throughout a polymer's internal morphology allowing for a rapid impregnation or extraction of an additive (Fig.1. 21).

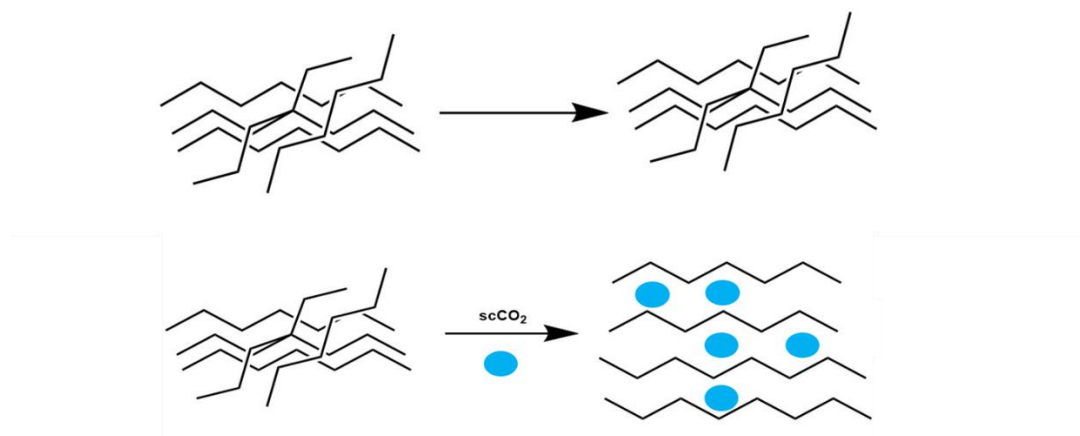


Figure 1.21 – Illustration of the swelling effect scCO_2 has on polymers (bottom), enabling access to the internal morphology of the polymer.

1.4.1 Supercritical Induced Plasticisation

The ability of scCO_2 to permeate into polymers, increasing the free volume between the chains, induces plasticisation. The increased free volume between the chains grants them additional degrees of movement at a lower temperature compared to ambient pressure. This phenomenon can be tracked by tracking how the glass transition temperature (T_g) falls via DSC studies.¹⁵⁹⁻¹⁶¹

Other techniques used to confirm scCO_2 plasticisation, and the corresponding recrystallisation, include NMR¹⁶², X-ray diffraction (XRD)¹⁶³, dielectric spectroscopy¹⁶⁴ and DMA.¹⁶⁵

A further benefit of utilising scCO_2 as the impregnation medium is that carbon dioxide's inherent chemical inertness means that the overall integrity of PET is not compromised, as shown by TGA and DSC studies pre and post-impregnation where the thermal properties of the polymer were retained.¹⁶⁶ This is in addition to the simple removal of carbon dioxide from the polymer afterwards, by reducing the pressure and converting it back into a gas, meaning no residue of

the solvent remains post-impregnation – an important consideration for materials that may be used for food packaging or medical equipment.¹⁶⁷

Once the desired process has been completed, simply releasing the pressure yields a dry, pure material which does not require any further cleaning. The facile removal of scCO_2 has driven studies of polymer synthesis in the supercritical fluid, as this removes the need for an energy-intensive drying step to remove the solvent.¹⁶⁸⁻¹⁷³

The simple removal of scCO_2 from a substrate to give a dry product, as well as the unique ability of scCO_2 to swell polymers at mild temperatures, is of particular interest as it has been identified as a possible route to overcome barriers currently faced in pyrolysis and solvolysis of plastics.

1.5 Aims and Objectives

It is laudable that so many routes currently exist to recycle PET and keep this valuable material out of the natural environment. However, it is clear that significant challenges remain to be overcome -especially where separation of the final product from the rest of the pyrolysis/solvolysis system is concerned.

The work in this thesis will focus on employing the aforementioned swelling of polymers and facile removal of scCO_2 to address two key challenges seen in PET recycling.

Challenge #1: PET yields products in the solid and gaseous phases when it undergoes microwave pyrolysis. This creates difficulties in removing the solid product from whichever susceptor was employed to ensure uniform heating.

Potential solution: scCO₂'s ability to swell polymers is utilised to impregnate PET with degradable microwave susceptors to explore if microwave pyrolysis can be conducted to yield a pure final product with minimal char formation.

Challenge #2: Solvolysis of PET leads to energy intensive purification steps, often using excessive amounts of toxic/hazardous solvents.

Potential solution: using scCO₂ as the main solvent for the depolymerisation will allow reduction of nucleophile (methanol, ethylene glycol) to single-digit stoichiometric amounts. Dry crude product should be isolated by depressurising the reactor and releasing gaseous CO₂. Isolation of pure monomer is expected to be achieved through either scCO₂ extraction or a second transesterification step.

To achieve these two aims, two parallel projects were devised, each with a list of objectives.

Project One: Enhancing the Dielectric Properties of PET via scCO₂ impregnation with degradable microwave susceptors, for improved microwave pyrolysis.

Objectives:

1. Identify a suitable degradable microwave susceptor with sufficient scCO₂ solubility for impregnation into PET.
2. Confirm successful impregnation via change in mass and an enhanced dielectric response.
3. Conduct microwave pyrolysis of PET which has been impregnated with degradable susceptors and determine if an appreciable increase in performance is achieved (increase in absorbed power, superior heating rate, better conversion).

Experimental work towards objectives one and two will be covered in Chapter 3; and Chapter 4 will discuss the results obtained for objective 3.

Project Two: Solvolytic depolymerisation of PET in scCO₂, with low-wastage product recovery

Objectives:

1. Devise a system which can successfully depolymerise PET in scCO₂.
2. Confirm depolymerisation, and probe selectivity of the process, by deploying a host of analysis techniques (GC-MS, HPLC, MALDI)
3. Explore novel isolation routes for pure PET-derived monomers via scCO₂ extraction, or melt transesterification treatment of the crude product

All experimental work towards these objectives will be discussed in Chapter 5.

2 Materials and Methodology

2.1 Overview

The work undertaken in this thesis explores the utilisation of lesser-known technologies towards novel routes for plastic recycling. In particular, the use of microwave heating and supercritical carbon dioxide require the design of equipment capable of withstanding high temperatures and elevated pressures respectively. Moreover, the behaviour of plastics and various substrates during a microwave process was probed by measuring their dielectric properties from room temperature to 340°C.

In addition to this, the products of the supercritical impregnation experiments, microwave pyrolysis, and the chemical depolymerisations laid out in later chapters were analysed by a range of mass spectrometry, nuclear magnetic resonance and thermal techniques in order elucidate what physical and chemical transformations had taken place.

2.2 Materials

2.2.1 Supercritical Impregnation of Polyethylene Terephthalate with Various Organic Microwave Susceptors

Polyethylene Terephthalate (Amorphous Grade Film, 0.2 mm thickness, $M_w = 46,209$ g/mol, Goodfellow Cambridge, Huntingdon, UK), Ethylene Glycol (99.9 % Reagent Plus®, Sigma-Aldrich, St. Louis, USA), 1,6-Hexanediol (Sigma-Aldrich), Terephthalic Acid (Sigma-Aldrich), Bis(2-Hydroxyethyl) terephthalate (Sigma-Aldrich), Carbon Dioxide (Air Products, SCF grade 5.5, 99.9995%). All were used as received.

2.2.2 Microwave Pyrolysis of Polyethylene Terephthalate

Polyethylene Terephthalate (Amorphous Grade, 0.2 mm thickness, $M_w = 46,209$ g/mol, Goodfellow Cambridge) and Ethylene Glycol (99.9 % Reagent Plus®, Sigma-Aldrich, St. Louis, USA), were used in the pyrolysis of unmodified PET and PET modified by impregnation with ethylene glycol in a supercritical carbon dioxide medium. Both were used as received.

2.2.3 Chemical Depolymerisations

Polyethylene Terephthalate (Amorphous Grade Film, 0.2 mm thickness, $M_w = 46,209$ g/mol, Goodfellow Cambridge, Huntingdon, UK), Methanol (99.9 % Analytical Reagent Grade, Fisher Scientific, Loughborough, UK), Carbon Dioxide (Air Products, SCF grade 5.5, 99.9995%) and 1,5,7-Triazabicyclo 4.4.0 Dec-5-Ene (98%, Sigma-Aldrich, St. Louis, USA) were all used as received.

2.3 Supercritical Experiments

2.3.1 Double-Ended High-Pressure View Cell

To visibly observe the solubility of various organic compounds in scCO_2 a fixed volume view cell (100 ml) was employed, with a maximum working pressure of 300 bar and a maximum working temperature of 150°C (Fig 2.1). The view cell contains two sapphire windows at either end of its body, through which light can be shone, allowing phase behaviour in supercritical carbon dioxide solutions to be observed. The windows are secured in place by EDPM O-rings placed around their circumference before they are slotted inside the detachable holders.

These detachable window holders are secured to the main body of the view cell by clamp which is hand-tightened around the components with the reverse end of a stainless-steel key. This key is screwed into the main body before and experiment to complete the seal. Carbon dioxide is transported to and from the view cell *via* high-pressure steel piping (1/8th or 1/16th of an inch

diameter) purchased from Swagelok®, the flow of which is controlled by the opening and closing of HiP taps purchased from Staffordshire Hydraulics®. The view cell body itself was developed in house at the University of Nottingham (Fig. 2.2).

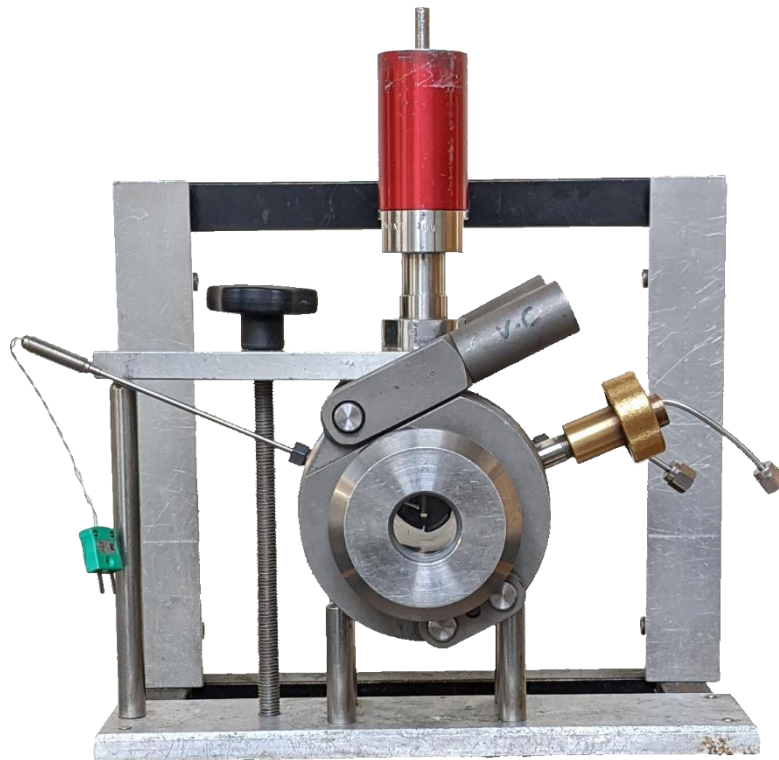


Figure 2.1 – Image of the view cell (front).

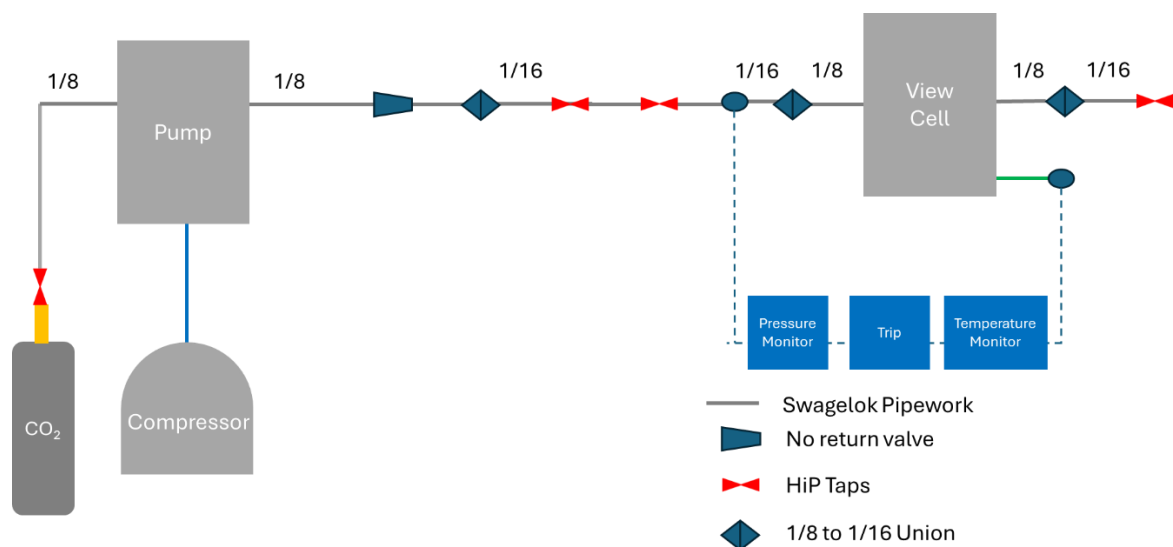


Figure 2.2 – Line diagram illustrating the high-pressure set-up for the view cell.

2.3.2 High Pressure Autoclaves

All supercritical impregnation and depolymerisation experiment were undertaken in bespoke high-pressure autoclaves, which were developed in-house at the University of Nottingham. The maximum working temperature of these autoclaves is 300 bar, whilst the maximum working temperature is dependent on the type of O-ring used: 150°C or 320°C for Ethylene Propylene Diene Monomer (EPDM) or Kalrez® respectively (Fig 2.3).

These O-rings are used to join the head and base of the autoclave together in an airtight seal, supported by a clamp which is hand-tightened around the two components with the reverse end of a stainless-steel key. This key is then screwed into the head before an experiment to complete the seal. Carbon dioxide is transported to and from the autoclave through high-pressure steel piping (1/8th or 1/16th of an inch diameter) purchased from Swagelok®, the flow of which is controlled by the opening and closing of HiP taps purchased from Staffordshire Hydraulics® (Fig. 2.4).



Figure 2.3 – Image of a high-pressure autoclave (front) with the base and head detached.

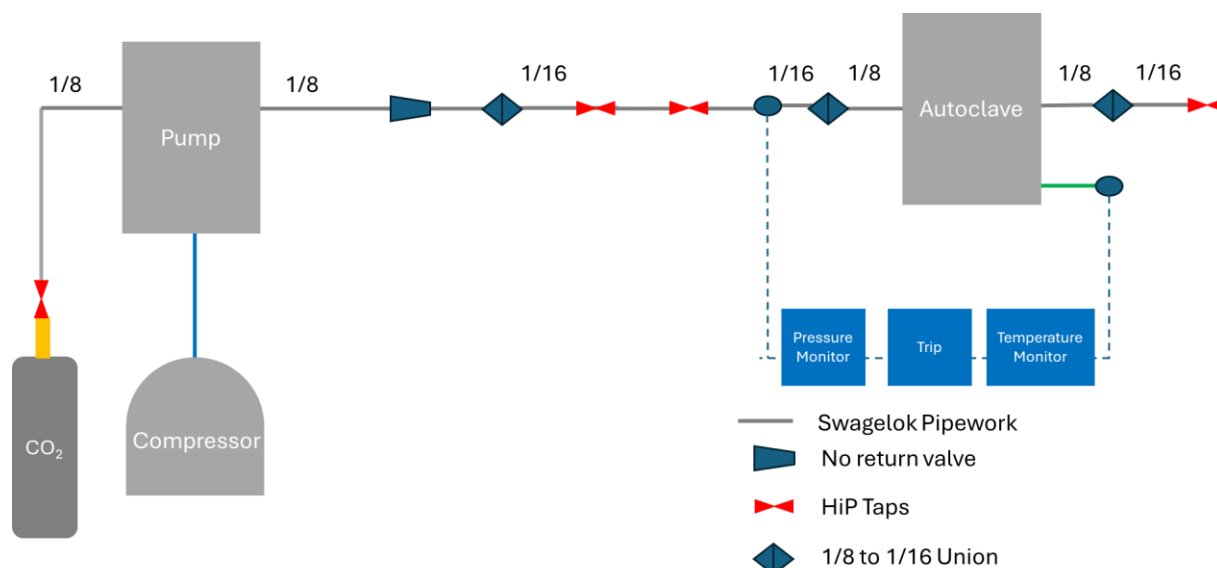


Figure 2.4 - Line diagram illustrating the high-pressure set-up for an autoclave.

2.4 Dielectric Property Measurements

2.4.1 Heat and Hold Cavity Perturbation

A cavity perturbation method was used in which a sample was placed in a quartz tube (4 mm internal diameter), which was mounted such that it could be moved between a temperature-controlled furnace and a cylindrical TE cavity with resonant frequencies spanning from 400 to 3000 MHz (Fig. 2.5) (Fig. 2.6). Samples were held in the furnace for at least 5 minutes to achieve thermal equilibrium before being moved into the cavity using a step-motor, where the frequency shift and quality factor were measured using a vector network analyser. The sample was then returned to the furnace, and the sequential heat-hold-measure process was repeated for the required temperature range – typically room temperature to 340°C for polyethylene terephthalate. The maximum temperature for various organic susceptor candidates was dictated by their boiling or sublimation points.



Figure 2.5 – Image of the heat-and-hold cavity perturbation set-up.

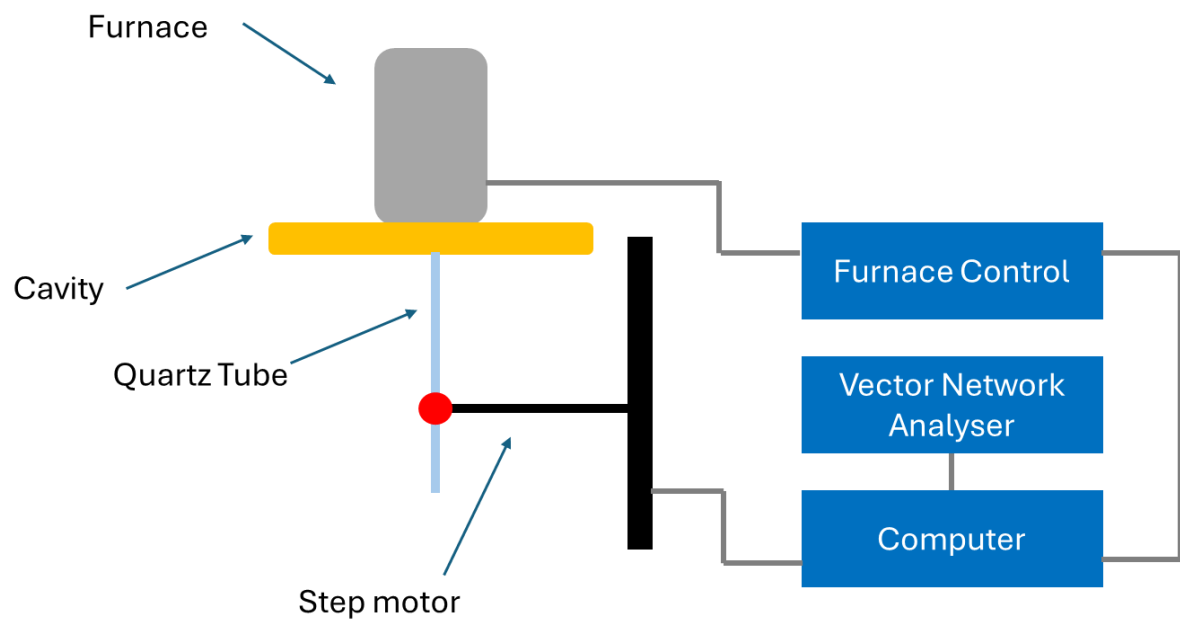


Figure 2.6 – Line diagram illustrating the heat-and-hold cavity perturbation set-up.

2.4.2 Simultaneous Heating and Measurement

The system consists of a cylindrical microwave cavity where 2 different resonant modes co-exist at the same time (Fig. 2.7) (Fig. 2.8). Mode TE₁₁₁ is used for microwave heating with incident power up to 100 W and electronically controlled to be applied depending on the heating slope required. This mode has a maximum electric field in the centre, which corresponds to the sample position. The TM₀₁₀ resonant mode coexists in the same cavity, and this is used to measure the changes of the resonant frequency to measure the sample permittivity. Both modes coexist in the same cavity but are de-coupled with an excitation strategy that guarantees that the heating mode does not interfere in the permittivity measuring mode. With this strategy, simultaneous heating and dielectric characterisation can be done, ensuring that the sample is only heated by microwave energy.

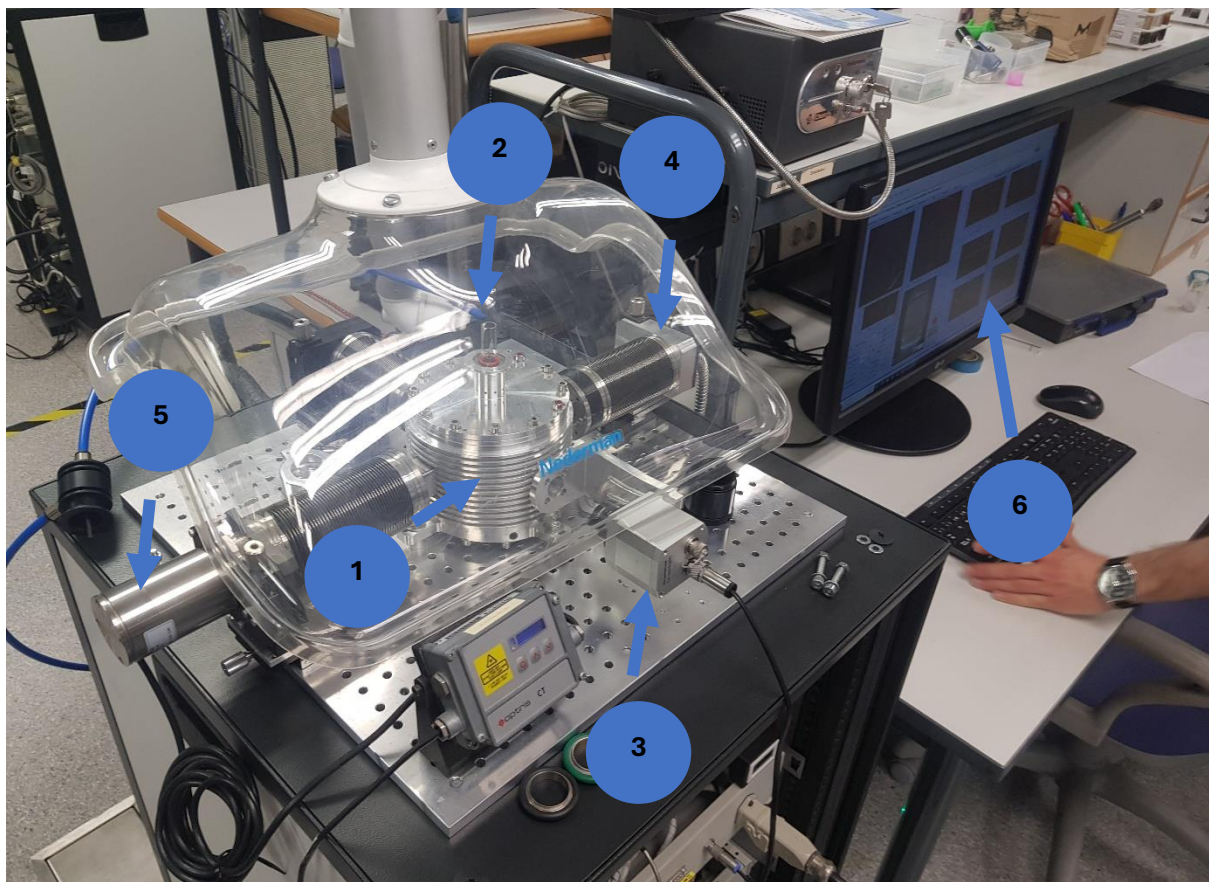


Figure 2.7 - Image of the simultaneous heating and measurement dielectric set-up. 1: Cavity, 2: Quartz Tube, 3: IR Pyrometer, 4: Microwave Source, 5: Video Camera, 6: Computer. Dielectric probe is directly underneath the cavity and cannot be pictured.

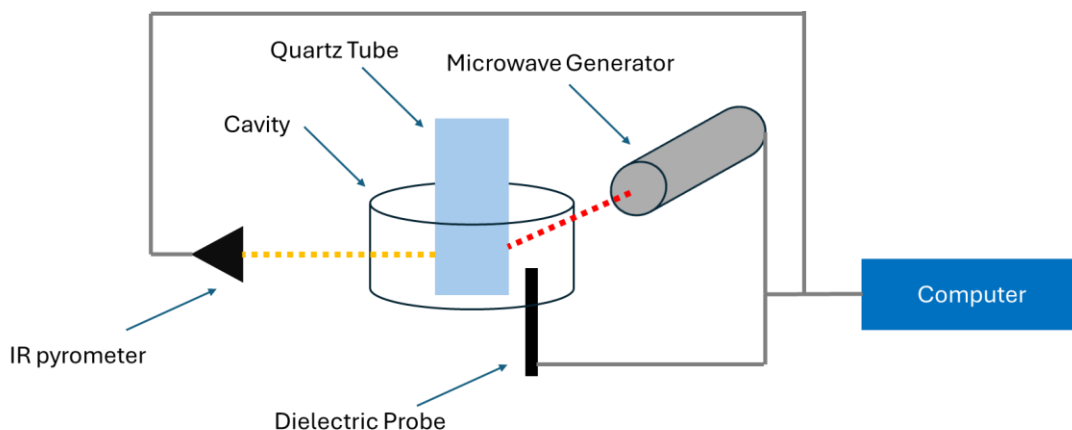


Figure 2.8 – Line diagram illustrating the simultaneous heating and measurement dielectric set-up.

2.4.3 Coaxial Probe

An Agilent 85070E high temperature coaxial probe was inserted into a sample of various liquid organic susceptor candidates to measure their dielectric properties across a frequency range of 500 MHz to 20 GHz, by determining the amplitude and the phase of the reflected signal from the sample. (Fig. 2.9) Samples were heated conventionally to a target temperature incrementally, at which the dielectric properties were measured by the probe. This was repeated until the desired temperature range had been covered. The maximum temperature the organic susceptor candidates were heated to was dictated by their boiling points.

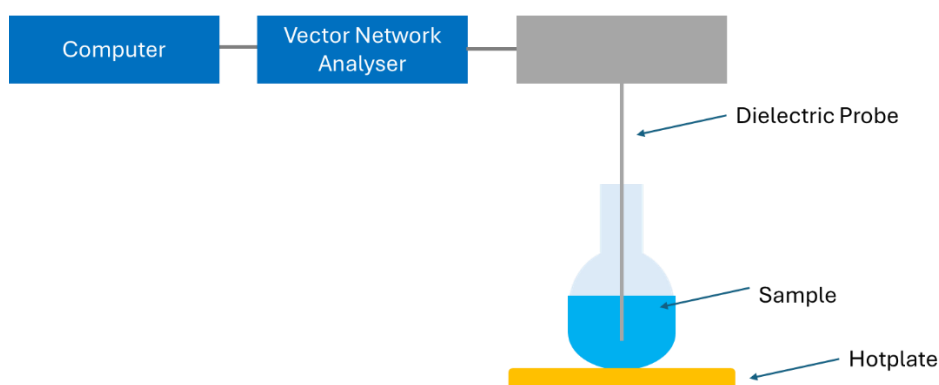


Figure 2.9 – Line diagram illustrating the coaxial probe set-up.

2.5 Microwave Pyrolysis

Cavity Configuration and Process Monitoring

The microwave power (0.80 – 1.60 kW) was provided by a 2.0 kW Sairem generator (2.45 GHz).

The microwave power was directed to cavity through WR430 waveguides.

A three-stub HOMER autotuner (ISM 2450 MHz) was attached to the waveguide for power recording. The HOMER measures the magnitude and phase of the reflected microwaves, in addition to the power and frequency, and uses this data to adjust the stub position for impedance matching, minimising the reflected power. This tuner was connected to a computer with HOMER software to control the tuner and record the incident, absorbed and reflected power results. The tuner was run in autotune mode during all experiments.

Pyrolysis experiments took place in a quartz tube within a single-mode cavity placed between the end of the waveguides and a sliding short. The sliding short was set to a length of 110 mm to place the microwave hotspot in the middle of the cavity.

The temperature was recorded at the interior wall of the sample by a CT 3MH1 SF IR pyrometer (150 -1000°C). The overhead temperature was recorded by a K-type thermocouple inserted into the top of the quartz tube through a silicone suba seal and the data was logged on a Lascar EL-USB-TC-LCD Temperature Data Logger. The pyrolysis was visually monitored by a Microsoft H5D-00014 LifeCam Cinema Webcam.

The conditions of the pyrolysis rig, and recovery of the pyrolysis products, differed between pyrolysis of unmodified PET, and PET that had been impregnated with ethylene glycol.

Product Collection: Pyrolysis of Unmodified PET

Product was collected by two cold traps in ice. The system was purged with nitrogen for 15 minutes at 100 cc/min before pyrolysis to remove oxygen which was maintained throughout the experiment. The microwave was turned on once 15 minutes had elapsed (Fig. 2.10).

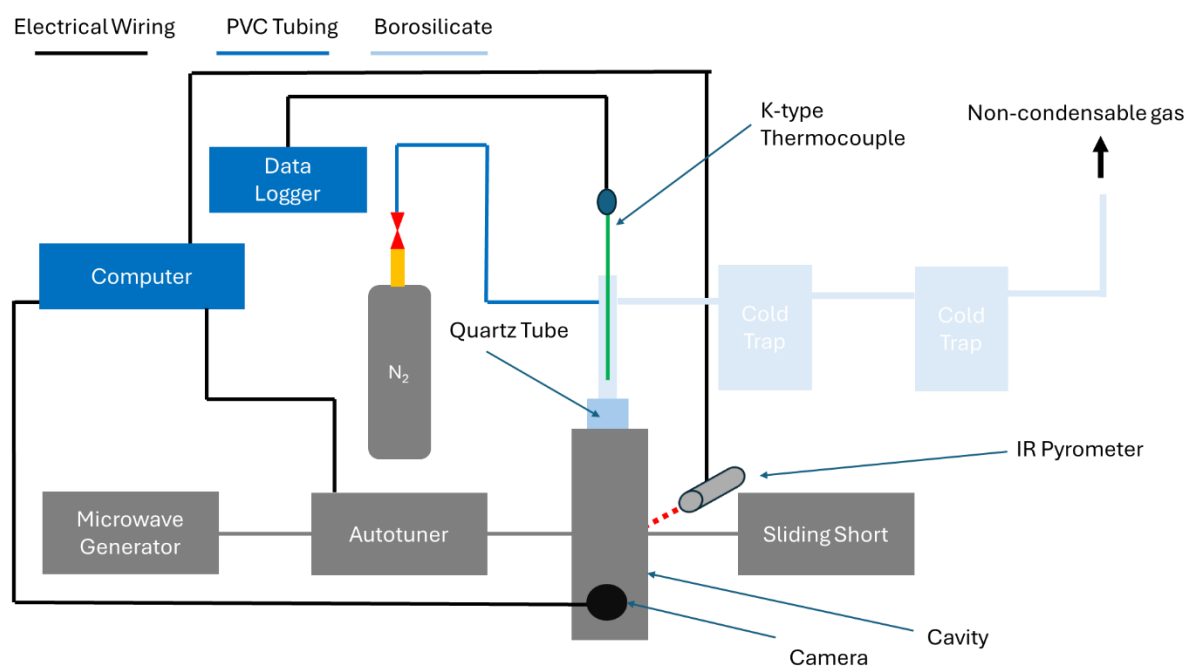


Figure 2.10 – Line diagram illustrating the set-up for microwave pyrolysis of unmodified PET.

Product Collection: Pyrolysis of Impregnated PET

Product was collected by one cold trap in ice and a second cold trap containing a limewater solution. The system was purged with nitrogen for 15 minutes at 100 cc/min before pyrolysis to remove oxygen which was maintained throughout the experiment. Internal pressure was reduced (450 mbar) to aid product transport by a vacuum pump operated with a CVC 3000 vacuum controller. The external wall of the quartz reactor, and the overhead borosilicate glassware was heated to 120 °C, to prevent premature condensation of pyrolysis fumes in the quartz tube seen in pyrolysis of unmodified PET, by HTWAT051-002 Omega silicone heating tape as monitored by the overhead K-type thermometer and the Lascar EL-USB-TC-LCD Temperature Data Logger (Fig. 2.11).

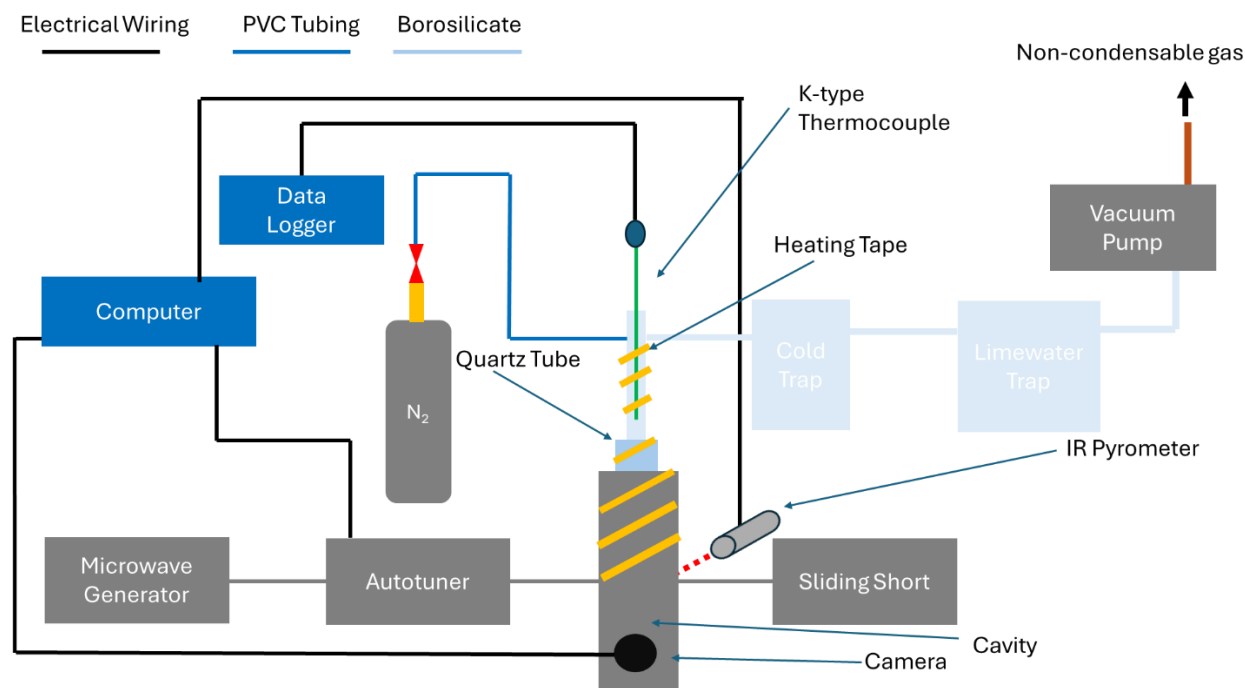


Figure 1.11 – Line diagram illustrating the set-up for microwave pyrolysis of PET impregnated with ethylene glycol.

2.6 Analytical Methods and Instrumentation

2.6.1 Thermogravimetric Analysis

The presence of organic susceptors within the PET structure was determined by TGA (Q500, TA instruments, Leatherhead, UK) at a heating rate of 10°C in the temperature range 20 to 250°C on platinum pans. The furnace was constantly purged with nitrogen at a flow rate of 50 ml/min.

2.6.2 Differential Scanning Calorimetry

PET's thermal properties (glass transition temperature, crystallisation temperature, melting point) were determined by differential scanning calorimetry (DSC) (Q2000, TA Instruments, Leatherhead, UK) at a heating rate of 10 °C /min in the temperature range of 0 to 300°C. Tzero pans and lids (TA Instruments, Brussels, Belgium) were used for the analysis of the samples, using empty pans as the reference. The DSC cell was constantly purged with nitrogen gas at a flow rate of 50 ml min⁻¹.

2.6.3 Dynamic Mechanical Analysis

PET mechanical properties were investigated by dynamic mechanical analysis (DMA) (T T DMA, Mettler Toledo formerly Triton Technologies, UK). Samples of PET were heated at a rate of 3°C/min in the temperature range of 20 to 200°C. Experiments were carried out in tension mode with a pre-load force of 1.5 N, and a displacement amplitude of 0.01 mm.

2.6.4 X-ray Scattering

Absolutely-calibrated small and wide-angle X-ray scattering (SAXS/WAXS) experiments were performed using the Xenocs3 instrument at the Chemical Sciences Division, Oak Ridge National Laboratory. The combined q range is between 0.001 and 0.2 Å⁻¹; here $q = 4\pi/\lambda \sin(\theta)$, λ is the wavelength and θ is ½ of the scattering angle. X-ray energy was 9.25 keV ($\lambda = 12.4/9.25$ Å). X-ray photon flux was $\approx 5 \times 10^9$ mm⁻²s⁻¹. Samples were analysed in standard X-ray capillaries.

2.6.5 Nuclear Magnetic Resonance

Pyrolysis or supercritical depolymerisation products of PET, as well as monomer standards, had their structures determined by ¹H and ¹³C nuclear magnetic resonance spectroscopy (NMR). Samples were dissolved in CDCl₃ or DMSO and analysed using a Bruker DPX 400 MHz spectrometer or a Bruker DPX 500 MHz spectrometer. Chemical shifts were assigned in parts per million (ppm). All spectra were obtained at ambient temperature (22 ± 1 °C). MestReNova 14.0.1 copyright 2020 (Mestrelab Research S.L.) was used for analysing the obtained spectra.

2.6.6 Atmospheric Pressure Chemical Ionisation (APCI)

Mass spectrometry chromatograms were obtained by atmospheric chemical pressure ionisation (APCI, Bruker Impact II, Germany). Solid samples were injected into the nebuliser, where it was carried by a flow of nitrogen into the corona where they were ionized by an electron discharge. Experiments were run in both positive and negative mode.

2.6.7 Infrared Spectroscopy

Solid pyrolysis or supercritical depolymerisation products of PET, as well as monomer standards, had their IR spectra recorded on a Bruker Alpha FTIR Instrument in an attenuated total reflectance (ATR) set-up. ATR was chosen due to the poor solubility of microwave pyrolysis products in organic solvents.

2.6.8 Gel Permeation Chromatography

Pyrolysis products, supercritical depolymerisation products and PET monomer standards

Gel permeation chromatography (GPC) was performed with DMF (HPLC grade, Sigma-Aldrich) as the eluent at 80 °C using an Agilent PL-gel D column in series with an Agilent PL-gel E column at a flow rate of 1 ml/min. Sample detection was achieved using a UV source ($\lambda=254$ nm) and a differential refractometer (dRI). The system was calibrated using narrow dispersity polystyrene standards ($1.02 \times 10^6 - 504$ g/mol).

PET

GPC was performed with Dichlorobenzene (DCB) (HPLC Grade, Sigma-Aldrich) (DCB) as the eluent at 140°C using an Agilent PL-gel D column at a flow rate of 1 ml/min. Sample detection was achieved using a UV source ($\lambda=254$ nm) and a differential refractometer (dRI). The system was calibrated using narrow dispersity polystyrene standards ($1.02 \times 10^6 - 504$ g/mol).

2.6.9 Matrix-assisted laser desorption ionization–time of flight mass spectrometry (MALDI-TOF)

Higher molecular weight pyrolysis or supercritical depolymerisation products of PET were identified using MALDI-TOF, which was conducted using a Bruker Autoflex Max spectrometer in positive, reflective mode. trans-2-[3-(4-tert-Butylphenyl)-2-methyl-2-propenylidene] malononitrile (DCTB) in acetonitrile was used as matrix with lithium bromide as a cationisation salt. All samples were dissolved in tetrahydrofuran, before being mixed with the matrix in acetonitrile.

2.6.10 High Pressure Liquid Chromatography – Mass Spectrometry (HPLC-MS)

Supercritical depolymerisation products of PET, as well as monomer standards, underwent HPLC-MS analysis on a Thermo Ultimate 3000s HPLC fitted with a Thermo Accucore Aq C18 column (dimensions: 150 × 4.6 mm; particle size: 2.7 µm) and a UV/vis detector (254 nm) connected a Bruker ESI-TOF MicroTOF II.

A mobile phase consisting of milliQ water, (A) and acetonitrile (B), with formic acid (0.01%) to maintain a constant pH, in was used in the below gradient (flow rate: 1 mL min⁻¹):

min	A (%)	B (%)
0	95	5
2	90	10
4	85	15
6	80	20
8	60	40
10	65	45
12	50	50
14	45	55
16	40	60
18	35	65
20	30	70
22	25	75
24	20	80
26	0	100

2.6.11 Gas Chromatography Mass Spectrometry (GC-MS)

Samples were dissolved in chloroform (HPLC grade, Fisher Scientific) at various concentrations (0.50 mg/mL, 0.25 mg/mL, 0.10 mg/mL, 0.05 mg/mL). Samples were run on an AccuTOF GCx

mass spectrometer (Jeol Ltd) with electron impact ionisation using a 30 m stabilwax GC capillary column with a diameter of 0.25 mm and a film thickness of 0.25 μm (Restek). The injector port temperature was 290 °C. The column oven was held at 50 °C for 4 minutes, then heated from 50 °C to 300 °C at 10 °C/min, and was purged constantly with helium.

3 Enhancement of Polyethylene Terephthalate's Dielectric Properties via Supercritical Carbon Dioxide Impregnation

Overview

This chapter will discuss the impregnation of PET with various degradable organic susceptors. After identification of a susceptor, a material with a strong ability to heat when exposed to microwaves, successful impregnation is shown through a combination of gravimetric methods, control experiments and thermal analysis. The impact on the dielectric response of PET is discussed using two different forms of cavity perturbation, and effect of scCO₂ impregnation on the dielectric constant and the dielectric loss factor is elucidated by additional thermal analyses and x-ray scattering.

3.1 Introduction

The high volumes of waste plastic produced globally on an annual basis, as well as the legacy waste that occupies landfills and pollutes the natural environment, has created a need for recycling technologies that are capable of high turnover. Moreover, the thermal stability and chemical inertness of many plastics which makes them such useful materials, necessitates harsh conditions, such as high temperatures, for their degradation.

Microwave heating reaches the required high temperature in seconds – enabling the high turnover needed to keep pace with the immense volume of waste plastic. Furthermore, the electrical nature of microwave heating means it will be a compatible with the transition away from fossil fuels to increasingly renewable energy sources (solar, wind, hydroelectric).

The strength of interaction of microwaves with differing media can be understood by measurement of dielectric properties. A key barrier to overcome when developing a microwave pyrolysis procedure for plastic recycling is the poor dielectric properties exhibited by many

commercially available polymers, which is attributed to their high molecular weight and the presence of crystalline regions in the polymer morphology.¹⁷⁴

A variety of examples can be found in the literature where a polymer's poor dielectric properties are compensated for by doping the material with a microwave susceptor; a material with strong dielectric properties which heats well when exposed to a microwave field.¹⁷⁵⁻¹⁷⁹ In Chapter 1, this was demonstrated as a viable route to degrade end-of-life plastic to valuable materials, but two major limitations remain:

1. Many susceptors are mechanically mixed with plastic pre-pyrolysis. This has been seen to result in a non-uniform distribution of susceptor material throughout the plastic, leading to either incomplete pyrolysis of the material or the formation of hotspots which may damage the reactor.
2. In scenarios where the pyrolysis products are the same phase as the susceptor itself, a challenging purification step is necessary post-pyrolysis which can consume large amounts of solvent or energy.

In this work, the dielectric properties of PET are successfully enhanced by impregnation of ethylene glycol via scCO_2 . Moreover, competing influences on the dielectric properties of PET from the ethylene glycol and the supercritical fluid itself were identified, and the mechanisms behind these observations are discussed.

3.1.1 Microwave Heating and Dielectric Properties

Microwaves are a non-ionising form of radiation found between frequencies of 300 MHz to 300 GHz, with corresponding wavelengths between 1 m and 1 mm, in the electromagnetic spectrum. Like all electromagnetic radiation, microwaves consist of two separate components, electric and magnetic, which are perpendicular to one another and in phase (Fig 3.1).¹⁸⁰

Despite existing at a broad range of frequencies, international agreements have determined specific microwave frequencies for industrial, domestic, and medical uses in order to avoid disrupting communications -these are 2.45 GHz ($\lambda=0.12$ m) and 915 MHz ($\lambda= 0.32$ m) in the United Kingdom.¹⁸¹

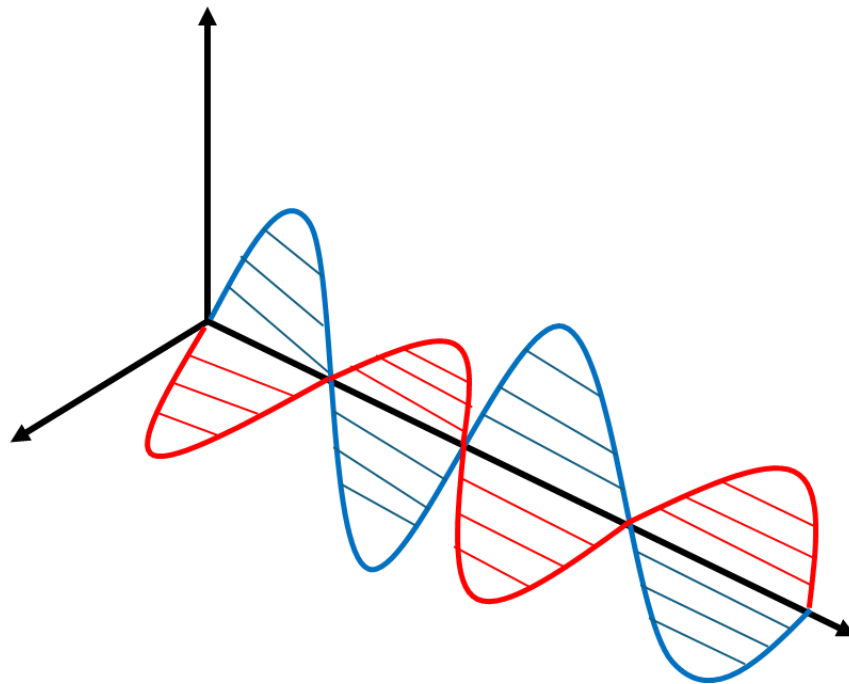


Figure 3.1 - Schematic of electromagnetic radiation. Electric component is shown in red, magnetic in blue. They are in-phase and perpendicular to one another.

3.1.1.1 Selective Heating and the Microwave Heating Mechanisms

One of the advantages of microwave heating is its selective nature. This arises from the need for a material to possess discrete electrical charges or have a non-uniform distribution in its electron density cloud, in order to undergo polarisation when exposed to the electrical component of microwave field.

This selectivity of microwaves has led to materials being classed into three separate categories.

Conductors reflect microwaves making them ideal materials to construct channels to guide the

radiation to a desired point, such as waveguides. **Insulators** are described as being “transparent” to microwaves, as the radiation propagates through them with negligible heating taking place. **Absorbent material**, also referred to as **dielectric material**, is heated by microwave radiation. It is this dielectric material which contains one, or both, of the discrete electrical charges or the non-uniform electron density.¹⁸²

Absorbers are heated because of polarisation or conduction losses. During polarisation, microwave energy is dissipated from a material as heat when electron density, otherwise referred to as charge density, interacts with the electrical component of an electromagnetic field. These dipoles will align with the electric component of the electromagnetic EM field upon exposure, whose alternating nature induces movement in the dielectric material (Fig. 3.2). Heat is then released from the intermolecular collisions which arise from this microwave-induced movement.¹⁸³

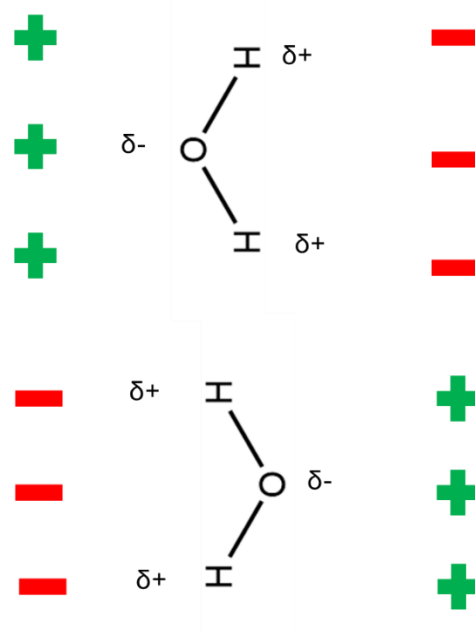


Figure 3.2 – Representation of the polarisation loss mechanism. As the relative positions of the positive and negative ends of the electric field alternate, the dipoles seen in a polar molecule (water is used here) will re-orientate to match the electric field's alignment. The molecule must rotate to achieve this, with heat being released because of the intermolecular collisions.

Interfacial polarisation, also known as the Maxwell-Wagner mechanism, occurs in heterogeneous materials where charged particles that are free to move are contained within an

insulating (microwave transparent) section of the material (Fig 3.3). Upon exposure to the microwave, the charged particles will accumulate at the interface of the insulating portion of the material, which causes secondary polarisation at the boundary of the two phases leading to polarisation within the non-conducting region.¹⁸⁰

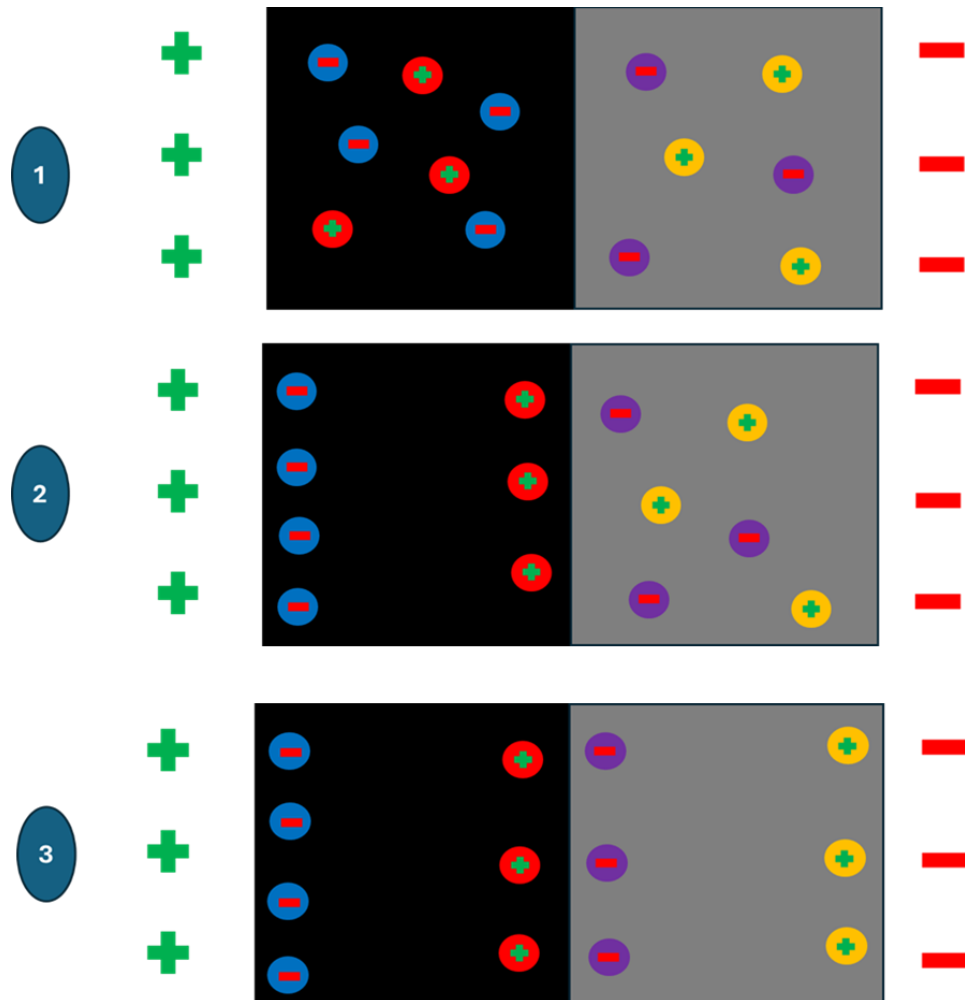


Figure 3.3 – Schematic of Maxwell-Wagner Polarisation.

1. An electric field is applied across a conducting region (black) and an adjacent non-conducting region (grey).
2. Charged particles in the conducting region are polarised, creating an electrical imbalance at the interface with the non-conducting region.
3. The microwave-induced charge imbalance at the interface generates secondary polarisation across the non-conducting region.

The second mechanism by which microwaves cause heat loss are conduction losses (Fig 3.4).

These are seen when an electric field is applied to a material containing free charge carriers. An

electrical gradient is set up inside the material, resulting in movement of the free charge carriers, and heating taking place because of the intermolecular collisions (electrical resistance). Conduction losses can be seen in solids, or solutions with free charge carriers dissolved in them, such as brine. ¹⁸⁰

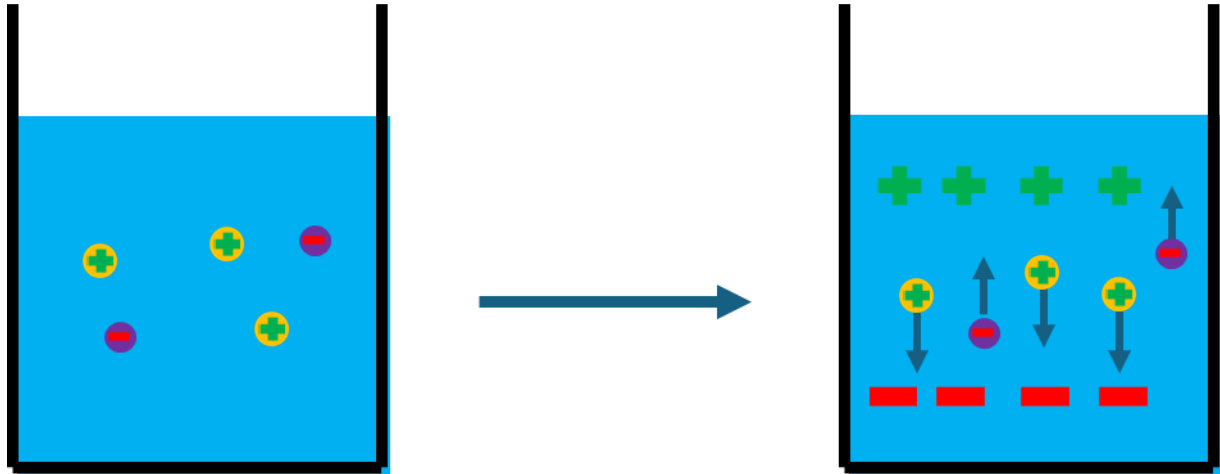


Figure 3.4 – Representation of the conduction heating mechanism. Delocalised charge carriers will propagate through a liquid medium when an EM field is applied, generating heat by collisions.

3.1.1.2 Volumetric Heating and Penetration Depth

Microwaves are able to heat a dielectric material by hundreds of degrees Celsius in seconds due to another unique property: volumetric heating. ¹⁸³ The radiation permeates a material uniformly, enabling it to heat the core of a material at a comparable rate to its surface (Fig 3.5). This stands in contrast to conventional heating, where the part of the material closest to the source of heating is heated first and the temperature of the material is steadily increased by conduction and/or convection.



Figure 3.5 – Volumetric heating enables a material to be heated by hundreds of degrees in seconds as there is little to no temperature gradient between the core and surface (left), whereas the large temperature gradient which is initially present in conventional heating results in a much slower heating rate (right).

It is important to note one caveat to volumetric heating: penetration depth. Penetration depth (D_p), is defined as the point beneath the surface of a material that the power flux drops to $1/e$ (≈ 0.368) of its incident value (Eq. 3.1).¹⁸⁰ Simply, penetration depth quantifies how far below the surface of a dielectric material microwaves can penetrate.

$$D_p = \frac{\lambda_0}{2\pi\sqrt{(2\varepsilon')}} \frac{1}{\sqrt{[(1 + (\frac{\varepsilon''}{\varepsilon'})^2)^{0.5} - 1]}}$$

Equation 3.1 – Calculation of penetration depth. The radiation wavelength, as well as the dielectric constant and dielectric loss factor of the material, will influence this value.

ε' = dielectric constant, ε'' = dielectric loss factor, λ_0 = wavelength of microwave passing through the medium

Penetration depth is dependent on the dielectric constant, the dielectric loss factor, and the wavelength of the microwave. The stronger the dielectric constant of a material, the shorter its penetration depth as an increasing amount of energy from the microwave is “stored” by the material (Tab. 3.1). Consideration of the penetration depth shows that knowledge of a material’s dielectric properties is key to explaining what processes occur during microwave heating.¹⁸⁰

Table 3.1 – Penetration depth values for metals, polymers and susceptors. The large range in values demonstrates why quantifying a material's dielectric properties is crucial to understanding its performance under microwave irradiation. ⁸⁹

Material	Penetration Depth (m)
Water	0.03
Silicon Carbide	0.02
Alumina	12.65
Copper	2.70×10^{-6}
Iron	1.30×10^{-6}
Polystyrene	76.20
Polyvinyl Chloride	4.03

3.1.1.4 Dielectric Properties

Dielectric properties describe how materials interact with microwave radiation. Dielectric materials are able to interact with microwave radiation because of the presence of a permanent, or induced, dipole. Applying an electric field to a dielectric material will result in some energy storage from the charge polarisation. This energy storage can be mathematically described by the dielectric permittivity (ϵ) (Eq. 3.2).

$$\varepsilon = \varepsilon' - j\varepsilon''$$

Equation 3.2 - Determination of dielectric permittivity of a given material

The dielectric permittivity is described by two parts: the real part (ε') is known as the dielectric constant, which quantifies the amount of stored energy; whereas the imaginary part (ε''), known as the dielectric loss factor, which describes the amount of stored microwave energy that is then dissipated as heat. Here, j is an imaginary constant ($\sqrt{-1}$).^{180, 182} The dielectric constant and loss factor are related to one another by a ratio known as the dielectric loss tangent ($\tan \delta$). It is used to assess the overall ability of a material to be heated by a microwave field at a specific frequency (Eq. 3.3).

$$\tan \delta = \frac{\varepsilon''}{\varepsilon'}$$

Equation 3.3 - Dielectric Loss tangent of a given material.

3.1.1.5 Frequency, Temperature and Density Dependence of Dielectric Properties

3.1.1.5.1 Frequency

Unless a material exhibits low loss when exposed to microwaves, there will be strong variation of the dielectric properties with frequency. The relationship between the dielectric constant and loss factor with frequency is well demonstrated by the Debye equation (Eq. 3.4).

$$\varepsilon = \varepsilon_{\infty} + \frac{\varepsilon_s - \varepsilon_{\infty}}{1 + j\omega\tau}$$

Equation 3.4 – The Debye Equation

ε_s and ε_{∞} represent the dielectric constant at static and very high frequencies respectively, whilst τ describes the relaxation time – the time taken for a molecule to revert to its equilibrium position once the electrical field ceases. The relaxation time will also vary significantly with

temperature, as is influenced by intermolecular interactions which will weaken with increasing temperature. Here, j is an imaginary constant ($\sqrt{-1}$) and ω corresponds to the relaxation frequency.¹⁸⁰

The Debye equation may be further separated into two components which describe the factors influencing the dielectric constant (Eq. 3.5) and loss factor specifically (Eq. 3.6).

$$\epsilon' = \epsilon_{\infty} + \frac{\epsilon_s - \epsilon_{\infty}}{1 + (\omega\tau)^2}$$

Equation 3.5 – Dielectric constant portion of the Debye Equation.

$$\epsilon'' = \frac{(\epsilon_s - \epsilon_{\infty})\omega\tau}{1 + (\omega\tau)^2}$$

Equation 3.6 – Dielectric loss factor portion of the Debye Equation.

The frequency dependence of the dielectric constant and loss factor is can also be represented graphically (Fig. 3.6).

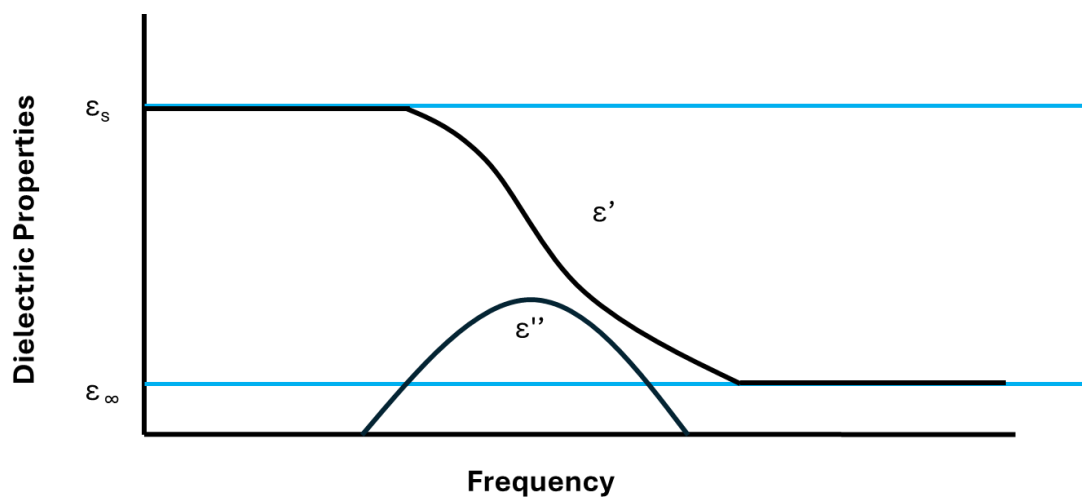


Figure 3.6 – Graphical representation of how dielectric constant (ϵ') and dielectric loss factor (ϵ'') vary with frequency, as described in the Debye equation.

Both at low and high frequencies the dielectric constant is seen to be largely constant, although there is a significant decrease in its magnitude with increasing frequency.

3.1.1.5.2 Temperature

As stated above, increasing temperature will reduce the relaxation time for a given sample, as the intermolecular forces are weakened. This has the corresponding effect of increasing the microwave frequency at which the equilibrium position is reached, shifting the Debye curves to the right.

Consequently, an increase in the dielectric constant can be seen with increasing temperature.

An increase in the dielectric loss factor can only be seen when the measured frequency is greater than that of the relaxation frequency.^{184, 185}

3.1.1.5.3 Density

The density at which a sample is packed for dielectric analysis will affect the overall permittivity, making it an important consideration. More densely packed samples of the same chemical compound will have superior permittivity, due to smaller air pockets, which will result in an enhanced dielectric constant and loss factor. It is important to be aware of packing density, as it will impact the results of an experiment.¹⁸⁶

3.1.2 Measurement of Dielectric Properties

The dielectric properties of a material may be measured by a range of different techniques. How lossy a material is expected to be, its state of matter and the frequencies of interest are all important considerations when selecting the most appropriate method for determining dielectric properties.

3.1.2.1 Cavity Perturbation

Cavity perturbation measures shift in a resonant frequency (f) (Eq. 3.7) and Q-factor (Q) (Eq 3.8) when a sample is inserted into the electric field within it. The Q-factor is a ratio of the energy stored within the cavity and the energy dissipated by the heating of a sample. The dielectric loss factor can be calculated by determining the shift in the Q-factor, whilst the corresponding shift in resonant frequency can be used to elucidate the dielectric constant.¹⁸⁰

$$\varepsilon' = 1 + 2J_1^2(x_{1,m}) \frac{(f_0 - f_1)}{f_0} \frac{V_c}{V_s}$$

Equation 3.7 – Determination of the dielectric constant by cavity perturbation.

$$\varepsilon'' = J_1^2(x_{1,m}) \left(\frac{1}{Q_1} - \frac{1}{Q_0} \right) \frac{V_c}{V_s}$$

Equation 3.8 – Determination of the dielectric loss factor by cavity perturbation.

It is important that the volume of the sample (V_s) is small in comparison to the volume of the cavity (V_c) to avoid significantly altering the distribution of the EM field within the cavity. $J_1(x_{1,m})$ is the second order of the first kind root of the Bessel function.^{187, 188}

Cavity perturbation is suitable for a range of different materials: solids, films, pellets and powders for example provided that they exhibit low dielectric loss, and the volume of the sample is much smaller than that of the cavity.^{189, 190} However, values for the dielectric properties are only obtained at a few discrete frequencies, and these are dependent on the size of the cavity. In this work, dielectric properties were measured at 2470 MHz as this is the frequency at which microwave pyrolysis was undertaken in Chapter 4.

Cavity perturbation was utilised to determine the dielectric properties of both unmodified polymers and polymers impregnated with organic microwave susceptors, as well as potential organic microwave susceptors which were solid at room temperature.

3.1.2.2 Open-Ended Probe

The open-ended probe technique is able to calculate the dielectric properties of a material by calculating the changes in phase and amplitude of the wave reflected back to the probe from the sample, with respect to the incident wave. This technique is very suitable for measuring the dielectric properties of materials with a high dielectric loss factor and, unlike cavity perturbation, has the additional benefit of measuring dielectric properties across a broadband spectrum of frequencies between 500 MHz – 10 GHz.^{191, 192}

One constraint of this technique is the phase of the sample itself. In order to obtain an accurate measurement, it is necessary for the probe to be in uniform contact with the boundary of the material, without the presence of air bubbles. This is possible when the sample undergoing analysis is a free-flowing liquid or gel, but significantly more challenging for a solid.¹⁹³

A probe was employed in this work to measure the dielectric properties of potential organic microwave susceptors, which were liquid at room temperature and believed to be polar enough to exhibit the necessary high dielectric loss factor.

3.1.3 Microwave Heating of Polymers

Despite many polymers, such as PET, possessing permanent dipoles and therefore theoretically being susceptible to microwave heating via the dipolar mechanism, polymeric materials typically possess very poor dielectric properties under standard conditions.⁸⁶ The presence of permanent dipoles is outweighed by the fact that many polymers consist of very high molecular weight chains, and can form very stable, semi-crystalline structures. These steric barriers

hinder the re-orientation of the dipoles present in the polymer when exposed to an alternating microwave field, resulting in very inefficient heating.

One established approach to overcome this challenge is to dope a polymer with a microwave susceptor.¹⁹⁴⁻¹⁹⁸ However, a non-uniform distribution of susceptor throughout the polymer can cause incomplete pyrolysis, or the formation of heat spots. There are also challenges surrounding isolation of the pyrolysis products from the susceptor.¹⁹⁹

Polymers have also been degraded by microwave-assisted depolymerisation in conventional organic solvents, where microwave heating is used as an energy source to drive the reaction.^{118, 200, 201} However, challenges concerning additional hazards associated with organic solvents and complex purification of products remain.

Ideally, development of a system where a polymer could be efficiently degraded by microwaves, which avoided challenging susceptor separation could yield a quick and low-waste route for the recycling of plastics. Two methods of achieving this can be envisioned:

1. Immobilise a susceptor or catalyst onto a surface in the microwave reactor so that pyrolysis products may be easily isolated e.g. a honeycomb that may be lifted out of the pyrolysis reactor, leaving pure product.
2. Incorporate a susceptor into the polymer which will be degraded itself during pyrolysis, removing the need for an isolation step entirely.

Although the first strategy possesses a clear advantage when reusability is considered, there is the potential for the activity of an immobilised susceptor or catalyst to decrease with time because of degradation or poisoning.^{202, 203} Addition of a susceptor designed to be degradable would avoid this longer-term issue, and selecting a susceptor candidate that is cheap, abundant and can be produced sustainably will mitigate the lack of reusability concern.

Furthermore, immobilised catalysts and susceptors have been explored in the literature, whereas there is significantly less precedent for degradable microwave susceptors – and the novelty aspect makes research in this area additionally appealing.²⁰⁴

A key barrier to overcome in this project was identifying, and implementing, a route to successfully impregnate PET with a degradable susceptor. The ability of scCO₂ to swell polymers at mild temperatures makes it an ideal candidate to investigate as a medium for PET impregnation.

3.1.4 Supercritical Carbon Dioxide Impregnation

One of the common routes for modifying a polymer in scCO₂ is the impregnation of a guest species with an additional desirable property e.g. colourants for dyeing, plasticisers for lowering of the glass transition temperature.

Impregnation of azo-dyes into poly(methyl methacrylate) (PMMA) inspired a series of impregnation studies on PET to incorporate dyes.¹⁵⁴ Sicardi *et al* successfully impregnated disperse blue and yellow dyes into a roll of PET film at 250 bar and up to 110 °C in 4 hours, with dye uptake being confirmed and quantified by UV spectrometry.²⁰⁵

Excellent mass transport is demonstrated in scCO₂, which arises from the combination of the supercritical fluid's high diffusivity and the swelling of PET. This aids diffusion of a guest molecule into the polymer, which is shown below by comparison studies with more traditional aqueous impregnation mediums.

De Giorgi *et al* studied the effect of dye uptake by variation of scCO₂ pressure and temperature, followed by comparison with an aqueous system which contained a dispersing agent.²⁰⁶ At constant temperature (80 °C and 100 °C) a significant increase in dye uptake was observed when pressure was increased from 172 bar to 241 bar, with a smaller increase seen when pressure was further increased to 275 bar. Regarding temperature, an increase in dye uptake

was recorded at 172 bar when the temperature was increased from 80 ° C to 100 ° C, but the uptake was constant at the two temperatures when pressure was increased to 241 bar and above.

At constant temperature, increasing the pressure of scCO₂ will improve the solvating power of the supercritical fluid by increasing its density. For an isobaric system, increasing temperature has been seen to reduce the solvating power of scCO₂, due to a reduction in density, but this can be offset by a corresponding increase in polymer chain mobility – which enhances diffusion.¹⁵⁹ The increase in solvating power when pressure is increased explains the substantial improvement in uptake when pressure was increased to 241 bar from 172, as both PET swelling and dye solubility was believed to be improved, whilst increasing temperature at the higher pressure (241 bar and above) is believed to have had no discernible effect as the supercritical solution was already saturated with dye at these pressures.

Three dispersed dyes were then impregnated into PET at 80 ° C and 241 bar. In order to achieve a comparable dye uptake in an aqueous system, it was necessary to heat water to 100 ° C as well as adding a dispersing agent to ensure adequate mixing of dye in the water. In addition to the lower temperature, and simpler impregnation mixture, use of scCO₂ also avoided the need to dispose of, or clean up, water post-impregnation.²⁰⁶

A similar study was then undertaken by Sicardi *et al*²⁰⁷, and they found that the diffusion coefficient of the dye was enhanced by 1 to 3 orders of magnitude over an aqueous system when pressure and temperature of scCO₂ were varied between 150 to 250 bar and 100 ° C to 120 ° C respectively. Dye uptake was also confirmed spectrophotometrically, and the enhancement in uptake was once again attributed to the plasticising effect of scCO₂ on PET.

Kazarian was able to undertake further the analysis of scCO₂-dyed PET by demonstrating that confocal Raman spectroscopy could be used to both map the distribution of the dye throughout

the polymer, as well as depth profiling confirming the presence of dye up to 100 μm below the surface.²⁰⁸

Once the principle of scCO_2 impregnation of PET had been proven with dyes in the above studies, further investigations were carried to understand the *in situ* behaviour of the impregnation process, in particular how a guest molecule would partition between the supercritical and polymer phases.

A supercritical impregnation system can be thought of as having three components:

1. The guest species, such as a dye, a plasticiser or a degradable microwave susceptor.
2. The host species, a polymer in these examples. This may also be referred to as the polymer phase when describing partitioning (see below).
3. The supercritical phase.

The impregnation process may be considered as four stages:

1. Pressurisation of the autoclave, accompanied by swelling of the host species
2. Initial dissolution of guest species into the supercritical fluid
3. Movement of the guest species from the supercritical phase into the host species until an equilibrium point is reached
4. Depressurisation of the autoclave

Partitioning describes how a guest molecule moves between the solute it is dissolved in, and the host species (Fig 3.7). The final equilibrium is dictated by the relative affinities the guest molecule exhibits for the two phases.²⁰⁹ It is possible to alter the solvating power of scCO_2 by modifying the pressure and temperature, thereby changing the density, or by the addition of a co-solvent which will vary the polarity. In this way, scCO_2 can be used to “tune” the impregnation process by selecting a pressure and temperature, or by adding a co-solvent, which will give a partition co-efficient favouring the host phase over the supercritical phase.²¹⁰

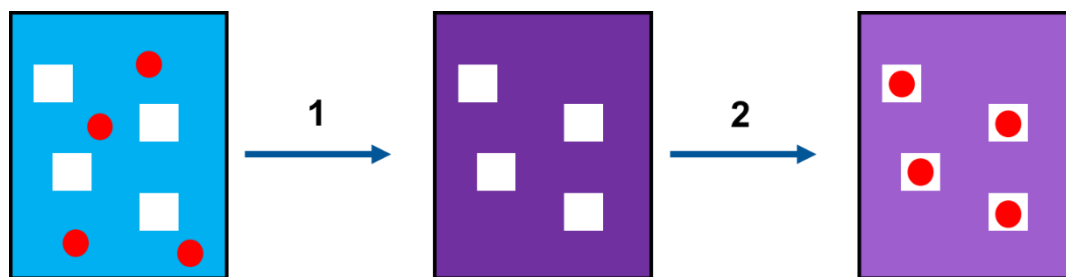


Figure 3.7 – Illustration of a guest species partitioning between the supercritical phase and the host.

1. Dissolution of guest species (red) in the supercritical fluid (blue) to form a solution (purple).
2. Guest species partitions between the supercritical solution (purple) and the host (white).

To understand the second step of a supercritical impregnation process, the solubility of a guest species has to be quantified, which has been done on previously studied dispersed dyes in scCO_2 . Original experiments consisted of a high-pressure cell with sapphire windows, enabling on-line study of the impregnation process by UV-Vis spectrometry. The absorbance value recorded for a particular guest molecule dissolved in scCO_2 could then be compared to values in a calibration curve to determine its concentration in the supercritical fluid.²¹¹

Flow experimental set ups, where CO_2 is passed through a container of dyestuff, whose solubility can then be monitored by on-line techniques, became more prominent as they enable faster and simpler measuring of dye solubilities at a range of conditions (pressure, temperature, flow rate).^{212, 213}

Use of mass flow meters within a high-pressure line enabled the on-line monitoring of scCO_2 density and temperature, with the addition of a pressure transducer in work published by Ferri *et al.*²¹⁴ A known amount of dye was placed in an extractor which scCO_2 was flowed through, and the solubility of the dye could be determined by quantifying the amount present in the solvent trap (ethanol) placed at the outlet by UV-vis spectroscopy.

The same group then carried this work forward and used the now known solubilities of these dyes in scCO_2 to calculate the partition co-efficient of their impregnation into PET at a range of temperatures and pressures.

The partition co-efficient, which is key to understanding how to saturate a host species, can be calculated by dividing the concentration of the guest species in the host post-impregnation by the concentration of the guest species in the solute during impregnation (Eq. 3.9).^{215, 216}

$$k = \frac{\text{concentration of guest in host}}{\text{concentration of guest in supercritical phase}}$$

Equation 3.9 – Partition co-efficient calculation.

Ferri *et al.* carried out supercritical dyeing of PET across a range of pressures (180-240 bar) and temperatures (80-120 ° C), with the concentration of dye in PET once again being determined by UV-Vis spectroscopy used in tandem with a calibration curve of stock dye solutions.²¹⁷

The partitioning of the dyes was found to be more sensitive to temperature than pressure. Above 180 bar, in an isothermal system, no significant increase of dye partitioning into PET could be observed, but large increases in the partitioning which favoured PET impregnation could be seen. The authors attribute this to the enhanced chain mobility of PET at higher temperatures, because of a stronger degree of plasticisation, allowing further diffusion of the dye into the polymer.

The extensive work carried out on supercritical dyeing of PET was followed by experimenting with a range of different guest species which could impart their desirable properties onto PET. Naturally occurring antioxidants derived from mango and olive leaf extracts have been successfully impregnated into PET/PP films to improve their ability to preserve foodstuffs²¹⁸⁻²²⁰. PET fabrics have been successfully impregnated with chitosan directly in scCO₂²²¹, or by immobilisation of an epoxy species which was itself impregnated into PET via scCO₂²²², to imbibe the polymer with anti-bacterial properties. Zinc oxide/PET composites have also been generated by scCO₂ impregnation, and these exhibit a spectrum of useful electrical and optical properties.²²³

3.1.5 Aims and Objectives

The overall aim of the work in this chapter is the identification of a degradable microwave susceptor, and successfully impregnating said susceptor into PET via scCO₂ to enhance PET's dielectric response with a view to improving its performance during microwave pyrolysis.

Specific experimental objectives are as follows:

1. Identify an organic species able to behave as a microwave susceptor, with affinities for scCO₂ and PET which will enable its dissolution in the supercritical phase but favour partitioning into the polymer phase
2. Successfully impregnate PET with an appropriate degradable susceptor, which will be confirmed by mass difference, thermal analysis and dielectric properties
3. Investigate the timescale for impregnation by use of *in situ* analysis

3.2 Experimental Procedures

3.2.1 Solubility testing of Organic Susceptor Candidates in Supercritical Carbon Dioxide

Organic susceptor candidate (0.5 g) was added to a glass sample holder and placed inside the view cell (100 mL). The view cell was charged with CO₂ (55 bar) at room temperature, after which the cell was heated to 65°C or 85°C with stirring at a rate of 300 rpm. Additional CO₂ was then added to top the pressure up to the desired level. It was then observed whether organic susceptor candidates dissolved in the supercritical fluid either instantly or over several hours. If dissolution did successfully occur, pressure was slowly lowered until the solubility limit, defined as the cloud point, was observed.

3.2.2 Supercritical Impregnation of Polyethylene Terephthalate with Organic Susceptor Candidates

Polyethylene terephthalate (0.5 g) and an organic susceptor candidate (0.5 g or 5.0 g) were placed inside the bottom of a high-pressure autoclave (60 mL), which was then sealed. The autoclave was charged with CO₂ (55 bar) at room temperature, and was heated to the desired temperature (32 °C, 65°C or 85°C) with a stirring rate of 300 rpm. If required, additional CO₂ was then added to the autoclave to reach the desired pressure. After the allotted residence time had passed, the heating was deactivated, and the CO₂ was vented once the internal temperature of the autoclave had reached 25°C. The PET film was removed from the bottom of the autoclave and rinsed with deionised water to remove any organic material deposited on the surface.

3.2.3 Coaxial Probe Dielectric Measurements

An Agilent 85070E high temperature coaxial probe was inserted into liquid organic susceptor candidates (10 mL). Samples were heated conventionally from room temperature in 20°C increments, at which the dielectric properties were measured by the probe. This was repeated

until the maximum temperature was reached, dictated by the boiling point of the susceptor candidate.

3.2.4 Heat and Hold Cavity Perturbation Dielectric Measurements

Samples of either PET films (0.1 g) or solid organic susceptor candidates (0.1 g) had their dielectric constant and dielectric loss factor measured at room temperature, after which they were heated in 20 °C increments up to a maximum temperature. Dielectric property measurements were taken at each temperature increment, with the maximum temperature being dictated by the melting point in the case of PET, and the boiling or sublimation points in the case of organic susceptor candidates.

3.2.5 Dynamic Cavity Perturbation Dielectric Measurements

Samples of PET films (10.0 g) had their dielectric constant and dielectric loss factor measured at room temperature, after which they were heated at a constant rate of 0.17 °C/min whilst the dielectric properties were measured continuously. Heating was discontinued once the melting point of PET had been reached.

3.2.6 Thermogravimetric Analysis (TGA)

PET samples were heated from room temperature to 250 °C at 10 °C/min under a constant flow of nitrogen.

3.2.7 Differential Scanning Calorimetry (DSC)

PET samples were heated and cooled across a temperature range of 0 °C to 300 °C at 10 °C/min under a constant flow of nitrogen. Before beginning the initial heating run, the DSC furnace was cooled to 0 °C and allowed to equilibrate for 10 minutes.

3.2.8 Dynamic Mechanical Analysis

PET samples were heated at a rate of 3°C/min in the temperature range of 20 to 200°C in tension mode.

3.2.9 Small and Wide-Angle X-Ray Scattering (SAXS/WAXS)

PET samples were analysed by absolutely calibrated small and wide-angle X-ray scattering (SAXS/WAXS) in the q range of 0.001 and 0.2 Å⁻¹. The X-ray energy was 9.25 keV ($\lambda = 12.4/9.25$ Å). X-ray photon flux was $\approx 5 \times 10^9$ mm⁻² s⁻¹. Samples were analysed in standard X-ray capillaries.

3.3 Results and Discussions

3.3.1 Identification of a Suitable Degradable Microwave Susceptor

In order to enhance the dielectric properties of PET, and be suitable for introduction into PET via scCO_2 impregnation, a degradable microwave susceptor must satisfy two conditions:

1. Display superior dielectric properties to PET, in particular its dielectric loss factor as this quantifies how well a material will heat in a microwave field.
2. Exhibit scCO_2 solubility which will enable its dissolution, whilst possessing an excellent affinity for PET to enable partitioning out of the supercritical phase.

Many of the microwave susceptors or catalysts discussed in the literature (silicon carbides, zeolites, iron oxide particles) are inorganic in nature and highly resilient to the temperatures seen in microwave pyrolysis of plastics. As the focus of this work was on degradable susceptors, organic species were identified as a more suitable class of compounds to explore.

To ensure these susceptors would have an excellent affinity for PET during scCO_2 impregnation, monomers of PET, and some analogues, were selected as potential susceptor candidates, specifically: terephthalic acid (TPA), ethylene glycol, bis(2-hydroxyethyl) terephthalate (BHET) and 1,6-hexanediol (1,6-HD) (Fig 3.8).

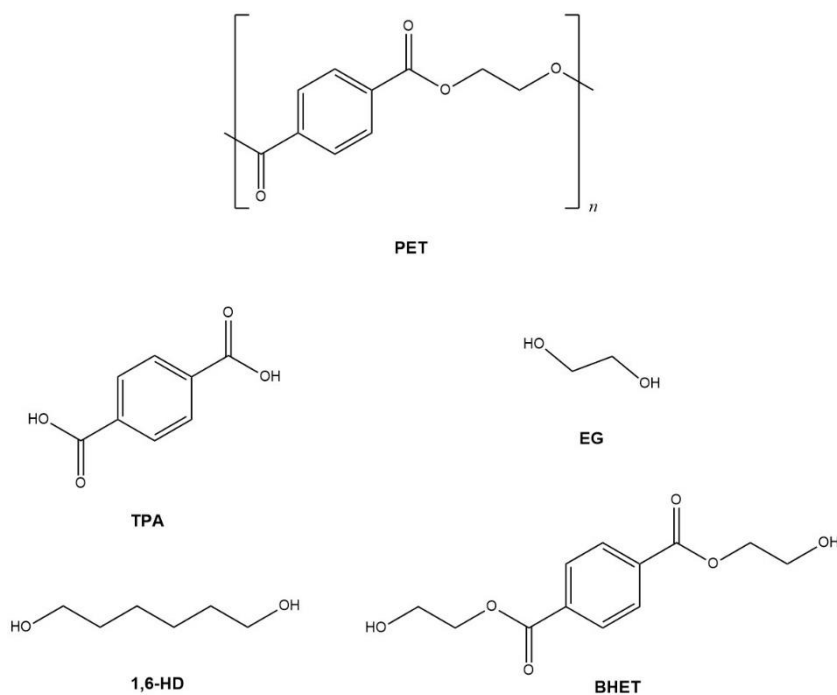


Figure 3.8 – Chemical structures of organic susceptor candidates terephthalic acid (TPA), ethylene glycol (EG), 1,6-hexanediol (1,6-HD) and bis(2-hydroxyethyl) terephthalate (BHET). PET is also shown (top) to illustrate structural similarities with susceptor candidates.

The dielectric constant (ϵ') and the dielectric loss factor (ϵ'') of these compounds, and PET, were obtained either by heat and hold cavity perturbation (PET, TPA, BHET and 1,6 -HD) or coaxial probe (ethylene glycol) and the dielectric response of the susceptor candidates was compared with that of PET (Fig. 3.9 – Fig 3.14) (Tab. 3.2).

Table 3.2 shows that at room temperature, all the potential susceptor candidates exhibit a dielectric loss factor greater than PET by 1 to 4 orders of magnitude, apart from TPA.

TPA is an exception to this as, despite five repeats, negligible dielectric loss factor was recorded. TPA is able to undergo a range of intermolecular interactions, including hydrogen bonding and π - π stacking, giving rise to a highly ordered crystalline structure.²²⁴ It is postulated here that this ordered structure impedes virtually all molecular rotation when exposed to a microwave field, and TPA was dropped from susceptor consideration as a result.

As well as displaying superior dielectric properties to PET at room temperature, the remaining potential susceptors (BHET, 1,6 -HD, ethylene glycol) retain both superior dielectric constant

(Fig. 3.9) (Fig 3.10) and dielectric loss factor (Fig. 3.11) (Fig. 3.12) up to their respective boiling points. The same trend is seen when the dielectric loss tangent is plotted against temperature (Fig. 3.13) (Fig. 3.14). As ethylene glycol demonstrated a much stronger dielectric response than all other materials tested, the dielectric constant, loss factor and tangent results have all been plotted with ethylene glycol (Fig. 3.9) (Fig. 3.11) (Fig. 3.13) and once again with the ethylene glycol result omitted to better show how BHET and 1,6-HD differ from PET (Fig. 3.10) (Fig. 3.12) and (Fig. 3.14)

As all these compounds possess a far smaller molar mass than PET, and contain polar functional groups, it is not surprising they are more able to undergo the polarisation heating mechanism (Fig. 3.2) than PET itself, explaining why they exhibit a stronger dielectric response.

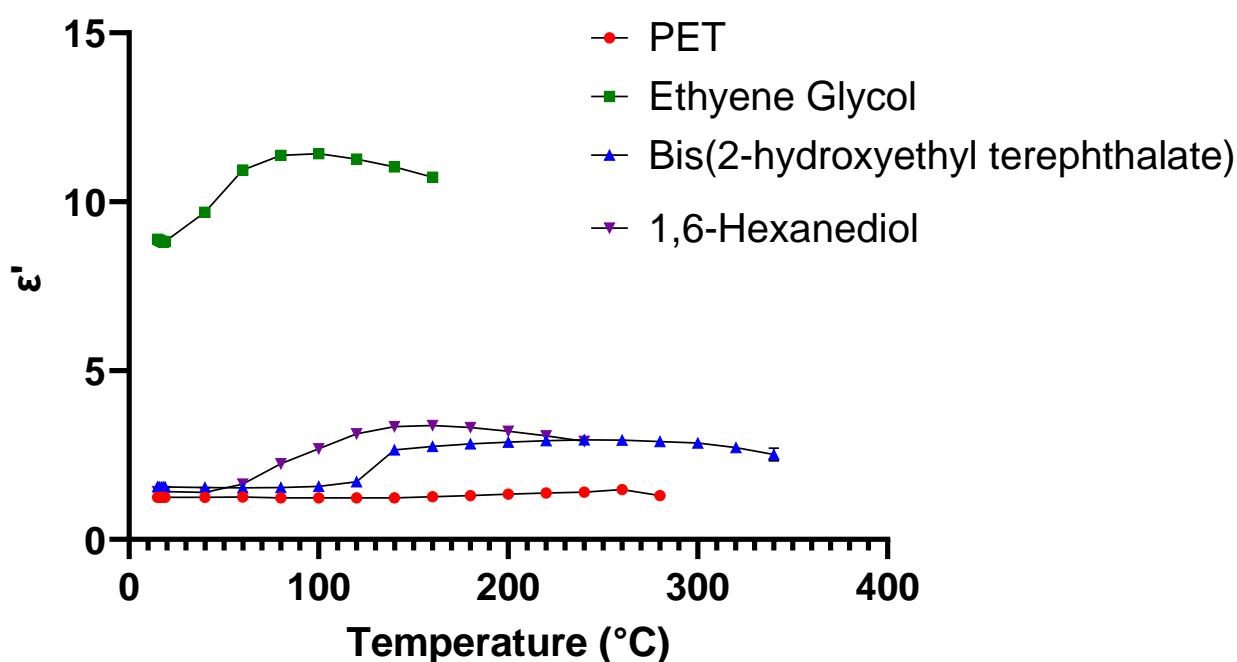


Figure 3.9 – Dielectric constant vs temperature of PET^a, ethylene glycol^b, 1,6-hexanediol^a and bis(2-hydroxyethyl) terephthalate^a. All three susceptor candidates demonstrate a considerably stronger dielectric constant over that of PET over the studied temperature range for the measured frequency (2.47 GHz). Error bars indicate standard error of the mean value.

a - measured by cavity perturbation b - measured by coaxial probe

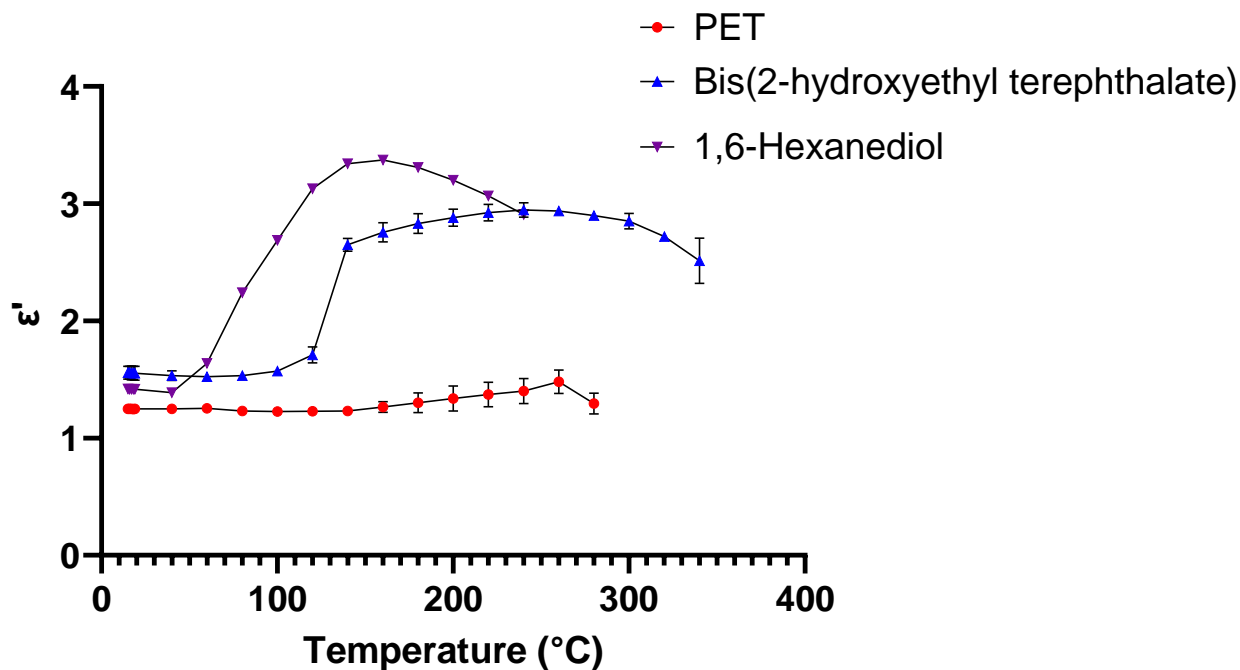


Figure 3.10 – Dielectric constant vs temperature of PET^a, 1,6-hexanediol^a and bis(2-hydroxyethyl) terephthalate^a with ethylene glycol omitted to better illustrate how 1,6-HD and BHET differ from PET. Error bars indicate standard error of the mean value.

a - measured by cavity perturbation b - measured by coaxial probe

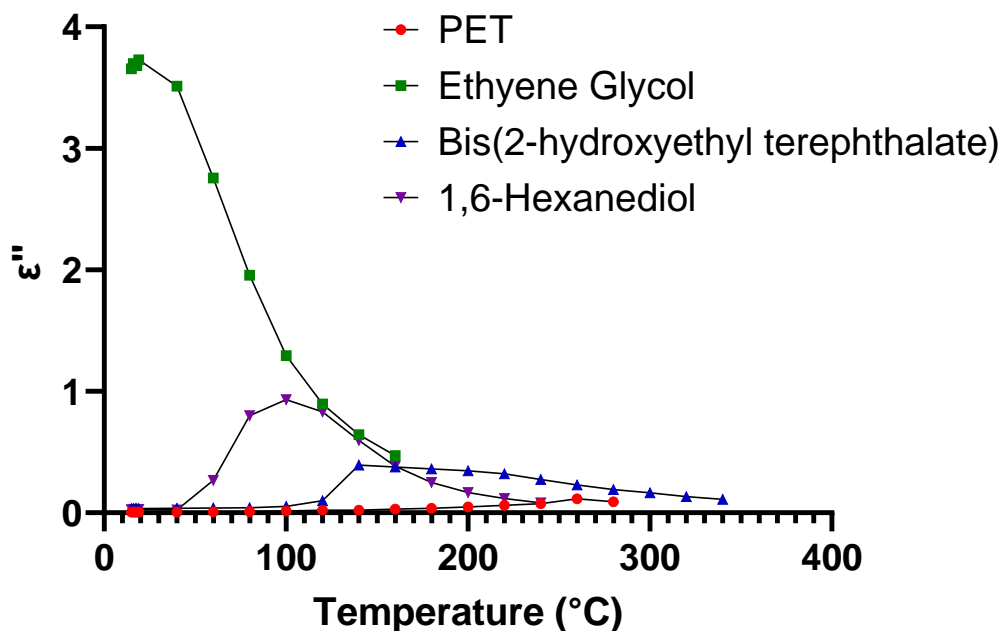


Figure 3.11 – Dielectric loss factor vs temperature of PET^a, ethylene glycol^b, 1,6-hexanediol^a and bis(2-hydroxyethyl) terephthalate^a. All three susceptor candidates demonstrate a considerably stronger dielectric loss factor over that of PET over the studied temperature range for the measured frequency (2.47 GHz). Error bars indicate standard error of the mean value.

a - measured by cavity perturbation b - measured by coaxial probe

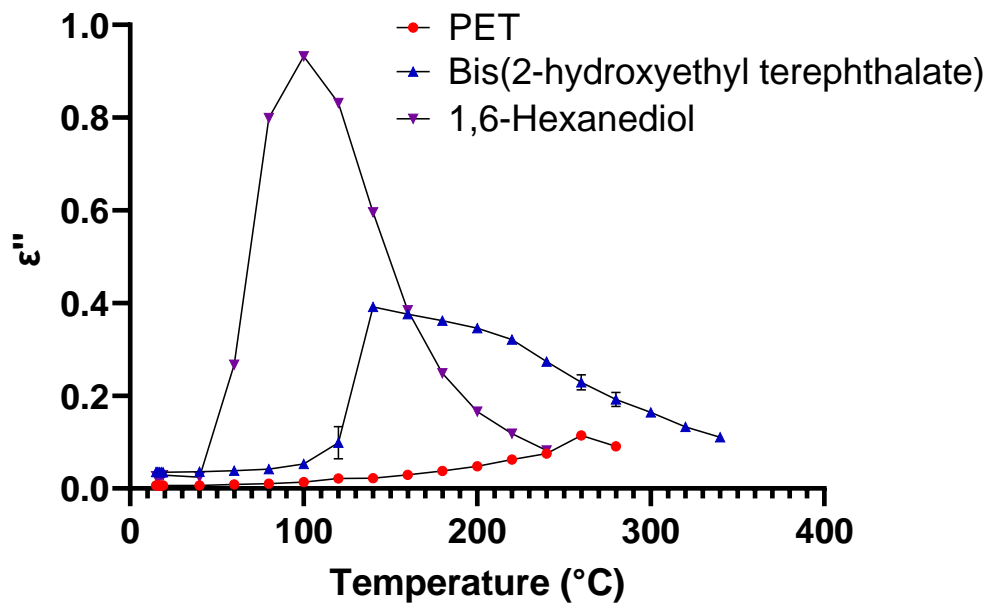


Figure 3.12 – Dielectric loss factor vs temperature of PET^a, 1,6-hexanediol^a and bis(2-hydroxyethyl) terephthalate^a with ethylene glycol omitted to better illustrate how 1,6-HD and BHET differ from PET. Error bars indicate standard error of the mean value.

a - measured by cavity perturbation b - measured by coaxial probe

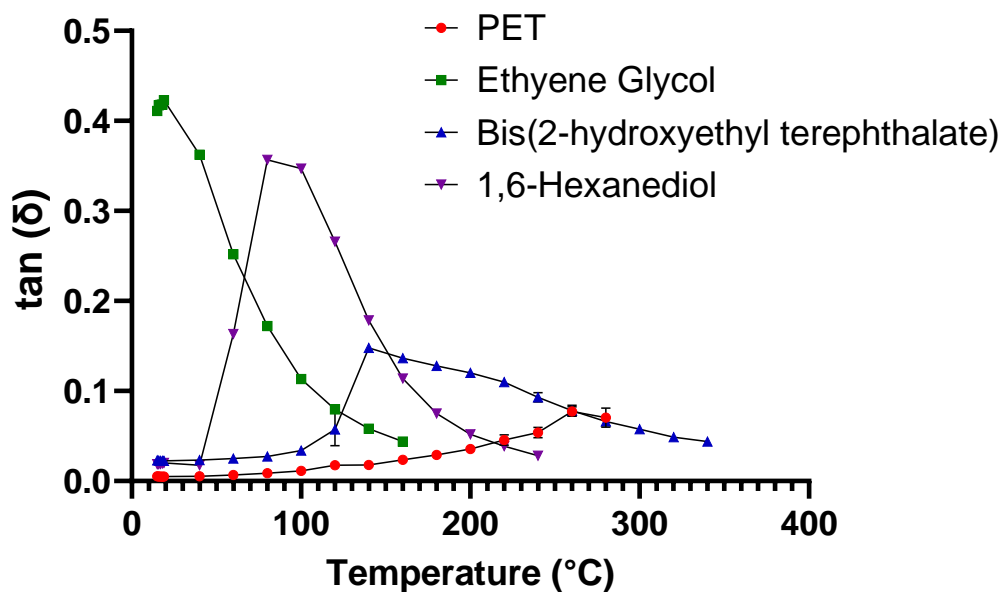


Figure 3.13 – Dielectric loss tangent vs temperature of PET^a, ethylene glycol^b, 1,6-hexanediol^a and bis(2-hydroxyethyl) terephthalate^a. All three susceptor candidates demonstrate a considerably stronger overall dielectric response over that of PET over the studied temperature range for the measured frequency (2.47 GHz). Error bars indicate standard error of the mean value.

a - measured by cavity perturbation b - measured by coaxial probe

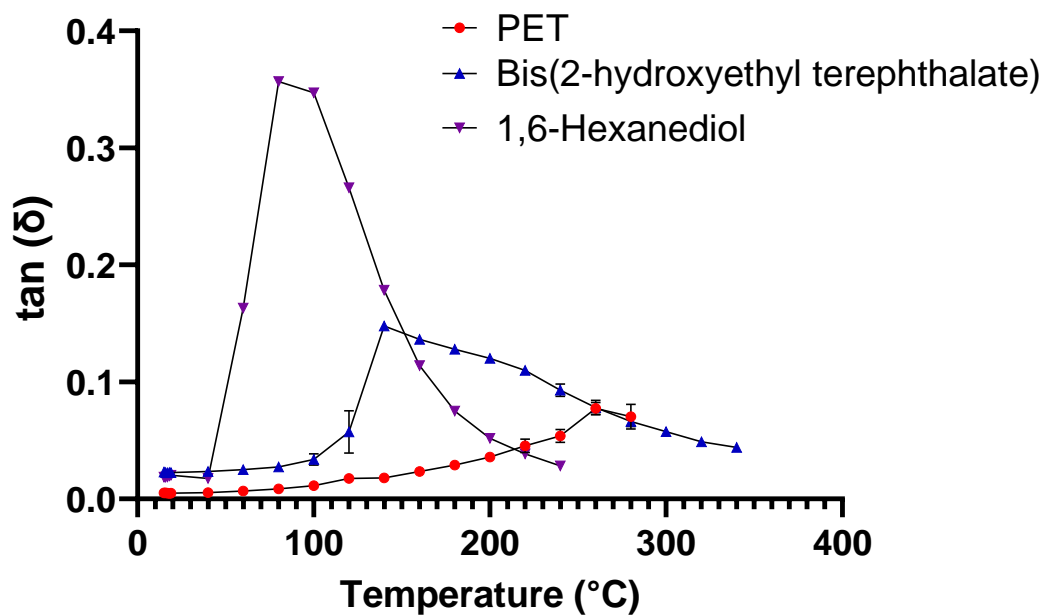


Figure 3.14 – Dielectric loss tangent vs temperature of PET^a, 1,6-hexanediol^a and bis(2-hydroxyethyl) terephthalate^a with ethylene glycol omitted to better illustrate how 1,6-HD and BHET differ from PET. Error bars indicate standard error of the mean value.

a - measured by cavity perturbation b - measured by coaxial probe

Table 3.2 – Room temperature dielectric constant, loss factor and the corresponding tan delta of PET and the organic susceptor candidates. It can be seen that all of the potential susceptors possess a superior dielectric response compared to PET, with ethylene glycol, a polar liquid at room temperature, displaying the strongest dielectric properties (20 °C, 2.47 GHz).

a- measured by cavity perturbation b- measured by coaxial probe

Compound	ϵ'	ϵ''	$\tan \delta$
PET ^a	1.25	6.19×10^{-3}	5.00×10^{-3}
Ethylene Glycol ^b	13.00	12.70	0.98
BHET ^a	1.56	3.51×10^{-2}	2.26×10^{-2}
1,6-HD ^a	1.42	2.77×10^{-2}	1.87×10^{-2}
TPA ^a	1.52	negligible	negligible

To probe the suitability of the susceptors for supercritical impregnation into PET, the scCO_2 solubility of BHET, 1,6-HD and ethylene glycol was then investigated in a fixed-volume view cell. At 278 bar and 65 °C, ethylene glycol gradually exited the sample holder (Fig. 3.15 left) and form a slurry cloudy emulsion with scCO_2 (Fig. 3.15 right) – ethylene glycol was seen to be immiscible with scCO_2 at lower pressures. The sample holder is highlighted by a red circle so EG can be seen easily, note the increasing cloudiness between the left and right images as ethylene glycol exits the sample holder (Fig. 3.15).

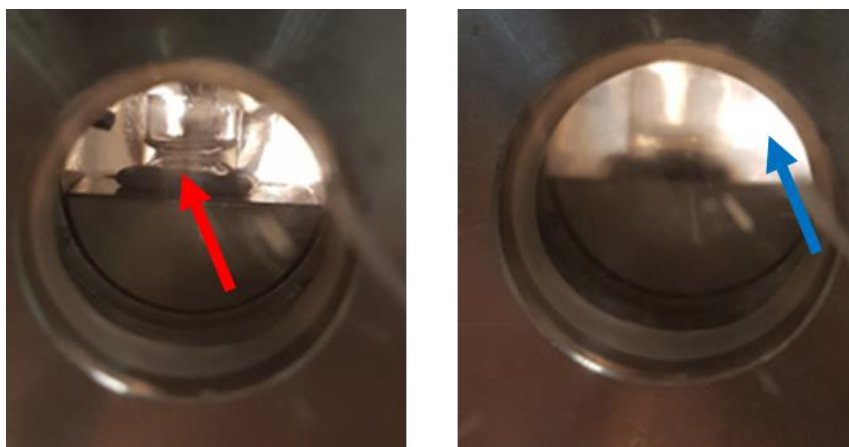


Figure 3.15 - EG can be seen in sample holder in scCO_2 (red arrow) as impregnation conditions (278 bar, 65 °C) are reached (left). As EG was held in scCO_2 at these conditions, it gradually exited the sample holder and formed a slurry-like emulsion with scCO_2 (blue arrow, right).

BHET and 1,6-HD remained in the sample holder at 278 bar and 65 °C. When the temperature was increased to 85 °C, BHET and 1,6-HD remained in the sample holder for 24 hours and were therefore dropped from consideration as microwave susceptor because of observed immiscibility with scCO_2 (Fig. 3.16).

Only ethylene glycol was carried forward for supercritical impregnation experiments with PET, owing to it possessing superior dielectric properties to PET as well as exhibiting some miscibility with scCO_2 .

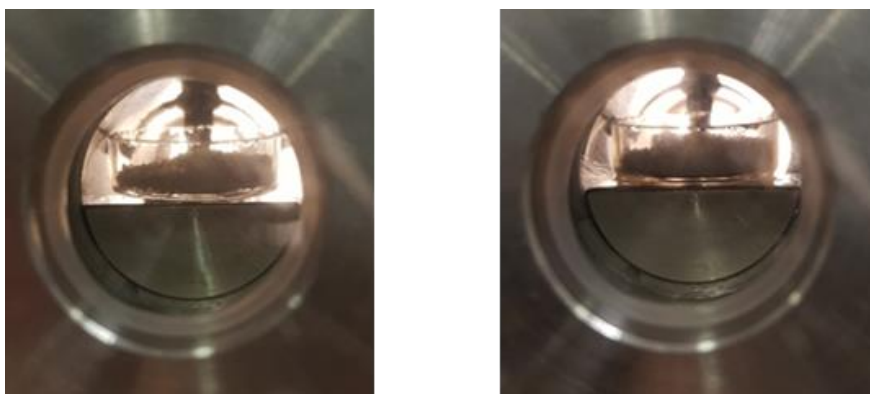


Figure 3.16 – BHET is shown in the sample holder in scCO₂ (278 bar, 65 °C) after 0 hours (left) and 24 hours (right). It remained completely insoluble; the same behaviour was seen for 1,6-HD.

3.3.2 Supercritical Impregnation of PET

Conditions for the supercritical impregnation experiments were informed by the solubility of ethylene glycol in scCO₂ acquired from the view cell. A constant pressure of 278 bar was used for all experiments, as this was shown to be the minimum pressure required to begin to dissolve ethylene glycol in scCO₂. Whilst three temperatures (32 °C, 65 °C, 85 °C) were chosen as this will change the density of the supercritical fluid, thereby influencing the miscibility of the susceptors.

Initial experiments were conducted with ethylene glycol at 278 bar, 40 °C for 3 or 24 hours. To validate that successful impregnation of ethylene glycol had occurred, a range of controls were devised:

- Control 1 – soak PET in pure scCO₂ at impregnation conditions and compare change in weight percentage ($\Delta W\%$) to the corresponding ethylene glycol impregnation experiments.
- Control 2 – soak PET in the presence of ethylene glycol at impregnation conditions, but replace scCO₂ with water, to confirm the swelling effect of the supercritical fluid is necessary.

- Control 3 – soak PET in bulk ethylene glycol at impregnation conditions, to again confirm the swelling effect of scCO₂ is required.

The PET film recovered from these experiments was dried and weighed immediately after impregnation (t=0 hrs) and one day afterwards (t=24 hrs), to allow any residual carbon dioxide in the polymer to evolve. It can be seen that not only was the swelling effect of scCO₂ on PET present, but necessary as impregnation of ethylene glycol could be seen to be occurring only when scCO₂ was used as the medium (Tab. 3.3).

Table 3.3 - Percentage change ($\Delta W\%$) of PET after supercritical impregnation with ethylene glycol, or one of three control experiments designed to illustrate that the swelling ability of scCO₂ is required to impregnate ethylene glycol (40 °C, 3 hrs). PET was weighed immediately after the experiment, and again after 24 hours to allow residual CO₂ to evaporate.

Experiment	($\Delta W\%$) 0 hrs post-impregnation	($\Delta W\%$) 24 hrs post-impregnation
scCO ₂ ethylene glycol impregnation	+ 11.48	+ 5.49
scCO ₂ control	+ 8.16	+ 1.43
Water: Ethylene Glycol Control	+ 0.00	+ 0.00
Bulk Ethylene Glycol Control	+ 0.00	+ 0.00

After 24 hours, PET soaked in scCO₂ alongside ethylene glycol retained a percentage weight increase 4.06 % greater than PET soaked in pure scCO₂. Furthermore, CO₂ could be seen to permeate into PET as the polymer exhibited an 11.48% and 8.16% increase in weight for the supercritical impregnation and control experiments respectively, with these values falling to 5.49% and 1.43% after 24 hours as CO₂ diffused out from the films.

With supercritical impregnation of PET being confirmed, the temperature range was expanded to 32 °C, 65 °C and 85 °C to explore its influence on the impregnation process.

PET was soaked with an equal mass of ethylene glycol (i.e. 0.5 g of PET to 0.5 g ethylene glycol), here after referred to as a 1:1 mass ratio, in scCO₂ for three hours at the three different temperatures, and control experiments in pure scCO₂ were also conducted to confirm

impregnation had taken place (Tab 3.4). Results exhibited a similar trend to those in table 3.3 as PET samples from impregnation experiments exhibit a greater mass percentage increase when compared to the controls both immediately post-impregnation (0 hrs) and after one day (24 hrs).

Table 3.4 – Percentage weight change ($\Delta W\%$) of PET films immediately (0 hrs) and one day (24 hrs) after being soaked in pure $scCO_2$ (control) or soaked in $scCO_2$ alongside an equal mass of ethylene glycol (impregnation) for 3 hours.

		Control		Impregnation	
Susceptor		($\Delta W\%$) 0 hrs post-impregnation	($\Delta W\%$) 24 hrs post-impregnation	($\Delta W\%$) 0 hrs post-impregnation	($\Delta W\%$) 24 hrs post-impregnation
Ethylene Glycol	32°C	+7.95	+0.97	+11.11	+3.49
	65°C	+7.77	+1.40	+8.18	+2.89
	85°C	+6.12	+1.39	+8.01	+1.67

Impregnation was further confirmed by PET films being heated in a TGA up to 250 °C, as this was sufficient to boil off ethylene glycol (b.p. = 196 °C) but below the decomposition temperature of PET of 340 °C (Fig. 3.17).^{225, 226} Once again, control experiments of PET soaked in pure $scCO_2$ at impregnation conditions were analysed under identical conditions in the TGA to discriminate between mass loss due to residual CO_2 and mass loss because of susceptor evaporation.

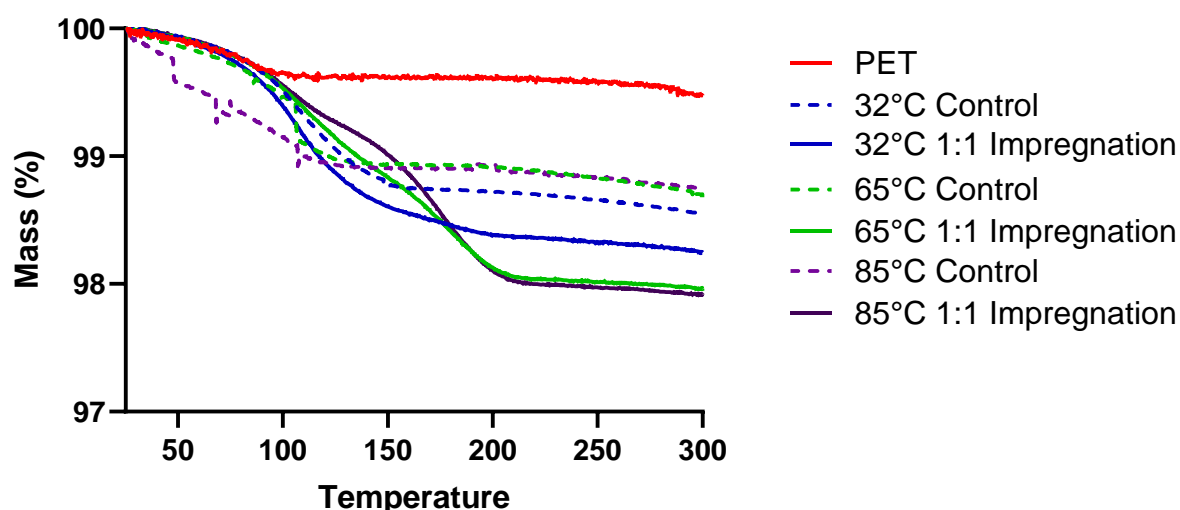


Figure 3.17-TGA of PET films impregnated with ethylene glycol at three temperatures (32, 65 and 85 °C) and the corresponding controls.

Impregnation pressure = 278 bar, Impregnation time = 3 hours, TGA heating rate = 10 °C/min.

Table 3.5 – Percentage weight change ($\Delta W\%$) of TGA analyses of PET impregnation and control experiments shown in figure 3.11. Impregnation pressure = 278 bar, Impregnation time = 3 hours, TGA heating rate = 10 °C/min

Impregnation Temperature	Experiment Type	($\Delta W\%$)
32 °C	Control	-1.34
	Impregnation	-1.68
65 °C	Control	-1.17
	Impregnation	-1.98
85 °C	Control	-1.17
	Impregnation	-2.07

All control experiments level off in terms of mass loss by 200 °C, whereas PET impregnated with ethylene glycol continues to lose mass up to 216 °C. (Fig. 3.17) (Tab. 3.5) Furthermore, the magnitude of lost mass is greater for the impregnated samples.

The presence of partitioning was confirmed by comparing results obtained from ethylene glycol impregnation into PET with 1,2-dimethoxy ethane (1,2-DME). This methoxy analogue of ethylene glycol (Fig. 3.18) was shown to be completely soluble in $scCO_2$ at 278 bar and differing temperatures (32 °C and 65 °C), unlike ethylene glycol which produced the slurry in view cell experiments. As 1,2-DME demonstrated excellent miscibility with $scCO_2$, impregnation experiments were undertaken with PET. 24 hours post-impregnation, PET soaked in $scCO_2$ alongside 1,2-DME was found to exhibit an effectively identical $\Delta W\%$ to PET soaked in pure $scCO_2$ (Tab. 3.6).



Figure 3.18 – Chemical structure of 1,2-dimethoxy ethane (left) and ethylene glycol (right).

These results are consistent with what is known about partitioning, as discussed in section 3.1.4.2. The excellent solubility of 1,2-DME in scCO₂ at the studied pressure and temperature means it possesses a high affinity for the supercritical phase, and it is therefore unfavourable for it to partition into PET. Ethylene glycol on the other hand, was shown to be significantly less miscible with scCO₂, which suggests that any glycol which may have been successfully dissolved in the supercritical phase would have been more able to partition into the polymer.

Table 3.6 – Percentage weight change ($\Delta W\%$) of PET impregnated with 1,2-DME. The results obtained are comparable to PET soaked in pure scCO₂ confirming that 1,2-DME's solubility in scCO₂ prevents it from partitioning into PET. Impregnation pressure = 278 bar, Impregnation time = 3 hours.

Impregnation Temperature	Experiment Type	($\Delta W\%$)
32 °C	Control	+0.97
	Impregnation	+1.10
65 °C	Control	+1.40
	Impregnation	+0.74

Informed by promising dielectric results, which will be discussed in the next section, the amount of ethylene glycol used per impregnation experiment was increased from an equivalent mass with respect to the PET film (0.5 g to 0.5 g) to a mass excess of 10 times that of PET film (5.0 g to 0.5 g) – here after referred to as a 10:1 mass ratio. Once again, a clear increase in $\Delta W\%$ can be seen when the impregnated PET films are compared with those soaked in pure scCO₂, both at 0 hours and 24 hours post-impregnation (Table. 3.7). TGA analysis also shows a clear increase in mass loss up to 250 °C for impregnated films, an identical trend to what is seen for PET films impregnated with a 1:1 mass ratio of ethylene glycol (Fig. 3.19) (Tab. 3.7).

Although it is common to calculate the partition co-efficient for a supercritical impregnation experiment, that has not been attempted in this case. Previous impregnation literature involving polycarbonate has taken great care to digitally control the depressurisation rate once the desired residence time has been reached, to avoid accidental removal of guest species when CO₂ is rapidly vented.²²⁷ Further work on the impregnation of linear low-density polyethylene

(LLDPE) investigated whether the rate of depressurisation affected the retention of guest species, and found significant differences in $\Delta W\%$ of LLDPE when the depressurisation rate was increased from 10 bar/min to 100 bar/min.²²⁸

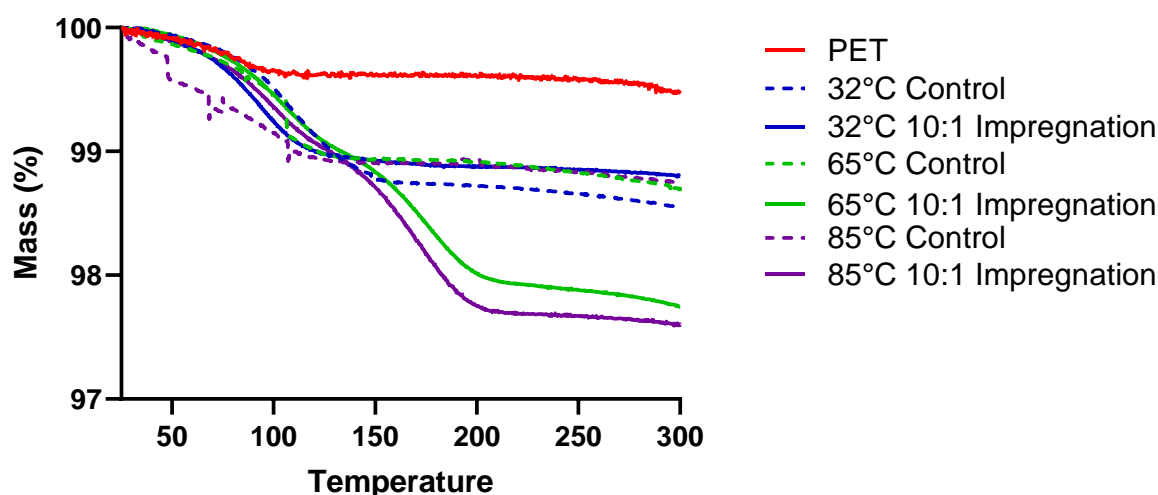


Figure 3.19- TGA of PET films impregnated with ethylene glycol at three temperatures (32, 65 and 85 °C), in a 1:10 mass ratio, and the corresponding controls.

Impregnation pressure = 278 bar, Impregnation time = 3 hours, TGA heating rate = 10 °C/min.

Table 3.7 – Percentage weight change ($\Delta W\%$) of PET impregnated with ethylene glycol in the presence of a 10-mass excess in $scCO_2$ at three temperatures. Impregnation pressure = 278 bar, Impregnation time = 3 hours.

Susceptor	Impregnation Temperature	Control		Impregnator	
		($\Delta W\%$) 0 hrs post-impregnation	($\Delta W\%$) 24 hrs post-impregnation	($\Delta W\%$) 0 hrs post-impregnation	($\Delta W\%$) 24 hrs post-impregnation
Ethylene Glycol	32°C	+7.95	+0.97	+9.62	+1.47
	65°C	+7.77	+1.40	+10.58	+1.93
	85°C	+6.12	+1.39	+9.70	+2.82

The high-pressure autoclaves utilised for these experiments were vented manually by opening a HiP tap. In these vessels monitoring the rate of CO_2 removal is not possible, and thus accurately controlling the rate of depressurisation cannot be done. For this reason, partition co-efficients have not been calculated, due to lack of precise reproducibility. The presence of susceptor within PET can however be confirmed by the gravimetric analyses, as well as through dielectric experiments described below.

3.3.3 Dielectric Analysis

Dielectric analysis undertaken on the dynamic cavity in this section was performed with the assistance of members of Professor Felipe Penaranda Foix's research group at Universitat Politècnica de València, Valencia, Spain. Members of Professor Penaranda Foix's group also plotted the corresponding data and provided it to PhD candidate Bradley Hopkins.

Following gravimetric confirmation of impregnation, dielectric experiments were performed to determine whether the impregnation successfully enhanced PET's dielectric response. The dielectric constant, dielectric loss factor and dielectric loss tangent were quantified at both elevated temperatures (Fig. 3.21) (Fig. 3.23) (Fig. 3.25) as well as room temperature (Fig. 3.22) (Fig. 3.24) (Fig. 3.26).

No significant difference in the dielectric constant can be seen for PET impregnated with a 1:1 mass ratio, but the dielectric loss factor increases by an order of magnitude after impregnation at all three temperatures (Fig. 3.21) (Fig. 3.23). Figures showing a close-up view of the dielectric constant and loss factor at room temperature are also included (Fig. 3.22) (Fig. 3.24), to better illustrate that there does not appear to be a significant difference in the dielectric constant (shown by overlapping error bars), whereas the dielectric loss factor does appear to have been enhanced. This improvement in the dielectric loss factor also indicates that impregnation has successfully occurred as ethylene glycol, a small polar molecule, is much more able to undergo polarisation when exposed to the alternating microwave field than PET.

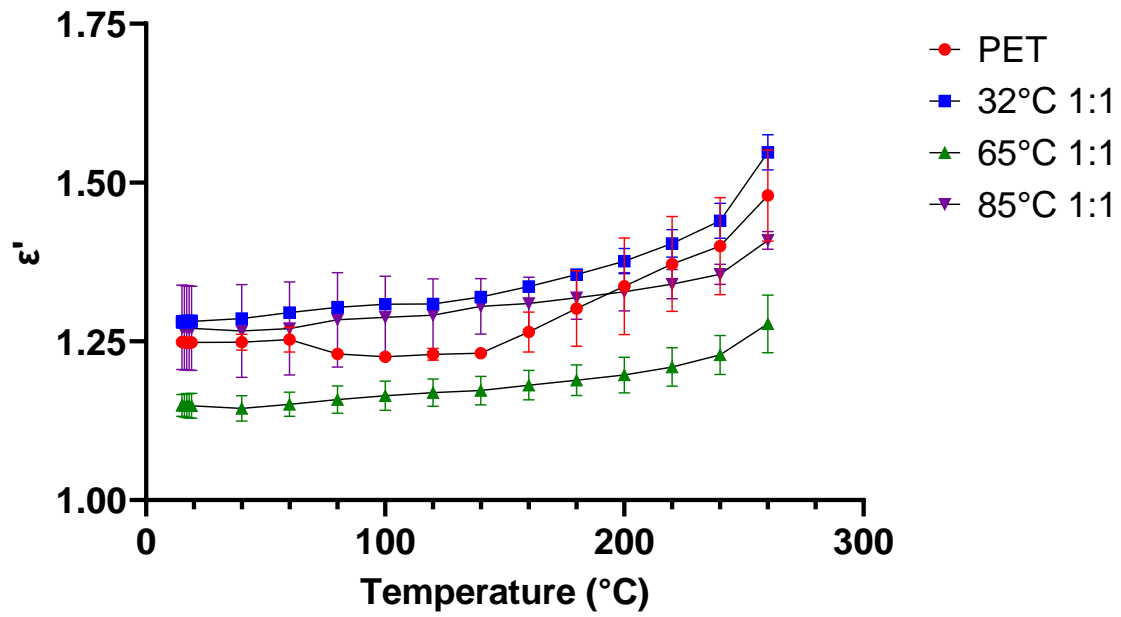


Figure 3.21 – Heat and hold dielectric constant results of PET contrasted with PET impregnated at 32, 65 and 85 °C with ethylene glycol in a 1:1 EG: PET mass ratio. Error bars indicate standard error of the mean value.

Impregnation pressure = 278 bar, Impregnation time = 3 hours, Frequency = 2470 MHz.

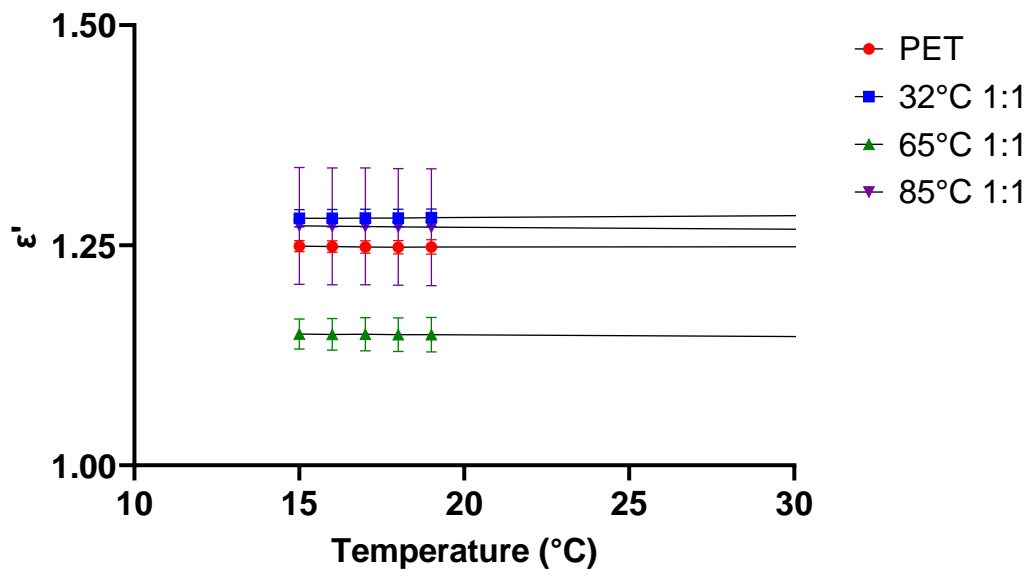


Figure 3.22 – Close up of heat and hold dielectric constant room temperature results from figure 3.21 of PET contrasted with PET impregnated at 32, 65 and 85 °C with ethylene glycol in a 1:1 EG: PET mass ratio. Error bars indicate standard error of the mean value.

Impregnation pressure = 278 bar, Impregnation time = 3 hours, Frequency = 2470 MHz.

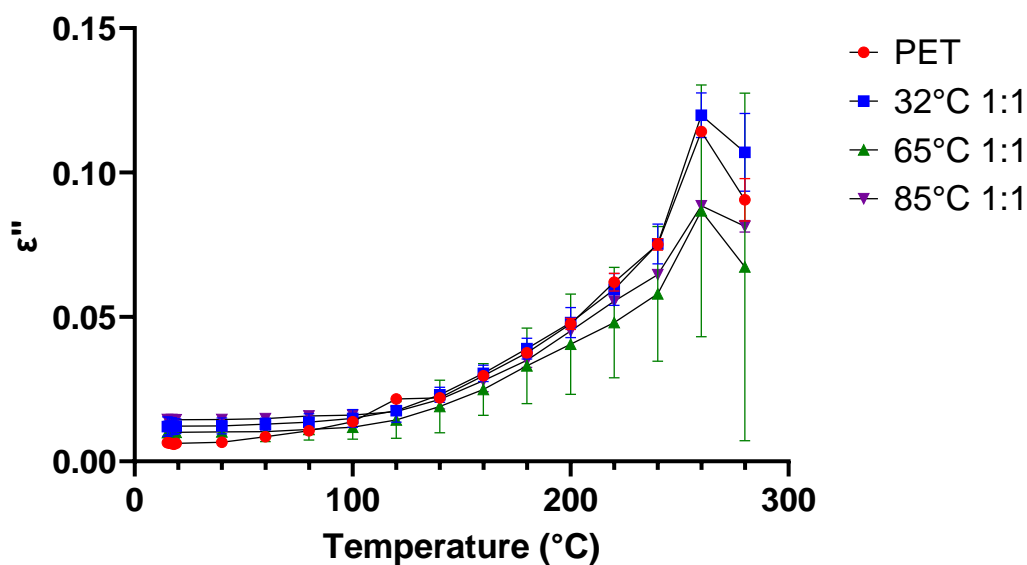


Figure 3.23 - Heat and hold dielectric loss factor results of PET contrasted with PET impregnated at 32, 65 and 85 °C with ethylene glycol in a 1:1 EG: PET mass ration. Error bars indicate standard error of the mean value.

Impregnation pressure = 278 bar, Impregnation time = 3 hours, Frequency = 2470 MHz

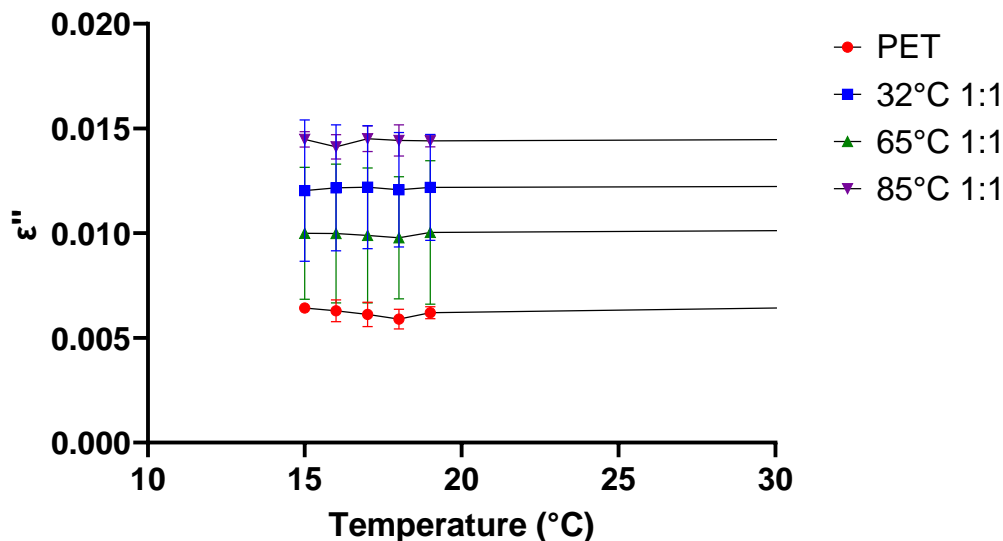


Figure 3.24 – Close up of heat and hold dielectric loss factor room temperature results in figure 3.23 of PET contrasted with PET impregnated at 32, 65 and 85 °C with ethylene glycol in a 1:1 EG: PET mass ration. Error bars indicate standard error of the mean value.

Impregnation pressure = 278 bar, Impregnation time = 3 hours, Frequency = 2470 MHz

When the dielectric response is expressed as $\tan \delta$, an enhancement can once again be seen at room temperature (Fig. 3.26), which diminishes at temperatures above 80 °C (Fig. 3.25).

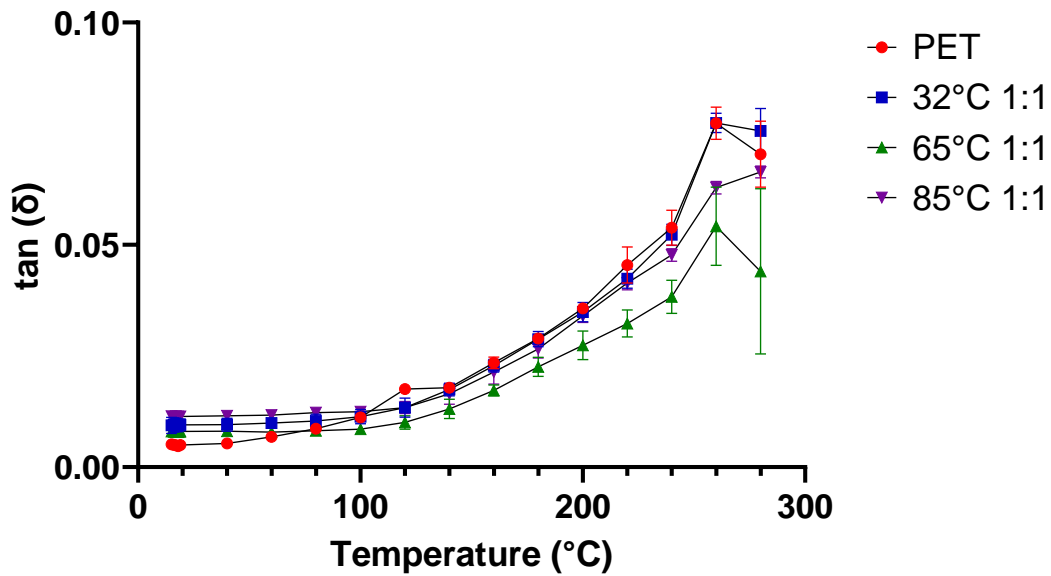


Figure 3.25 - Heat and hold dielectric loss tangent results of PET contrasted with PET impregnated at 32, 65 and 85 °C with ethylene glycol in a 1:1 EG: PET mass ration. Error bars indicate standard error of the mean value.

Impregnation pressure = 278 bar, Impregnation time = 3 hours, Frequency = 2470 MHz.

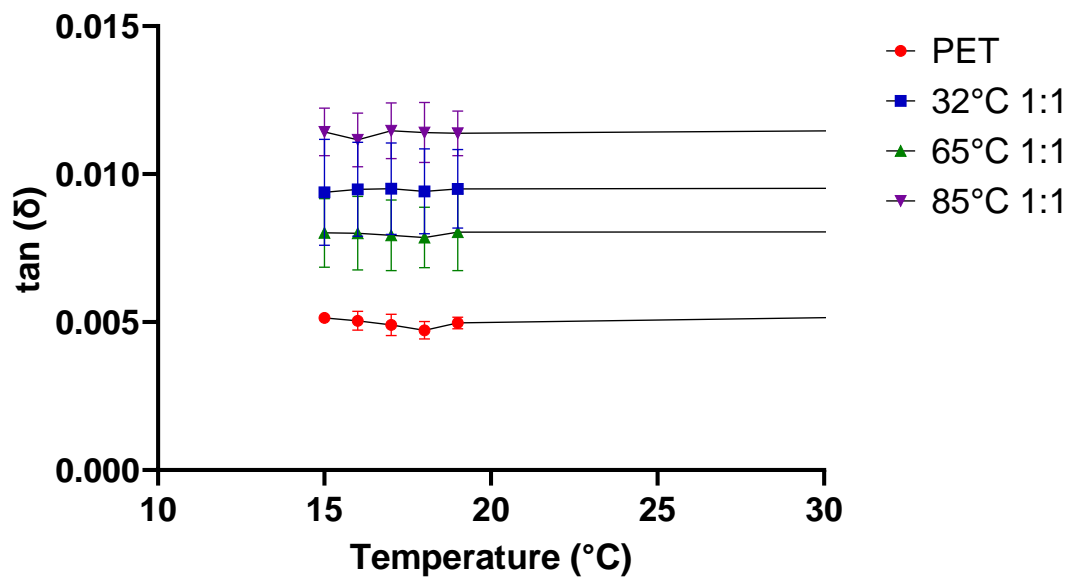


Figure 3.26 – Close up of heat and hold dielectric loss tangent room temperature results in figure 3.25 of PET contrasted with PET impregnated at 32, 65 and 85 °C with ethylene glycol in a 1:1 EG: PET mass ration. Error bars indicate standard error of the mean value.

Impregnation pressure = 278 bar, Impregnation time = 3 hours, Frequency = 2470 MHz.

When the PET films were heated above room temperature, and particularly once 80 °C is reached, the dielectric loss factor and dielectric loss tangent of the impregnated PET becomes indistinguishable from that of the unmodified polymer (Fig. 3.23) (Fig. 3.25). Between each of the temperature increments where the dielectric properties are measured, there was approximately a time delay of 5 minutes as the furnace heated the sample. This was adequate time for the ethylene glycol impregnated into the polymer to desorb and evaporate, which would have been aided as the polymer chains become increasingly mobile at elevated temperatures. It was hypothesised that the ethylene glycol that had been successfully impregnated, as shown by the gravimetric analyses and the room temperature dielectric response, was able to desorb from the polymer once a sufficient temperature had been reached during. The fact that ethylene glycol has been shown to desorb from PET when heated in the TGA (Fig. 3.17) (Fig. 3.19), provides evidence for this reasoning.

To probe if the room temperature enhancements seen in the dielectric properties were also present when PET was exposed to a microwave field, dielectric measurements were undertaken on a dynamic, dual-mode cavity capable of simultaneously heating a sample with microwave radiation whilst continuously measuring the dielectric response of PET samples.

Whilst different values for the dielectric properties were obtained which is attributed to the higher mass and packing density of the samples, an identical trend can be seen for the dielectric loss factor, dielectric constant and dielectric loss tangent (Tab. 3.8). Much like the heat-and-hold cavity perturbation experiments, unmodified PET demonstrates the poorest dielectric properties at room temperature whilst the magnitude of both the dielectric loss factor and loss tangent increases with impregnation temperature. A small increase in the dielectric constant can also be seen with increasing impregnation temperature.

Table 3.8 – Room temperature dynamic dielectric results of PET contrasted with PET impregnated with ethylene glycol at 32, 65 and 85 °C.

Impregnation pressure = 278 bar, Impregnation time = 3 hours, Frequency = 2470 MHz.

	ϵ'	ϵ''	$\tan(\delta)$
PET	1.76	1.00×10^{-2}	5.68×10^{-3}
32 °C	1.82	1.42×10^{-2}	7.78×10^{-3}
65 °C	1.90	1.70×10^{-2}	8.96×10^{-3}
85 °C	2.03	2.57×10^{-2}	1.26×10^{-2}

To understand what effects exposure to scCO₂ alone could have on the dielectric response of PET, independent of the ethylene glycol impregnation, PET films soaked in pure scCO₂ were also subjected to dynamic dielectric measurements. Unlike films soaked in the presence of ethylene glycol, no improvement in the dielectric constant, loss factor or loss tangent could be seen at room temperature (Tab. 3.9).

Table 3.9 – Room temperature dynamic dielectric results of PET and PET soaked in scCO₂ at 32, 65 and 85 °C.

Impregnation pressure = 278 bar, Impregnation time = 3 hours, Frequency = 2470 MHz.

	ϵ'	ϵ''	$\tan(\delta)$
PET	1.76	1.00×10^{-2}	5.68×10^{-3}
32 °C	1.67	9.70×10^{-3}	5.81×10^{-3}
65 °C	1.77	1.02×10^{-2}	5.77×10^{-3}
85 °C	1.77	1.00×10^{-2}	5.63×10^{-3}

Impedance in the dielectric response of PET exposed to pure scCO₂ is believed to be a consequence of recrystallisation which is able to take place when a polymer is swollen and plasticised by scCO₂.¹⁵⁹ A crystalline domain is more ordered and tightly packed in comparison to an amorphous region of polymer, thus crystallinity will restrict the ability of the polymer chains to move when exposed to an alternating microwave field and limit heating.²²⁹

These control experiments provide further evidence that ethylene glycol was successfully impregnated into PET, as the impregnated samples display their enhanced dielectric properties despite the fact that scCO_2 -induced recrystallisation of the PET has been shown to hamper the dielectric response. This supposition is supported by literature precedent mentioned in section 3.1.4.1, as well as the thermal and x-ray scattering data in section 3.3.4.

As with the gravimetric experiments above, the amount of ethylene glycol was again increased from a 1:1 mass ratio with respect to PET to a 10:1 mass ratio, to assess if there was scope to further improve the dielectric properties by heat and hold cavity perturbation.

As with the 1:1 impregnation experiments, the dielectric constant, loss factor and loss tangent for PET impregnated with ethylene glycol with a 10:1 mass ratio is shown (Fig. 3.27) (Fig. 3.29) (Fig. 3.31) which corresponding figures demonstrating how these dielectric properties compare to unmodified PET at room temperature (Fig. 3.28) (Fig. 3.30) (Fig. 3.32).

Unlike the 1:1 impregnation experiments, the error bars for the dielectric constants of the impregnated PET do not overlap with those of unmodified PET at room temperature (Fig. 3.28) and this enhancement is maintained as the samples are heated (Fig. 3.27). The dielectric loss factor (Fig. 3.29) and loss tangent (Fig. 3.31) for PET impregnated at 65°C and 85 °C also show a statistically significant increase over unmodified PET up to 100 °C. All impregnated samples show an increase in loss factor and loss tangent at room temperature too (Fig. 3.30) (Fig. 3.32). In Chapter 4, microwave pyrolysis experiments will be used to demonstrate that these enhancements in the dielectric response of PET do impact how the polymer performs when it is microwaved.

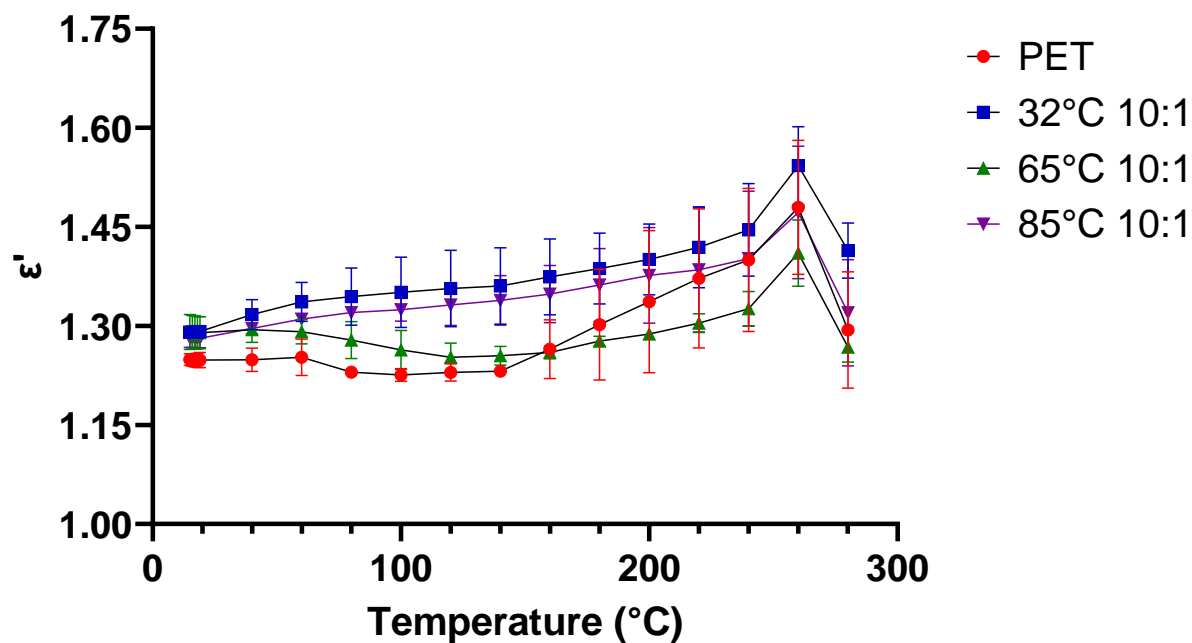


Figure 3.27 - Heat and hold dielectric constant results of PET contrasted with PET impregnated at 32, 65 and 85 °C with ethylene glycol in a 10:1 EG: PET mass ration. Error bars indicate standard error of the mean value.

Impregnation pressure = 278 bar, Impregnation time = 3 hours, Frequency = 2470 MHz

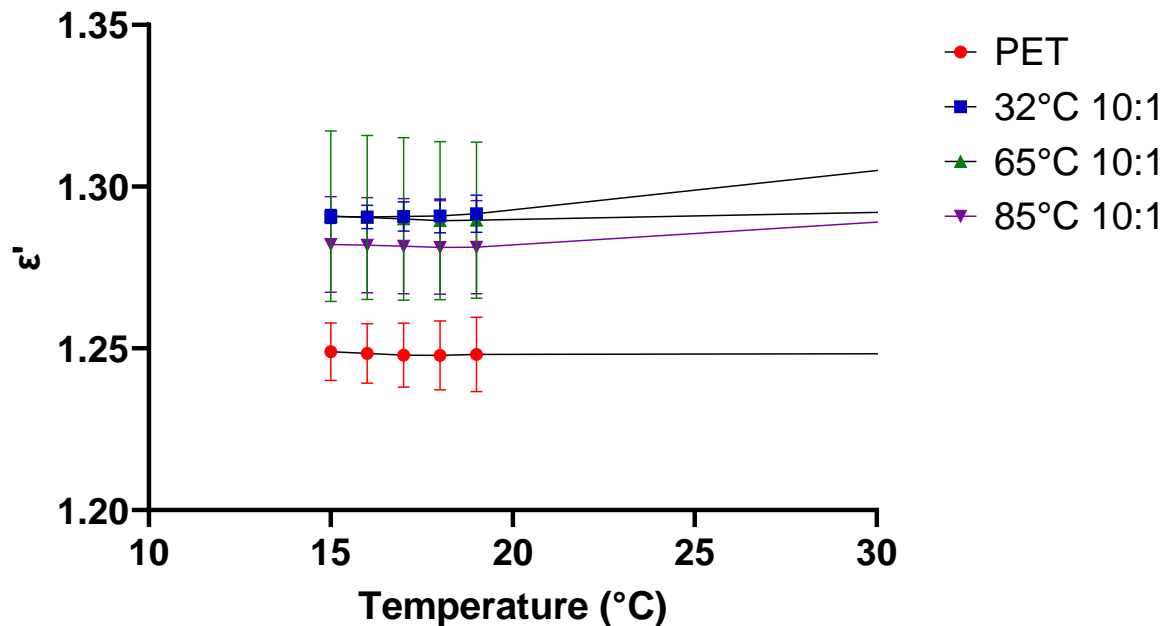


Figure 3.28 – Close up of heat and hold dielectric constant results of PET at room temperature from figure 3.27 contrasted with PET impregnated at 32, 65 and 85 °C with ethylene glycol in a 10:1 EG: PET mass ration. Error bars indicate standard error of the mean value.

Impregnation pressure = 278 bar, Impregnation time = 3 hours, Frequency = 2470 MHz

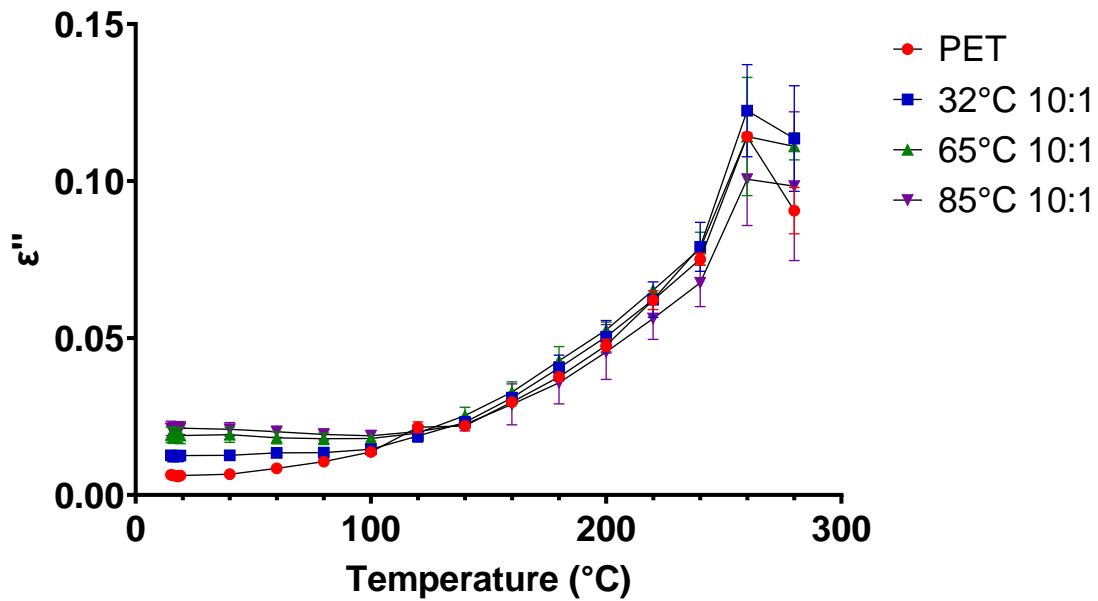


Figure 3.29 - Heat and hold loss factor results of PET contrasted with PET impregnated at 32, 65 and 85 °C with ethylene glycol in a 10:1 EG: PET mass ration. Error bars indicate standard error of the mean value.

Impregnation pressure = 278 bar, Impregnation time = 3 hours, Frequency = 2470 MHz

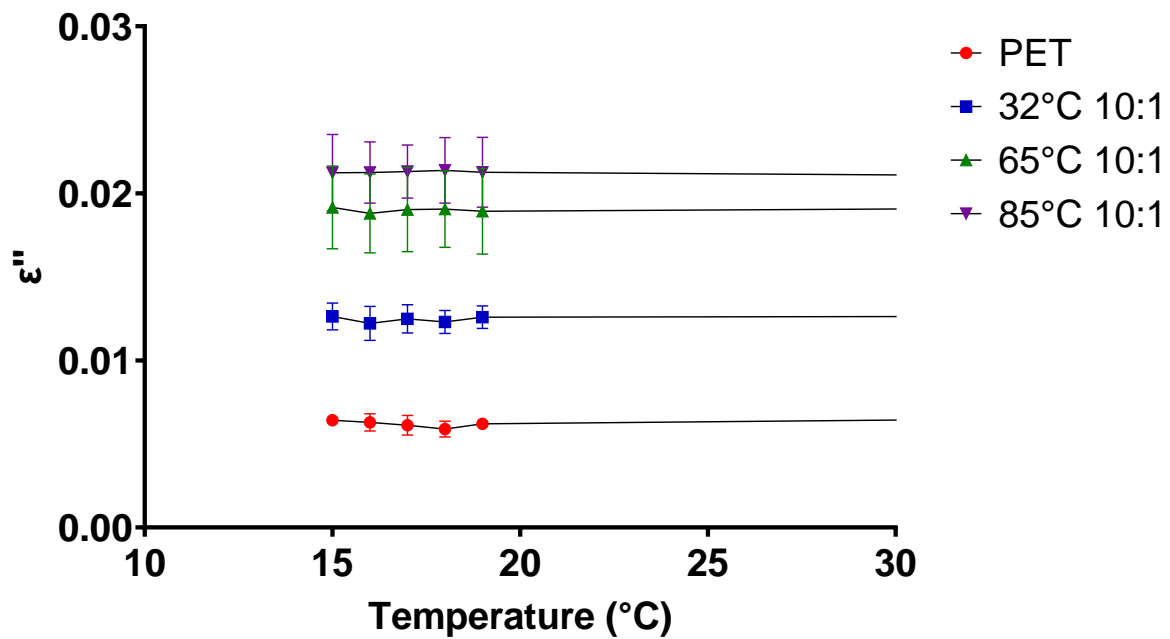


Figure 3.30 – Close up of heat and hold loss factor results of PET at room temperature from figure 3.29 contrasted with PET impregnated at 32, 65 and 85 °C with ethylene glycol in a 10:1 EG: PET mass ration. Error bars indicate standard error of the mean value.

Impregnation pressure = 278 bar, Impregnation time = 3 hours, Frequency = 2470 MHz

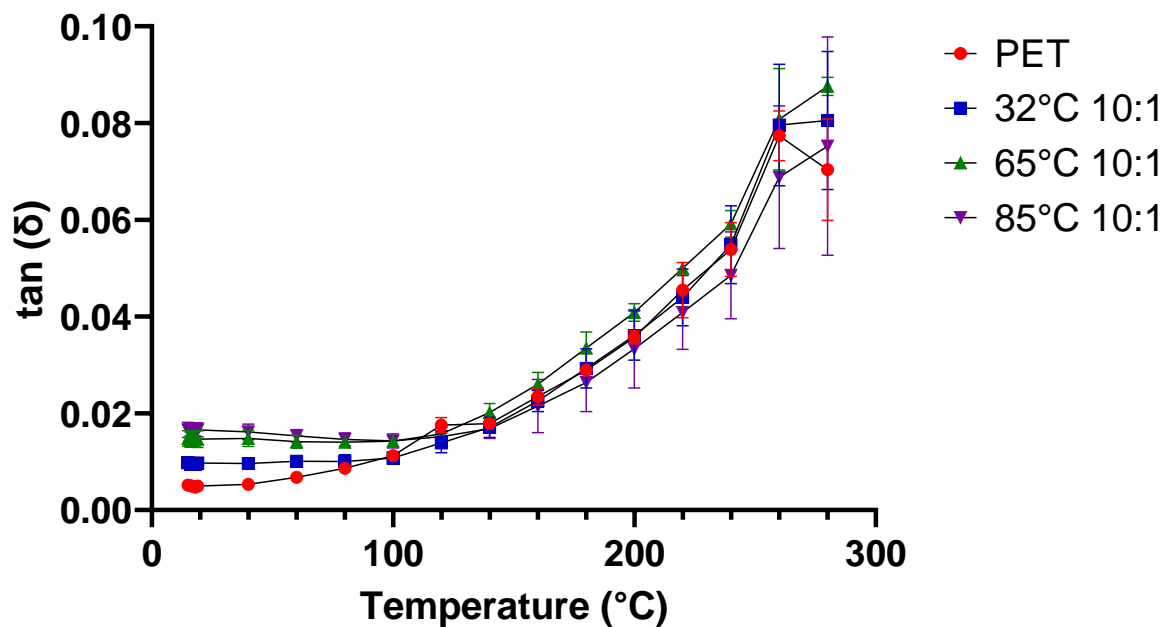


Figure 3.31 - Heat and hold loss tangent results of PET contrasted with PET impregnated at 32, 65 and 85 °C with ethylene glycol in a 10:1 EG: PET mass ration. Error bars indicate standard error of the mean value.

Impregnation pressure = 278 bar, Impregnation time = 3 hours, Frequency = 2470 MHz

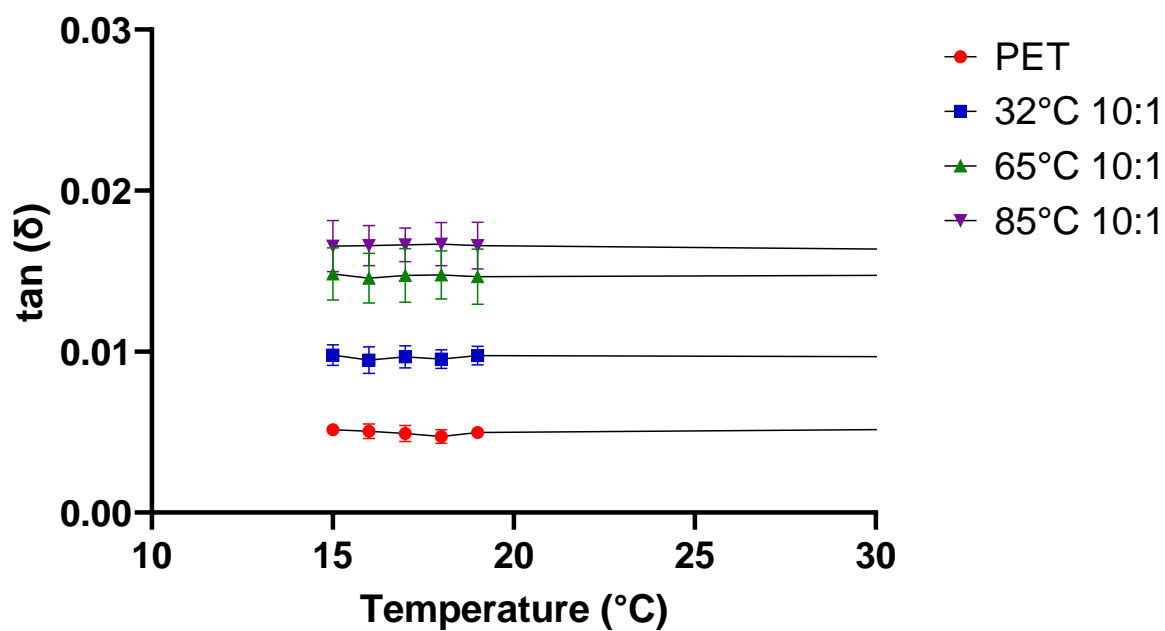


Figure 3.32 – Close up of heat and hold loss factor results of PET at room temperature from figure 3.31 contrasted with PET impregnated at 32, 65 and 85 °C with ethylene glycol in a 10:1 EG: PET mass ration. Error bars indicate standard error of the mean value.

Impregnation pressure = 278 bar, Impregnation time = 3 hours, Frequency = 2470 MHz

3.3.4 Thermal Characterisation and X-ray Scattering

Small and Wide-Angle X-ray analysis (SAXS/WAXS) in this section was performed by Dr Wim Bras at Oak Ridge National Laboratory, Tennessee, USA. PhD Candidate Bradley Hopkins provided samples of PET that was unmodified and treated in scCO₂ for analysis

To improve understanding of the mechanisms behind the dielectric property results in the previous section and confirm the presence of the hypothesised scCO₂-induced crystallites, differential scanning calorimetry (DSC), dynamic mechanical analysis (DMA) as well as small and wide-angle x-ray scattering (SAXS/WAXS) were performed.

As a semi-crystalline polymer, it is possible to track changes in crystallinity of PET by measuring its glass transition temperature.²³⁰ Two common methods of doing so are DSC^{231, 232} and DMA^{233, 234}.

The glass transition temperatures of PET impregnated with ethylene glycol in 1:1 and 10:1 mass ratio was measured by these techniques, alongside PET soaked in pure scCO₂ at impregnation conditions to act as a control. The results obtained for DSC and DMA of PET impregnated in a 1:1 mass ratio can show clear evidence of a re-crystallisation occurring when PET is soaked in pure scCO₂ (control) and a plasticisation effect when soaked in a scCO₂-ethylene glycol mixture (impregnation) (Tab. 3.10).

For impregnations at 32 °C and 65 °C, a reduction in the T_g of approximately 4 °C can be seen in the DSC, suggesting that the presence of ethylene glycol in the impregnation system enables plasticisation. In addition, experiments at 85 °C showed no significant difference indicating that recrystallisation at this higher temperature is so favoured when PET is swollen in the supercritical fluid that the presence of ethylene glycol is unable to inhibit it.

DMA shows a similar trend when corresponding impregnation and control experiments are compared, but the degree of difference is greater. Unlike in the DSC, a significant decrease in

the T_g for PET impregnated at 85 °C can be observed, indicating that plasticisation does take place at this temperature.

Table 3.10 – Glass transition temperature (T_g) and melting point (T_m) of PET after soaking in $scCO_2$ (control) or impregnation with ethylene glycol (impregnation) at 32, 65 and 85 °C.

DSC heating rate = 10 °C/min

DMA heating rate = 3 °C/min, Frequency = 1.0 Hz, tension mode

Impregnation Temperature		T_g (DSC)	T_g (DMA)	T_m (DSC)
N/A	PET	72.68	76.70	246.61
32 °C	Control	96.48	95.4	245.78
	Impregnation	93.05	90.90	247.07
65 °C	Control	119.16	101.4	246.94
	Impregnation	114.77	88.20	248.47
85 °C	Control	130.77	106.70	246.29
	Impregnation	130.75	87.30	248.45

The difference in the magnitude of the results between DSC and DMA can be explained when considering the properties being measured. A DSC identifies phase transitions by measuring changes in heat flow as a function of temperature. This produces strong peaks for crystallisation and melting, but a much weaker signal for the glass transition as no change in phase takes place. DMA identifies phase changes by measuring changes in mechanical properties as a function of temperature. The modulus (the overall measure of a material's stiffness) of PET falls by an order of magnitude when the polymer passes through its glass transition, producing a much stronger signal compared to DSC (Fig. 3.33).

No significant change in the DSC or DMA T_g results for PET soaked in $scCO_2$ in the presence of ethylene glycol can be seen as the ethylene glycol: PET ratio is increased from 1:1 (Tab. 3.10) to 10:1 (Tab. 3.11), and this may be due to the partial miscibility of ethylene glycol in carbon

dioxide demonstrated in section 3.3.1 limiting the amount of glycol able to partition into the polymer regardless of its abundance.

Table 3.11 - Glass transition temperature (T_g) and melting point (T_m) of PET after soaking in $scCO_2$ (control) or impregnation with a 10-mass excess of ethylene glycol (impregnation) at 32, 65 and 85 °C.

DSC heating rate = 10 °C/min DMA heating rate = 3 °C/min, Frequency = 1.0 Hz, tension mode

Impregnation Temperature		T_g (DSC)	T_g (DMA)	T_m (DSC)
N/A	PET	72.68	76.70	246.61
32 °C	Control	96.48	95.4	245.78
	Impregnation	94.72	93.40	248.34
65 °C	Control	119.16	101.4	246.94
	Impregnation	111.32	87.67	248.86
85 °C	Control	130.77	106.70	246.29
	Impregnation	127.49	85.76	247.20

Variation in the T_g of PET shown in the thermal analysis provided evidence of the presence of $scCO_2$ -induced crystallites. To directly observe the hypothesised crystallites, small and wide-angle x-ray scattering (SAXS/WAXS) were both applied to PET films before and after treatment in $scCO_2$.

SAXS results for unmodified PET (Fig. 3.34) indicate that the PET is indeed entirely amorphous in structure, as no characteristics can be seen over the explored scattering vector. Once PET has been exposed to $scCO_2$, lamellar peaks can be seen to appear at 0.1 \AA^{-1} demonstrating that crystalline domains have been formed during supercritical treatment.

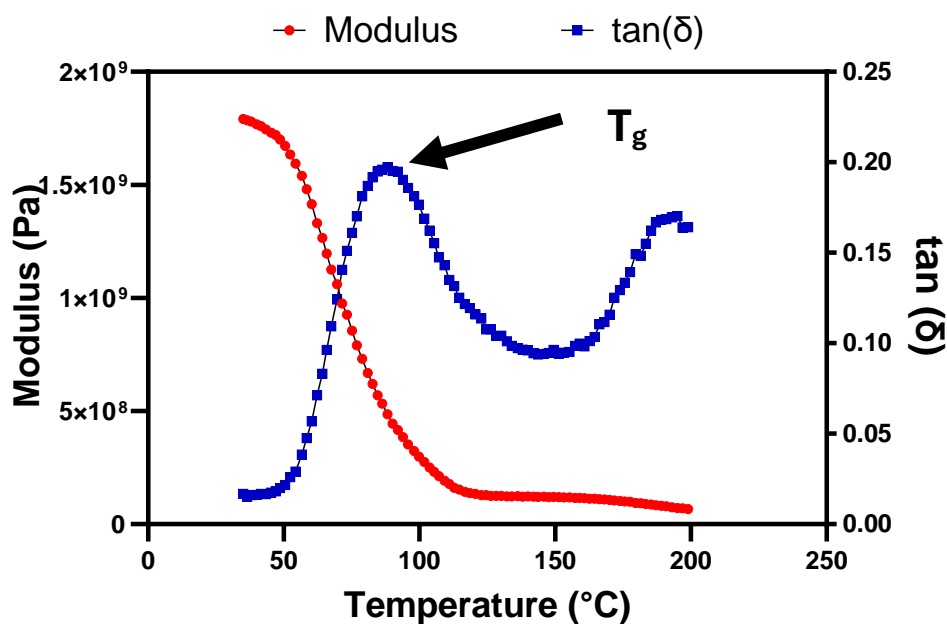


Figure 3.33 – A typical DMA trace of PET in tension mode. The drop in modulus (red), which describes the stiffness of a material, by an order of magnitude produces a strong signal when the glass transition temperature is exceeded (indicated by arrow on blue line).

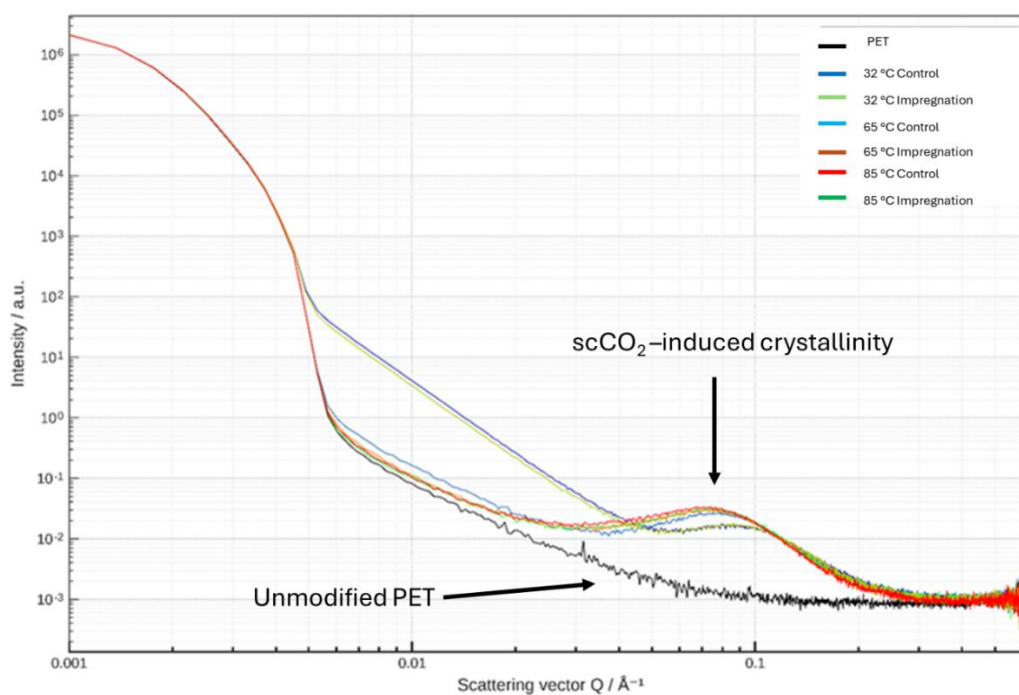


Figure 3.34 – SAXS scattering pattern of unmodified PET, PET soaked in pure scCO_2 (control) and PET impregnated with ethylene glycol (impregnation) at 32, 65 and 85 °C.

The broadness of all these peaks point to a range of crystalline domains of varying sizes, as peak width in SAXS is known to be inversely proportional to ordering.²³⁵ The impregnation and control experiments at 32 °C give rise to a slightly narrower and less intense peak than experiments

which took place at 65 °C and 85 °C, implying that a lower diversity in crystallite size has been formed and that a smaller degree of crystallisation has taken place. This would be consistent with previous knowledge about scCO₂ plasticisation as the PET chains would have fewer degrees of freedom when swollen at 32 °C, hindering recrystallisation.

Little difference can be seen in the scattering vectors of the corresponding control and impregnation experiments (Fig 3.34). This suggests that any enhancements seen in the dielectric properties in section 3.3.3 are largely arising from the presence of ethylene glycol within the PET, rather than the presence of ethylene glycol preventing recrystallisation when PET is swollen in an ethylene glycol-scCO₂ mixture – as evidenced by the significant reduction in T_g demonstrated by DMA results above.

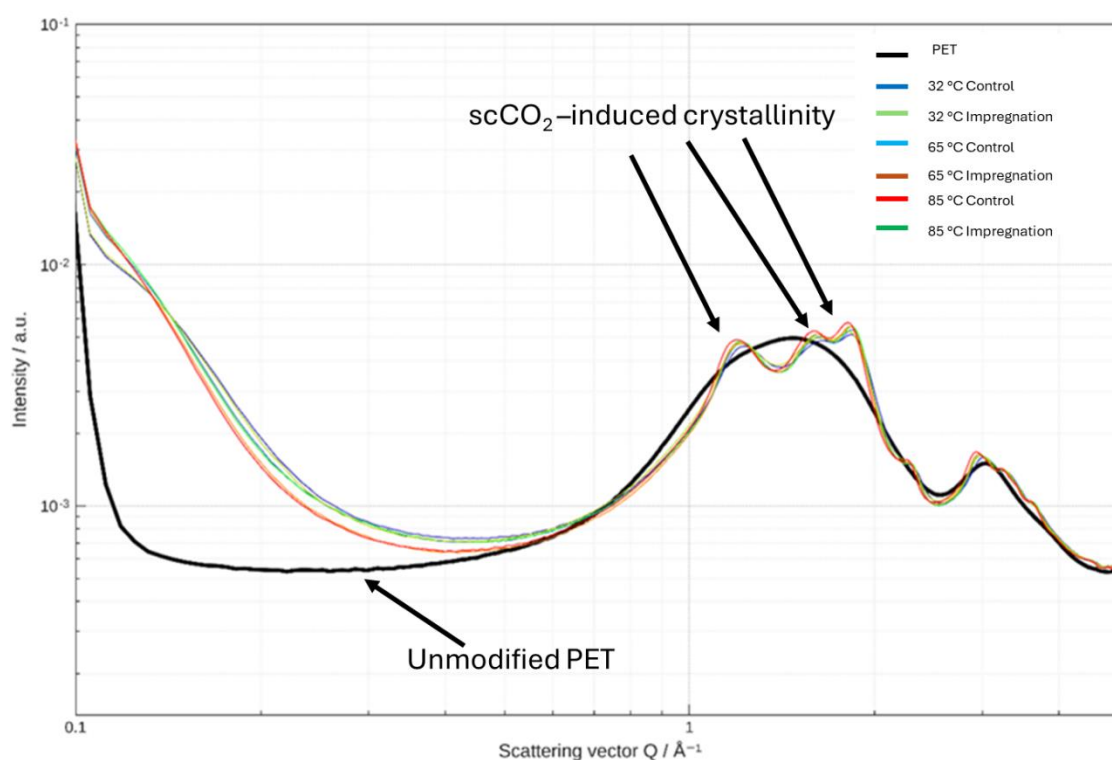


Figure 3. 35 - WAXS scattering pattern of unmodified PET, PET soaked in pure scCO₂(control) and PET impregnated with ethylene glycol (impregnation) at 32, 65 and 85 °C.

WAXS results agree with SAXS. Broad humps arise when unmodified PET scatters the x-ray beam, once again showing that a featureless, amorphous structure is present (Fig. 3.35).

Treatment of PET in scCO₂ results in a narrowing of these peaks, confirming the formation of a more ordered, crystalline structure. However, these peaks are still relatively broad, and no sharp peaks indicative of a discrete crystalline domain of specific size can be seen. WAXS also points towards a broad range of crystalline domains of different sizes being formed in these supercritical impregnation experiments and, once again, no clear differences in the morphology of corresponding impregnation and control experiments can be seen.

When the DSC, DMA and SAXS/WAXS results are considered together, they conclusively prove that recrystallisation does take place when PET has been treated in scCO₂. However, whilst there is a depression in the T_g when ethylene glycol is introduced into the supercritical impregnation system, the lack of obvious differences in the SAXS/WAXS results would suggest that the presence of ethylene glycol in PET post-impregnation is the dominant factor behind dielectric property enhancement, rather than any hinderance in recrystallisation.

3.4 Conclusion

Successful impregnation of PET with ethylene glycol has been demonstrated by a combination of gravimetric analyses (weighing by difference, TGA) and dielectric experiments (heat-and-hold, dynamic heating and measurements). Alongside impregnation, the potential for PET recrystallisation during scCO₂ treatment was observed by thermal analysis (DSC and DMA) and X-ray scattering. It is thought that the recrystallisation should impede the dielectric response of PET. However, a clear improvement in the polymer's dielectric response was seen post-impregnation on two different dielectric cavities, with 85 °C being identified as the optimum impregnation temperature. These results are carried forward to Chapter 4, where PET impregnated is scaled up from a 60 mL autoclave to 1 L, followed by microwave pyrolysis.

4 Microwave Pyrolysis of Polyethylene Terephthalate

Overview

The work in this chapter is a continuation of that discussed in the previous chapter. PET impregnated with ethylene glycol at 278 bar and 85 °C was found to demonstrate the best enhancement of the polymer's dielectric properties. A scale up of this impregnation, from 0.5 g PET to 90 g PET, by use of a 1 litre high-pressure autoclave was successfully undertaken. This modified PET then underwent microwave pyrolysis at a series of input powers. PET with no pre-treatment was subjected to identical pyrolysis conditions, and absorbed power, temperature, heating rate, product conversion and product selectivity all being compared. The products from the pyrolysis were also subjected to a host of analytical techniques (GC-MS, MALDI, APCI, IR, NMR) to elucidate their structures.

4.1 Introduction

4.1.1 Current State of PET Microwave Pyrolysis

4.1.1.1 Nature of Products and Mechanism of Degradation

Unlike most other plastics, microwave pyrolysis of PET, without susceptors or any co-feedstock, yields just solid and gaseous products.²³⁶ The solid, non-char, products are typically a terephthalate-based compound (terephthalic acid, monovinyl terephthalate, divinyl terephthalate, benzoic acid), whilst the gaseous component consists of CO₂ and ethylene. Increasing pyrolysis temperature has been shown to reduce the proportion of char in the final product, by favouring formation of further gas – typically CO₂ and CO.²³⁷

Studies have been undertaken to understand the mechanisms at play when PET is pyrolysed, through a combination molecular modelling²³⁸, TGA experiments²³⁹, and diffuse reflectance infrared Fourier transform spectroscopy (DRIFT).²⁴⁰ All of the studies undertaken to probe the pyrolysis mechanisms of PET do so using conventional heating. Whilst it is important to

acknowledge there could be some uncertainty when directly comparing work carried out in a conventional heating environment to a microwave one, particularly if a catalyst or susceptor is present, the conclusions of the mechanistic literature do correlate well to the products obtained from microwave pyrolysis.

PET pyrolysis is believed to be initiated by homolytic chain scission of the glycolic unit, as Density Functional Theory (DFT) calculations determined the C-C bonds in this portion of the repeat unit exhibit the lowest bond dissociation energy (BDE) (Fig. 4.1).^{238, 241} Homolytic cleavage appears to dominate in the early stages of pyrolysis (Fig 4.2), after which concerted and cross-linking reactions become more abundant (Fig. 4.3).²⁴² *in-situ* DRIFT analyses also identified the growth of an -OH stretching band corresponding to carboxylic acid formation as decomposition took place (Fig. 4.4), whereas the bands which corresponded to aromatic C-H stretching and bending all remained unchanged.²⁴⁰ This has been taken as further evidence that all of the chemical transformations taking place during PET pyrolysis occur in the glycolic and ester regions of the repeating unit, whilst the aromatic ring remains unaltered.

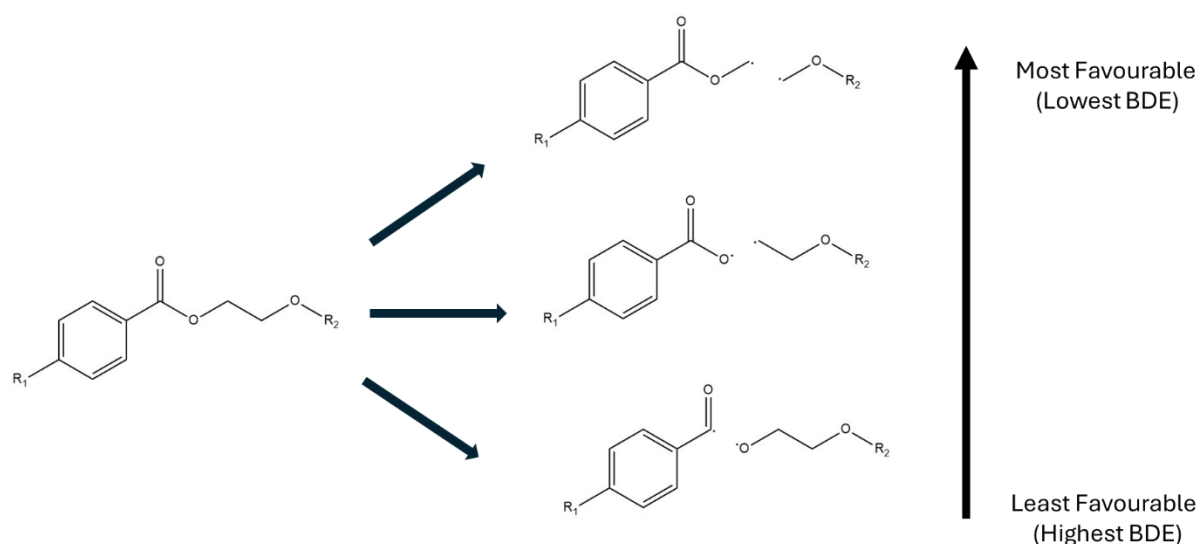


Figure 4.1 – Bond dissociation energies of PET in kJ/mol, calculated by density functional theory. Scission of the C-C bond in the glycolic portion of the repeat unit is most favourable (334.4 kJ/mol) with bonds requiring more energy to be broken as the aromatic ring is approached.

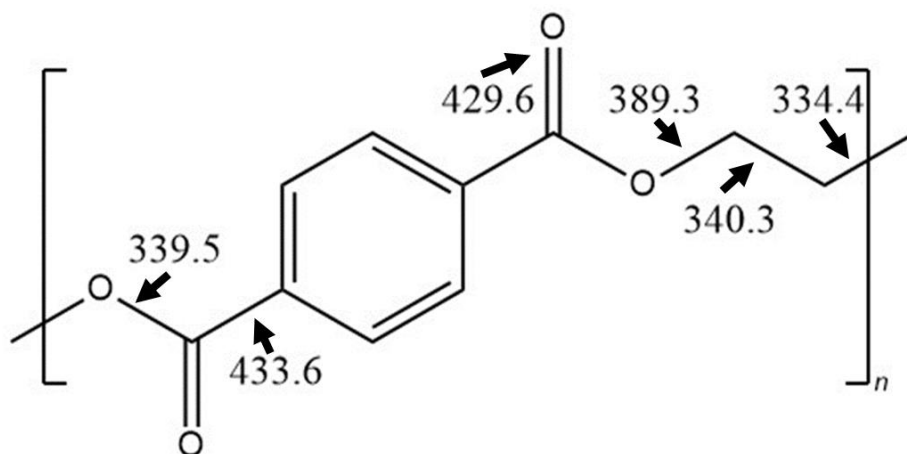


Figure 4.2 – Homolytic scission at various locations in the PET repeating unit. The potential scenarios are ranked in terms of the BDEs in figure 4.3.

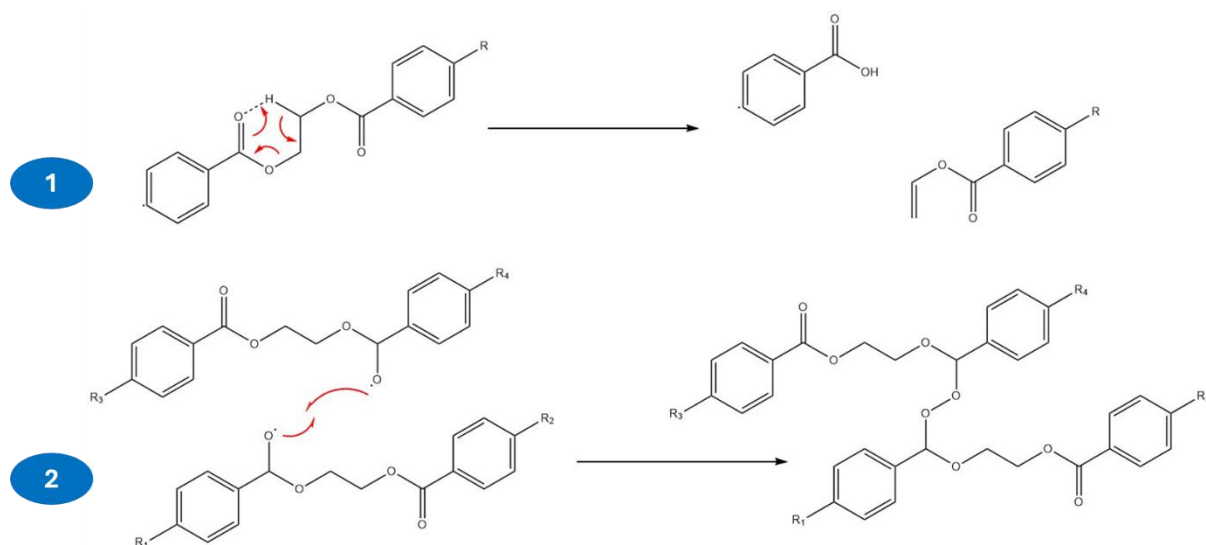


Figure 4.3 – Mechanisms believed to take place during PET pyrolysis, besides homolytic chain scission illustrated in figure 4.2.

1. Concerted reaction to produce fragments with carboxylic acid and vinyl ester end groups
2. Cross-linking reaction between two PET chains - a potential route to char formation.

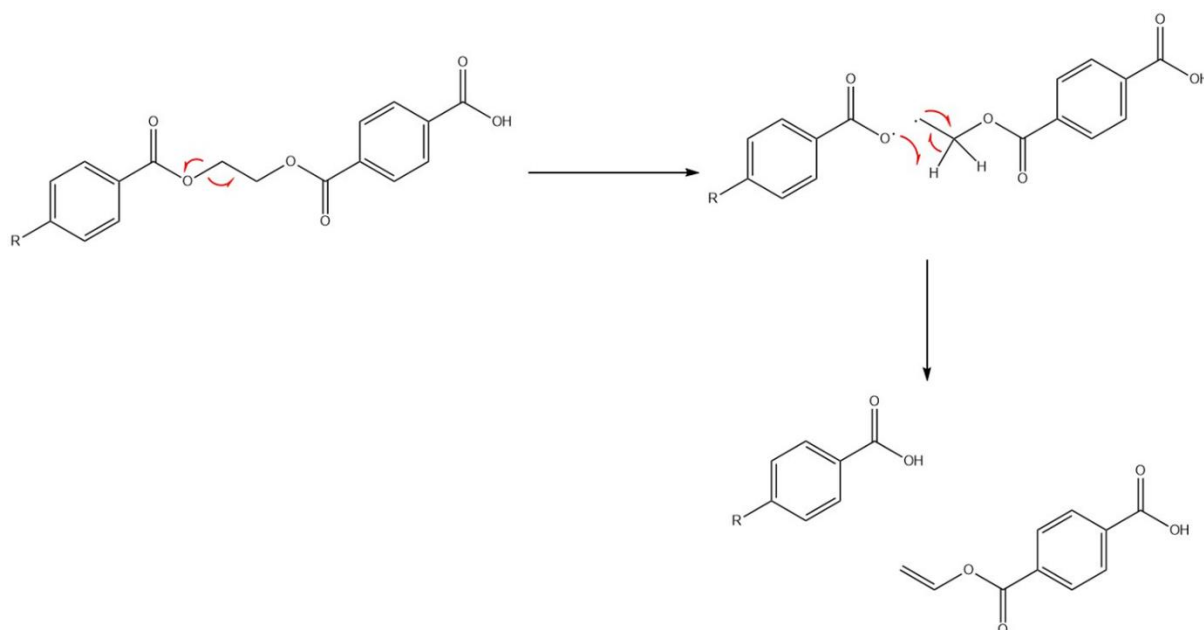


Figure 4.4 – A possible, alternate route to carboxylic acid and vinyl ester-terminated chain fragments to the one proposed in figure 4.3. -homolytic chain scission of the C-O bond in the glycolic region followed by a hydrogen abstraction step.

The identity of the gaseous products (CO_2 , CO and ethylene) have been identified by either bubbling pyrolysis gases through limewater or GC-MS. Solid products from PET pyrolysis are usually subjected to elemental analysis or GC-MS, assuming they are of low enough molecular weight to be soluble in the volatile solvents required by GC-MS.

4.1.1.2 Routes for PET Pyrolysis

The high volumes of char which can be formed when PET heated in a microwave field by itself has necessitated the addition of susceptors, or co-pyrolysis strategies, to disfavour char formation by increasing the heating rate or introducing synergistic effects between the different feedstocks.

Silicon carbides (SiC) also exhibit excellent microwave absorbing properties and have been utilised in the microwave pyrolysis of PET water bottles.²³⁶ 30 g of PET was pyrolyzed at 500 °C with increasing loads of SiC (20, 25, 30, 35 and 40 g) and the heating rate was found to fall with increasing load (104.64 °C/min at 25 g loading fell to 41.46 °C/min at 30 g loading) which was

attributed to a fall in the specific energy of the process. However, solid and gas product yields increased from 4 % and 8 % respectively at a 25 g SiC loading to 25 % and 35 % when SiC loading was increased to 40 g. Despite the addition of further SiC impeding the heating rate of the pyrolysis initially, it was shown to aid conversion of the PET at higher amounts. Although this work crafted an interesting discussion on the different outcomes of varying susceptor load, little work was done to analyse the products of the pyrolysis. Only elemental analysis was performed on the solid products, and as they abundance of carbon, hydrogen and oxygen matched those of benzoic acid, 4-vinylbenzoic acid, monovinyl terephthalate and divinyl terephthalate the authors summarised that these were the products of their process.

Use of biochar, produced from the carbonisation of corn or Douglas fir trees, has been demonstrated as a route to remove char formation altogether.²⁴³ When pyrolysed with a 3:1 char to PET loading at 600 °C, PET was degraded to liquid and gaseous products, 20 wt% and 80 wt% respectively for corn biochar; 23 wt% and 77 wt% for Douglas fir.

Biomass itself, due to the water present in its structure, has also been explored as a susceptor for microwave pyrolysis.¹⁷⁵ PET and rice husk (RH) were first heated with microwaves at an input power of 450 W, and heating rates of 38 °C/min and 148 °C/min respectively were measured.

The two materials were then mixed at varying ratios and the resulting heating rate was quantified, with the most rapid heating (163 °C/min) arising from a PET: RH mixture of a 1:3 ratio. However, despite this high heating rate, a char yield of 31.1 wt% was produced alongside gaseous products totalling 39.9 wt %. When the PET:RH ratio was adjusted to 5:1, a far lower heating rate (63 °C/min) was seen, but lower char yields (18.6 wt%) with a concurrent improvement in gas yield (55.2 %). The same pyrolysis temperature (600 °C) was reached for all pyrolysis, and the distribution of bio-oil yielded at these ratios was unchanged (29.7 – 26.2 wt %) respectively, suggesting that the lower heating rate of the pyrolysis for the 5:1 ratio, and the

longer residence time that arises as a result, facilitates greater transformation of the char to gaseous material.

Co-pyrolysis of PET and LDPE (1:3 loading ration by mass) has also been performed with susceptors generated by the carbonisation of coconut husks (CHC).²⁴⁴ CHC was shown to provide a competitive heating rate (42.99 °C/min) to SiC (33.14 °C/min) and activated carbon (56.18 °C/min), and maintained this heating rate for a least five pyrolysis cycles. After the first cycle, a reduction in char and oil yield was observed for pyrolysis using CHC susceptors, with a corresponding increase in gas yield. All experiments were conducted at a temperature of 550 °C with an input power of 500 W; GC-MS analysis determined the oil consisted of various mono-aromatic species, whilst the gas phase was made up of CO, CO₂, CH₄ and H₂.

In order to study how susceptor choice could be used to tune product selectivity, *Zhao et al* undertook experiments where a mixed feedstock of PET and sawdust was pyrolysed alongside three different susceptors: carbon powder, ferroferric oxide (Fe₃O₄) and calcium oxide (CaO).²⁴⁵ Pyrolysis experiments were conducted at a temperature of 630 °C for 1 hour, with input power being dynamically adjusted to maintain a constant temperature, after which pyrolysis products were extracted into dichloromethane (DCM) and analysed by GC-MS.

For an equivalent mass-loading of PET and sawdust (1: 1), almost half of the products are benzoic acid and its derivatives when carbon powder was used as the susceptor. The formation of terephthalic acid derivatives (7.9 wt %) during co-pyrolysis was also noted, and the authors hypothesise that this probably results from the hydrolysis of the ester bond by water released during biomass pyrolysis forming terephthalic acid.

Valuable hydrocarbons were found in the liquid product (30 wt %), with molecular weights of 140 to 260 Da, when a 1: 4 PET: sawdust underwent pyrolysis with carbon powder. CaO was seen to promote the formation of ketones and hydrocarbons, with a reduction of benzoic-acid

derived material now only accounting for 15 wt% of the pyrolysed material, whilst Fe_3O_4 favoured the formation of ester-based products over that of benzoic acid and its derivatives.

All of the above examples demonstrate successful routes to degrade PET by microwave pyrolysis. Due to the different phases of material produced (solid, liquid, gas), as well as the diversity present within the liquid and gaseous products, microwave pyrolysis can be considered a form of molecule recycling by Sheldon's hierarchy of recycling⁴⁵ as there is not an obvious route back to PET from the pyrolysis products.

4.1.2 Drawbacks of Susceptor Use and Pushing the Boundaries of Product Analysis

4.1.2.1 Drawbacks of Microwave Susceptors

Microwave susceptors have proven invaluable as a route to making microwave pyrolysis of plastic a viable route for generating value-added chemicals from waste material. The multiple sources of susceptors have been outlined in the previous section (metals, biomass, SiC, activated carbon) and they all have their own benefits and limitations. However, two general challenges can be drawn out from the current microwave literature regarding susceptors:

1. Susceptors are often mechanically mixed with the pyrolysis feedstock.^{195, 246} This has been shown to result in a non-uniform distribution of susceptor material, leading to hotspot and cold spot formation.²⁴⁷⁻²⁴⁹ Incomplete pyrolysis can arise from an uneven distribution of susceptors, harming process yields, and reactor damage is also possible if hotspots reach sufficiently high temperatures.²⁵⁰

2. A challenge surrounding use of susceptors that is particularly pertinent to PET is separation.²⁵¹ All the susceptors discussed above have been solids and PET, when not undergoing co-pyrolysis, has been seen to produce large quantities of solid when degraded. This can make isolation of the product from the susceptor challenging.

There is currently scope in the literature to explore developing a pyrolysis process which utilises degradable susceptors, and potential candidates were studied in Chapter 3 with ethylene glycol impregnation into PET via scCO₂ showing promising enhancements in the dielectric response.

scCO₂ impregnation could enable the challenge concerning non-uniform distribution of susceptor in a pyrolysis feedstock. The swelling of PET when exposed supercritical fluid grants superior access to the internal structure of the polymer, which could enable a more even distribution of susceptor.

4.1.2.2 Expanding the Library of Analysis Techniques

Despite the wide range of feedstocks and susceptors reviewed in this chapter, the analytical portfolio for pyrolysis products remains limited. Heavy use of GC-MS, IR and elemental analysis are seen when elucidating the nature of pyrolysis oils or non-char solid products. IR and elemental analysis are suitable for identifying a wide range of chemical species, but GC-MS is generally limited to lower molecular weight products (< 500 Da) as a sample must be volatile within the working temperature of the GC-MS oven – typically ≤ 300 °C.

As a result, the presence of any higher molecular weight products, such as oligomers of the starting polymer, may be missed in the analytical portion of the work. There are some examples of GPC analysis for biomass pyrolysis²⁵²⁻²⁵⁴, but GC-MS is far more routine for plastics, whilst MALDI is virtually never used for pyrolysis analytical work. These two techniques, when used in conjunction with GC-MS, would provide a more detailed picture of the pyrolysis product make up, as a far wider molecular weight window would be covered.

4.1.3 Aims and Objectives

The literature reviewed here demonstrates that whilst microwave pyrolysis is a viable route to degrading plastic waste, general observations or conclusions can be difficult to draw out due to the wide range of feedstock mixtures, susceptor types and processing conditions explored. However, at least two challenges concerning the use of susceptors, hot spot formation and difficulties separating susceptors from product post-pyrolysis, are acknowledged in the literature. There is also a heavy reliance on GC-MS, IR and elemental analysis to elucidate the identity of pyrolysis products, with techniques aimed at detecting higher molecular weight species, such as GPC and MALDI, being used more sparingly.

Accordingly, this chapter has two overall aims:

1. Demonstrate that PET which has undergone scCO_2 impregnation of ethylene glycol is able to absorb microwave power more strongly than the unmodified polymer, resulting in a superior heating rate for the same input power.
2. Deploy a portfolio of analytical techniques appropriate for a range of molecular weights (GPC, APCI, GC-MS), alongside those aimed at functional group identification (IR, NMR).

The specific objectives are:

1. Carry out a successful scale up of the scCO_2 impregnation of ethylene glycol into PET described in Chapter 3. Impregnation experiments will be conducted in a 1 litre high-pressure autoclave, as opposed to 60ml, to modify PET in quantities more appropriate for microwave processing. Dielectric analysis will then be performed to confirm impregnation has taken place.

2. Subject PET impregnated with ethylene glycol to microwave pyrolysis, as well as PET that has not been modified, at a series of input powers and residence times.

Comparisons between the performance of modified and unmodified PET (absorbed power, heating rate, maximum temperature, conversion, specific energy) for the same input power will then be carried out.

3. Determine the identity of all valuable pyrolysis products obtained from PET, by executing a holistic approach to their analysis. GC-MS, APCI, and GPC are all suitable for increasing molecular weight ranges respectively, whilst IR and NMR will be used to thoroughly probe the functional groups present.

4.2 Experimental

4.2.1 Supercritical Impregnation of Polyethylene Terephthalate with Ethylene Glycol

PET was deposited into the base of a high-pressure autoclave (1 L), and either an equivalent mass of ethylene glycol was added, or a 10-mass excess with respect to PET (Fig. 4.5) (Fig. 4.6) (Tab. 4.1). The autoclave was then charged with CO₂ (55 bar) and heated to 85 °C. Once the temperature had been reached, CO₂ was added until a pressure of 278 bar was reached. After 3 hours the heating was discontinued, and the autoclave was vented once it had cooled below the critical temperature (31.1 °C) of CO₂. The PET was then removed from the autoclave, and the residual ethylene glycol on the surface was washed off with deionised water and left to dry at room temperature until no liquid could be wiped from the surface.

Table 4.1 – Ratios of PET to ethylene glycol used in various scale-up scCO₂ impregnation experiments.

PET (g)	Ethylene Glycol (ml)	PET: Ethylene Glycol Mass Ratio
90 g	82	1:1
15 g	136	1:10



Figure 4.5 – Image of the 1 litre high-pressure autoclave scaled up impregnation experiments were conducted in.

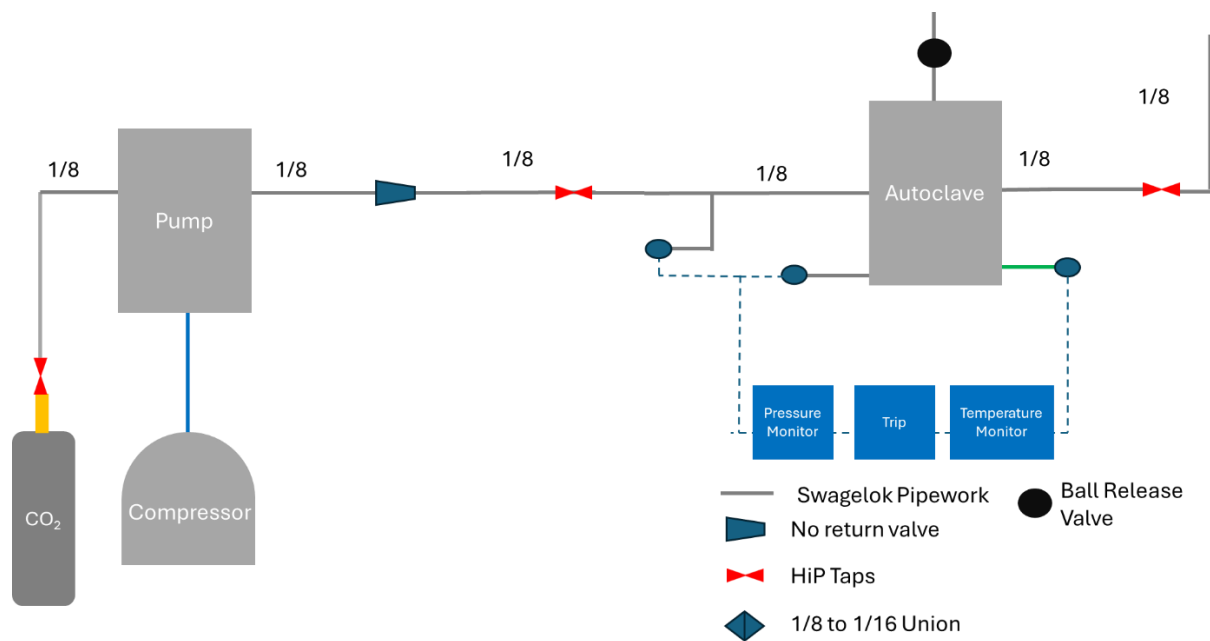


Figure 4.6 – Line diagram of 1 litre high-pressure autoclave set up pictured in Figure 4.5.

4.2.2 Microwave Pyrolysis of Polyethylene Terephthalate

PET films (15 g) were cut into rectangles of similar size and placed in a quartz tube with the face of the rectangles placed perpendicular to the path of microwave propagation. PET then underwent microwave pyrolysis at various input powers, until no further pyrolysis fumes were visibly evolving from the sample. The temperature was recorded at the interior wall of the sample by an Optris CT 3MH1 SF IR pyrometer (150 -1000°C). The overhead temperature was recorded by a K-type thermocouple and the data was logged on a Lascar EL-USB-TC-LCD Temperature Data Logger. The input power and absorbed power was recorded by an S-Team HOMER Autotuner (ISM 2450 MHz), and physical changes to PET were observed by a Microsoft H5D-00014 LifeCam Cinema Webcam. Microwaves were generated across a range of input powers (0.80 – 1.60 kW) by a 2.0 kW Sairem generator, which were guided to the sample by WR340 (R26) waveguides.

Products were collected by two cold traps in ice. The system was purged with nitrogen for 15 minutes at 100 ml/min before pyrolysis to remove oxygen which was maintained throughout the experiment. (Fig. 4.7) (Fig. 4.8)

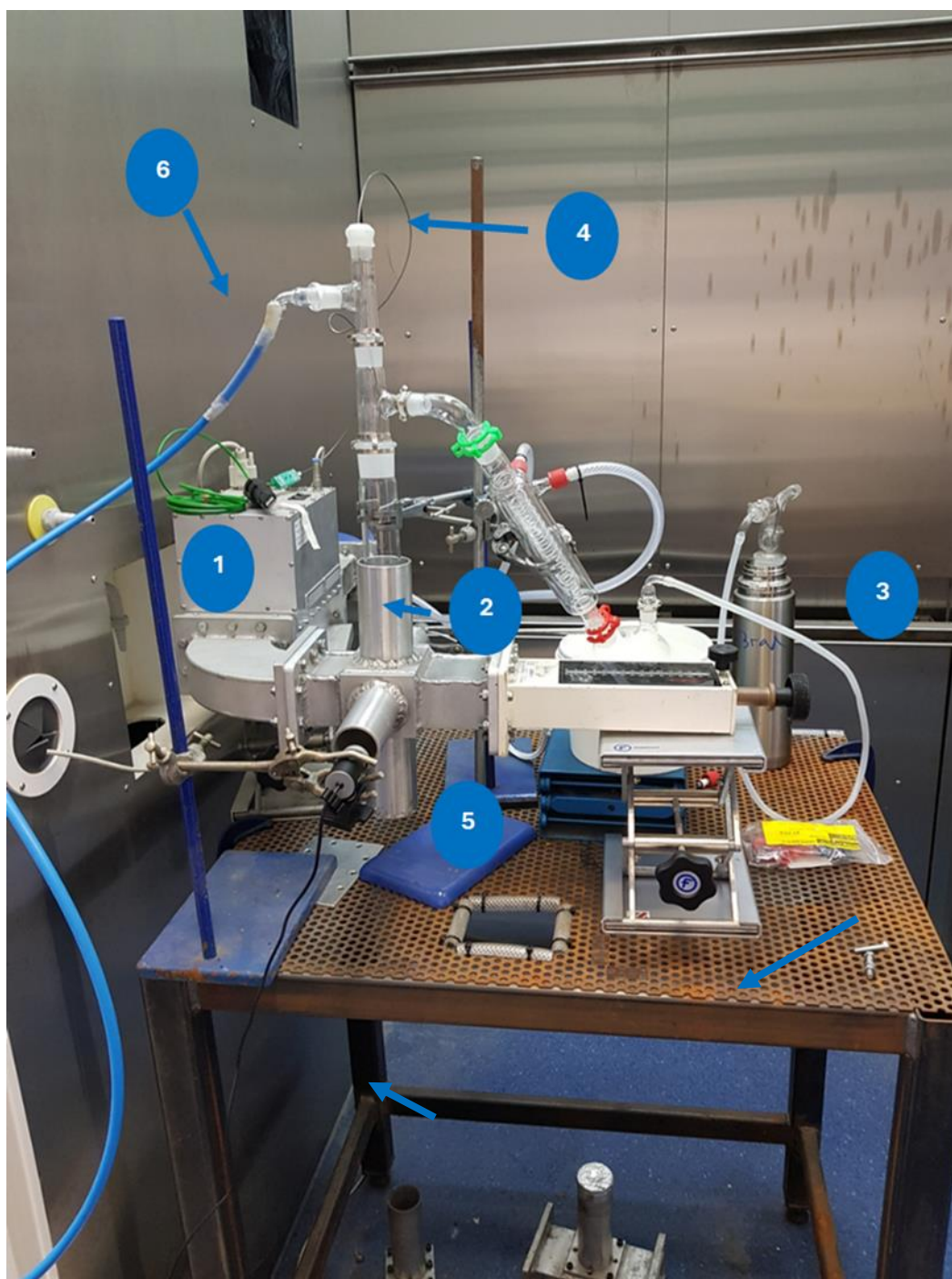


Figure 4.7 – 1: HOMER autotuner, 2: Choke containing a quartz reactor tube where the PET sample was situated, 3: Sliding short, 4: K-type thermocouple, 5: web camera, 6: N₂ line.

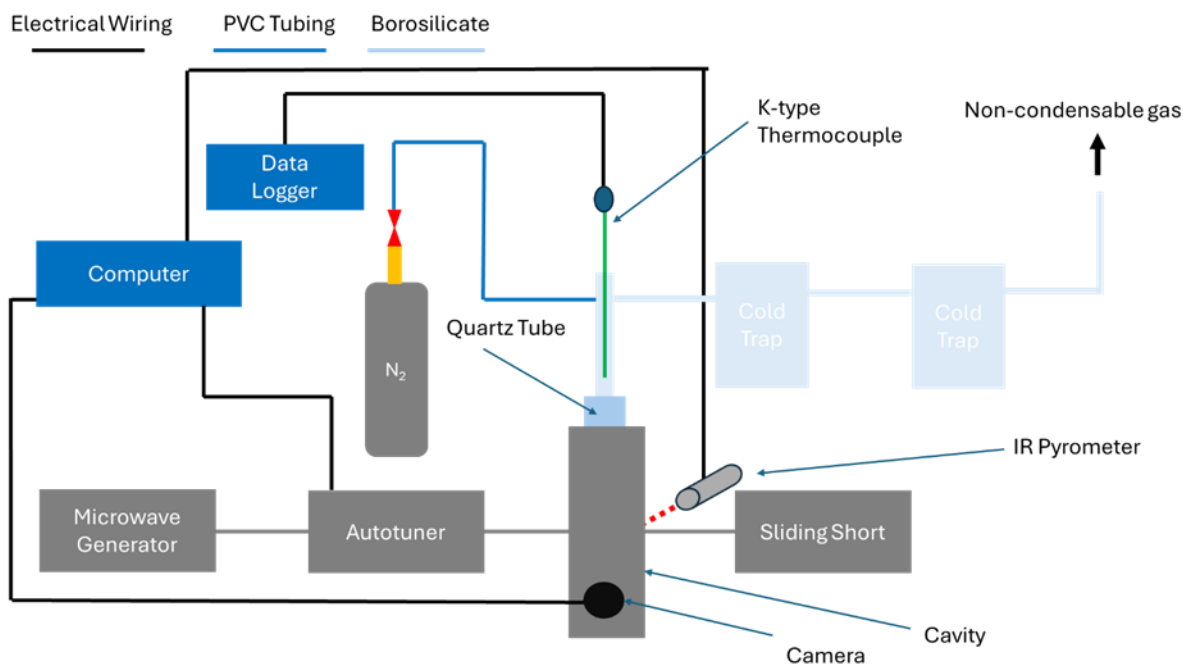


Figure 4.8 – Line diagram of set-up pictured in Figure 4.7.

4.2.3 Microwave Pyrolysis of Polyethylene Terephthalate Impregnated with Ethylene Glycol

The configuration of the pyrolysis rig for these experiments was identical to the previous section, except for the addition of two components to aid the transition of pyrolysis products out of the quartz tube, and towards the product traps.

1. The external wall of the quartz reactor, and the overhead borosilicate adaptor was heated to 120 °C by HTWAT051-002 Omega silicone heating tape.
2. After purging the system with nitrogen for 15 minutes at 100 ml/min before pyrolysis to remove oxygen, pressure was then reduced to 450 mbar by use of a vacuum pump operated with a CVC 3000 vacuum controller, which was maintained throughout the experiment.

The second cold trap used in the previous section was also replaced with a limewater trap to confirm the generation of CO₂ (Fig. 4.9) (Fig. 4.10).

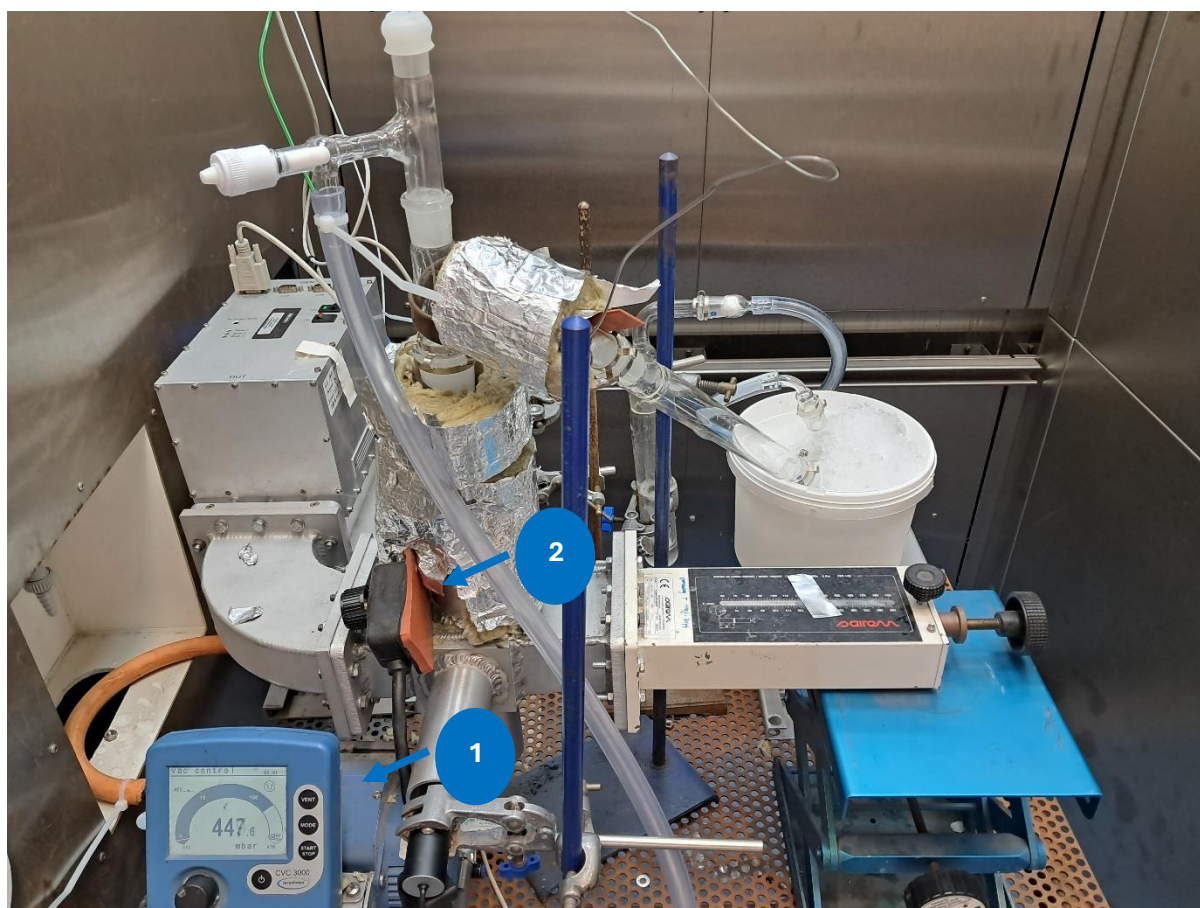


Figure 4.9 – 1: Vacuum pump, 2: Heating tape enclosed in wool insulation. All other components are identical to figure 4.7.

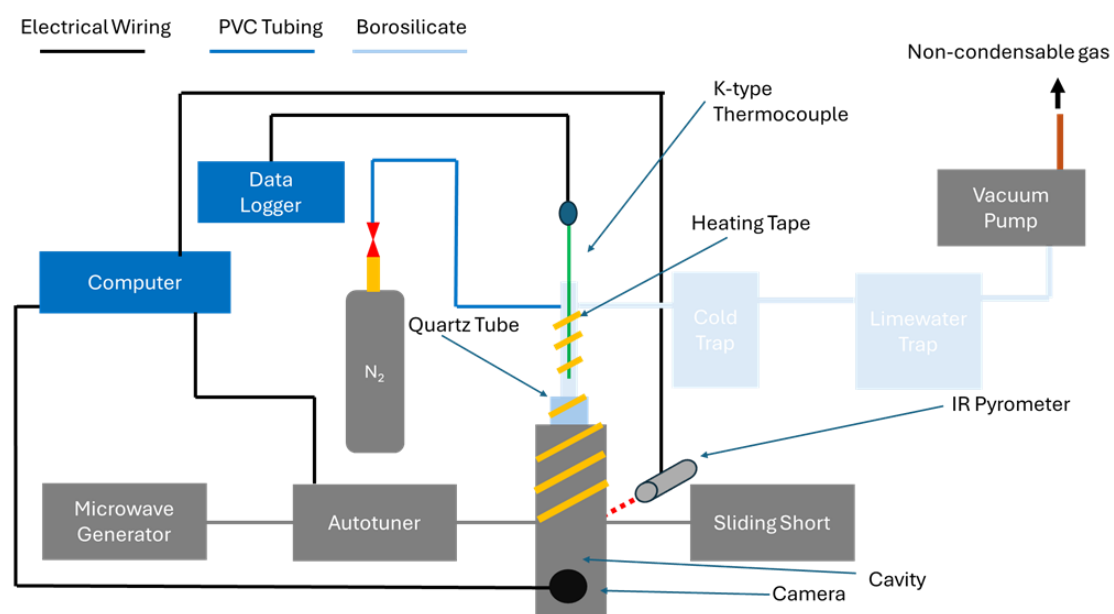


Figure 4.10 – Line diagram of set-up pictured in Figure 4.9.

4.2.4 Nuclear Magnetic Resonance (^1H NMR, ^{13}C NMR)

Pyrolysis products of PET had their structures determined by ^1H and ^{13}C , nuclear magnetic resonance spectroscopy (NMR). Samples were dissolved in d-DMSO and analysed using a Bruker DPX 400 MHz spectrometer or a Bruker DPX 500 MHz spectrometer. Chemical shifts assigned in parts per million (ppm). All spectra obtained at ambient temperature ($22 \pm 1^\circ\text{C}$). MestReNova 14.0.1 copyright 2020 (Mestrelab Research S.L.) was used for analysing the obtained spectra.

4.2.5 Gas Chromatography-Mass Spectrometry (GC-MS)

Lower molecular weight PET pyrolysis products were extracted into chloroform (HPLC grade, Fisher Scientific), and made up to various concentrations (0.50 mg/ml, 0.25 mg/ml, 0.10 mg/ml, 0.05 mg/ml). Samples were run on an AccuTOF GCx mass spectrometer (Jeol Ltd) with electron impact ionisation using a 30 m stabilwax GC capillary column with a diameter of 0.25 mm and a film thickness of 0.25 μm (Restek). The injector port temperature was 290°C . The column oven was held at 50°C for 4 minutes, then heated from 50°C to 300°C at $10^\circ\text{C}/\text{min}$, and was purged constantly with helium.

4.2.6 Matrix-assisted laser desorption/ionization – Time of Flight Spectrometry (MALDI-ToF)

Higher molecular weight pyrolysis products of PET were identified using MALDI-TOF, which was conducted using a Bruker Autoflex Max spectrometer in positive, reflective mode. trans-2-[3-(4-tert-Butylphenyl)-2-methyl-2-propenylidene] malononitrile (DCTB) in acetonitrile was used as matrix with lithium bromide as a cationisation salt. All samples were dissolved in tetrahydrofuran, before being mixed with the matrix in acetonitrile.

4.2.7 Atmospheric Pressure Chemical Ionisation (APCI)

Mass spectrometry chromatograms were obtained by atmospheric chemical pressure ionisation (APCI, Bruker Impact II, Germany). Solid samples were injected into the nebuliser, where it was carried by a flow of nitrogen into the corona where they were ionized by an electron discharge. Experiments were run in both positive and negative mode.

4.2.8 Infrared Spectroscopy

Pyrolysis products of PET, as well as monomer standards, had their IR spectra recorded on a Bruker Alpha FTIR Instrument in an attenuated total reflectance (ATR) set-up. Data in the wavenumber range 4000 -400 cm^{-1} was collected.

4.3 Results and Discussion

4.3.1 Scale Up of PET Impregnation in Supercritical Carbon Dioxide with Ethylene Glycol

The successful impregnations of PET with ethylene glycol described in section 3.3.2 were scaled up to provide an appropriate amount of PET for microwave pyrolysis experiments in a timely manner. It can be seen from the dielectric results discussed in section 3.3.3 that the strongest enhancement in PET's dielectric properties was achieved when impregnation was carried out at 85 °C. Accordingly, this temperature was selected for the scale up experiments. To probe this, scaled up PET impregnations were undertaken at 1: ethylene glycol: PET mass ratios, as well as a 10:1 ethylene glycol: PET mass ratio.

Scaled-up scCO₂ impregnations were carried out in a 1 litre high pressure autoclave (Fig. 4.11). For impregnations carried out with an equivalent PET: ethylene glycol mass ratio, 90 g of PET was swollen in scCO₂ for 3 hours in the presence of 82 ml of ethylene glycol. A slightly opaquer film was removed from the autoclave and was washed with deionised water, then dried at room temperature until no liquid could be wiped from the surface. For the 10:1 ethylene glycol: PET mass ratio, 15 g of PET was swollen in scCO₂ alongside 136 ml of ethylene glycol.



Figure 4.11 – PET impregnated with ethylene glycol immediately post scCO₂ impregnation.

To confirm successful impregnation, heat and hold cavity perturbation was performed on the PET post-impregnation (Fig 4.12). The enhancement in the dielectric loss factor described in the previous chapter can be seen for the scaled-up samples too.

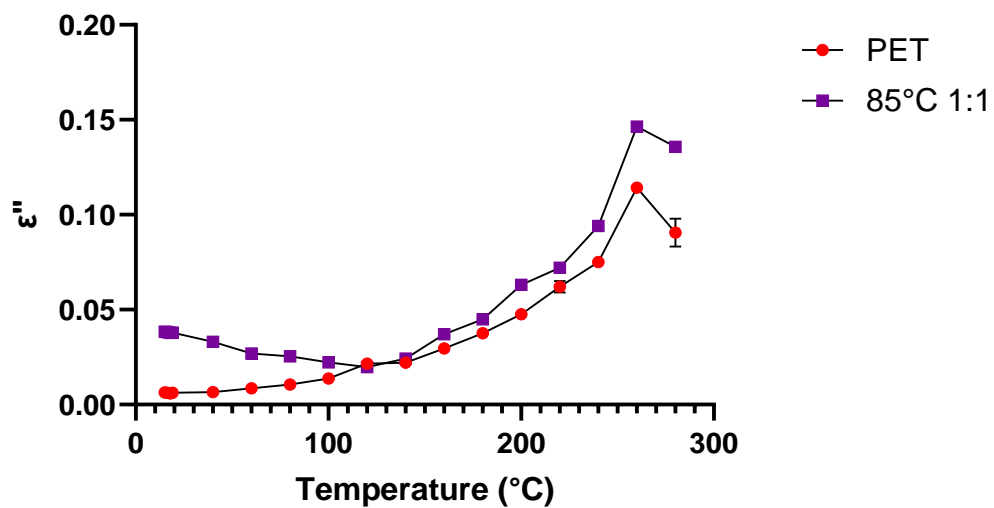


Figure 4.12 – Dielectric loss factor of PET before and after impregnation in the 1 litre autoclave.

Pressure = 278 bar, Temperature = 85 °C, time = 3 hours

4.3.2 PET Performance During Microwave Pyrolysis

During microwave pyrolysis, the incident power, as well as that absorbed and reflected by the polymer, was continuously measured by a Homer Autotuner. It can be seen from the equation for power density (Eq. 4.1) that it is directly proportional to the dielectric loss factor. Therefore, PET which has been impregnated with ethylene glycol is expected to absorb energy from the microwave field more strongly than the original polymer.

$$Pd = 2\pi f \epsilon_0 \epsilon'' |E|^2$$

Equation 4.1 – Calculation for power density of a material in a microwave field.

$\pi = \text{pi}$, $f = \text{microwave frequency}$, $\epsilon_0 = \text{permittivity of free space } (8.85 \times 10^{-12} \text{ m}^{-3} \text{ kg}^{-1} \text{ s}^4 \text{ A}^2)$, $\epsilon'' = \text{dielectric loss factor}$, $E = \text{electric field strength}$

PET pyrolysis was conducted at three input powers (0.8, 1.2 and 1.6 kW), whilst the power absorbed by the sample, and the corresponding heating profile, was measure continuously. The physical changes to the sample were also monitored via video camera.

4.3.2.1 Physical Changes During Pyrolysis

Pyrolysis was conducted until one of two end points was reached. Fumes could be observed evolving from the pyrolysing material during the experiment, which then condensed to a yellow powder. In one series of experiments, the microwave was discontinued once these fumes could no longer be seen to evolve. A second series continued heating the sample for 1 minute after fume evolution had ceased, to explore if a longer residence time influenced PET conversion or product selectivity. The physical changes described in the next paragraph were seen for unmodified PET as well as PET impregnated in scCO₂.

Initially, the PET films were cut into rectangles of similar size and place in a quartz tube with the face of the rectangles placed perpendicular to the path of microwave propagation (Fig. 4.13 -1). The polymer could then be seen to melt once a temperature of 150 °C had been reached and

was completely molten by 250 °C (Fig. 4.13 -2). Above 300 °C, the molten PET began to turn brown, and fumes could be seen to evolve from the molten polymer, indicating degradation had begun (Fig. 4.13 -3). The temperature was seen to peak in the range 450 to 480 °C and the liquid phase could be seen to gradually darken until a black fluid was present in the bottom of the quartz tube, whilst fumes were still evolving (Fig. 4.13 -4).

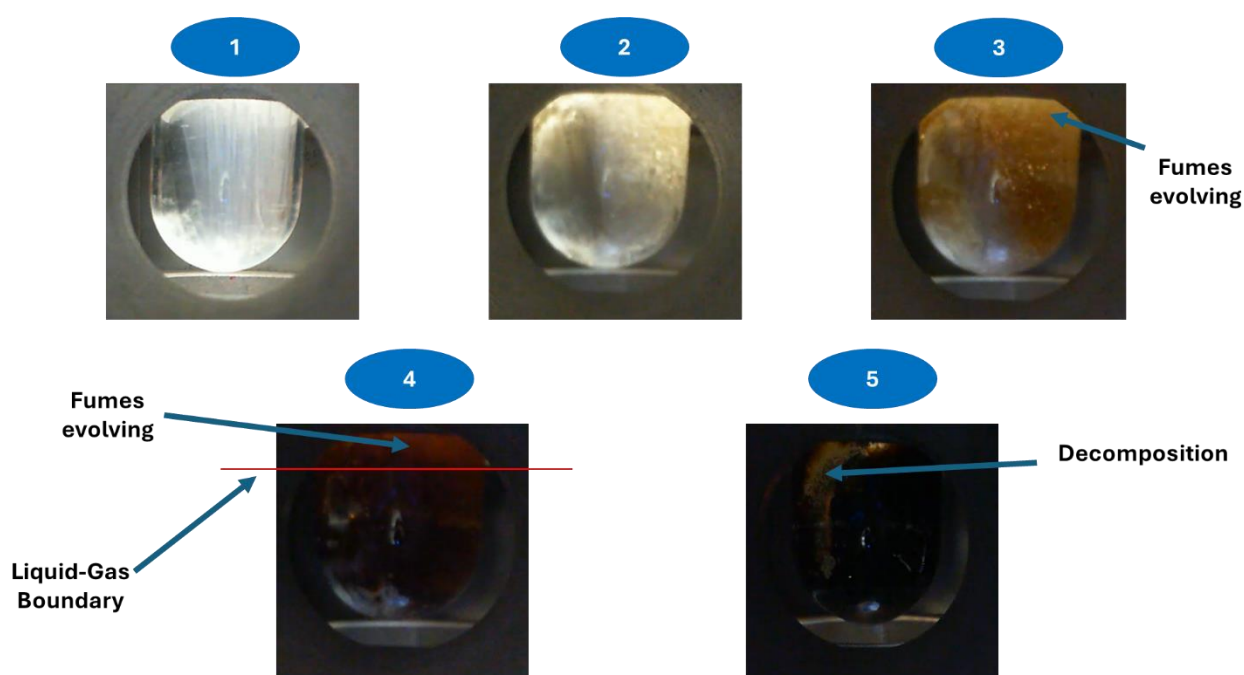


Figure 4.13 – The stages of PET decomposition during microwave pyrolysis.

- 1- Initial loading of PET films into quartz reactor.
- 2- Melting of PET to a white fluid.
- 3- Beginning of decomposition can be seen as molten PET begins to darken, and fumes begin to evolve from the liquid.
- 4- Molten PET turns black as decomposition proceeds, this was seen to solidify and form char once heating was discontinued, fumes were seen to cease at this stage.
- 5- When heating was continued after fumes had ceased to be evolved, the liquid was seen to solidify in the bottom of the quartz reactor and appeared to decompose.

In the first series of experiments, the microwave was discontinued once fumes no longer evolve from this black liquid (Fig. 4.13 -4), whilst heating continued for an additional minute in the

second series. When heating for an additional minute took place, the black liquid could be seen to solidify and decompose (Fig. 4.13 -5).

4.3.2.2 Absorbed Power and Temperature Profiles

The power absorbed by the polymer was monitored continuously, and the performance of unmodified PET was compared with PET impregnated with ethylene glycol at 1:1 and 10:1 mass ratios at the same input power (0.8, 1.2 and 1.6 kW).

It can be seen that the absorbed power peaks at a higher value for samples impregnated with PET when contrasted with the unmodified polymer at all three studied input powers (Fig. 4.14) (Fig. 4.15) (Fig. 4.16). The absorbed power also peaks more quickly for PET samples impregnated in scCO_2 which illustrates a stronger initial interaction with the microwave field. Both of these observations are likely due to the presence of ethylene glycol within the polymer, as this small polar molecule demonstrated much stronger dielectric properties than PET in section 3.3.1. During pyrolysis, the temperature of the quartz reactor's interior wall was also measured to track how the heating rate of the various samples varied (Fig. 4.17 – 4.22). A general trend can be seen where the impregnated PET samples all exhibit a superior heating rate over their unmodified counterparts. The exception to this can be seen in figures 4.17 and 4.18 where the PET samples impregnated with a 1:1 mass ratio of ethylene glycol to PET heat more slowly, and to a lower maximum temperature, in comparison to both the unmodified PET and the PET impregnated with a 10:1 mass ratio of ethylene to glycol to PET.

Difficulties in recording temperature accurately, and repeatably, for microwave pyrolysis experiments has been accepted as an ongoing challenge. If the volume of the pyrolysis reactor is far larger than the area where temperature is being recorded, variation in the measured temperature can occur if the placement of the temperature probe changes.

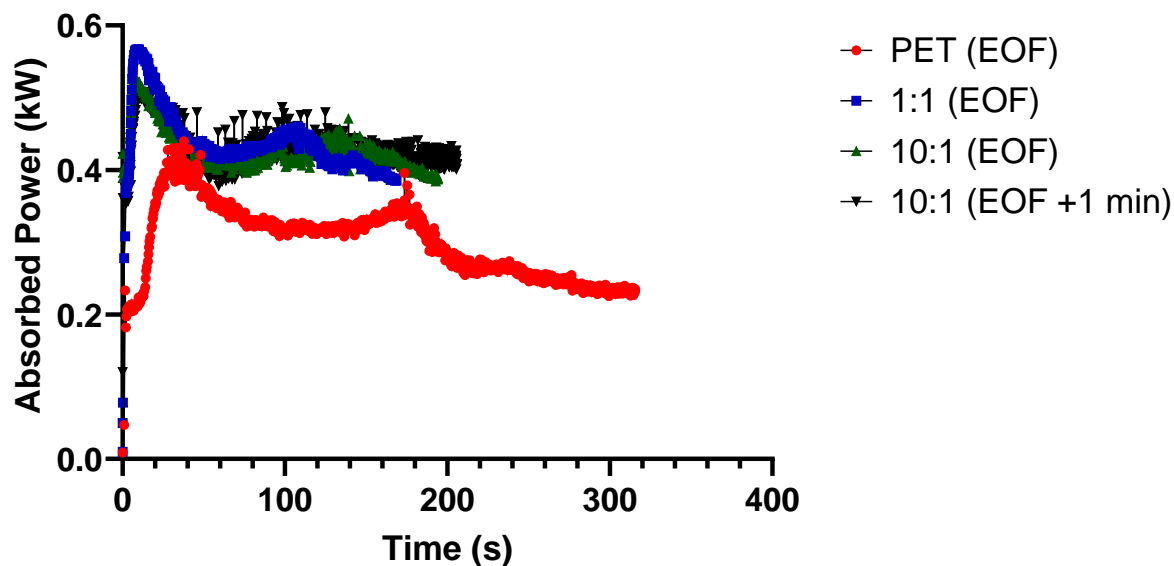


Figure 4.14 – Absorbed power profiles for PET samples for an input power of 0.80 kW.

1:1. 10:1 = EG: PET mass ratio

EOF = Microwave discontinued after pyrolysis fumes ceased to evolve.

EOF + 1 min = Microwave discontinued 1 minutes after pyrolysis fumes ceased to evolve

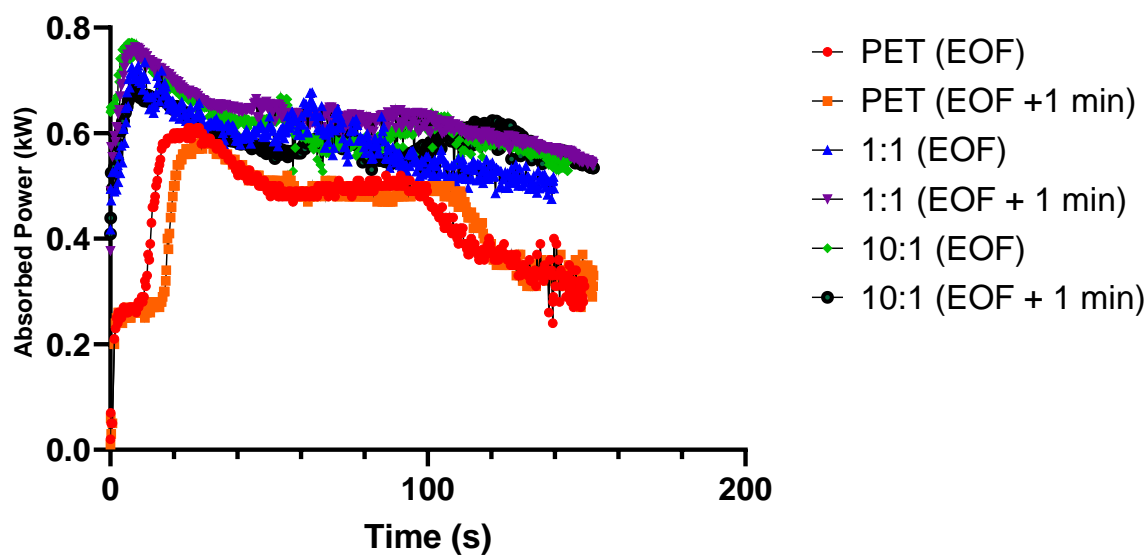


Figure 4.15 – Absorbed power profiles for PET samples for an input power of 1.20 kW.

1:1. 10:1 = EG: PET mass ratio

EOF = Microwave discontinued after pyrolysis fumes ceased to evolve.

EOF + 1 min = Microwave discontinued 1 minutes after pyrolysis fumes ceased to evolve.

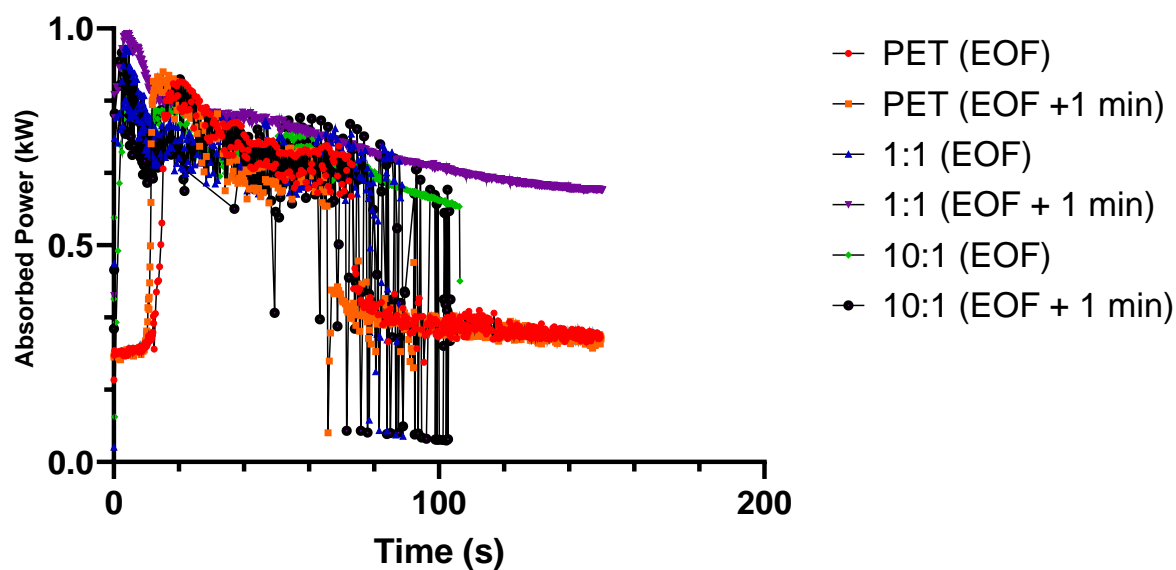


Figure 4.16 – Absorbed power profiles for PET samples for an input power of 1.60 kW.

Insert – Close up of initial 20 seconds to more clearly show the faster absorption of microwave power by impregnated PET.

1:1, 10:1 = EG: PET mass ratio

EOF = Microwave discontinued after pyrolysis fumes ceased to evolve.

EOF + 1 min = Microwave discontinued 1 minutes after pyrolysis fumes ceased to evolve.

Despite the well understood difficulties surrounding the accurate measurement of temperature, a clear improvement in the heating rate of the impregnated PET can be seen for all impregnated PET samples over their unmodified counterparts (Fig 4.17 – 4.22) which does demonstrate that scCO₂ impregnation of degradable susceptors into PET does have the potential to improve the performance of the polymer during microwave pyrolysis.

As all the improvement in heating of PET was seen in the first minute of the pyrolysis experiments, close ups of the recorded temperature during this time have also been presented for the three input powers: 0.80 kW (Fig. 4.18), 1.20 kW (Fig. 4.20) and 1.60 kW (Fig. 4. 22).

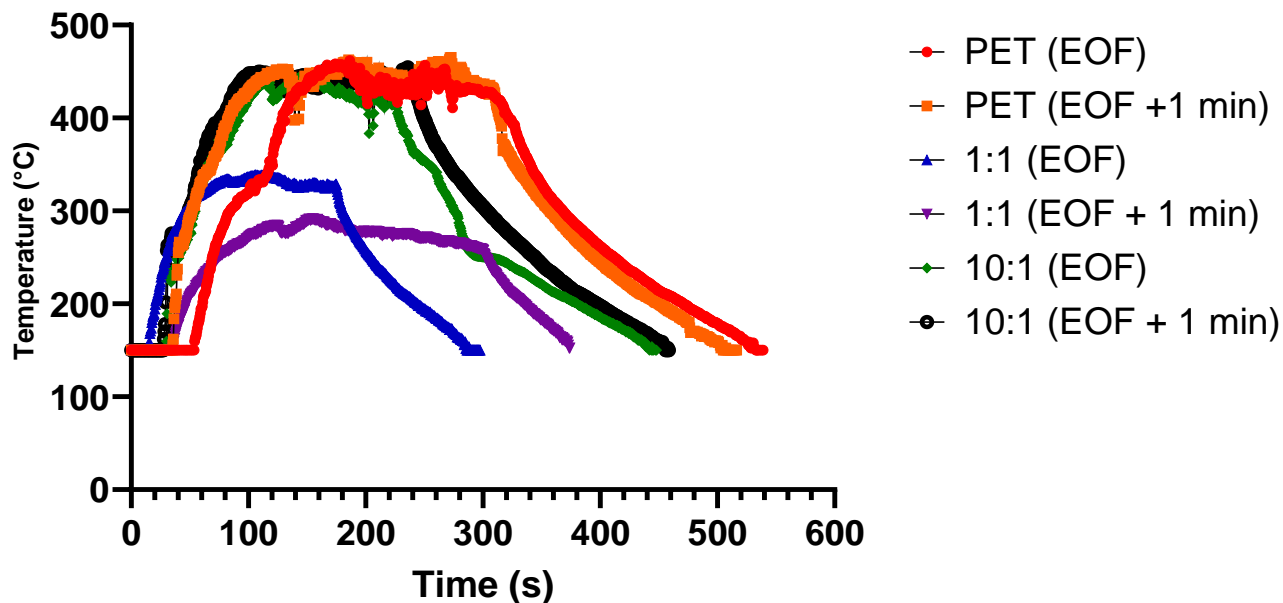


Figure 4.17 – Temperature profile of PET samples for an input power of 0.80 kW..

1-1. 10-1 = EG: PET mass ratio

EOF = Microwave discontinued after pyrolysis fumes ceased to evolve.

EOF + 1 min = Microwave discontinued 1 minutes after pyrolysis fumes ceased to evolve.

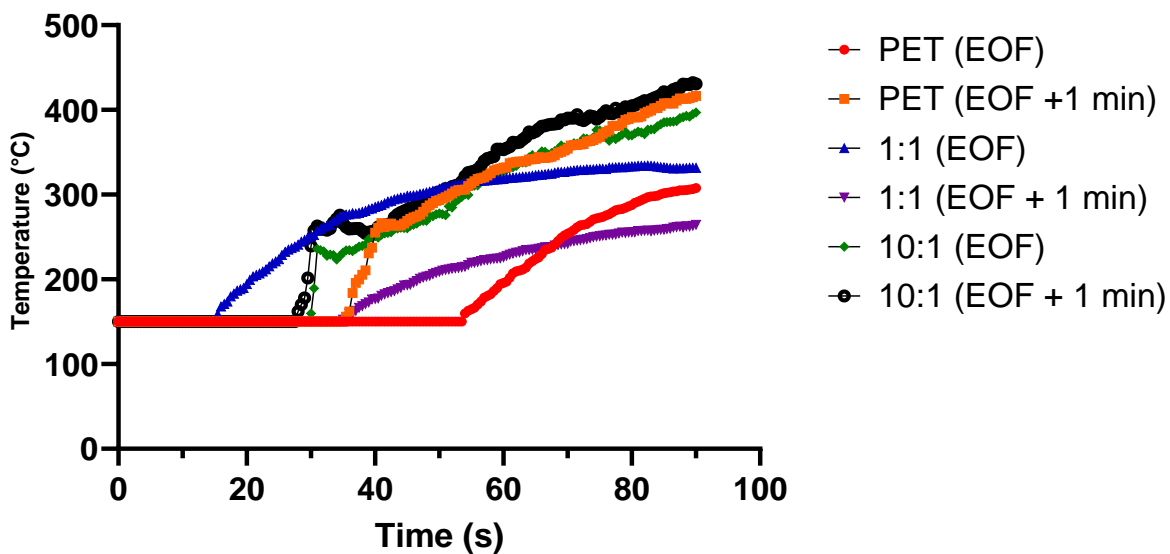


Figure 4.18 - Close up of initial 90 seconds in figure 4.17 to more clearly show the superior heating rate of impregnated PET.

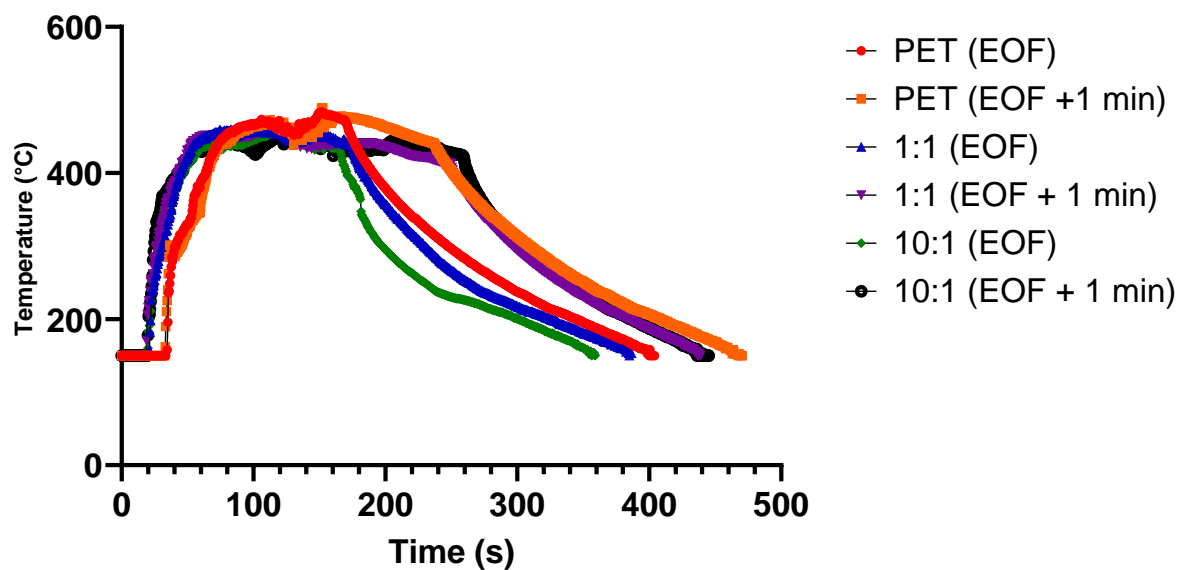


Figure 4.19 – Temperature profile of PET samples for an input power of 1.20 kW.

1-1. 10-1 = EG: PET mass ratio

EOF = Microwave discontinued after pyrolysis fumes ceased to evolve.

EOF + 1 min = Microwave discontinued 1 minutes after pyrolysis fumes ceased to evolve.

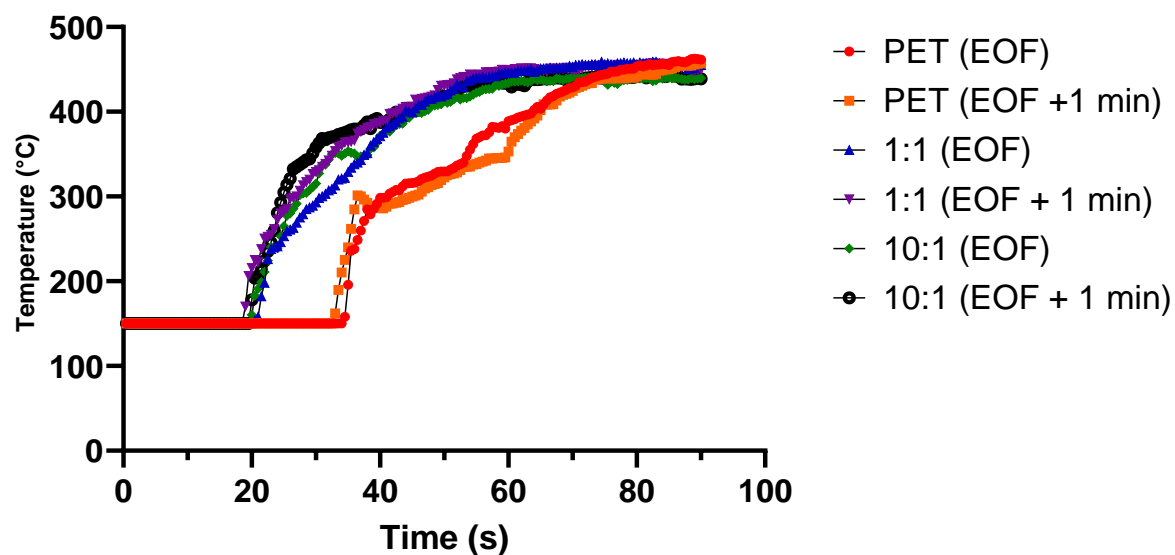


Figure 4.20 - Close up of initial 90 seconds in figure 4.19 to more clearly show the superior heating rate of impregnated PET.

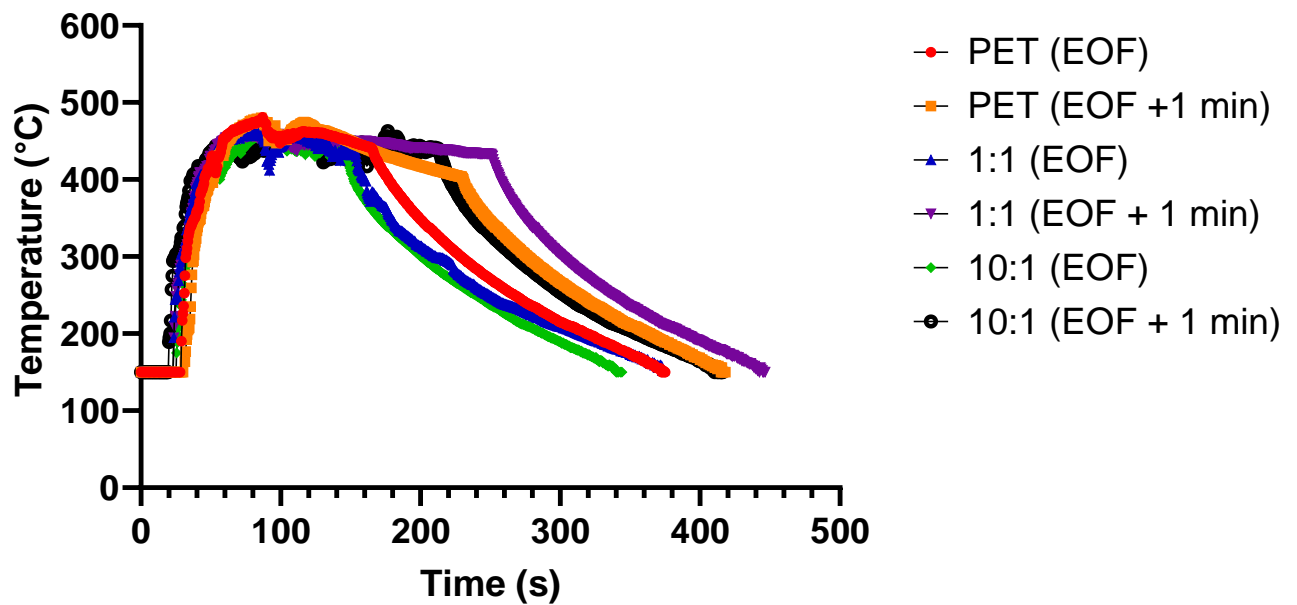


Figure 4.21 – Temperature profile of PET samples for an input power of 1.60 kW.

1-1, 10-1 = EG: PET mass ratio

EOF = Microwave discontinued after pyrolysis fumes ceased to evolve.

EOF + 1 min = Microwave discontinued 1 minutes after pyrolysis fumes ceased to evolve.

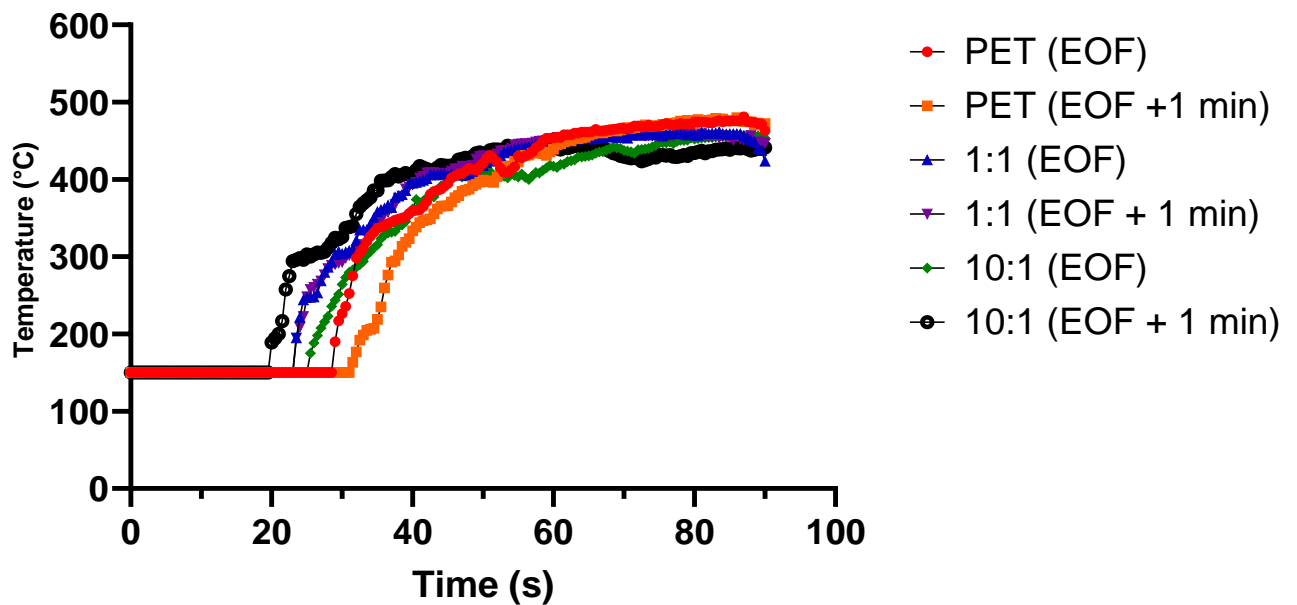


Figure 4.22 - Close up of initial 90 seconds in figure 4.21 to more clearly show the superior heating rate of impregnated PET.

4.3.2.3 Mass Balance and Pyrolysis Rig Design

When PET (unmodified and impregnated) underwent microwave pyrolysis, the resulting products could be broken down into 4 materials which were recovered from different locations in the pyrolysis rig (Tab 4.2).

Table 4.2 – Location of product fractions at the end of pyrolysis experiments

Product	Unmodified/Impregnated PET	Location
Char	Unmodified	Bottom of Quartz Tube
	Impregnated	Bottom of Quartz Tube
Wax	Unmodified	Interior Wall of Quartz Tube
	Impregnated	Interior Wall of Quartz Tube
Powder	Unmodified	Dispersed Throughout Rig
	Impregnated	Round Bottomed Flask + Air Condenser
Gas	Unmodified	Released to Fume Cupboard (not collected)
	Impregnated	Limewater Trap + Released to Fume Cupboard

After unmodified PET had been pyrolysed, two challenges concerning product recovery were presented:

1. A waxy product condensed on the interior wall of the quartz reactor and could only be separated from the char via extraction into dimethylformamide (DMF) – a highly toxic solvent.
2. A powder was also recovered from the pyrolysis rig, but it condensed across several pieces of glassware – complicating recovery.

To simplify solid product recovery after pyrolysis of impregnated PET, a combination of heating and reduced pressure was employed. Heating tape was used to heat the external wall of the quartz reactor, and the overhead borosilicate adaptor to 120 °C before the pyrolysis took place. The pressure within the rig was also reduced to 450 mbar by use of a vacuum pump. It was hypothesised that heating the quartz reactor beforehand would minimise the amount of material that condensed within it, and, in combination with the reduced pressure, solid

pyrolysis product would be pulled into the first cold trap where the bulk of the material would condense.

A full mass balance is available (Fig. 4.23), with raw data located in the appendix, and it can be seen that the amount of waxy solid falls, with a corresponding increase in the mass of powder product obtained, when modified PET is pyrolysed. This swing towards powdered product could be a result of two possibilities:

1. The external heating and reduced pressure facilitating movement of pyrolysis fumes out of the quartz reactor before they condense, reducing the amount of wax on the interior walls.
2. Impregnated ethylene glycol could be altering the chemistry taking place during pyrolysis, changing the nature of the products.

The different product fractions have been expressed as the percentage of the mass of the original PET they make up (Fig. 4.24). The wax and powder products have been combined into a single fraction expressed as “solid”, and no large changes in the solid % of total can be seen between unmodified and impregnated PET. This suggests that the increase in powder product, and the fall in waxy product, seen in Tables 4.2 and 4.3 is due to the additional heating and reduced pressure enabling the pyrolysis fumes to exit the quartz reactor before they condense, rather than the impregnated ethylene glycol influencing the chemistry taking place during pyrolysis.

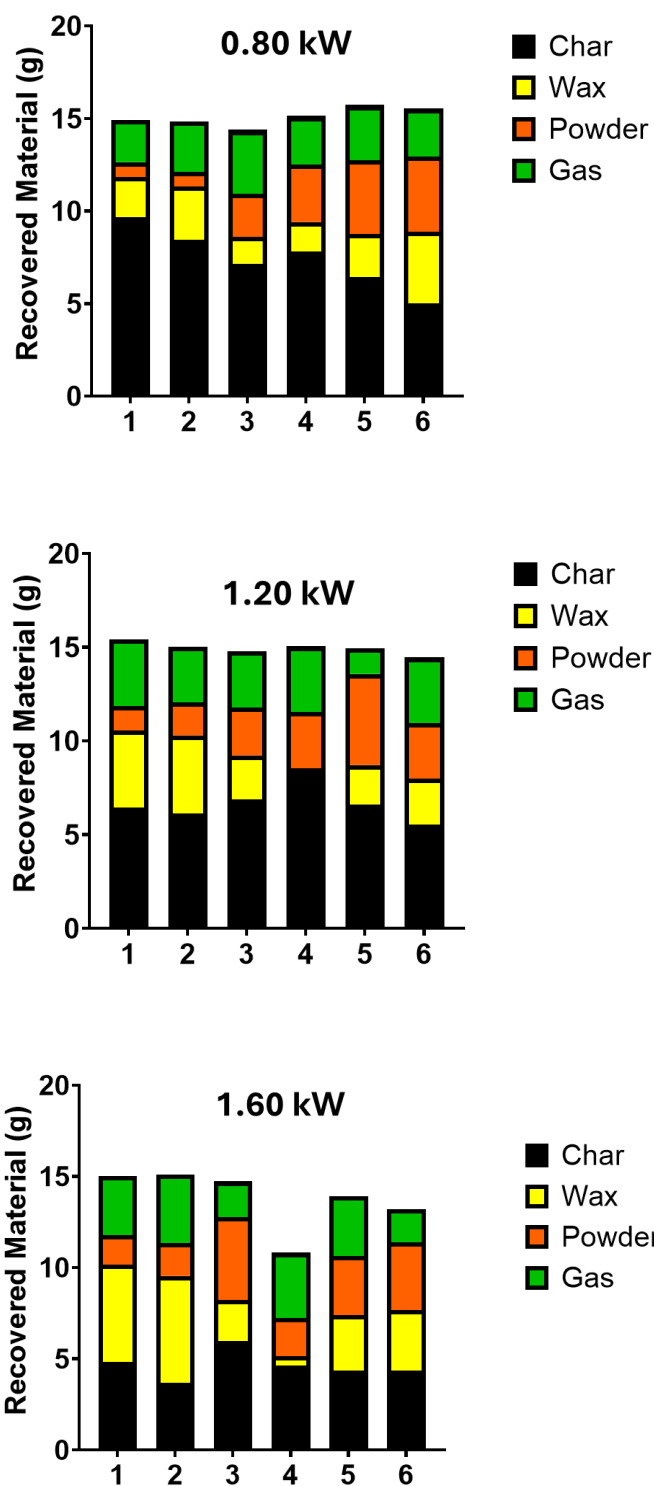


Figure 4.23 – Graphical representation of the different product fractions of PET pyrolysis by mass.

Experiment no.	1	2	3	4	5	6
PET: EG Impregnation Ration	1:0	1:0	1:1	1:1	1:10	1:10
Pyrolysis Residence Time	EOF	EOF + 1 min	EOF	EOF + 1 min	EOF	EOF + 1 min

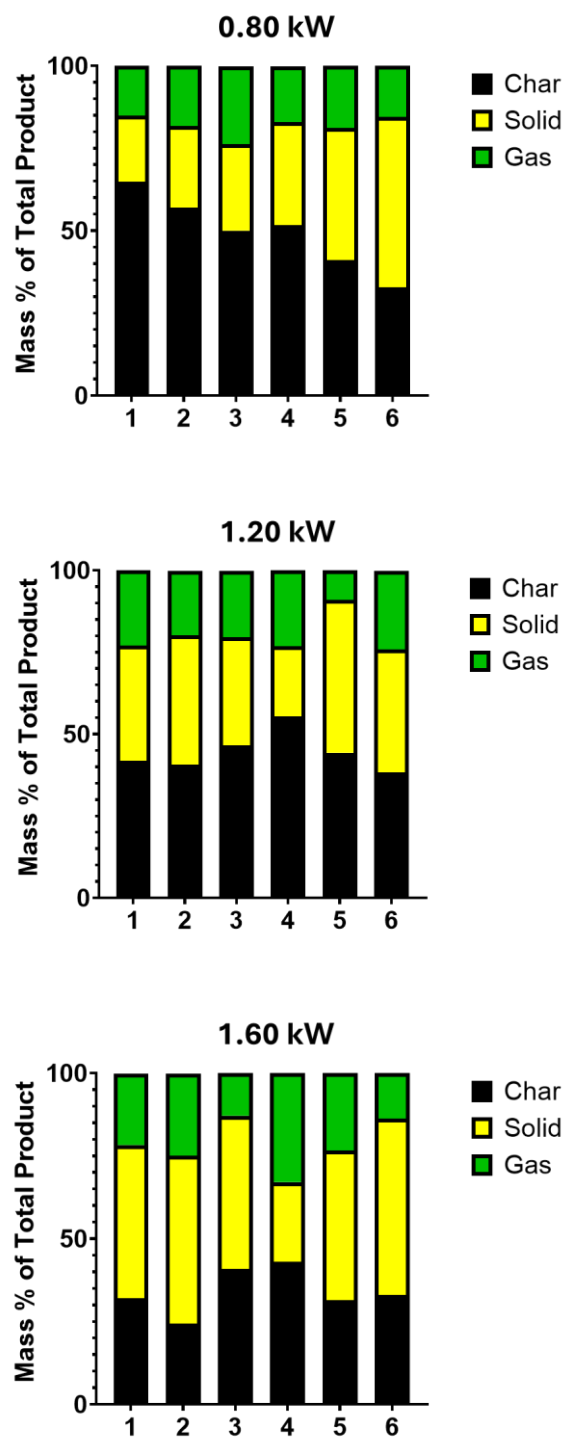


Figure 4.24 - Percentage split of the different product fractions of PET pyrolysis illustrated in figure 4.23.

Experiment no.	1	2	3	4	5	6
PET: EG Impregnation Ration	1:0	1:0	1:1	1:1	1:10	1:10
Pyrolysis Residence Time	EOF	EOF + 1 min	EOF	EOF + 1 min	EOF	EOF + 1 min

4.3.2.4 PET Conversion and Specific Energy

Results discussed in section 4.3.2.2 illustrate that impregnating PET with ethylene glycol can result in an improvement in the ability of the polymer to absorb power from a microwave field, yielding a superior heating rate. However, a key test of whether the enhanced heating produces an improvement in the degradation of PET to value-added products, specifically a shift away from char production and an increase in the solid and gas products, remains. It is also of interest to determine the specific energy (energy input per unit mass) of the pyrolysis experiments, to determine if the improved power absorption and heating rates exhibited by the impregnated PET resulted in improvements in conversion, or a reduction in specific energy for the same degree of conversion.

Conversion of PET by microwave pyrolysis was calculated (Eq. 4.2); specific energy was also calculated for pyrolysis experiments (Eq. 4.3), and the values were plotted against one another (Fig. 4.24)

$$\text{Conversion (\%)} = 100\% \times \left(\frac{\text{PET (g)} - \text{Char (g)}}{\text{PET (g)}} \right)$$

Equation 4.2 – Conversion of PET during microwave pyrolysis to value-added products

$$\text{Specific Energy (kJ g}^{-1}\text{)} = \frac{\text{Average Absorbed Power (kW)} \times \text{time (s)}}{\text{PET (g)}}$$

Equation 4.3 – Calculation of specific energy consumed during microwave pyrolysis

Conversion of PET can be seen to increase as the input power is increased in for unmodified PET, but impregnating PET with ethylene glycol does not appear to enhance the conversion at the same input power (Fig. 4.24). There is also no discernible trend for changes to the specific energy of the pyrolysis. Impregnating PET with ethylene glycol in scCO₂ does not appear to

impart any improvement to the pyrolysis, apart from an initial increase in power absorption and a faster heating rate.

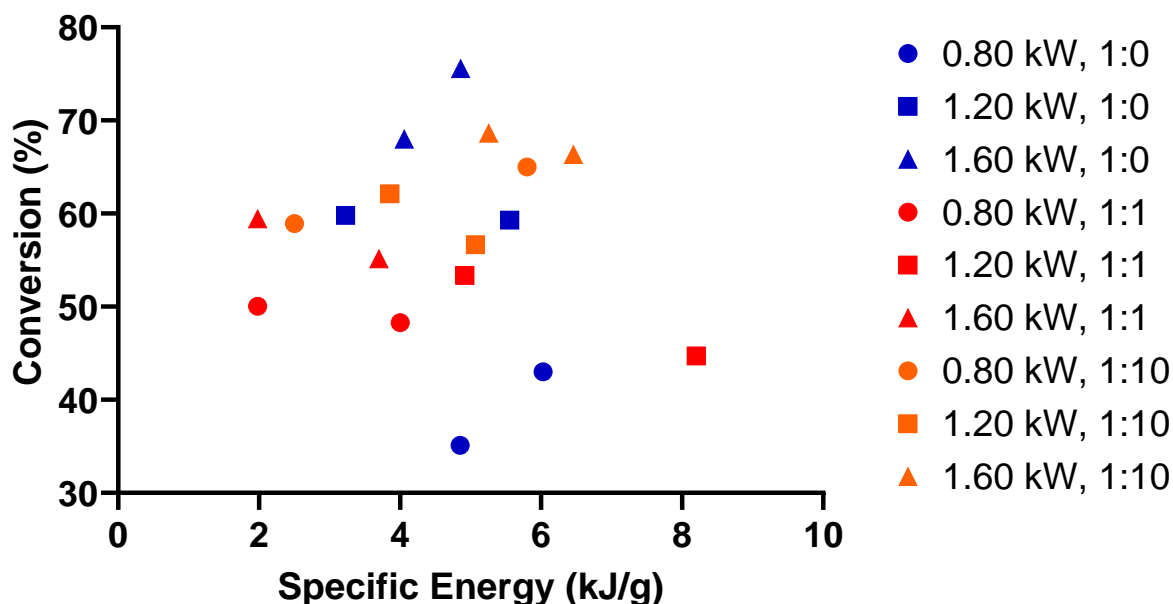


Figure 4.24 – Plot of pyrolysis specific energy against PET conversion.

An explanation for these results can be formulated when the TGA and dielectric measurements from section 3.3 are considered. Both heat-and-hold and dynamic dielectric measurements showed a clear enhancement in the dielectric loss factor and dielectric loss tangent at room temperature after PET had been impregnated with ethylene glycol, but no significant difference could be seen for a temperature above 100 °C. TGA experiments illustrated that ethylene glycol could be desorbed from PET by heating the films, and this was hypothesised to be why any differences in the dielectric response could not be seen above 100 °C.

Despite the potential for ethylene glycol to desorb from the PET, pyrolysis experiments were undertaken as the generator used to produce the microwaves is capable of far higher input powers than the analytical equipment used for analysis. This was expected to result in a faster heating rate, and it was hypothesised that this faster heating rate would make it possible to “outrun” the desorption of the ethylene glycol. Specifically, the much shorter residence time inherent to microwave pyrolysis, as opposed to the residence times for dielectric or TGA

experiments, could allow ethylene glycol impregnated into PET to improve the ability of the polymer to be heated by microwaves before it evaporates or degrades due to the high temperatures. Some evidence in support of this theory can be seen - the initial improvement in absorbed power and the concurrent faster heating rate, but this does not result in an improved conversion of PET or a reduction in specific energy consumption.

4.3.3 Analysis of the Products

As stated in the previous section, the products from PET pyrolysis can be considered as four fractions: char, waxy solid, powder solid and gas. Char is a low value material which is commonly re-used as a susceptor in microwave pyrolysis, and the gaseous products are difficult to capture and store safely on the laboratory scale. For these reasons, characterisation post-pyrolysis was focussed on the waxy and powder products.

4.3.3.1 Functional Groups and Structural Feature

From ^1H NMR of the waxy and powder products of unmodified PET in d_6 -DMSO, it can be seen that a mixture of species is present in, and there appears to be no chemical difference between the fractions (Fig 4.25) (Fig.4.26). Closer inspection of the aryl region of the NMR suggests that several aromatic-based materials are present, consistent with the PET pyrolysis literature reviewed earlier in this chapter (Fig 4.2).

The singlet at $\delta = 13.2$ ppm confirms the presence of a proton in a highly polar environment, such as a carboxylic acid functional group. Standards of benzoic acid (BA) and terephthalic acid (TPA) were also characterised by ^1H NMR and comparison with the aryl region of pyrolysis products formed during pyrolysis illustrated that both species were present.

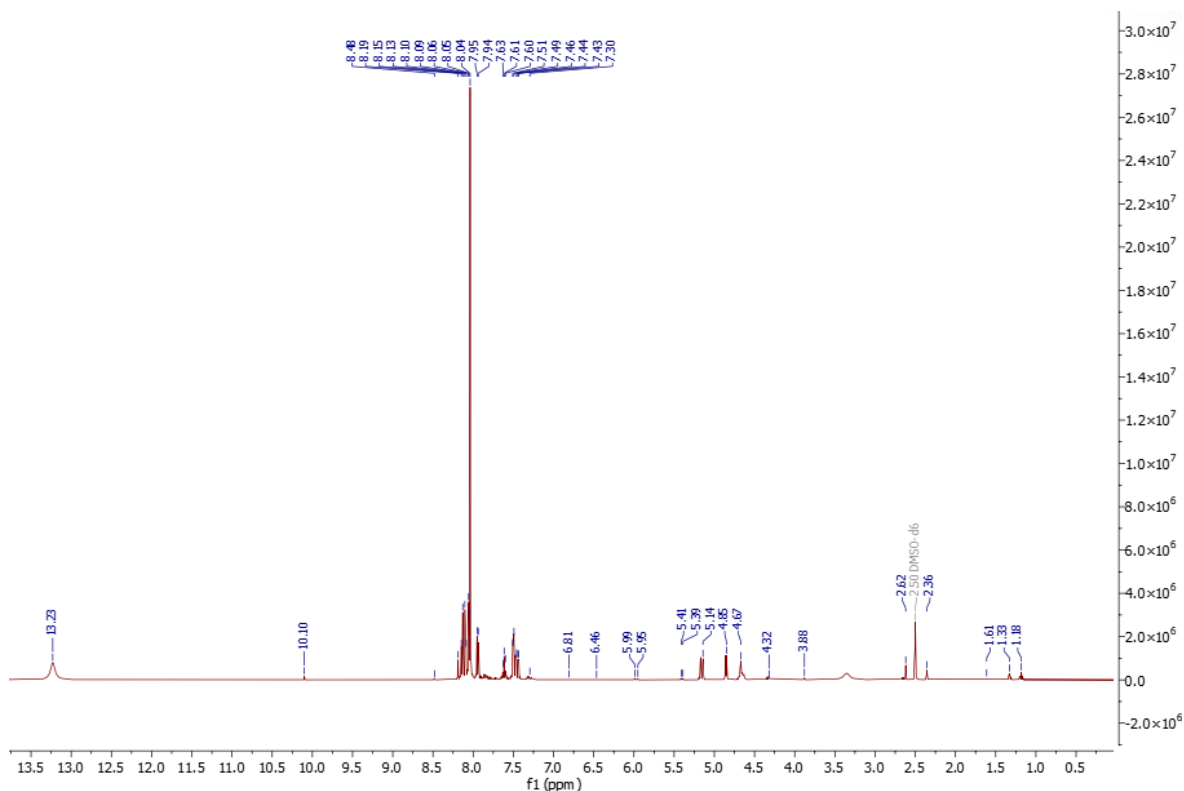


Figure 4.25 – ^1H NMR of the wax fraction obtained from unmodified PET degraded by microwaves with an input power of 0.8 kW. This spectrum is representative of all unmodified PET degraded via microwave pyrolysis in this work.

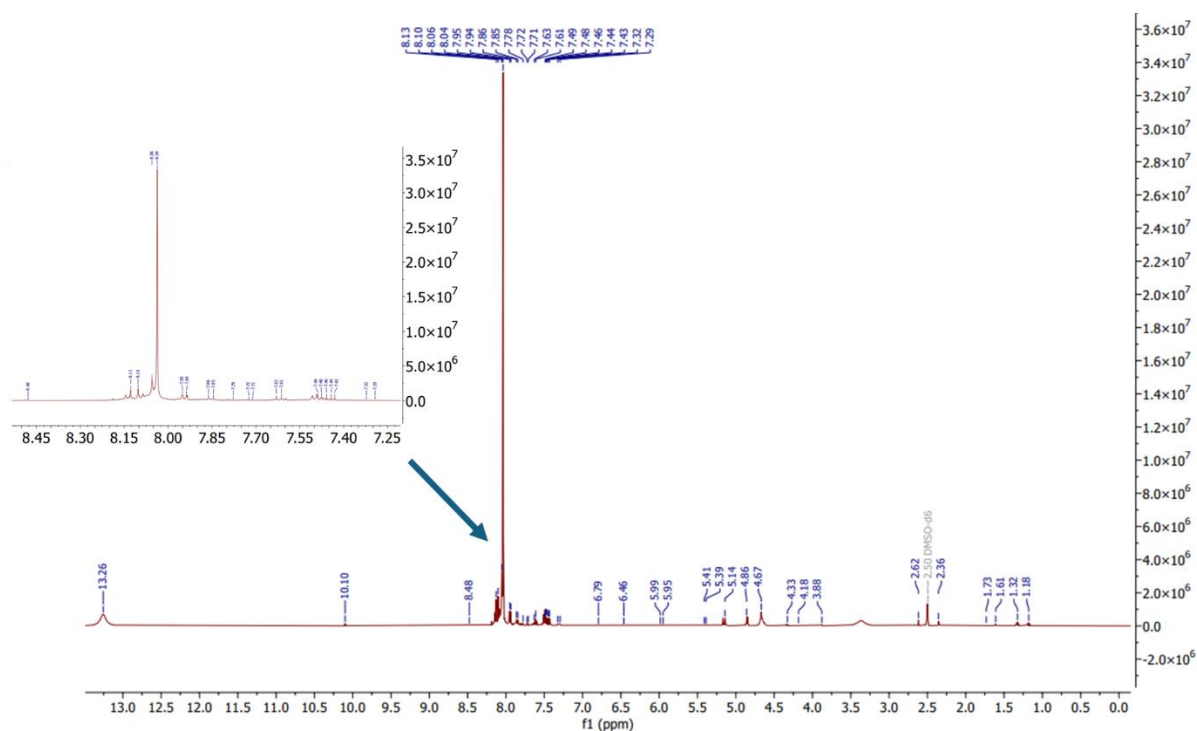


Figure 4.26 - ^1H NMR of the wax fraction obtained from PET impregnated with ethylene glycol in a 1:1 mass ratio degraded by microwaves with an input power of 0.8 kW. This spectrum is representative of all modified PET degraded via microwave pyrolysis in this work. Insert: Expansion of the aryl region of the spectrum. The multitude of peaks in this region indicate several aromatic-based species are contained in the product

All of the pyrolysis products produced a very similar IR spectrum, and a representative example is shown (Fig. 4.27). Bands can be seen at 3062 and 2963 cm^{-1} which is consistent with a carboxylic acid -OH stretch, and bands of similar wavenumbers, 3069 and 2986 cm^{-1} , can be seen in the spectrum of BA and TPA respectively (Appendix). Further to this, C-H stretching bands are visible at 2873, 2825, 2665 and 2547 cm^{-1} . Whilst C-H stretching bands themselves are not that useful for determining the overall structure of a molecule, the fact that these multiple C-H bands can be seen, alongside typical C=C stretching bands (1400-1680 cm^{-1}), does indicate that several combinations of alkane and alkene structures are present in the pyrolysis products. An aromatic ester band can also be seen at 1258 cm^{-1} which is consistent with the PET repeating unit.

The information imparted from the NMR and IR was used to aid in the interpretation of mass spectra in the next section.

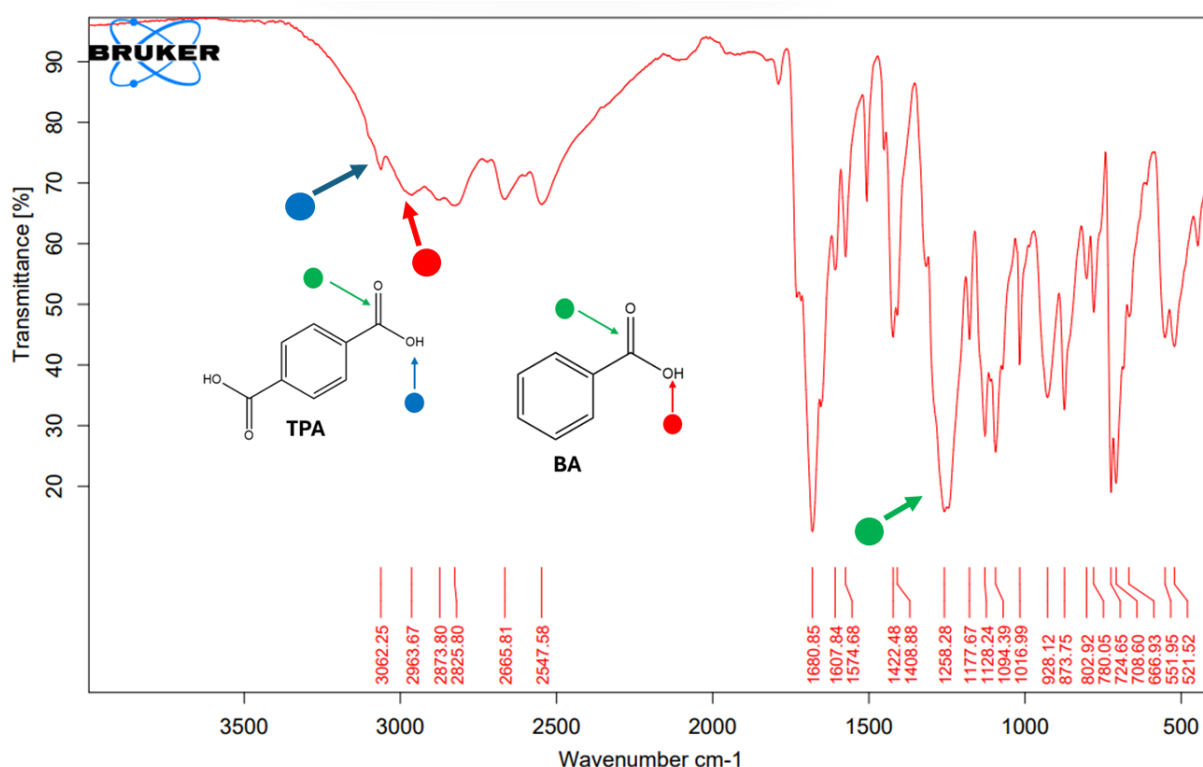


Figure 4.27 – IR spectrum of the wax fraction obtained from unmodified PET degraded by microwaves with an input power of 0.8 kW. A plethora of peaks can be seen, but key peaks indicating the presence of aromatic ester linkages, as well as carboxylic acid end groups have been indicated.

4.3.3.2 – Mass Spectrum

GC-MS was used to determine the molecular weights of the pyrolysis products. DMF and DMSO were the only solvents able to dissolve the entire pyrolysis wax or powder. Unfortunately, these solvents are incompatible with routine mass spectrometry instruments due to their high boiling point (GC-MS, ESI) and their highly polar nature enabling swelling of pipework fittings (HPLC).

MALDI-ToF produced no peaks when a *trans*-2-[3-(4-*tert*-Butylphenyl)-2-methyl-2-propenylidene]malononitrile (DCTB) matrix and lithium bromide cationisation agent was used (Fig. 4.28). APCI was also attempted as no solvent is required, but a complicated mixture of peaks was produced in both positive and negative modes (Fig. 4.29). Without the chromatography element of GC-MS or HPLC, it was not possible to confirm the number of different species present in the chromatogram, so APCI was not relied on here.

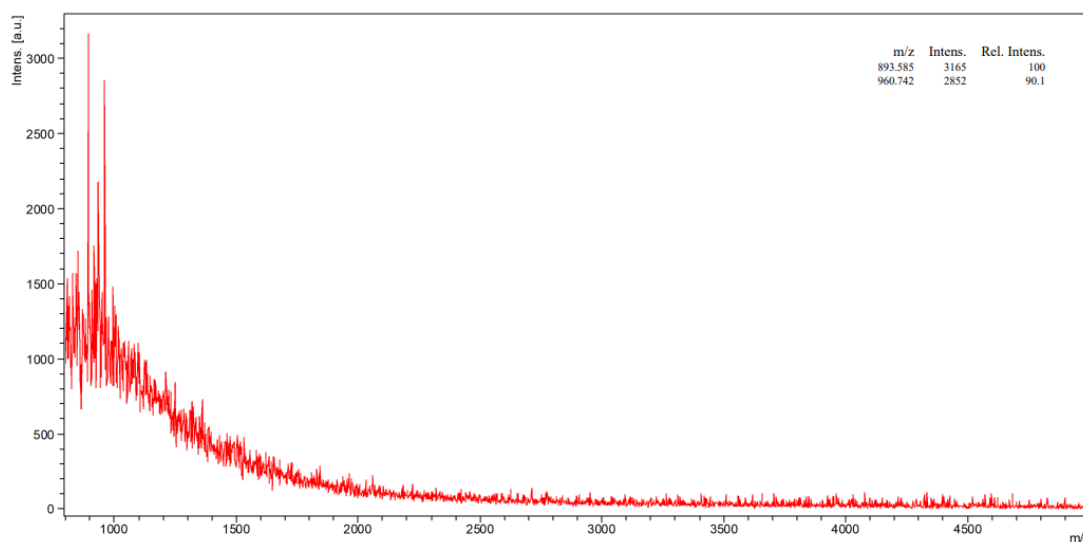


Figure 4.28– MALDI spectrum of attempted analysis of powder fraction obtained from unmodified PET degraded by microwaves with an input power of 0.8 kW. No strong peaks clear of the baseline were achieved, indicating that either no oligomers remained or that they flew poorly after interacting with the laser.

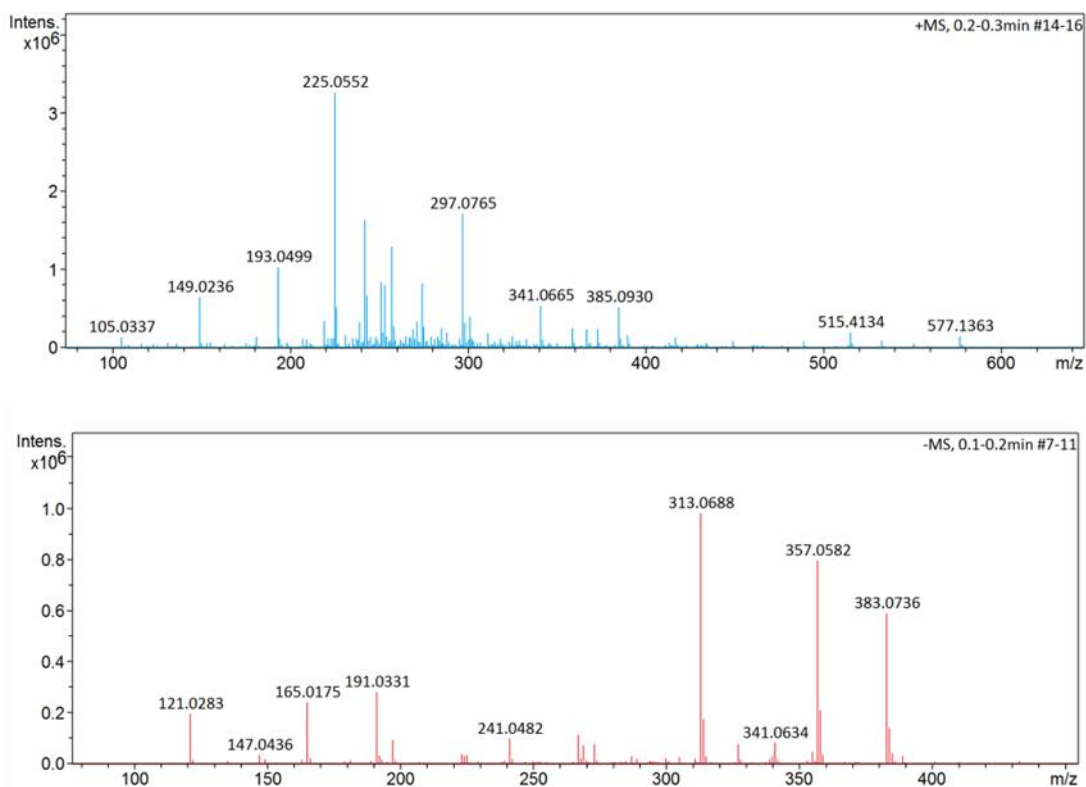


Figure 4.29 – Mass spectra obtained from APCI of the wax fraction obtained from unmodified PET degraded by microwaves with an input power of 0.8 kW. Positive mode (top) and negative mode (bottom) show an array of peaks, but it is unclear how many different species are present due to the lack of chromatography and the lability of the ester linkages when exposed to the corona discharge.

It was serendipitously discovered that a lower-molecular weight fraction could be extracted from the bulk waxy and powder products into chloroform, which is compatible with GC-MS.

Identical to the NMR, the waxy and powder fractions gave similar TICCs (Fig. 4.30) (Fig. 4.31).

Proposed identities for the chemical species have been formulated (Tab. 4.3) (Tab. 4.4) (Tab. 4.5) (Tab. 4.6).

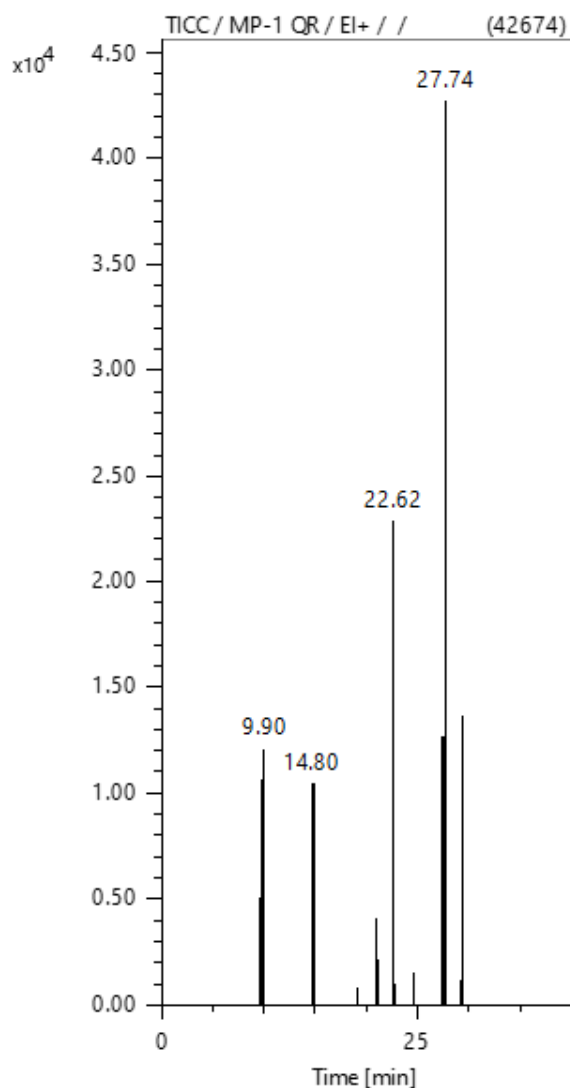


Figure 4.30 - TICC obtained from GC-MS of the wax fraction obtained from unmodified PET degraded by microwaves with an input power of 0.8 kW.

Benzoic acid is confirmed as one product, as the peaks in the TICC of the pyrolysis fractions have matching retention times with the standard confirming what the IR and NMR above illustrated (Appendix). A series of species based on the PET repeating unit have also been suggested, but standards of these were not available for confirmation with IR and NMR analysis.

Despite indications of its presence in the NMR and IR, TPA cannot be observed in the GC-MS. This is expected as TPA is highly insoluble in chloroform and was not extracted into the fraction of the products analysed by GC-MS.

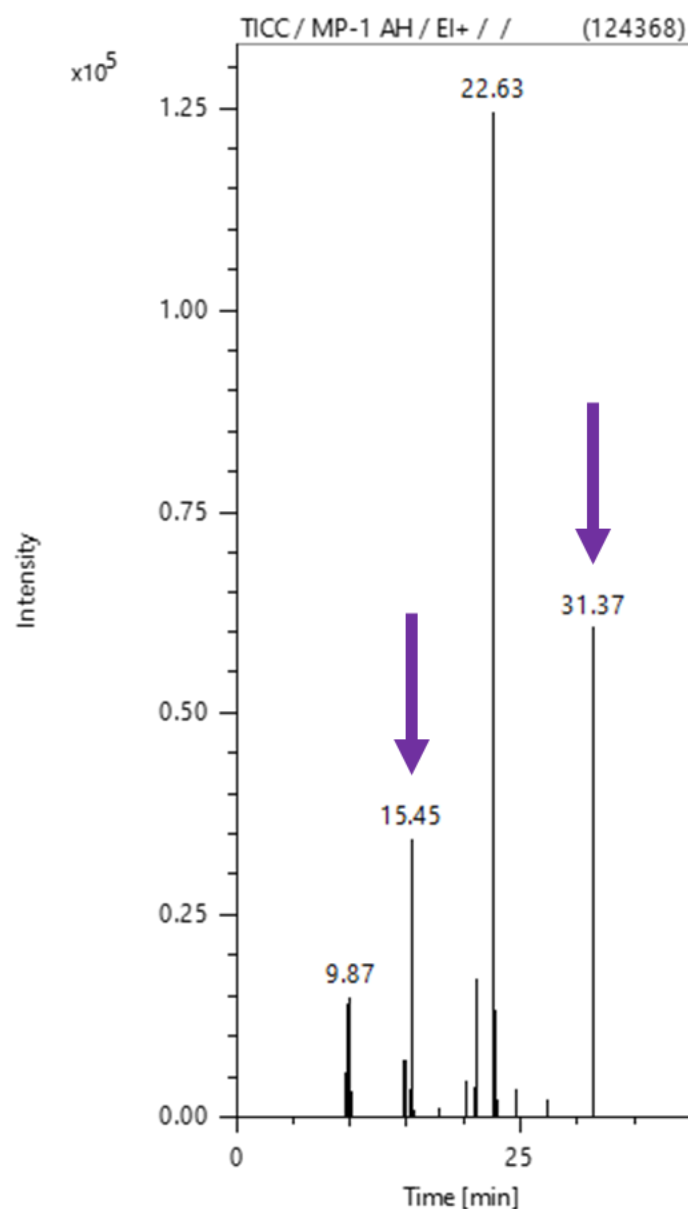


Figure 4.31 - TICC obtained from GC-MS of the powder fraction obtained from unmodified PET degraded by microwaves with an input power of 0.8 kW. Additional peaks not seen in wax fraction are circled.

A range of peaks are present in the TICC, highlighting that a complex mixture of products is formed during pyrolysis. Not all of the corresponding mass spectra for the peaks in the TICC contain an obvious molecular ion, making it difficult to confirm the identity of the species coming off the column. This is possibly due to the lability of the ester linkages in the PET backbone, resulting in degradation of the material when it undergoes ionisation in the GC-MS. The four peaks with the greatest intensity have had their mass spectra interpreted, with the proposed structures presented below (Tab. 4.3) (Tab. 4.4) (Tab. 4.5) (Tab. 4.6). Where a

molecular ion could be seen, it has been highlighted in bold in the first row of the appropriate table. If a clear molecular ion could not be observed, a structure for the base peak has been presented in the first row instead. Without being able to perform a mass spectrometry technique which uses a soft ionisation technique, such as ESI or HPLC, it is difficult to say what real product a base peak corresponds to. Additional work is needed to obtain a complete understanding as to the nature of these pyrolysis products, which is discussed in Chapter 6.

Table 4.3 – Proposed structures for material retained on the GC-MS column for 9.90 minutes. The molecular ion is shown in bold on the first row, with fragments visible in the mass spectrum listed underneath.

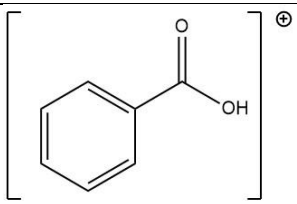
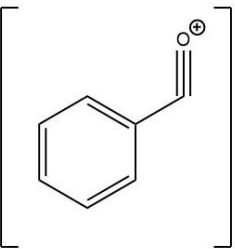
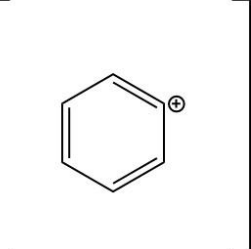
Retention Time (min)	m/z	Identity
9.90	122.02	 <chem>[O-]C(=O)c1ccccc1</chem> [⊕]
9.90	105.12	 <chem>[O+]#Cc1ccccc1</chem>
9.90	77.03	 <chem>[c+]1ccccc1</chem>

Table 4.4 - Proposed structures for material retained on the GC-MS column for 14.80 minutes. The base peak is shown on the first row, with additional fragments visible in the mass spectrum listed underneath.

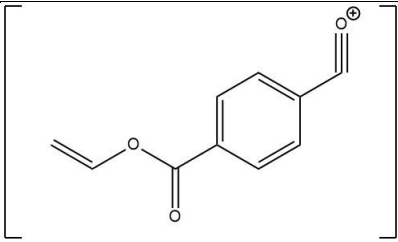
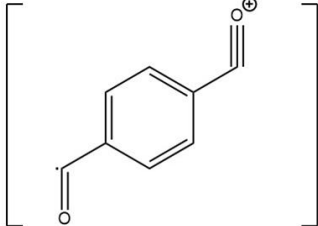
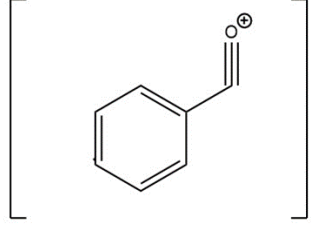
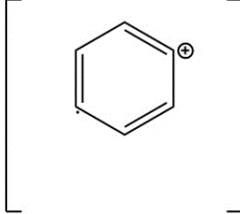
Retention Time (min)	m/z	Identity
14.80	175.03	
14.80	132.01	
14.80	104.02	
14.80	76.02	

Table 4.5 - Proposed structure for material retained on the GC-MS column for 22.62 minutes. The base peak is shown in bold on the first row. No other fragments are listed as additional peaks in the mass spectrum are of low intensity and difficult to distinguish from the baseline.

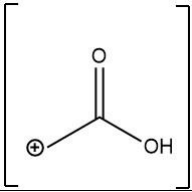
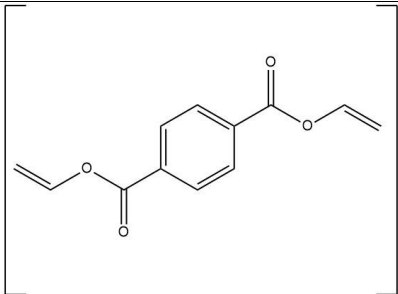
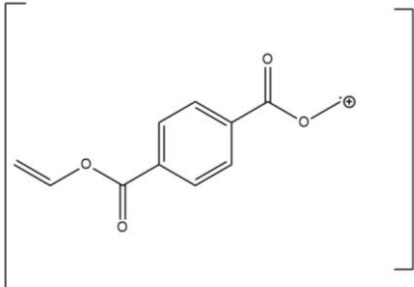
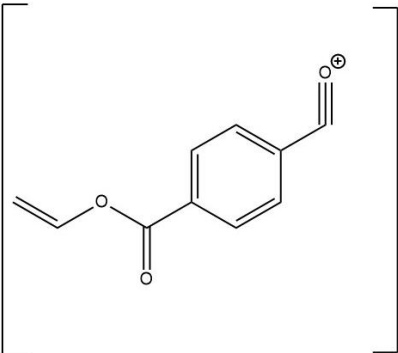
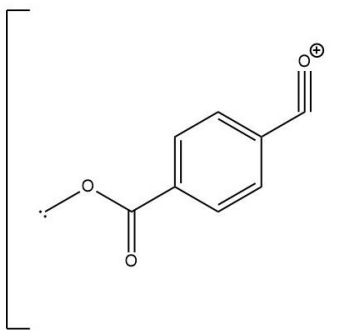
Retention Time (min)	m/z	Identity
22.62	59.03	

Table 4.6 - Proposed structures for material retained on the GC-MS column for 27.74 minutes. The molecular ion is shown in bold on the first row, with fragments visible in the mass spectrum listed underneath.

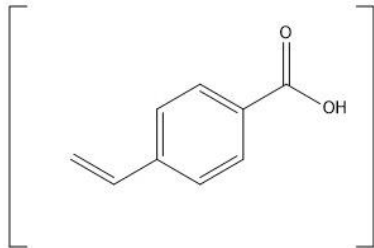
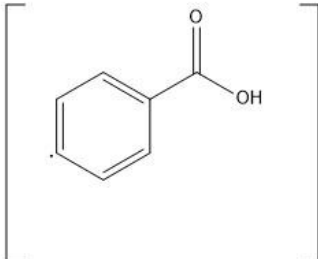
Retention Time (min)	m/z	Identity
27.74	218.17	
27.74	203.03	
27.74	175.05	
27.74	161.02	

The mixture of species in the wax and powder fractions is largely identical, apart from two species that can be seen in the powder fraction that are not present in the wax at retention

times 15.45 and 32.37 minutes (Fig. 4.32) (Tab. 4.7). This is constant across the range of input powers used for the pyrolysis.

Additional work is still required to elucidate the structure of the product retained on the column for 31.37 minutes.

Table 4.7 – Proposed structures for the additional peaks seen in the powder fraction from Figure 4.29. retained on the GC-MS column for 15.45 minutes. The molecular ion is shown in bold, with fragments listed underneath.

Retention Time (min)	m/z	Identity
15.45	149.00	
15.45	121.01	

The wax fraction also appears unchanged for PET which was impregnated with ethylene glycol before pyrolysis. However, the peaks seen at 27.74, 29.32 and 32.37 minutes in the powder fraction of unmodified PET are not present in the corresponding TICC for impregnated PET, and a new peak at 25.74 minutes is visible (Fig. 4.32). The proposed structure for this peak, based on the fragmentation pattern in the mass spectrum, is presented in Table 4.8. It incorporates one intact glycolic unit in its structure, which may suggest that the impregnated ethylene glycol is influencing the degradation mechanisms at play. However, further investigation is needed to confirm this.

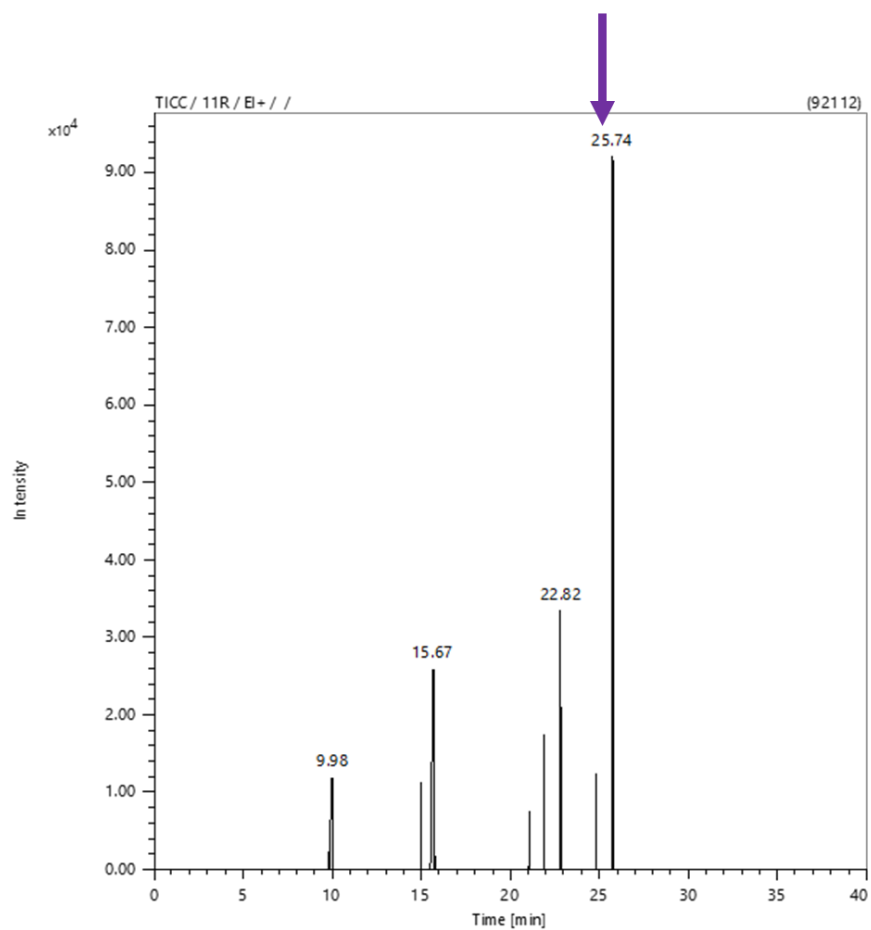
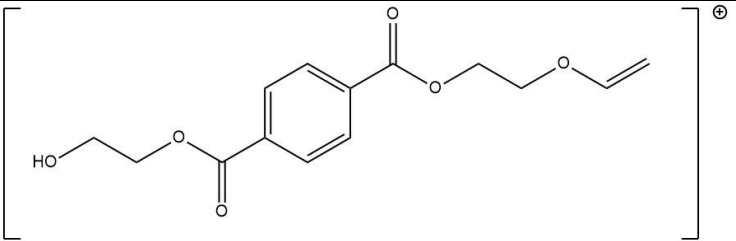
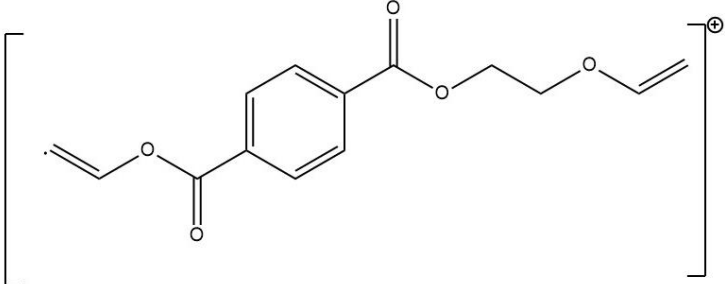
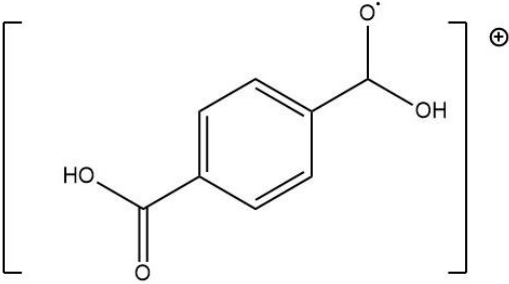
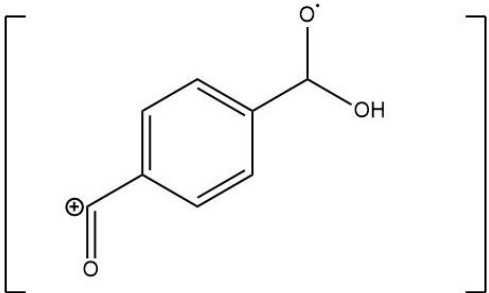


Figure 4.32 - TICC obtained of the powder fraction from PET impregnated with ethylene glycol in a 1:1 mass ration degraded by microwaves with an input power of 0.8 kW. The new peak at 25.74 minutes is circled.

Table 4.8 - Proposed structures for the peak at 25.74 minutes seen in the powder fraction from figure 4.30. *m/z*. Molecular ion shown in bold, with fragments seen in the corresponding mass spectrum shown in normal text.

Retention Time (min)	<i>m/z</i>	Identity
25.74	279.14	
25.74	261.08	
25.74	167.03	
25.74	150.03	

Overall, there is limited evidence to suggest that the impregnated ethylene glycol significantly alters the pathway of PET degradation during microwave pyrolysis. Analysis was severely hindered by two factors:

1. A complex mixture of compounds appears to have been produced via microwave pyrolysis of PET, demonstrated by the range of peaks in the ^1H NMR, IR and GC-MS spectra, meaning that chromatography is required for any meaningful analysis.
2. The only solvents capable of dissolving the entire wax and powder product were DMF or DMSO, which are incompatible with routine chromatography – mass spectroscopy techniques due to their high boiling points.

4.4 Conclusions

Microwave pyrolysis was conducted on PET that had received no prior modification, and PET that had been impregnated with ethylene glycol in scCO_2 . A clear enhancement in the ability of PET to absorb microwave power, and a corresponding increase in the heating rate, was demonstrated by PET which had been impregnated with ethylene glycol. This confirms dielectric data discussed in Chapter 3.

Both the physical and chemical composition of the pyrolysis products was analysed. The distribution of char, wax, powder and gas does not appear to significantly change when PET is impregnated with ethylene glycol. There is some limited GC-MS evidence that suggests the selectivity of the products may vary when impregnated PET is microwaved, but further work is required to resolve the complicated ^1NMR and GC-MS results.

5 Supercritical Depolymerisation of Polyethylene Terephthalate

Overview

This chapter will begin by critically reviewing the current state of the art in the field of PET solvolysis, specifically by discussing the major drawbacks surrounding the isolation of monomers from crude reaction mixtures. Application of scCO_2 as both the medium for PET depolymerisation, and as a solvent for extracting monomers in high purities, will be demonstrated. Finally, the supercritical solvolysis processes described here will be compared to the current state of the art through previously defined sustainability metrics.

5.1 Introduction

5.1.1 Solvolysis of Polyethylene Terephthalate

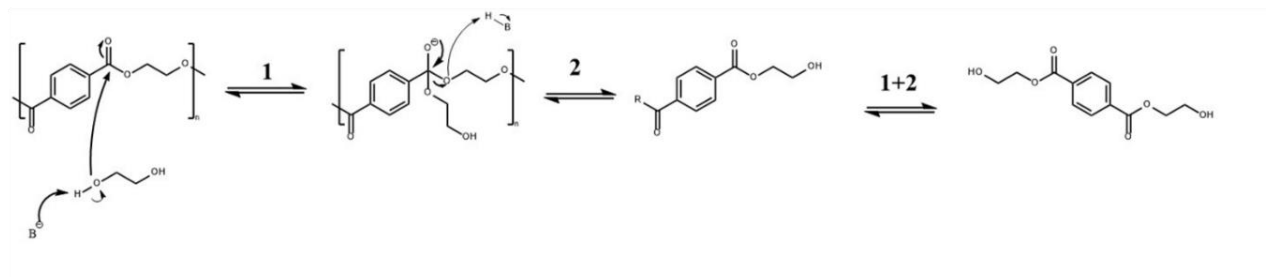
Several routes to depolymerise PET have been published. As mentioned in chapter one, closed-loop recycling pathways typically use one of ethylene glycol, water or methanol as these provide a direct mechanistic pathway to PET's constituent monomers (Fig. 1.17).

It is common to see these recycling approaches referred to as solvolysis, as the attacking species (nucleophile) also serves as the solvent for the depolymerisation, with the large excess helping to drive the reaction forward. All solvolysis routes for PET proceed by the transesterification mechanism, which is reversible (Fig. 5.1). Transesterification reactions obey Le Chatelier's Principle, meaning their equilibrium may be influenced to favour product formation. Strategies that exploit this to favour PET degradation will be discussed below.

Reported reaction temperatures are high (170-220 °C), as these are necessary to break down the otherwise chemically inert PET backbone. Ethylene glycol is a suitable solvolysis medium at

these temperatures due to its high boiling point (194 °C), but use of methanol (methanolysis) or water (hydrolysis) requires a pressurised vessel.

Forward Reaction:



Back Reaction:

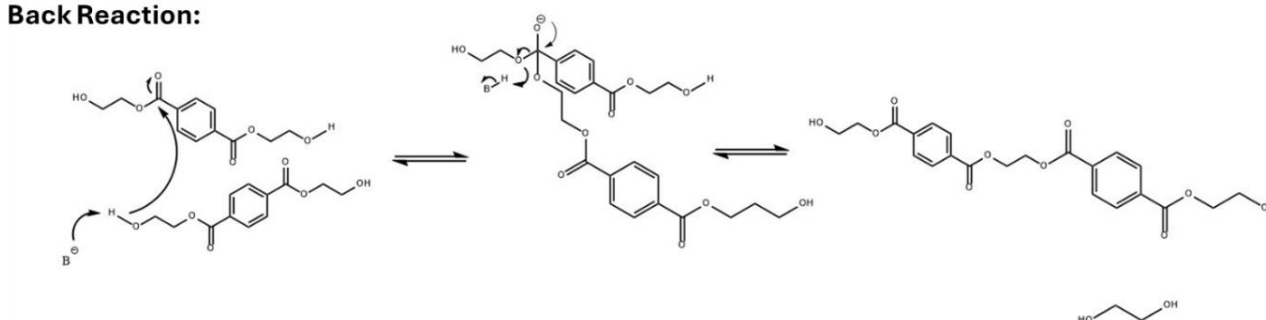


Figure 5.1 – Scheme of how base-catalysed (B) glycolysis of PET proceeds. The desired reaction, where PET is depolymerised is shown (top) as is the undesirable reverse reaction (bottom). Adapted from Clayden's Organic Chemistry.¹¹⁷

The poor solubility of PET in many organic solvents has been identified as a limiting factor to its depolymerisation. The depolymerisation process has been envisaged as proceeding by the shrinking core model, where the reaction only occurs at the interface between the polymer and the solvent, with the particle size being reduced gradually by surface erosion (Fig. 5.2).²⁵⁵ PET depolymerisation proceeding by the shrinking core model was confirmed in early examples of acid-catalysed hydrolysis, where PET was successfully depolymerised by aqueous solutions of either nitric²⁵⁶ or sulfuric acid²⁵⁷ undertaken by Yoshioka *et al.* This group found that the rate of PET hydrolysis could be increased by three factors:

1. Decreasing pH
2. Decreasing PET particle size
3. Increasing temperature

The first two of these variables will improve the surface area-to-volume ratio (S:V) ratio of the reacting species, and the authors concluded that the reaction must be restricted to the surface of the polymer.

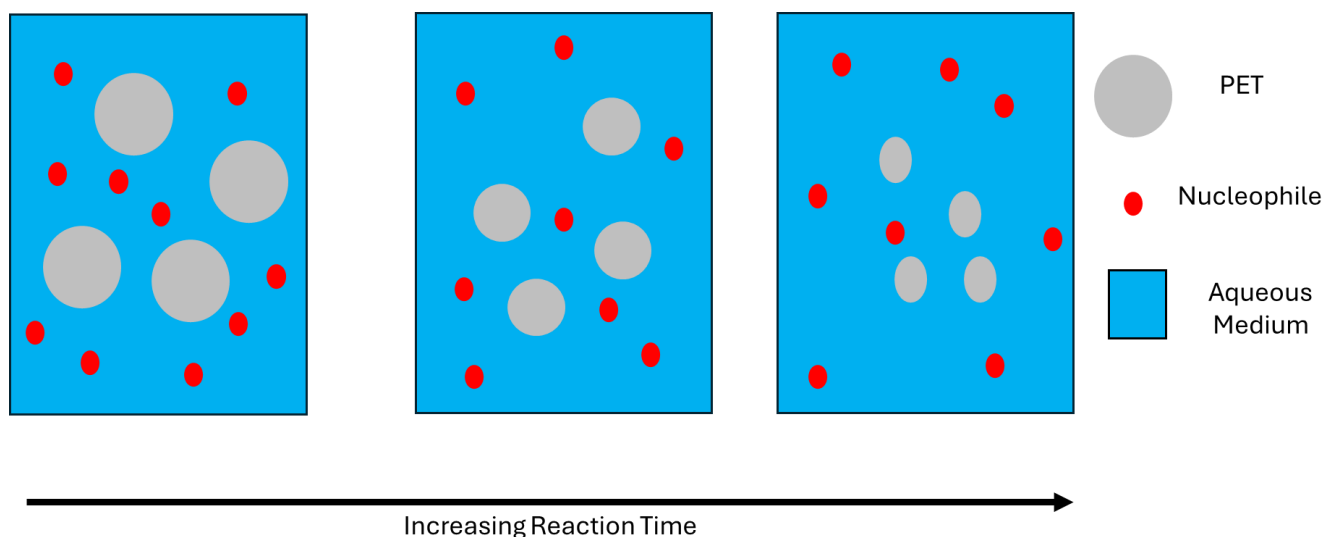


Figure 5.2 – Representation of PET degradation by the Shrinking Core Model. The PET particles can be seen to get gradually smaller with reaction time, as they are degraded at the interface with the aqueous medium only.

Use of co-solvents alongside the solvolytic agent have also been published with the intention of enhancing the solubility of PET in the solvolysis medium or swelling the polymer to improve the S: V to get around the limitation of the shrinking core model.

Kurokawa *et al* investigated the use of toluene as a co-solvent in the methanolysis of PET.²⁵⁸ At 200°C in pure methanol, with an aluminium triisopropoxide (AIP) catalyst, yields of 64% and 63% were achieved for dimethyl terephthalate and ethylene glycol respectively in 2 hours. With a 20% volume toluene reaction mixture, these yields increased to 88% and 87% for the same conditions.

Another example carried out glycolysis of PET in a range of highly polar or aromatic solvents and this lowered the reaction time to below 20 minutes.²⁵⁹ The authors probed the intermolecular interactions at play via IR experiments to explain the improved reaction rate. For aniline and nitrobenzene, a clear shift in the bands which correspond to the aromatic ring of these co-solvents could be seen when PET was dissolved in them, indicating that these solvents were

able to undergo π - π interactions with the polymer as they permeated its structure, and it began to swell. The same shift in IR bands could not be seen for DMSO, but DFT calculations proposed that hydrogen bonding could take place between PET and DMSO, facilitating swelling of the polymer as seen for the aromatic solvents. The swelling effect of DMSO was believed to be substantial as PET was completely depolymerised, with an 82% yield of BHET, in 1 minute with a zinc acetate catalyst at 190 °C.

As mentioned above, strategies aimed at removing product *in situ*, to manipulate reaction equilibrium, thereby favouring the generation of additional product, have been developed to enhance reaction yields. Glycolysis of PET was undertaken in the presence of xylene at temperatures of 170 – 245 °C for 3 hours.²⁶⁰ PET was completely degraded in this timeframe, yielding 80% BHET with the remainder of the products consisting of BHET dimer. Here the authors proposed that the depolymerised products were preferentially moving into the xylene phase of the reaction mixture, preventing them from re-forming PET oligomers. An additional benefit of xylene was the easy isolation of reaction products as they were seen to crystallise out of solution once the reaction had been cooled.

Tanaka *et al* pioneered a novel approach of favouring the forward reaction of PET methanolysis by trapping ethylene glycol via a secondary reaction with a co-solvent (Fig. 5.3).²⁶¹ After methanolysis had successfully produced dimethyl terephthalate (DMT) and ethylene glycol from PET, ethylene glycol underwent a further transesterification with dimethyl carbonate (DMC) to yield ethylene carbonate (EC) and methanol, effectively removing ethylene glycol from the system. Due to the stability of EC's five-membered ring, the reverse reaction between the glycol and DMT was suppressed. This approach was validated by the higher yields of dimethyl terephthalate and EC, when compared with the yields of DMT and ethylene glycol achieved when no co-solvent was present or THF was used as a co-solvent (Tab. 5.1).



Figure 5.3 – Scheme of methanolysis procedure described by Tanaka ⁵, the formation of ethylene carbonate (EC) by a secondary reaction between ethylene glycol and dimethyl carbonate prevents the backwards reaction, favouring PET depolymerisation.

The authors experimented with the ratios of DMC: methanol, with the optimum (1.5 mL: 0.2 mL) successfully depolymerising PET after 5 hours at ambient temperature with a 5% loading of catalyst. The authors do not conclusively explain why PET is degraded at such a low temperature (28 °C) however. One significant claim they do make is that DMC, as a relatively benign chemical, is an improvement over previous ambient temperature depolymerisations of PET, as they were dependent on halogenated solvents.

Table 5.1 – Percentage yields of PET monomers obtained via methanolysis with no co-solvent, THF as a co-solvent or DMC as a co-solvent. The swelling effect of THF and DMC can be seen in the improved yields, whilst the trapping of EG in EC prevents back reactions, producing the highest yield (28 °C, 5 hrs).

Co-Solvent	DMT Yield	EG Yield	EC Yield
N/A	18 %	22%	N/A
THF ^a	47%	53%	N/A
DMC ^a	86%	14%	75%

^a- Methanol: Co-solvent Ratio = 1:3

Pham and Cho reported one such example where methanol and dichloromethane (DCM) were mixed in equimolar amounts, with a 50 molar excess with respect to PET. ²⁶² When potassium carbonate (K₂CO₃) was used as a catalyst, PET was degraded at 25 °C in 24 hours with a DMT yield of 93.1%. Once again, the authors do not postulate a concrete reason as to why the reaction is able to proceed at ambient temperature, as opposed to the usual harsh

temperatures (170 – 240 °C). Potassium carbonate is a moderate base, with the potassium cation and carbonate anion expected to dissociate well (Fig. 5.4). Potassium carbonate also exhibits excellent solubility in methanol (3.11 g/100g of MeOH).²⁶³ The excellent solubility of potassium hydroxide in methanol, combined with its moderate basicity enables the base-catalysed methanolysis of PET to take place (Fig.5.5).

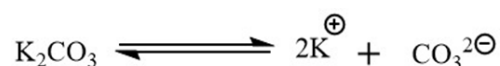


Figure 5.4 – Dissociation of potassium carbonate to its conjugate acid and base when dissolved in an aqueous medium.

The availability of potassium carbonate's conjugate acid in methanol, combined with the swelling effect of DCM on PET and the long reaction time, could all be essential factors to enable the depolymerisation to occur at 25 °C.

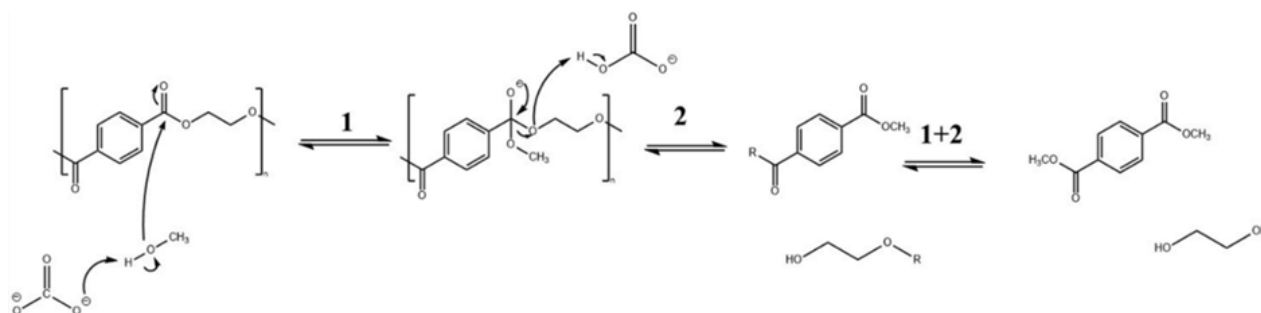


Figure 5.5 – Mechanistic pathways for base-catalysed methanolysis of PET.

Whilst these contributions to the literature have undeniably advanced the state of PET solvolysis, either by increasing turnover through reduced reaction times or lowering the energy costs through temperature reduction, questions still remain around how wasteful PET solvolysis is. In order to overcome the limitations of the shrinking core-model, or lower the reaction temperature, increasingly complicated solutions of solvents/co-solvents/catalysts have been developed. This creates a mixture of chemicals that need to be disposed of or purified once the reaction has taken place.

5.1.2 Is PET Solvolysis Sustainable from a Solvent Waste Point of View?

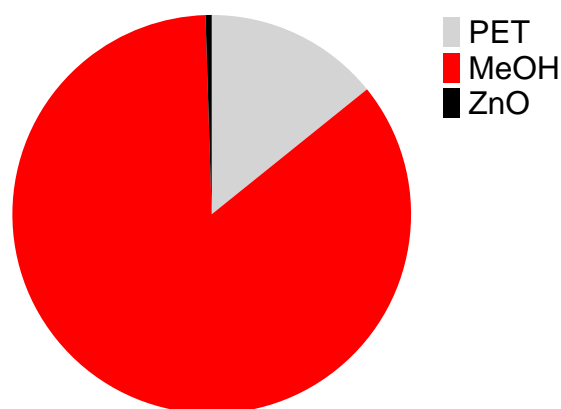
The simplest PET solvolysis reaction mixture needs to contain three components: PET, the solvent (also the nucleophile) and a catalyst. To ensure a favourable S:V and, drive product formation, very large excesses of the solvolytic agent are typically employed. Whilst PET is not soluble in the solvents commonly used, the monomers produced by the reaction are – requiring an additional purification step.

Two common approaches are seen in the literature for the isolation of monomers from the reaction mixture:

1. Cooling of the reaction mixture ($\approx 12\text{ }^{\circ}\text{C}$) to precipitate monomers, typically used to isolate DMT from a crude PET methanolysis reaction mixture.^{258,121}
2. Addition of a large excess of water to precipitate the monomers, which can then be filtered off from the solvent. This purification is reported for use after both glycolysis and methanolysis of PET.^{102, 122}

When determining how wasteful a given process is, and by extension how sustainable or “green” it is, these purification steps cannot be ignored. The final fate of the reaction and purification solvents (disposal, cleaning, re-use) also must be taken into account.

The least wasteful PET solvolysis route from a solvent mass point of view would be one which uses no additional solvent for purification. *Du et al* published a successful methanolysis of PET catalysed by zinc oxide nanoparticles (ZnO), where DMT, obtained from PET at $170\text{ }^{\circ}\text{C}$ after 15 minutes, was isolated by simply cooling the reaction.²⁶⁴ The relative proportions of PET, solvent and catalyst used in the procedure by mass are shown (Fig. 5.6), and the large excess of solvolytic agent compared to the polymer is stark.



E-Factor = 6.04

Figure 5.6 – A representation of how the total mass of the solvolytic system of ZnO-catalysed methanolysis of PET

The E-Factor (Eq. 5.1) has been calculated for this methanolysis reaction. E-factor was coined by Roger Sheldon in 1992 to encourage chemists to measure how much waste a reaction generated and not be solely concerned with the product yield.²⁶⁵ The simple equation shown below allows for a quick diagnosis of how wasteful a reaction is, in addition to enabling easy comparisons between different reactions. A process with an E-factor of 0 would be considered to possess a “perfect score”.

$$\text{E-Factor} = \frac{\text{mass of total waste}}{\text{mass of product}}$$

Equation 5.1 – Calculation of E-factor.

Where the quantity of solvent used in the purification step has been reported, E-factor has been calculated for the reaction alone, and with purification solvents being considered (Fig. 5.7). This has been done to demonstrate just how wasteful many solvolytic routes for PET recycling become after monomer isolation is performed. For example, when glycolysis of PET described by *Chen et al* is considered, the E-factor does not appear unreasonable (2.02) as 80 g of PET was depolymerised using 160 g of ethylene glycol (Fig. 5.7a).¹²² But when the 800 g of water used in the purification of the BHET monomer is taken into account a far less favourable value is obtained (12.02) (Fig. 5.7b).

In the previous section, several examples of PET solvolysis were reviewed where the primary aim was to reduce the reaction time or lower the temperature. These objectives were achieved by addition of a second solvent to the reaction mixture, which generates a new challenge concerning the separation of these different solvents out from the depolymerised products, and then from each other. Pie charts have been constructed (Fig. 5.7) demonstrating how large excesses of these solvents are required to first of all depolymerise PET and then isolate the products.

Like many research articles, the work referenced above does not describe how the reaction mixture was cleaned/disposed or whether it was re-used. It is presumable that some method of solvent removal would be required to enable separation on the laboratory scale, however. In 2011 Phillip Jessop outlined four grand challenges for green chemistry, the final of which was the elimination of distillation as a purification strategy.²⁶⁶ He argues that the high energy costs, and the need for at least one of the solvents to be volatile require that alternative approaches to purification need to be identified.

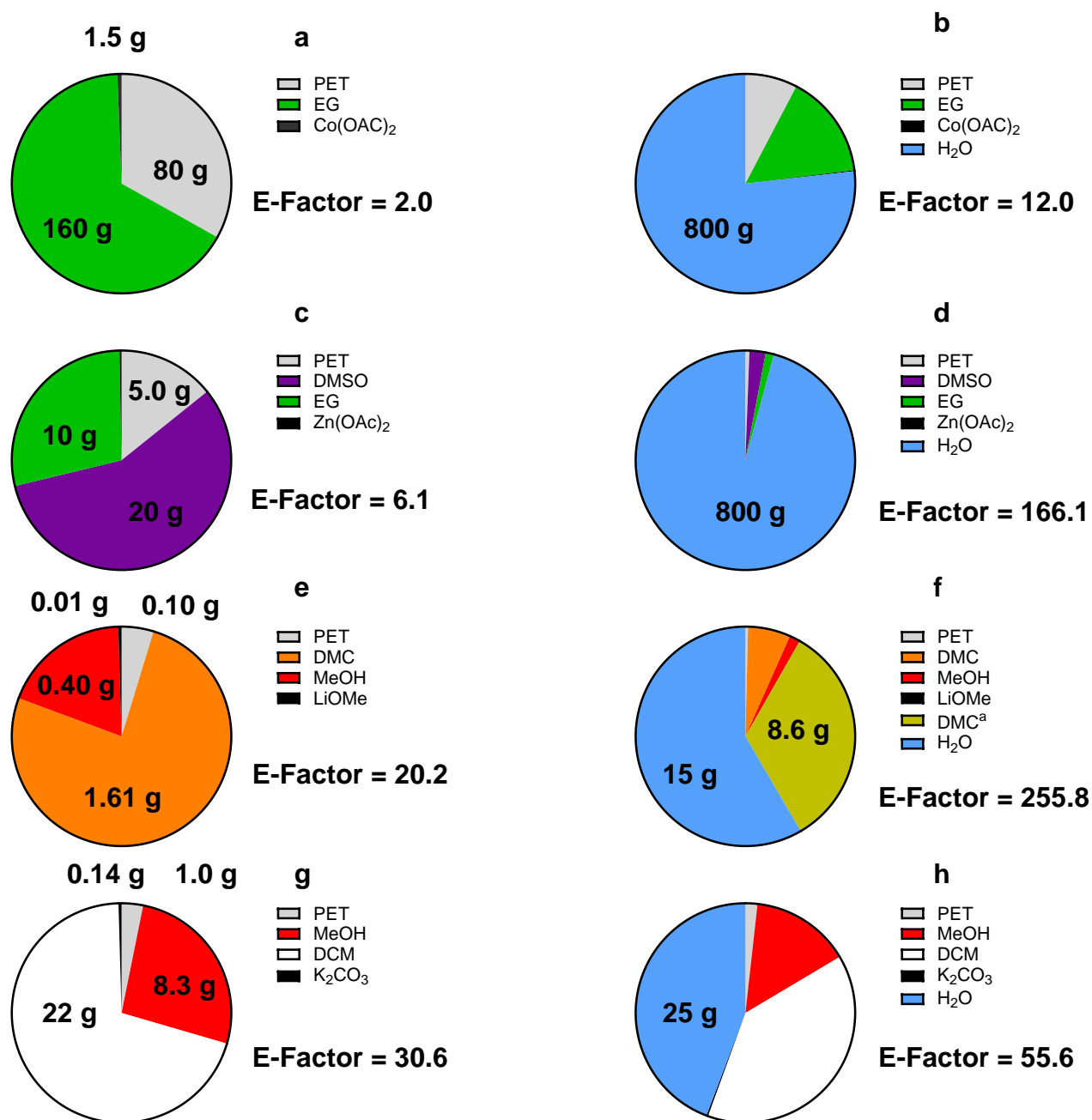


Figure 5.7 – Graphical representations of the total mass distribution of solvolytic systems for PET depolymerisation reaction mixtures (a,c,e,g) and the same reactions also accounting for use of purification solvents (b,d,f,h). The corresponding E-factors indicate these processes are far less sustainable once purification is considered.

a,b - Studies of Glycolysis of Poly(ethylene terephthalate) Recycled from Postconsumer Soft-Drink Bottles, .Influences of Glycolysis Conditions ¹²²

c,d - Ultrafast Homogeneous Glycolysis of Waste Polyethylene Terephthalate via Dissolution-Degradation Strategy ²⁵⁹

e,f - Capturing ethylene glycol with dimethyl carbonate towards depolymerisation of polyethylene terephthalate at ambient temperature ²⁶¹

g,h - Low-energy catalytic methanolysis of poly(ethylene terephthalate) ²⁶²

5.1.3 PET Solvolysis in Supercritical Carbon Dioxide

Utilising scCO_2 as the medium for solvolysis of PET would enable the challenges surrounding the large volumes of waste solvent generated to be overcome. Specifically, the simple isolation of CO_2 from the crude reaction mixture by reducing the pressure and converting it back into a gas removes the need for any distillation. Moreover, the tuneable density of scCO_2 opens routes to selectively dissolving one component of a reaction mixture and removing it via supercritical extraction – eliminating the need for precipitation, or extraction of monomers into halogenated solvents.

When the experimental work outlined in this chapter was conceptualised, only one publication describing a protocol to depolymerise PET in scCO_2 had been published where Li *et al* reported hydrolysis of the polymer with a sulfated titanium dioxide solid acid catalyst.²⁶⁷ Conversion of PET exceeded 90%, with 94% and 87% molar yields of TPA and ethylene glycol respectively, after 6 hours at 150 bar and 160 °C. Whilst the authors acknowledge the benefits the swelling effect of scCO_2 has on the reaction rate, by enabling better access to the polymer's internal structures thereby overcoming the limitations of the shrinking core model, they do not take advantage of the potential to also use scCO_2 as a medium for monomer purification. Although the quantities of solvents used in the isolation of TPA and ethylene glycol are not specified, the authors do confirm that ethylene glycol is washed out of the crude with water, and TPA is removed with DMSO. These multiple purification steps would add additional solvent removal, cleaning and disposal steps to an industrial process, and would produce less favourable numbers from an E-factor calculation. It is also noteworthy that the exceptionally high boiling point of DMSO (189 °C) makes isolation of TPA by distillation challenging.

Over the course of this project, interest in utilising sub and supercritical CO_2 has started to gain momentum in the literature. It has already been outlined in Chapter 1 how supercritical methanolysis of PET is an efficient, catalyst-free route to DMT and ethylene glycol. However, the

extreme conditions required to achieve the supercritical state of methanol ($T_c=240\text{ }^{\circ}\text{C}$, $T_p=80.8\text{ bar}$) create a high energy demand and present significant safety issues. Addition of scCO_2 to a supercritical methanolysis reaction has been investigated in order to increase monomer yields and reduce the required temperature.

Liu and Yin found that a DMT yield of only 25% was achieved when PET underwent methanolysis at $270\text{ }^{\circ}\text{C}$ with a methanol-to-PET mass ratio of 6:1 after 20 minutes.²⁶⁸ However, when the reactor was charged with an initial 15 bar of CO_2 before heating, a 75% yield was achieved in the same residence time – increasing to 95% after 40 minutes (Fig. 5.8). Interestingly, if the initial pressure of CO_2 was increased above 15 bar, the yield of DMT was seen to fall: 70% DMT yield resulted from methanolysis with an initial CO_2 pressure of 50 bar. It was postulated that CO_2 , once it had reached its supercritical state at reaction conditions, was able to swell PET and improve methanol's access to the polymer – leading to the enhanced yields. The reduction in DMT yield at initial CO_2 pressures $>15\text{ bar}$ was attributed to the increasing proportion of CO_2 diluting methanol's concentration, reducing the likelihood of methanol coming into contact with PET and initiating degradation of the polyester backbone.

Addition of scCO_2 has also been shown as a pathway to catalyst-free methanolysis of PET, whilst keeping methanol sub-critical.²⁶⁸ Shen *et al* built-on Liu and Yin's work by increasing the initial loading of CO_2 into the autoclave from 15 to 20 bar, allowing 100% PET conversion, with a 79% DMT yield, at $220\text{ }^{\circ}\text{C}$ after 50 minutes – below the critical point of methanol.

PET has also been converted into TPA and ethylene glycol via hydrolysis with a zeolite catalyst in scCO_2 .²⁶⁹ Full conversion was achieved after 5 hours at $210\text{ }^{\circ}\text{C}$ under a pressure of 75 bar, with a 72.3% yield of DMT. The authors used the Arrhenius equation to calculate the activation energy for the PET hydrolysis at several different pressures and found that an increase from ambient pressure to 75 bar decreased the activation energy, but it then increased for hydrolysis conducted at 125 bar (Tab. 5.2).

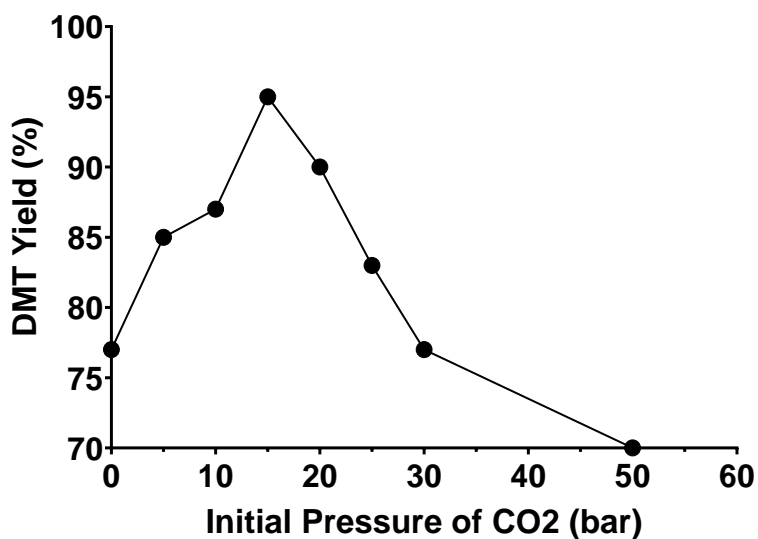


Figure 5.8 – Effect of initial CO₂ pressure on DMT yield. Temperature = 270 °C, Time = 40 minutes, 6:1 weight ratio of methanol to PET.

Table 5.2 – Activation energies for hydrolysis of PET catalysed by Z5₇₀ zeolite under differing pressures.

Pressure (bar)	Activation Energy (kJ/mol)
0	249.9
25	209.6
75	189.9
125	200.1

The authors postulate that below 125 bar the only effect of scCO₂ on the polymer is to swell it, improving access for reacting species, whereas the supercritical fluid begins to induce crystallisation once 75 bar is exceeded, which is in line with literature precedent discussed in Chapter 3. It is noteworthy that they only study the hydrolysis at three pressures (25 bar, 75 bar and 125 bar) and they refer to all of them as supercritical conditions. CO₂ at 25 bar and ≈ 200 °C is gaseous, whilst increasing the pressure to 75 bar will just breach the critical pressure of CO₂, meaning that only the highest studied pressure is reasonably inside the supercritical region of

CO₂. The authors do not explicitly state that they are using CO₂ in at least two different states of matter, and this may go some way toward explaining why they see differences in the activation energy.

Researchers at the University of Kansas and the National Renewable Energy Laboratory (NREL) explored whether subcritical CO₂ could be used to improve hydrolysis of PET to TPA and ethylene glycol.²⁷⁰ They found that charging a high-pressure cell with 14 bar of CO₂ before heating the hydrolysis reaction mixture to 200 °C gave a high yield of TPA (83%). This is believed to be a result of an *in situ* formation of carbonic acid between CO₂ and water (Fig. 5.9), which can then go on to catalyse PET hydrolysis.²⁷¹ The critical role of carbonic acid was confirmed by running control experiments where CO₂ was replaced with an equivalent pressure of nitrogen, and far lower yields were obtained.

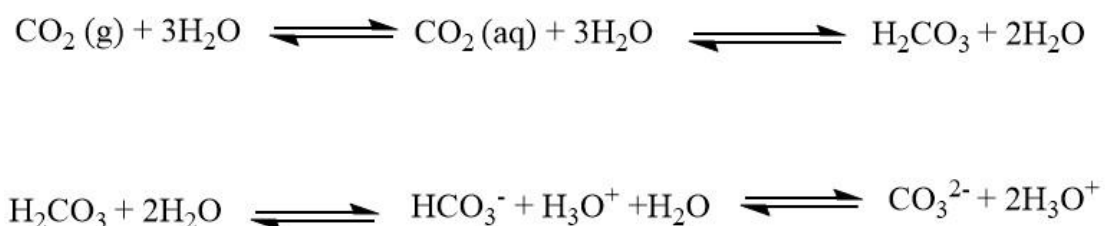


Figure 5.9 – Carbonic acid formation (top) when CO₂ is dissolved in water. The carbonic acid formed *in situ* then dissociates to bicarbonate (HCO₃⁻) and carbonate (CO₃²⁻) ions, which is accompanied by a lowering of the pH.²⁷⁰

scCO₂ has also been studied as a pre-treatment to aid enzymatic hydrolysis of PET.²⁷² A

significant limiting factor to this hydrolysis is the polymer surface area available for the enzyme to act on. PET was soaked in scCO₂ for 2 hours at 250 °C, the autoclave was charged with 60 bar CO₂ prior to this heating, with new pores being induced in the PET morphology via swelling. These pores were confirmed visually by transmission electron microscopy (TEM), and the scCO₂-treated PET produced a yield of TPA double that of the untreated PET for the same hydrolysis conditions of 55 °C and 288 hours.

Pie charts illustrating the relative masses of PET, catalysts, nucleophile/solvent and scCO_2 are shown (Fig. 5.10) and it can be seen that movement toward a more favourable distribution of the masses in the reaction system (a smaller proportion made up by organic solvents that are hard to recycle or dispose of) has taken place when compared to solvolysis examples that depend on conventional solvents only (Fig. 5.7). Unfortunately, the previous literature on scCO_2 solvolysis reviewed here does not specify the amount of organic solvent used in the purification of the monomers, so E-factor was not calculated for purifications.

5.1.3.1 Limitations of the Current Literature

PET solvolysis using scCO_2 as the primary medium, or as a co-solvent, has been clearly demonstrated by the above examples. However, they all suffer from the same issues surrounding the use of additional solvents to purify the monomer post-depolymerisation seen across the chemical recycling literature. The publications discussed above all mention how the swelling effect scCO_2 has on PET can lead to shorter reaction times and enhanced yields, but they do not make the point about how the simple removal of CO_2 from a reaction system makes the solvent easily recyclable, and therefore outcompetes more traditional solvolysis routes in terms of solvent wastage, or how the established use of scCO_2 as a medium for extraction could present a route to generating pure monomer without additional purification solvents.

None of the above publications confirm how much solvent is used to separate TPA or ethylene glycol from the crude reaction mixture, but they all make use of water or DMSO. Both of these solvents have high boiling points (189 °C for DMSO, 100 °C for water), meaning that either a second anti-solvent would be required to precipitate the products or energy-consuming distillation would be needed.

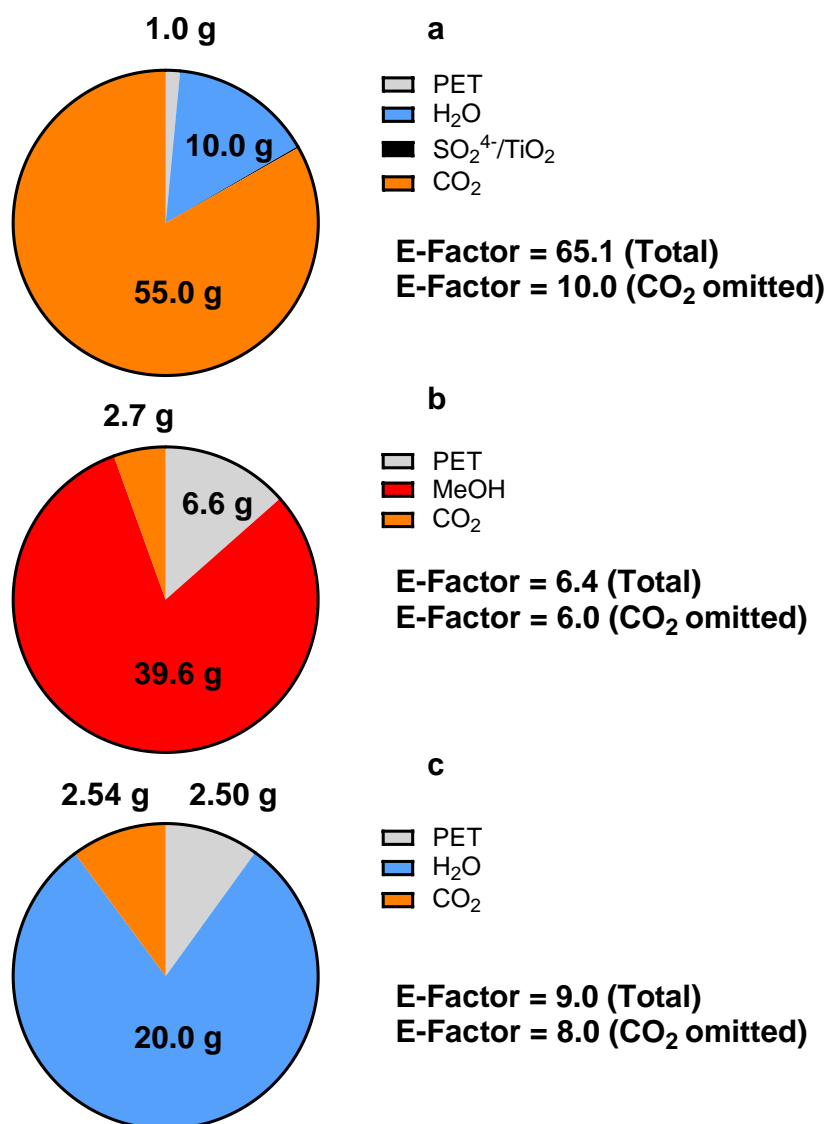


Figure 5.10 - A representation of how the total mass distribution of scCO₂-assisted solvolysis of PET vary (a,b,c) .

The corresponding E-factors have also been calculated for the depolymerisation step, but no calculation is included for purification as the quantities of solvent used were not specified. However, due to the simple recyclability of CO₂ an E-Factor calculation has been included where CO₂ is omitted from the waste portion of the equation.

a - Reaction Kinetics and Mechanism of Catalysed Hydrolysis of Waste PET Using Solid Acid Catalyst in Supercritical CO₂²⁶⁷

b – CO₂ -enhanced PET depolymerization by catalyst free methanolysis²⁶⁶

c - Subcritical CO₂–H₂O hydrolysis of polyethylene terephthalate as a sustainable chemical recycling platform²⁷³

None of the above publications confirm how much solvent is used to separate TPA or ethylene glycol from the crude reaction mixture, but they all make use of water or DMSO. Both of these solvents have high boiling points (189 °C for DMSO, 100 °C for water), meaning that either a

second anti-solvent would be required to precipitate the products or energy-consuming distillation would be needed.

Pie charts have been devised which illustrate the relative mass proportions of the CO₂ solvolysis reaction components (Fig. 5.10). Generally, a more favourable distribution of the relative masses can be seen when these CO₂-assisted solvolysis reactions are compared to the conventional protocols in section 5.1.2, as there is a lower reliance on organic solvents which need to be disposed of or cleaned post-reaction. Furthermore, if CO₂ is disregarded from the E-factor calculation, due to its simple removal from a reaction mixture facilitating recyclability, then values far closer to 0 are achieved – demonstrating that these processes are considerably less wasteful.

5.1.4 Supercritical Extraction as a Route Towards Monomer Purification

Both the conventional and CO₂ assisted solvolysis routes make use of traditional solvents, commonly water, DMSO or chloroform, to remove monomers from the crude reaction mixture. scCO₂ itself is a proven medium for extraction of materials, and it is currently underexplored as a pathway to producing pure monomers from polymer solvolysis.

The tuneable density of scCO₂ enables selective dissolution of one component in a reaction mixture, which can then be easily removed by flowing CO₂ through the reaction vessel. The high diffusivity of scCO₂, and the excellent mass transfer properties this imparts, allows for short extraction times when compared to a more conventional extraction technique - such as Soxhlet. scCO₂ extraction boasts an additional benefit over Soxhlet extraction as it avoids the need to heat hazardous organic solvents above their boiling point for extended periods of time.²⁷⁴

Early examples of scCO₂ extraction concern removal of vegetable oils from rapeseed and sunflower seeds.^{275, 276} Yields up to 46% were achieved at 300 bar and 40 °C, showing that

scCO₂ was a viable alternative to hexane. The facile removal of CO₂ from the oils by lowering the pressure avoided the health concerns that arise from residual hexane in vegetable oils for human consumption.

Perhaps the most widely known use of scCO₂ extraction is the production of decaffeinated coffee.²⁷⁷ The reusability of CO₂, alongside the fact that both the extracted caffeine and remaining decaffeinated coffee can be sold as valuable products, has created a cost-effective process.²⁷⁸ When water is employed as a co-solvent, high yields of caffeine (>90 %) can be produced in two hours.^{279, 280}

scCO₂ has also been applied to the field of plastic recycling, as a strategy for additive removal from plastic materials. If these additives are not separated from the bulk material, they can damage the plastic properties in mechanical recycling, through undesirable side reactions during melt extrusion, or act as contaminants during chemical recycling.²⁸¹

Additives designed to protect PP from degradation (Irfagos 168 and Irganox 1010) have been removed in a scCO₂ medium after 30 minutes at 50 °C across a range of pressures (76 bar to 405 bar).²⁸² Similar results have been observed for the removal of polybrominated diphenyl ethers (PBDE), a common flame retardant, from polystyrene (PS).²⁸³ Over 97% of the PBDE was removed when PS soaked in d-limonene was exposed to scCO₂ at 200 bar and 65 °C for 40 minutes.

To explore the viability of scCO₂ on a realistic sample, *Singh et al* doped plastic cups made from PP, PET and PLA with a range of contaminants that these materials could reasonably come into contact with during their lifetime.²⁸⁴ The United States Food and Drug Administration (FDA) has compiled a list of contaminants (they describe them as surrogates) that plastic materials have been known to be exposed to by consumers, and they recommend researchers working on recycling test that their novel technologies are able to remove these species.²⁸⁵ When the plastic materials were decontaminated in scCO₂ at 80 °C for 10 minutes, PP displayed the

highest decontamination efficiency (85.0%) whereas PET and PLA possessed decontamination efficiencies of 69.9% and 76.7% respectively. Small increases in these values were seen when the extraction time was increased to 60 minutes, but the same trend, where PP was decontaminated more thoroughly than PLA or PET, was retained. This is believed to be due to CO₂ exhibiting poorer diffusivity into PET and PLA, meaning it is less able to swell these polymers compared to PP at the same conditions.²⁸⁶

5.1.5 Aims and Objectives

Use of scCO₂ as a medium for PET solvolysis and removal of plastic additives in separate scenarios has been demonstrated in the literature. However, there are two drawbacks to the current state of CO₂-assisted PET solvolysis.

1. Although CO₂ is often described as the solvent in CO₂-assisted solvolysis, a significant amount of water or methanol is used as well. This nullifies the simple removal of the supercritical solvent through depressurisation, as the residual water or methanol must still be isolated from the products.
2. Purification of the monomers post-solvolysis still requires large amounts of traditional solvents. This creates additional solvent waste that must be cleaned up and disposed.

Accordingly, the overall aim of the work discussed in this chapter is to demonstrate a route for CO₂-assisted solvolysis, by reducing the nucleophile concentration to (close to) stoichiometric quantities whilst using scCO₂ as the major component of the solvolysis system. Further to this, the solvent-demanding purification steps will be eliminated. This will be accomplished either by judicious selection of the supercritical conditions, to selectively dissolve a single monomer which may then undergo scCO₂ extraction, or by treating the crude reaction mixture with ethylene glycol to produce BHET without any pre-treatment.

The specific objectives are as follows:

1. Identify a solvolytic system capable of depolymerising PET in a scCO_2 medium. As PET itself is not soluble in scCO_2 , but can be swollen, it is necessary to devise a system where the nucleophile and catalyst form a homogeneous solution with the supercritical fluid, so they may be efficiently transported into contact with PET.
2. Successfully depolymerise PET to monomers in the aforementioned supercritical solvolytic system, to give a low-waste, closed-loop route for PET recycling.
3. Ascertain a scCO_2 pressure and temperature where one monomer is selectively dissolved over all other reaction components, then undertake a series of scCO_2 experiments to prove this as a viable method for monomer isolation.

5.2 Experimental

5.2.1 Solubility Testing of Supercritical Solvolytic Systems

Methanol (0.13 mol, 5.26 mL) was mixed with TBD (0.36 g, 2.59×10^{-3} mol) and placed into a glass sample holder. This sample holder was placed into a double-ended high pressure view cell (100 ml), which was charged with CO₂ (55 bar) at room temperature. The view cell was then heated to 85 °C, and the pressure was steadily increased until the MeOH-TBD solution exited the sample holder and formed a homogeneous solution with scCO₂.

5.2.2 Methanolysis of Polyethylene Terephthalate in Supercritical Carbon Dioxide

Methanol in three molar ratios with respect to the PET repeating unit (Tab. 5.3) was mixed with (TBD) (0.36 g, 2.59×10^{-3} mol) and deposited into the base of a high-pressure autoclave (60 mL). PET (5 g, 2.60×10^{-2} mol) was added and the autoclave was charged with CO₂ (55 bar) at room temperature. The autoclave was then heated to the target temperature (140 °C, 160 °C, 170 °C, 180 °C) where the pressure was made up to 172 bar. The autoclave was held at reaction conditions for the desired residence time (0.5 hrs, 1.0 hrs, 3.0 hrs) before the heating was discontinued. The autoclave was allowed to cool to room temperature, and CO₂ was vented once a temperature of 25 °C was reached. A dry, brown, lumpy solid was recovered from the autoclave base via extraction into chloroform. The solvent was removed *in vacuo* and conversion was calculated.

Table 5.3 – Methanol: PET ratios of the solvolysis experiments attempted in this chapter.

PET (g)	MeOH: PET (molar equivalents of MeOH: PET repeat units)	MeOH (moles)	MeOH (ml)
5.00	5:1	1.30×10^{-1}	5.26
5.00	3:1	7.80×10^{-2}	3.16
5.00	1:1	2.60×10^{-2}	1.05

5.2.3 Transesterification of Crude Methanolysis Product to BHET

Crude methanolysis product (3 g), prepared from PET degraded with a 5:1 molar excess of methanol at 180 °C, was heated to 130 °C with an excess of ethylene glycol (2.64 ml, 4.68×10^{-3} mol) for 2 or 4 hours. The product was cooled to room temperature, giving a beige solid which was then suspended in deionised water (10 mL). A white, lumpy product was extracted by gravity filtration.

5.2.4 Solubility Testing of PET monomers in Supercritical Carbon Dioxide

PET monomer (0.5 g) was added to a glass holder and placed inside the view cell (100 mL). The view cell was charged with CO₂ (55 bar) at room temperature, after which the cell was heated to 65°C. Once this temperature was reached, pressure was steadily increased by pumping in additional CO₂ until the monomer formed a homogeneous solution with scCO₂, or the maximum working pressure (278 bar) was reached.

5.2.5 Supercritical Extraction of Dimethyl Terephthalate and PET Oligomers

Crude methanolysis product (5 g), prepared from PET degraded with a 5:1 molar excess of methanol at 180 °C, was placed in the bottom of a high-pressure autoclave (60 mL) which was then charged with CO₂ (55 bar) at room temperature. The autoclave was then heated to 65 °C, and the pressure was made up to 248 bar. These conditions were held for 1 hour, after which

scCO₂ extraction was performed for various times (15 minutes, 30 minutes, 60 minutes) to yield a dry, free-flowing white powder collected from a liquid nitrogen trap at the end of the extraction pipework.

5.2.6 Nuclear Magnetic Resonance (¹H NMR, ¹³C NMR)

Supercritical depolymerisation products of PET, as well as monomer standards, were dissolved in d-CDCl₃ (30 mg/ml) and were analysed by ¹H and ¹³C, nuclear magnetic resonance (NMR) spectroscopy. Experiments were carried out on a Bruker DPX 400 MHz spectrometer or a Bruker DPX 500 MHz spectrometer. Chemical shifts were assigned in parts per million (ppm). All spectra obtained at ambient temperature (22 ± 1 °C). MestReNova (Mestrelab Research S.L.) was used for analysing the obtained spectra.

5.2.7 Gas Chromatography-Mass Spectrometry (GC-MS)

Crude methanolysis products, and monomer standards, were dissolved in chloroform (HPLC grade, Fisher Scientific) at various concentrations (0.50 mg/mL, 0.25 mg/mL, 0.10 mg/mL, 0.05 mg/mL). Samples were run on an AccuTOF GCx mass spectrometer (Jeol Ltd) with electron impact ionisation using a 30 m stabilwax GC capillary column with a diameter of 0.25 mm and a film thickness of 0.25 µm (Restek). The injector port temperature was 290 °C. The column oven was held at 50 °C for 4 minutes, then heated from 50 °C to 300 °C at 10 °C/min, and was purged constantly with helium.

5.2.8 High Pressure Liquid Chromatography – Mass Spectrometry (HPLC-MS)

Supercritical depolymerisation products of PET, as well as monomer standards, underwent HPLC-MS analysis on a Thermo Ultimate 3000s HPLC fitted with a Thermo Accucore Aq C18 column (dimensions: 150 × 4.6 mm; particle size: 2.7 µm) and a UV/vis detector (254 nm)

connected a Bruker ESI-TOF MicroTOF II. A mobile phase consisting of formic acid (0.01%) in milliQ water, (A) and acetonitrile (B) was used in the below gradient (flow rate: 1 mL/min):

min	A (%)	B (%)
0	95	5
2	90	20
4	85	15
6	80	20
8	60	40
10	55	45
12	50	50
14	45	55
16	40	60
18	35	65
20	30	70
22	25	75
24	20	80
26	0	0

5.2.9 Gel Permeation Chromatography (GPC)

GPC analysis of PET was performed by Dr Daniel Lester at the Polymer Research Technology Platform at the University of Warwick

Supercritical depolymerisation products

Supercritical depolymerisation products were dissolved in DMF (20 mg/ml) and gel permeation chromatography (GPC) was performed with DMF (0.21 % w/v LiBr) (HPLC grade, Sigma-Aldrich) as the eluent at 80 °C using an Agilent PL-gel D column in series with an Agilent PL-gel E column at a flow rate of 1 mL/min. Sample detection was achieved using a differential refractometer (dRI). The system was calibrated using low dispersity poly(methyl methacrylate standards (1.02x10⁶ – 504 g/mol).

PET

PET (25 mg) was dissolved in o-cresol (4 mL) at 100°C overnight, then diluted 1:3 with dichlorobenzene (1.5 mg/ml) and filtered through 10 um frit. GPC was performed with Dichlorobenzene (DCB) (HPLC Grade, Sigma-Aldrich) (DCB) as the eluent at 140°C using an Agilent PL-gel D column at a flow rate of 1 mL/min. Sample detection was achieved using a UV source (λ =254 nm) and a differential refractometer (dRI). The system was calibrated using narrow dispersity polystyrene standards (1.02x10⁶ – 504 g/mol).

5.3 Results and Discussion

5.3.1 Identification of an scCO₂ Solvolytic System for PET

As PET is known to be insoluble in scCO₂, although it can be swollen, it is necessary to develop a system capable of depolymerising PET in a bulk scCO₂ solvent. Water, methanol and ethylene glycol are commonly used as nucleophiles for PET solvolysis as they produce monomers that can be directly polymerised back to PET.

Water and ethylene glycol are sparingly soluble in scCO₂ as they are highly polar molecules, so methanol was selected for testing in the first instance; methanol has excellent miscibility with scCO₂. TBD is an excellent catalyst for solvolysis of PET in conventional solvolysis, due to its high basicity which enables it to deprotonate nucleophiles, increasing reactivity (Fig. 5.11).^{132, 287}

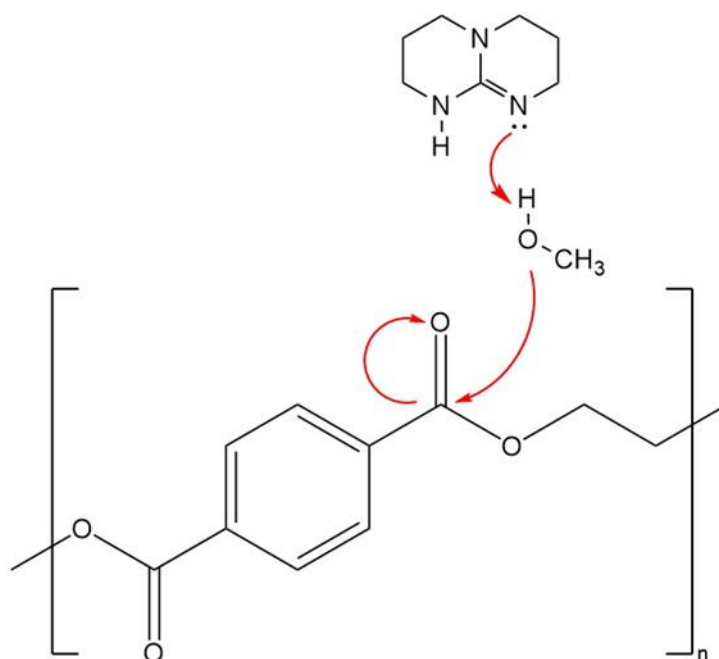


Figure 5.11 – The initial step of TBD-catalysed methanolysis of PET. The lone pair of electrons on the nitrogen in TBD imparts excellent basicity, enabling deprotonation of methanol to produce a highly reactive methoxide.

TBD was exposed to scCO₂ in the high-pressure view cell, so a visible determination of its solubility could be made (Fig. 5.12). The TBD remained in the sample holder when the view cell was charged with 55 bar of CO₂ at room temperature and remained insoluble in scCO₂ across a

range of pressures and temperatures up to 274 bar and 85 °C, as can be seen in the red circle (Fig. 5.12).

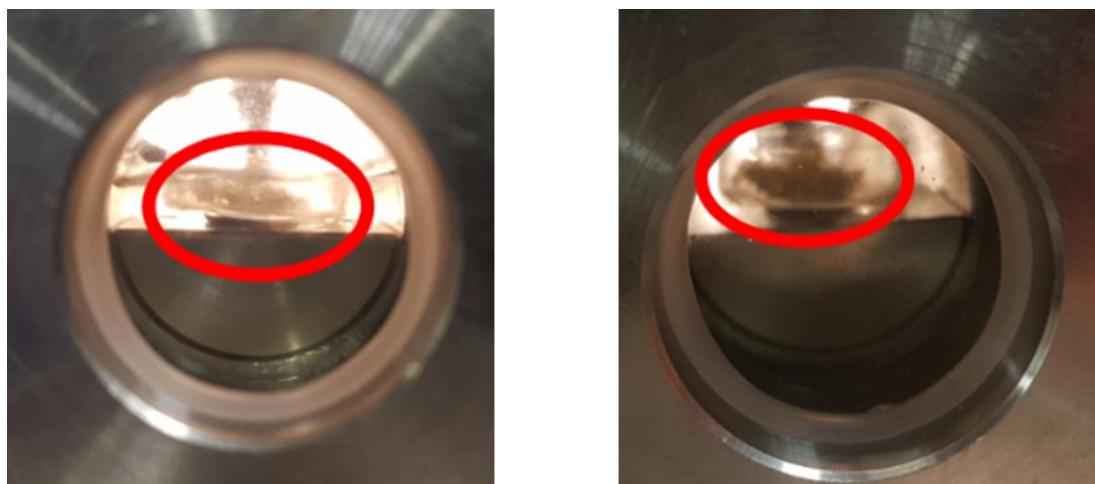


Figure 5.12 – Solubility test of TBD in scCO₂. Solid catalyst is visible when the view cell is charged with 55 bar CO₂ at room temperature (left) and was seen to remain in the sample holder at 274 bar and 85 °C (right), demonstrating insolubility in scCO₂.

TBD, however, is readily soluble in methanol, and a solution of TBD in methanol, was prepared and placed in the high-pressure view cell (Fig. 5.13). The proportions of TBD and methanol were representative of those used to depolymerise PET (0.36 g TBD in 5.26 ml of methanol). Once again, the view cell was charged with 55 bar of CO₂ at room temperature, and heated to 85 °C. Unlike the TBD sample, the solution began to exit the sample holder and form a cloudy solution with the supercritical phase at 103 bar and 45 °C. Once the temperature had reached 85 °C, pressure was steadily increased until the cloudy solution formed a clear, homogeneous solution at 172 bar (Fig. 5.13). This confirmed that TBD could be solubilised in scCO₂ when methanol is used as a co-solvent.

As mentioned in the aims and objectives, it is important to find a solvolytic system where both the nucleophile and catalyst form a homogeneous solution with scCO₂, so they are efficiently transported to PET. For this reason, pressure was increased until the cloudy solution was replaced with a clear, homogeneous one.



Figure 5.13 – Solubility test of a TBD-methanol solution in $scCO_2$. The solution is clearly insoluble in CO_2 of pressure 55 bar at room temperature (left) but was seen to be fully soluble in $scCO_2$ at 172 bar and 85 °C (right).

5.3.2 Supercritical Methanolysis of PET

With a homogeneous reaction system identified, TBD-catalysed depolymerisation of methanol was attempted. A typical temperature of 180 °C and a residence time of 3 hours was found in the literature, and the reaction was conducted as outlined in section 5.2.1 with a 5-molar excess of methanol with respect to PET repeating units.¹³²

5.3.2.1 Conversion for TBD-catalysed Methanolysis of PET in $scCO_2$

Here, conversion of PET is defined as the total mass of the crude product soluble in chloroform ($CHCl_3$) as both monomers and the catalyst are soluble in this solvent, but PET is not. Any insoluble fraction was separated by filtration, dried overnight and then weighed. Conversion of PET was then calculated (Eq. 5.2).

$$Conversion (\%) = 100 \left(\frac{Initial\ Mass\ of\ PET\ (g) - Mass\ of\ Insoluble\ Fraction}{Initial\ Mass\ of\ PET\ (g)} \right)$$

Equation 5.2 – Calculation to determine conversion of PET by TBD-catalysed supercritical methanolysis.

For TBD-catalysed methanolysis in $scCO_2$ at 180 °C for 3 hours, with a 5-times molar excess of methanol to PET, 100 % conversion was achieved, and this degree of conversion was

maintained at lower temperatures (170 °C, 160°C and 140 °C), shorter reaction times (1 hour and 30 minutes) and at smaller molar excesses of methanol.

Full conversion of PET was further confirmed by GPC analysis. The polymer was determined to possess a starting molecular weight of (M_w) of 46,209 g/mol by GPC analysis. (Appendix) When crude methanolysis product was analysed by GPC, peaks in the chromatogram were seen cross the lower limit of the calibration (total permeation), indicating that whilst some of the products may possess a molecular weight of approximately 1000 g/mol, the majority were significantly smaller than this. (Appendix)

5.3.2.2 Selectivity of TBD-catalysed Methanolysis of PET in $scCO_2$

A damp, beige solid was recovered from the autoclave post-reaction, then dissolved in d_3 - $CHCl_3$ and analysed via NMR. Peaks corresponding to DMT are shown by blue dots, whilst ethylene glycol peaks are shown by red dots (Fig 5.14). Peaks with the correct chemical shifts and multiplicity for DMT and ethylene glycol can be seen in the NMR of the crude product, in addition to the expected peaks for TBD - highlighted in red (Fig. 5.15).

When the individual peaks which correspond to DMT are inspected more closely, several shoulders can be observed, highlighted in blue (Fig. 5.15). Furthermore, the relative height of these shoulders compared to the DMT peak increases when the ratio of methanol to PET in the depolymerisation is lowered (Fig. 5.16). This was hypothesised to arise from incomplete depolymerisation of PET to monomers DMT and ethylene glycol, and that short chain oligomers or analogues of DMT had also been formed. Despite this, conversion of PET is still defined as 100 % as a polymer which was insoluble in $CHCl_3$ has been reduced to small molecules capable of being dissolved and processed in a conventional organic solvent. This will be confirmed by GC-MS and HPLC-MS in the following sections.

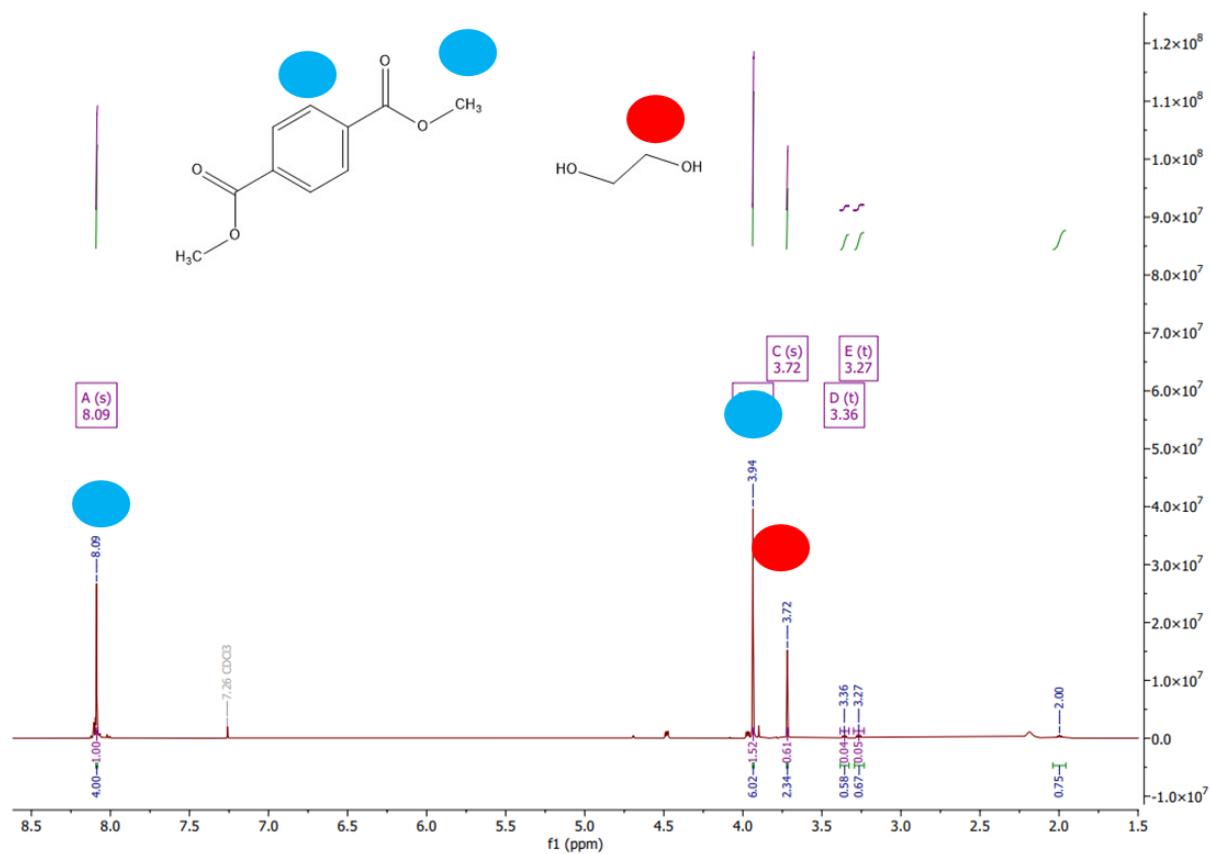


Figure 5.14 – ^1H NMR exhibits peaks with the correct chemical shift, integral values and multiplicity for DMT (blue) and ethylene glycol (red). Alcoholic -OH peak is not seen for ethylene glycol due to proton exchange with the solvent.

Temperature = 180 °C, time = 3 hours, MeOH: PET = 5:1

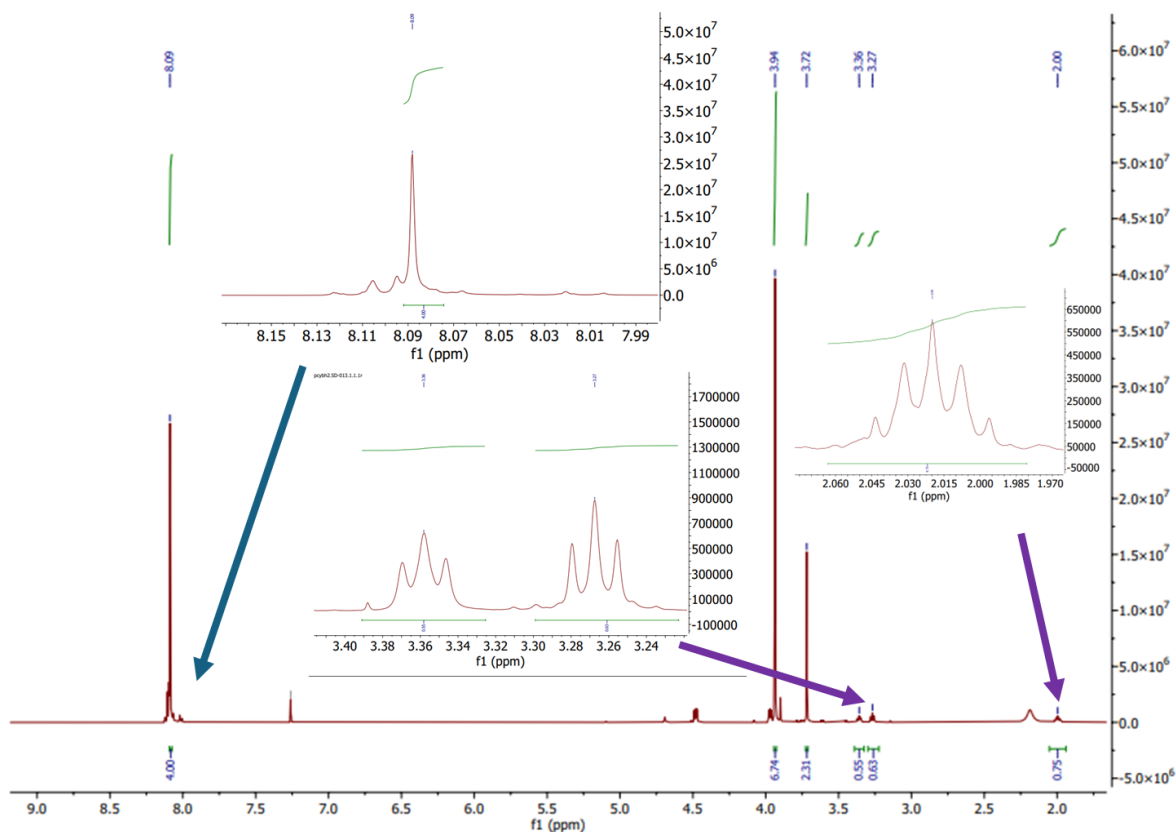


Figure 5.15 – Closer inspection of DMT's aryl peak in the ^1H NMR (blue) reveals the presence of shoulder peaks. Peaks which arise due to the presence of TBD (purple) can also be seen.

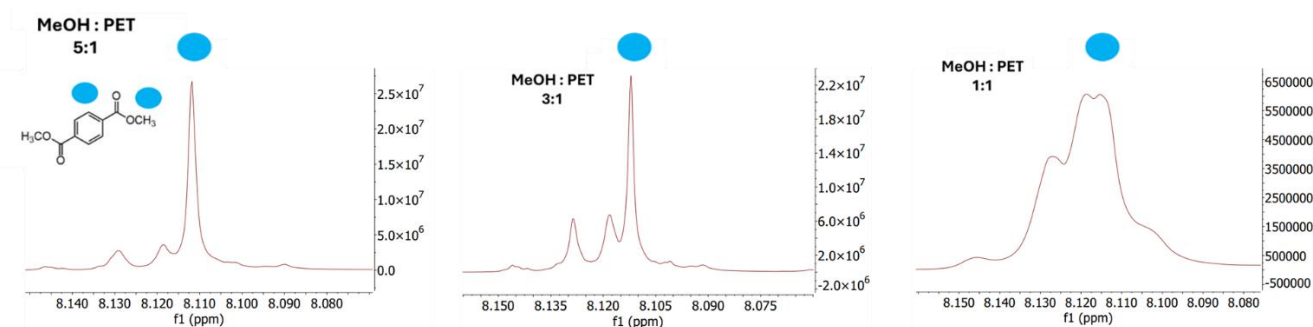


Figure 5.16 – The relative intensity of the shoulders to the DMT aryl peak can be seen to increase as the methanolic content of the reaction mixture is reduced, indicating that a greater proportion of the crude product consists of a mixture of low molecular weight products.

5.3.2.2.1 GC-MS

The total ion current chromatogram (TICC) for scCO_2 methanolysis contains four peaks of interest when PET is degraded with a 5:1 molar excess of MeOH to the PET repeating unit

(Fig. 5.17). The peaks at retention times of 14.25 and 22.87 minutes are exact matches for DMT

and ethylene glycol standards, and analysis of the fragmentation pattern in their mass spectra confirmed the identity of these monomers. (Appendix)

Other peaks at retention times of 18.05 and 27.00 are postulated to arise from the additional low molecular weight products whose peaks were highlighted in the ^1H NMR (Fig 5.15) (Fig. 5.16). The identities of these low molecular weight products are proposed based on the molecular ion in their corresponding mass spectra and analysis of the fragmentation pattern (Tab 5.4). The peak which can be seen at retention times 21.29 minutes is attributed to TBD, once again confirmed by running a standard of the catalyst and analysing the fragmentation pattern in the mass spectrum (Fig. 5.17).

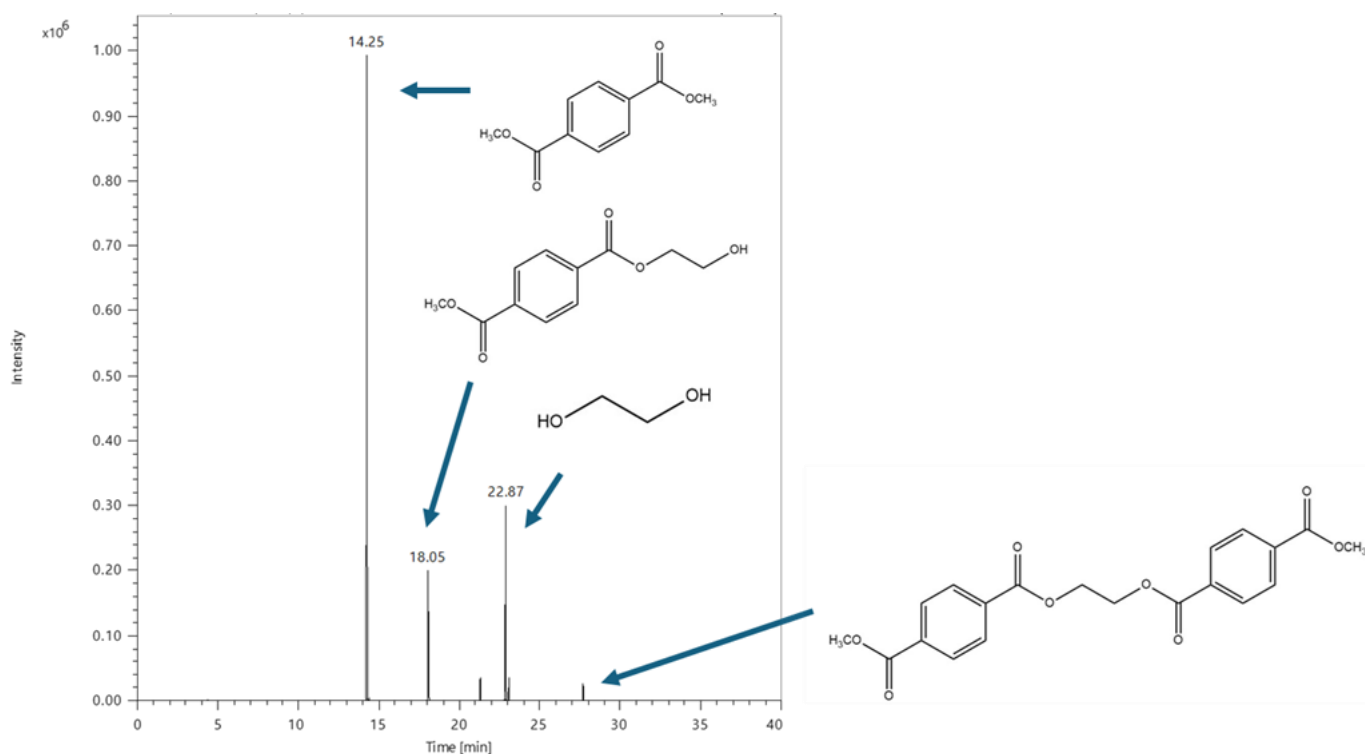


Figure 5.17 – TICC of crude methanolysis product. Peaks which correspond to DMT and EG were confirmed by comparison with standards, whilst the oligomer peaks at $t=18.05$ and 27.68 minutes are proposed based on the m/z which correspond to those retention times.

The identities of the low molecular weight products can be derived mechanistically from the depolymerisation of PET with methanol (Fig. 5.18). Attack on the ester linkage by methoxide, and the following elimination step, will yield products with a methyl ester (red arrow in Fig. 5.18) or an alcoholic end group (blue arrow in Fig. 5.18) only. DMT and ethylene glycol monomers will

be produced (blue box in Fig. 5.18) if there is a large enough excess of methanol to attack every ester linkage in the PET backbone. The 5:1, 3:1 and 1:1 methanol: PET molar ratios used here do not appear to be sufficient to degrade PET all the way to DMT and ethylene glycol, but the additional lower molecular weight products are consistent with the mechanistic pathway. They will also become more abundant, as seen in the GC-MS, at lower methanol: PET ratios as the PET backbone will be degraded to a lesser extent.

The increasing abundance of the additional low molecular weight products can be tracked via GC-MS as the methanol: PET ratio is altered. The relative intensities of the peaks which correspond to DMT, and ethylene glycol, reduce in comparison to the peaks corresponding to the other low molecular weight products as the methanol loading is reduced (Fig. 5.19). This shows that, although PET is fully converted to low molecular weight products by TBD-catalysed methanolysis in scCO_2 there is insufficient methanol in the system to drive the reaction to 100 % monomer (DMT and ethylene glycol) products. As transesterification is known to be an equilibrium, this is not a surprising result. Whilst the selectivity is not 100 % for the monomers, these results are still positive as PET has been degraded to compounds that are far easier to process in conventional solvents. Strategies to “close the loop” and process the crude product to a state where it could be converted back to PET will be demonstrated in section 5.3.3.

The identities of the molecular ions for the peaks seen at 14, 18 and 27 minutes in the TICC, along with the various fragments they give rise to when they undergo ionisation are available (Tab. 5.4) (Tab 5.5) (Tab. 5.6).

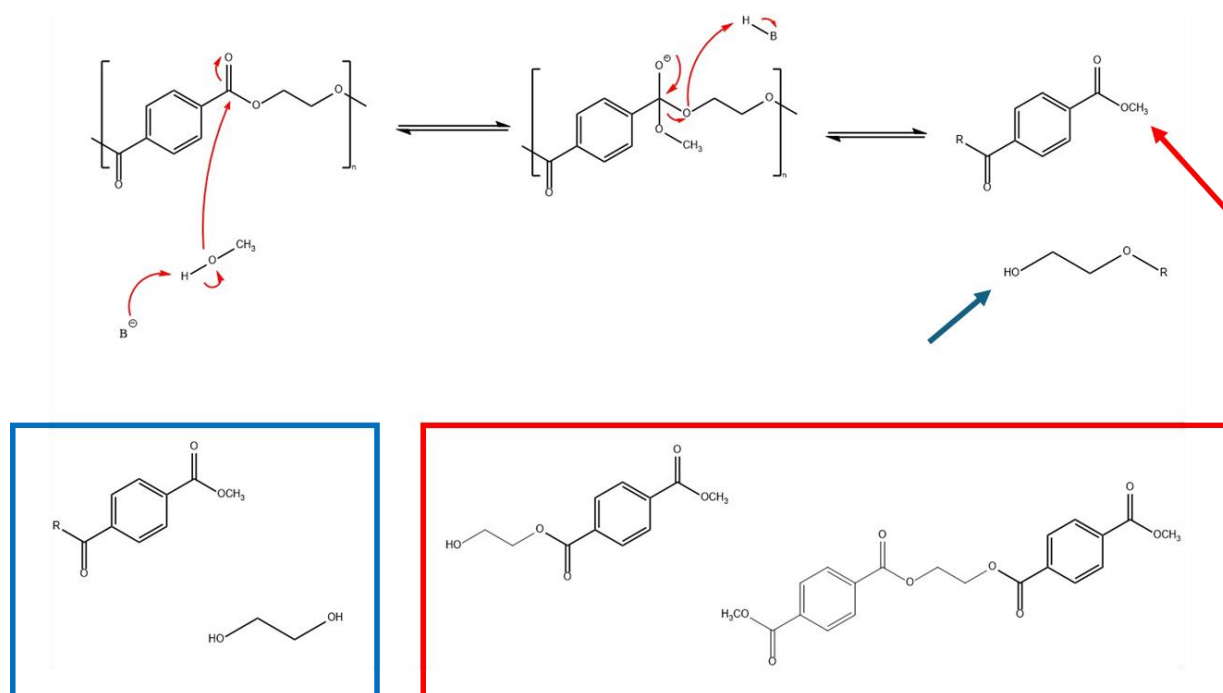


Figure 5.18 – A base-catalysed methanolysis of PET, with the resultant end groups highlighted (top). DMT and ethylene glycol monomers which would result if all ester linkages in the backbone underwent methanolysis (blue box), and other low molecular weight products which would arise from partial backbone degradation – that can be seen in the GC-MS – are illustrated (red box).

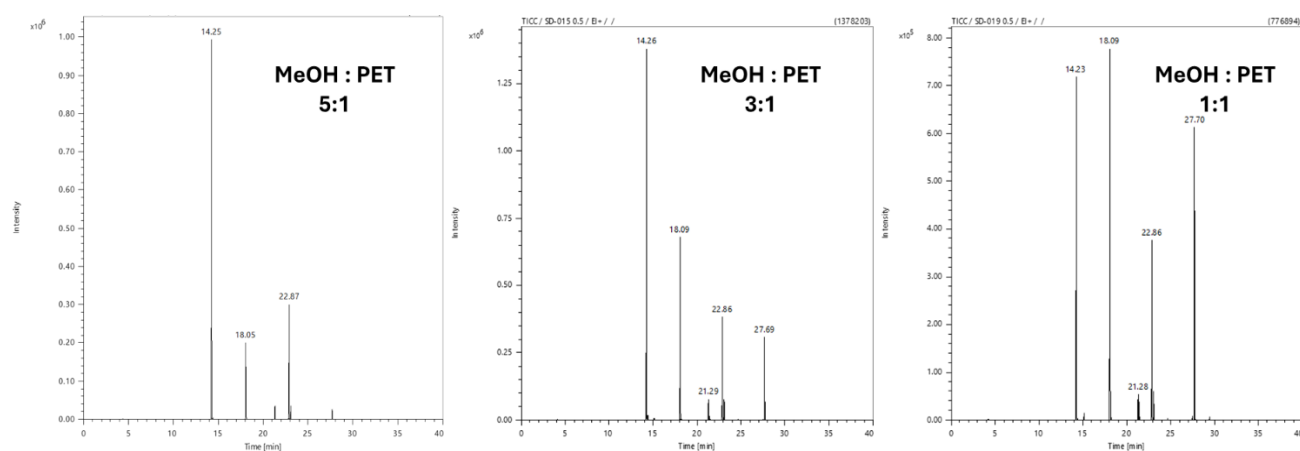


Figure 5.19 – TICC shows the relative intensities of peaks which correspond to oligomers ($t = 18.07$ and 27.68 min) increasing in comparison to DMT and ethylene glycol ($t = 14.25$ and 22.87 min) as the amount of methanol in the solvolytic system is reduced.

Table 5.4 – Identity of species seen to have a retention time of 14.25 minutes in the GC-MS. Molecular ion is shown on the first row. with small m/z that arise from EI identified based on fragmentation of parent peaks. Mass spectrum available in Appendix.

Retention Time (min)	m/z	Identity
14.25	195.0923	
14.25	179.9913	
14.25	163.9125	
14.25	135.7716	
14.25	120.6696	
14.25	103.5579	

Table 5.5 – Identity of species seen to have a retention time of 18.07 minutes in the GC-MS. Molecular ion is shown on the first row with small m/z that arise from EI identified based on fragmentation of parent peaks. Mass spectrum available in Appendix.

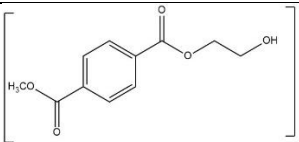
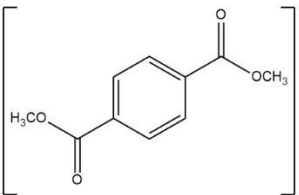
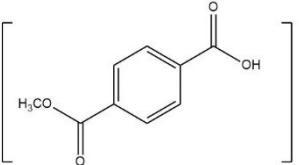
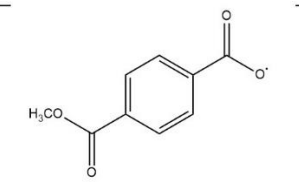
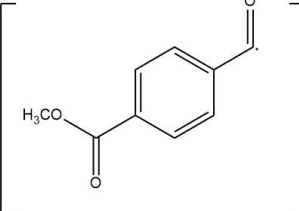
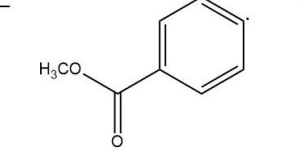
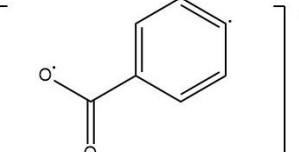
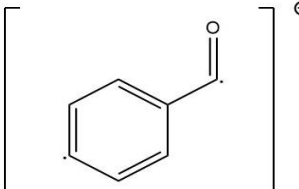
Retention Time (min)	m/z	Identity
18.07	224.00	
18.07	195.0923	
18.07	182.0166	
18.07	179.9913	
18.07	163.9125	
18.07	135.7716	
18.07	120.6696	
18.07	103.5579	

Table 5.6 – Identity of species seen to have a retention time of 27.68 minutes in the GC-MS. Molecular ion is shown on the first row. with small m/z that arise from EI identified based on fragmentation of parent peaks. Mass spectrum available in Appendix.

Retention Time (min)	m/z	Identity
27.68	356.9501	
27.68	208.1545	
27.68	163.9125	
27.69	135.7716	

The stated molecular ion for the species which passes through the GC column at 18.07 minutes (Tab. 5.5) cannot be seen in the mass spectrum. However, the m/z for the 18.07 retention time includes a strong peak for 182.0166 m/z, which no other component from the crude product exhibits (Fig. 5.20). Therefore, this proposed molecular ion has been derived by application of the McLafferty arrangement.

The McLafferty arrangement is a well-known phenomenon that can take place when a molecule undergoes “hard” ionisation, such as the electron ionisation (EI) employed in GC-MS.²⁸⁸

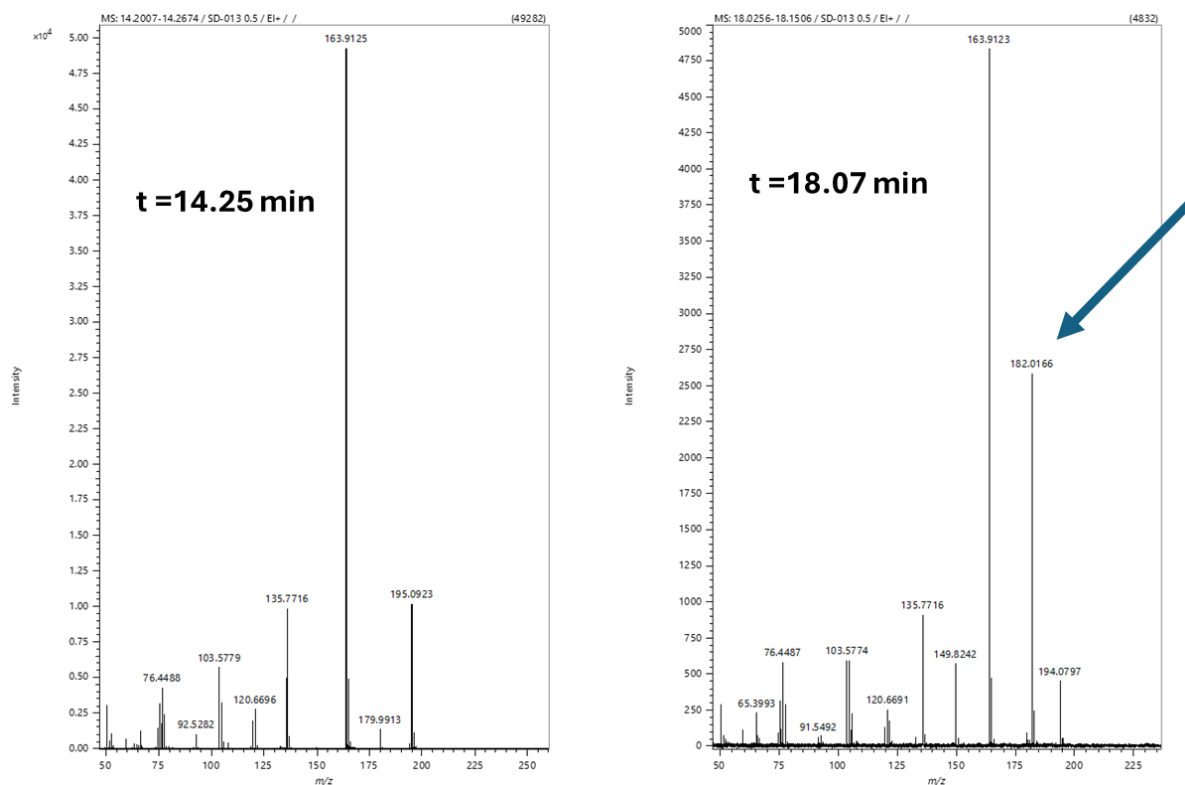


Figure 5.20 – Mass spectra which are collected at $t = 14.25$ and 18.07 minutes. A strong peak at 182.0166 m/z can be seen (blue arrow) for the mass spectrum at $t = 18.07$ minutes, and this is presented as evidence for the McClafferty rearrangement taking place.

A compound must contain a keto group, and a hydrogen at the γ position to provide a favourable orientation for proton transfer (Fig. 5.21). The structure of the molecular ion in Table 5.5 contains the necessary features to undergo the McClafferty rearrangement, which has been shown mechanistically to yield a fragment with a mass-to-charge ratio of 182.0166 m/z , which matches the peak highlighted in figure 5.20 by the blue arrow.

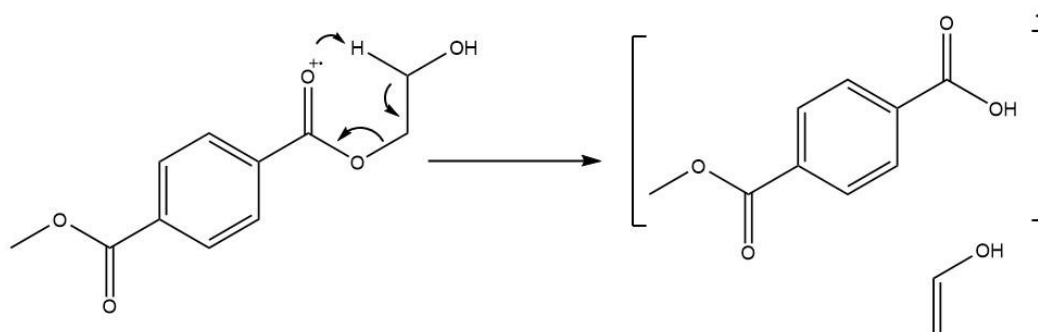


Figure 5.21 – Proposed McClafferty rearrangement of a PET oligomer to produce a species of correct exact mass to appear at 182.0166 m/z in the GC-MS mass spectrum.

GC-MS samples of the crude products were then prepared quantitatively to determine the amount of DMT produced by this system, and how it varied as the methanol: PET ratio was reduced. DMT standards were prepared at four concentrations and the average peak area from the TICC was plotted, and the peak area for DMT in the crude product (where PET was degraded at 180 °C, in either 3 hours or 30 minutes) was compared to estimate the selectivity towards DMT formation (Fig. 5.22).

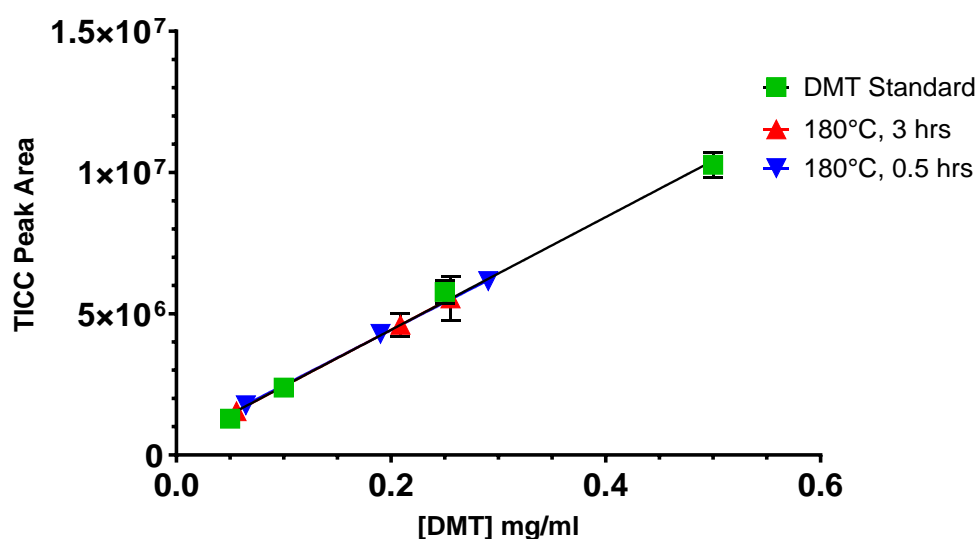


Figure 5.22 – Plot of peak area at 14.25 minutes in the TICC, and the corresponding concentration of DMT. A calibration was created by analysing standard solutions of DMT in CHCl_3 at concentrations of 0.50, 0.25, 0.10 and 0.05 mg/ml. Error bars indicate standard error of the mean.

Crude methanolysis products were then prepared in CHCl_3 at a concentration of 0.50 mg/ml, and the concentration of DMT was estimated using the calibration trendline.

It can be seen that selectivity for DMT falls with the methanol: PET ratio, and the yields have been calculated based on the concentration of DMT read off the x-axis (Fig 5.22). It is possible to calculate the moles, and therefore the mass of DMT from the solution concentration, enabling yield to be determined. (Tab 5.7)

Table 5.7 – Yields of DMT obtained after supercritical methanolysis of PET at various conditions, calculated by using trendline in figure 5.22.

MeOH: PET	DMT Yield (%) 180 °C, 3 hours	DMT Yield (%) 180 °C, 0.5 hours
5:1	37.2	42.2
3:1	30.4	27.7
1:1	8.2	9.4

Samples are ionised in GC-MS through bombardment with a high-energy electron beam. This is often referred to as a form of “hard” ionisation as the sample is broken down into several different fragments.²⁸⁹ On one hand, this can be advantageous as a sample’s identity can be confirmed by identifying which fragments correspond to peaks in the m/z . However, the complex fragmentation patterns can complicate analysis, and the real molecular ion of the sample may not appear in the mass spectrum if it is labile to fragmentation.

5.3.2.2.2 HPLC

To ensure the analysis of the above GC-MS experiments was correct, corresponding HPLC-MS analysis was also conducted on the depolymerised samples. The ion source in this setup ionises samples through applying a potential difference across the outlet of a capillary tube where the sample, dissolved in an appropriate solvent, is eluted. The potential difference creates charged droplets, which have been nebulised by a flow of gas, and the solvent gradually evaporates from these droplets – leaving ionised sample which has had its structure largely retained. This technique is referred to as electrospray ionisation (ESI), it is referred to as a “soft” ionisation technique due to the limited fragmentation it produces.²⁸⁹

An HPLC with a UV detector only was employed for this analysis. Terephthalate-based compounds are known chromophores as the π system in their aromatic rings enables them to absorb photons. Therefore, HPLC-MS was suitable to confirm the identities of these terephthalate-based oligomers. DMT could be easily identified by comparing the peak elution

time in the crude samples to a standard sample, highlighted by the blue arrow, (Fig. 5.23) and from the m/z of the corresponding mass spectrum (Fig. 5.24).

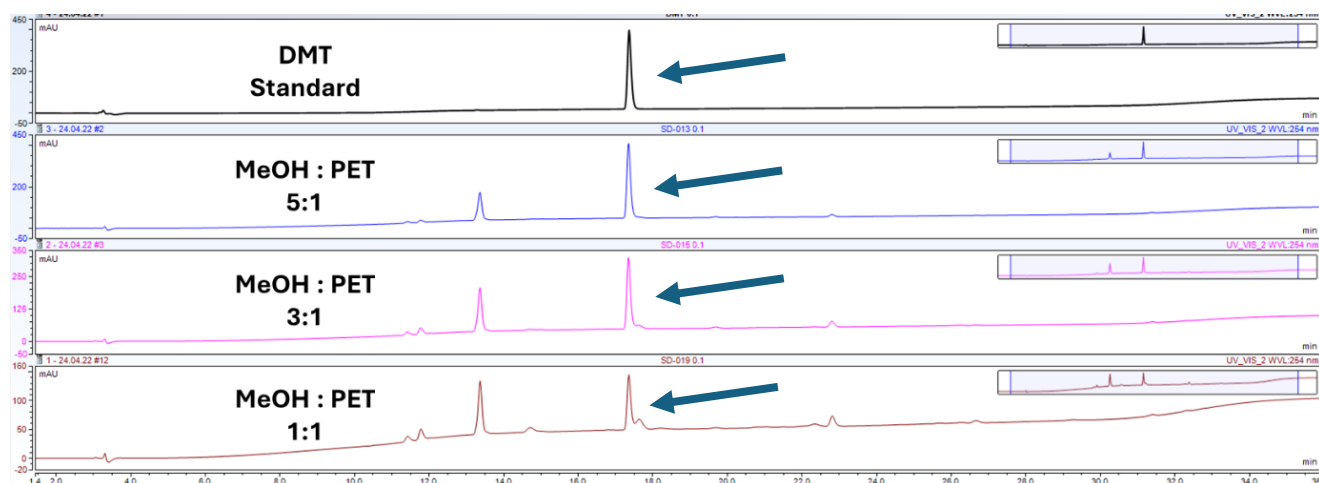


Figure 5.23 – Reverse phase HPLC chromatograms from a DMT standard, and crude methanolysis product.

Temperature = 180 °C, time = 3 hours

Several other peaks could be observed in the crude product chromatograms, further confirming that other low molecular weight products were present alongside DMT and ethylene glycol in the crude product. This is consistent with the shoulder peaks seen in the ^1H NMR and the TICC from the GC-MS. (Fig. 5.16) (Fig. 5.17). Moreover, an increase in peak number could be seen with decreasing methanol: PET ratio (Fig. 5.23), indicating that although conversion of PET remained at 100%, an increasing proportion of the products consists of oligomers as the methanol content of the solvolytic system decreases.

To identify the chemical structures of these low molecular weight components, the eluted samples underwent mass spectrometry analysis once they exited the column. The m/z ($M+H^+$) detected at the various elution times are shown and these were exact matches for molecular ions obtained from peaks in the GC-MS chromatogram (Fig. 5.24).

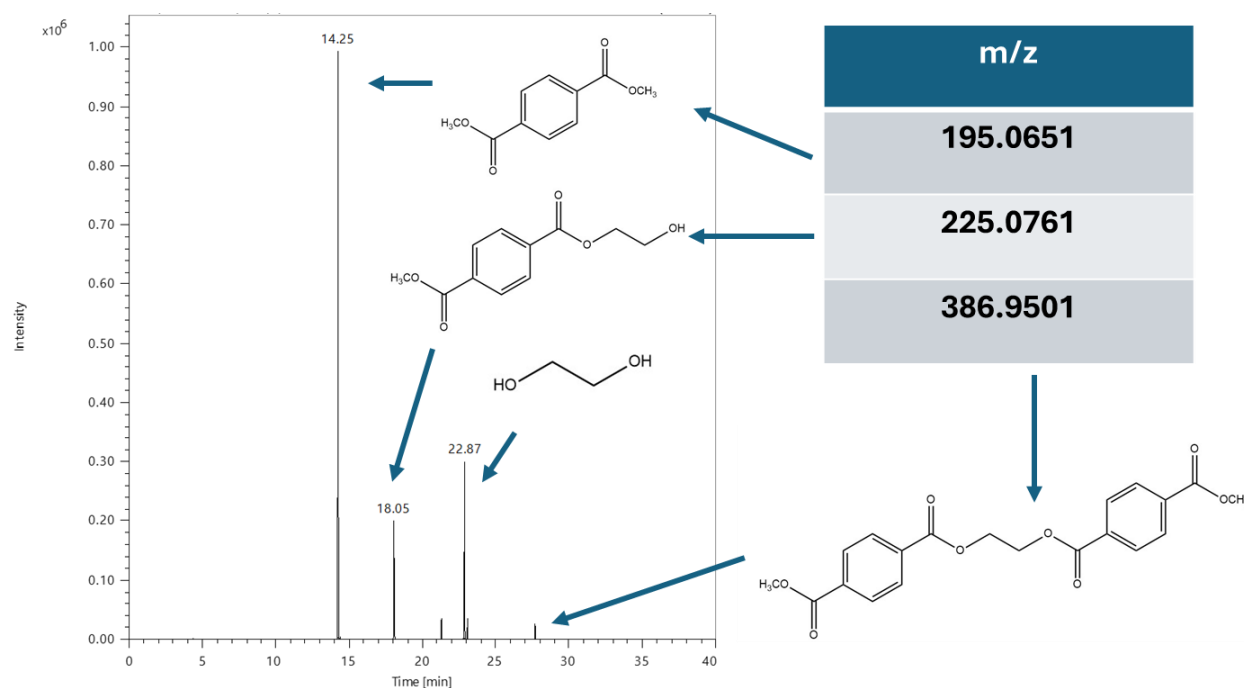


Figure 5.24 – TICC from GC-MS, as seen in Figure 5.18, overlaid with corresponding m/z obtained from HPLC-MS.

5.3.2.3 Broadening the Catalyst Scope

The majority of experimental work in this section was conceptualised by the PhD candidate Bradley Hopkins and performed by masters student Priya Patel under supervision from the PhD candidate. Inclusion of 2-aminopyridine and urea to the catalyst screening was suggested by Priya Patel.

To expand the range of studied catalysts, four species were identified which were postulated to be suitable for supercritical methanolysis of PET (Fig. 5.25). 4-Dimethylaminopyridine (DMAP) and *N*-methylimidazole (NMI) contain basic moieties like TBD and have been used as catalysts for PET solvolysis previously.²⁹⁰ 2-Aminopyridine (2-AP) is a lesser explored catalyst for this chemistry but was included to expand the studied range of basicity. Finally, urea was included although it is not a base, may be able to undergo hydrogen bonding with both PET and methanol which could align the species into a favourable orientation for reaction.²⁹¹

Hydrogen bonding has been proposed as a key factor in the excellent performance of TBD-catalysed systems^{133, 139}, as it enables the reacting species to be brought into a favourable

orientation and urea was included to test if hydrogen bonding alone would be enough to catalyse the reaction.

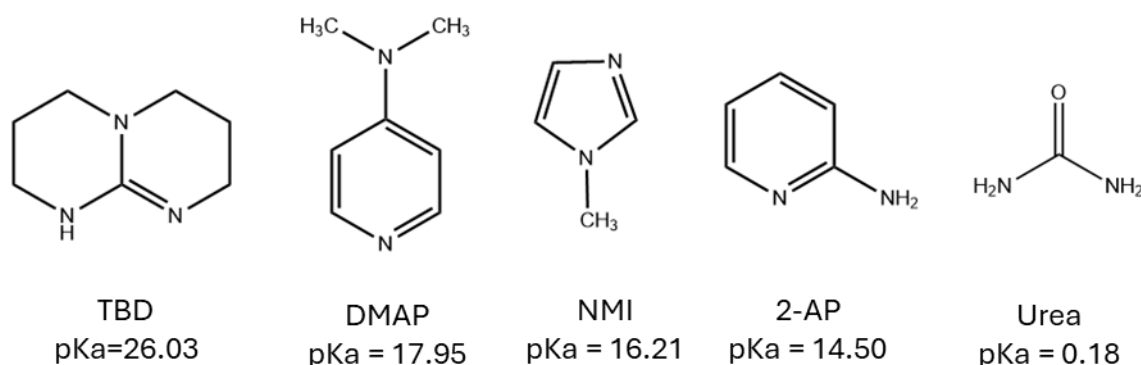


Figure 5.25 – Structures of organic, and urea, employed as catalysts for methanolysis of PET in $scCO_2$. pK_a values given here are for bases their conjugate acids in acetonitrile. ¹²⁸

We postulate the bases initially deprotonate prior to (or concurrent with) nucleophilic attack on the ester linkage. These bases, and urea, all are all weaker than TBD (see pK_a values of the conjugate acids in Figure 5.25) and will clearly change the equilibrium between methanol and methoxide (Fig 5.26) in the reactions. ^{292, 293}

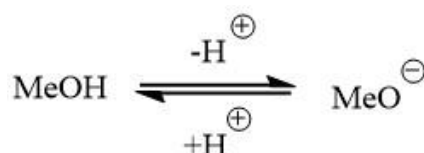


Figure 5.26 – Equilibrium between methanol and its conjugate base – methoxide. An organic base with a higher conjugate acid pK_a , should favour the forward reaction due to its greater ability to receive a proton from methanol.

To investigate how changing bases affects conversion, PET was degraded with a 5:1 molar excess of methanol for 1 hour at 4 different temperatures (Fig. 5.27). Identical to TBD catalysed methanolysis in the previous section, the crude reaction mixture was dissolved in chloroform and any insoluble fraction was removed by filtration. Conversion calculated (Eq. 5.1) (Fig. 5.27) illustrates how PET conversion varied with catalyst basicity and temperature (TBD data is also included in Figure 5.27 for reference).

DMAP and NMI-catalysed methanolysis produced comparable conversion to TBD-catalysed reactions at 180 °C, but conversion fell at 160 °C and 140 °C. 2-AP performance was

considerably poorer than all three other bases at the studied temperature, whilst urea-catalysed methanolysis resulted in 0% conversion at 180 °C (data omitted from Fig 5.27).

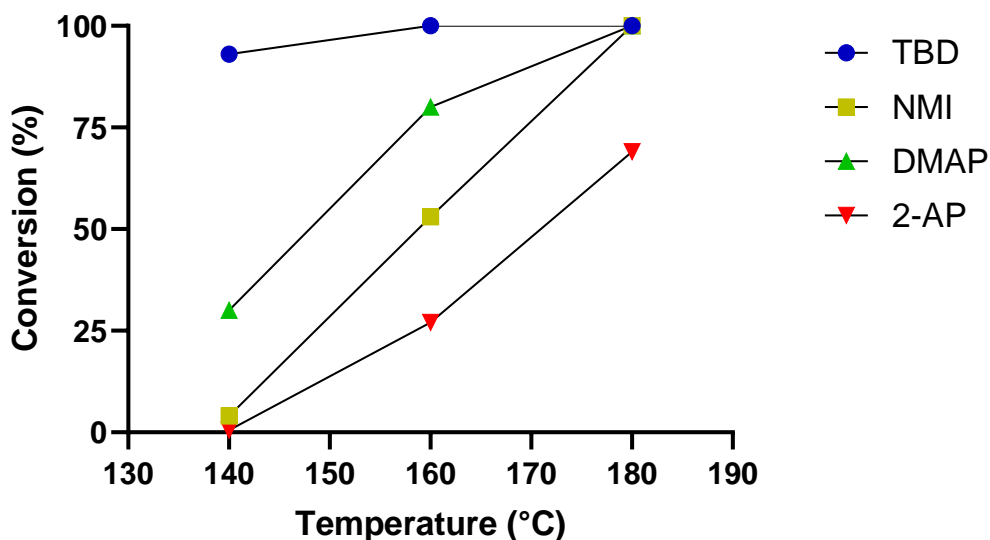


Figure 5.27 – PET conversion against both temperature and catalyst basicity.

PET conversion was shown to correspond to the basicity of the catalyst across the studied temperature range, which is consistent with the original hypothesis of the differing basicity of the catalysts altering the equilibrium between methanol and methoxide. The fact that 0% PET conversion was seen with urea at 180 °C demonstrates that hydrogen bonding alone is insufficient to catalyse nucleophilic attack of methanol on the polymer backbone at this temperature, and that formation of the methoxide is necessary.

5. 3.2.3.1 Product Analysis

The crude product recovered from the autoclave could be separated into two fractions, CHCl_3 soluble and CHCl_3 insoluble (Tab 5.8). The insoluble fraction recovered from CHCl_3 post-methanolysis could not be dissolved in any solvents compatible with GPC or mass spectrometry. Therefore, study of this fraction was limited to TGA and DSC. Comparison of the degradation profile (TGA) (Fig. 5.28), alongside the melting point (DSC) (Fig. 5.29) of the insoluble fraction with that of unmodified PET suggested that this fraction consisted of PET that is of roughly identical molecular weight to the starting material.

Table 5.8 – Recovered CHCl_3 –soluble and insoluble fractions from methanolysis with various catalysts.

Catalyst	Temperature (°C)	PET (g)	Soluble Fraction (g)	Insoluble Fraction (g)	Conversion (%)
None	180	5.10	0.00	5.10	0.00
DMAP	180	5.05	5.05	0.00	100
NMI	180	6.31	6.31	0.00	100
2-AP	180	6.53	4.97	1.56	69
Urea	180	5.97	0.46	5.51	0
DMAP	160	5.61	4.61	1.00	80
NMI	160	5.54	3.13	2.41	52
2-AP	160	5.52	1.79	3.73	27
DMAP	140	5.01	1.42	3.59	30
NMI	140	5.58	0.66	4.92	4.0
2-AP	140	5.38	0.30	5.08	0.5

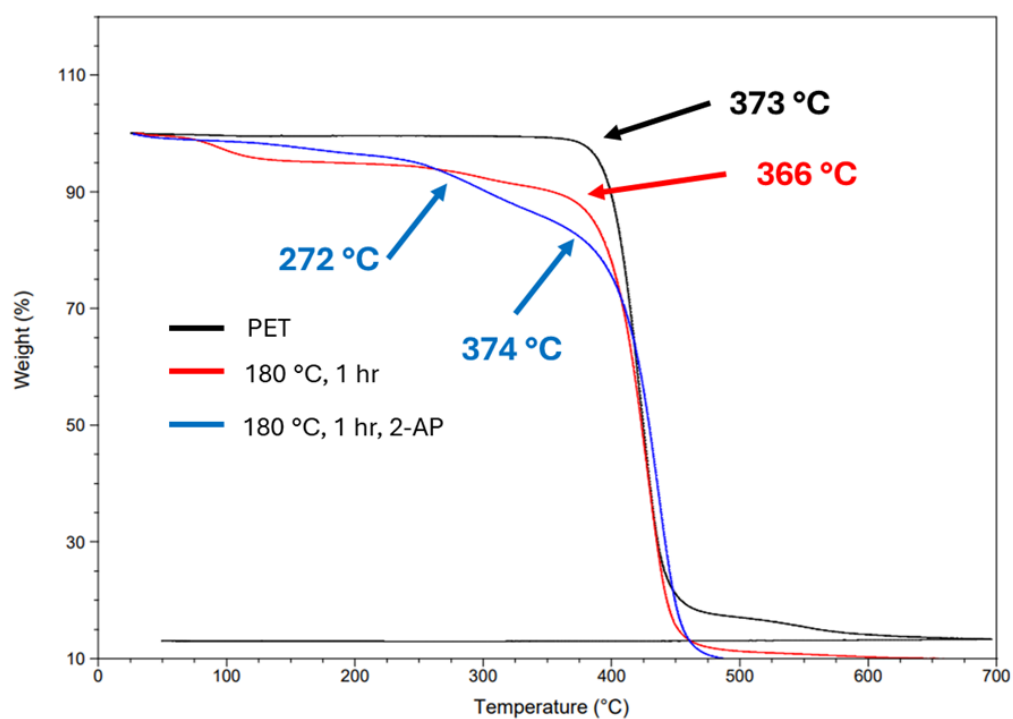


Figure 5.28 – TGA thermogram of unmodified PET (black), PET exposed to solvolysis conditions (see legend) with no catalyst (red) and PET exposed to solvolysis conditions with 2-AP catalyst. The onset temperature for the major degradation steps is indicated.

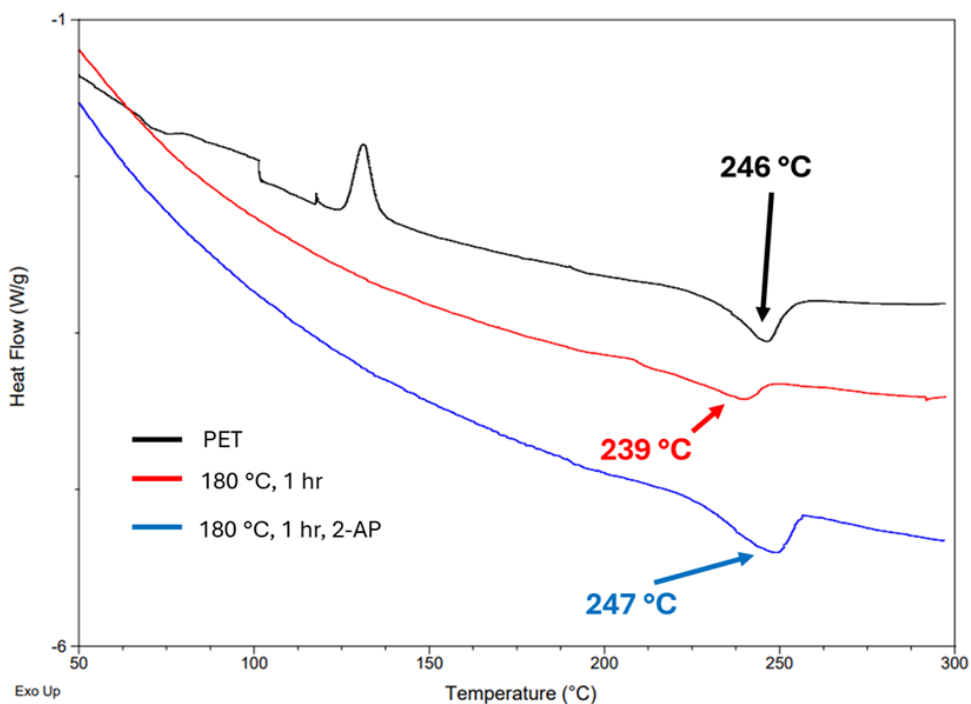


Figure 5.29 – DSC of unmodified PET (black), PET exposed to solvolysis conditions (see legend) with no catalyst (red) and PET exposed to solvolysis conditions with 2-AP catalyst. The melting temperature is indicated.

The GC-MS chromatograms for the methanolysis catalysed by these bases (DMAP, NMI, 2-AP) contain peaks with identical retention times to the TBD-catalysed series in the previous section. However, as the basicity of the catalyst is reduced (DMAP > NMI > 2-AP) (Fig. 5.30) and the temperature falls (Fig. 5.31), the relative intensity of the peak known to correspond to DMT (14 minutes) falls in comparison to peaks which correspond to the other low molecular weight products.

The relative peak intensities can be used to qualitatively track the extent of the reaction, and the reduction of the DMT peak confirms that the extent of PET depolymerisation falls with catalyst basicity or reaction temperature. This is consistent with expectations as the equilibrium between methanol and methoxide (Fig. 5.26) will favour methanol with a less basic catalyst, and lowering the temperature will simply reduce the energy available to drive the reaction.

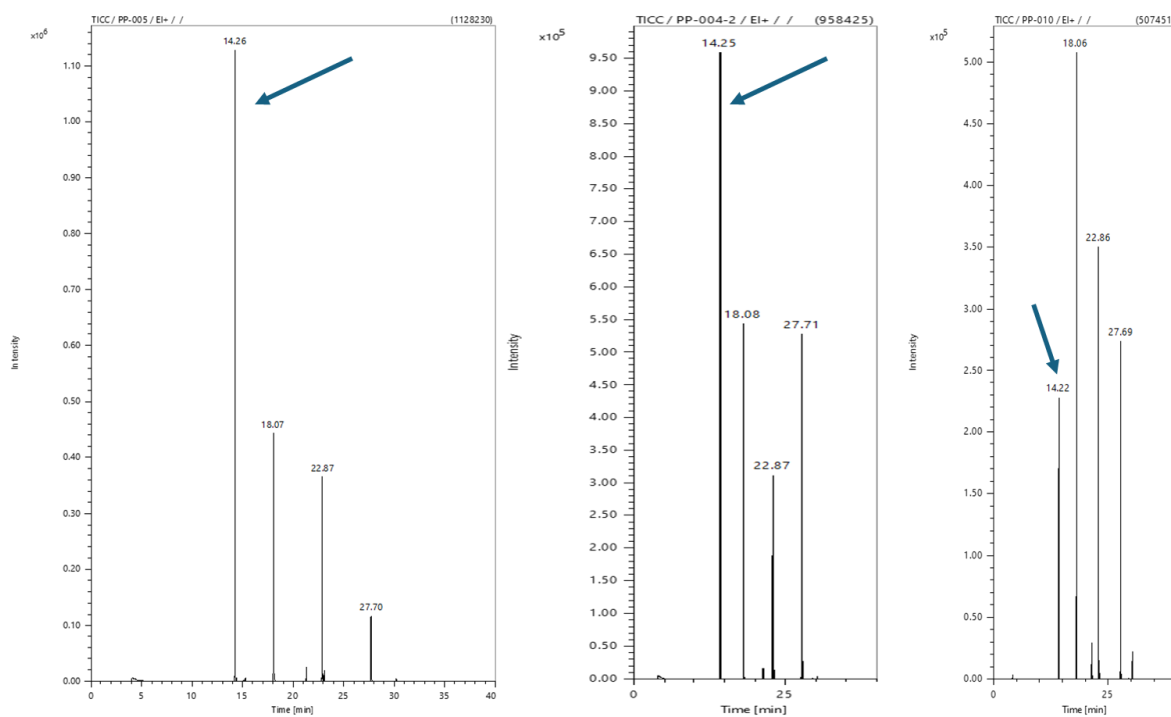


Figure 5.30 – GC-MS chromatograms obtained for DMAP (left), NMI (middle) and 2-AP (right) catalysed methanolysis of PET. The peak corresponding to DMT is highlighted.

Temperature = 180 °C, time = 1 hour Pressure = 172 bar

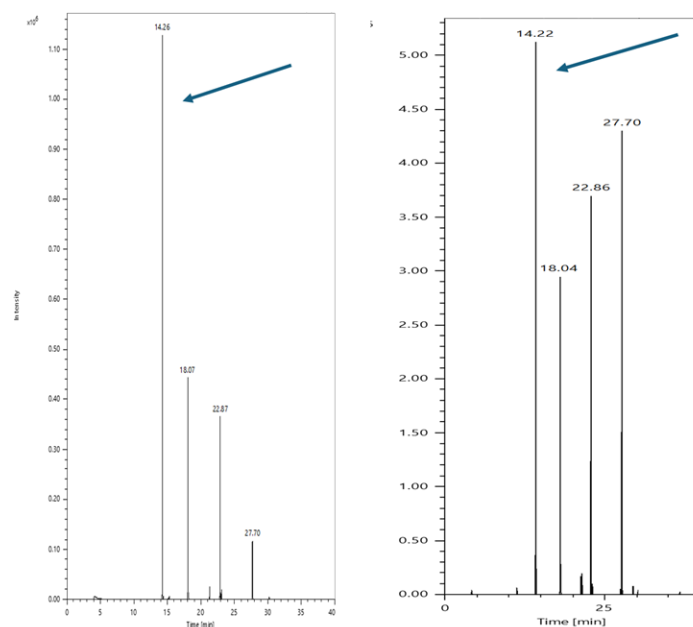


Figure 5.31 – GC-MS chromatograms obtained for DMAP- catalysed methanolysis at 180 °C (left) and 140 °C (right). The peak corresponding to DMT is highlighted.

Time = 1 hour, Pressure = 172 bar

5.3.3 Closing the Loop

The previous section demonstrates a convincing pathway for methanolysis of PET to monomers and other low molecular weight products in scCO_2 . This alone represents an improvement over the current state of the art, as much of the PET solvolysis literature that utilises sub or supercritical CO_2 only does so as a co-solvent. Unlike the conventional PET solvolysis routes, a dry product which does not need to be isolated from the bulk solvent is yielded by the supercritical methanolysis route here. However, it is still necessary to isolate pure low molecular weight products from the catalyst if a truly closed-loop route for PET recycling is to be developed.

Here, two routes to recover pure products, with significantly less solvent waste typically generated, will be discussed.

5.3.3.1 Transesterification to Bis(2-Hydroxyethyl) terephthalate

BHET is a direct pre-cursor to PET, which is typically produced by bulk polymerisation of this species. The characterisation in this chapter showed that DMT, ethylene glycol and other low molecular weight products are produced for TBD-catalysed methanolysis in scCO_2 . Despite the different chain lengths of these depolymerisation products, the end group is either the methyl ester of the DMT moiety or the alcoholic functional group derived from ethylene glycol (Fig. 5.32).



Figure 5.32 -The only two types of end groups seen in the PET methanolysis products. The ester functional group of DMT (left) and the alcoholic functional group derived from ethylene glycol (right).

As both end groups contain ester functionality, they are susceptible to transesterification. It is possible to derive a mechanistic pathway whereby all of these products can be converted to BHET via transesterification with ethylene glycol. Furthermore, TBD should be capable of

catalysing this reaction by the same route of the original methanolysis – deprotonation of ethylene glycol to its conjugate base.

Crude supercritical methanolysis product was heated until molten, along with a small molar excess of ethylene glycol. The crude melt was left for 2 or 4 hours, and the residual TBD from the methanolysis was left in the crude melt to catalyse its transesterification to BHET.

^1H NMR enables the transesterification reaction to be tracked, as peaks which correspond to the BHET standard can be seen to grow (Fig. 5.33). After two hours, a mixture of BHET, DMT, ethylene glycol and other PET oligomers can be seen in the NMR. If the aryl region is focused on, growth of a singlet at $\delta = 8.12$ ppm over the singlet at $\delta = 8.09$ ppm is observed. The former corresponds to aryl protons from BHET; the latter aryl protons on DMT. This subtle change in the spectrum shows that, after a two-hour transesterification, BHET has started to become more abundant, but DMT remains.

After 4 hours, the intensity of DMT's aryl peak in the ^1H NMR is significantly weaker and the peaks which correspond to BHET have become dominant (Fig. 5.34). To isolate BHET from the TBD catalyst and excess ethylene glycol, the product was suspended in a small amount of deionised water (20 mL), dissolving the catalyst, which was then separated by filtration. ^1H NMR confirmed the removal of TBD (Fig. 5.34).

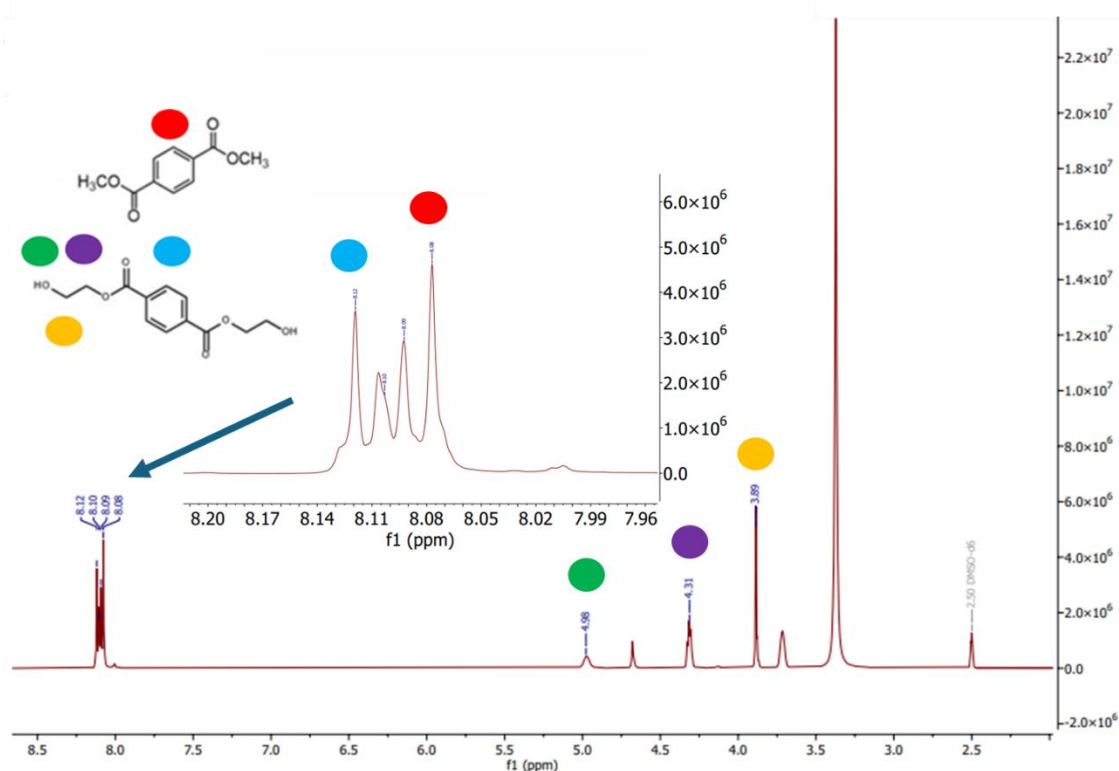


Figure 5.33 - ^1H NMR of crude methanolysis product after transesterification with a small excess of ethylene glycol. Note the appearance of an aryl peak which corresponds to BHET (blue), but DMT's aryl peak can also be seen too indicating conversion is not complete after 2 hours (red).

Temperature = 130 °C, time = 2 hours

Although a small amount of solvent was required in the final step of this closed-loop process, it is important to consider the quantities involved. 5 grams of PET have been successfully degraded using only 4.17 g of methanol by leveraging scCO_2 as a reaction medium. The crude product, once it has been converted by transesterification to BHET, has then been purified by a relatively small amount of water – 20 g. When this is contrasted against the literature that was reviewed at the start of this chapter, where less than 1 g of PET is degraded in tens of grams of organic solvent – followed by purification which can require up to 100 grams of water- the step forward this work represents becomes obvious.

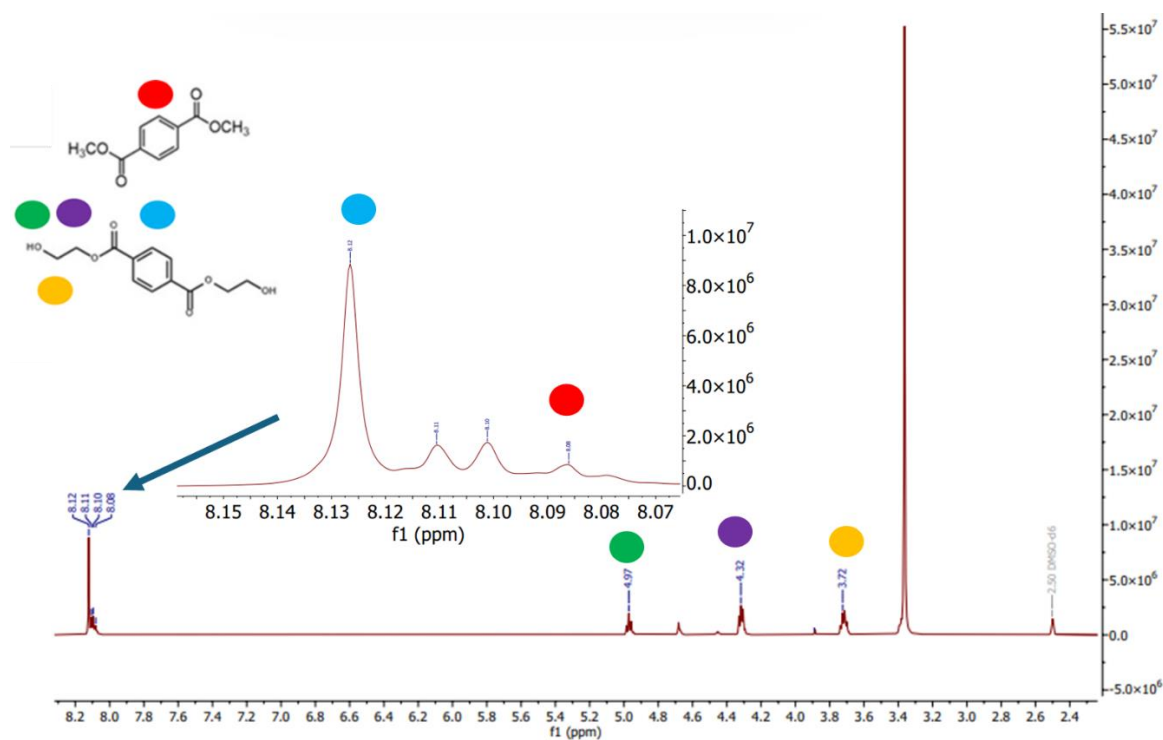


Figure 5.34 - ^1H NMR of crude methanolysis product after transesterification with a small excess of ethylene glycol. Note the appearance of an aryl peak which corresponds to BHET (blue), whilst the intensity of DMT's aryl peak has been significantly reduced (red).

Temperature = 130 °C, time = 4 hours

GC-MS analysis of the purified material produced a chromatogram that only contained a single peak at a retention time of 21.47 minutes (Fig.5.35). This matched the retention time of a BHET standard, and the mass spectra were also exact matches (Appendix).

A pie chart illustrating the quantities of material used in this route has been prepared (Fig. 5.36) and the proportion of PET to solvolytic or purification solvent is more favourable when compared to solvolysis carried out in conventional solvents (Fig. 5.8). This results in E-factor values far lower than those seen for the solvolysis of PET that relies on traditional solvents, or CO_2 -assisted solvolysis, reviewed earlier in this chapter.

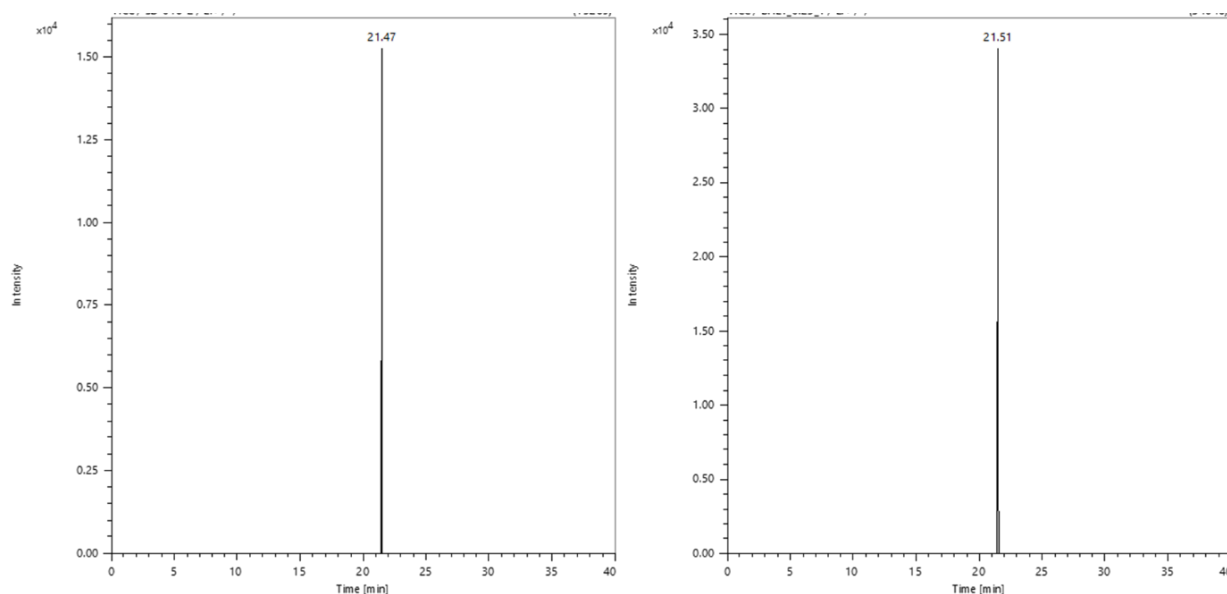


Figure 5.35 – TIC of product obtained from transesterification of crude methanolysis product with ethylene glycol (left) and a BHET standard (right).

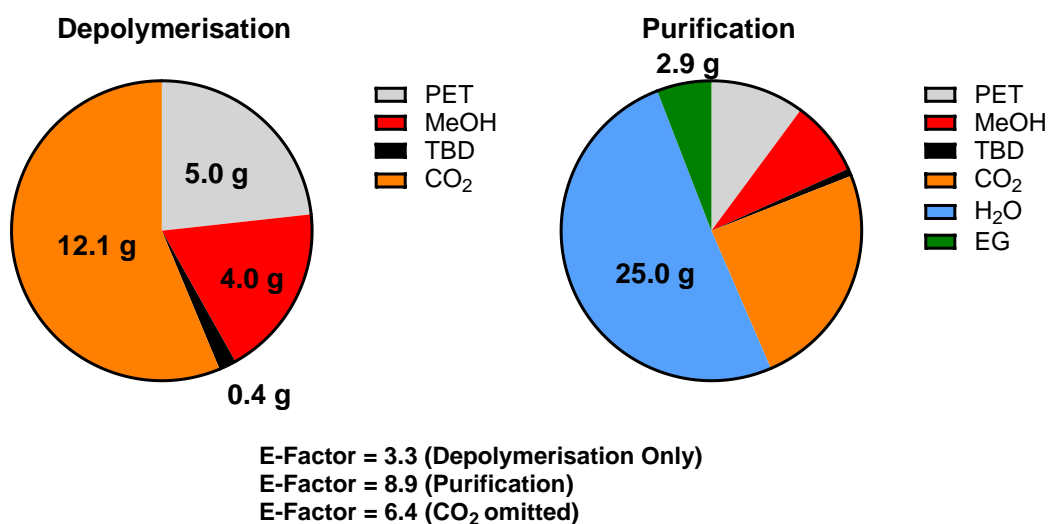


Figure 5.36 – Graphical representations of the total mass distribution of the solvolytic system for TBD-catalysed methanolysis of PET (left) and the corresponding mass distribution when the resulting crude product undergoes transesterification with ethylene glycol (right).

5.3.3.2 scCO₂ Extraction of Dimethyl Terephthalate

The possibility of using scCO₂ as an extraction medium has also been investigated. The solubilities of DMT, ethylene glycol and TBD in scCO₂ was measured in a fixed volume view cell; to identify a pressure and temperature where one compound would be selectively dissolved over the others.

TBD was shown to be insoluble when soaked in scCO₂ by itself in section 5.3.1. Ethylene glycol formed a slurry over several hours in scCO₂ at 241 bar and 65 °C, as shown in Chapter 3, whereas DMT was seen to dissolve in less than 1 minute at the same conditions. In Chapter 3, BHET was shown to be insoluble in scCO₂, even after 24 hours. This would suggest that the limit of solubility of low molecular weight PET derivatives in scCO₂ lies somewhere between DMT and BHET. Therefore, it was hypothesised that DMT could be selectively removed from the crude material over the other low molecular weight products via scCO₂ extraction.

To explore the use of scCO₂ extraction for post-depolymerisation purification crude methanolysis product was placed in a high-pressure autoclave, and the autoclave was charged with scCO₂ - 241 bar and 65 °C. After soaking for 1 hour, scCO₂ was flowed through the autoclave, and a dry, white powder was collected in a liquid nitrogen trap (Fig. 5.37).

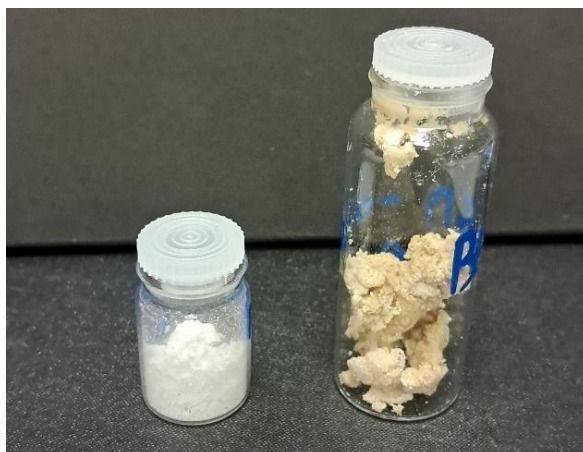


Figure 5. 37 - Dry, free-flowing white powder (left) was collected from crude methanolysis powder (right) via scCO₂ extraction.

Temperature = 65 °C, Pressure = 241 bar, time = 15, 30 or 60 minutes

An increasing yield of dry, white product was collected with increasing extraction time (Fig.5.38), whereas an increasingly damp residue was recovered from inside the autoclave. Following successful extraction, both the dry powder and damp residue were analysed to elucidate their identity.

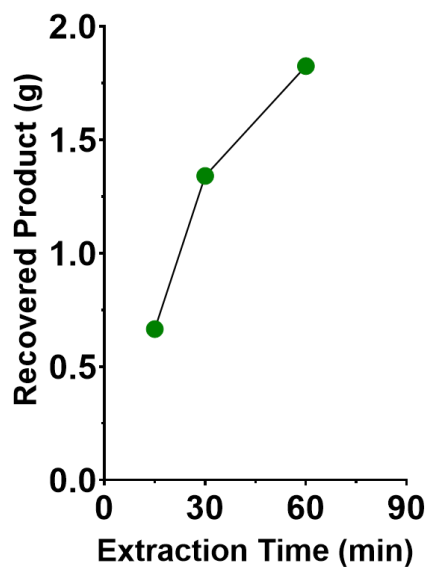


Figure 5.38- Mass of recovered dry, free-flowing white powder from crude methanolysis product via scCO₂ extraction at various residence times.

It can be seen from the ¹H NMR that scCO₂ extraction has selectively removed DMT over all other components in the crude methanolysis product (Fig. 5.39). By comparing the ¹H NMR of the extracted product with that of the remaining autoclave residue. It is clear that DMT is being selectively dissolved, and extracted, at 241 bar and 65 °C and it is also clear that no TBD is being extracted either. However, a peak which is known to correspond to the CH₂ backbone of ethylene glycol can also be seen in the ¹H NMR.

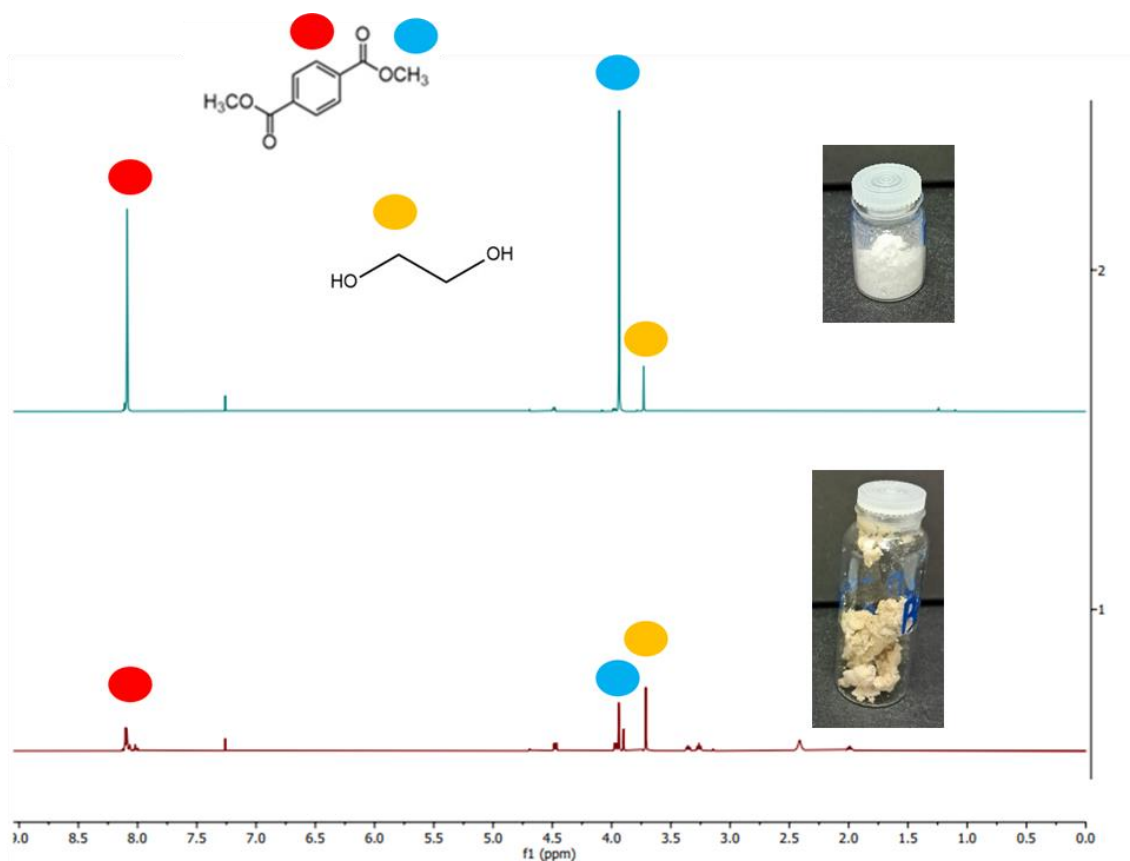


Figure 5.39 – ^1H NMR of the dry, white extracted product (top) and the corresponding residue remaining in the autoclave (bottom).

To determine if trace amounts of ethylene glycol, or an oligomer which links the terephthalate units by a CH_2 backbone, was also being extracted alongside DMT, GC-MS was performed (Fig. 5.40). The TICC of the extracted material contains peaks which correspond to DMT and the low molecular weight products only- no TBD or ethylene glycol appears to be visible (Fig. 5.41). Furthermore, the peak at 14.25 minutes occupies 93 % of the total peak area. From this result, it can be seen that the scCO_2 extraction purification route of this crude product is highly selective towards DMT (Tab. 5.9).

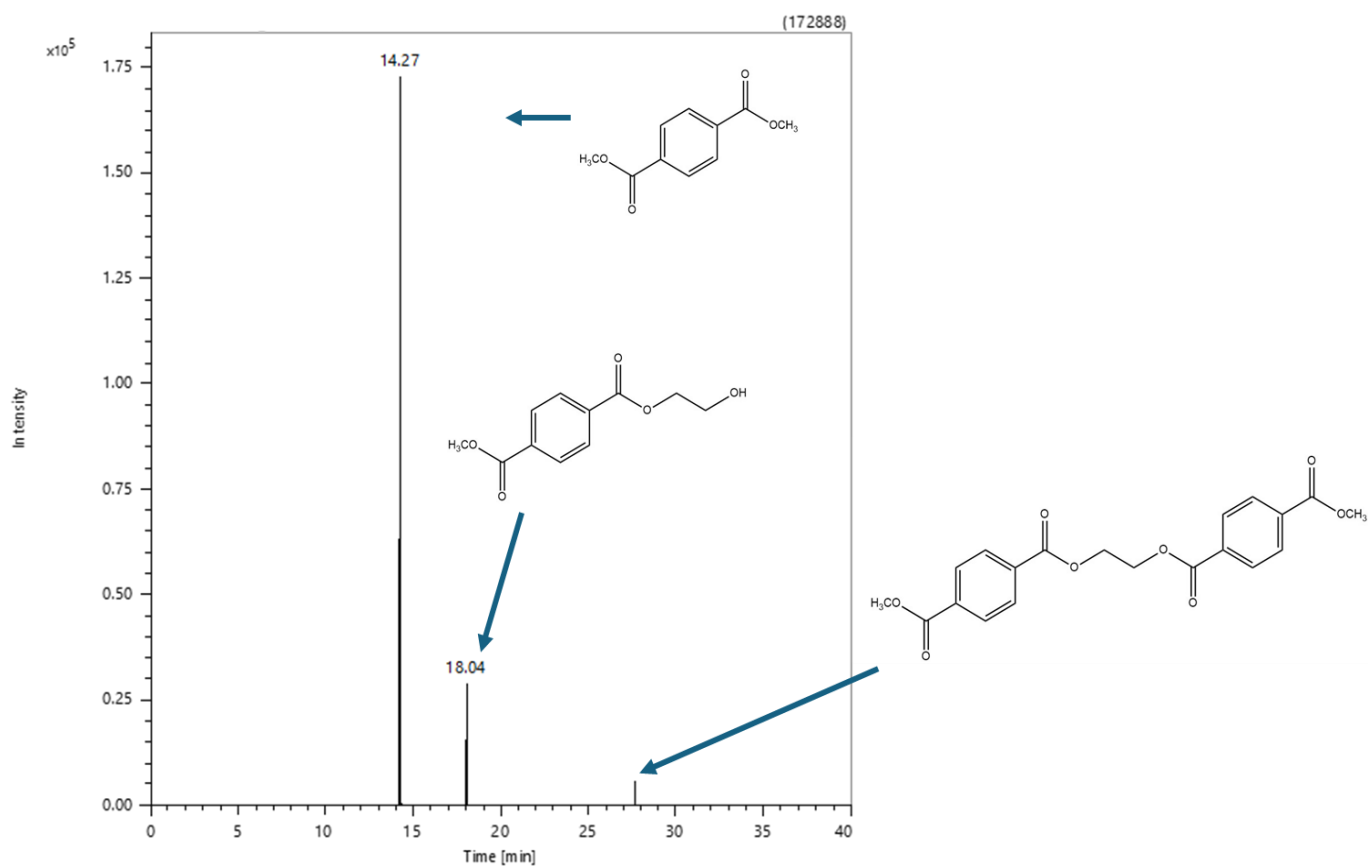


Figure 5.40- TICC of white powder produced from scCO₂ extraction. A strong selectivity for DMT over the oligomers can be seen, and no ethylene glycol or TBD appears to be removed from the autoclave during the scCO₂ extraction.

Temperature = 65 °C, Pressure = 274 bar, time = 30 or 60 minutes

Table 5.9 - Peak areas of each component in the extracted powder

Time [min]	Area	Area [% of Total]
14.25	596390	93
18.04	38648	6
27.65	7880	1

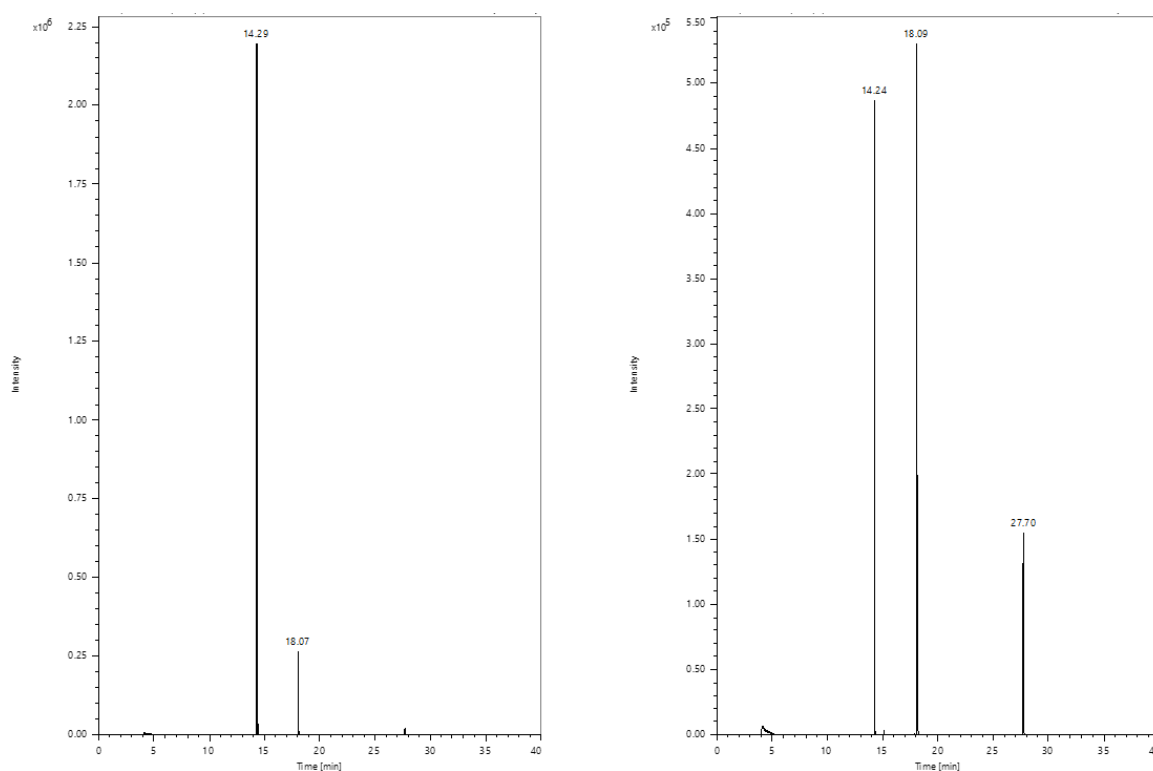
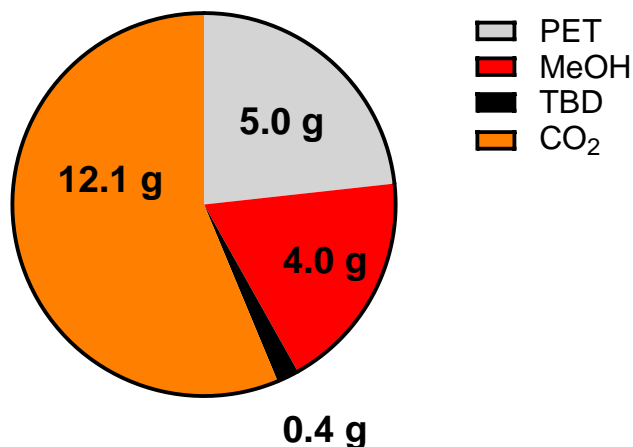


Figure 5.41 – GC-MS TIC of dry, free-flowing white powder extracted from the autoclave (left) and the corresponding residue remaining in the autoclave (right).

The relative mass proportions of the depolymerisation step are illustrated (Fig. 5.42). As the system used in this work for scCO₂ extraction is operated manually, preventing the flow rate of CO₂ being quantified, it is not possible to present a pie chart, or E-factor calculation inclusive of the purification. However, in a larger system it could be possible to collect and re-use the CO₂ once it has cycled through the reactor, as outlined by Nextek for plastic recycling.²⁹⁴ The transition from supercritical fluid to gas by reduction of CO₂ pressure makes its isolation from the extracted products simple, and if this were successful, it could be argued that CO₂ is no longer a waste material and therefore would be excluded from the E-factor calculation. This brings the E-factor value for this process very close to zero (Fig 5.42), which the original author of the E-factor, Roger Sheldon, stated was the best theoretical value any process could possess.



E-Factor = 3.3 (Depolymerisation Only)
E-Factor = 0.9 (CO₂ omitted)

Figure 5.42- Graphical representations of the total mass distribution of the solvolytic system for TBD-catalysed methanolysis of PET.

5.3.4 One Pot Depolymerisation-Extraction

The novel procedures for PET methanolysis and purification of low molecular weight products via scCO₂ extraction outlined in the above two sections were combined to create a one pot protocol, which avoids reducing CO₂ pressure back to ambient between the depolymerisation and extraction steps.

PET was degraded with a 5:1 MeOH:PET ratio and 180 °C for 30 minutes at 172 bar, as this was shown to fully degrade PET to low molecular weight products with a 42 % yield of DMT (Tab. 5.7). After 30 minutes, the temperature was reduced to 65 °C, and the pressure was increased to 241 bar, to selectively dissolve DMT over the other components in the reaction mixture, followed by following CO₂ through the system for 30 minutes.

¹H NMR confirms that low molecular weight products from PET depolymerisation have been successfully produced, and isolated from the reaction mixture, by this one pot process. Peaks with the correct chemical shift and multiplicity for DMT and the CH₂ from the glycolic unit are

visible, with minimal shouldering of the peaks (Fig. 5.43). Moreover, no peaks which correspond to TBD can be seen, confirming successful isolation of the products from the catalyst. ^1H NMR of the corresponding residue left in the autoclave post-extraction confirms that TBD remains in the autoclave during scCO_2 extraction, and that DMT is being selectively extracted over the additional low molecular weight products as illustrated by the substantial shouldering of the aryl and methyl peaks (Fig. 5.44).

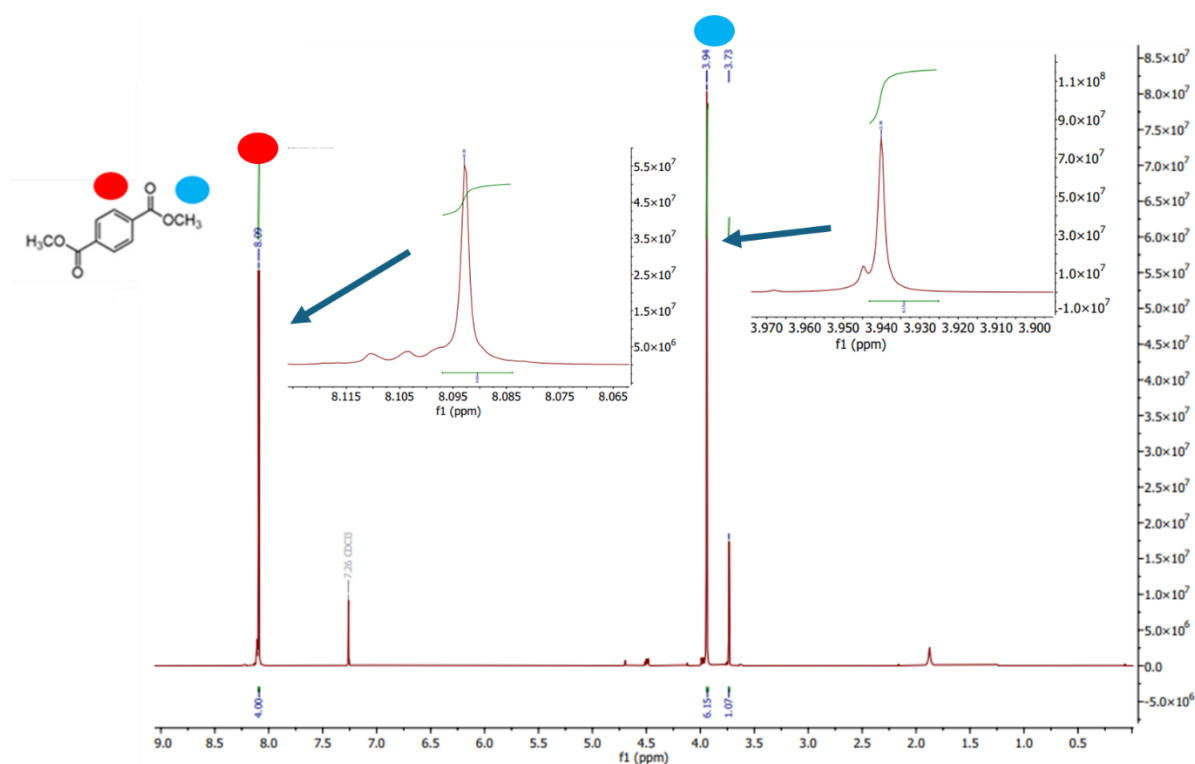


Figure 5.43 – ^1H NMR of the dry product removed from a high-pressure autoclave via scCO_2 extraction. Inserts illustrate minimal shouldering of DMT peaks.

Temperature = 65 °C, time = 30 minutes, Pressure = 207 bar

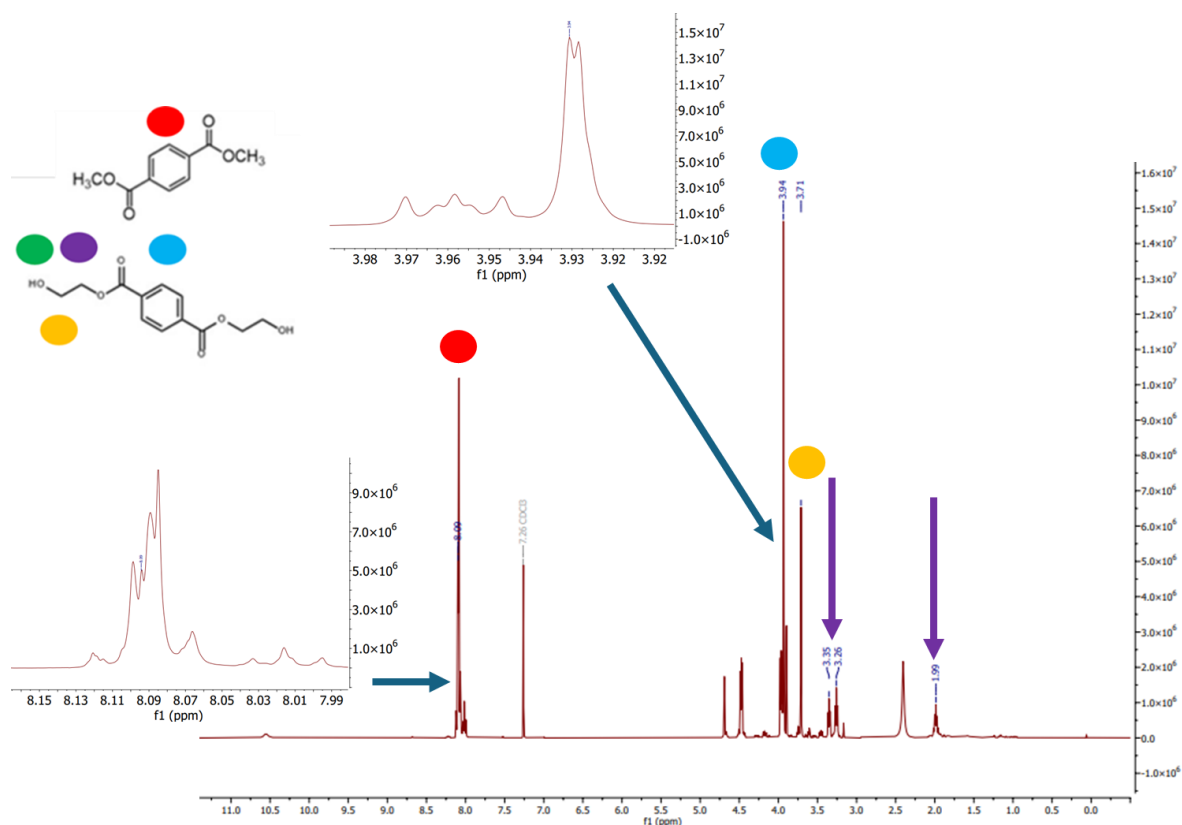


Figure 5.44 - ^1H NMR of the residue remaining in a high-pressure autoclave post scCO_2 extraction. Inserts illustrate substantially more shouldering of the DMT peaks in comparison to Figure 5.44, and TBD peaks are highlighted by purple arrows.

Temperature = 65 °C, time = 30 minutes, Pressure = 207 bar

GC-MS also confirms DMT is being selectively removed from the reaction mixture above all other components. The relative intensity of the peak in the chromatogram which corresponds to DMT (14.28 min) is far higher than the other components when the extracted material is analysed (Fig. 5.45). In comparison the peaks in the chromatogram of the residue from the autoclave, which correspond to the additional low molecular weight products, are more intense than that of DMT – matching the extensive shouldering seen in the ^1H NMR (Fig. 5.44).

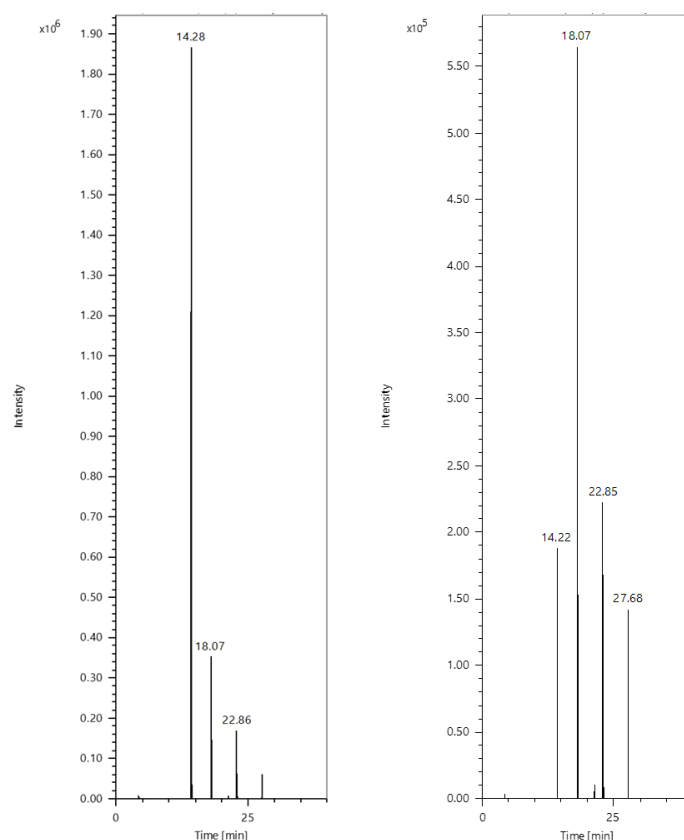


Figure 5.45 – TICC of the dry product removed from a high-pressure autoclave via scCO_2 extraction (left) and the corresponding residue remaining in the autoclave post-extraction (right).

Temperature = 65°C, time = 30 minutes, Pressure = 207 bar

5.3.5 Expanding the Scope to Real World Materials

Methanolysis of PET in scCO_2 , followed by product isolation *via* a separate scCO_2 extraction, was performed on a Starbucks cup, resulting in a dry, white powder product and a viscous green liquid (Fig. 5.48).

The Starbucks cup was degraded with a 5:1 MeOH :PET ratio at 180 °C for 30 minutes at 172 bar, followed by a 60 minute extraction at 65 °C and 207 bar as a separate step. ^1H NMR of the fraction collected after removal *via* scCO_2 extraction, and the fraction that remained in the autoclave, illustrated that an identical result was obtained in the one-pot procedure in this previous section (Fig. 5.48) (Fig. 5.49).



Figure 5.48 – (Top) Original Starbucks cup (left) and the damp solid product resulting from methanolysis in scCO_2 (right).

(Bottom) – Dry, white powder isolated from the crude product via scCO_2 extraction (left) and the corresponding viscous liquid left over in the autoclave (right).

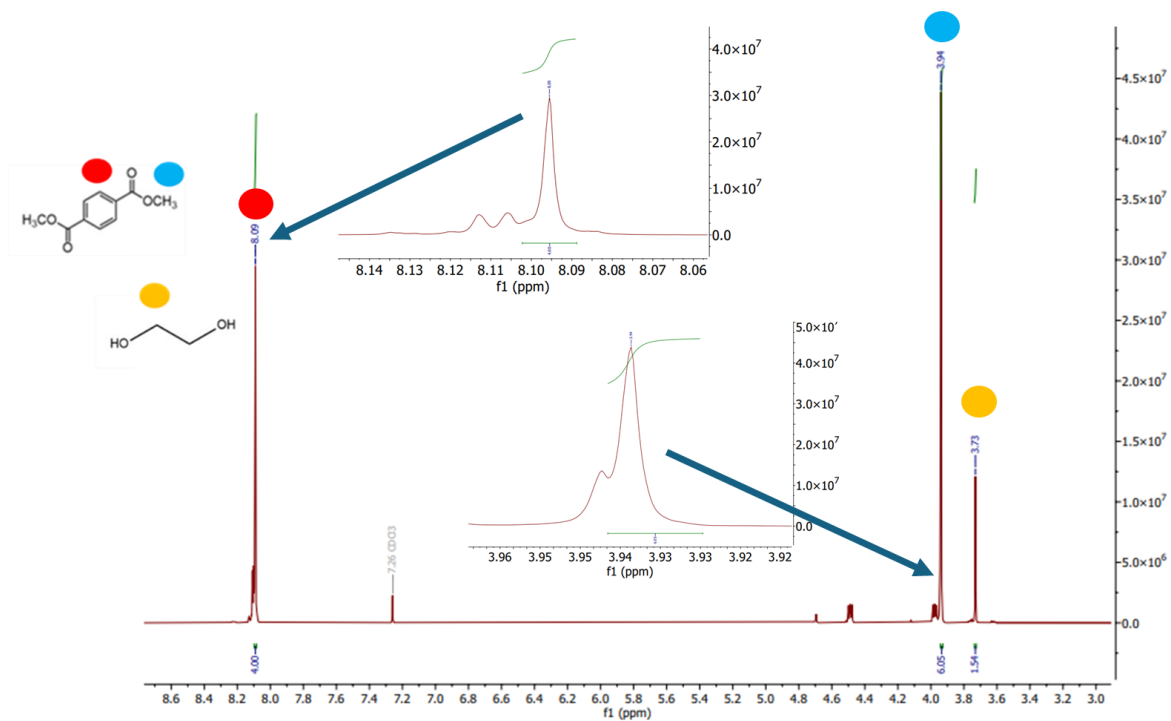


Figure 5.48 - ^1H NMR of the dry product removed from a high-pressure autoclave via scCO_2 extraction. Inserts illustrate minimal shouldering of DMT peaks.

Temperature = 65 °C, time = 60 minutes, Pressure = 207 bar

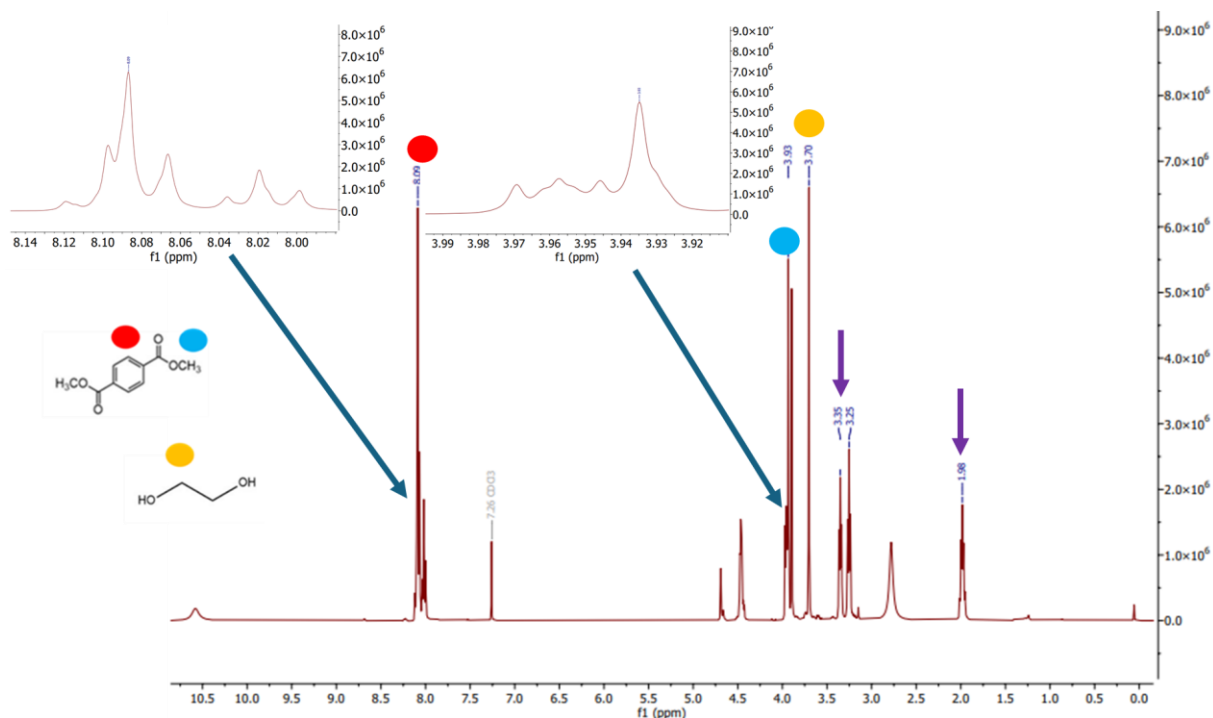


Figure 5.49 - ^1H NMR of the dry product removed from a high-pressure autoclave via scCO_2 extraction. Inserts illustrate minimal shouldering of DMT peaks. TBD peaks are indicated by purple arrows.

Temperature = 65 °C, time = 60 minutes, Pressure = 207 bar

5.4 Conclusions

In this chapter, the successful methanolysis of PET in scCO_2 has been demonstrated. Using scCO_2 as the primary solvent has enabled the development of a closed-loop recycling process with minimal chemical hazards, and almost no solvent waste. Furthermore, two purification strategies have been developed to produce material capable of being re-polymerised back to PET in high yields, also with minimal solvent waste being generated. The substantial reduction in waste solvent is quantified by calculating the E-factor for the methanolysis and purification protocols pioneered in this work and, comparing them to the state-of-the-art in the literature. Finally, the development of a one-pot depolymerisation-extraction protocol was shown as a way to streamline the recycling route, by removing the need to re-pressurise the reactor from ambient between the two steps. A real-world example of PET was also successfully recycled, proving that the protocols developed here can be applied to realistic PET products.

6 Conclusions and Future Work

Overview

Two projects have been envisioned and executed in this work in an attempt to address the urgent need to facilitate a circular approach to the treatment of waste plastic. Improvements over the state-of-the-art have been demonstrated and potential routes to build on this work will be outlined on a chapter-by-chapter basis below.

6.1 Enhancement of Polyethylene Terephthalate's Dielectric Properties via Impregnation in Supercritical Carbon Dioxide

Successful impregnation of ethylene glycol into PET was confirmed via weighing by difference and TGA experiments. An improvement in the dielectric properties of PET was demonstrated by two different methods of cavity perturbation (heat-and-hold and dynamic measurements), confirming that scCO_2 impregnation was a viable route for enhancing the dielectric properties of PET. Further to this, a competing recrystallisation of the polymer when swollen in scCO_2 was confirmed through DSC and DMA analysis, along with X-ray scattering experiments. This work was focused on proof of concept, and there is plenty of opportunities to broaden the scope of exploration.

Ethylene glycol was observed to be partially soluble in scCO_2 and was able to be impregnated into PET, whereas 1,2-DME was completely miscible with scCO_2 at the studied conditions and did not appear to partition into PET as a result of its strong affinity with scCO_2 . A constant pressure of 278 bar was maintained during all impregnation experiments, as this was perceived to be the minimum pressure required to begin to dissolve ethylene glycol in scCO_2 . Lowering the pressure slightly could be explored to reduce the affinity of ethylene glycol for scCO_2 even further, favouring the partitioning of what ethylene glycol does dissolve in the supercritical

phase into the polymer phase. The reduction of ethylene glycol's solubility in scCO_2 could be compensated for by more rapid stirring.

Broadening the scope of guest species studied is another possible way forward. Monomers of PET, with 1,6-HD, were selected for testing as potential microwave susceptors as they were expected to have an excellent affinity for PET once dissolved in scCO_2 . Some examples of potential susceptors are proposed which share structural similarities with ethylene glycol but include additional alkyl regions which would be expected to aid dissolution in scCO_2 (Fig. 6.1).

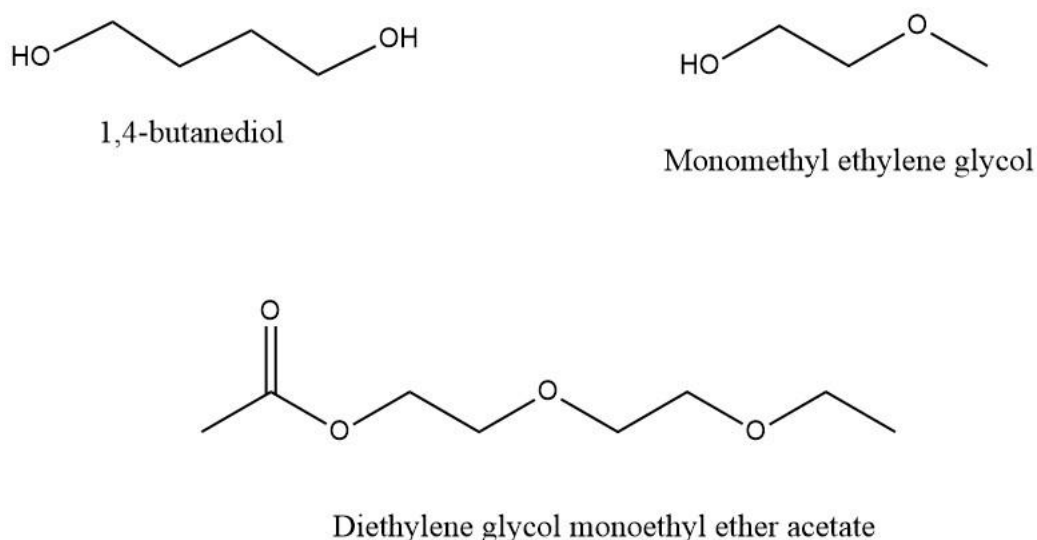


Figure 6.1 – Structures of potential susceptors that could be explored for scCO_2 impregnation into PET

Being unable to digitally control the depressuring rate of the autoclave, because of the manually operated taps, was a major limitation in this work. It prevented the calculation of reliable partition co-efficients, which meant that no trends as to how partitioning of ethylene glycol between scCO_2 and PET varied when the supercritical fluid's density was modified (by varying temperature at a constant pressure) could be quantified. Addition of a backpressure regulator (BPR) on the outlet line could aid in the controlled release of CO_2 at the end of an impregnation experiment (Fig. 6.2). Control of a BPR by way of appropriate software could allow for a gradual release of CO_2 , by slowly reducing the value of the pressure at which the BPR valve would open.

This would enable the development of a reproducible gradient at which the pressure was released from the autoclave.

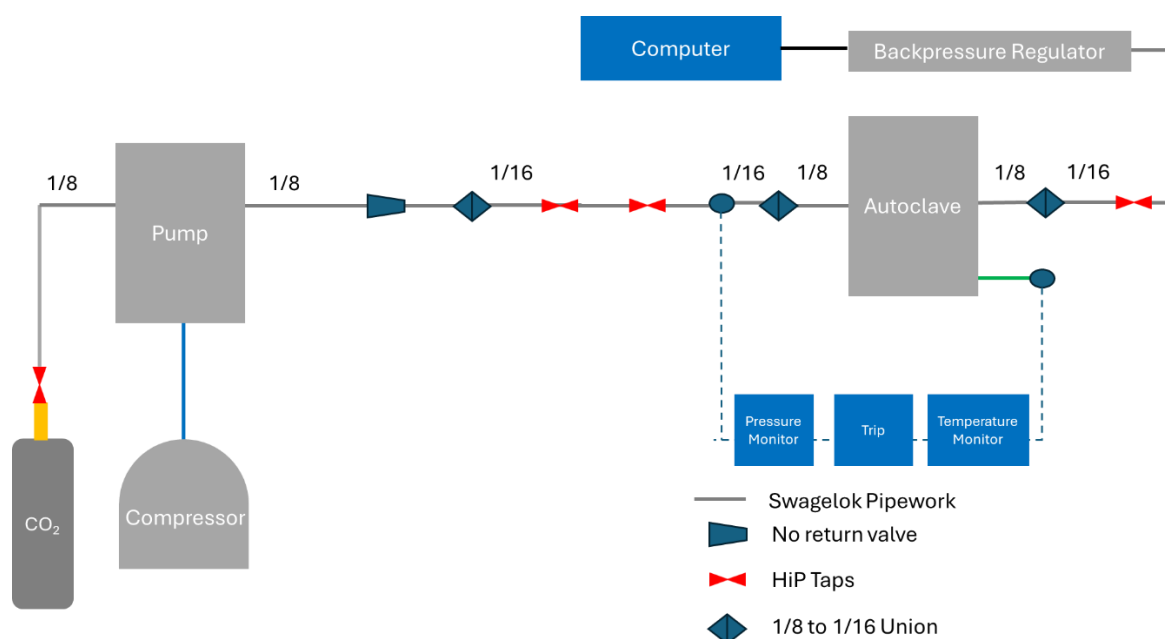


Figure 6.2 – Line diagram from Chapter 2 adapted to include a backpressure regulator at the end of the outlet line to control CO₂ release at the end of an experiment.

6.2 Microwave Pyrolysis of Polyethylene Terephthalate

Successful impregnation of ethylene glycol at the 0.5 g scale demonstrated in Chapter 3 led onto microwave pyrolysis experiments of PET in Chapter 4 at a scale of 15 g. A clear enhancement in the ability of PET to absorb microwave power was observed, and a corresponding increase in heating rate was observed. However, this did not appear to result in either an appreciable increase in PET conversion, or a reduction in specific energy for the same degree of conversion. This is postulated to be because of ethylene glycol desorbing from the PET once a temperature of 200 °C is exceeded, as evidence by TGA analysis. Two approaches are suggested here to overcome this limitation of using an organic molecule as a susceptor:

1. Investigate the use of organic material with a higher boiling point than ethylene glycol, such as glycerol, which would be expected to persist for a longer period in the quartz reactor.

2. Continuously inject fresh impregnated PET into the quartz reactor to replenish the glycol which has desorbed from the system or has degraded as a result of the temperature.

Product analysis was also complicated by the limited solubility of the pyrolysis products in solvents compatible with chromatographic techniques. Many HPLCs are not compatible with DMF or DMSO as they are capable of swelling the fittings in the instrument and causing leaks. GPC instruments often contain metal fittings between components, and these should be compatible with DMSO or DMF. Moving an HPLC column onto a GPC instrument could be one way around the analysis issues. Different fractions could then be collected manually and isolated from one another after passing through the column.

6.3 Supercritical Depolymerisation of Polyethylene Terephthalate

Successful depolymerisation of PET via methanolysis in scCO_2 was proven in Chapter 5. Two low-solvent waste routes to purify the crude product and generate a truly closed-loop process were also established. A greater understanding of how varying the temperature or catalyst impacts the yield of DMT, which can be used to track the degree of depolymerisation, could be attained by applying the quantitative GC-MS work to crude products.

Replacing methanol as the nucleophile for solvolysis with ethylene glycol, water, ethanol or an amine would allow a different terephthalate-based product to be produced. Proving that solvolysis in scCO_2 is a viable route to generate a range of useful products besides DMT.

scCO_2 extraction was also proven to be an appropriate strategy for removal of DMT and other low molecular weight products, but ethylene glycol has not yet been isolated from the catalyst. Once all terephthalate-based solvolysis products have been removed from the autoclave, injection of a co-solvent through use of a HPLC pump could be investigated as a route to selectively remove either ethylene glycol or TBD from the autoclave in a second extraction step.

7 References

1. R. Geyer, J. R. Jambeck and K. L. Law, *Science Advances*, 2017, **3**, 1700782.
2. Conversio, Global Plastics Flow, https://www.carboliq.com/pdf/19_conversio_global_plastics_flow_2018_summary.pdf, (accessed 9th June, 2024).
3. What is the Linear Economy?, <https://www.ellenmacarthurfoundation.org/what-is-the-linear-economy>, (accessed 9th June, 2024).
4. What is a Circular Economy?, <https://www.ellenmacarthurfoundation.org/topics/circular-economy-introduction/overview>, (accessed 9th June, 2024).
5. J. C. Warner and P. T. Anastas, *Green Chemistry: theory and Practice, 12 Principles of Green Chemistry*, Chemistry Oxford Press, Oxford, 1998.
6. UNCED, Agenda 21, <https://sdgs.un.org/publications/agenda21>, (accessed 9th June, 2024).
7. U. N. Department of Economic and Social Affairs, The 17 Goals, <https://sdgs.un.org/goals>, (accessed 9th June, 2024).
8. A. L. Brooks, S. Wang and J. R. Jambeck, *Science Advances*, 2018, **4**, 0131.
9. From Green Fence to red alert: A China timeline, <https://resource-recycling.com/recycling/2018/02/13/green-fence-red-alert-china-timeline/>, (accessed 9th June, 2024).
10. What Operation Green Fence has Meant for Recycling, <https://www.waste360.com/waste-management-business/what-operation-green-fence-has-meant-for-recycling>, (accessed 9th June 2024, 2024).
11. Why is UK recycling being dumped by Turkish roadsides?, <https://www.bbc.co.uk/news/av/uk-53181948>, (accessed 9th June, 2024).
12. D. González-Fernández, A. Cózar, G. Hanke, J. Viejo, C. Morales-Caselles, R. Bakiu, D. Barceló, F. Bessa, A. Bruge, M. Cabrera, J. Castro-Jiménez, M. Constant, R. Crosti, Y. Galletti, A. E. Kideys, N. Machitadze, J. Pereira de Brito, M. Pogojeva, N. Ratola, J. Rigueira, E. Rojo-Nieto, O. Savenko, R. I. Schöneich-

- Argent, G. Siedlewicz, G. Suaria, M. Tourgeli, D. González-Fernández, A. Cózar, G. Hanke, J. Viejo, C. Morales-Caselles, R. Bakiu, D. Barceló, F. Bessa, A. Bruge, M. Cabrera, J. Castro-Jiménez, M. Constant, R. Crosti, Y. Galletti, A. E. Kideys, N. Machitadze, J. Pereira de Brito, M. Pogojeva, N. Ratola, J. Rigueira, E. Rojo-Nieto, O. Savenko, R. I. Schöneich-Argent, G. Siedlewicz, G. Suaria and M. Tourgeli, *Nature Sustainability*, 2021, **4**, 474–483.
13. Z. Bilginsoy, Turkey bans polyethylene plastic imports, <https://apnews.com/article/middle-east-europe-turkey-global-trade-business-1ca9dad71a8b2e65406ae80a8f61326a>, (accessed 9th June, 2024).
 14. S. Gündoğdu and T. R. Walker, *Marine Pollution Bulletin*, 2021, **171**, 112772.
 15. <https://www.basel.int/TheConvention/Overview/tabid/1271/Default.aspx>, (accessed 9th June, 2024).
 16. Plastics Recycling, https://www.bpf.co.uk/Sustainability/Plastics_Recycling.aspx, (accessed 9th June, 2024).
 17. Recycling Roadmap, <https://www.bpf.co.uk/roadmap#Report%20isssuu%20iframe>, (accessed 11th June, 2024).
 18. Q. Huang, Z. Cheng, C. Yang, H. Wang, N. Zhu, X. Cao and Z. Lou, *Water Research*, 2022, **223**, 119035.
 19. R. C. Thompson, C. J. Moore, F. S. vom Saal and S. H. Swan, *Philosophical Transactions of the Royal Society*, 2009, **364**, 2153-2166.
 20. C. Campanale, C. Massarelli, I. Savino, V. Locaputo, V. F. Uricchio, C. Campanale, C. Massarelli, I. Savino, V. Locaputo and U. V. Felice, *International Journal of Environmental Research and Public Health*, 2020, **17**, 1212.
 21. X. Wang, X.-R. Jiang, F. Wu, Y. Ma, X. Che, X. Chen, P. Liu, W. Zhang, X. Ma and G.-Q. Chen, *Biotechnology Journal*, 2019, **14**, 1900132.
 22. H. Chen, H. Chen, S. Nan, H. Liu, L. Chen, L. Yu, H. Chen, H. Chen, S. Nan, H. Liu, L. Chen and L. Yu, *Bulletin of Environmental Contamination and Toxicology*, 2022, **109**, 882-892.
 23. M. D. Sharma, A. I. Elanjickal, J. S. Mankar and R. J. Krupadam, *Journal of Hazardous Materials*, 2020, **398**, 122994.

24. K. J. Groh, T. Backhaus, B. Carney-Almroth, B. Geueke, P. A. Inostroza, A. Lennquist, H. A. Leslie, M. Maffini, D. Slunge, L. Trasande, A. M. Warhurst and J. Muncke, *Science of The Total Environment*, 2019, **651**, 3253-3268.
25. A. Yasuhara, *Journal of Chromatography A*, 1997, **774**, 321-332.
26. C. M. Rochman, R. L. Lewison, M. Eriksen, H. Allen, A.-M. Cook and S. J. Teh, *The Science of the total environment*, 2014, **476-477**, 622-633.
27. K. Tanaka, H. Takada, R. Yamashita, K. Mizukawa, M.-a. Fukuwaka and Y. Watanuki, *Marine pollution bulletin*, 04/15/2013, **69**, 219-222.
28. M. C. Fossi, L. Marsili, M. Baini, M. Giannetti, D. Coppola, C. Guerranti, I. Caliani, R. Minutoli, G. Lauriano, M. G. Finoia, F. Rubegni, S. Panigada, M. Bérubé, J. U. Ramíre and C. Panti, *Environmental Pollution*, 2016, **209**, 68-78.
29. S. Vincoff, B. Schleupner, J. Santos, M. Morrison, N. Zhang, M. M. Dunphy-Daly, W. C. Eward, A. J. Armstrong, Z. Diana and J. A. Somarelli, *Environmental Science & Technology*, 2024, **58**, 10445-10457.
30. Y. Chen, Z. Cui, X. Cui, W. Liu, X. Wang, X. Li and S. Li, *Resources, Conservation and Recycling*, 2019, **146**, 348-357.
31. F. Perugini, M. L. Mastellone and U. Arena, *Environmental Progress*, 2005, **24**, 137-154.
32. C. C. Wiles, *Journal of Hazardous Materials*, 1996, **47**, 325-344.
33. S. Hohn, E. Acevedo-Trejos, J. F. Abrams, J. F. d. Moura, R. Spranz and A. Merico, *The Science of the total environment*, 2020, **746**, 141115.
34. R. Nisticò, *Polymer Testing*, 2020, **90**, 106707.
35. L. W. Chen and J. W. Chen, *Journal of Applied Polymer Science*, 2000, **75**, 1229-1234.
36. A. L. Jadhav, R. S. Malkar and G. D. Yadav, *ACS Omega*, 2020, **5**.
37. J. W. Chen and L. W. Chen, *Journal of Polymer Science Part A: Polymer Chemistry*, 1999, **37**, 1797-1803.
38. How to keep a sustainable PET recycling industry in Europe, <https://www.epbp.org/>, (accessed 25th September, 2024).

39. Deposit Return Scheme for drinks containers: joint policy statement, <https://www.gov.uk/government/publications/deposit-return-scheme-for-drinks-containers-policy-statements/deposit-return-scheme-for-drinks-containers-joint-policy-statement>, (accessed 8th July, 2024).
40. Deposit Return Scheme for drinks containers moves a step closer, <https://www.gov.uk/government/news/deposit-return-scheme-for-drinks-containers-moves-a-step-closer>, (accessed 20th July, 2024).
41. E. Commission, European Union Plastics Strategy, https://environment.ec.europa.eu/strategy/plastics-strategy_en, (accessed 8th July, 2024).
42. S. Rhein and K. F. Sträter, *GAIA - Ecological Perspectives for Science and Society*, 2021, **30**, 250-256.
43. H. R. Customs, Plastic Packaging Tax, <https://www.gov.uk/government/collections/plastic-packaging-tax>, (accessed 8th July, 2024).
44. KPMG, Plastic Taxes - A European Perspective, <https://kpmg.com/xx/en/home/insights/2022/11/plastic-taxes-a-european-perspective.html>, (accessed 8th July, 2024).
45. R. A. Sheldon and M. Norton, *Green Chemistry*, 2020, **22**, 6310-6322.
46. Closed and Open Loop Plastic Recycling, <https://www.bpf.co.uk/press/closed-and-open-loop-plastic-recycling.aspx>, (accessed 9th July, 2024).
47. Mechanical plastics recycling production anticipated to reach over 54 million tonnes by 2030, <https://www.amiplastics.com/insights/mechanical-plastics-recycling-production-anticipated-to-reach-over-54-million-tonnes-by-2030>, (accessed 9th July, 2024).
48. I. Vollmer, M. J. F. Jenks, M. C. P. Roelands, R. J. White, T. v. Harmelen, P. d. Wild, G. P. v. d. Laan, F. Meirer, J. T. F. Keurentjes and B. M. Weckhuysen, *Angewandte Chemie (International ed. in English)*, 2020, **59**, 15402-15423.
49. L. Dong, W. Zhi, J. Li and W. Li, *ACS Sustainable Resource Management*, April 26, 2024, **1**, 908-915.
50. L. Dong, Z. Huang, Y. Qin and W. Zhi, *Journal of Cleaner Production*, 2024, **447**, 141477.

51. J.-P. Lange, *ACS Sustainable Chemistry & Engineering*, 2021, **9**, 15722–15738.
52. M. Strangl, E. Ortner, T. Fell, T. Ginzinger and A. Buettner, *Journal of Cleaner Production*, 2020, **260**, 121104.
53. M. Roosen, T. D. Somer, R. Demets, S. Ügdüler, V. Meesseman, B. V. Gorp, K. Ragaert, K. M. V. G. C. Walgraeve, A. Dumoulin and S. D. Meester, *Waste Management*, 2021, **120**, 564-575.
54. J. F. Stevenson, *Extrusion of Rubber and Plastics. Comprehensive Polymer Science and Supplements*, Pergamom, Oxford, 1989.
55. Dynisco, An Introduction to Single Screw Extrusion, <https://www.azom.com/article.aspx?ArticleID=13566>, (accessed 13th July, 2024).
56. J. Maris, S. Bourdon, J.-M. Brossard, L. Cauret, L. Fontaine and V. Montembault, *Polymer Degradation and Stability*, 2018, **147**, 245-266.
57. J. Vera-Sorroche, A. Kelly, E. Brown, P. Coates, N. Karnachi, E. Harkin-Jones, K. Li and J. Deng, *Applied Thermal Engineering*, 2013, **53**, 405-413.
58. G. Gryn'ova, G. Gryn'ova, J. L. Hodgson, J. L. Hodgson, M. L. Coote and M. L. Coote, *Organic & Biomolecular Chemistry*, 2010, **9**, 480-490.
59. P. Oblak, J. G.-G. B. Zupančič, A. Aulova and I. Emri, *Polymer Degradation and Stability*, 2015, **114**, 133-145.
60. A. S. A. F.-F. T. Bögl, J. Fischer and W. Buchberger, *Polymer Degradation and Stability*, 2021, **192**, 109689.
61. J. D. Badia, E. Strömberg, S. Karlsson and A. Ribes-Greus, *Polymer Degradation and Stability*, 2012, **97**, 98-107.
62. The Future of Plastic, <https://cen.acs.org/sections/discovery-reports/the-future-of-plastic.html>, (accessed 13th July, 2024).
63. V. Sankar and A. Kumar, *Recycling of Polymers, methods, characterization and applications*, Wiley-VCH, Weinheim, 2017.
64. G. P. Thomas, Recycling of Polypropylene, <https://www.azocleantech.com/article.aspx?ArticleID=240#:~:text=This%20varies%20with%20the%20use,%20as%20clothes%20or%20playground%20equipment>, (accessed 13th July, 2024).

65. A. Holmes, How Many Times Can That Be Recycled?, <https://earth911.com/business-policy/how-many-times-recycled/>, (accessed 13th July, 2024).
66. A. Midilli, H. Kucuk, M. Haciosmanoglu, U. Akbulut and I. Dincer, *International Journal of Energy Research*, 2022, **46**, 4001-4032.
67. J.-K. Kim, Y.-S. Jeong, J.-W. Kim and J.-S. Kim, *Energy*, 2023, **276**, 127651.
68. S. Elkhailifa, T. Al-Ansari, H. R. Mackey and G. McKay, *Resources, Conservation and Recycling*, 2019, **144**, 310-320.
69. D. Mohan, C. U. P. Jr and P. H. Steele, *Energy Fuels*, 2006, **2020**, 848-889.
70. D. Yao, H. Yang, H. Chen and P. T. Williams, *Applied Catalysis B: Environmental*, 2018, **239**, 565-577.
71. H. Bamdad, K. Hawboldt and S. MacQuarrie, *Renewable and Sustainable Energy Reviews*, 2018, **81**, 1705-1720.
72. T. Bridgwater, *Johnson Matthey Technology Review*, 2018, **62**, 118-130.
73. F. Mayer, R. Bhandari and S. Gäth, *The Science of the Total Environment*, 2019, **672**, 708-721.
74. S. M. Al-Salem, A. Antelava, A. Constantinou, G. Manos and A. Dutta, *Journal of Environmental Management*, 2017, **197**, 177-198.
75. T. Kuppens, M. V. Dael, K. Vanreppelen, T. Thewys, J. Yperman, R. Carleer, S. Schreurs and S. V. Passel, *Journal of Cleaner Production*, 2015, **88**, 336-344.
76. D. V. Suriapparao, D. V. Suriapparao, R. Vinu and R. Vinu, *RSC Advances*, 2015, **5**, 57619-57631.
77. O. Soka and O. Oyekola, *Heliyon*, 2020, **6**, e04346.
78. K. Song, Y. Li, F. Huo, J. Liu, W. Hou, N. Wang, Q. Zhou, J. Xu and X. Lu, *The Canadian Journal of Chemical Engineering*, 2023, **101**, 4395-4408.
79. X. Yuan, S. Li, S. Jeon, S. Deng, L. Zhao and K. B. Lee, *Journal of Hazardous Materials*, 2020, **399**, 123010.
80. L. Xu, L.-y. Zhang, H. Song, Q. Dong, G.-h. Dong, X. Kong and Z. Fang, *Waste Management*, 2019, **92**, 97-106.

81. L. Chen, S. Wang, H. Meng, Z. Wu and J. Zhao, *Applied Thermal Engineering*, 2017, **111**, 834-846.
82. Ö. Çepelioğullar and A. E. Pütün, *Journal of Analytical and Applied Pyrolysis*, 2014, **110**, 363-374.
83. G. R. Mong, C. T. Chong, W. W. F. Chong, J.-H. Ng, H. C. Ong, V. Ashokkumar, M.-V. Tran, S. Karmakar, B. H. H. Goh and M. F. M. Yasin, *Fuel*, 2022, **324**, 124777.
84. N. Zhou, L. Dai, Y. Lv, H. Li, W. Deng, F. Guo, P. Chen, H. Lei and R. Ruan, *Chemical Engineering Journal*, 2021, **418**, 129412.
85. <https://www.webofscience.com/wos/woscc/summary/f664ed47-5a8a-4959-9546-bc75dcd39fb8-fbba4676/relevance/1>, (accessed 15th July, 2024).
86. A. J. Bur, *Polymer*, 1985, **26**, 963-977.
87. J. Kobayashi, M. Hori, N. Kobayashi, Y. Itaya, S. Hatano and S. Mori, *Journal of Chemical Engineering of Japan*, 2019, **52**, 656-661.
88. S. S. Lam, H. A. Chase, S. S. Lam and H. A. Chase, *Energies*, 2012, **5**, 4209-4232.
89. M. Bhattacharya and T. Basak, *Energy*, 2016, **97**, 306-338.
90. C. Ludlow-Palafox and H. A. Chase, *Industrial & Engineering Chemistry Research*, 2001, **40**, 4749-4756.
91. A. Undri, L. Rosi, M. Frediani and P. Frediani, *Fuel*, 2014, **116**, 662-671.
92. Z. Hussain, K. M. Khan, S. Perveen, K. Hussain and W. Voelter, *Fuel Processing Technology*, 2012, **94**, 145-150.
93. Z. Hussain, K. M. Khan and K. Hussain, *Journal of Analytical and Applied Pyrolysis*, 2010, **89**, 39-43.
94. M. Dai, H. Xu, Z. Yu, S. Fang, L. Chen, W. Gu and X. Ma, *Applied Thermal Engineering*, 2018, **136**, 9-15.
95. B. K. Kandola, A. R. Horrocks, D. Price and G. V. Coleman, *Journal of Macromolecular Science, Part C: Polymer Reviews*, 1996, **36**, 721-794.
96. H. Yu, J. Qu, Y. Liu, H. Yun, X. Li, C. Zhou, Y. Jin, C. Zhang, J. Dai and X. Bi, *Science of The Total Environment*, 2022, **806**, 150903.

97. A. Mohanty, D. K. Patel and S. K. Panigrahi, *International Journal of Thermal Sciences*, 2024, **196**, 108674.
98. V. Piemonte, S. Sabatini, F. Gironi, V. Piemonte, S. Sabatini and F. Gironi, *Journal of Polymers and the Environment*, 2013, **21**, 640-647.
99. A.-J. Minor, R. Goldhahn, L. Rihko-Struckmann and K. Sundmacher, *Chemical Engineering Journal*, 2023, **474**, 145333.
100. I. Omrani and R. M. Berenjegani, *ACS Applied Polymer Materials*, 2024, **6**, 10698–10705.
101. Y. Liu and X.-B. Lu, *Journal of Polymer Science*, 2022, **60**, 3256-3268.
102. S. R. Shukla and A. M. Harad, *Polymer Degradation and Stability*, 2006, **91**, 1850-1854.
103. R. Shamsi, M. Abdouss, G. M. M. Sadeghi and F. A. Taromi, *Polymer International*, 2009, **58**, 22-30.
104. M. M. Aslzadeh, G. M. M. Sadeghi and M. Abdouss, *Materialwissenschaft und Werkstofftechnik*, 2010, **41**, 682-688.
105. S. R. Shukla, P. U. Kapadi, S. T. Mhaske, M. N. Mali and A. More, *Journal of Vinyl and Additive Technology*, 2017, **23**, 152-160.
106. A. P. More, R. A. Kute, S. T. Mhaske, A. P. More, R. A. Kute and S. T. Mhaske, *Iranian Polymer Journal* 2013 23:1, 2013, **23**, 59-67.
107. Y. S. Parab, P. A. Wasekar, S. T. Mhaske, S. R. Shukla, Y. S. Parab, P. A. Wasekar, S. T. Mhaske and S. R. Shukla, *Polymer Bulletin*, 2014, **71**, 2695-2707.
108. N. D. Pingale and S. R. Shukla, *European Polymer Journal*, 2009, **45**, 2695-2700.
109. D. S. Achilias, G. P. Tsintzou, A. K. Nikolaidis, D. N. Bikiaris and G. P. Karayannidis, *Polymer International*, 2011, **60**, 500-506.
110. R. V. Shah, V. S. Borude and S. R. Shukla, *Journal of Applied Polymer Science*, 2013, **127**, 323-328.
111. R. V. Shah and S. R. Shukla, *Journal of Applied Polymer Science*, 2012, **125**, 3666-3675.

112. C. Jehanno, M. M. Pérez-Madrigal, J. Demarteau, H. Sardon and A. P. Dove, *Polymer Chemistry*, 2019, **10**, 172-186.
113. Y. Weng, C.-B. Hong, Y. Zhang and H. Liu, *Green Chemistry*, 2024, **26**, 571-592.
114. F. Cao, L. Wang, R. Zheng, L. Guo, Y. Chen and X. Qian, *RSC Advances*, 2022, **12**, 31564-31576.
115. T. E. Darai, A. Ter-Halle, M. Blanzat, G. Despras, V. Sartor, G. Bordeau, A. Lattes, S. Franceschi, S. Cassel, N. Chouini-Lalanne, E. Perez, C. Déjugnat and J. C. Garrigues, *Green Chemistry*, 2024, **26**, 6857-6885.
116. A. S. Joshi, Niloofar Alipourasiabi, Keerthi Vinnakota, M. R. Coleman, J. G. Lawrence, A. S. Joshi, Niloofar Alipourasiabi, Keerthi Vinnakota, M. R. Coleman and J. G. Lawrence, *RSC Advances*, 2021, **11**, 23506-23518.
117. J. Clayden, N. Greeves and S. Warren, *Organic Chemistry*, University Oxford Press, Oxford, Second edn., 2012.
118. A. Kržan, *Journal of Applied Polymer Science*, 1998, **69**, 1115-1118.
119. A. Kržan, *Polymers for Advanced Technologies*, 1999, **10**, 603-606.
120. H. Kurokawa, M. A. Ohshima, K. Sugiyama and H. Miura, *Polymer Degradation and Stability*, 2003, **79**, 529-533.
121. S. Mishra and A. S. Goje, *Polymer International*, 2003, **52**, 337-342.
122. C.-H. Chen, C.-Y. Chen, Y.-W. Lo, C.-F. Mao and W.-T. Liao, *Journal of Applied Polymer Science*, 2001, **80**, 943-948.
123. F. Hubert, G. Durand and G. Tersac, *Journal of Applied Polymer Science*, 1999, **72**, 329-340.
124. A. C. Sánchez and S. R. Collinson, *European Polymer Journal*, 2011, **47**, 1970-1976.
125. D. P. R. Kint, A. Alla, E. Deloret, J. L. Campos and S. Muñoz-Guerra, *Polymer*, 2003, **44**, 1321-1330.
126. A. Södergård and M. Stolt, *Progress in Polymer Science*, 2002, **27**, 1123-1163.
127. M. Arnoult, E. Dargent and J. F. Mano, *Polymer*, 2007, **48**, 1012-1019.

128. I. Kaljurand, A. Kütt, L. Sooväli, T. Rodima, V. Mäemets, I. Leito and I. A. Koppel, *The Journal of Organic Chemistry*, 2005, **70**, 1019-1028.
129. A. M. Hyde, R. Calabria, R. Arvary, X. Wang and A. Klapars, *Organic Process Research & Development*, 2019, **23**, 1860-1871.
130. M. K. Kiesewetter, E. J. Shin, J. L. Hedrick and R. M. Waymouth, *Macromolecules*, 2010, **43**, 2093-2107.
131. N. E. Kamber, W. Jeong, R. M. Waymouth, R. C. Pratt, B. G. G. Lohmeijer and J. L. Hedrick, *Chemical Reviews*, 2007, **107**, 5813-5840.
132. K. Fukushima, O. Coulembier, J. M. Lecuyer, H. A. Almegren, A. M. Alabdulrahman, F. D. Alsewailem, M. A. McNeil, P. Dubois, R. M. Waymouth, H. W. Horn, J. E. Rice and J. L. Hedrick, *Journal of Polymer Science Part A: Polymer Chemistry*, 2011, **49**, 1273-1281.
133. K. Fukushima, J. M. Lecuyer, D. S. Wei, H. W. Horn, G. O. Jones, H. A. Al-Megren, A. M. Alabdulrahman, F. D. Alsewailem, M. A. McNeil, J. E. Rice and J. L. Hedrick, *Polymer Chemistry*, 2013, **4**, 1610-1616.
134. E. Quaranta, D. Sgherza and G. Tartaro, *Green Chemistry*, 2017, **19**, 5422-5434.
135. T. Do, E. R. Baral and J. G. Kim, *Polymer*, 2018, **143**, 106-114.
136. A. Chuma, H. W. Horn, W. C. Swope, R. C. Pratt, L. Zhang, B. G. G. Lohmeijer, C. G. Wade, R. M. Waymouth, J. L. Hedrick and J. E. Rice, *Journal of the American Chemical Society*, 2008, **130**, 6749-6754.
137. L. Simón and J. M. Goodman, *The Journal of Organic Chemistry*, 2007, **72**, 9656-9662.
138. R. C. Pratt, B. G. G. Lohmeijer, D. A. Long, R. M. Waymouth and J. L. Hedrick, *Journal of the American Chemical Society*, 2006, **128**, 4556-4557.
139. H. W. Horn, G. O. Jones, D. S. Wei, K. Fukushima, J. M. Lecuyer, D. J. Coady, J. L. Hedrick and J. E. Rice, *The Journal of Physical Chemistry A*, 2012, **116**, 12389-12398.
140. Minoru Genta, Tomoko Iwaya, Mitsuru Sasaki, a. Motonobu Goto and T. Hirose, *Industrial & Engineering Chemistry Research*, 2005, **44**, 3894-3900.
141. M. Čolnik, Ž. Knez and M. Škerget, *Chemical Engineering Science*, 2021, **233**, 116389.

142. J. Hu and W. Deng, *Journal of Cleaner Production*, 2016, **113**, 931-946.
143. T. Adschiri, Y.-W. Lee, M. Goto and S. Takami, *Green Chemistry*, 2011, **13**, 1380-1390.
144. J. Xu, Z. Jiang, L. Li and T. Fang, *RSC Advances*, 2014, **4**, 23447-23455.
145. Y. Yang, Y. Lu, H. Xiang, Y. Xu and Y. Li, *Polymer Degradation and Stability*, 2002, **75**, 185-191.
146. M. Goto, M. Sasaki, T. Hirose, M. Goto, M. Sasaki and T. Hirose, *Journal of Materials Science*, 2006, **41**, 1509-1515.
147. S. Yamamoto, M. Aoki and M. Yamagata, *Research and Development, Kobe Steel Engineering Reports*, 1996, **46**, 60-63.
148. A. B. Said, C. Guinot, J.-C. Ruiz, A. Grandjean, P. Dole, C. Joly and Y. Chalamet, *The Journal of Supercritical Fluids*, 2016, **110**, 22-31.
149. N. Ajzenberg, F. Trabelsi and F. Recasens, *Chemical Engineering & Technology*, 2000, **23**, 829-839.
150. S. O. Essien, B. Young and S. Baroutian, *Trends in Food Science & Technology*, 2020, **97**, 156-169.
151. S. G. Kazarian, M. F. Vincent, F. V. Bright, C. L. Liotta and C. A. Eckert, *Journal of the American Chemical Society*, 1996, **118**, 1729-1736.
152. Y. Zhang, K. K. Gangwani and R. M. Lemert, *The Journal of Supercritical Fluids*, 1997, **11**, 115-134.
153. J. v. Schnitzler and R. Eggers, *The Journal of Supercritical Fluids*, 1999, **16**, 81-92.
154. B. L. West, S. G. Kazarian, M. F. Vincent, N. H. Brantley and C. A. Eckert, *Journal of Applied Polymer Science*, 1998, **69**, 911-919.
155. O. Muth, T. Hirth and H. Vogel, *The Journal of Supercritical Fluids*, 2000, **17**, 65-72.
156. M. D. Elkovitch and D. L. Tomasko, *Polymer Engineering & Science*, 2000, **40**, 1850-1861.
157. D. Li and B. Han, *Industrial & Engineering Chemistry Research*, 2000, **39**, 4506-4509.

158. L. N. Nikitin, M. O. Gallyamov, R. A. Vinokur, A. Y. Nikolaec, E. E. Said-Galiyev, A. R. Khokhlov, H. T. Jespersen and K. Schaumburg, *The Journal of Supercritical Fluids*, 2003, **26**, 263-273.
159. Y.-T. Shieh, Y.-H. Li, C.-C. Huang and T.-L. Wang, *The Journal of Supercritical Fluids*, 2010, **55**, 373-380.
160. M. A. Singh, R. Hutanu, M. Shea, R. Fraser, T. Plivelic and Y. P. Handa, *Journal of Polymer Science Part B: Polymer Physics*, 2000, **38**, 2457-2467.
161. W. Dan Ding, T. Kuboki, A. Wong, C. B. Park and M. Sain, *RSC Advances*, 2015, **5**, 91544-91557.
162. R. A. Assink, *Journal of Polymer Science: Polymer Physics Edition*, 1975, **13**, 1665-1673.
163. A. Y. Houde, S. S. Kulkarni and M. G. Kulkarni, *Journal of Membrane Science*, 1992, **71**, 117-128.
164. Y. Kamiya, K. Mizoguchi and Y. Naito, *Journal of Polymer Science Part B: Polymer Physics*, 1990, **28**, 1955-1964.
165. J. R. Fried, H.-C. Liu and C. Zhang, *Journal of Polymer Science Part C: Polymer Letters*, 1989, **27**, 385-392.
166. L. C. S. Herek, R. C. Oliveira, A. F. Rubira and N. Pinheiro, *Brazilian Journal of Chemical Engineering*, 2006, **23**, 227-234.
167. P. Alessi, A. Cortesi and I. Kikic, France, 1998.
168. Q. Xu, Y. Chang, J. He, B. Han and Y. Liu, *Polymer*, 2003, **44**, 5449-5454.
169. A. Galia, A. Muratore and G. Filardo, *Industrial & Engineering Chemistry Research*, 2003, **42**, 448-455.
170. S. Curia, A. F. Barclay, S. Torron, M. Johansson and S. M. Howdle, *Philosophical Transactions of the Royal Society A: Mathematical, Physical and Engineering Sciences*, 2015, **373**, 20150073.
171. R. R. Larder, E. Krumins, P. L. Jacob, K. Kortsen, R. Cavanagh, L. Jiang, C. Vuotto, I. Francolini, C. Tuck, V. Taresco and S. M. Howdle, *Polymer Chemistry*, 2022, **13**, 3768-3779.

172. K. Kortsen, H. R. Fowler, P. L. Jacob, E. Krumins, J. C. Lentz, M. R. A. Souhil, V. Taresco and S. M. Howdle, *European Polymer Journal*, 2022, **168**, 111108.
173. K. Kortsen, M. Reynolds-Green, B. Hopkins, A. McLellan, M. J. Derry, P. D. Topham, J. J. Titman, D. J. Keddie, V. Taresco and S. M. Howdle, *Chemical Communications*, 2023, **59**, 14536-14539.
174. A. J. Bur, *Polymer*, 1985, **26**, 963-977.
175. D. V. Suriapparao, D. A. Kumar and R. Vinu, *Sustainable Energy Technologies and Assessments*, 2022, **49**, 101781.
176. X. Jing, J. Dong, H. Huang, Y. Deng, H. Wen, Z. Xu and S. Ceylan, *Journal of Cleaner Production*, 2021, **291**, 125857.
177. Z. Jiang, Y. Liang, F. Guo, Y. Wang, R. Li, A. Tang, Y. Tu, X. Zhang, J. Wang, S. Li and L. Kong, *ChemSusChem*, 2024, **17**, e20240012.
178. Y. Zhang, W. Zhao, B. Li and G. Xie, *Journal of Energy Resources Technology*, 2018, **140**, 040802.
179. S. S. Alam, A. H. Khan, S. S. Alam and A. H. Khan, *International Journal of Environmental Science and Technology*, 2023, **21**.
180. M. R. C and M. R. J, *Industrial Microwave Heating*, Peter Perengius Ltd, London, 3rd edn., 1993.
181. B. Clarke, A. Gregory, D. Cannell, M. Patrick, S. Wylie, I. Youngs and G. Hill, *A Guide to characterisation of dielectric materials at RF and microwave frequencies*, Institute of Measurement and Control, National Physical Laboratory, London, 2003.
182. D. E. Clark and W. H. Sutton, *Annual Review of Materials Science*, 1996, **26**, 299-331.
183. M. Adam, University of Nottingham, 2017.
184. S. O. Nelson and S. Trabelsi, *Journal of Microwave Power and Electromagnetic Energy*, 2012, **46**, 93-107.
185. Camelia Gabriel, Sami Gabriel, Edward H. Grant, Ben S. J. Halstead and D. M. P. Mingos, *Chemical Society Reviews*, 1998, **27**, 213-224.

186. M. Tuhkala, J. Juuti and H. Jantunen, *Journal of Applied Physics*, 2013, **114**, 014108.
187. A. D. Smith, E. Lester, K. J. Thurecht, J. E. Harfi, G. Dimitrakis, S. W. Kingman, J. P. Robinson and D. J. Irvine, *Industrial & Engineering Chemistry Research*, 2010, **49**, 1703-1710.
188. B. Meng, J. Booske and R. Cooper, *IEEE*, 1995, **43**, 2633-2636.
189. J. P. Robinson, S. W. Kingman, R. Barranco, C. E. Snape and H. Al-Sayegh, *Industrial & Engineering Chemistry Research*, 2010, **49**, 459–463.
190. J. Robinson, E. Binner, D. B. Vallejo, N. D. Perez, K. A. Mughairi, J. Ryan, B. Shepherd, M. Adam, V. Budarin, J. Fan, M. Gronnow and F. Peneranda-Foix, *Chemical Engineering Journal*, 2022, **430**, 132975.
191. M. S. Venkatesh and G. S. V. Raghavan, *Canadian Biosystems Engineering*, 2005, **47**, 7.15-17.30.
192. S. O. Nelson, *Transactions of the ASAE*, 1999, **42**, 523-529.
193. S. O. Nelson and P. G. Bartley, *IEEE Transactions on Instrumentation and Measurement*, 1998, **47**, 133-137.
194. X. Shen, Z. Zhao, H. Li, X. Gao and X. Fan, *Materials Today Chemistry*, 2022, **26**, 101166.
195. X. Jie, W. Li, D. Slocombe, Y. Gao, I. Banerjee, S. Gonzalez-Cortes, B. Yao, H. AlMegren, S. Alshihri, J. Dilworth, J. Thomas, T. Xiao and P. Edwards, *Nature Catalysis*, 2020, **3**, 902-912.
196. D. V. Suriapparao and R. Vinu, *Journal of Analytical and Applied Pyrolysis*, 2015, **113**, 701-712.
197. K. N. Aishwarya and N. Sindhu, *Procedia Technology*, 2016, **25**, 990-997.
198. P. Rex, I. P. Masilamani and L. R. Miranda, *Journal of the Energy Institute*, 2020, **93**, 1819-1832.
199. H. Arshad, S. A. Sulaiman, Z. Hussain, Y. Naz and F. Basrawi, *MATEC Web of Conferences*, 2017, **131**, 02005.
200. M. A. Mohsin, M. A. Alnaqbi, R. M. Busheer and Y. Haik, *Catalysis in Industry*, 2018, **10**, 41-48.

201. E. Bäckström, K. Odelius and M. Hakkarainen, *Industrial & Engineering Chemistry Research*, 2017, **56**, 14814-14821.
202. R. Liu, M. Sarker, M. M. Rahman, C. Li, M. Chai, Nishu, R. Cotillon and N. R. Scott, *Progress in Energy and Combustion Science*, 2020, **80**, 100852.
203. M. Xie, M. Cheng, Y. Yang, Z. Huang, T. Zhou, Y. Zhao, P. Xiao, Q. Cen, Z. Liu and B. Li, *Chemical Engineering Journal*, 2024, **498**, 155120.
204. W. Ao, L. Cheng, X. Zhang, J. Fu, Y. Liu, J. Dai and X. Bi, *Journal of Analytical and Applied Pyrolysis*, 2022, **165**, 105564.
205. S. Sicardi, L. Manna and M. Banchero, *The Journal of Supercritical Fluids*, 2000, **17**, 187-194.
206. M. R. D. Giorgi, E. Cadoni, D. Maricca and A. Piras, *Dyes and Pigments*, 2000, **45**, 75-79.
207. S. Sicardi, L. Manna and M. Banchero, *Industrial & Engineering Chemistry Research*, 2000, **39**, 4707-4713.
208. S. G. Kazarian and K. L. A. Chan, *Analyst*, 2003, **128**, 499-503.
209. S. G. Kazarian and G. G. Martirosyan, *International Journal of Pharmaceutics*, 2002, **232**, 81-90.
210. H. Mhemdi, E. Rodier, N. Kechaou and J. Fages, *Journal of Food Engineering*, 2011, **105**, 609-616.
211. D. Tuma and G. M. Schneider, *The Journal of Supercritical Fluids*, 1998, **13**, 37-42.
212. C. B. Kautz, B. Wagner and G. M. Schneider, *The Journal of Supercritical Fluids*, 1998, **13**, 43-47.
213. B. Wagner, C. B. Kautz and G. M. Schneider, *Fluid Phase Equilibria*, 1999, **158-160**, 707-712.
214. A. Ferri, M. Banchero, L. Manna and S. Sicardi, *The Journal of Supercritical Fluids*, 2004, **30**, 41-49.
215. T. T. Ngo, C. L. Liotta, C. A. Eckert and S. G. Kazarian, *The Journal of Supercritical Fluids*, 2003, **27**, 215-221.

216. M.-W. Park and H.-K. Bae, *The Journal of Supercritical Fluids*, 2002, **22**, 65-73.
217. A. Ferri, M. Banchero, L. Manna and S. Sicardi, *The Journal of Supercritical Fluids*, 2006, **37**, 107-114.
218. P. Franco, L. Incarnato and I. D. Marco, *Journal of CO₂ Utilization*, 2019, **34**, 266-273.
219. M. Belizón, M. T. Fernández-Ponce, L. Casas, C. Mantell and E. J. M. d. l. Ossa-Fernández, *Journal of CO₂ Utilization*, 2018, **25**, 56-67.
220. C. C. Bastante, M. J. Cran, L. C. Cardoso, C. M. Serrano, E. J. M. d. l. Ossa and S. W. Bigger, *The Journal of Supercritical Fluids*, 2019, **145**, 181-191.
221. T. Baba, K. Hirogaki, I. Tabata, S. Okubayashi, K. Hisada and T. Hori, *Sen'i Gakkaishi*, 2010, **66**, 63-69.
222. W.-X. Ma, C. Zhao, S. Okubayashi, I. Tabata, K. Hisada and T. Hori, *Journal of Applied Polymer Science*, 2010, **117**, 1897-1907.
223. M. R. Mauricio, F. C. G. Manso, M. H. Kunita, D. S. Velasco, A. C. Bento, E. C. Muniz, G. M. d. Carvalho and A. F. Rubira, *Composites Part A: Applied Science and Manufacturing*, 2011, **42**, 757-761.
224. J. J. McKinnon, A. S. Mitchell and M. A. Spackman, *Chemical Communications*, 1998, **19**, 2071-2072.
225. Ethylene Glycol SDS,
<https://www.sigmaaldrich.com/GB/en/sds/sial/324558?userType=anonymous>,
(accessed 3rd April, 2025).
226. P. Das and P. Tiwari, *Thermochimica Acta*, 2019, **679**, 178340.
227. D. Varga, S. Alkin, P. Glusnitz, B. Péter-Szabó, E. Székely and T. Gamse, *The Journal of Supercritical Fluids*, 2016, **116**, 111-116.
228. A. Rojas, D. Cerro, A. Torres, M. J. Galotto, A. Guarda and J. Romero, *The Journal of Supercritical Fluids*, 2015, **104**, 76-84.
229. M. Al-Hussein, G. Strobl, M. Al-Hussein and G. Strobl, *The European Physical Journal E*, 2001, **6**, 305-314.
230. N. M. Alves, J. F. Mano, E. Balaguer, J. M. M. Dueñas and J. L. G. Ribelles, *Polymer*, 2002, **43**, 4111-4122.

231. A. Hensel, J. Dobbertin, J. E. K. Schawe, A. Boller and C. Schick, *Journal of thermal analysis*, 1996, **46**, 935–954.
232. J. M. Hutchinson, *Thermochimica Acta*, 1998, **324**, 165-174.
233. C. A. Gracia-Fernández, S. Gómez-Barreiro, J. López-Beceiro, J. T. Saavedra, S. Naya and R. Artiaga, *Polymer Testing*, 2010, **29**, 1002-1006.
234. W. Sun, A. P. Vassilopoulos and T. Keller, *International Journal of Adhesion and Adhesives*, 2014, **52**, 31-39.
235. M. Alauhdin, T. M. Bennett, G. He, S. P. Bassett, G. Portale, W. Bras, D. Hermida-Merino and S. M. Howdle, *Polymer Chemistry*, 2019, **10**, 860-871.
236. Y. Liu, W. Fu, T. Liu, Y. Zhang and B. Li, *Journal of Analytical and Applied Pyrolysis*, 2022, **161**, 105414.
237. M. Sogancioglu, G. Ahmetli and E. Yel, *Energy Procedia*, 2017, **118**, 221-226.
238. S. Feng, Z. Zhen, X. Xu, J. Xu, Q. Huang, Z. Zhou, X. Li and H. Zhang, *Proceedings of the Combustion Institute*, 2024, **40**, 105462.
239. R. K. Singh, B. Ruj, A. K. Sadhukhan and P. Gupta, *Journal of Environmental Management*, 2019, **239**, 395-406.
240. G. Wang, Z. Zhang, D. Xu, B. Xing, L. Zhu and S. Wang, *Science of The Total Environment*, 2023, **897**, 165359.
241. J. Huang, H. Meng, X. Luo, X. Mu, W. Xu, L. Jin and B. Lai, *Chemosphere*, 2022, **291**, 133112.
242. E. M. Zakharyan, A. L. Maksimov, E. M. Zakharyan and A. L. Maksimov, *Russian Journal of Applied Chemistry*, 2024, **96**, 892–941.
243. C. Wang, H. Lei, M. Qian, E. Huo, Y. Zhao, Q. Zhang, W. Mateo, X. Lin, X. Kong, R. Zou and R. Ruan, *Sustainable Energy & Fuels*, 2020, **4**, 4614-4624.
244. X. Wang, Y. Peng, R. Zhou, L. Fan, Q. Zhang, X. Cui, Q. Wu, Y. Zeng, X. Tian, L. Ke, R. Ruan and Y. Wang, *Chemical Engineering Journal*, 2024, **488**, 150732.
245. Z. Zhao, S. M. A. Abdo, X. Wang, H. Li, X. Li and X. Gao, *Journal of Analytical and Applied Pyrolysis*, 2021, **158**, 105239.

246. D. V. Suriapparao, H. K. Tanneru and B. R. Reddy, *Environmental Research*, 2022, **215**, 114378.
247. J. P. Robinson, S. W. Kingman, C. E. Snape, S. M. Bradshaw, M. S. A. Bradley, H. Shang and R. Barranco, *Chemical Engineering Research and Design*, 2010, **88**, 146-154.
248. D. A. Jones, T. P. Lelyveld, S. D. Mavrofidis, S. W. Kingman and N. J. Miles, *Resources, Conservation and Recycling*, 2002, **34**, 75-90.
249. F. Mushtaq, T. A. T. Abdullah, R. Mat and F. N. Ani, *Bioresource Technology*, 2015, **190**, 442-450.
250. P. H. M. Putra, S. Rozali, M. F. A. Patah and A. Idris, *Journal of Environmental Management*, 2022, **303**, 114240.
251. J. Ren, X. La, J. Wang and J. Jiang, *Fuel*, 2024, **372**, 132220.
252. Z. Du, Y. Li, X. Wang, Y. Wan, Q. Chen, C. Wang, X. Lin, Y. Liu, P. Chen and R. Ruan, *Bioresource Technology*, 2011, **102**, 4890-4896.
253. M. Tayier, Y. Zhao, D. Duan, R. Zou, Y. Wang, R. Ruan and Y. Liu, *Journal of Wood Chemistry and Technology*, 2020, **40**, 190-199.
254. C. Dong, C. Feng, Q. Liu, D. Shen and R. Xiao, *Bioresource Technology*, 2014, **162**, 136-141.
255. S. Kumar and C. Guria, *Journal of Macromolecular Science, Part A: Pure and Applied Chemistry*, **42**, 237-251.
256. T. Yoshioka, N. Okayama and A. Okuwaki, *Industrial & Engineering Chemistry Research*, 1998, **37**, 336-340.
257. T. Yoshioka, T. Motoki and A. Okuwaki, *Industrial & Engineering Chemistry Research*, 2001, **40**, 75-79.
258. H. Kurokawa, M.-a. Ohshima, K. Sugiyama and H. Miura, *Polymer Degradation and Stability*, 2003, **79**, 529-533.
259. B. Liu, X. Lu, Z. Ju, P. Sun, J. Xin, X. Yao, Q. Zhou and S. Zhang, *Industrial & Engineering Chemistry Research*, 2018, **57**, 16239–16245.
260. G. Güçlü, A. Kas , göz, S. Özbudak, S. Özgümüs , and M. Orbay, *Journal of Applied Polymer Science*, 1998, **69**, 2311-2319.

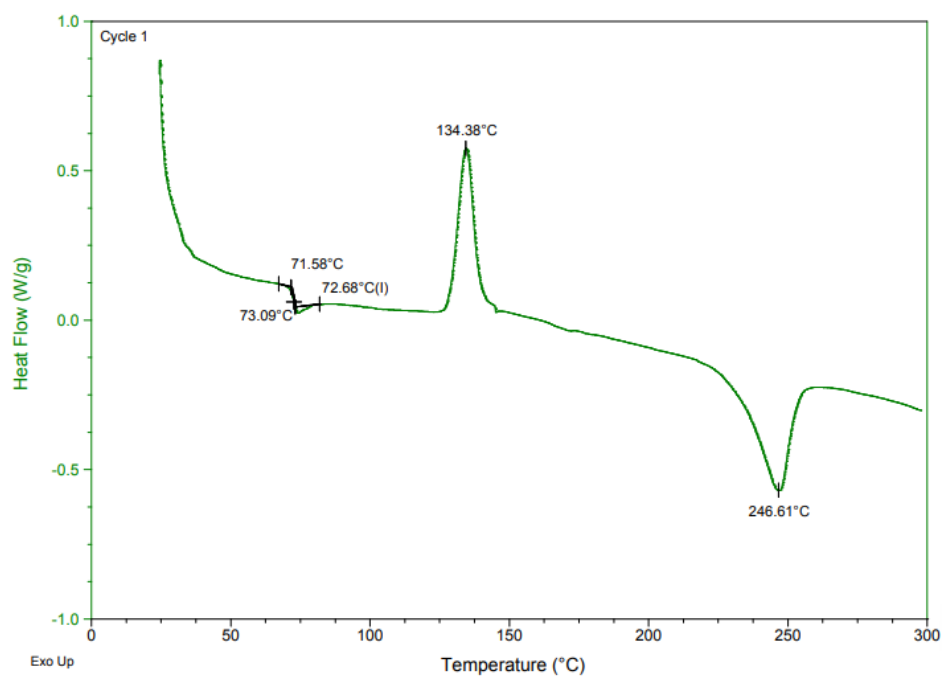
261. S. Tanaka, J. Sato and Y. Nakajima, *Green Chemistry*, 2021, **23**, 9412-9416.
262. D. D. Pham and J. Cho, *Green Chemistry*, 2021, **23**, 511-525.
263. A. Y. Platonov, A. N. Evdokimov, A. V. Kurzin and H. D. Maiygorova, *J. Chem. Eng. Data*, 2022, **47**, 1175-1176.
264. J.-T. Du, Q. Sun, X.-F. Zeng, D. Wang, J.-X. Wang and J.-F. Chen, *Chemical Engineering Science*, 2020, **220**, 115642.
265. R. A. Sheldon, *Organic synthesis; past, present and future*, Chemistry and Industry London, 1992.
266. P. G. Jessop, *Green Chemistry*, 2011, **13**, 1391-1398.
267. X.-K. Li, H. Lu, W.-Z. Guo, G.-P. Cao, H.-L. Liu and Y.-H. Shi, *AIChE Journal*, 2015, **61**, 200-214.
268. J. Liu and J. Yin, *Industrial & Engineering Chemistry Research*, 2022, **61**, 6813–6819.
269. P. Gao, W.-H. Qiao, Z.-Y. Hu, B.-C. Yang, C.-Y. Cao, Y. Fu, Y. Xia, C.-X. Wang, G.-P. Cao and H. Lv, *Polymer Degradation and Stability*, 2024, **219**, 110590.
270. D. Osei, L. Gurralla, A. Sheldon, J. Mayuga, C. Lincoln, N. A. Rorrer and A. R. C. Morais, *Green Chemistry*, 2024, **26**, 6436-6445.
271. X. Wang and T. Bürgi, *Angewandte Chemie International Edition*, 2021, **60**, 7860-7865.
272. L. Gurralla, R. Anowar and A. R. C. Morais, *ACS Sustainable Chemistry & Engineering*, 2024, **12**, 7713–7723.
273. *Chemical Engineering Science*, 2021/04/06, **233**.
274. K. Clark and S. Lee, *Polymer Engineering & Science*, 2004, **44**, 1636-1641.
275. E. Stahl, E. Schuetz and H. K. Mangold, 1980, **28**, 1153–1157.
276. J. P. Friedrich and G. R. List, 1982, **30**, 192–193.
277. C. B. Mehr, R. N. Biswal, J. L. Collins and H. D. Cochran, *The Journal of Supercritical Fluids*, 1996, **9**, 185-191.

278. <https://www.missioncoffeeworks.com/blogs/news/exploring-the-co2-decaffeination-process-in-specialty-coffee>, (accessed 26th August, 2024).
279. P. Elisabeth, M. Yoshioka, Y. Yamauchi, M. Saito, P. Elisabeth, M. Yoshioka, Y. Yamauchi and M. Saito, *Analytical Sciences* 1991, **7**, 427-431.
280. H. Peker, M. P. Srinivasan, J. M. Smith and B. J. McCoy, *AIChE Journal*, 1992, **38**, 761-770.
281. L. Delva, S. Hubo, L. Cardon and K. Ragaert, *Waste Management*, 2018, **82**, 198-206.
282. N. J. Cotton, K. D. Bartle, A. A. Clifford and C. J. Dowle, *Journal of Applied Polymer Science*, 1993, **48**, 1607-1619.
283. S. Peng, S. Liang, M. Yu and X. Li, *Journal of Material Cycles and Waste Management* 2013 16:1, 2013, **16**, 178-185.
284. S. Singh, J. Pereira, T. Brandão, A. L. Oliveira and F. Poças, *Journal of the Science of Food and Agriculture*, 2023, **103**, 1127-1138.
285. Guidance for Industry: Use of Recycled Plastics in Food Packaging (Chemistry Considerations, <https://www.fda.gov/regulatory-information/search-fda-guidance-documents/guidance-industry-use-recycled-plastics-food-packaging-chemistry-considerations>, (accessed 11th August 2024)
286. S. Kanehashi, A. Kusakabe, S. Sato and K. Nagai, *Journal of Membrane Science*, 2010, **365**, 40-51.
287. E. Fritz-Langhals, *Organic Process Research & Development*, 2022, **26**, 3015–3023.
288. D. Williams and I. Fleming, *Spectroscopic Methods in Organic Chemistry* McGraw-Hill Education UK, 6th Edition edn., 2008.
289. S. P. J. Higson, *analytical chemistry*, Oxford University Press Oxford, 4th Edition edn., 2006.
290. A. J. Spicer, A. Brandolese and A. P. Dove, *ACS Macro Letters*, 2024, **13**, 189–194.
291. B. Shao, X. Zhu, K. N. Plunkett and D. A. V. Bout, *Polymer Chemistry*, 2017, **8**, 1188-1195.

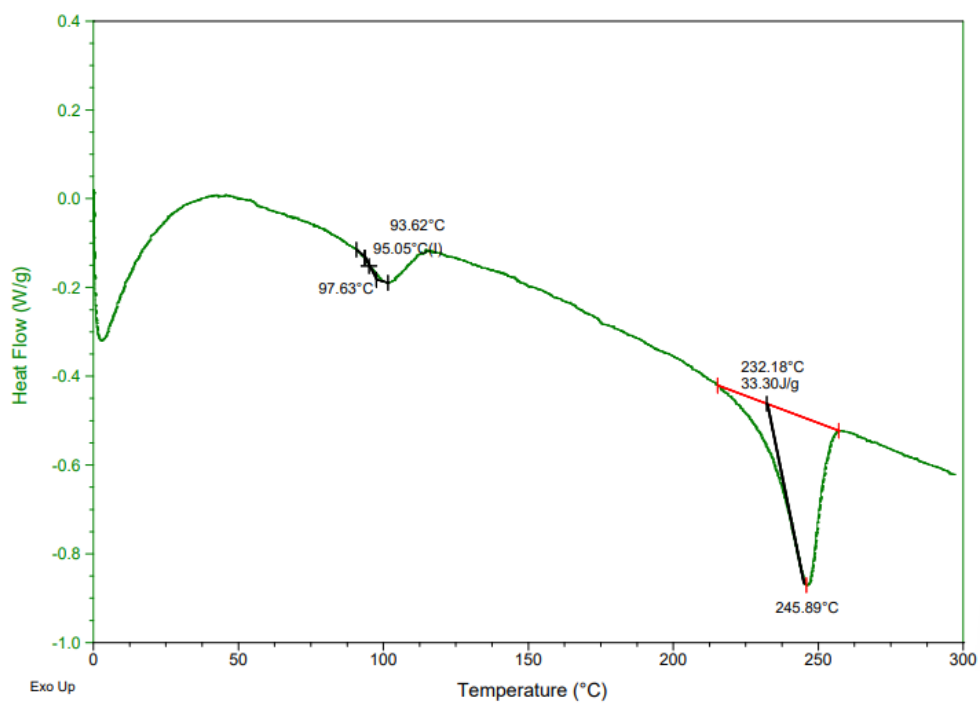
292. M. Lõkov, S. Tshepelevitsh, A. Heering, P. G. Plieger, R. Vianello and I. Leito, *European Journal of Organic Chemistry*, 2017, **2017**, 4475-4489.
293. C. Jehanno, C. Jehanno, M. M. Pérez-Madrigal, M. M. Pérez-Madrigal, J. Demarteau, J. Demarteau, H. Sardon, H. Sardon, A. P. Dove and A. P. Dove, *Polymer Chemistry*, 2018/12/21, **10**.
294. <https://global-recycling.info/archives/6400>, (accessed 21st September, 2024).

Appendix

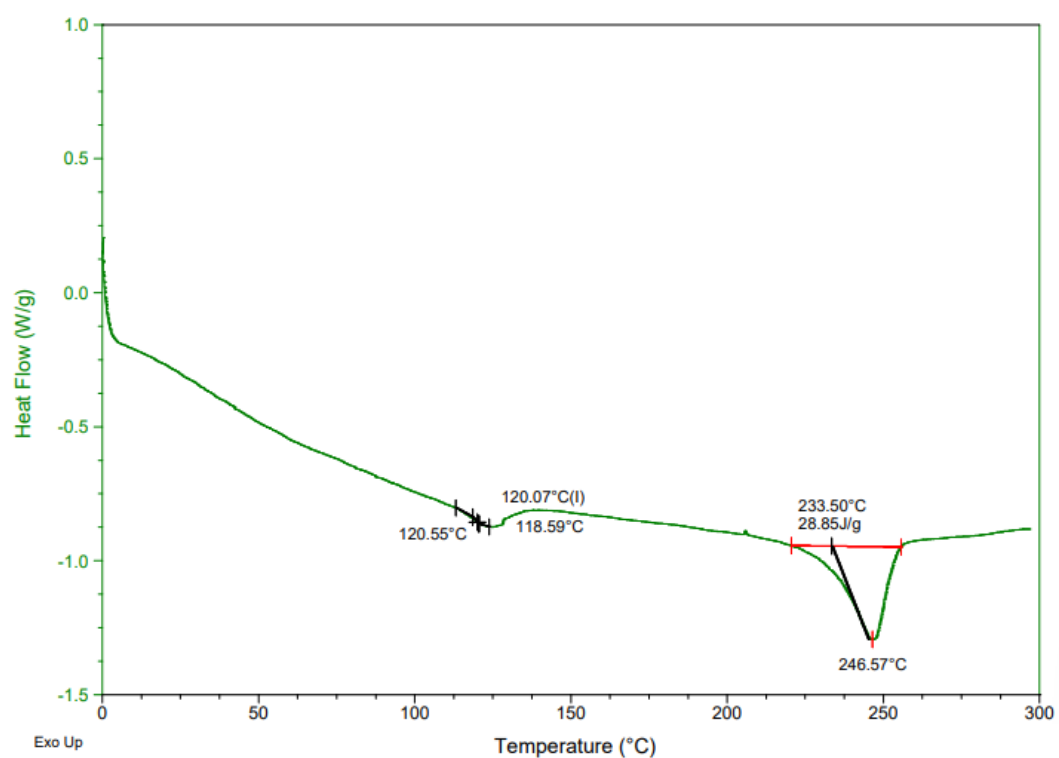
Chapter 3



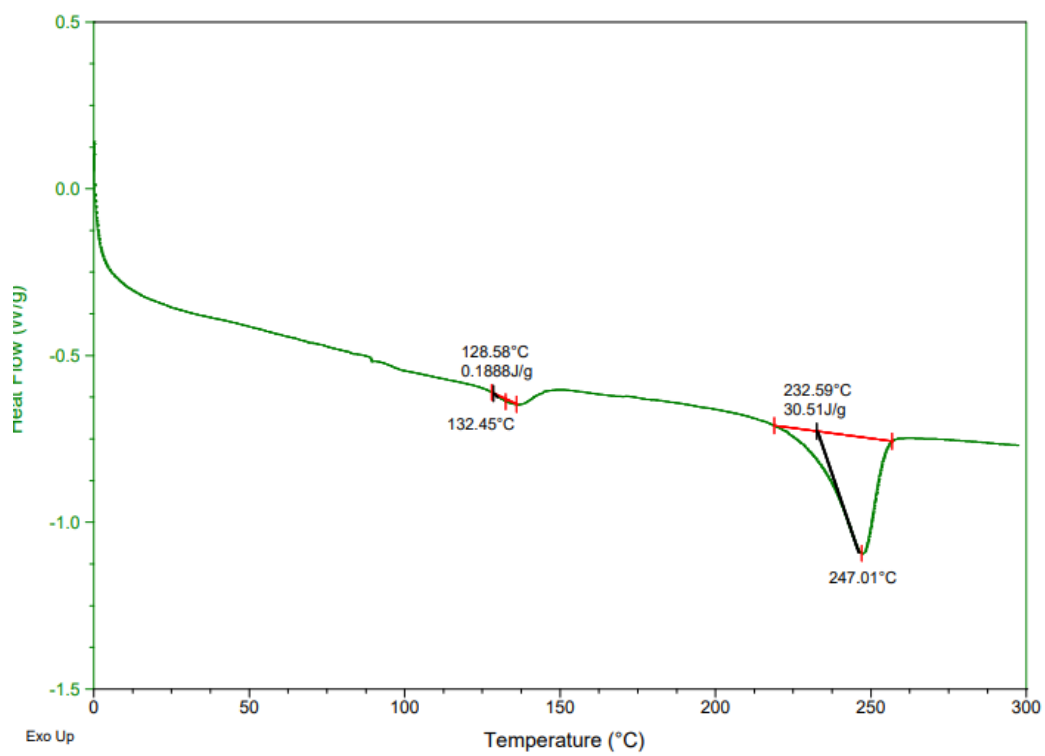
S1 – DSC of unmodified amorphous unmodified PET



S2 – DSC of PET soaked in pure scCO₂ (278 bar, 32 °C) for 3 hours.



S3- DSC of PET soaked in pure scCO_2 (278 bar, 65 °C) for 3 hours.



S4 - DSC of PET soaked in pure scCO_2 (278 bar, 85 °C) for 3 hours.

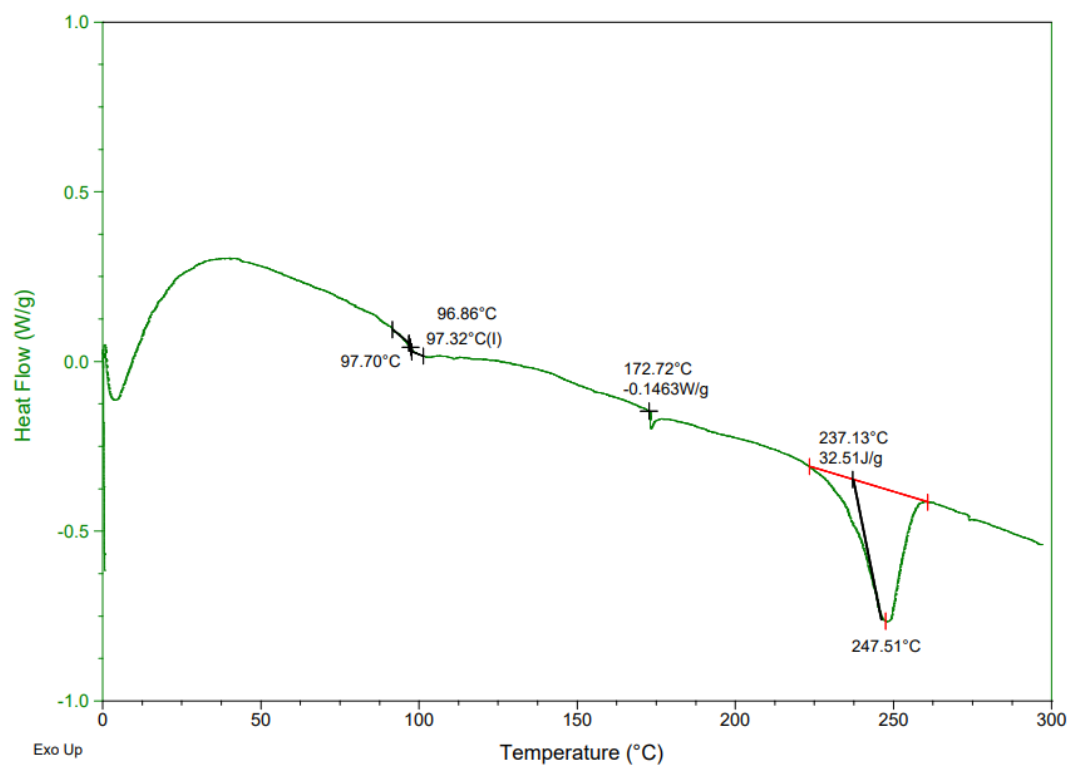


Figure S5- DSC of PET impregnated in a 1:1 ratio of ethylene glycol in $scCO_2$ (278 bar, 32 °C) for 3 hours

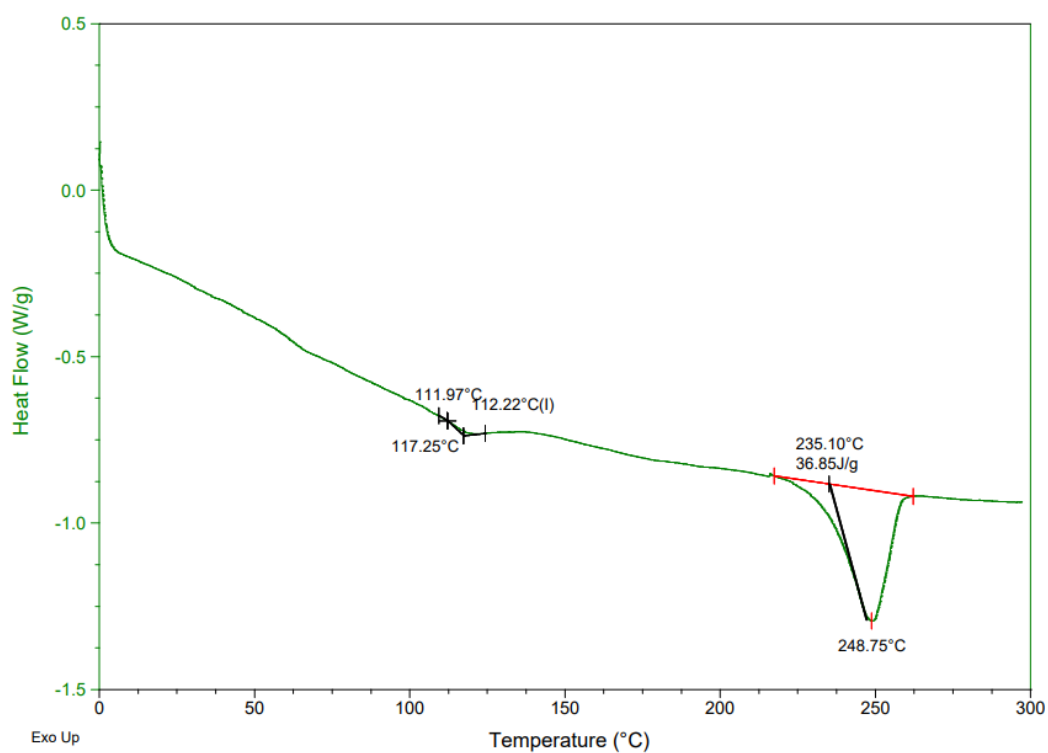
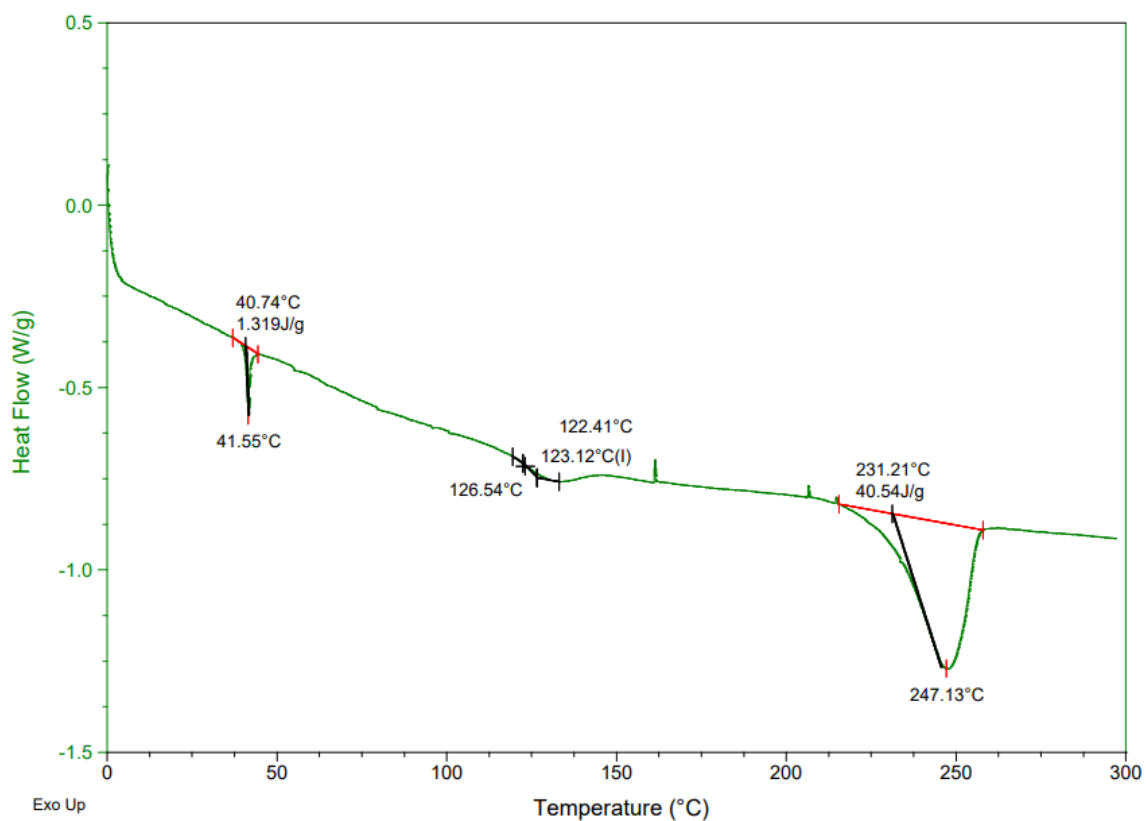
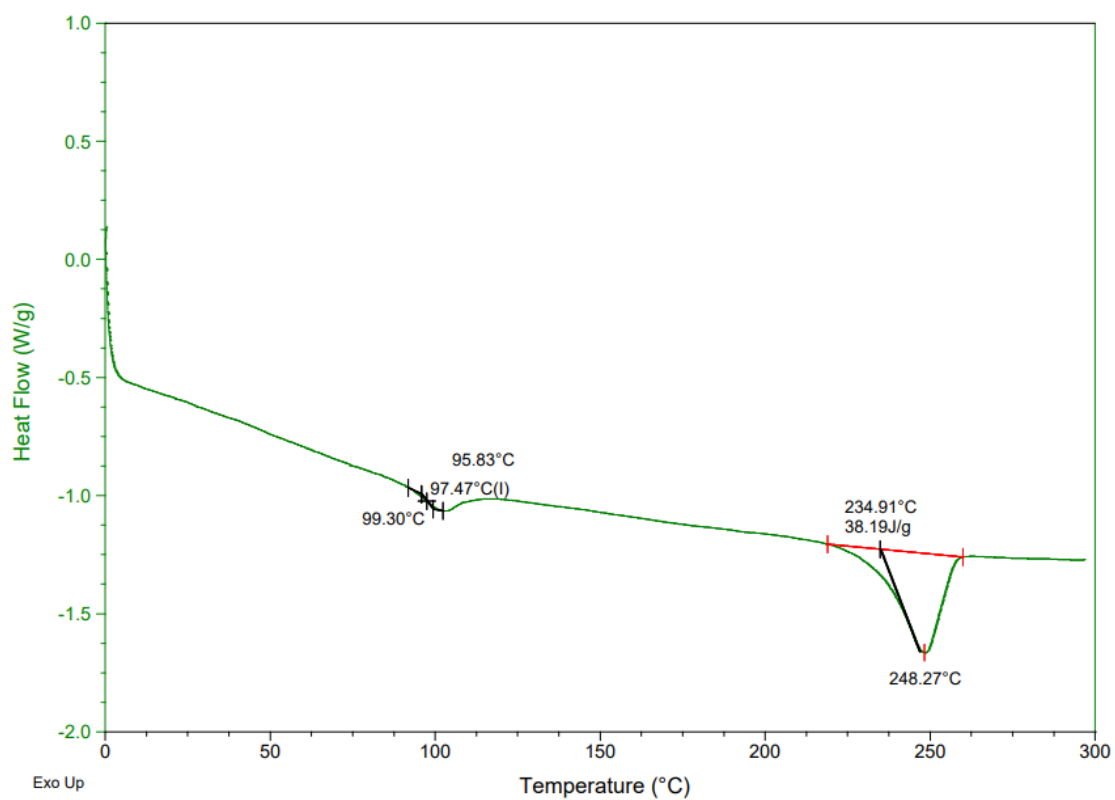


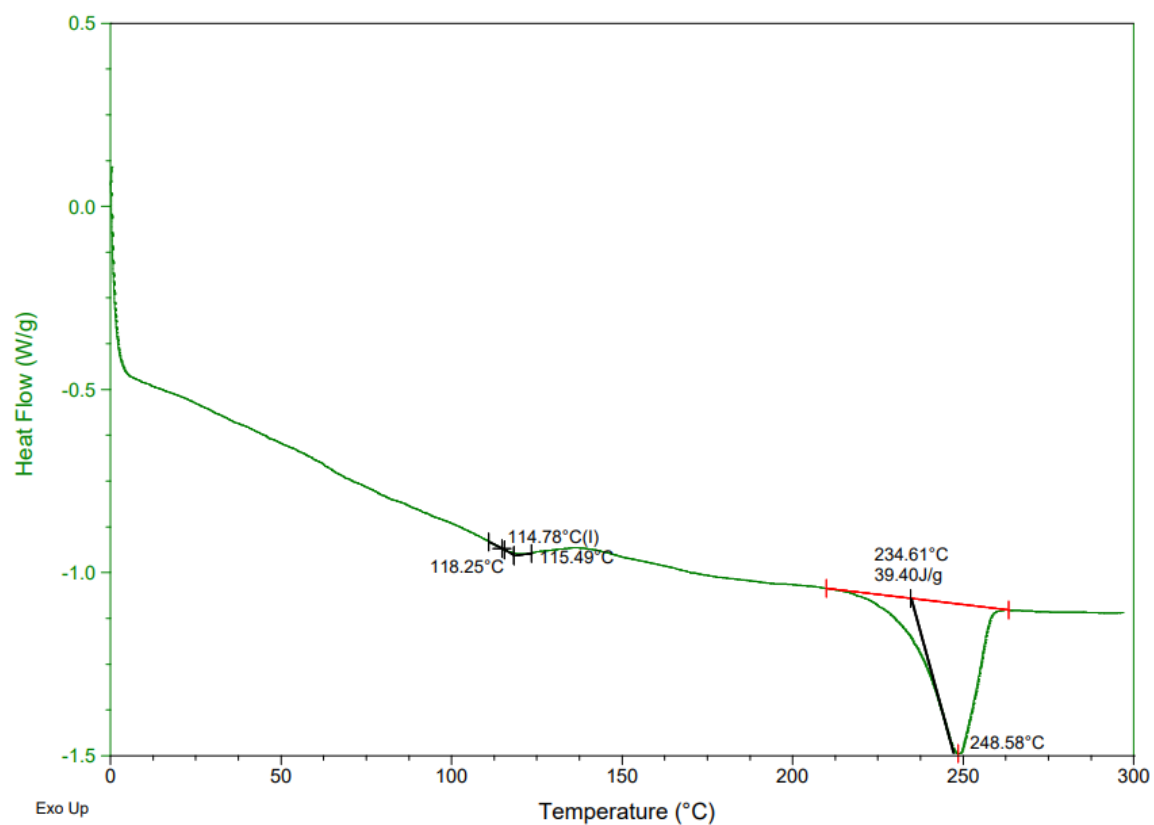
Figure S6- DSC of PET impregnated in a 1:1 ratio of ethylene glycol in $scCO_2$ (278 bar, 65 °C) for 3 hours.



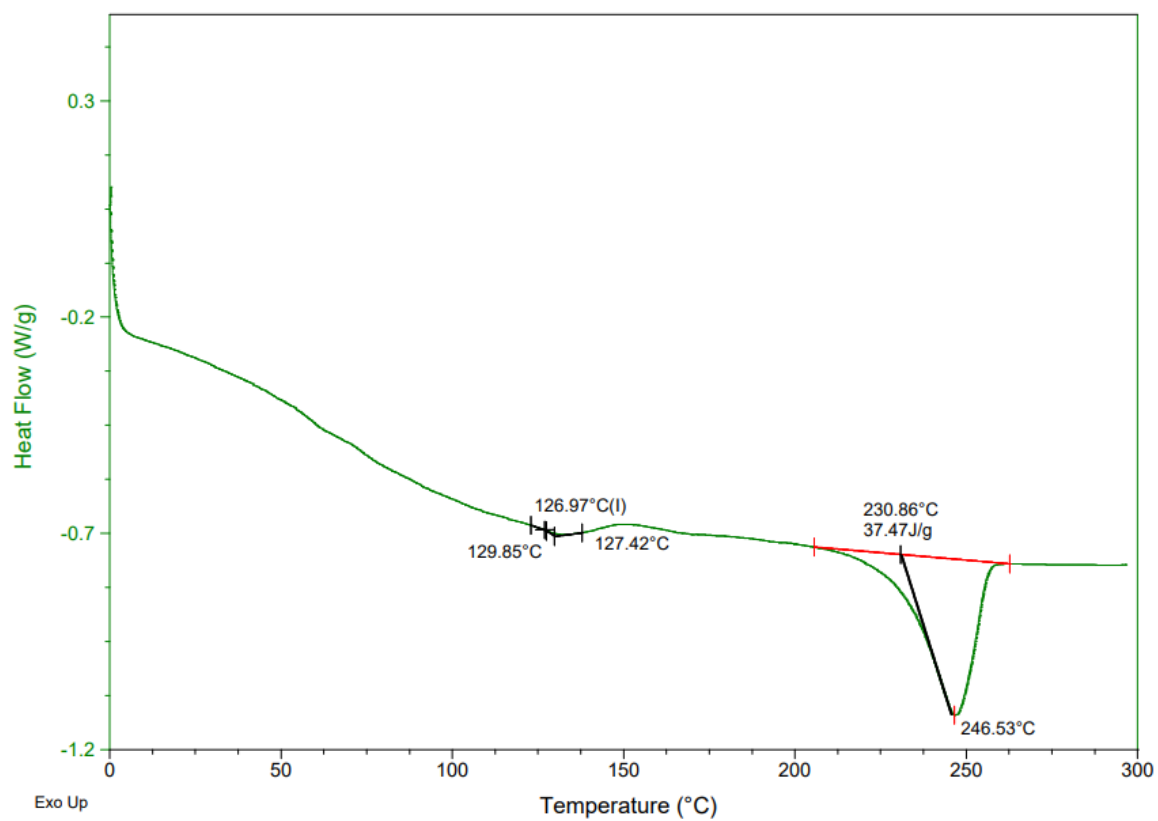
S7 - DSC of PET impregnated in a 1:1 ratio of ethylene glycol in $scCO_2$ (278 bar, 85 °C) for 3 hours.



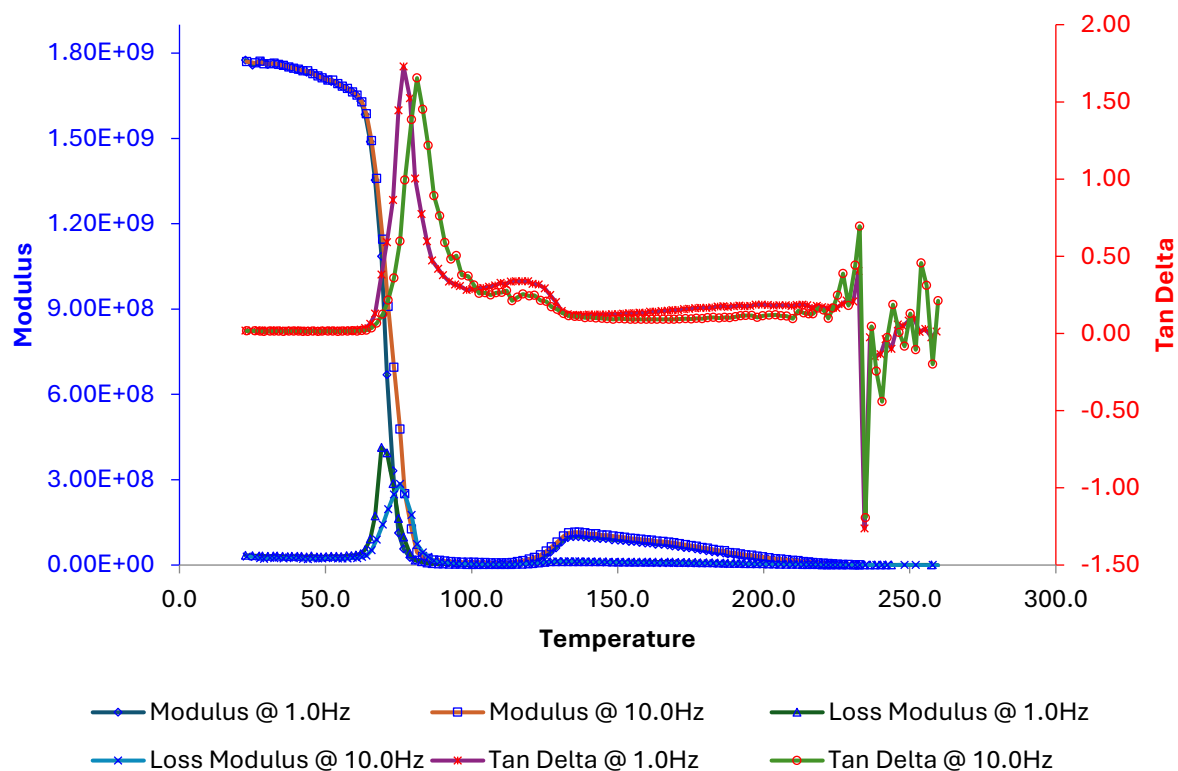
S8- DSC of PET impregnated in a 10:1 ratio of ethylene glycol in $scCO_2$ (278 bar, 32 °C) for 3 hours.



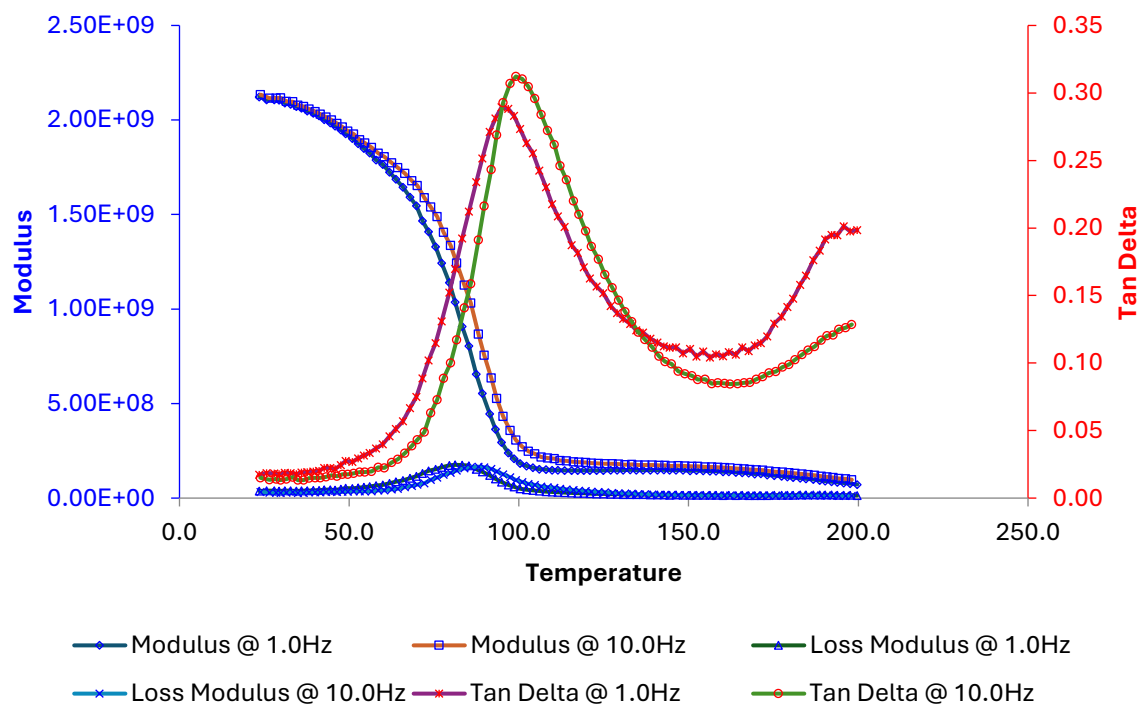
S9- DSC of PET impregnated in a 10:1 ratio of ethylene glycol in scCO_2 (278 bar, 65 °C) for 3 hours.



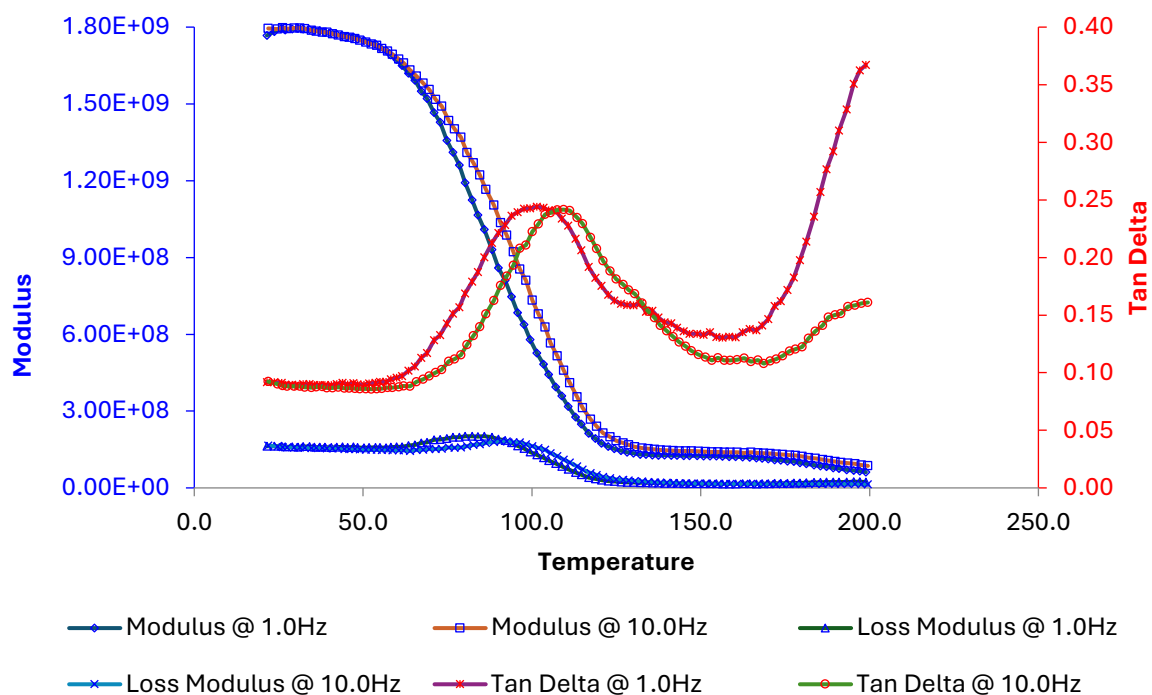
S10- DSC of PET impregnated in a 10:1 ratio of ethylene glycol in scCO_2 (278 bar, 85 °C) for 3 hours.



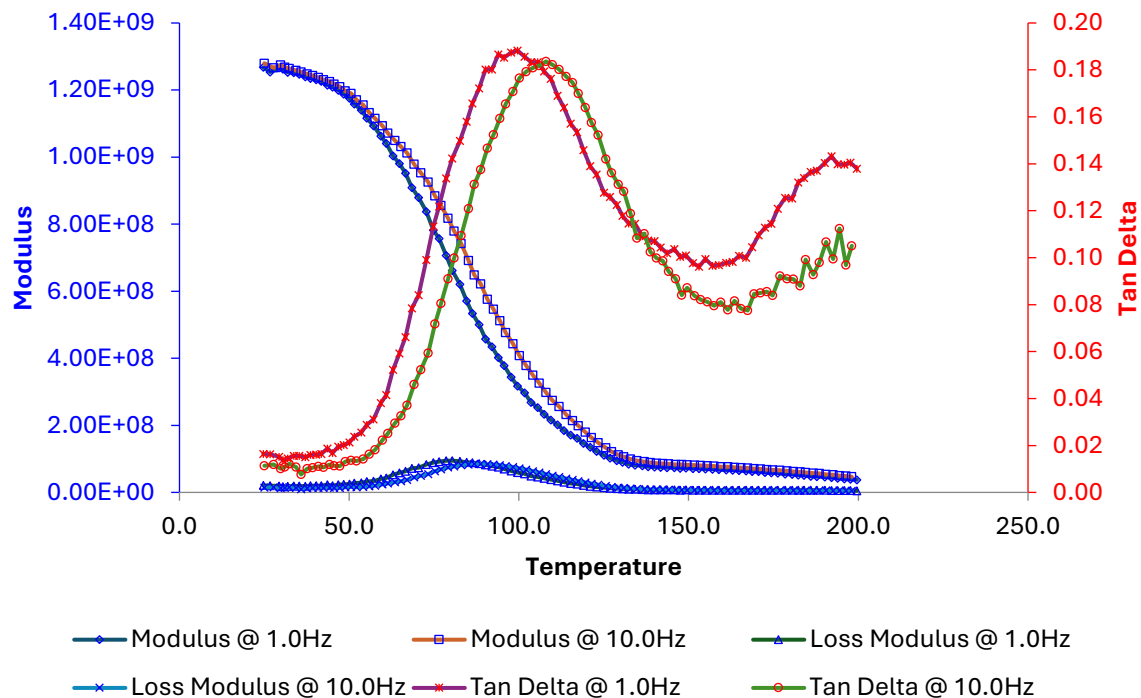
S11 – DMA trace of unmodified amorphous PET.



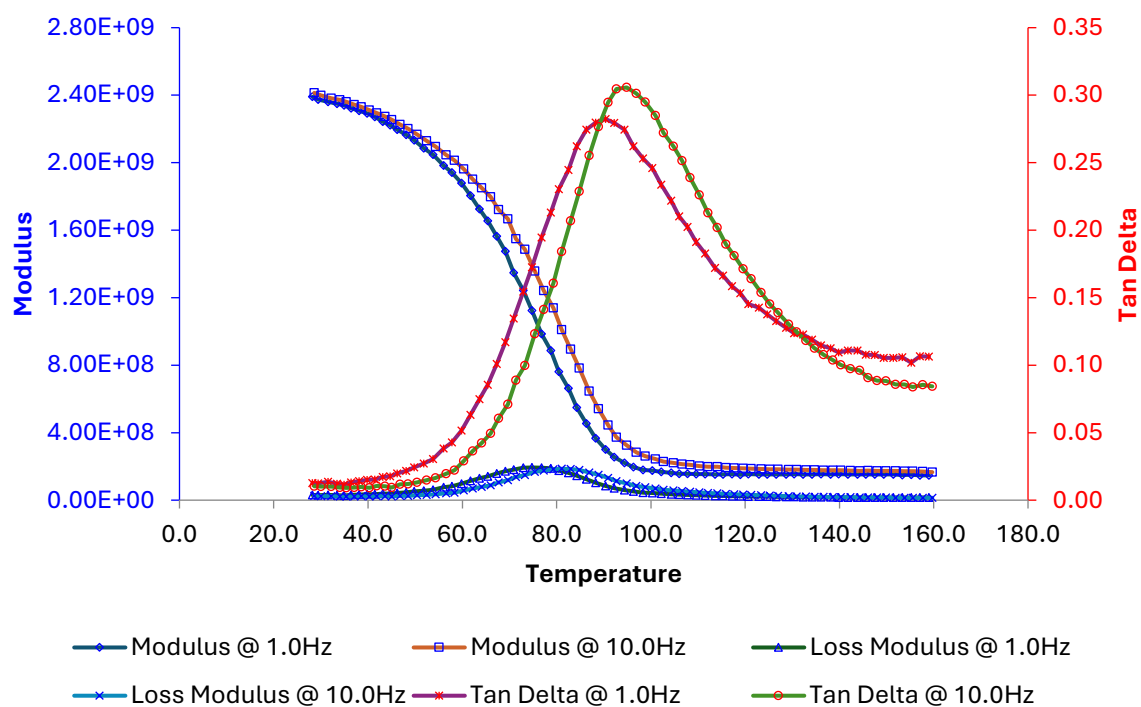
S12 – DMA trace of PET soaked in pure scCO₂ (278 bar, 35 °C) for 3 hours



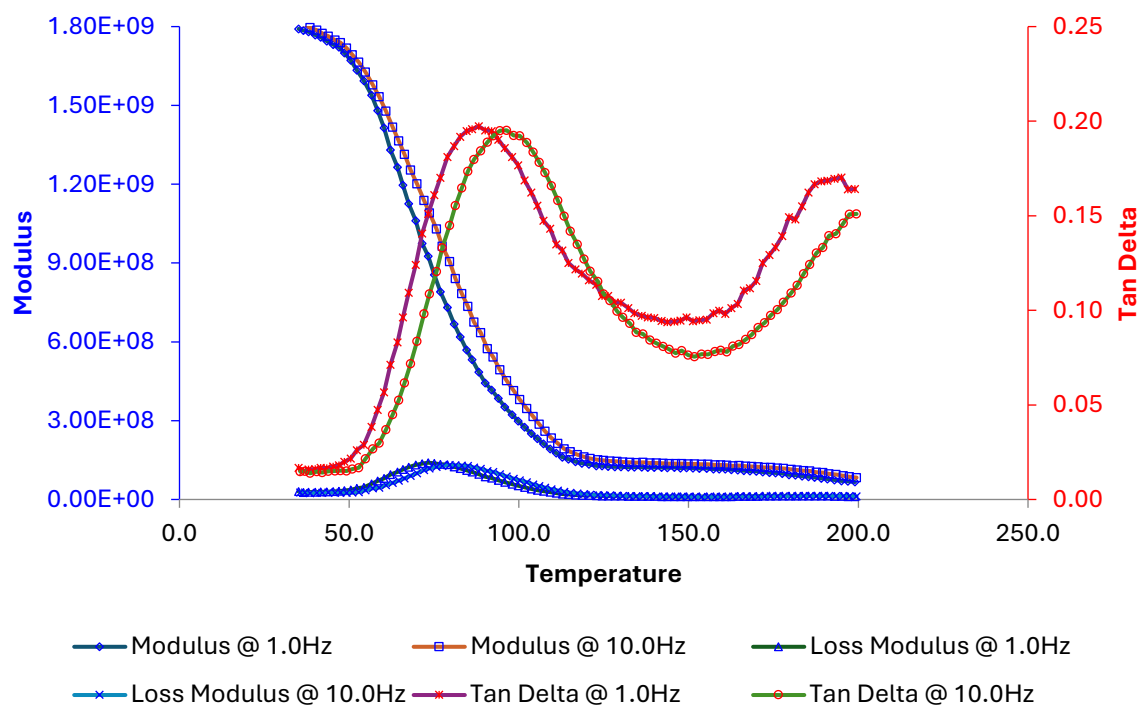
S13 – DMA trace of PET soaked in pure scCO₂ (278 bar, 65 °C) for 3 hours.



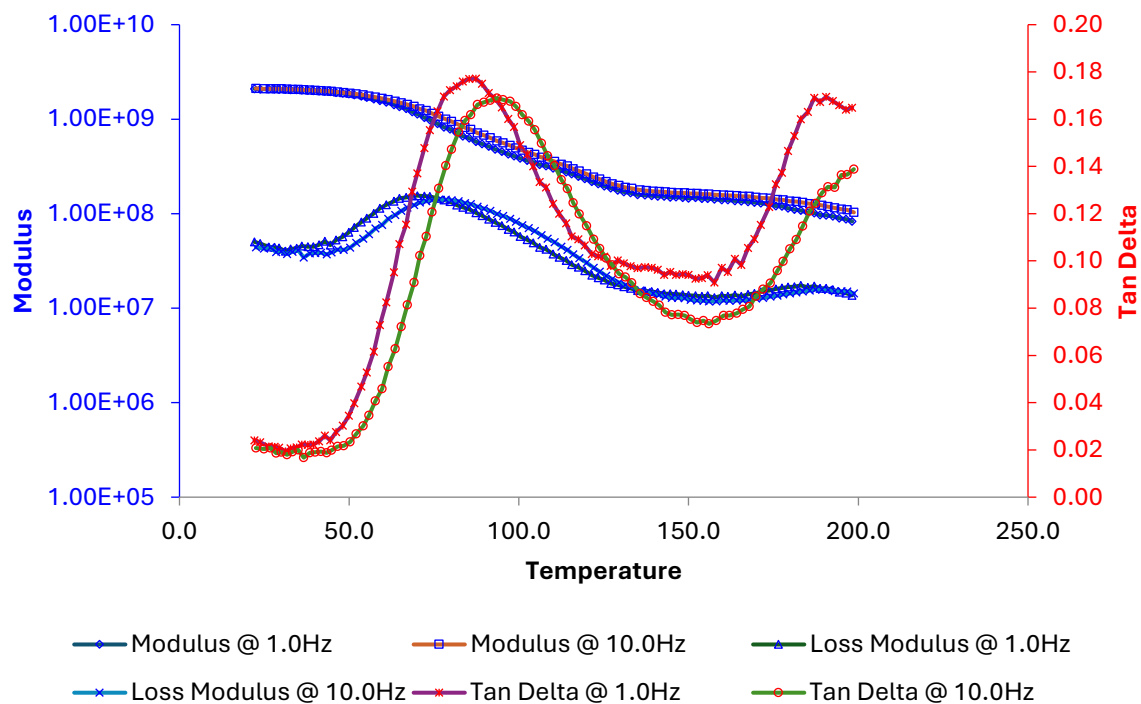
S14 – DMA trace of PET soaked in pure scCO₂ (278 bar, 85 °C) for 3 hours.



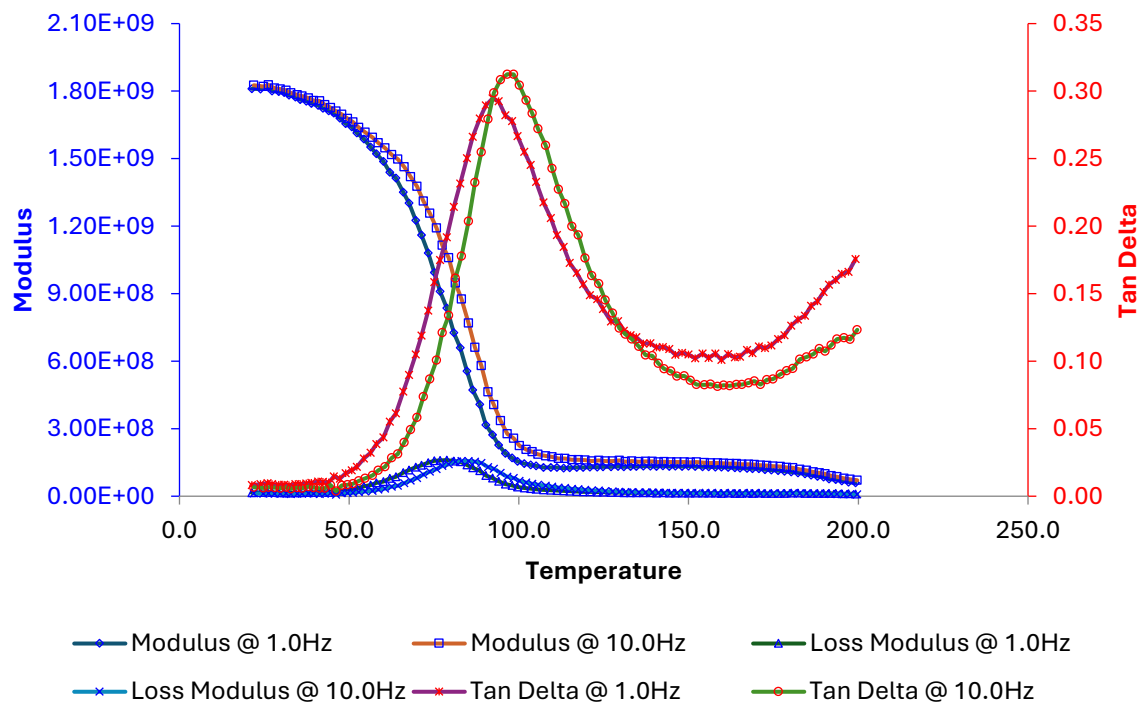
S15 – DMA trace of impregnated in a 1:1 ratio of ethylene glycol in $scCO_2$ (278 bar, 32 °C) for 3 hours.



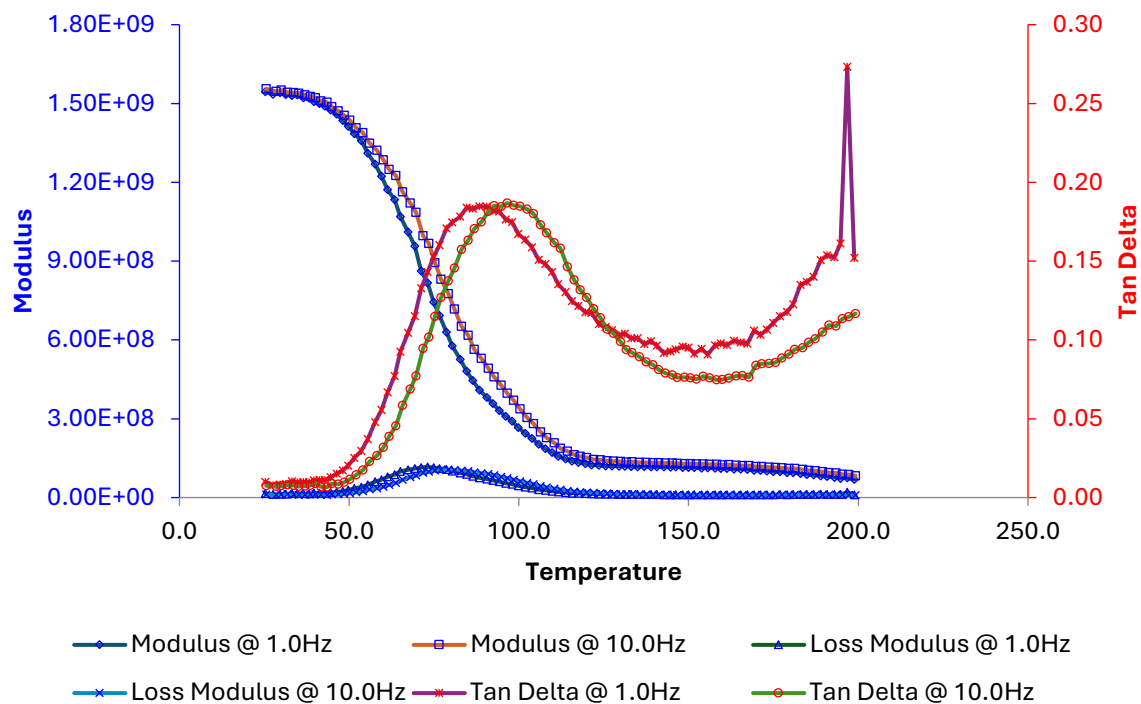
S16 – DMA trace of impregnated in a 1:1 ratio of ethylene glycol in $scCO_2$ (278 bar, 65 °C) for 3 hours.



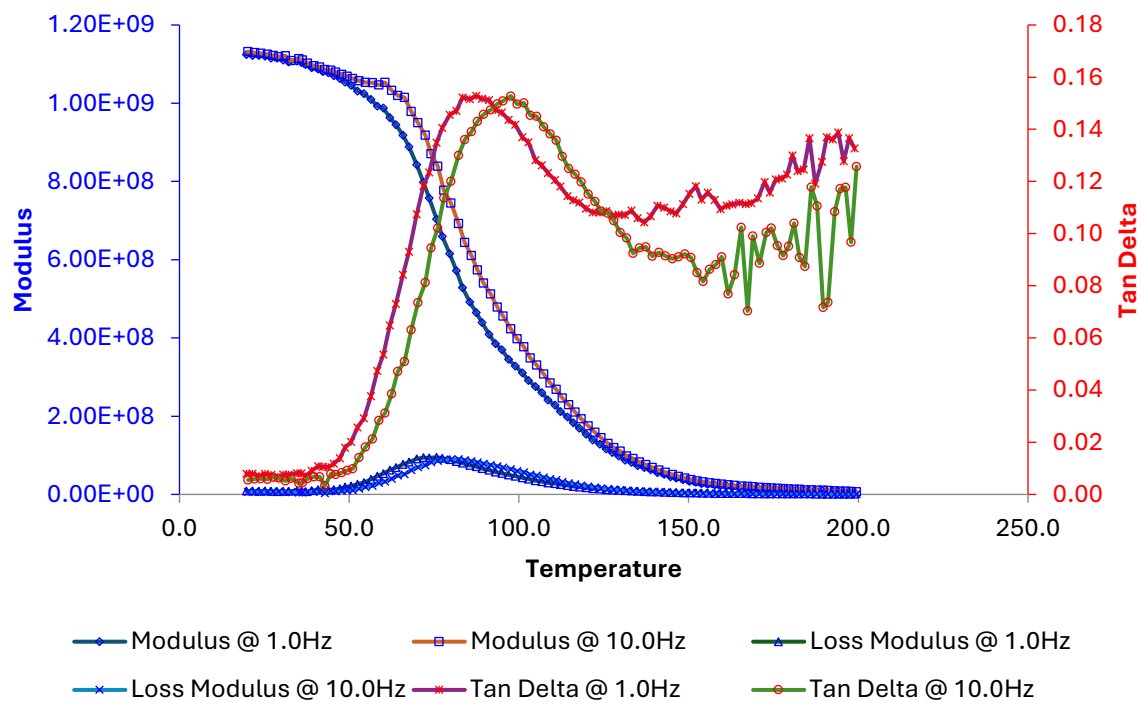
S17- DMA trace of impregnated in a 1:1 ratio of ethylene glycol in $scCO_2$ (278 bar, 85 °C) for 3 hours.



S18- DMA trace of PET impregnated in a 10:1 ratio of ethylene glycol in $scCO_2$ (278 bar, 32 °C) for 3 hours.

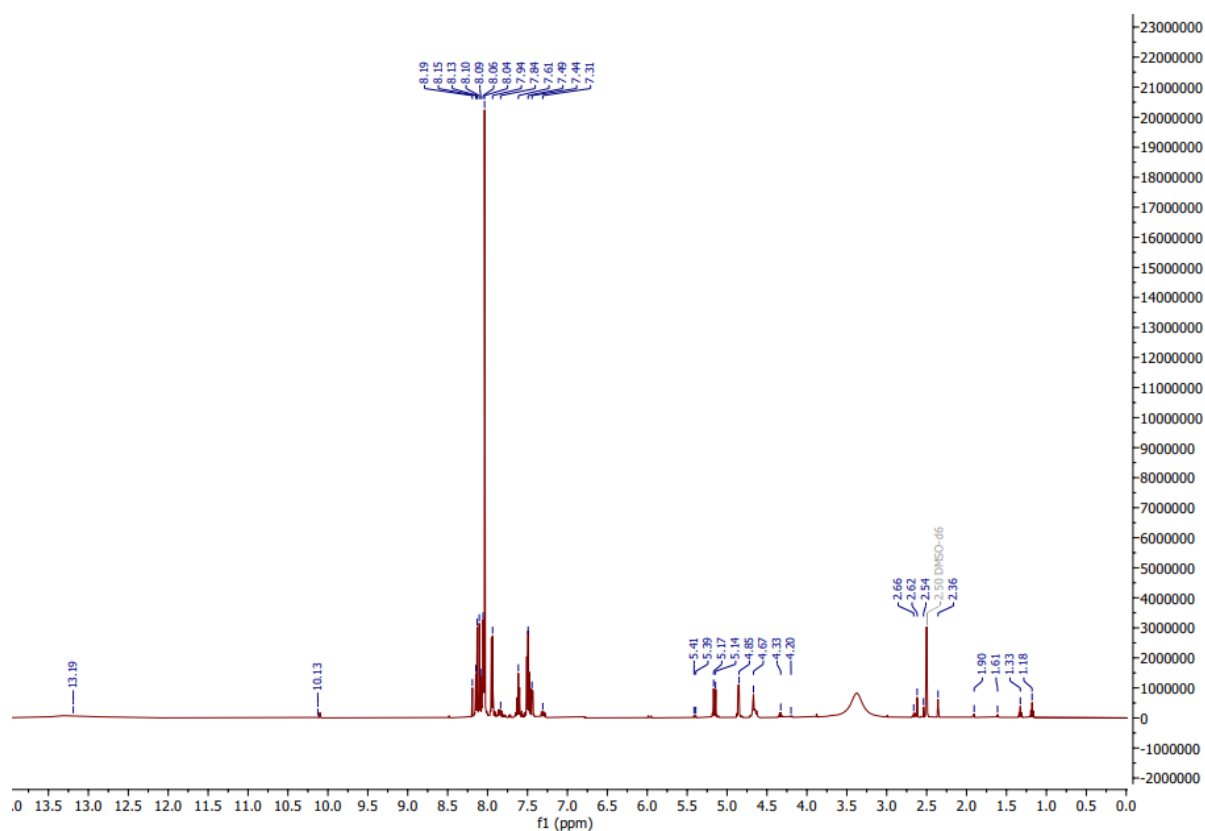


S19- DMA trace of PET impregnated in a 10:1 ratio of ethylene glycol in $scCO_2$ (278 bar, 65 °C) for 3 hours.

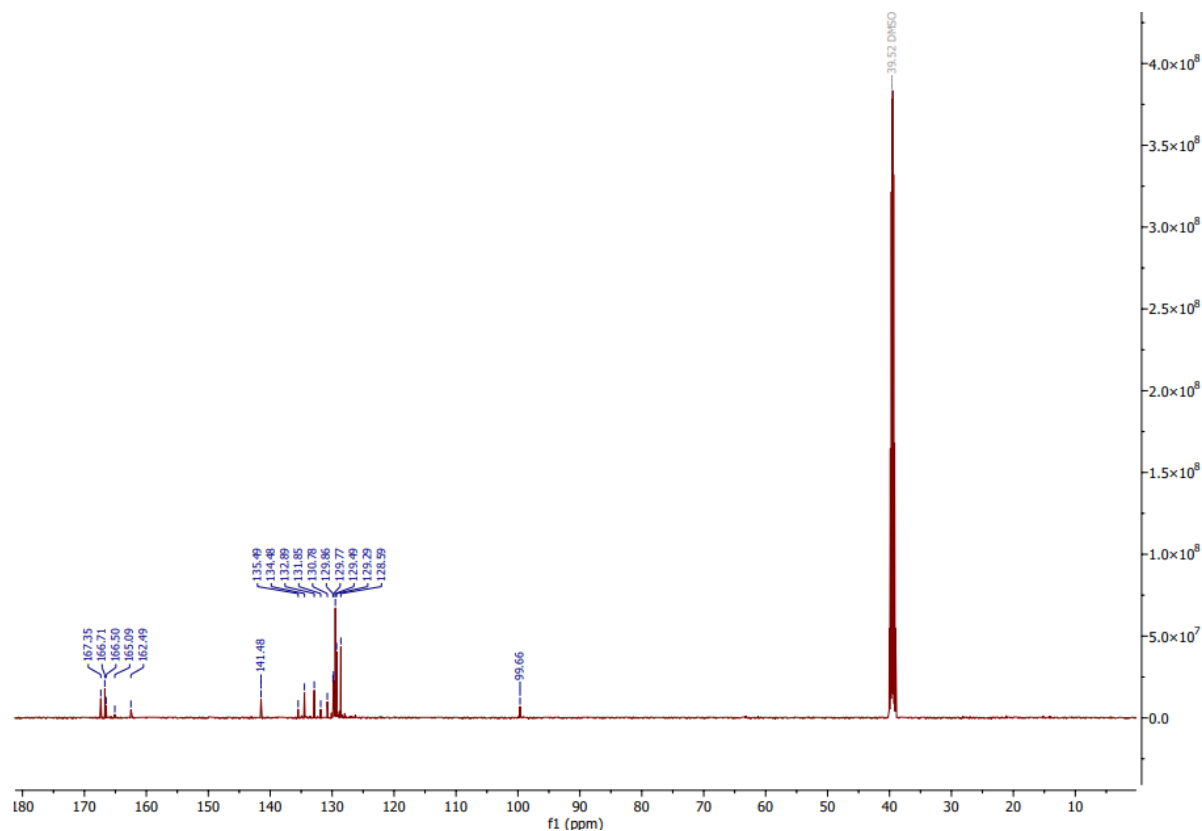


S20- DMA trace of PET impregnated in a 10:1 ratio of ethylene glycol in $scCO_2$ (278 bar, 85 °C) for 3 hours.

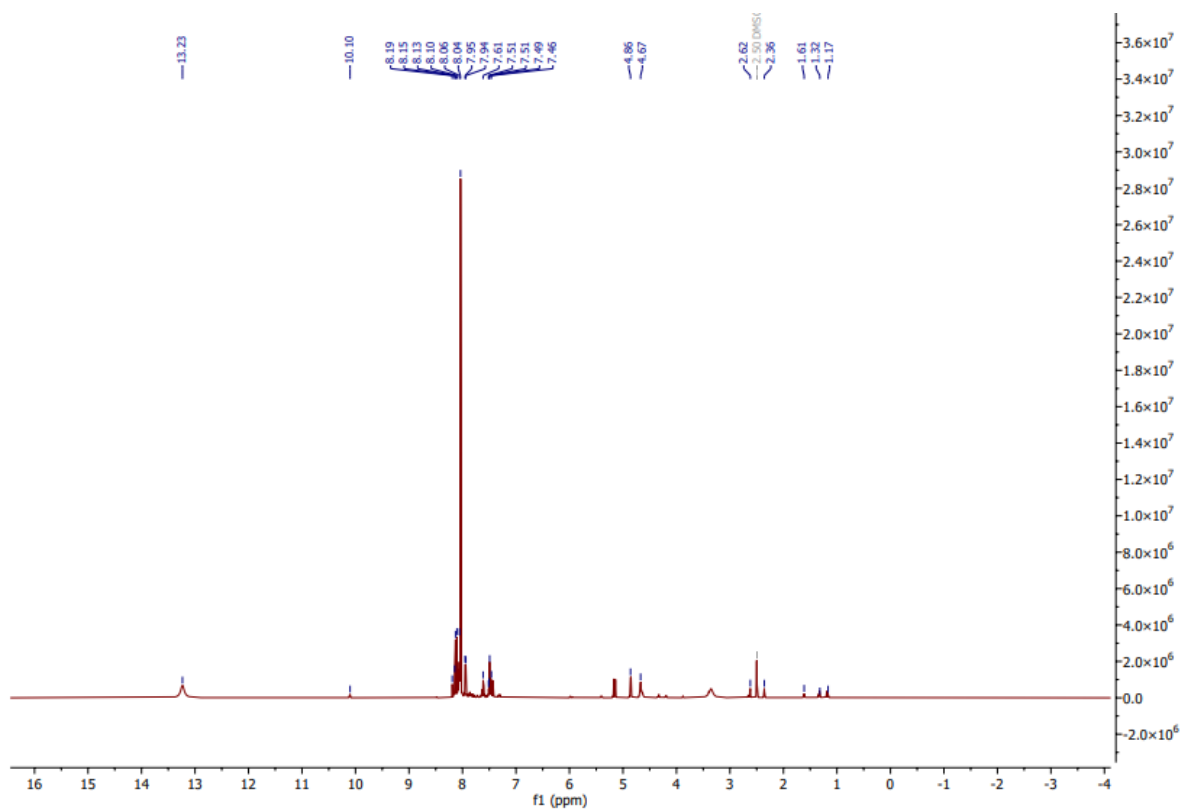
Chapter 4



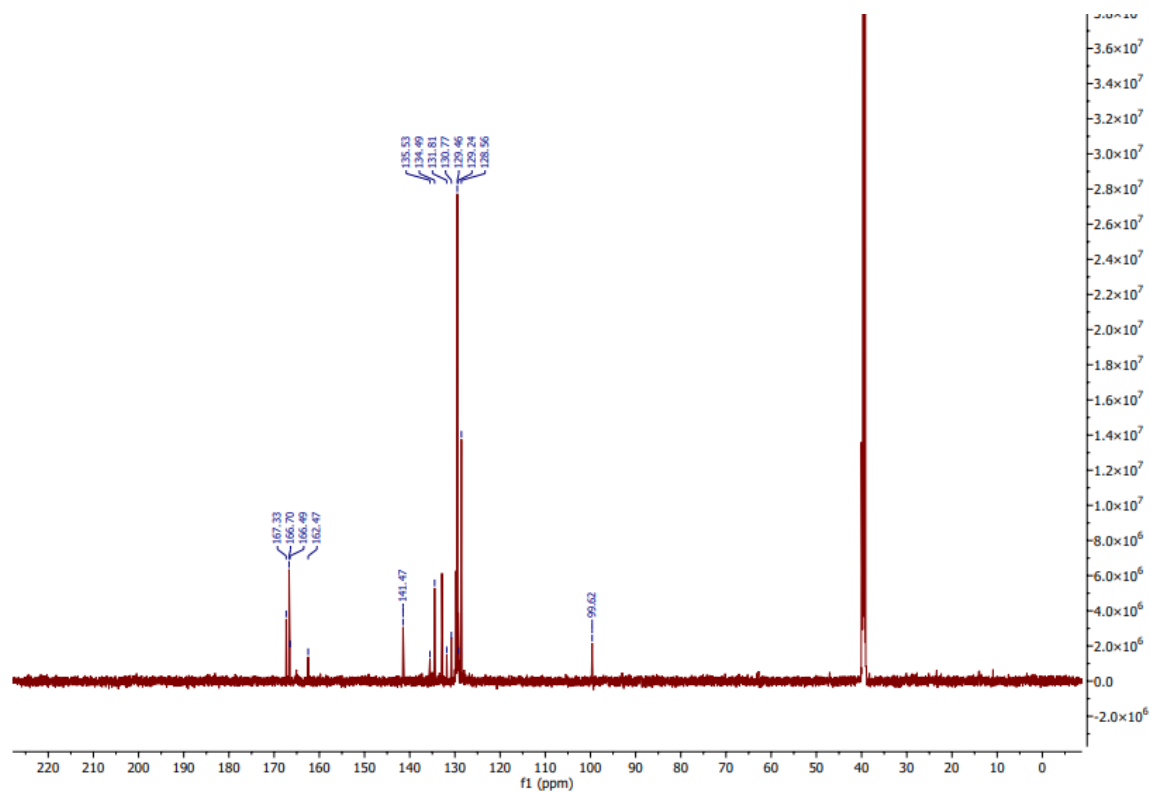
S21- ¹H NMR of unmodified PET degraded with microwaves of 0.8 kW input power.



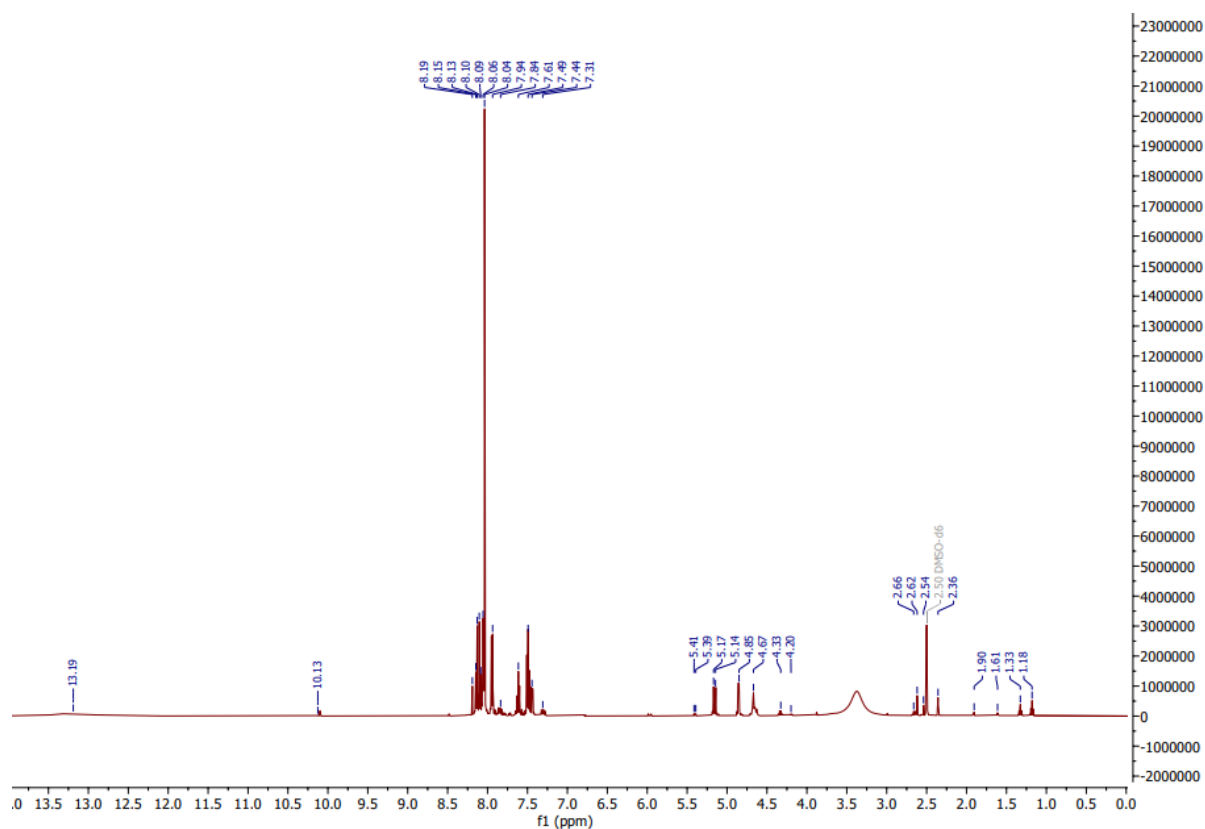
S22- ¹³C NMR of unmodified PET degraded with microwaves of 0.8 kW input power.



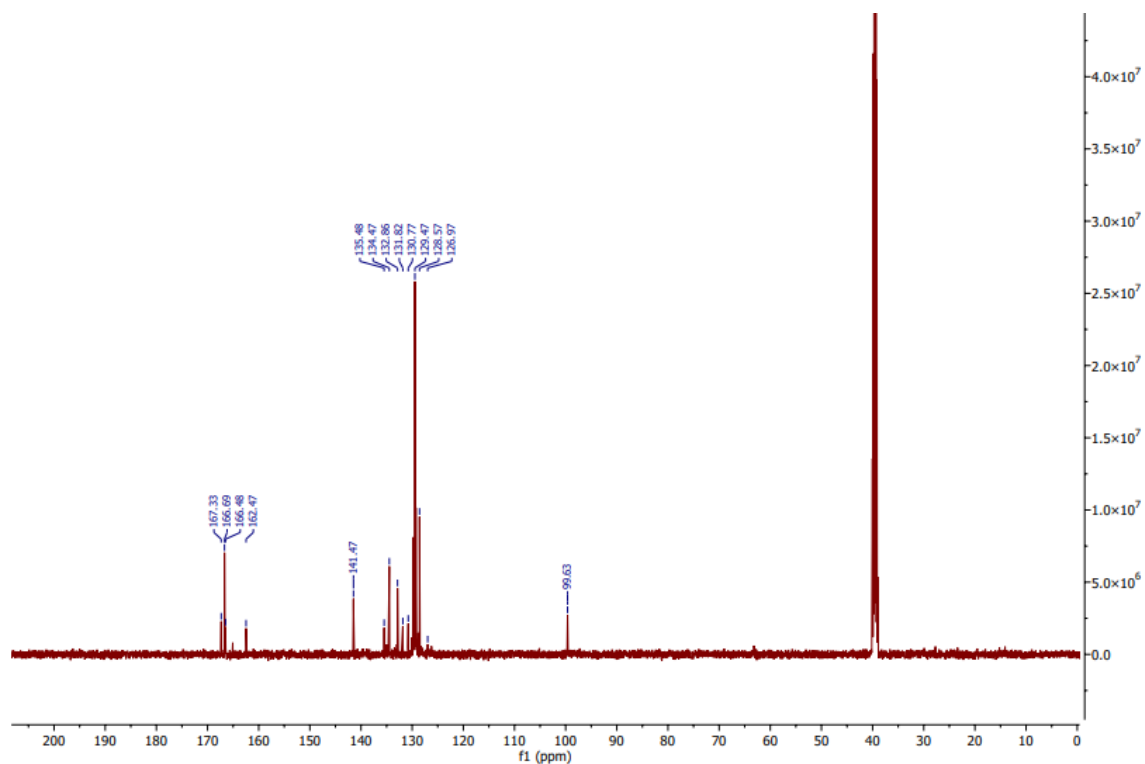
S23- ^1H NMR of unmodified PET degraded with microwaves of 1.2 kW input power.



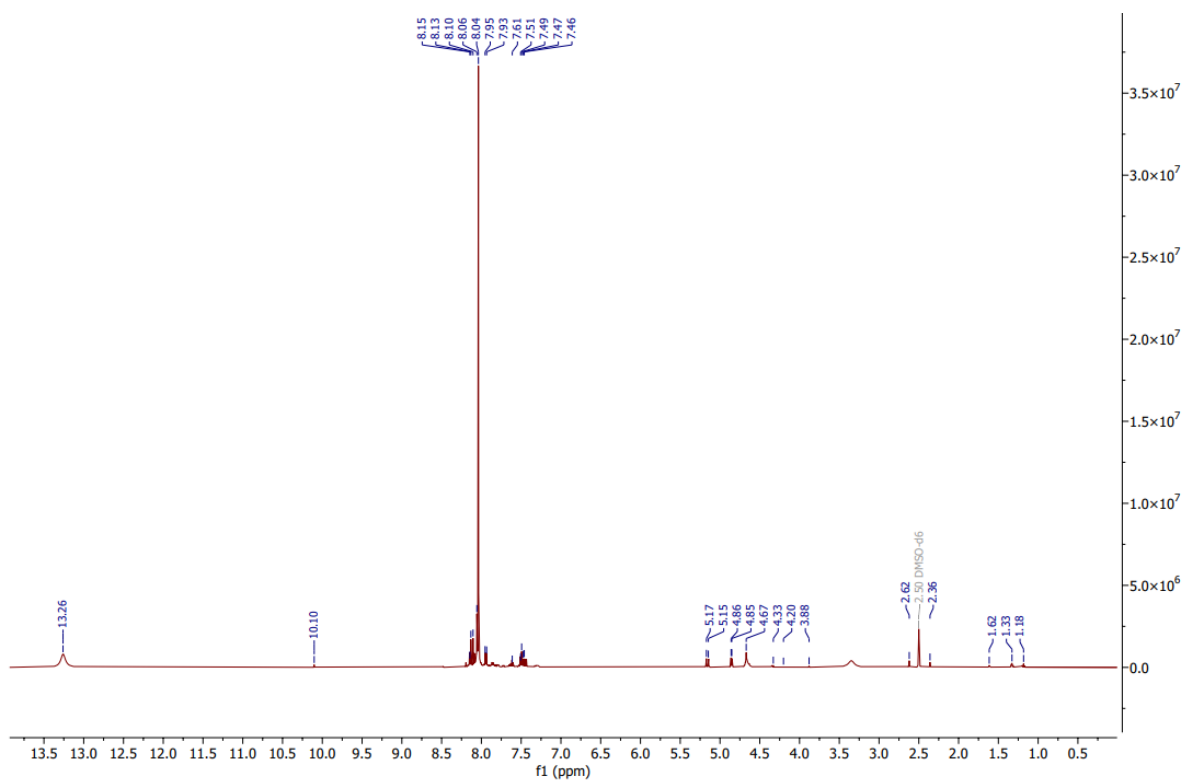
S24- ^{13}C NMR of unmodified PET degraded with microwaves of 1.2 kW input power.



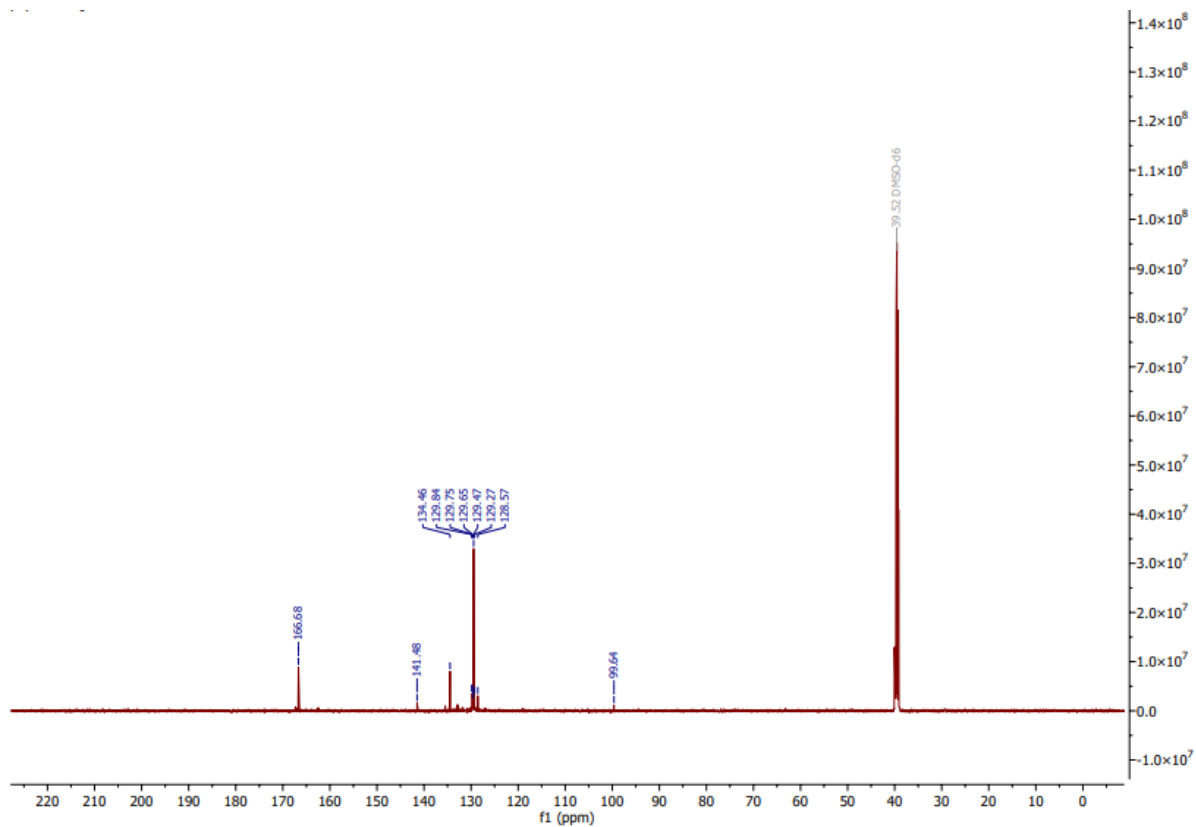
S25- ¹H NMR of unmodified PET degraded with microwaves of 1.6 kW input power.



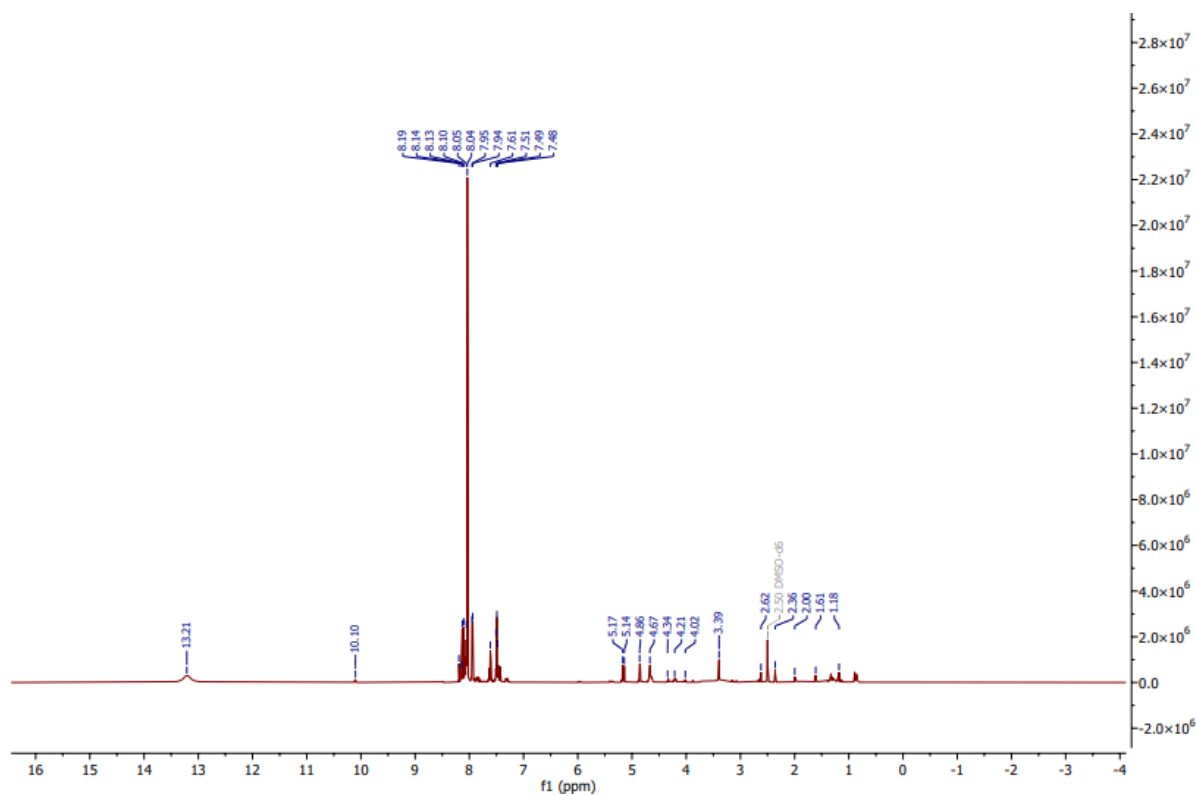
S26- ¹³C NMR of unmodified PET degraded with microwaves of 1.6 kW input power.



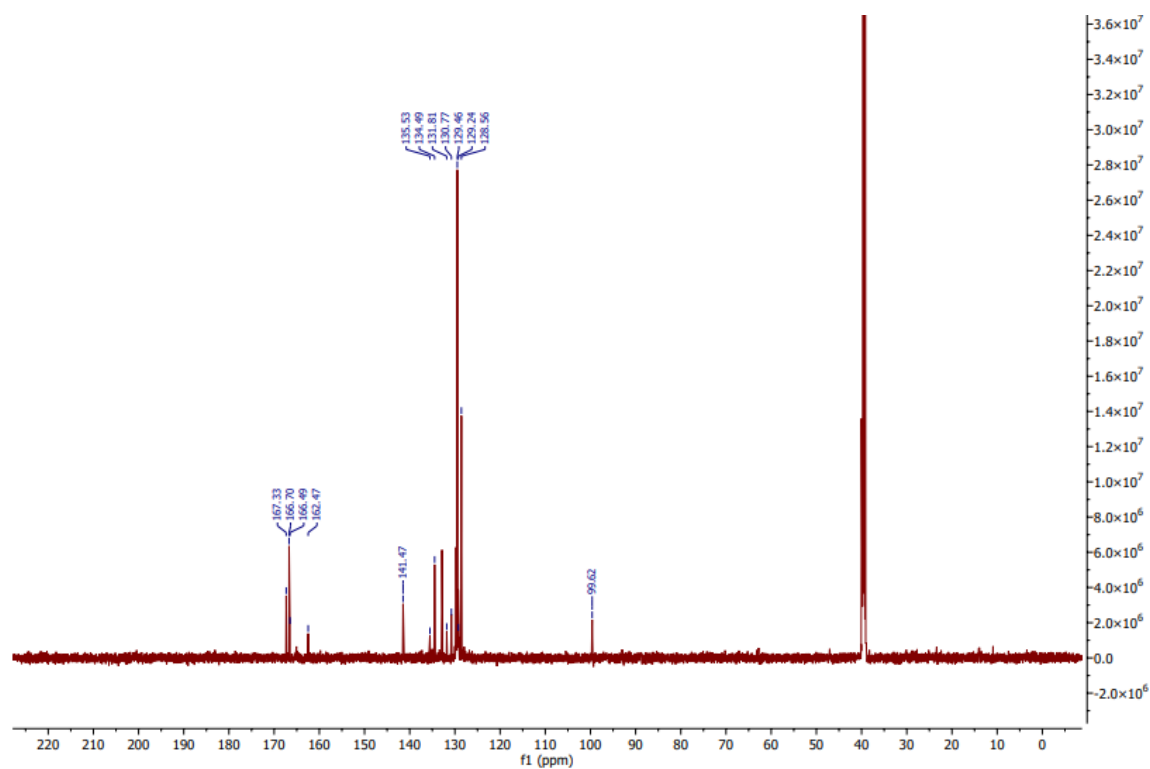
S27- ¹H NMR of PET impregnated with ethylene glycol in a 1:1 mass ratio degraded with microwaves of 0.8 kW input power.



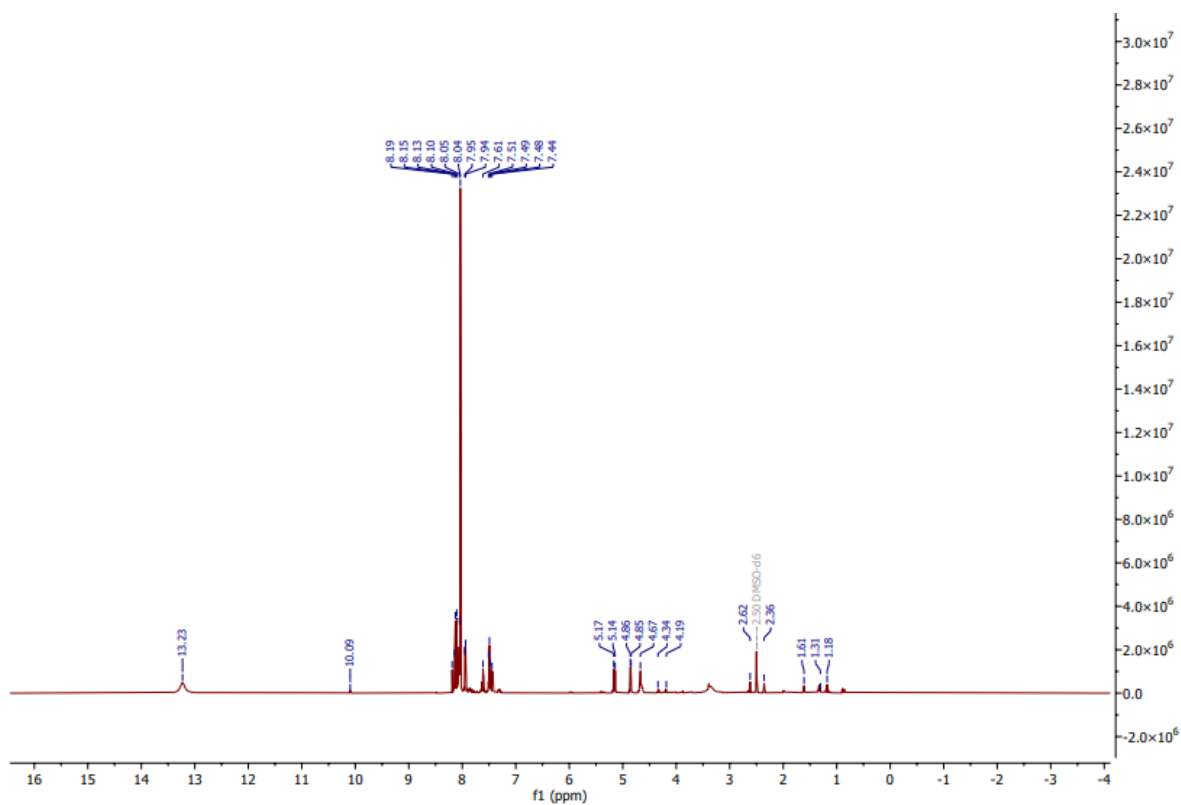
S28- ¹³C NMR of PET impregnated with ethylene glycol in a 1:1 mass ratio degraded with microwaves of 0.8 kW input power.



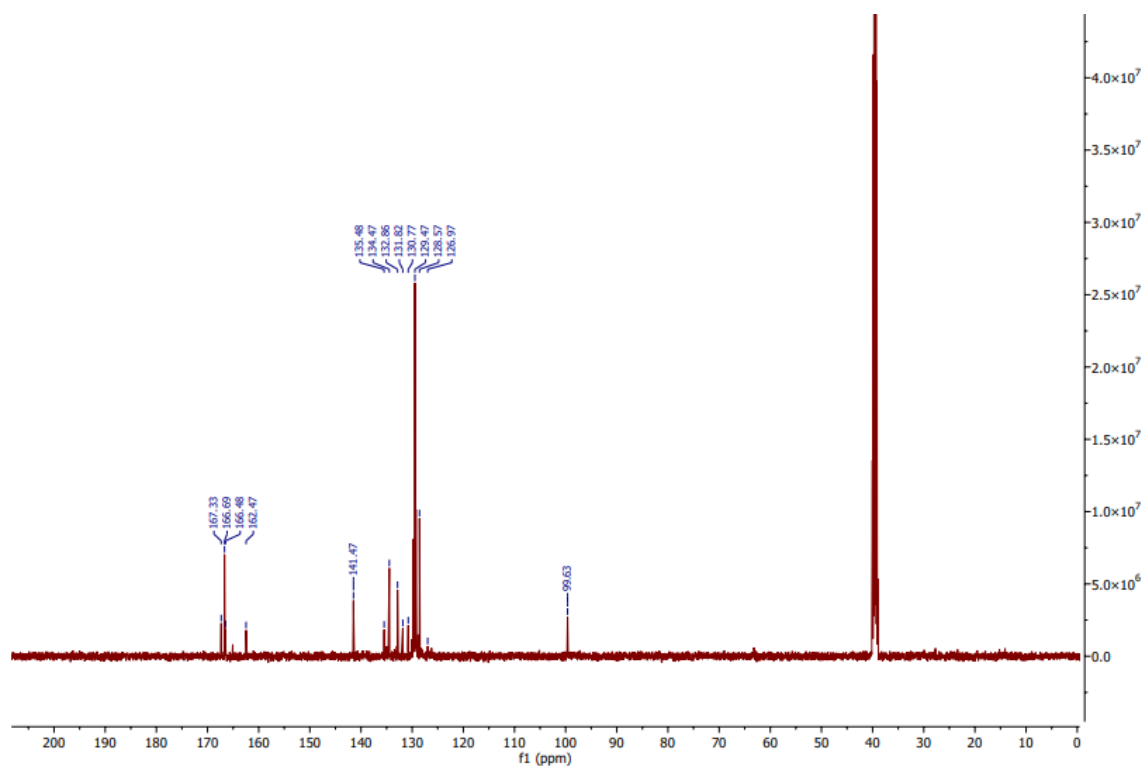
S29- ¹H NMR of PET impregnated with ethylene glycol in a 1:1 mass ratio degraded with microwaves of 1.2 kW input power.



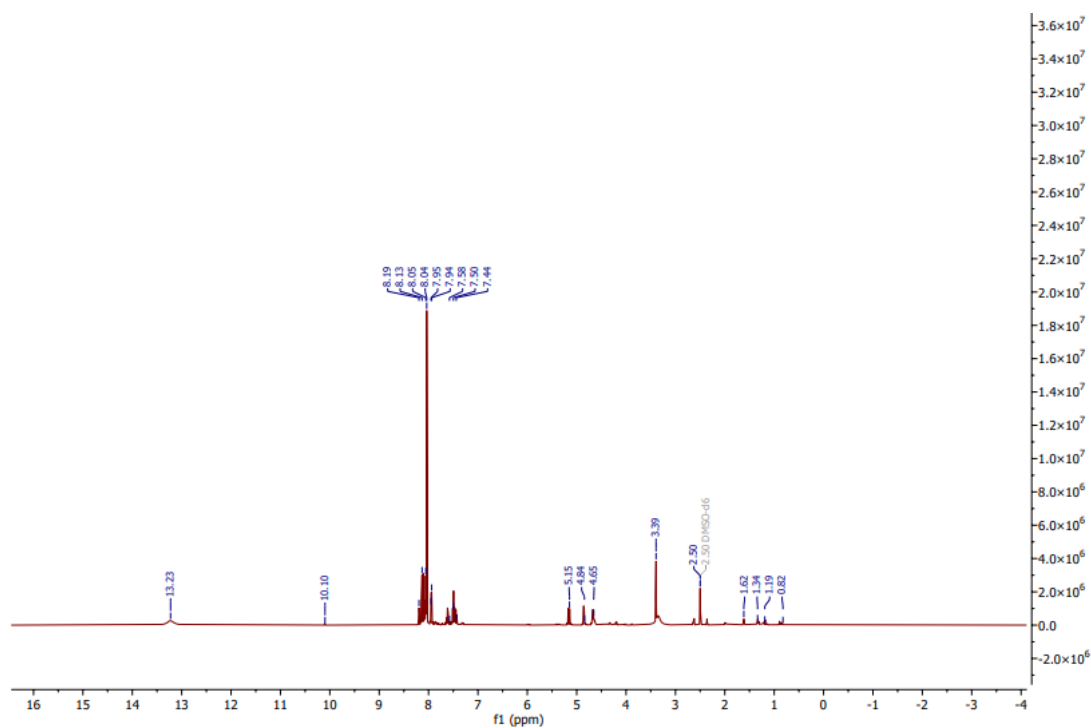
S30- ¹³C NMR of PET impregnated with ethylene glycol in a 1:1 mass ratio degraded with microwaves of 1.2 kW input power.



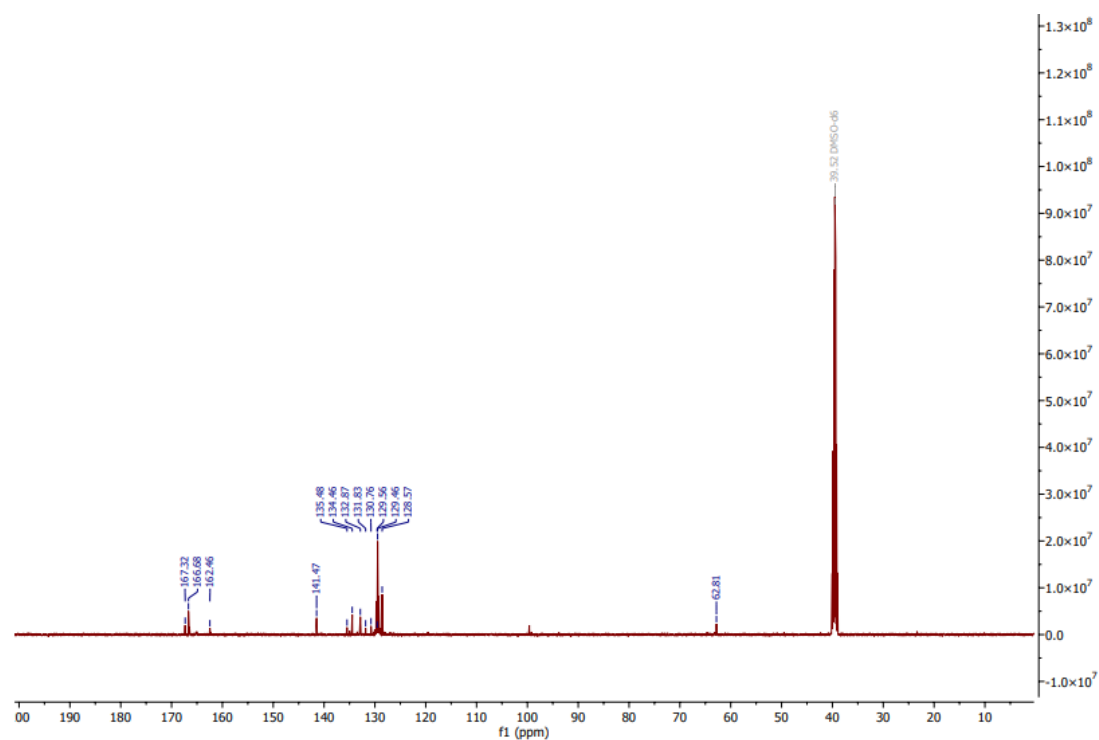
S31- ¹H NMR of PET impregnated with ethylene glycol in a 1:1 mass ratio degraded with microwaves of 1.6 kW input power.



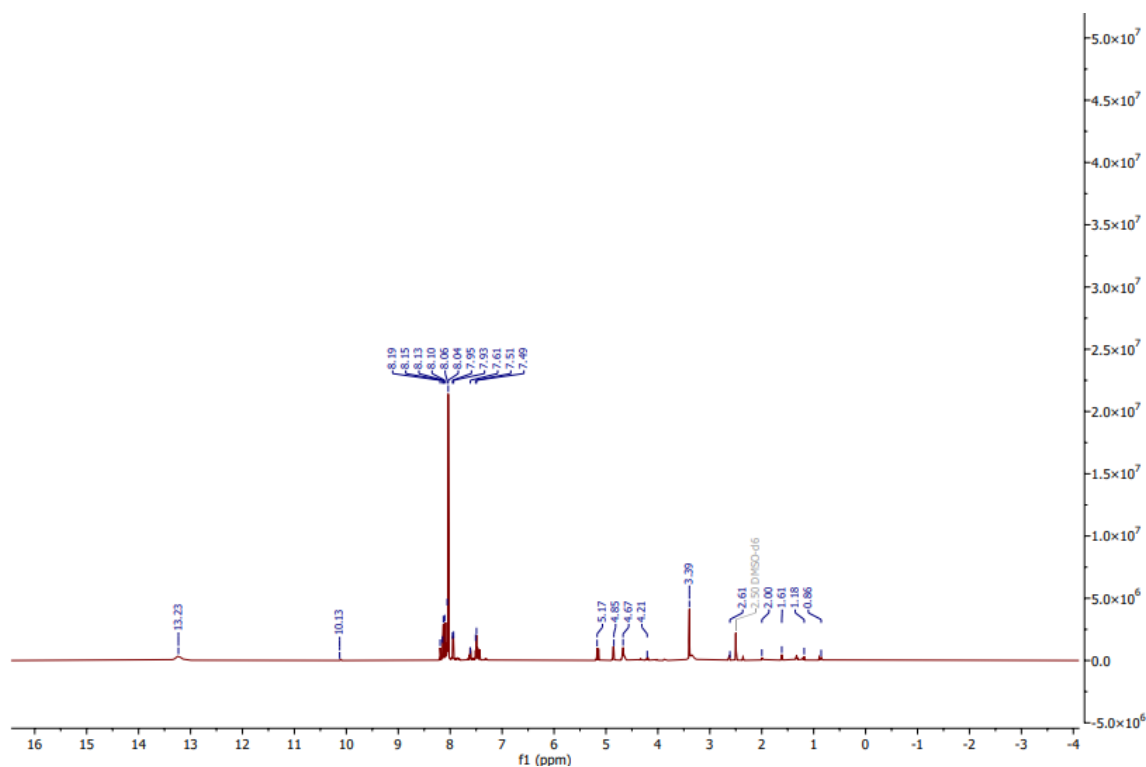
S32- ¹³C NMR of PET impregnated with ethylene glycol in a 1:1 mass ratio degraded with microwaves of 1.6 kW input power.



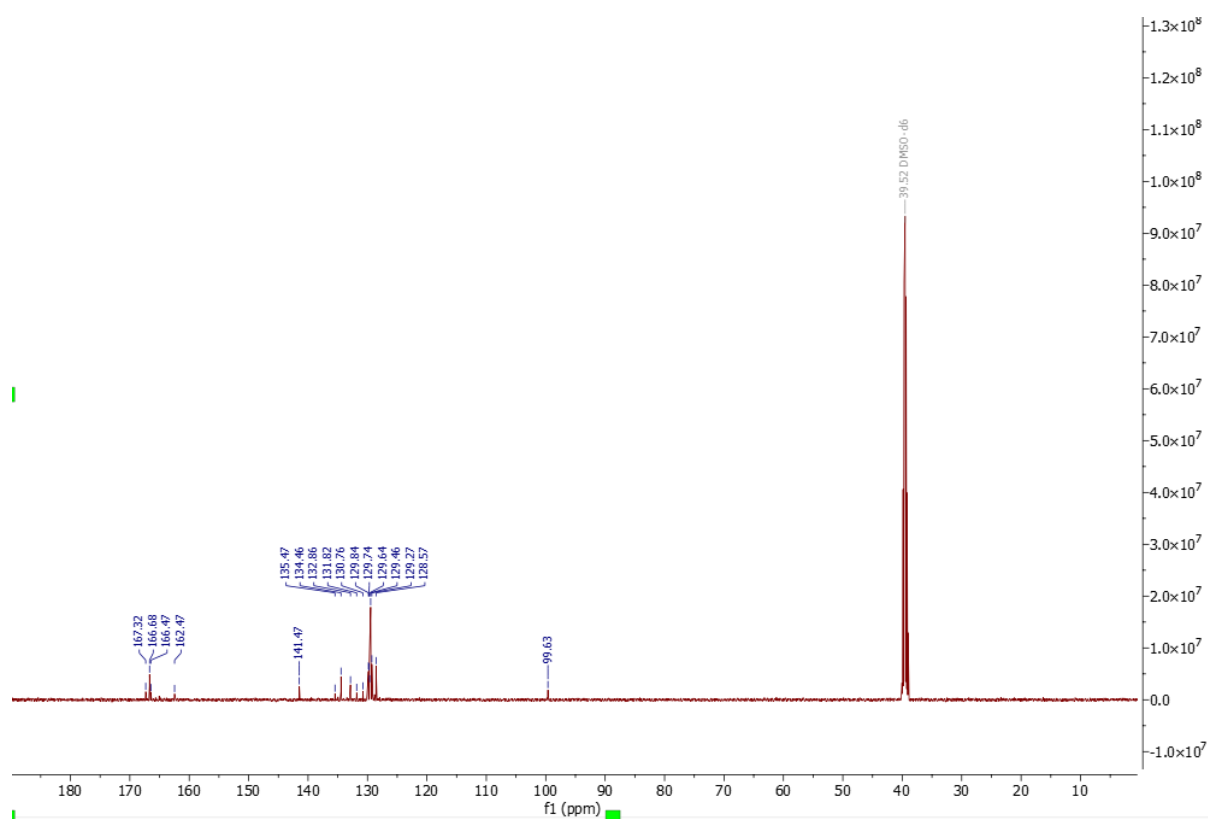
S33- ¹H NMR of PET impregnated with ethylene glycol in a 10:1 mass ratio degraded with microwaves of 0.8 kW input power.



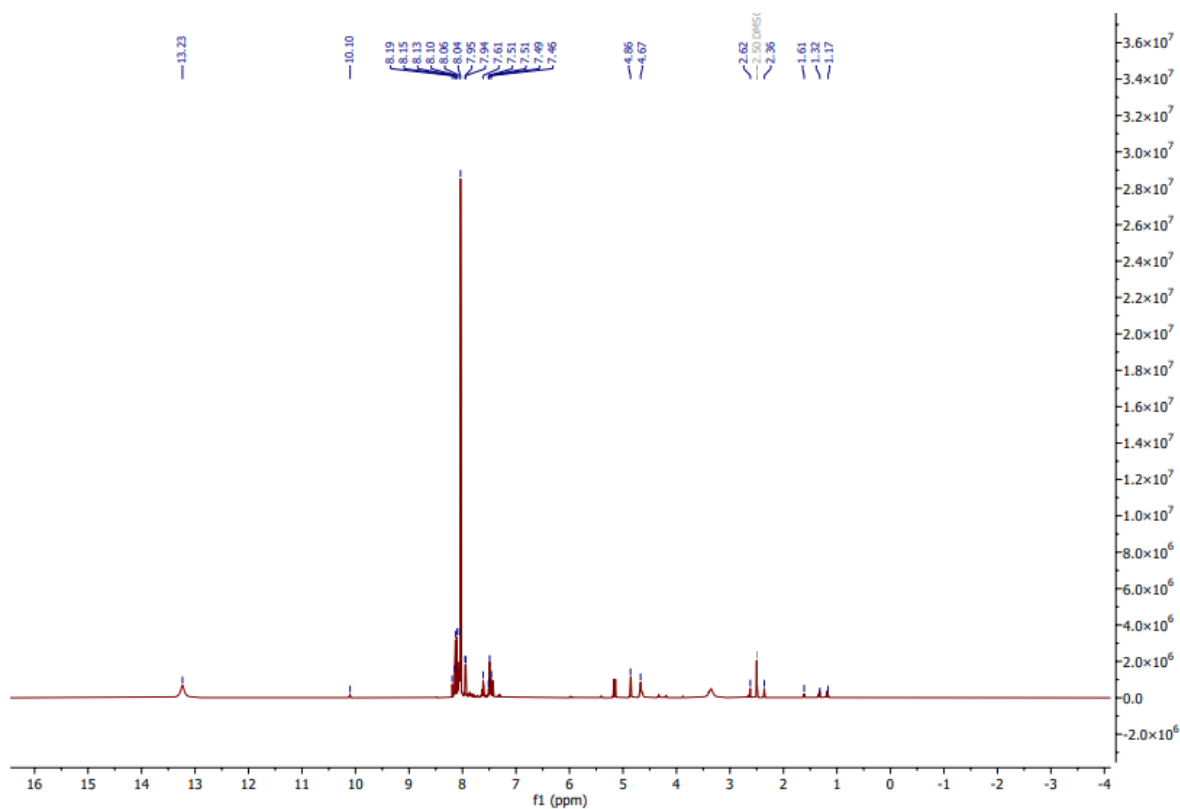
S34- ¹³C NMR of PET impregnated with ethylene glycol in a 10:1 mass ratio degraded with microwaves of 0.8 kW input power.



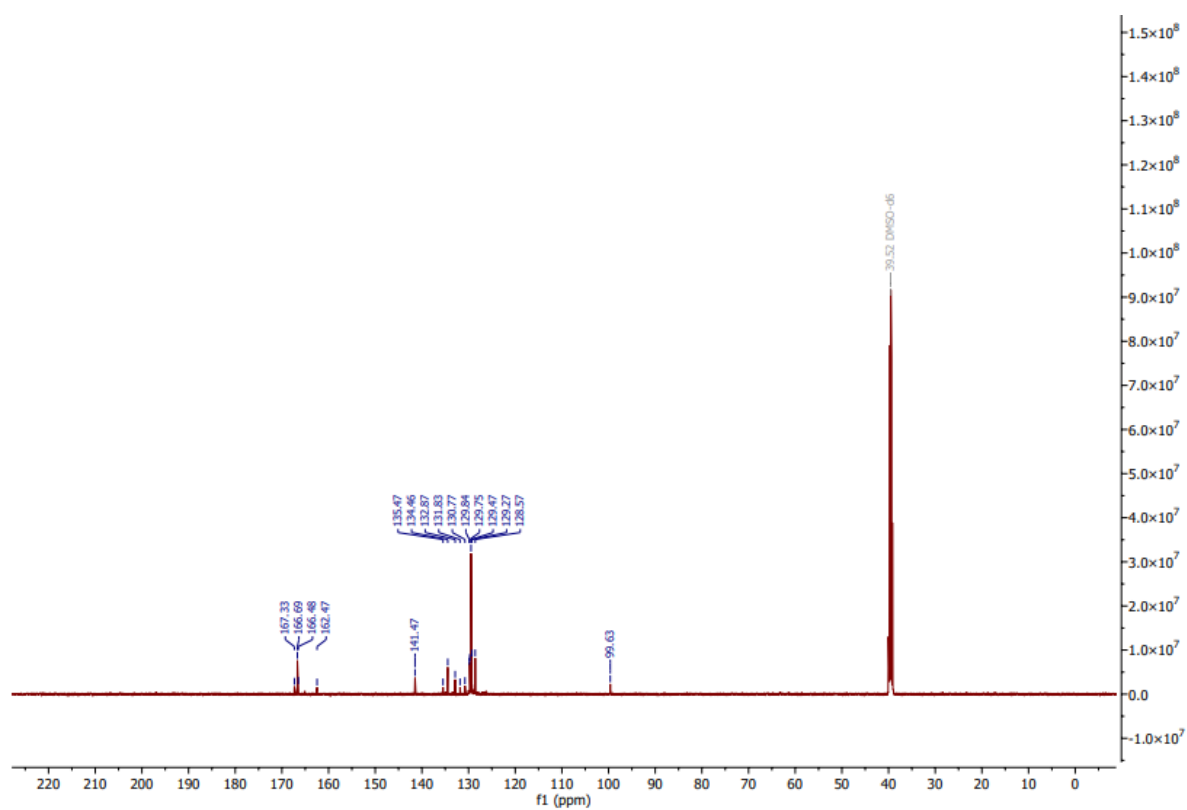
S35- ¹H NMR of PET impregnated with ethylene glycol in a 10:1 mass ratio degraded with microwaves of 1.2 kW input power.



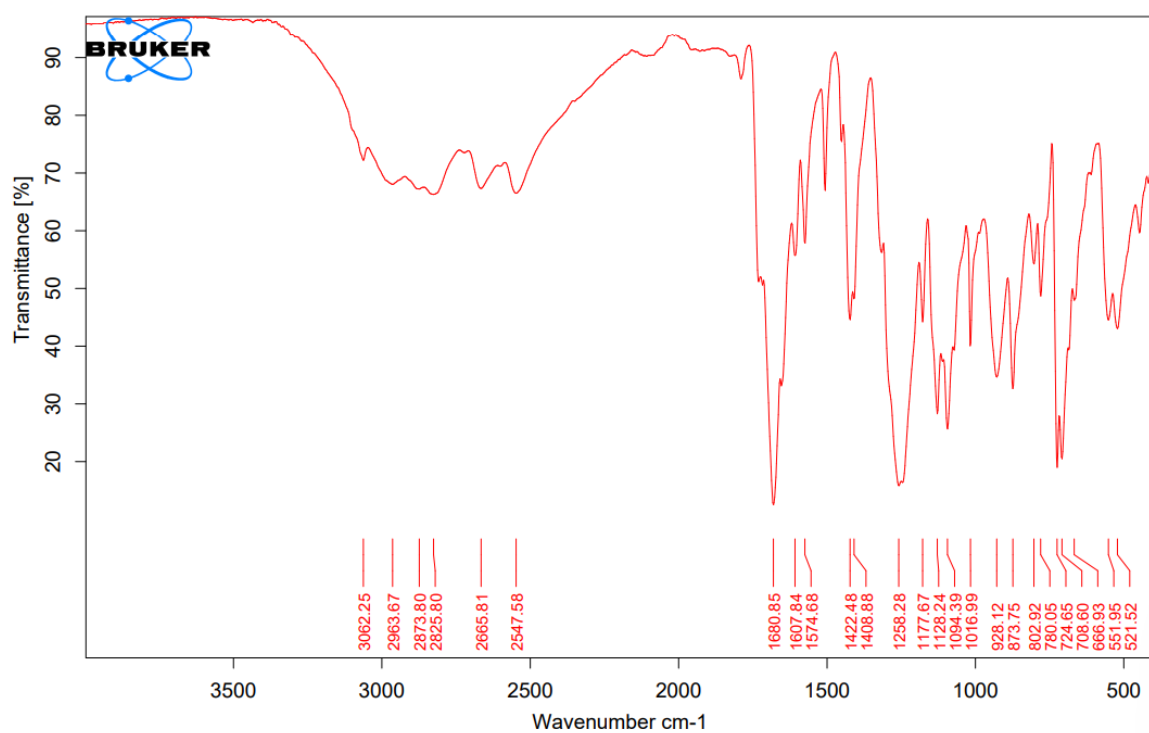
S36- ¹³C NMR of PET impregnated with ethylene glycol in a 10:1 mass ratio degraded with microwaves of 1.2 kW input power.



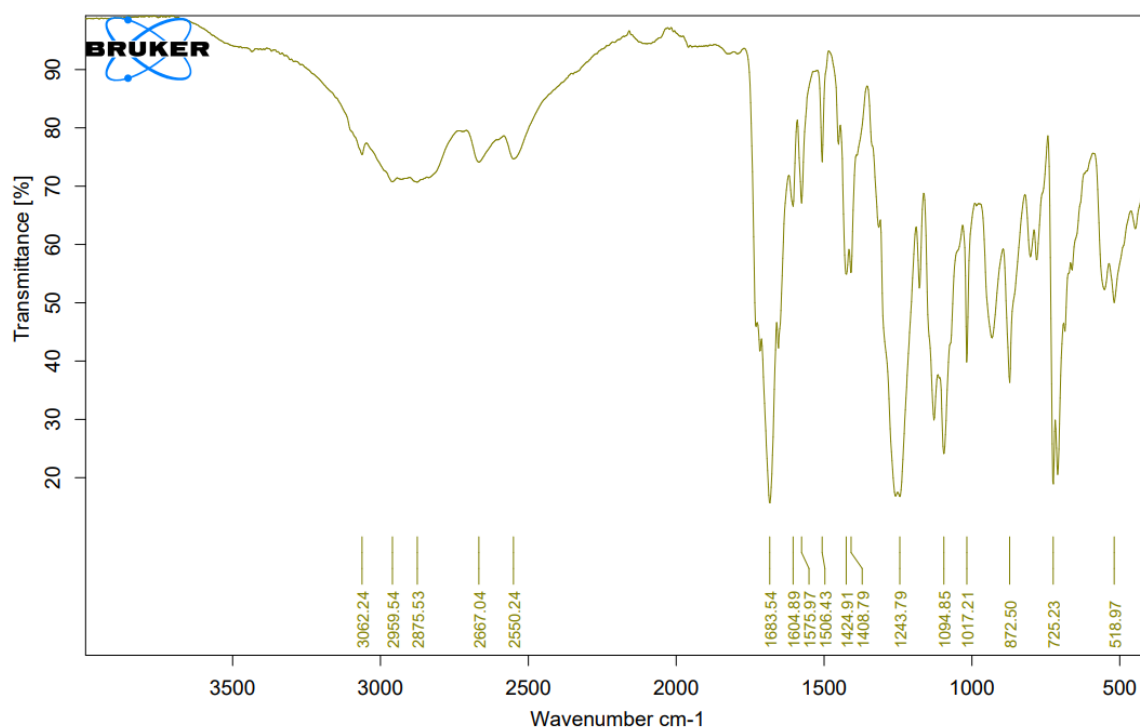
S37- ^1H NMR of PET impregnated with ethylene glycol in a 10:1 mass ratio degraded with microwaves of 1.6 kW input power.



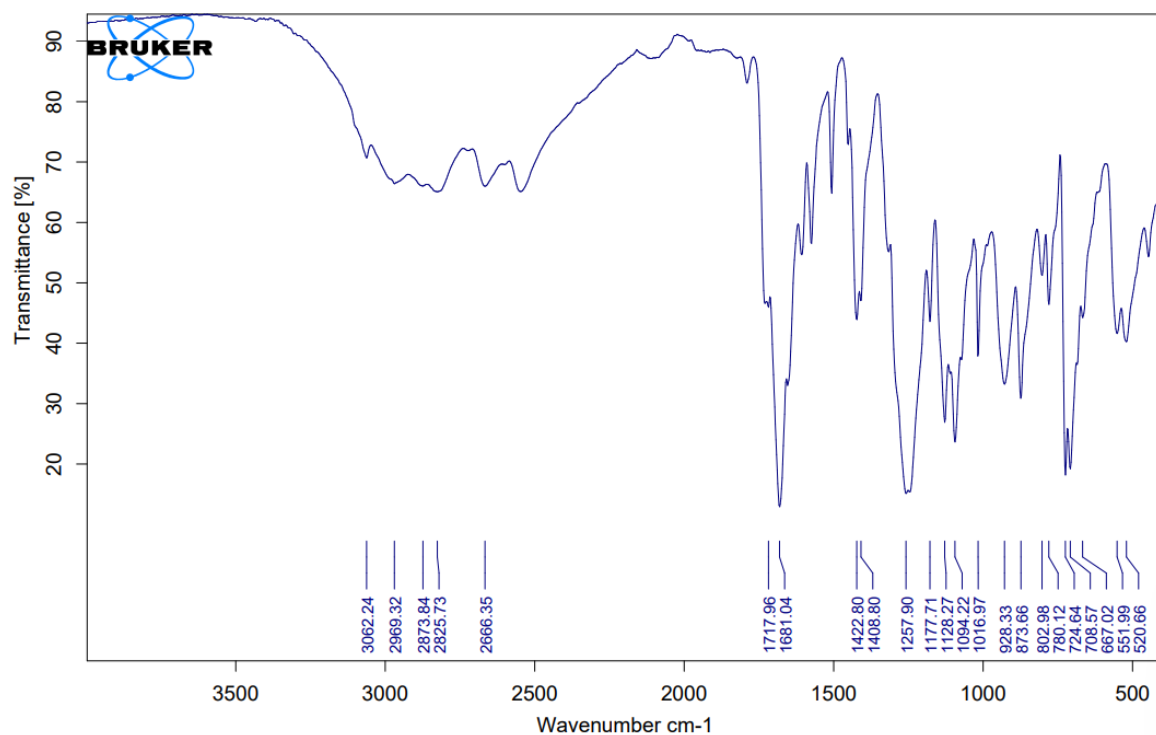
S38- ^{13}C NMR of PET impregnated with ethylene glycol in a 10:1 mass ratio degraded with microwaves of 1.6 kW input power.



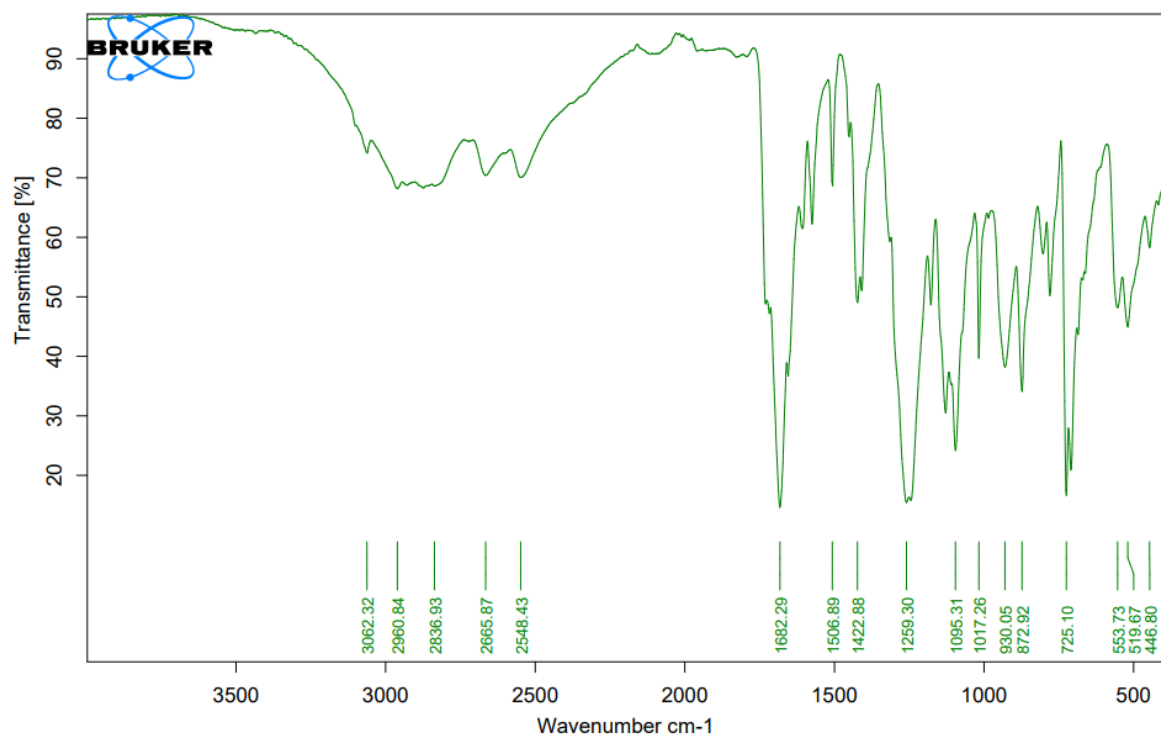
S39- IR of unmodified PET degraded with microwaves of 0.8 kW input power.



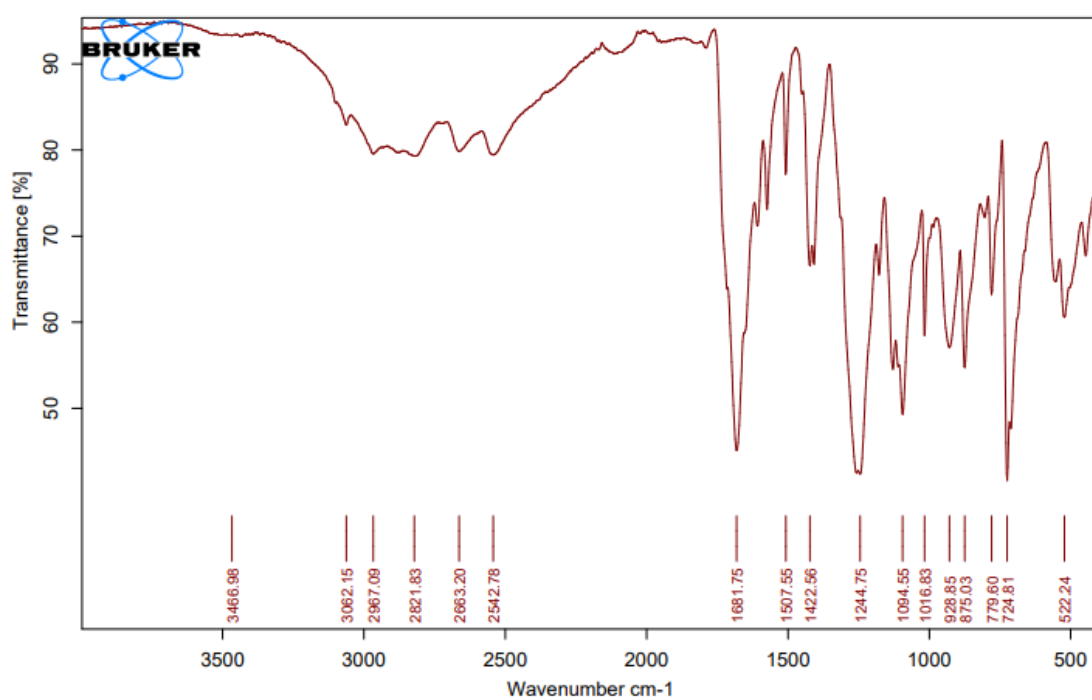
S40- IR of unmodified PET degraded with microwaves of 1.2 kW input power.



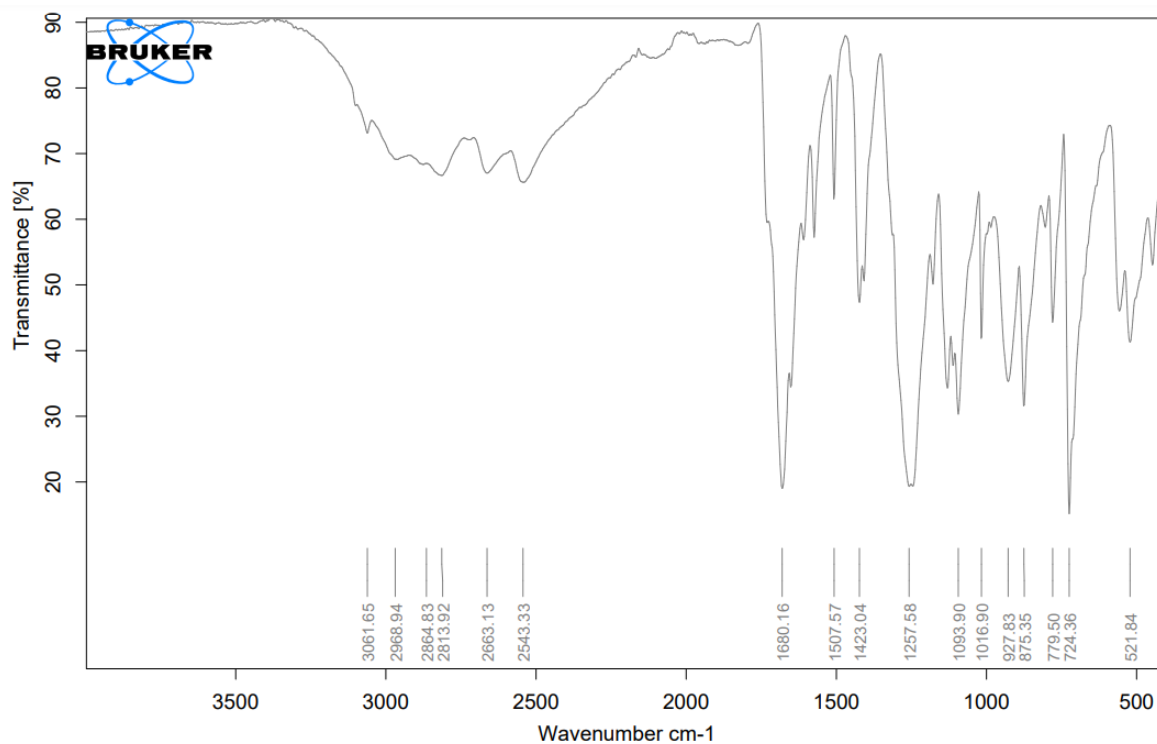
S41- IR of unmodified PET degraded with microwaves of 1.6 kW input power.



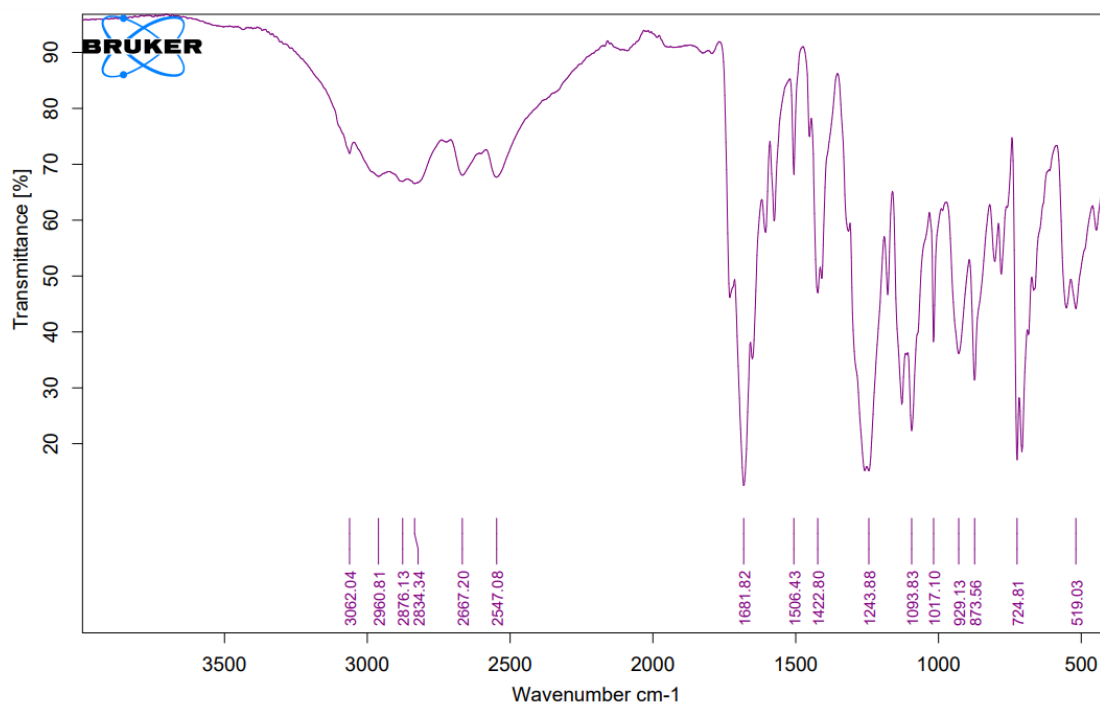
S42- IR of unmodified PET of PET impregnated with ethylene glycol in a 1:1 mass ratio degraded with microwaves of 0.8 kW input power.



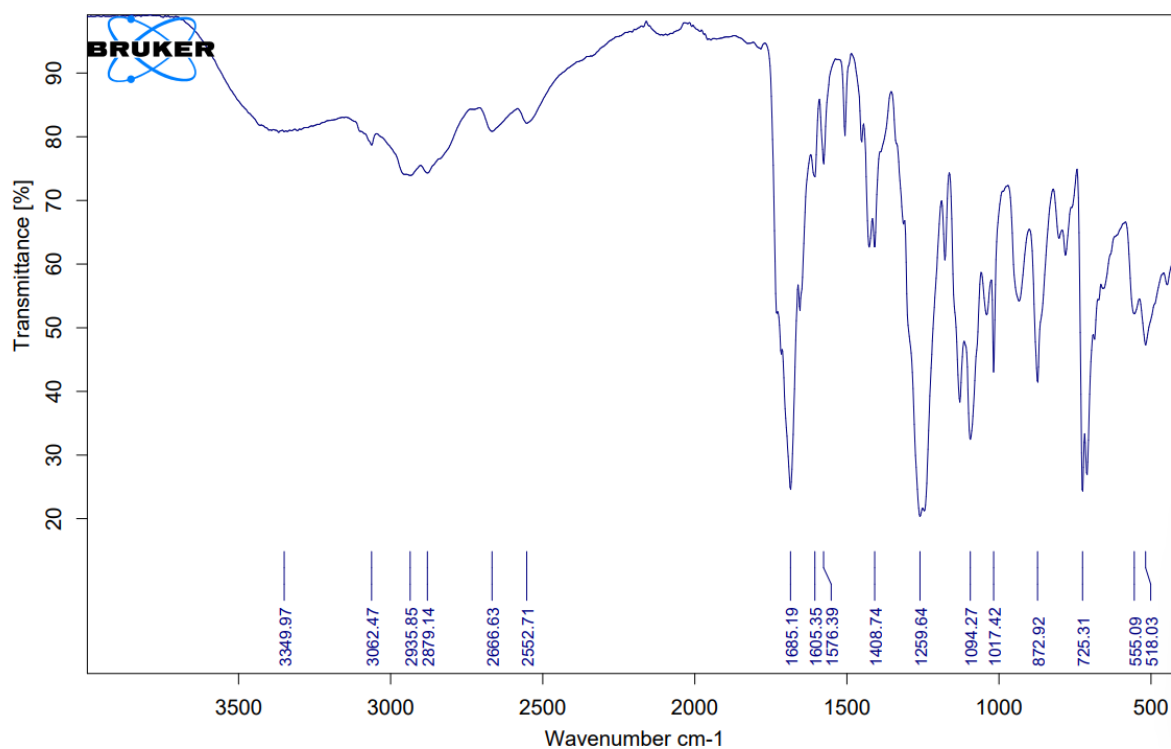
S43- IR of unmodified PET of PET impregnated with ethylene glycol in a 1:1 mass ratio degraded with microwaves of 1.2 kW input power.



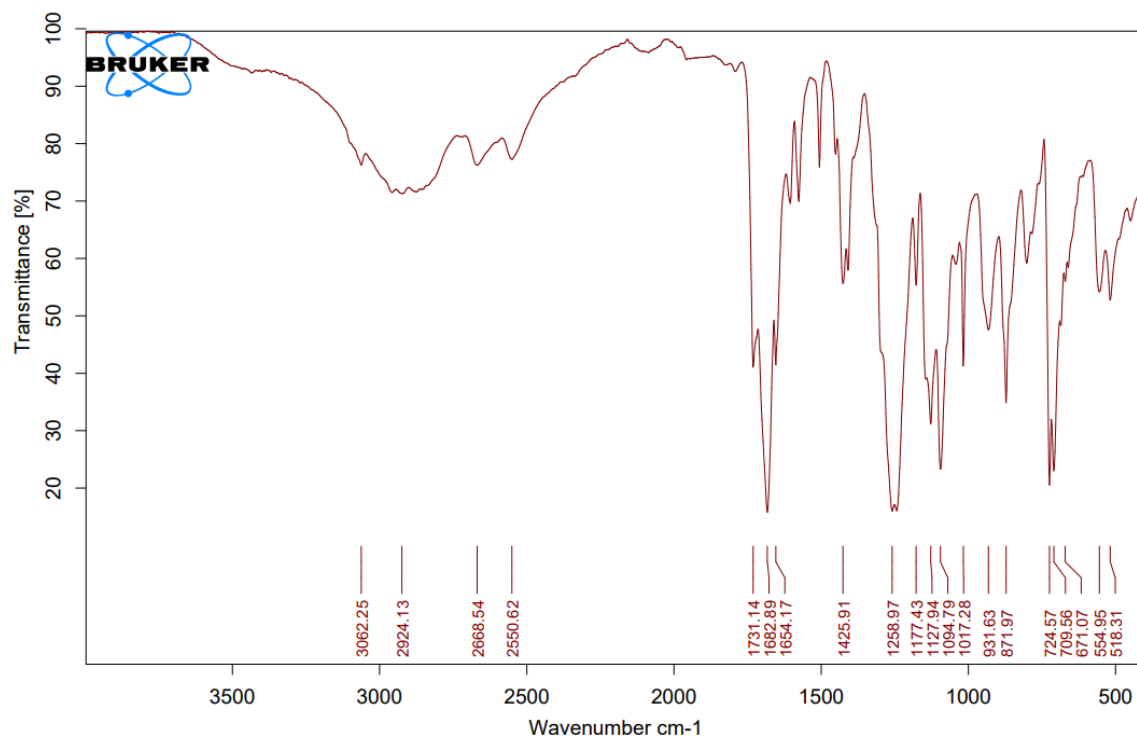
S44- IR of unmodified PET of PET impregnated with ethylene glycol in a 1:1 mass ratio degraded with microwaves of 1.6 kW input power.



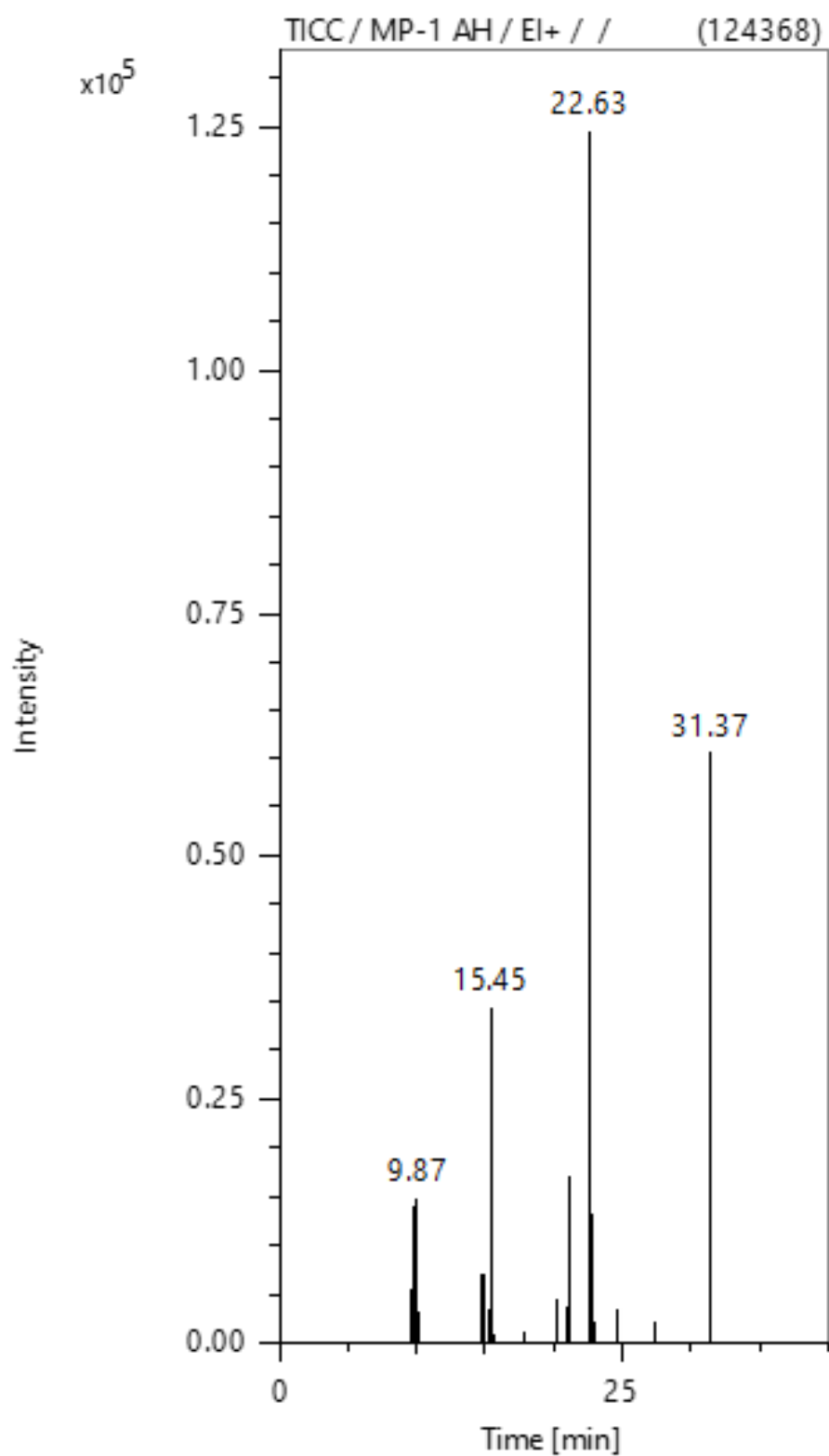
S45- IR of unmodified PET of PET impregnated with ethylene glycol in a 10:1 mass ratio degraded with microwaves of 0.8 kW input power.



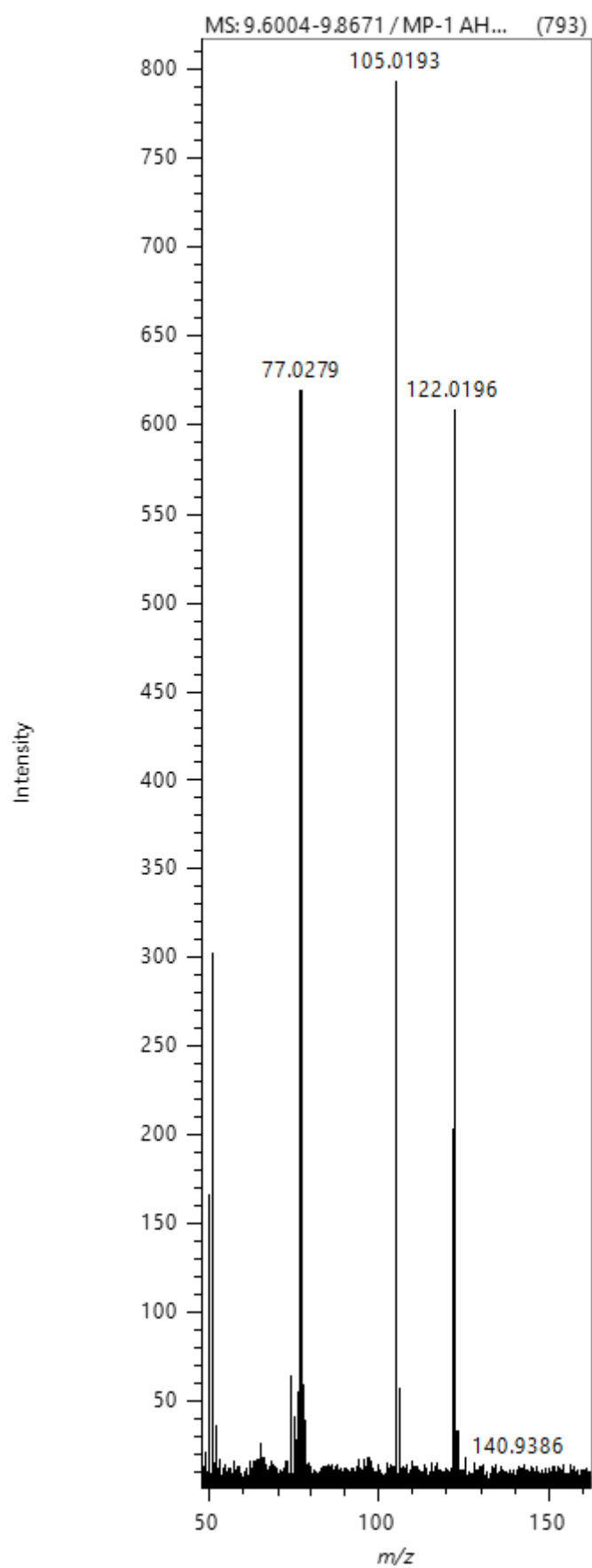
S46- IR of unmodified PET of PET impregnated with ethylene glycol in a 10:1 mass ratio degraded with microwaves of 1.2 kW input power.



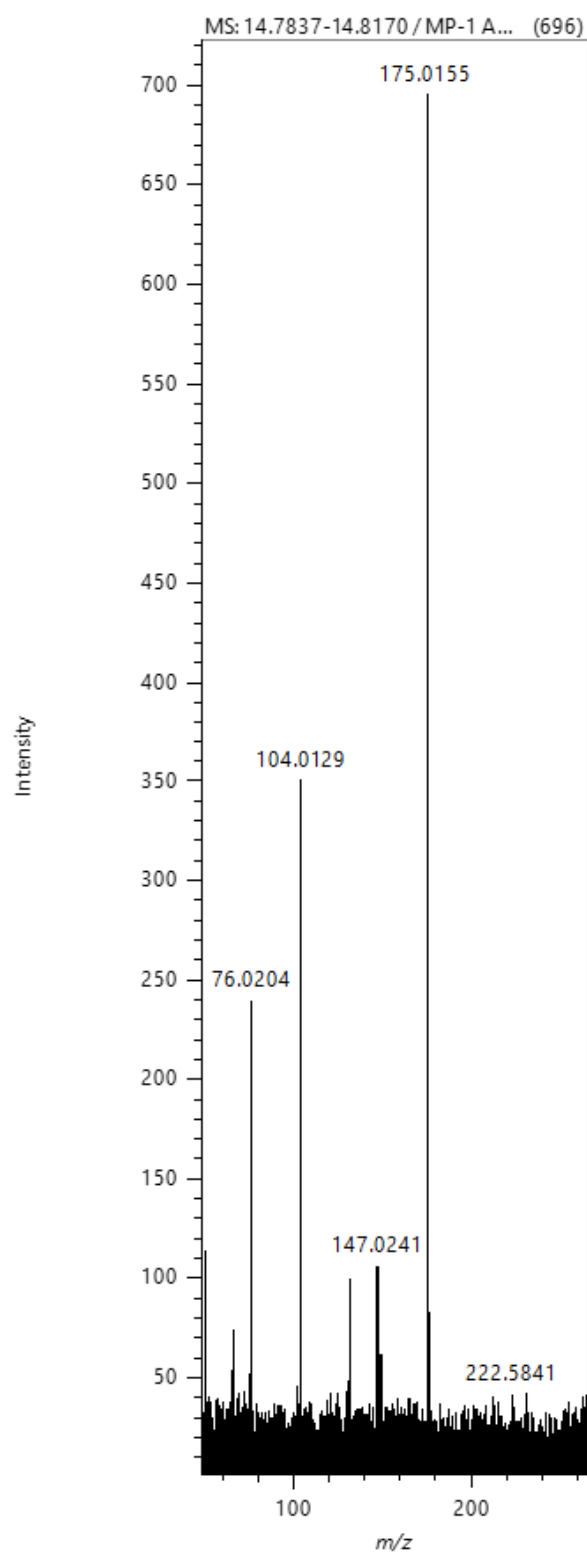
S47- IR of unmodified PET of PET impregnated with ethylene glycol in a 10:1 mass ratio degraded with microwaves of 1.6 kW input power.



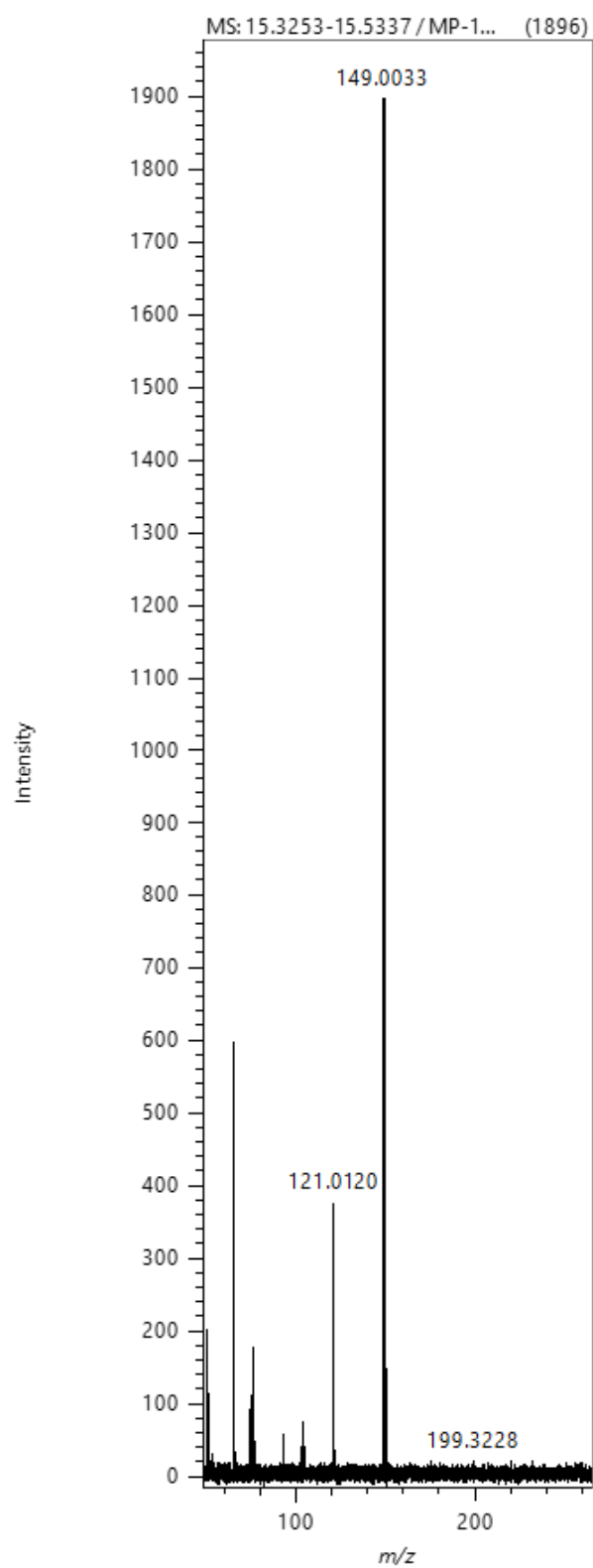
S48- GC-MS TICC of unmodified PET degraded with microwaves at an input power of 0.8 kW (powder fraction).



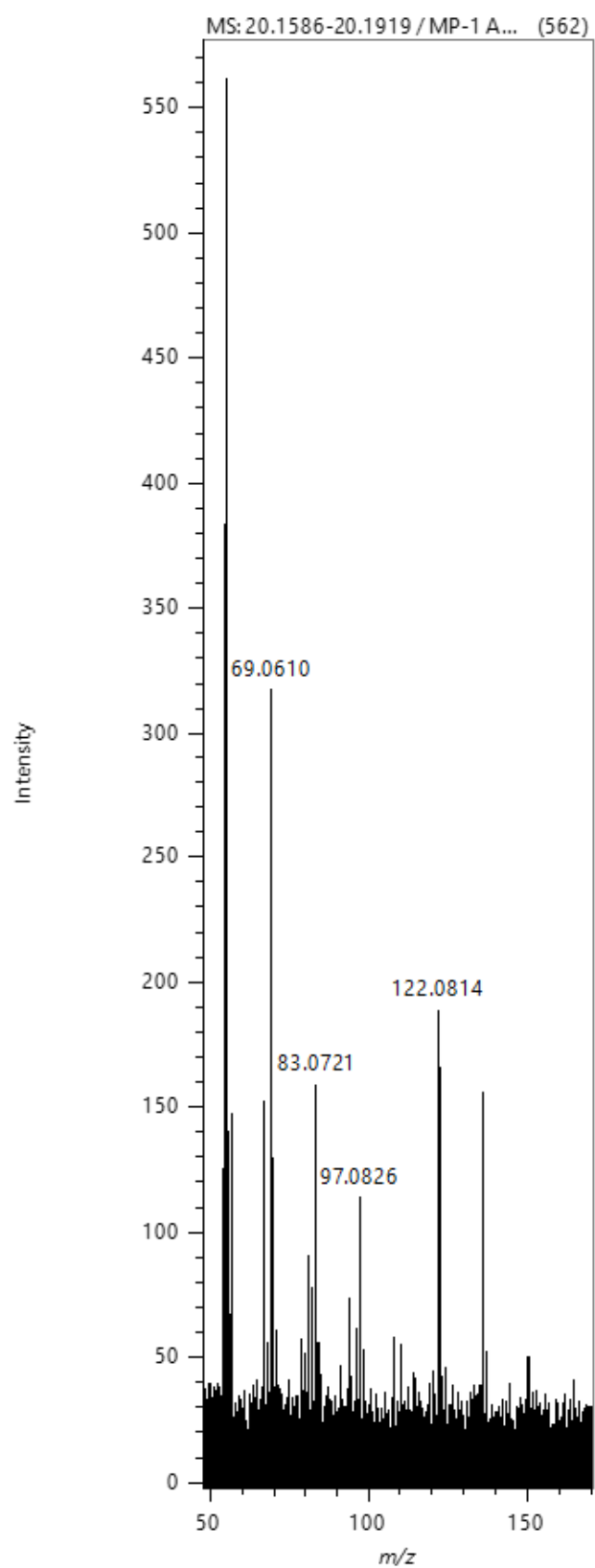
S49- GC-MS m/z of unmodified PET degraded with microwaves at an input power of 0.8 kW (powder fraction) t=9.87 minutes).



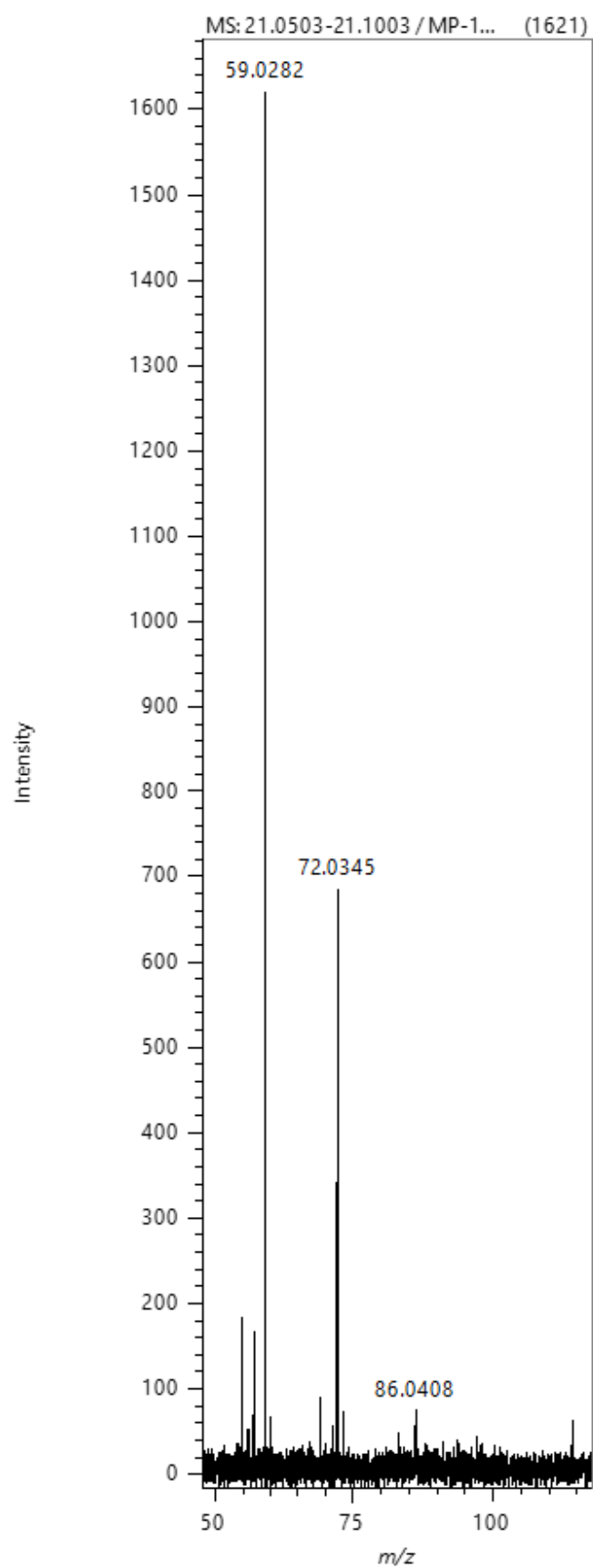
S50- GC-MS m/z of unmodified PET degraded with microwaves at an input power of 0.8 kW (powder fraction) t=9.87 minutes).



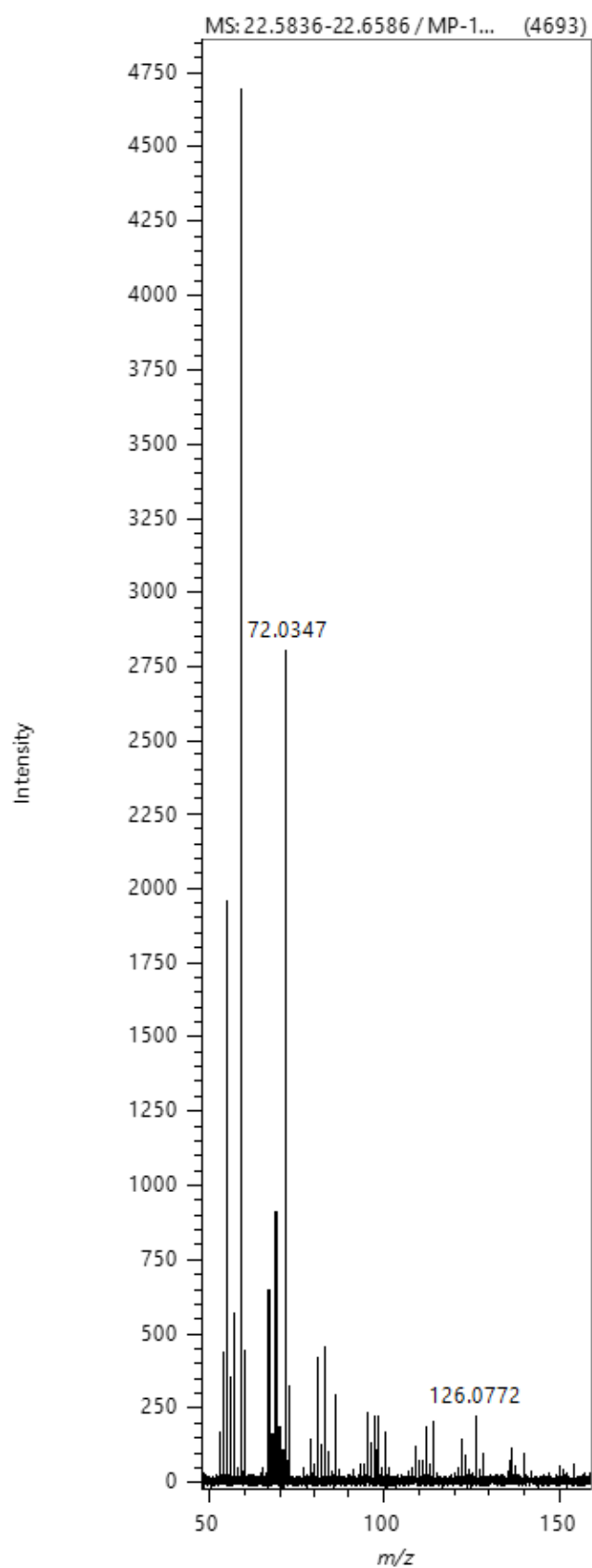
S51- GC-MS m/z of unmodified PET degraded with microwaves at an input power of 0.8 kW (powder fraction) $t=15.45$ minutes).



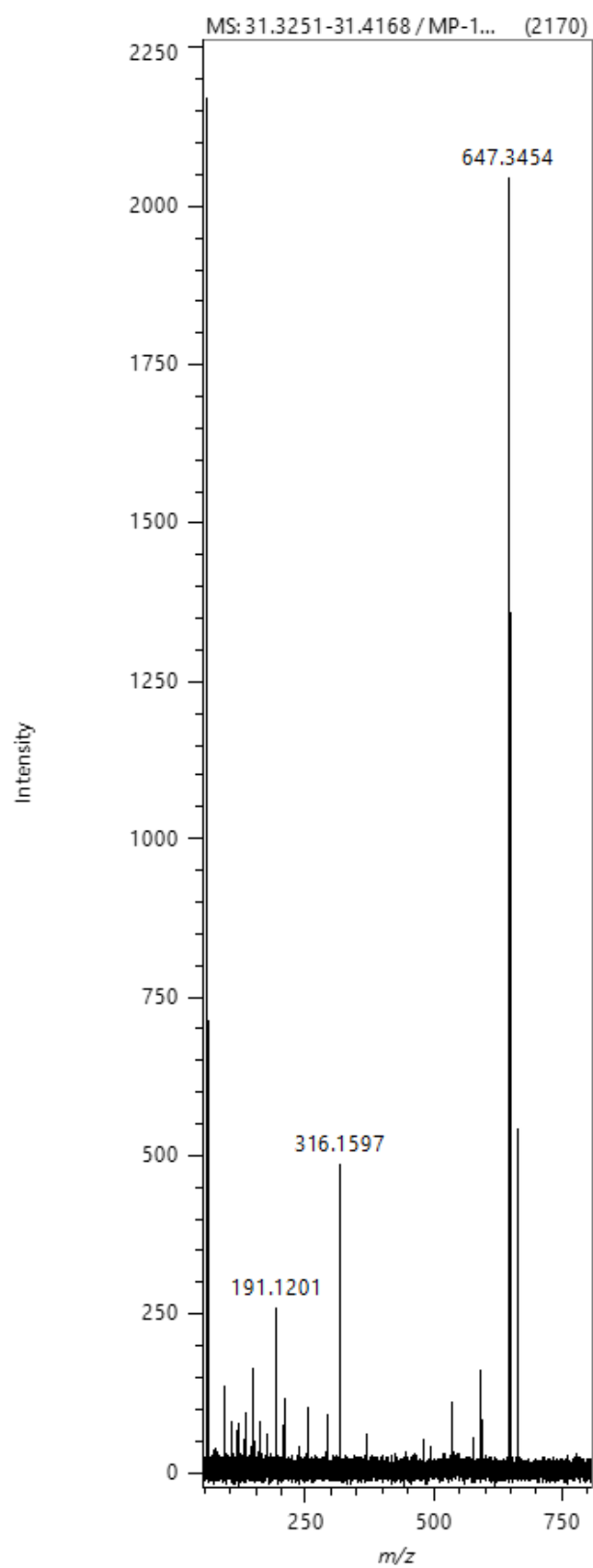
S52- GC-MS m/z of unmodified PET degraded with microwaves at an input power of 0.8 kW (powder fraction) $t=20.18$ minutes).



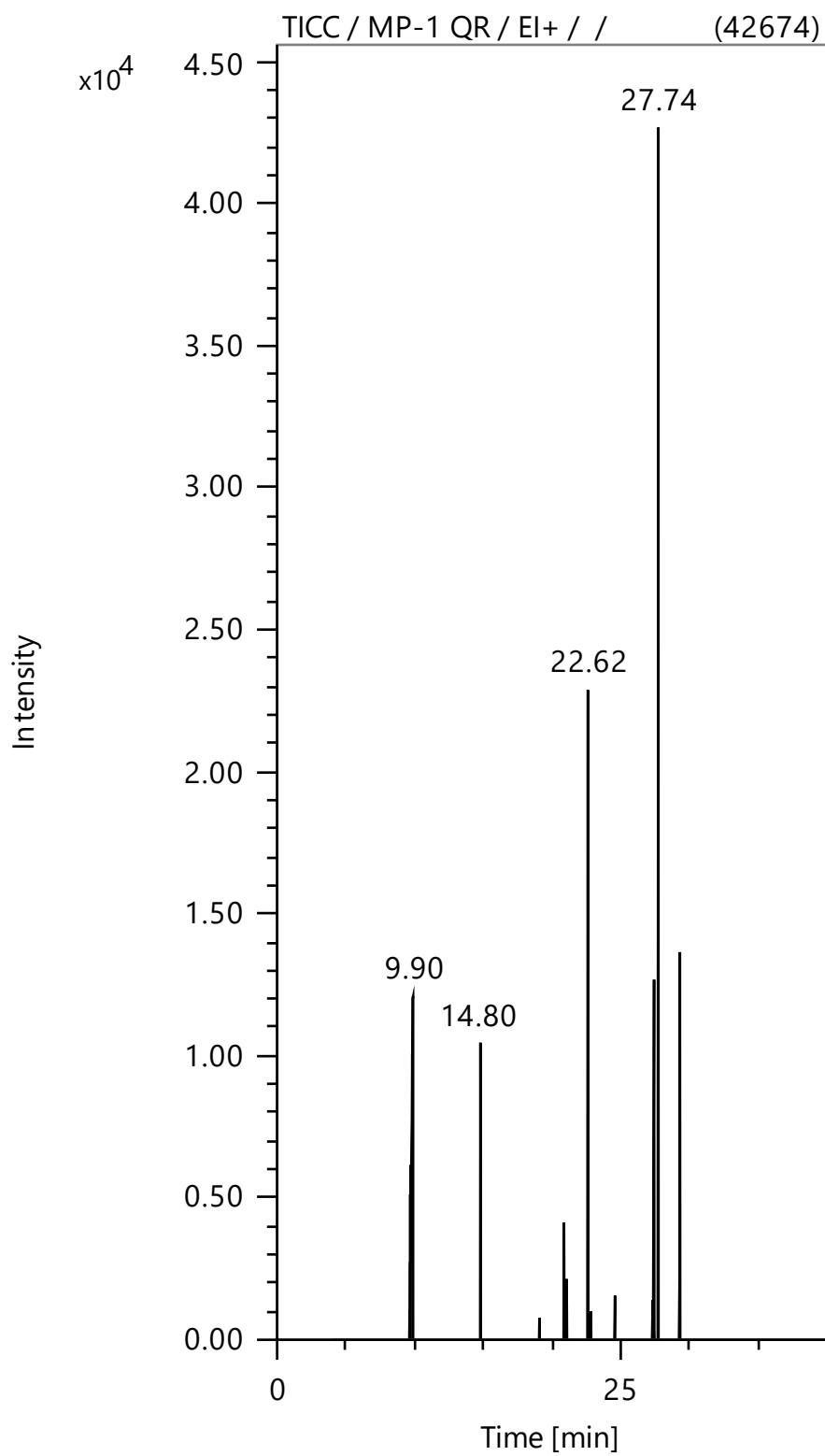
S53- GC-MS m/z of unmodified PET degraded with microwaves at an input power of 0.8 kW (powder fraction) $t=21.88$ minutes).



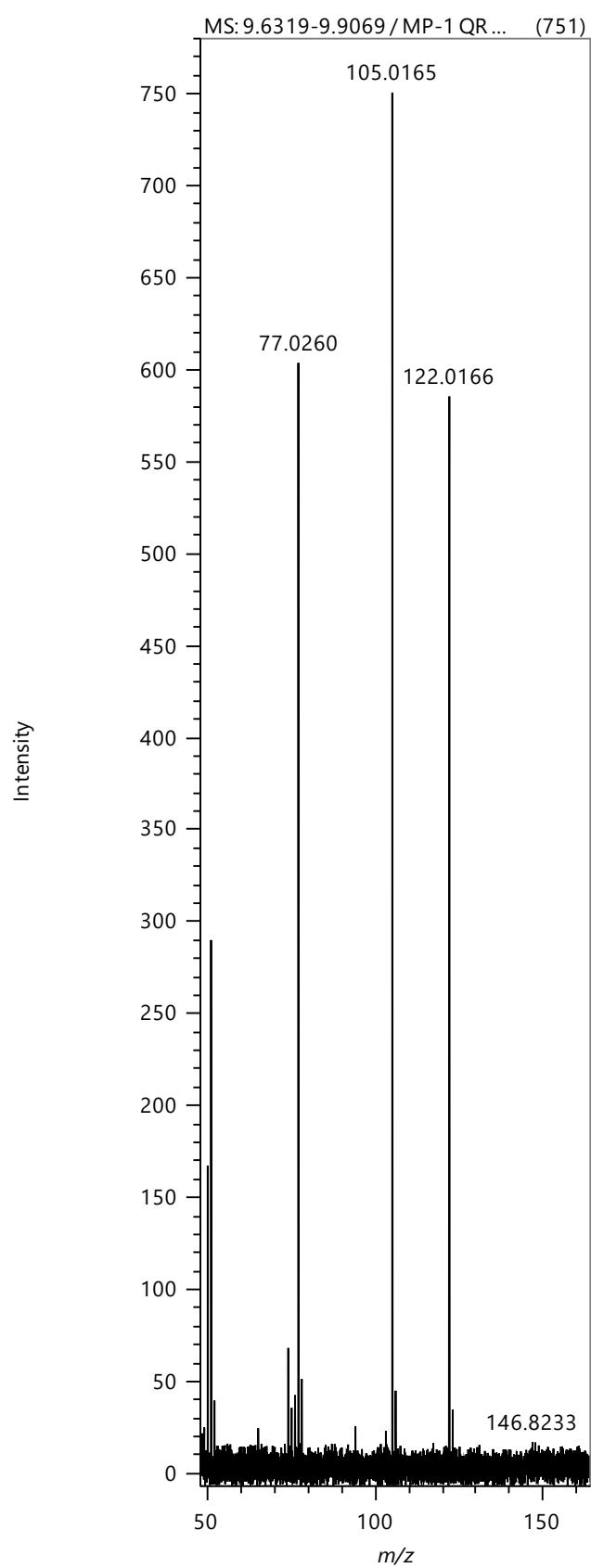
S54- GC-MS m/z of unmodified PET degraded with microwaves at an input power of 0.8 kW (powder fraction) t=22.60 minutes).



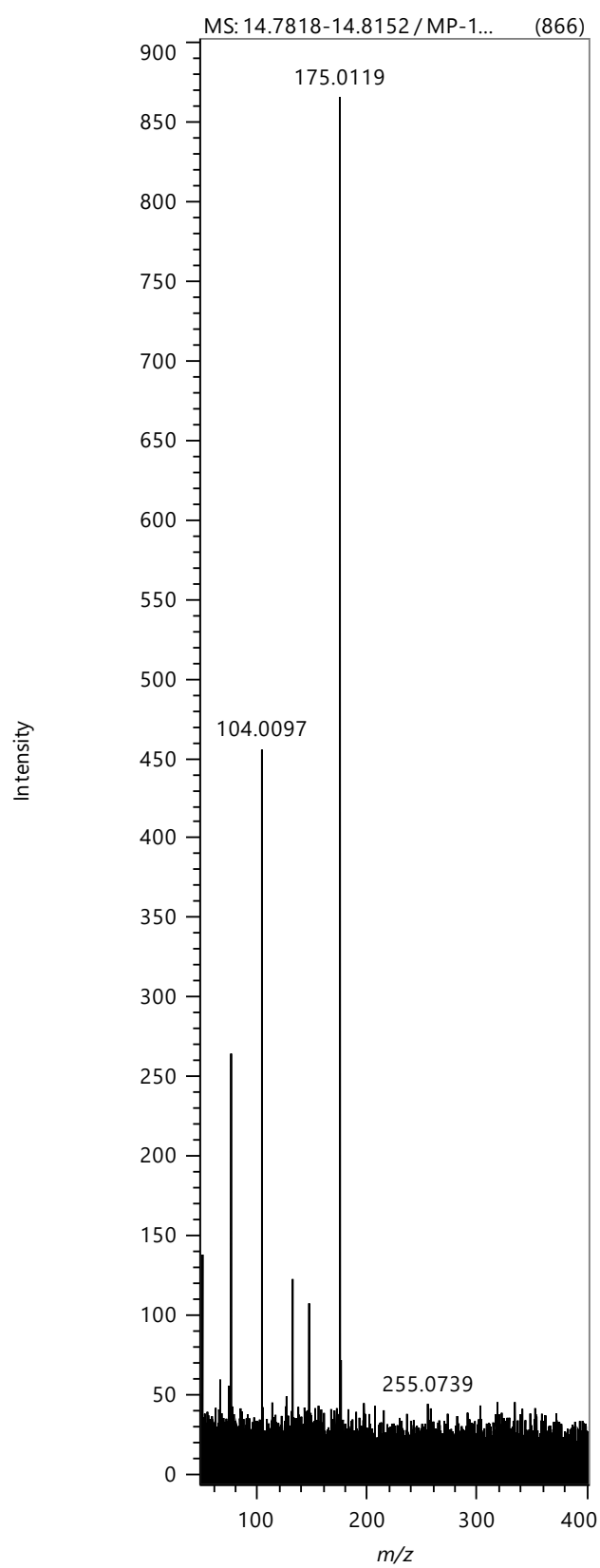
S55- GC-MS m/z of unmodified PET degraded with microwaves at an input power of 0.8 kW (powder fraction) $t=31.37$ minutes).



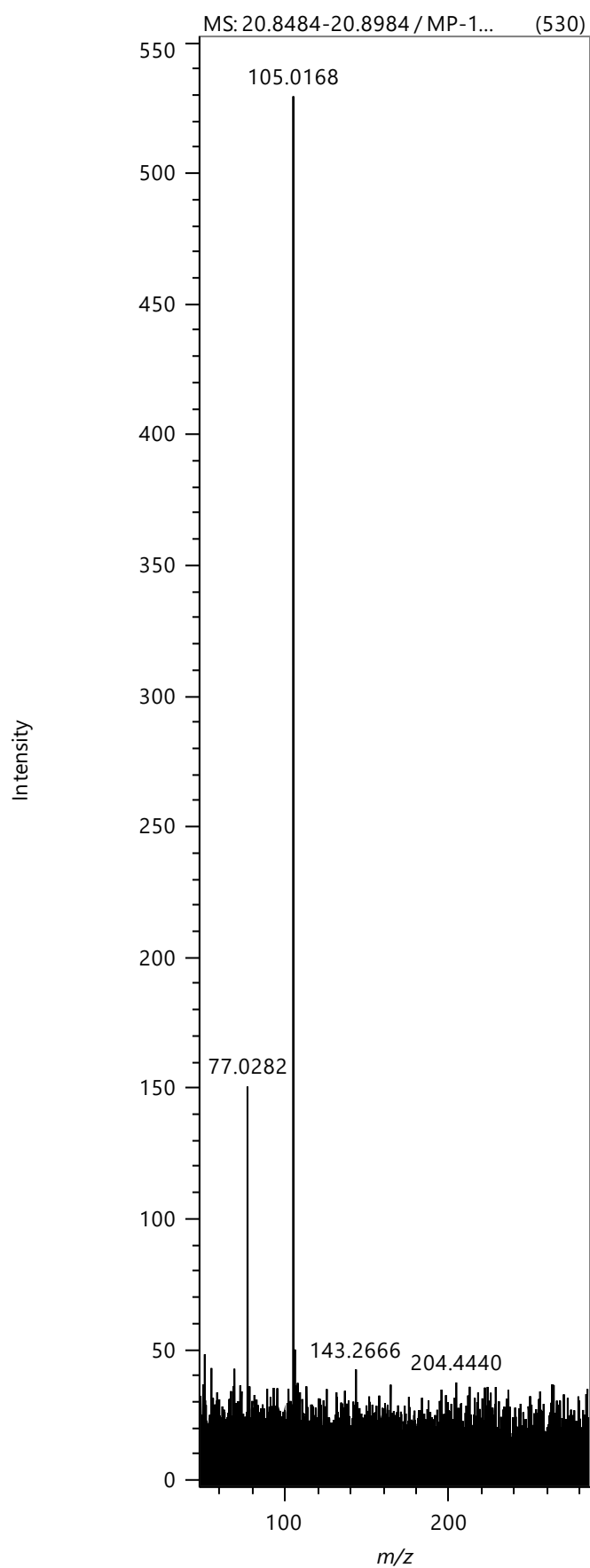
S56- GC-MS TICC of unmodified PET degraded with microwaves at an input power of 0.8 kW (wax fraction).



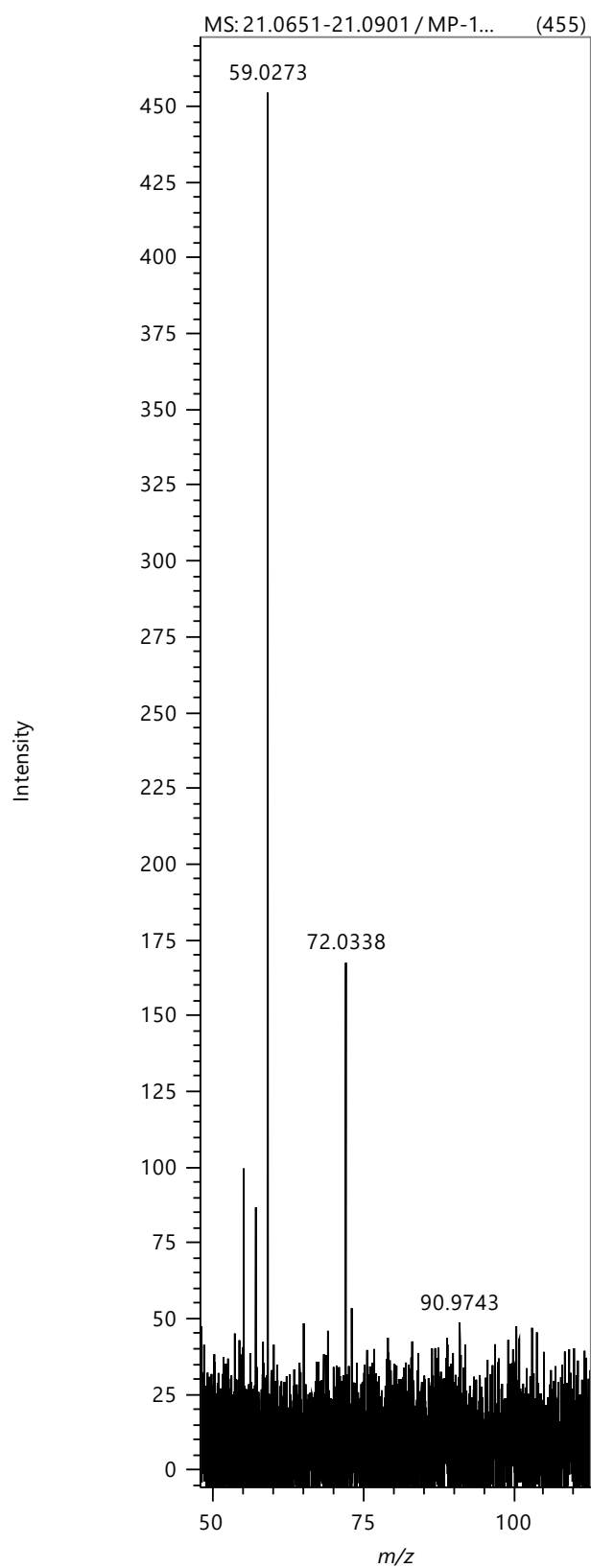
S57- GC-MS m/z of unmodified PET degraded with microwaves at an input power of 0.8 kW (powder fraction) t=9.90 minutes).



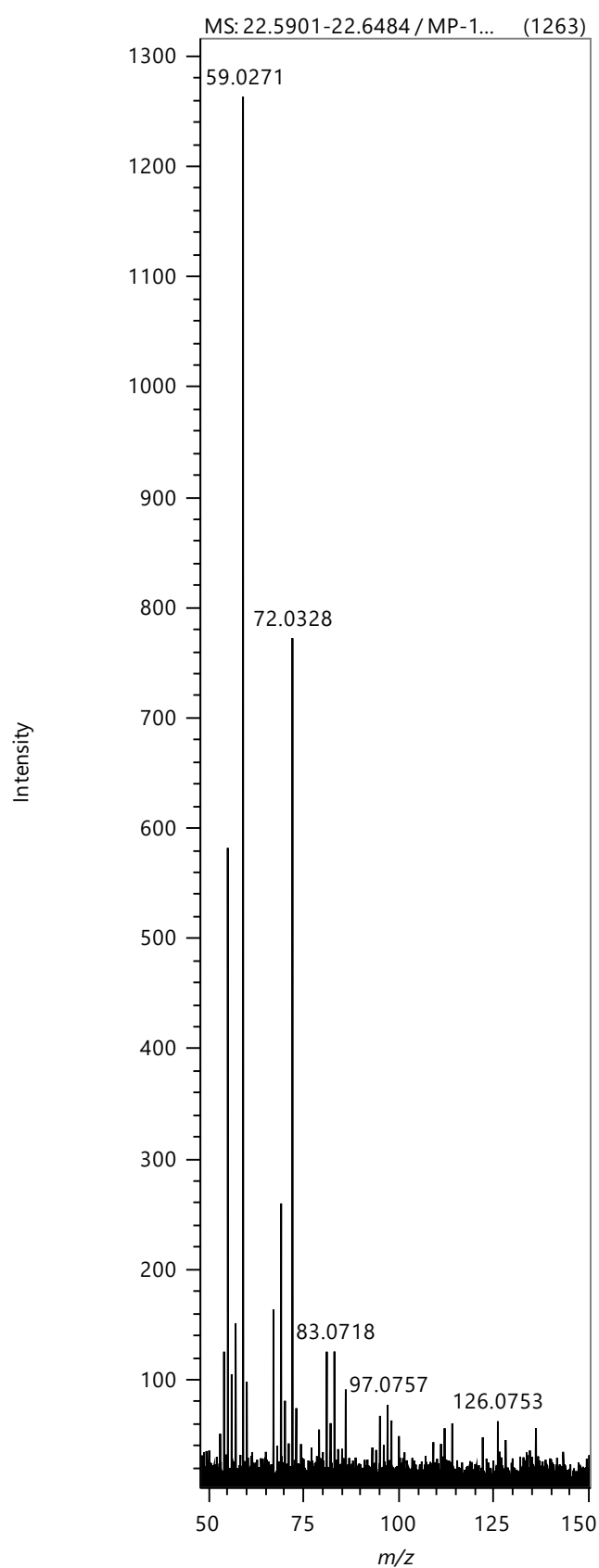
S58- GC-MS m/z of unmodified PET degraded with microwaves at an input power of 0.8 kW (powder fraction) t=14.80 minutes).



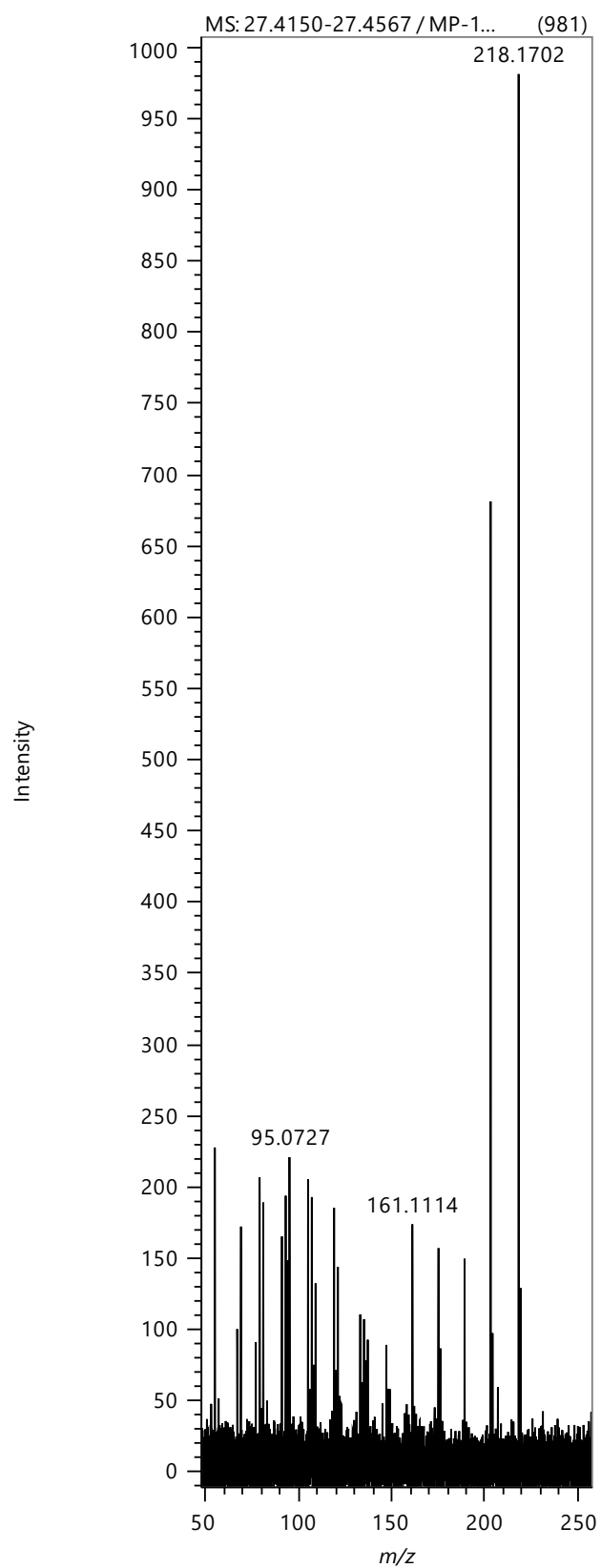
S59- GC-MS m/z of unmodified PET degraded with microwaves at an input power of 0.8 kW (powder fraction) $t=20.85$ minutes).



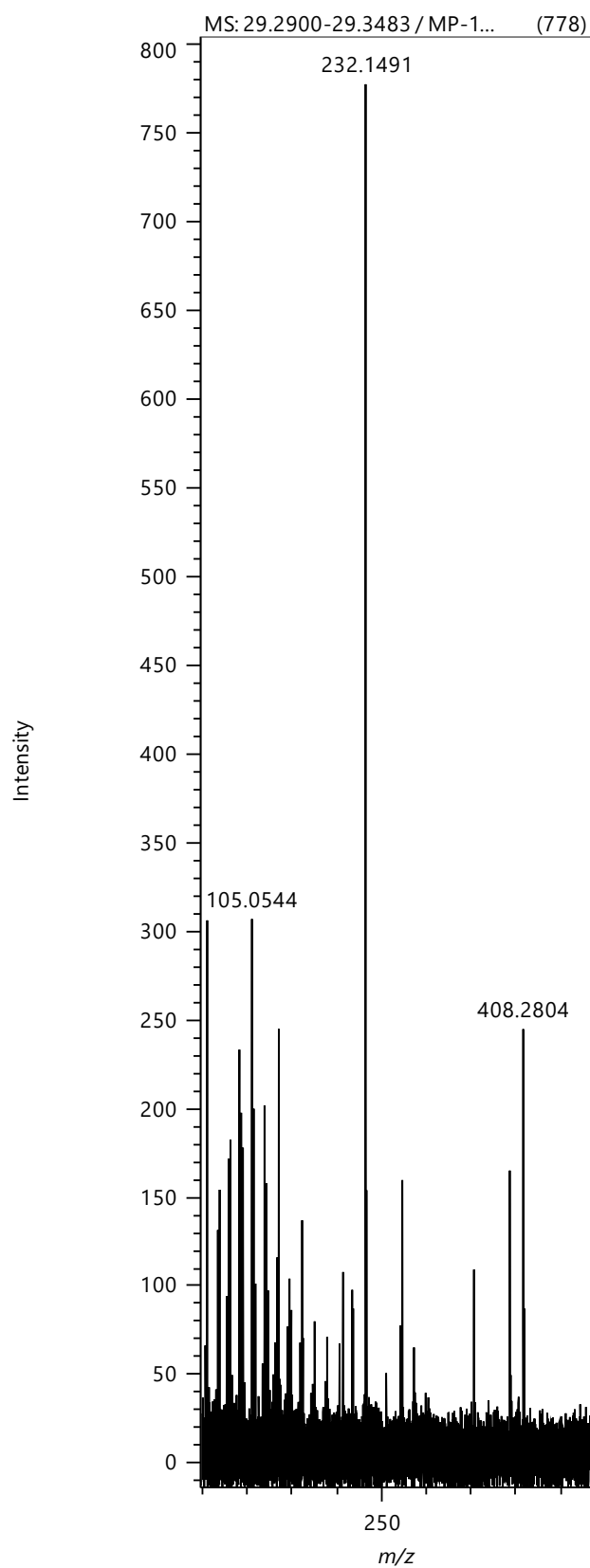
S60- GC-MS m/z of unmodified PET degraded with microwaves at an input power of 0.8 kW (powder fraction) $t=21.80$ minutes).



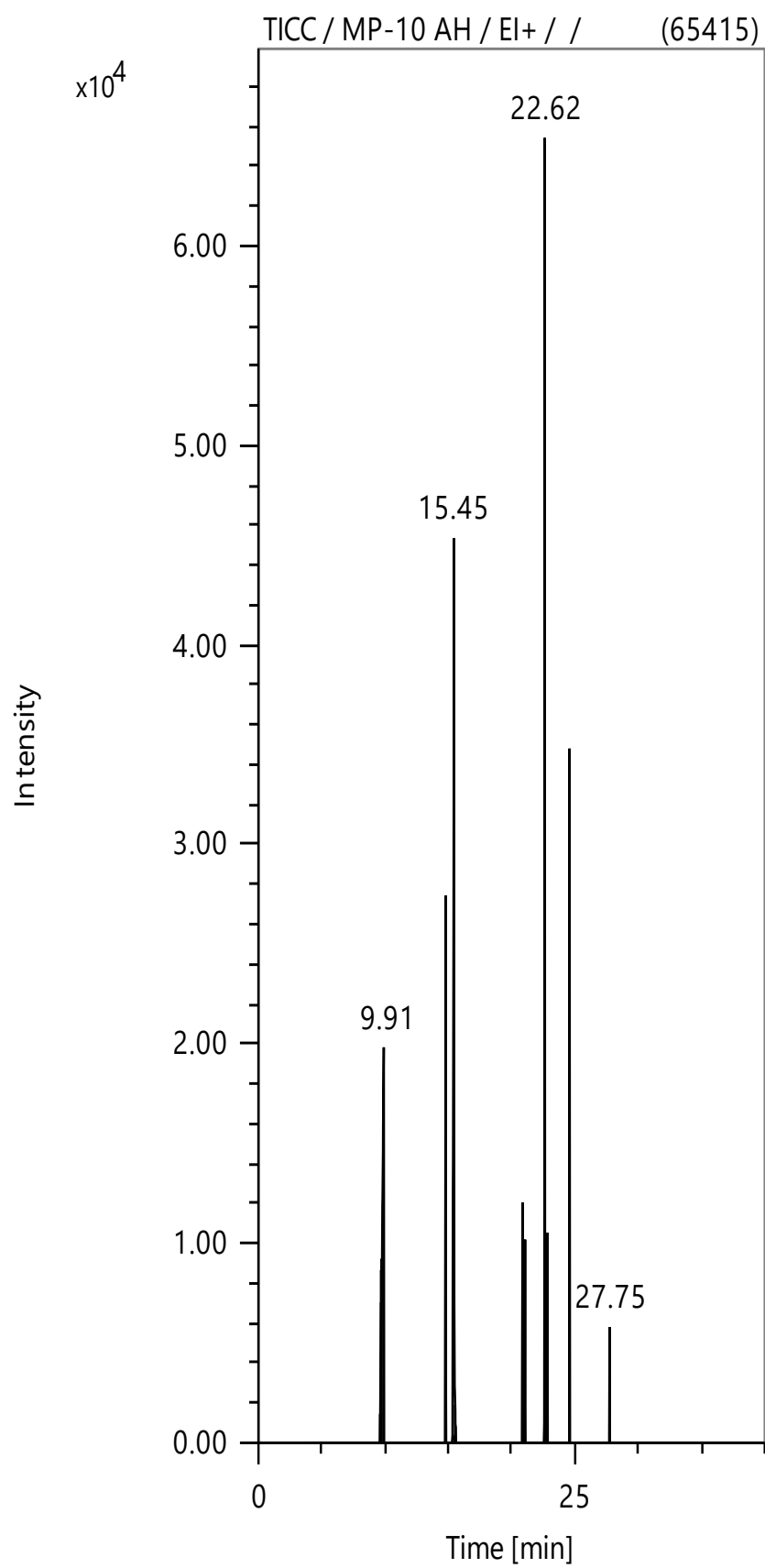
S61- GC-MS m/z of unmodified PET degraded with microwaves at an input power of 0.8 kW (powder fraction) t=22.62 minutes).



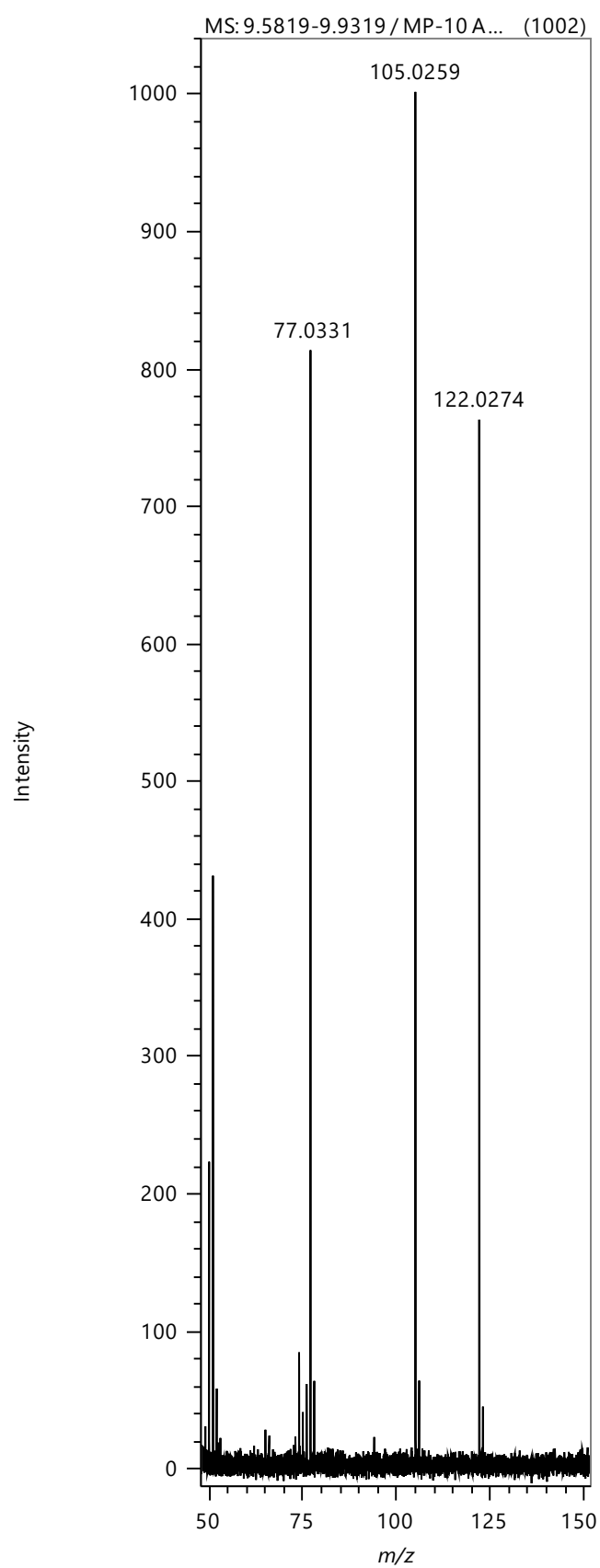
S62- GC-MS m/z of unmodified PET degraded with microwaves at an input power of 0.8 kW (powder fraction) t=27.42 minutes).



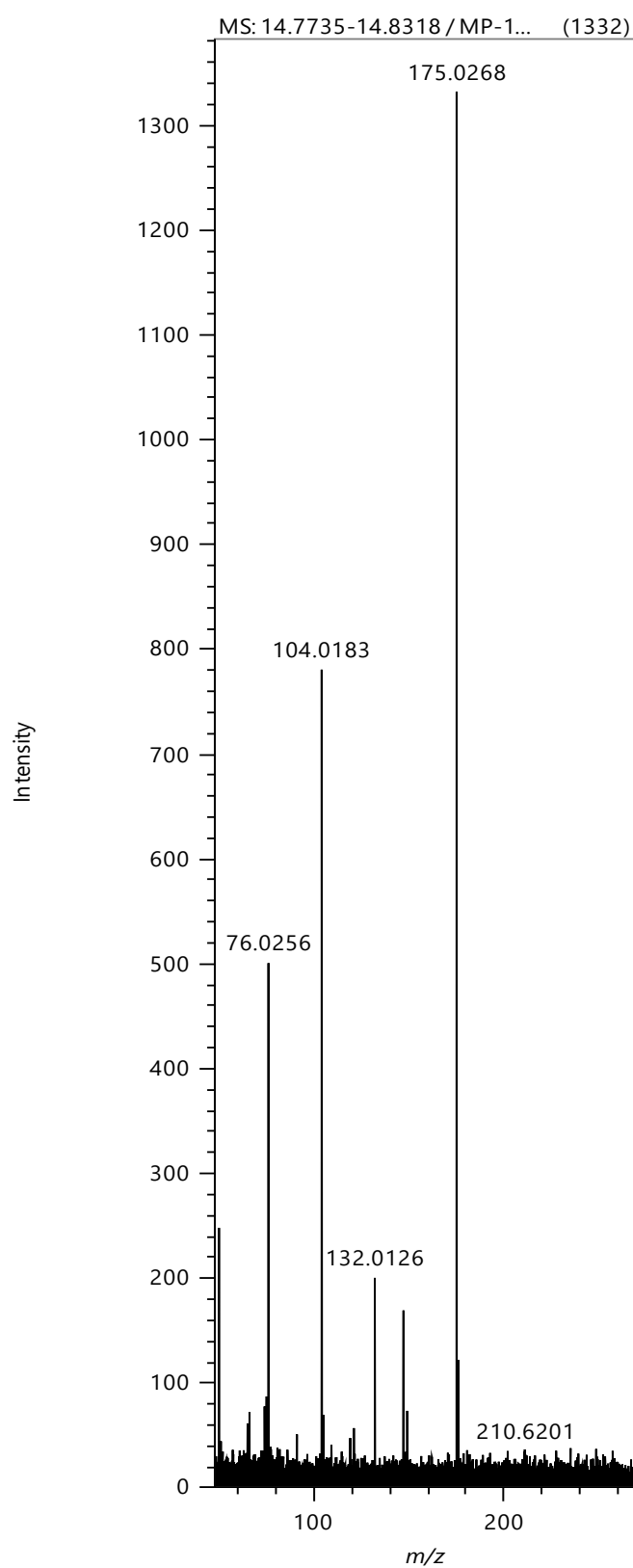
S63- GC-MS m/z of unmodified PET degraded with microwaves at an input power of 0.8 kW (powder fraction) t=29.27 minutes).



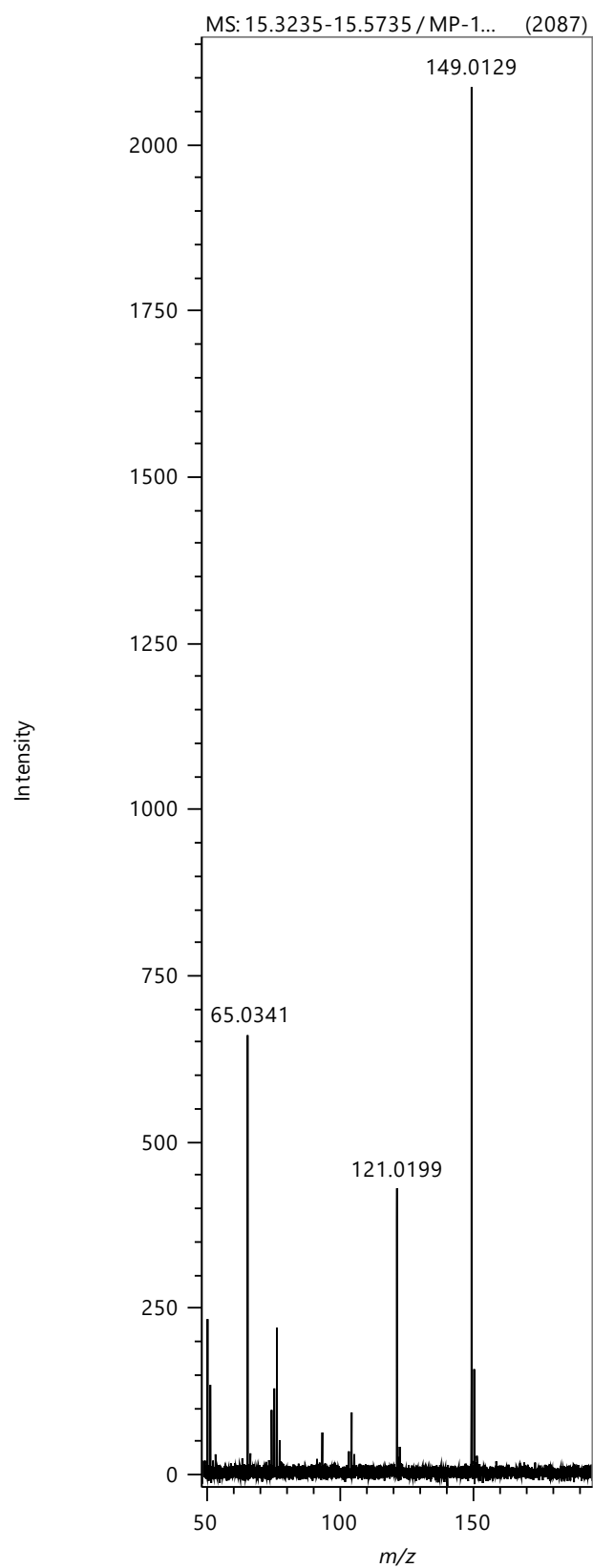
S64- GC-MS TICC of unmodified PET degraded with microwaves at an input power of 1.6 kW (powder).



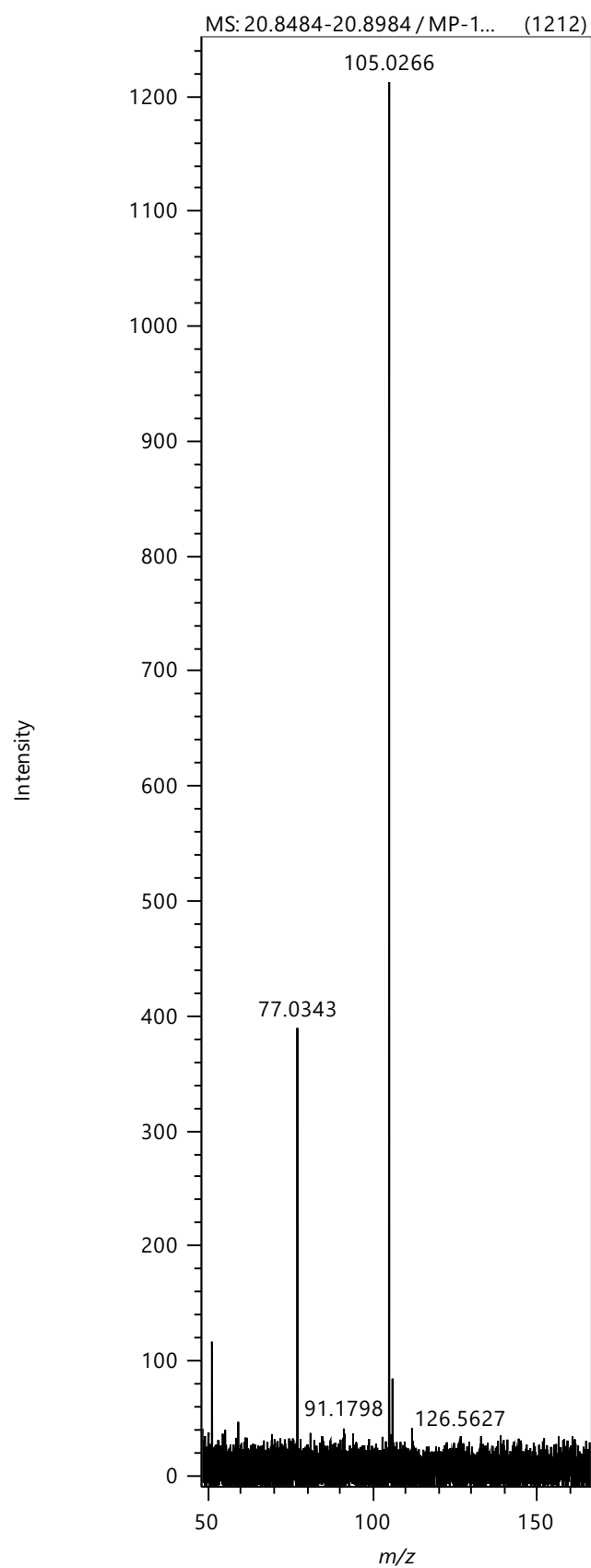
S65- GC-MS m/z of unmodified PET degraded with microwaves at an input power of 1.6 kW (powder fraction) $t=9.80$ minutes).



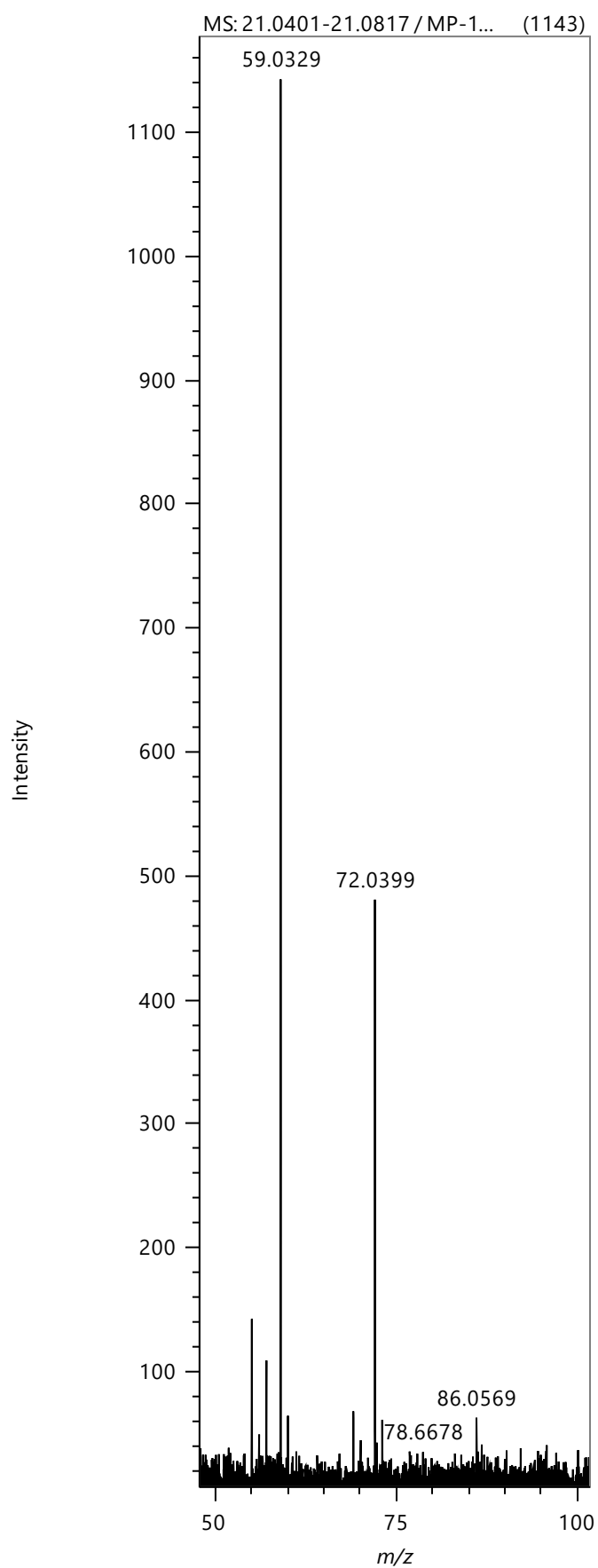
S66- GC-MS m/z of unmodified PET degraded with microwaves at an input power of 1.6 kW (powder fraction) t=14.80 minutes).



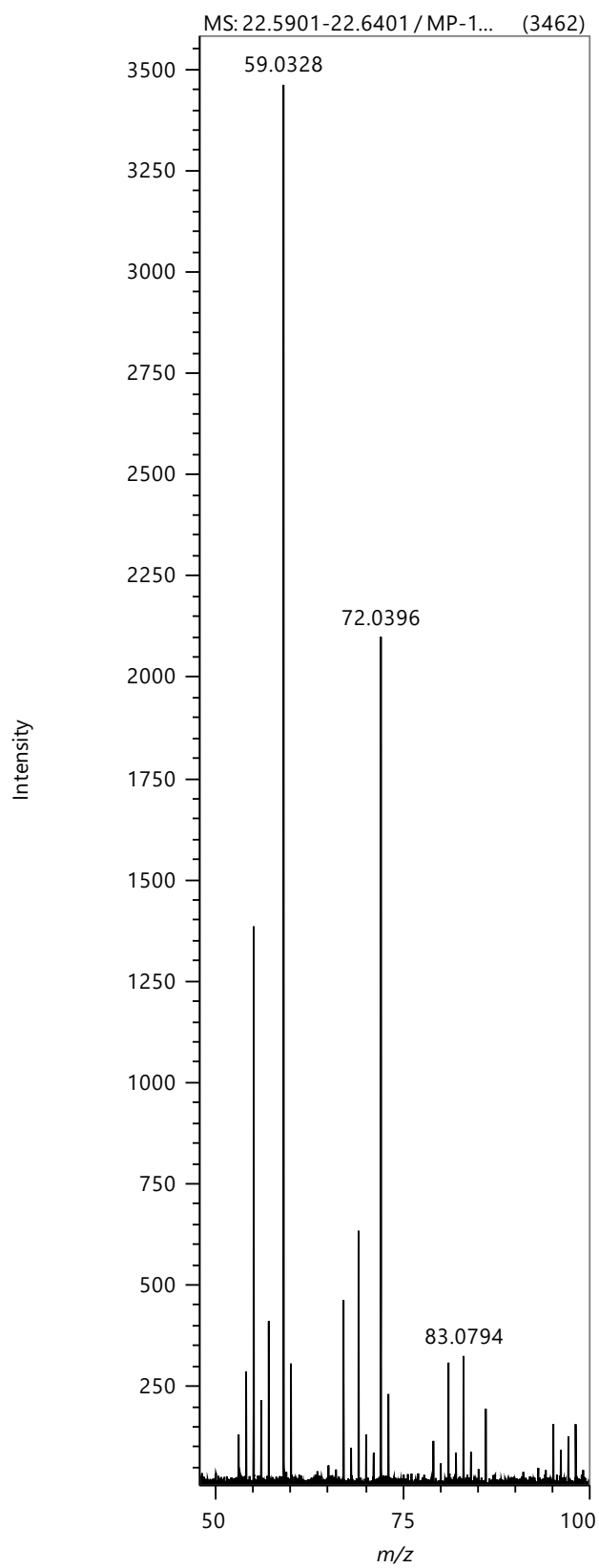
S67- GC-MS m/z of unmodified PET degraded with microwaves at an input power of 1.6 kW (powder fraction) $t=15.48$ minutes).



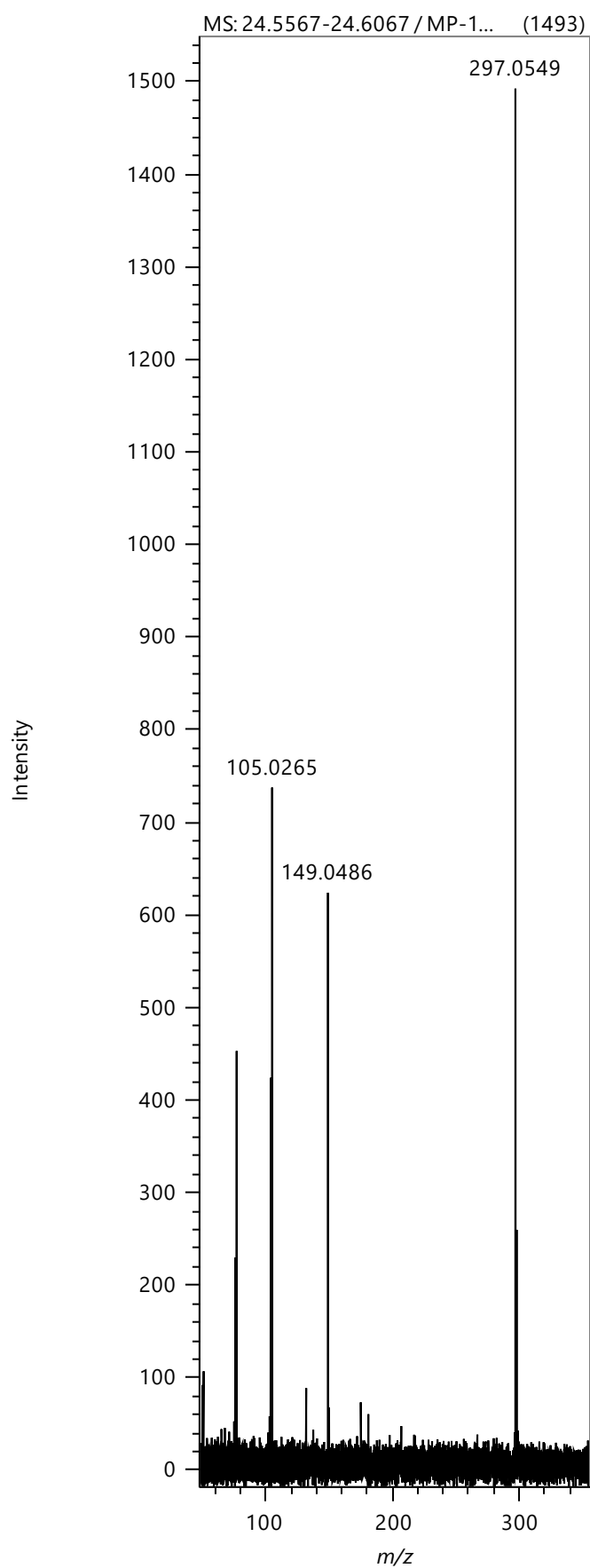
S68- GC-MS m/z of unmodified PET degraded with microwaves at an input power of 1.6 kW (powder fraction) t=20.87 minutes).



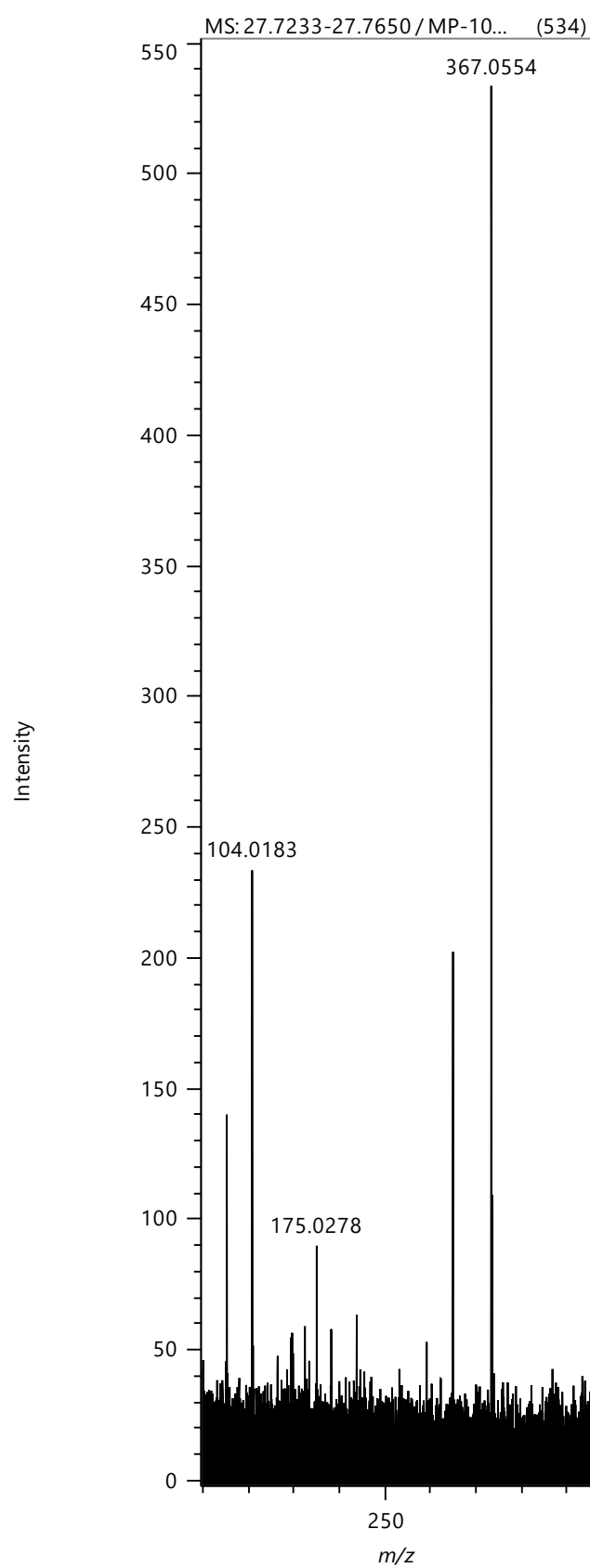
S69- GC-MS m/z of unmodified PET degraded with microwaves at an input power of 1.6 kW (powder fraction) $t=21.06$ minutes).



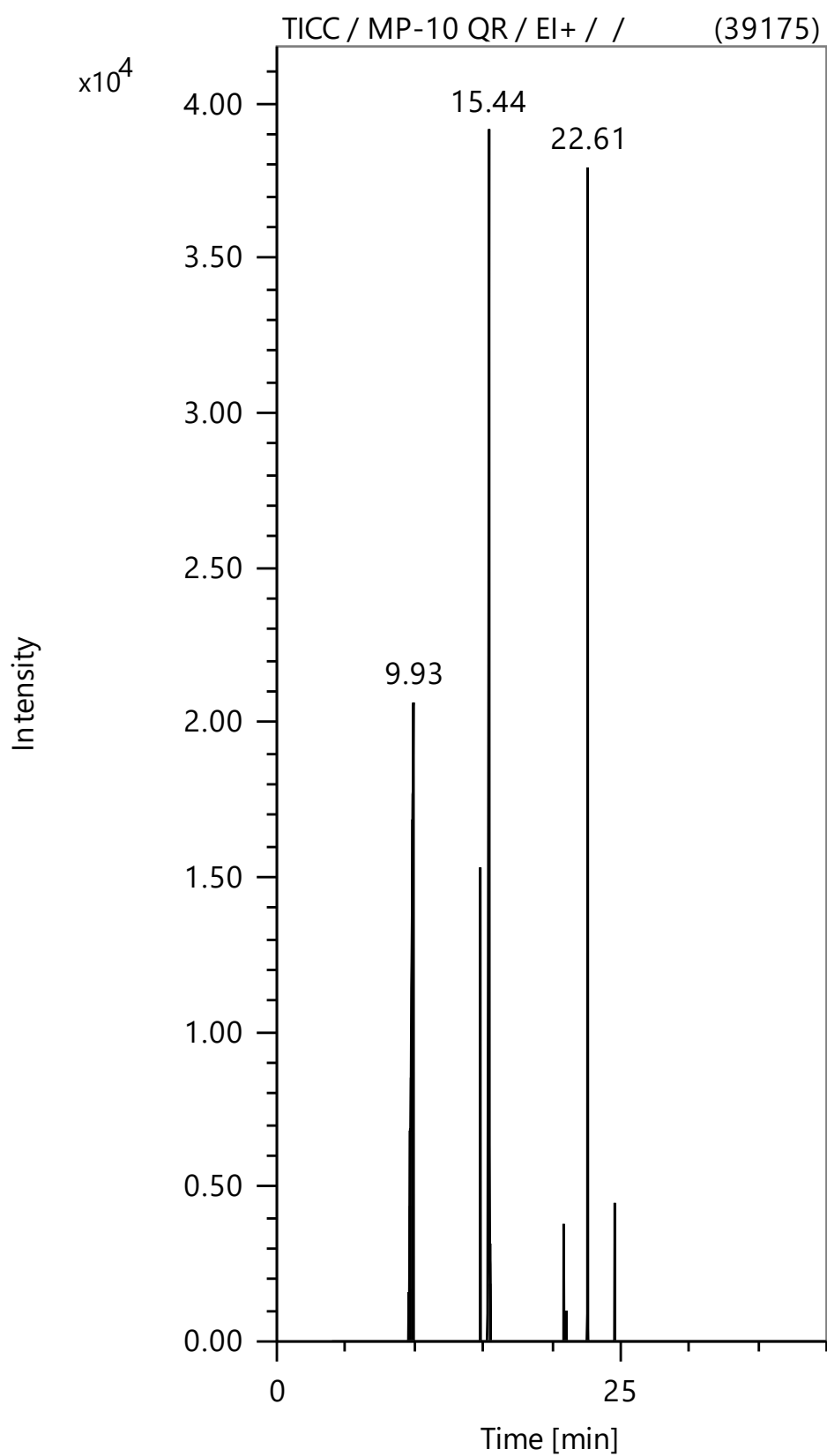
S70- GC-MS m/z of unmodified PET degraded with microwaves at an input power of 1.6 kW (powder fraction) t=22.61 minutes).



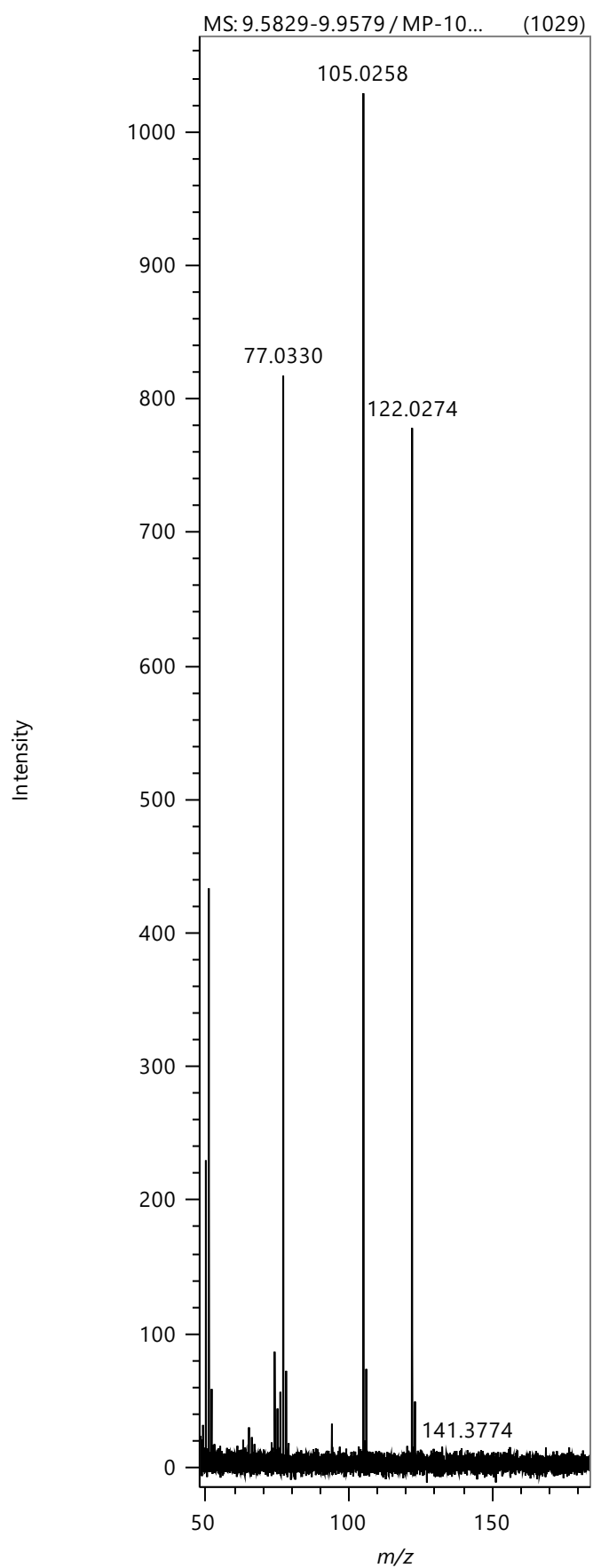
S71- GC-MS m/z of unmodified PET degraded with microwaves at an input power of 1.6 kW (powder fraction) t=24.58 minutes).



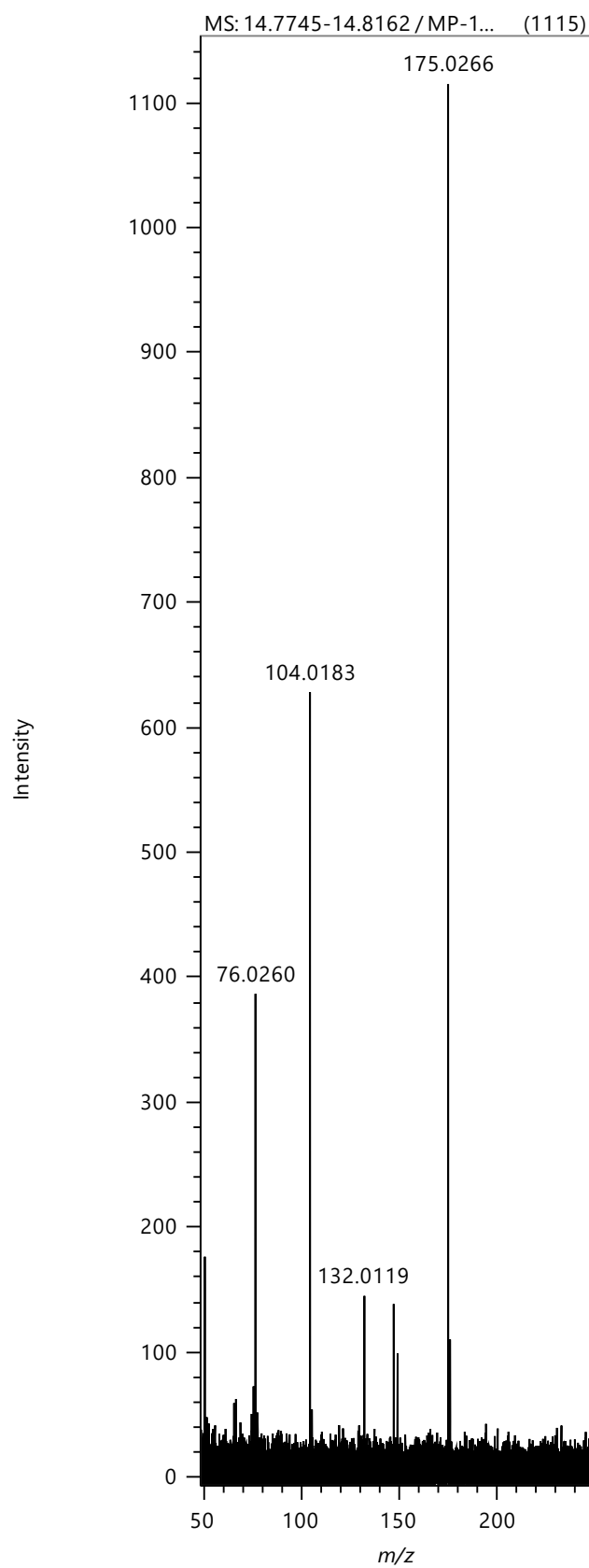
S72- GC-MS m/z of unmodified PET degraded with microwaves at an input power of 1.6 kW (powder fraction) $t=27.74$ minutes).



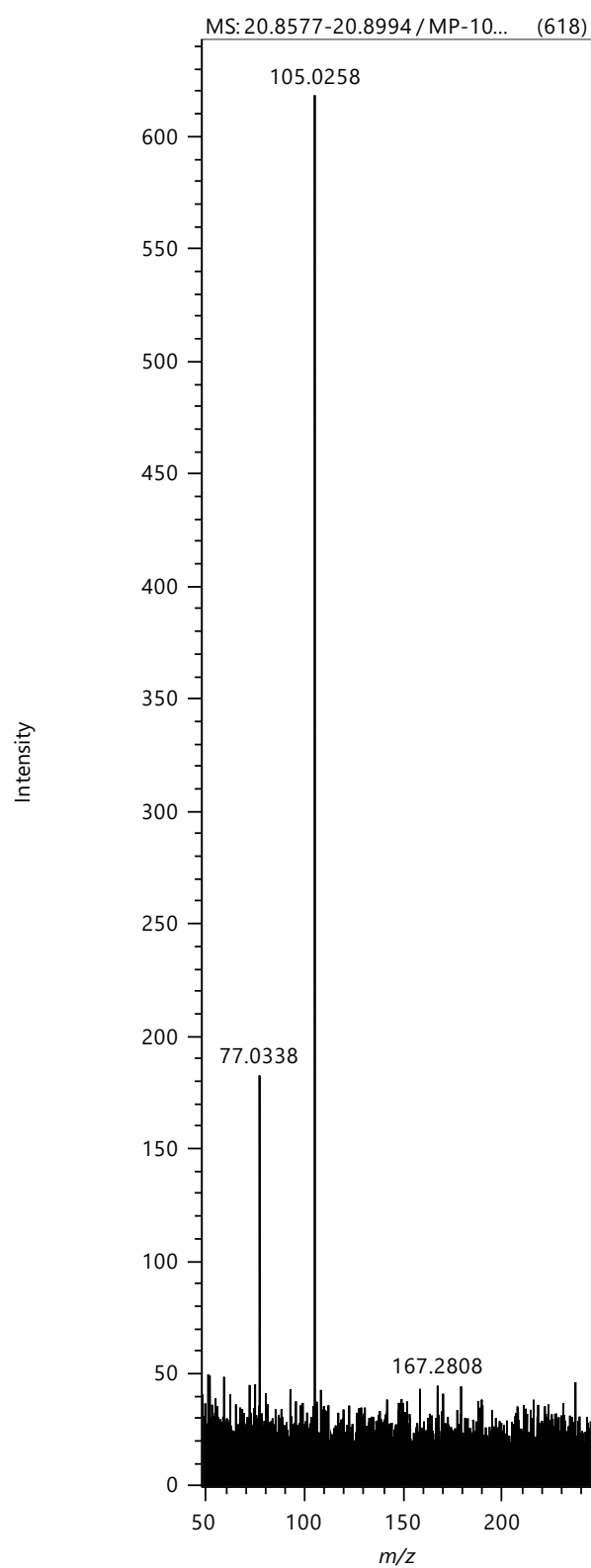
S73- GC-MS TICC of unmodified PET degraded with microwaves at an input power of 1.6 kW (wax fraction).



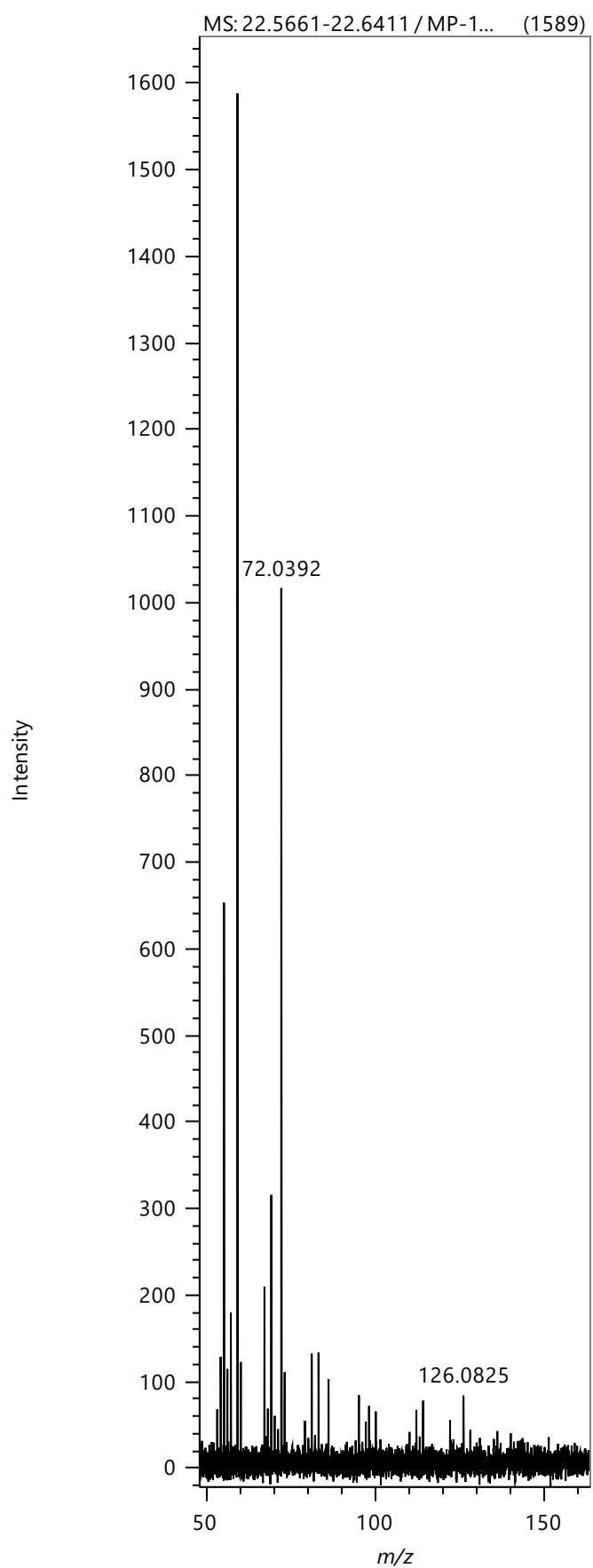
S74- GC-MS m/z of unmodified PET degraded with microwaves at an input power of 1.6 kW (wax fraction) t=9.93 minutes).



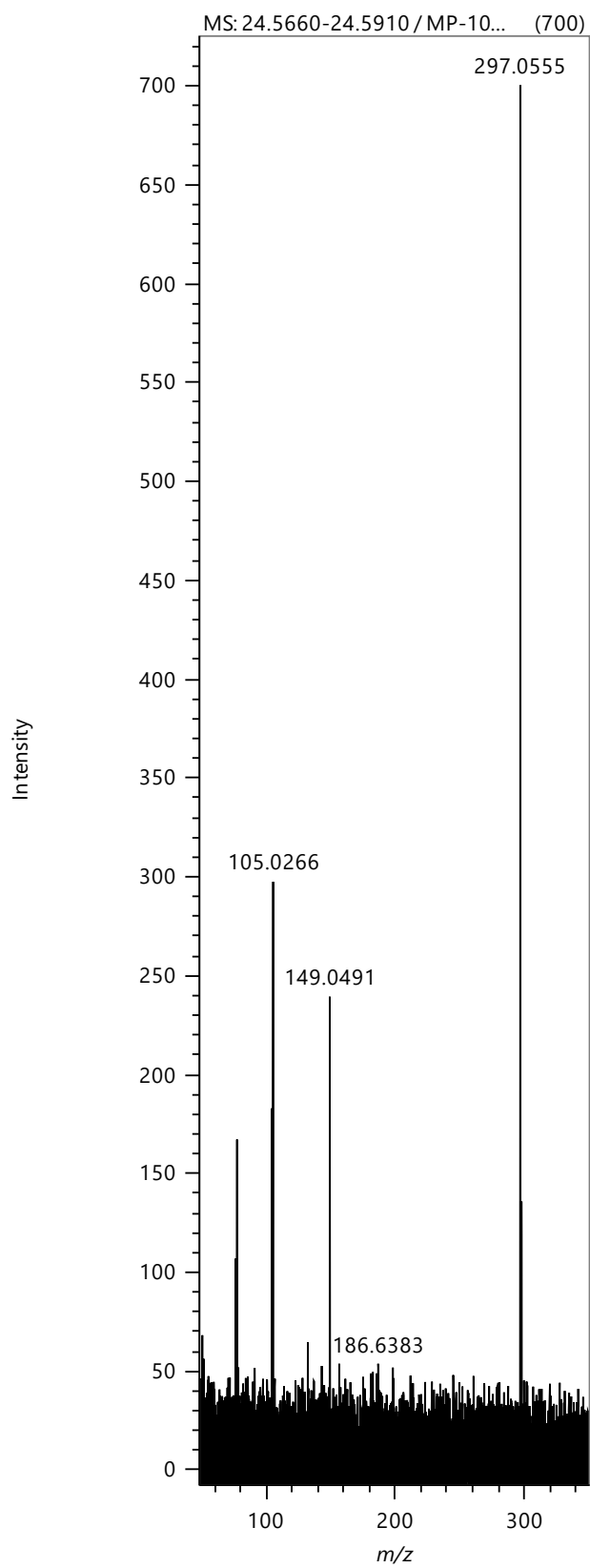
S75- GC-MS m/z of unmodified PET degraded with microwaves at an input power of 1.6 kW (wax fraction) t=14.79 minutes).



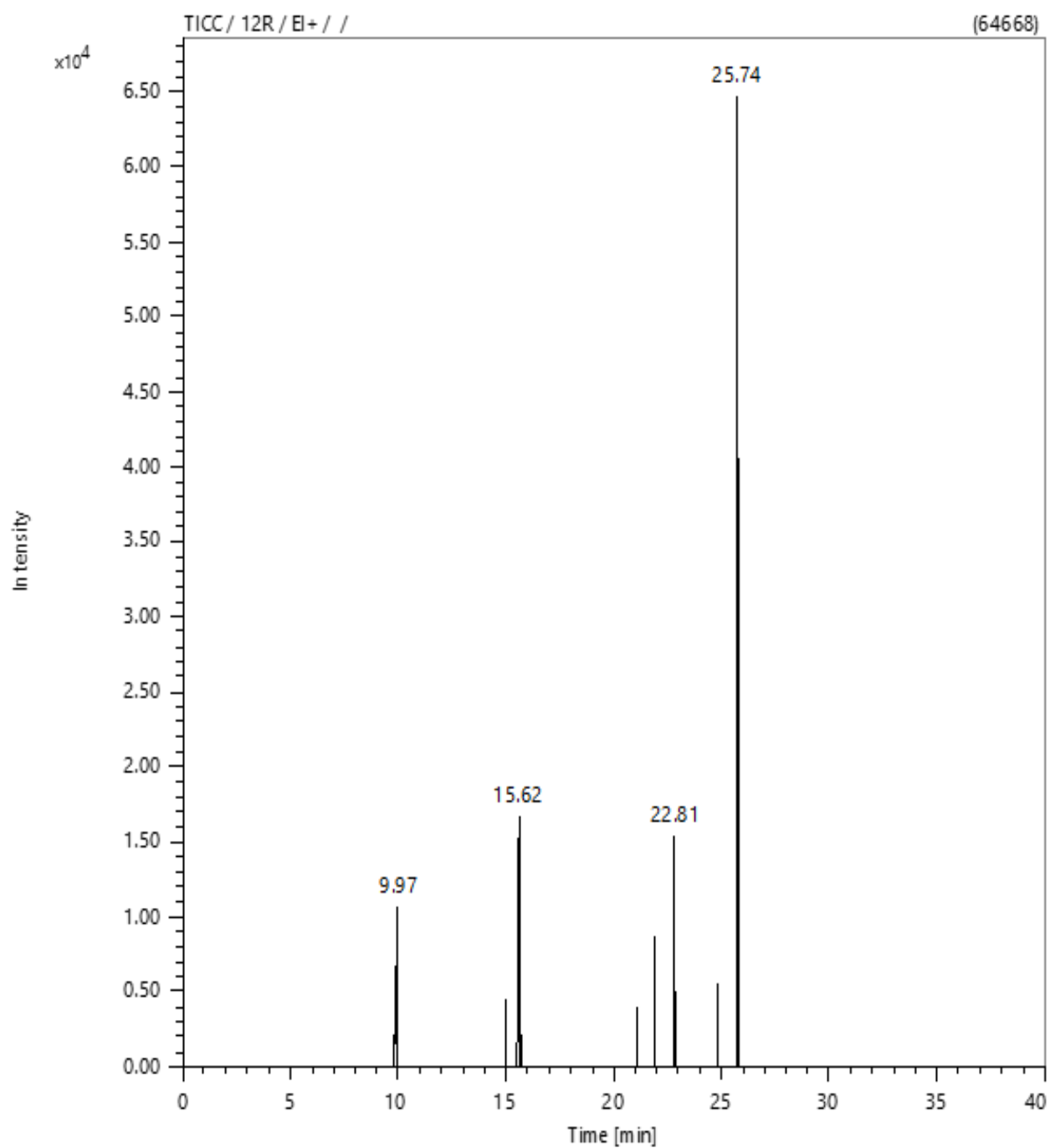
S76 -GC-MS m/z of unmodified PET degraded with microwaves at an input power of 1.6 kW (wax fraction) $t=20.87$ minutes).



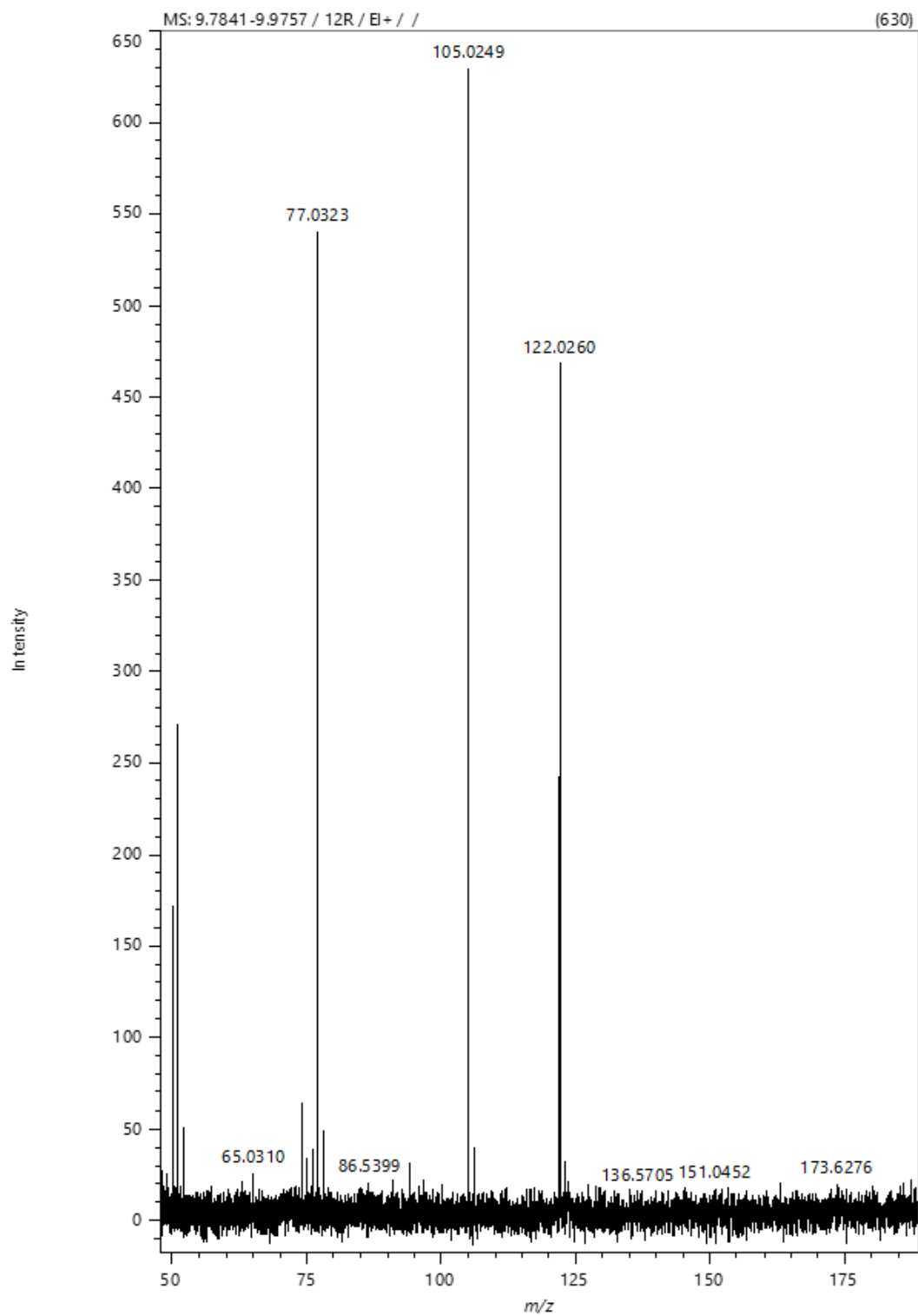
S77- GC-MS m/z of unmodified PET degraded with microwaves at an input power of 1.6 kW (wax fraction) $t=22.61$ minutes).



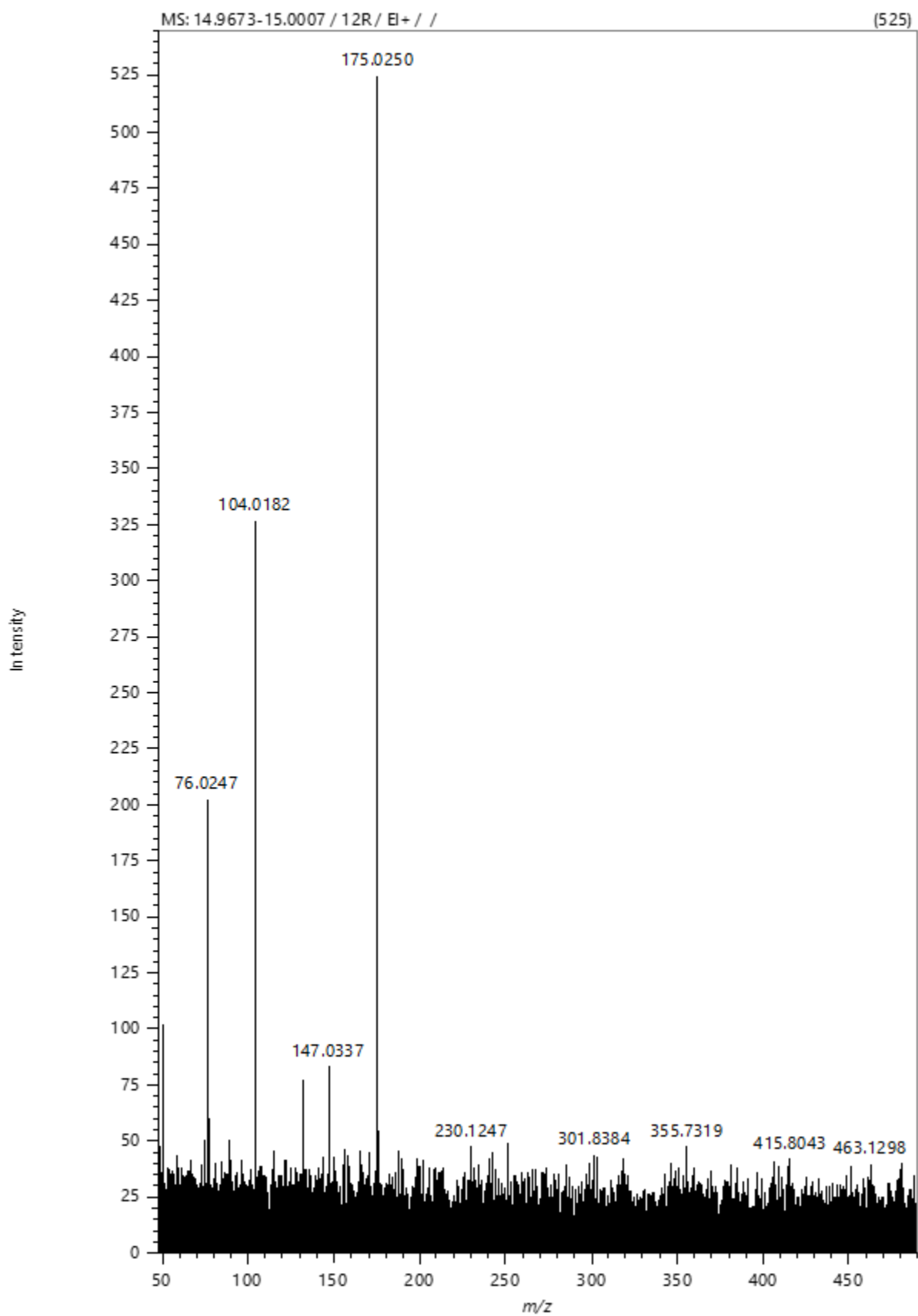
S78- GC-MS m/z of unmodified PET degraded with microwaves at an input power of 1.6 kW (wax fraction) t=24.58 minutes).



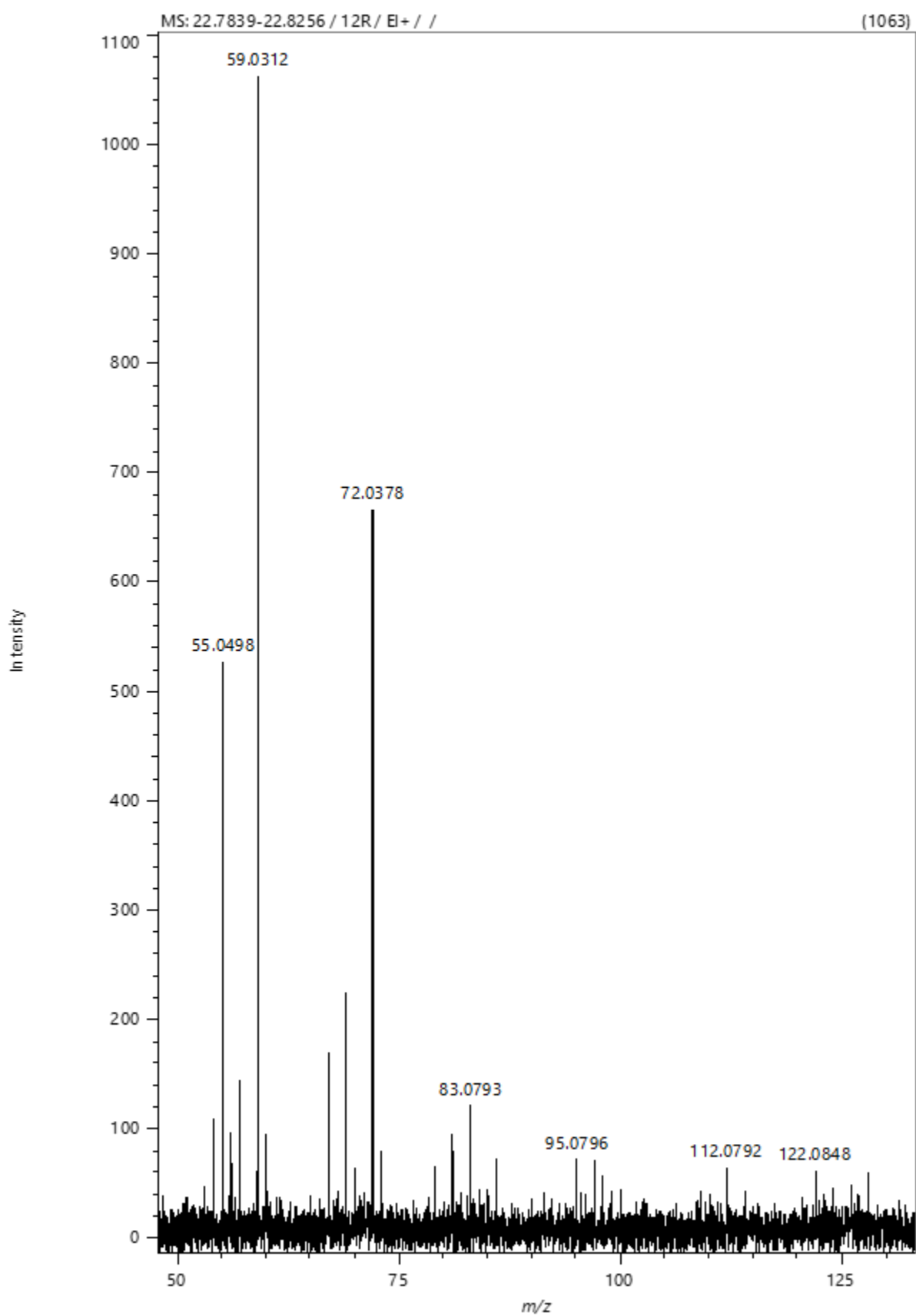
S79- GC-MS TICC of PET impregnated with ethylene glycol in a 1:1 mass ratio degraded with microwaves at an input power of 0.8 kW (powder).



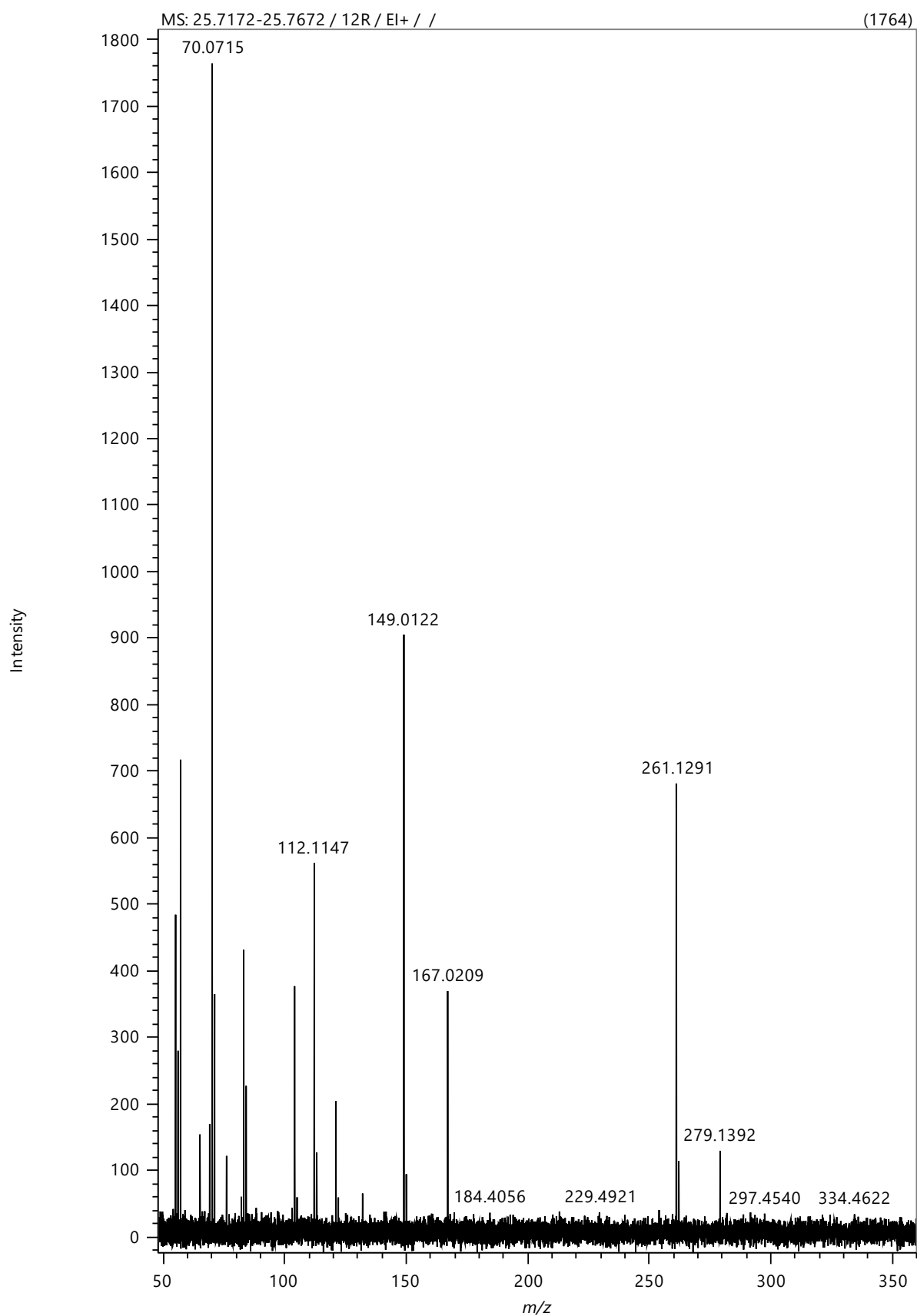
S80- GC-MS m/z of PET degraded with ethylene glycol impregnated with a 1:1 mass ratio with microwaves at an input power of 0.8 kW (powder fraction) $t=9.97$ minutes).



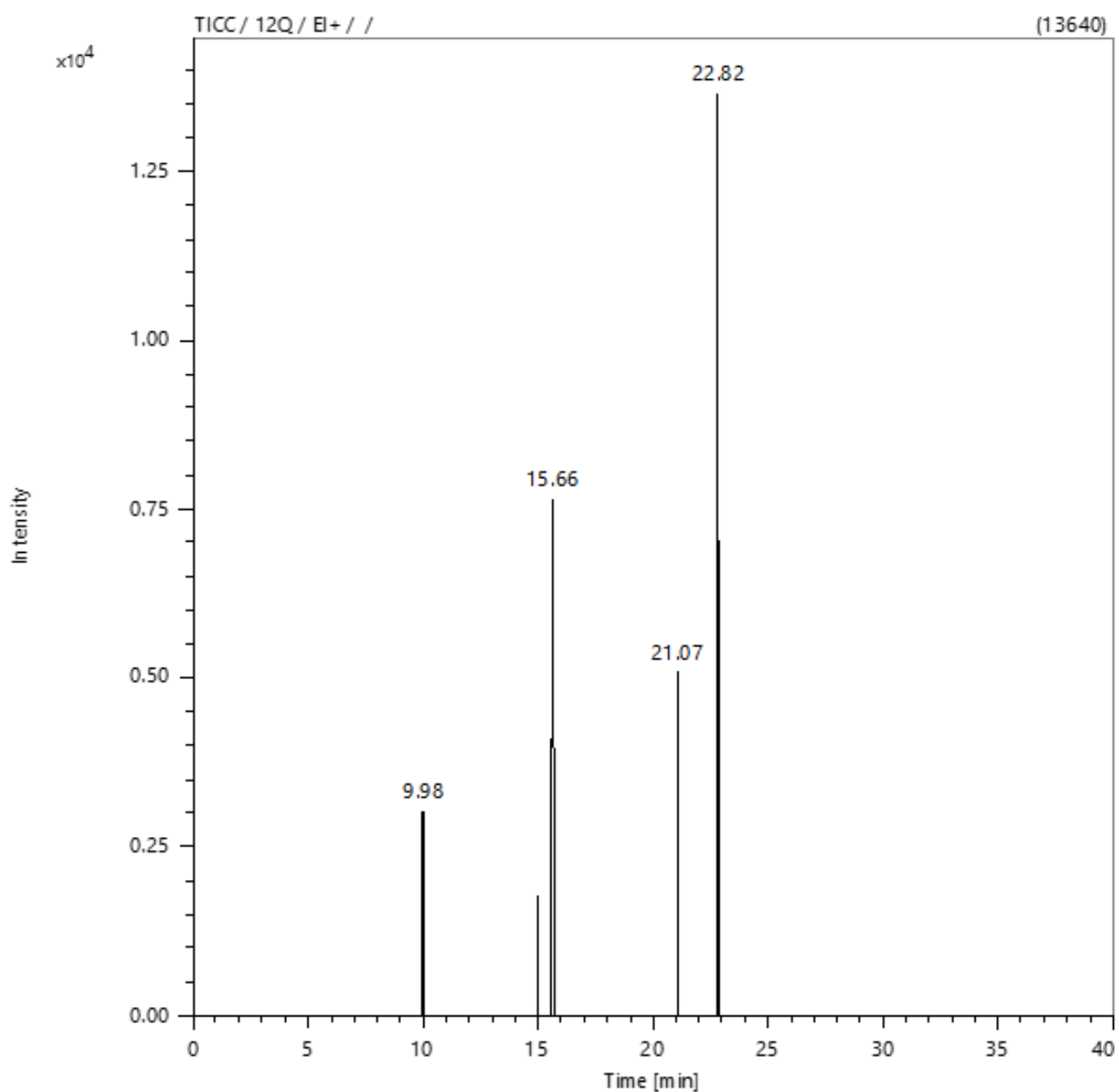
S81- GC-MS m/z of PET degraded with ethylene glycol impregnated with a 1:1 mass ratio with microwaves at an input power of 0.8 kW (powder fraction) $t=14.98$ minutes).



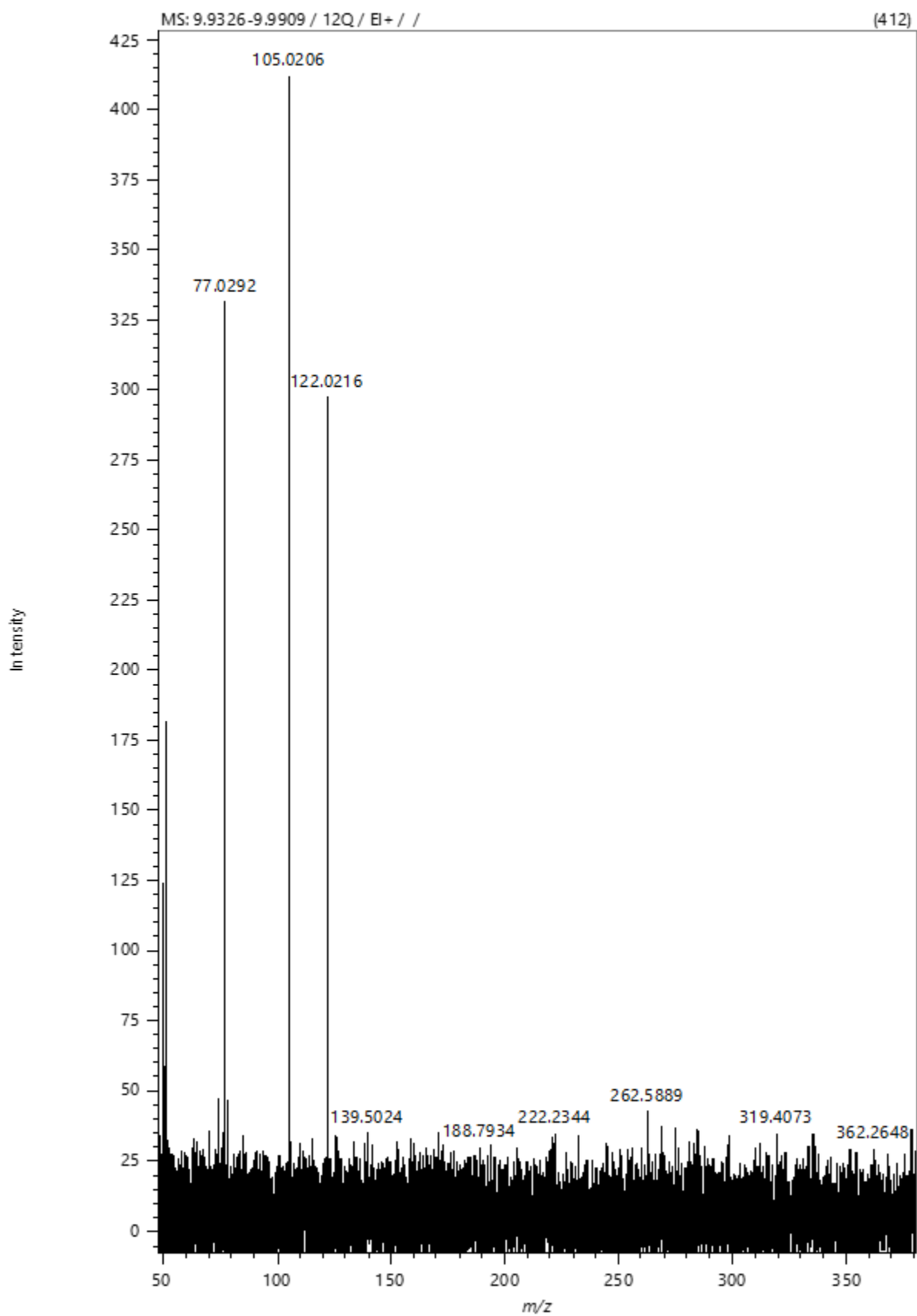
S82- GC-MS m/z of PET degraded with ethylene glycol impregnated with a 1:1 mass ratio with microwaves at an input power of 0.8 kW (powder fraction) $t=22.81$ minutes).



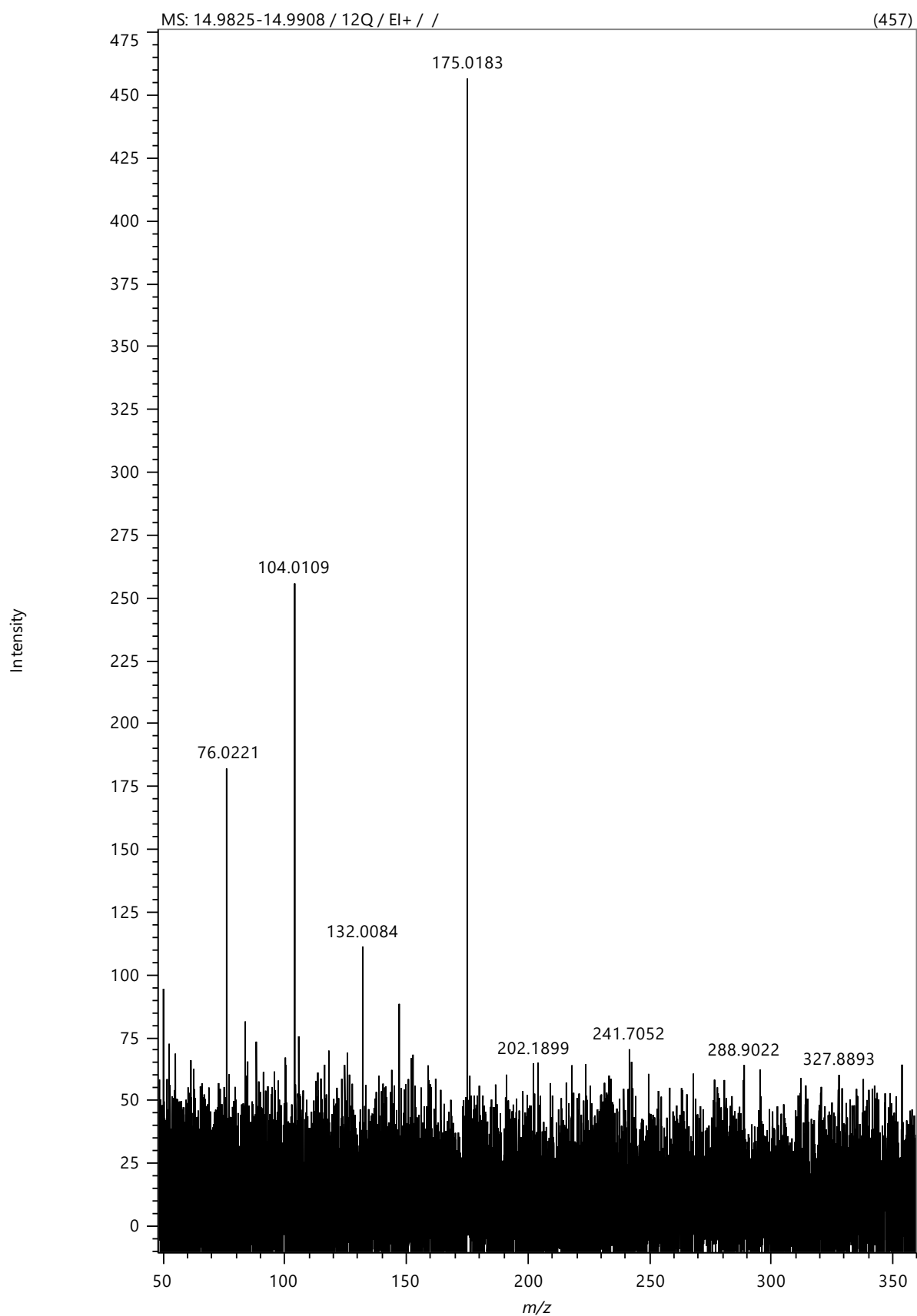
S83- GC-MS m/z of PET degraded with ethylene glycol impregnated with a 1:1 mass ratio with microwaves at an input power of 0.8 kW (powder fraction) t=25.74 minutes).



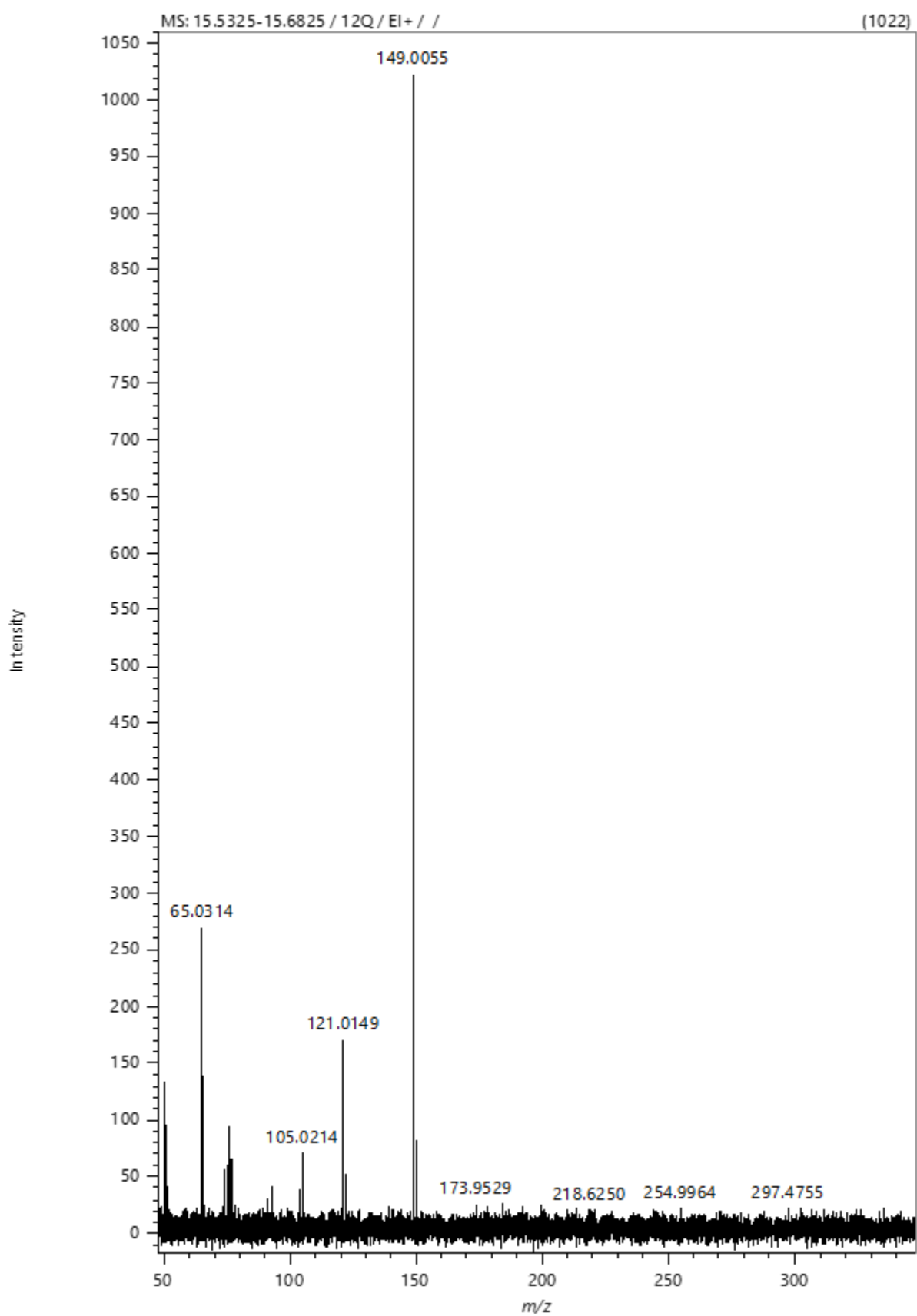
S84- GC-MS TICC of PET impregnated with ethylene glycol in a 1:1 mass ratio degraded with microwaves at an input power of 0.8 kW (wax fraction).



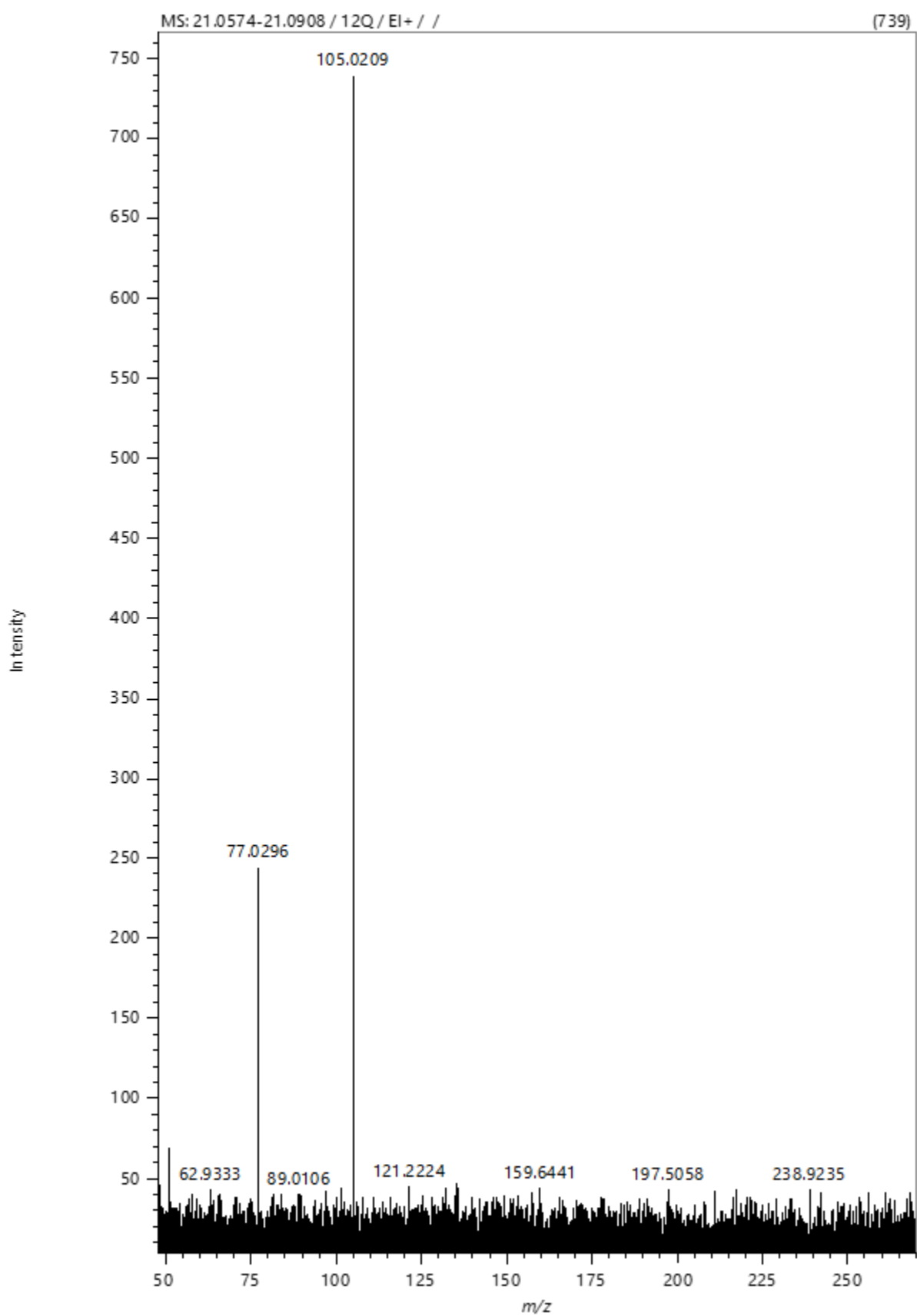
S85- GC-MS m/z of PET degraded with ethylene glycol impregnated with a 1:1 mass ratio with microwaves at an input power of 0.8 kW (powder fraction) $t=9.98$ minutes.



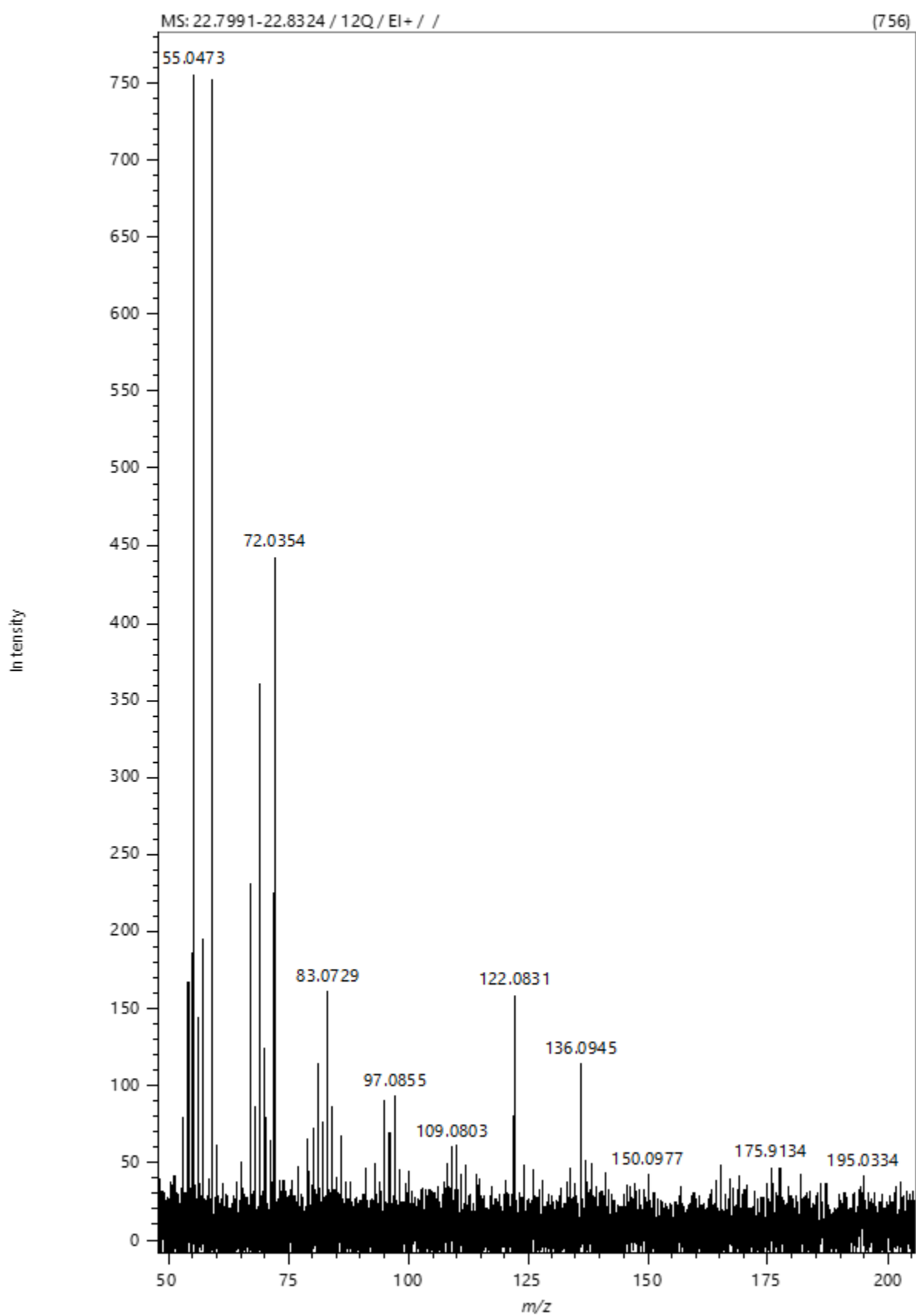
S86- GC-MS m/z of PET degraded with ethylene glycol impregnated with a 1:1 mass ratio with microwaves at an input power of 0.8 kW (powder fraction) t=14.98 minutes.



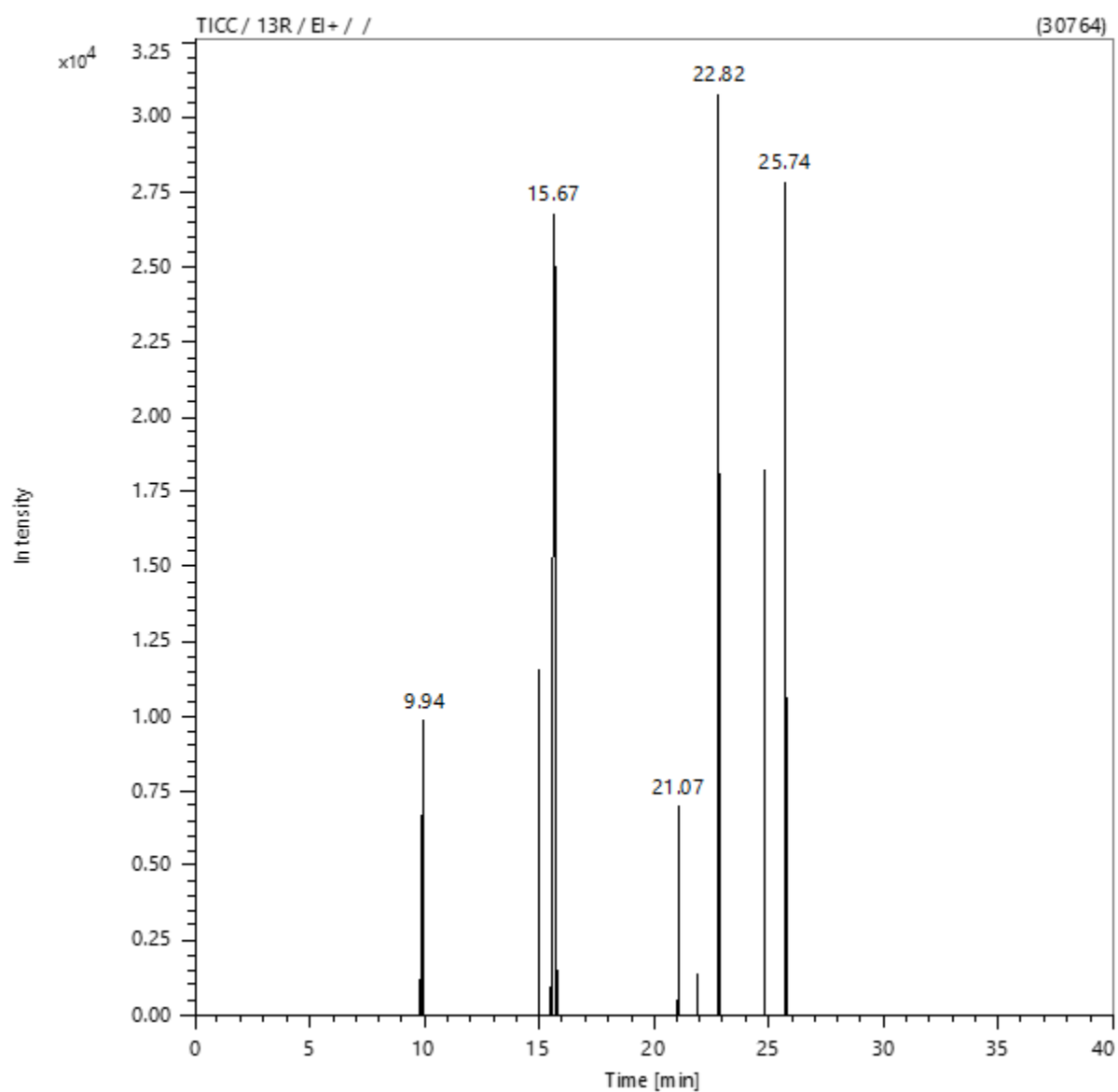
S87- GC-MS m/z of PET degraded with ethylene glycol impregnated with a 1:1 mass ratio with microwaves at an input power of 0.8 kW (powder fraction) $t=15.66$ minutes.



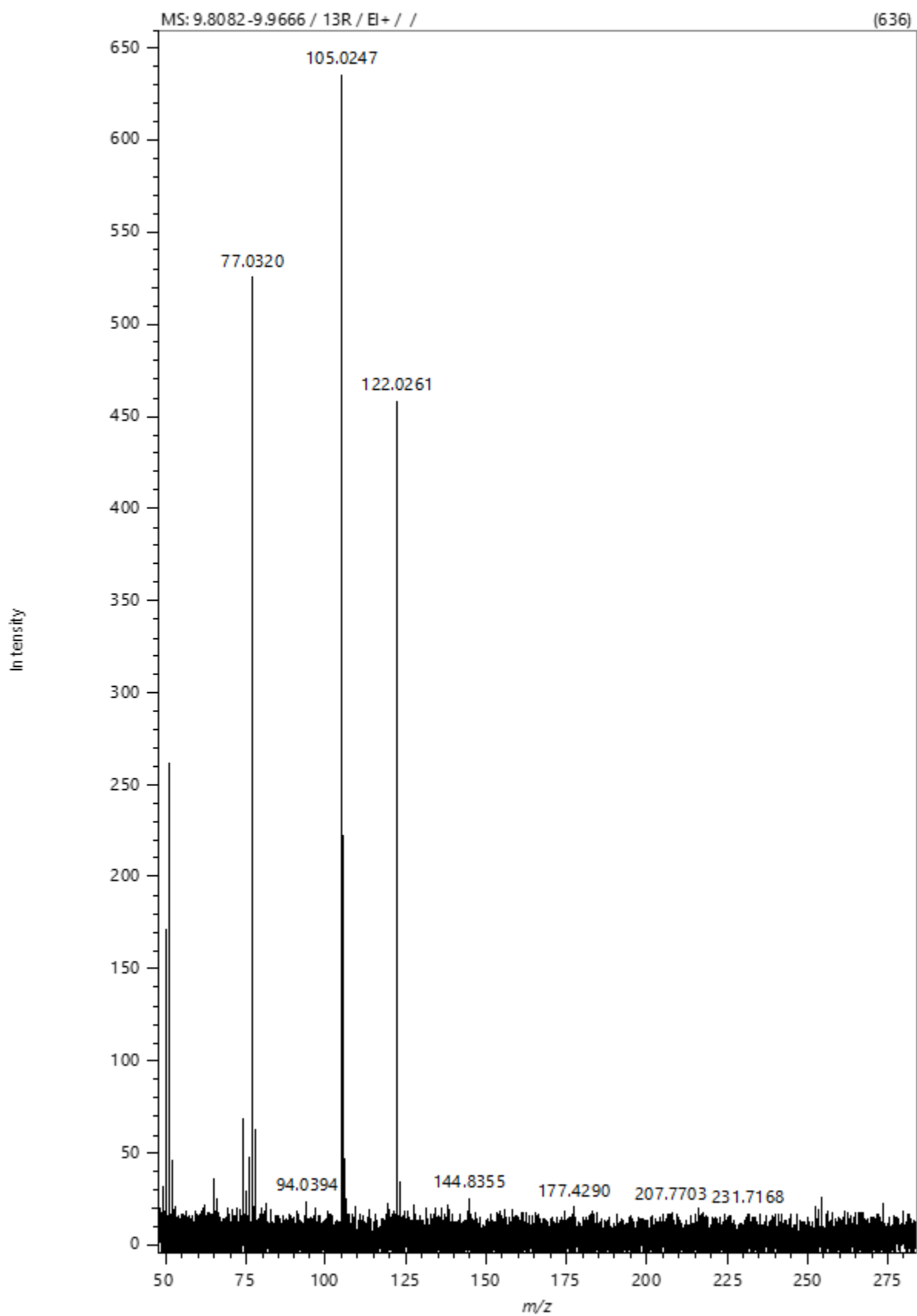
S88- GC-MS m/z of PET degraded with ethylene glycol impregnated with a 1:1 mass ratio with microwaves at an input power of 0.8 kW (powder fraction) t=21.07 minutes.



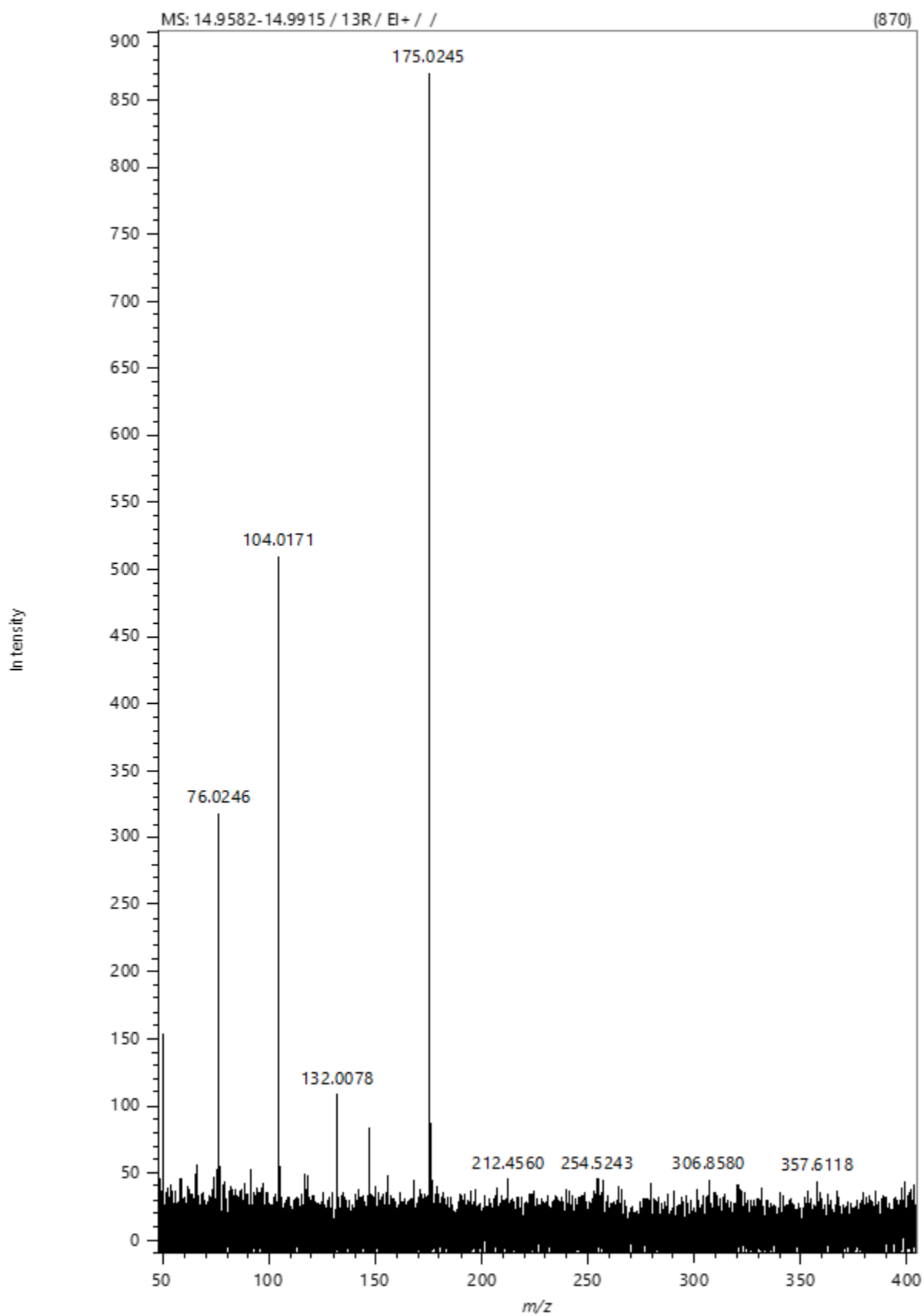
S89- GC-MS m/z of PET degraded with ethylene glycol impregnated with a 1:1 mass ratio with microwaves at an input power of 0.8 kW (powder fraction) $t=22.82$ minutes.



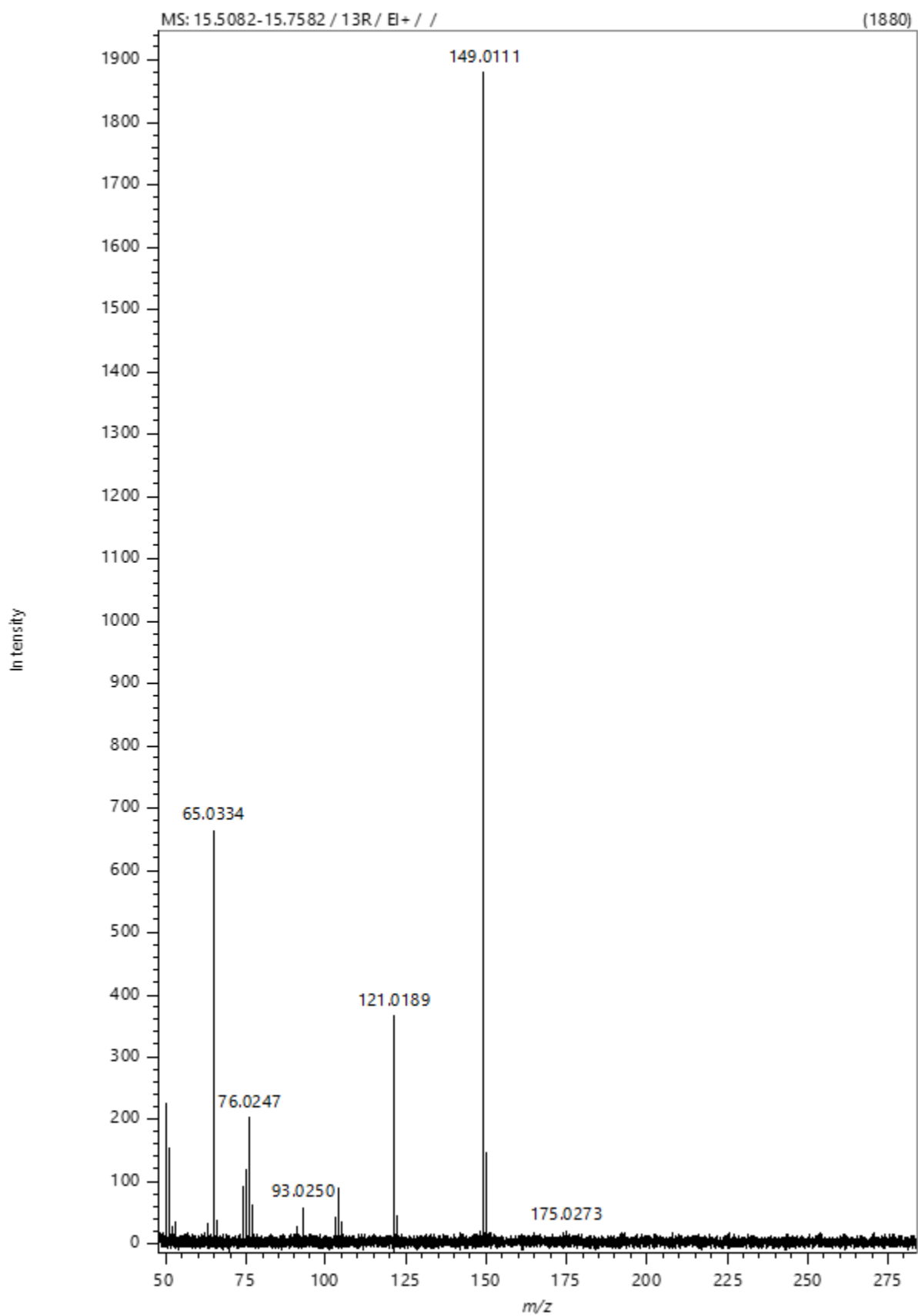
S90- GC-MS TICC of PET impregnated with ethylene glycol in a 1:1 mass ratio degraded with microwaves at an input power of 1.6 kW (powder fraction).



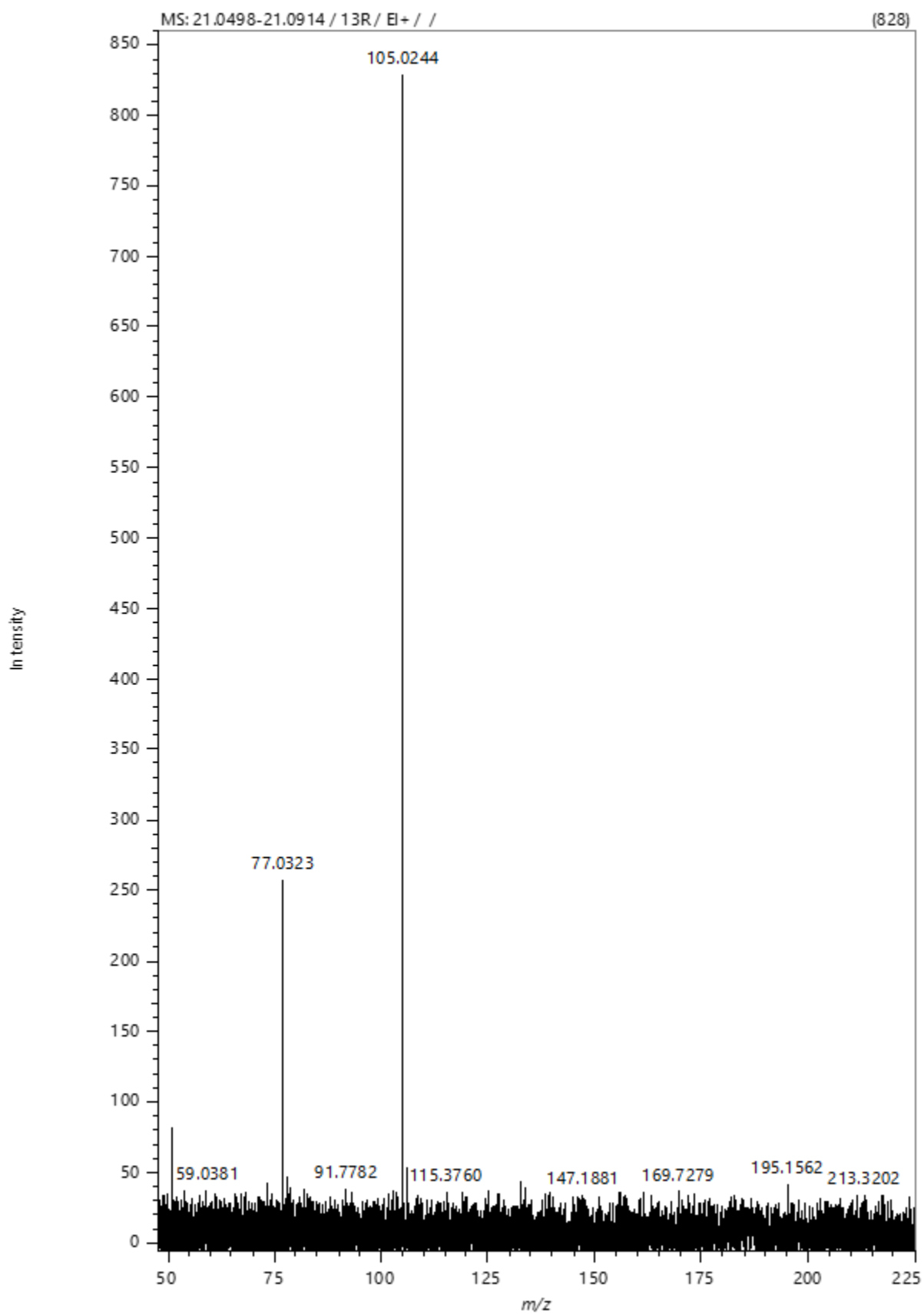
S91- GC-MS m/z of PET degraded with ethylene glycol impregnated with a 1:1 mass ratio with microwaves at an input power of 1.6 kW (powder fraction) t=9.94 minutes.



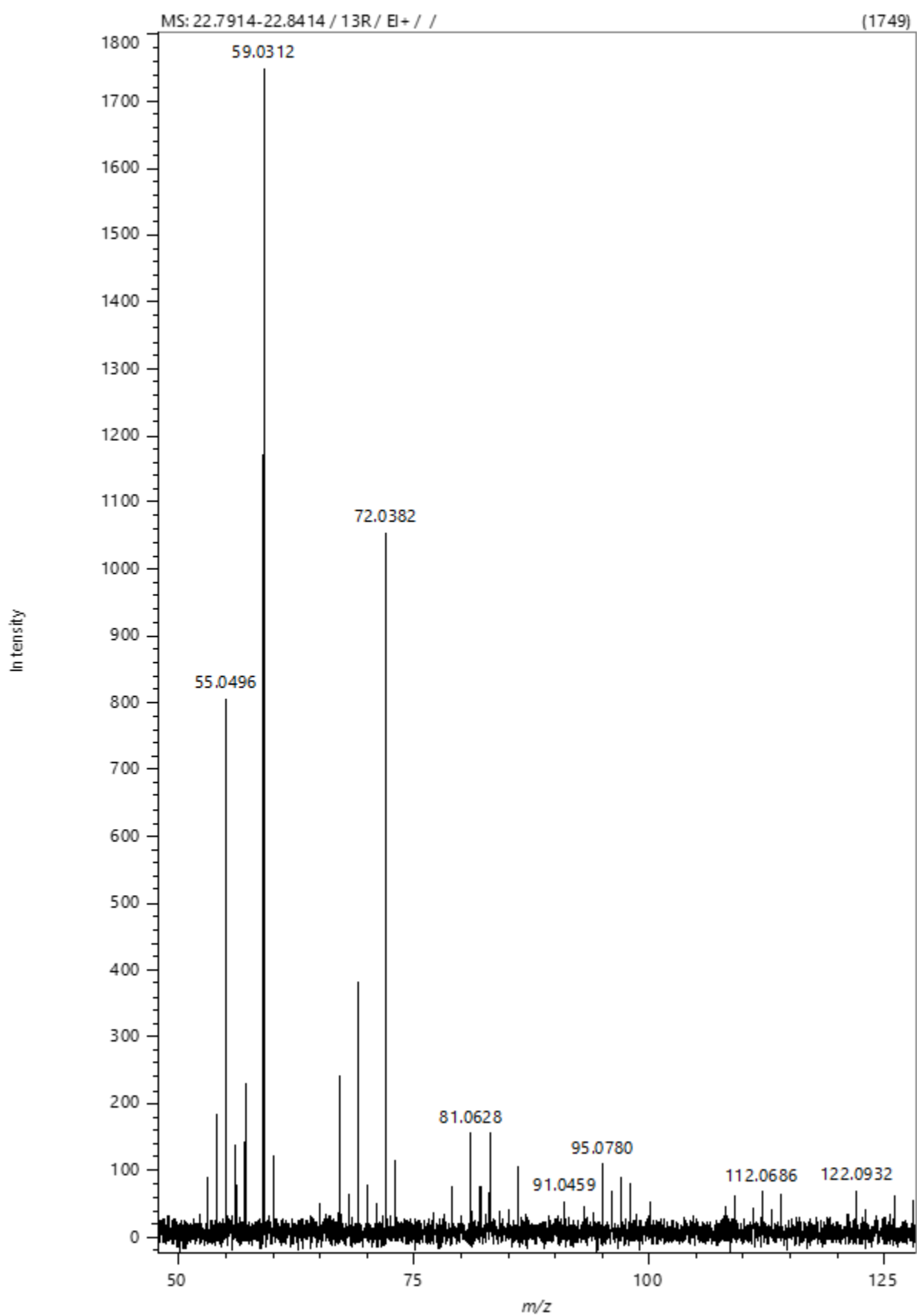
S92- GC-MS m/z of PET degraded with ethylene glycol impregnated with a 1:1 mass ratio with microwaves at an input power of 1.6 kW (powder fraction) $t=14.98$ minutes.



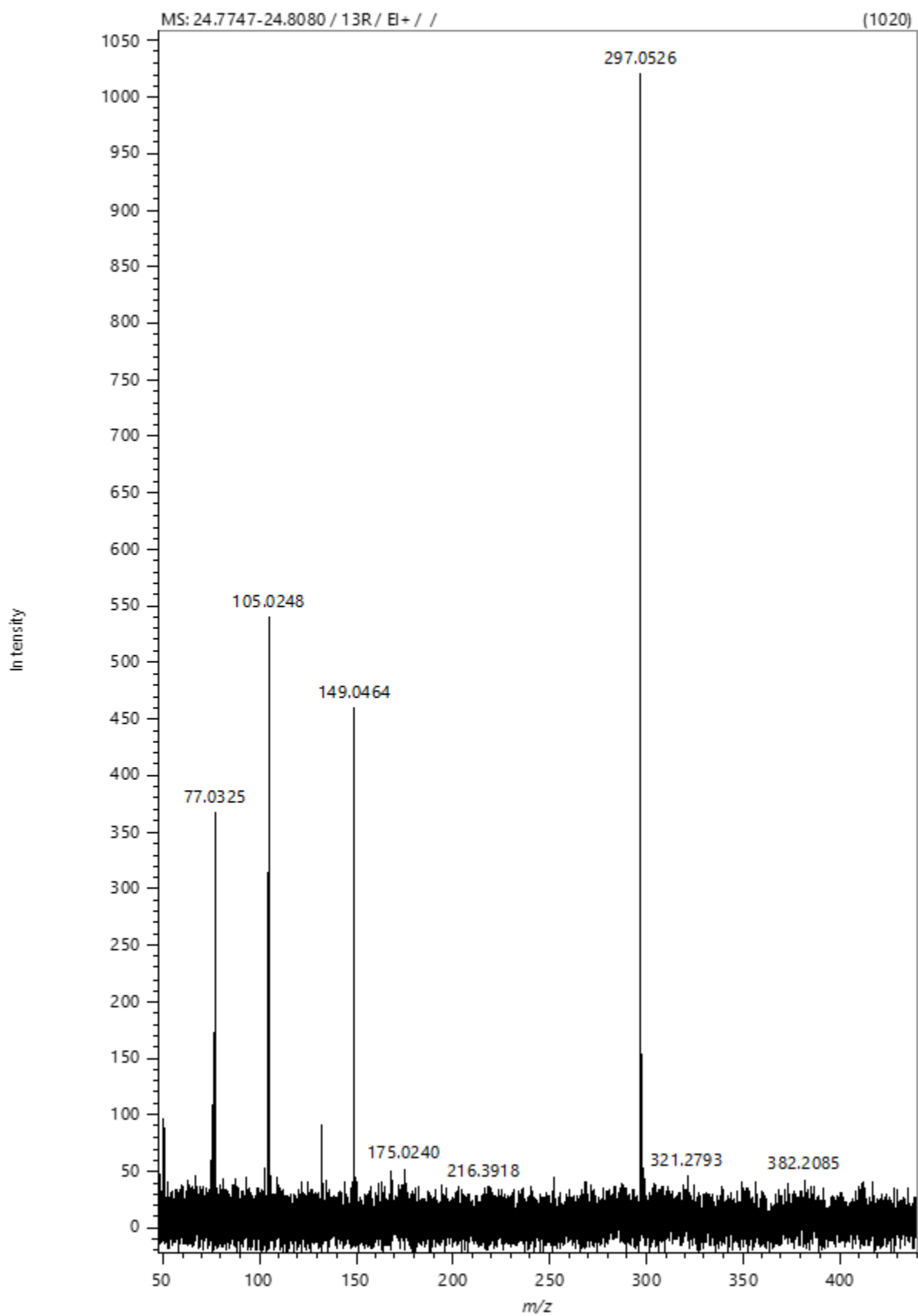
S93- GC-MS m/z of PET degraded with ethylene glycol impregnated with a 1:1 mass ratio with microwaves at an input power of 1.6 kW (powder fraction) $t=15.67$ minutes.



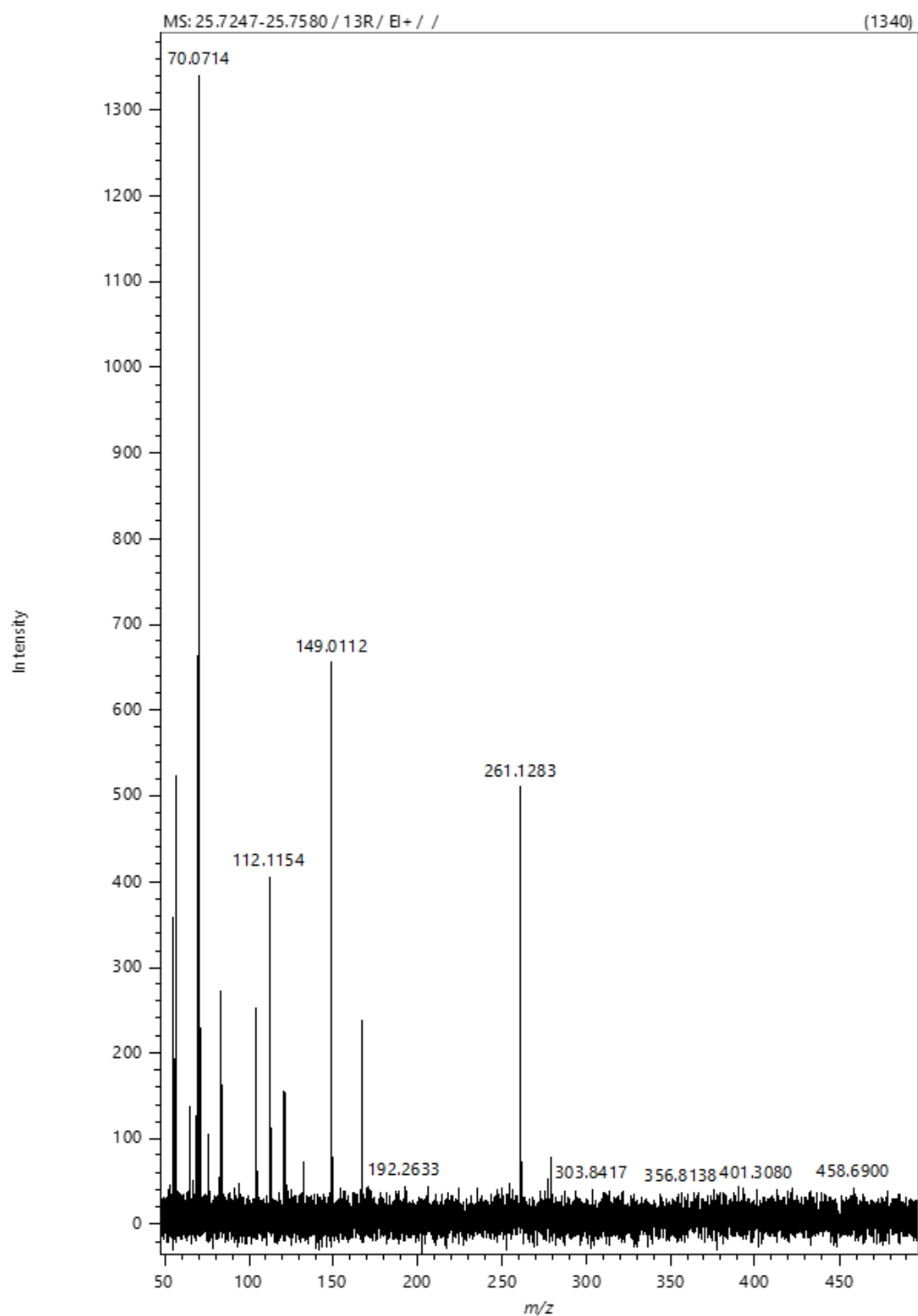
S94- GC-MS m/z of PET degraded with ethylene glycol impregnated with a 1:1 mass ratio with microwaves at an input power of 1.6 kW (powder fraction) $t=21.07$ minutes.



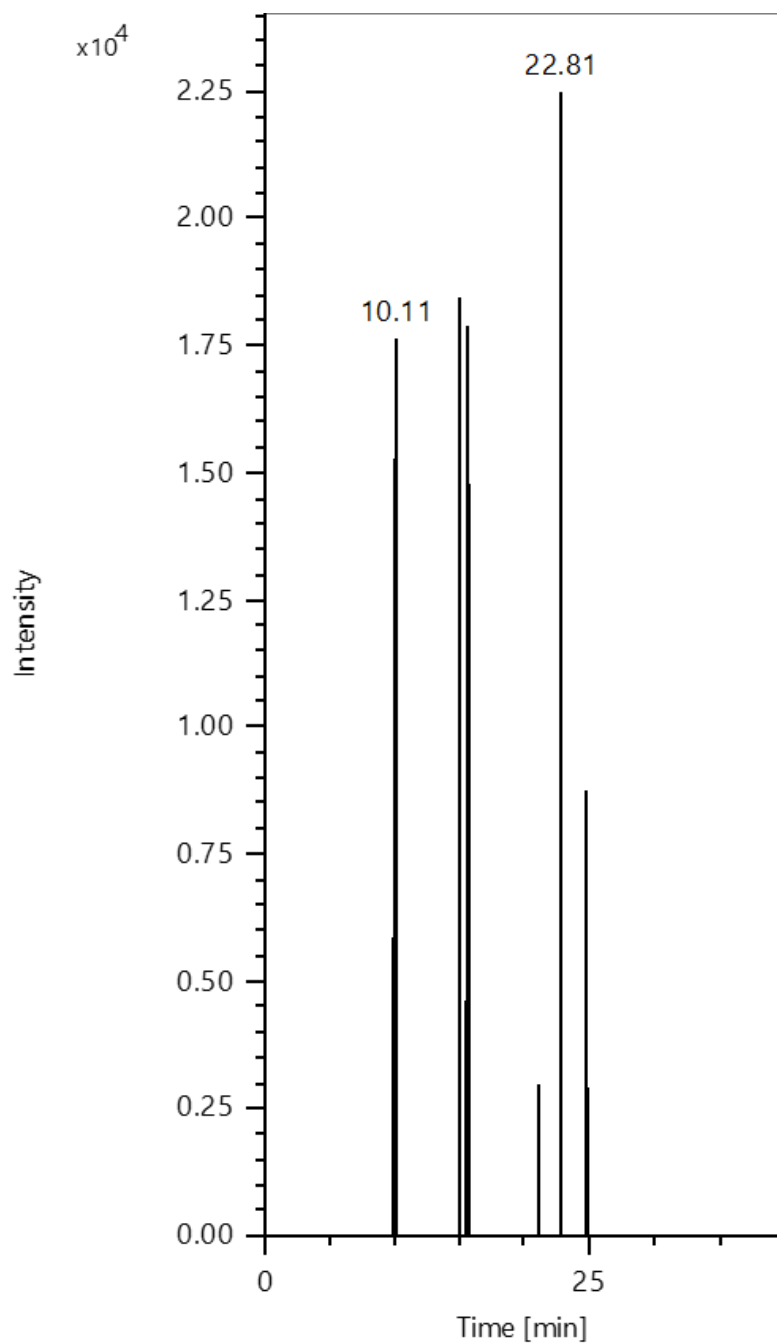
S95- GC-MS m/z of PET degraded with ethylene glycol impregnated with a 1:1 mass ratio with microwaves at an input power of 1.6 kW (powder fraction) t=22.82 minutes.



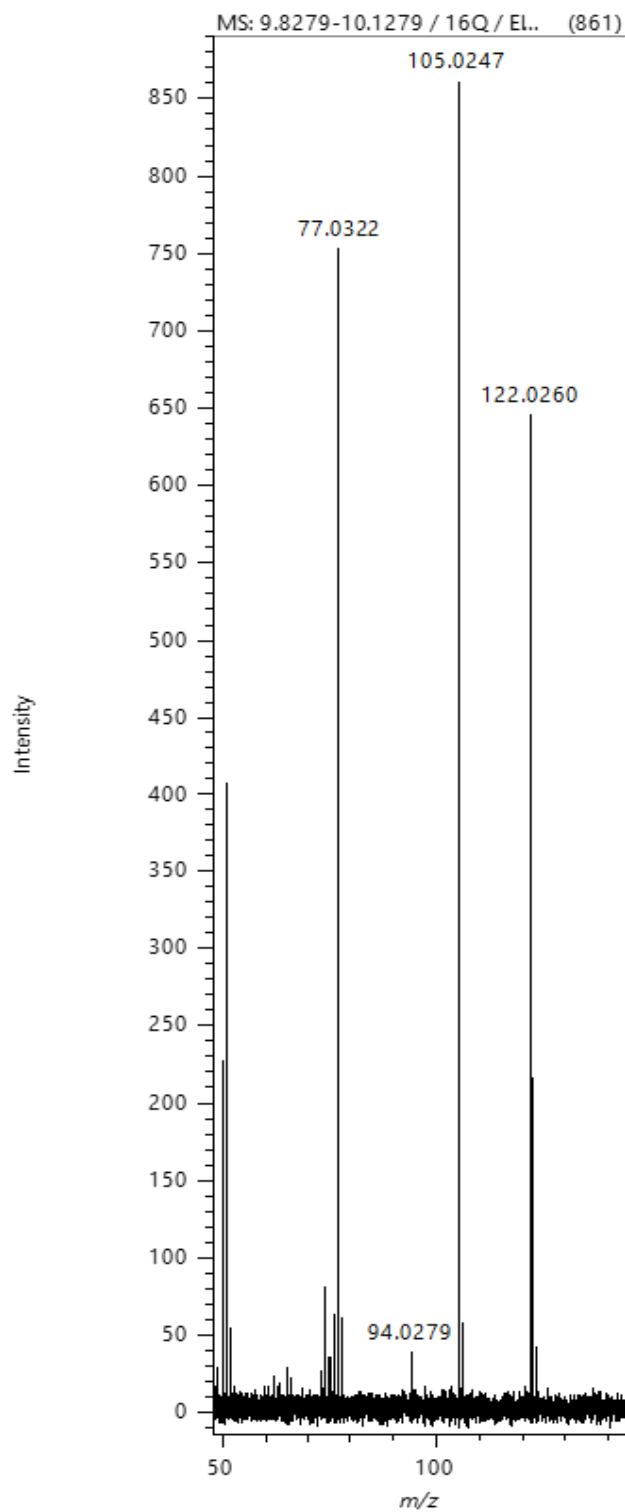
S96- GC-MS m/z of PET degraded with ethylene glycol impregnated with a 1:1 mass ratio with microwaves at an input power of 1.6 kW (powder fraction) $t=24.79$ minutes.



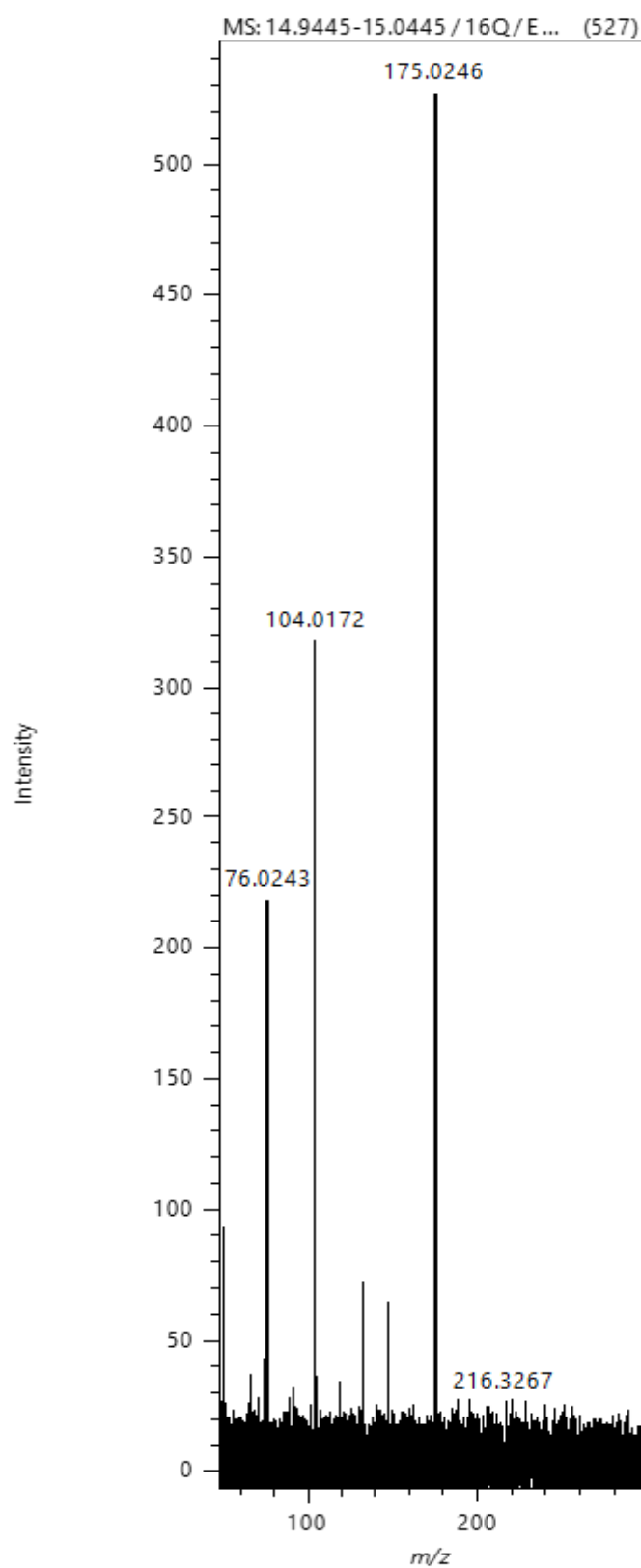
S97- GC-MS m/z of PET degraded with ethylene glycol impregnated with a 1:1 mass ratio with microwaves at an input power of 1.6 kW (powder fraction) $t=25.74$ minutes.



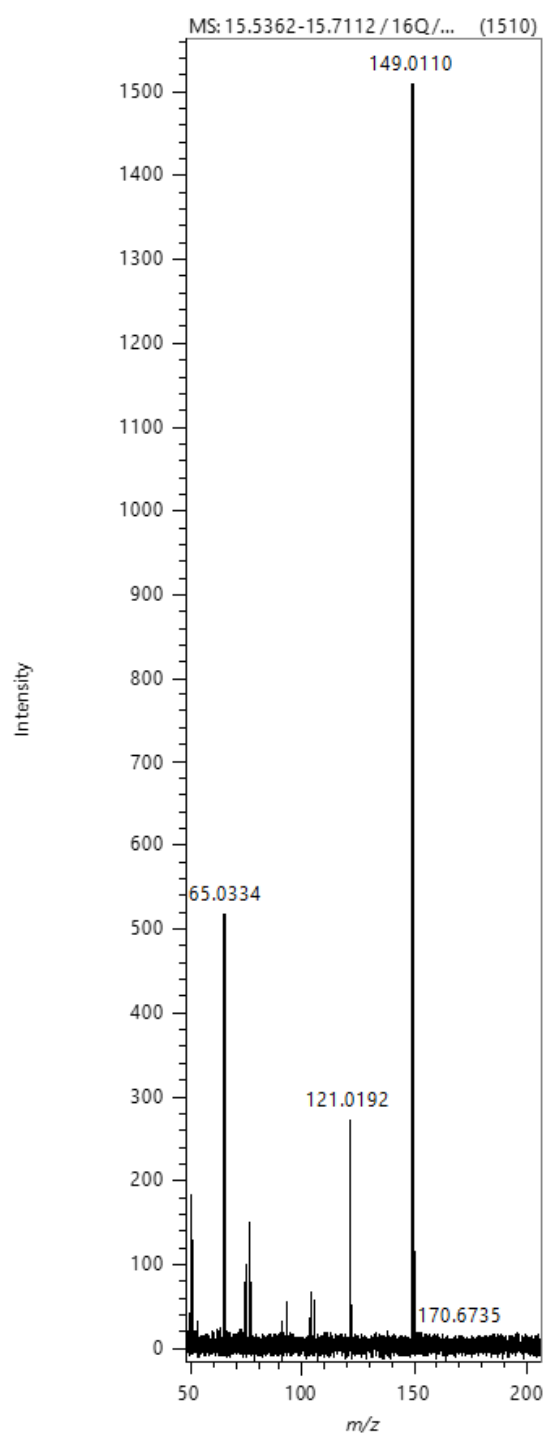
S98- GC-MS TICC of PET impregnated with ethylene glycol in a 1:1 mass ratio degraded with microwaves at an input power of 1.6 kW (wax fraction).



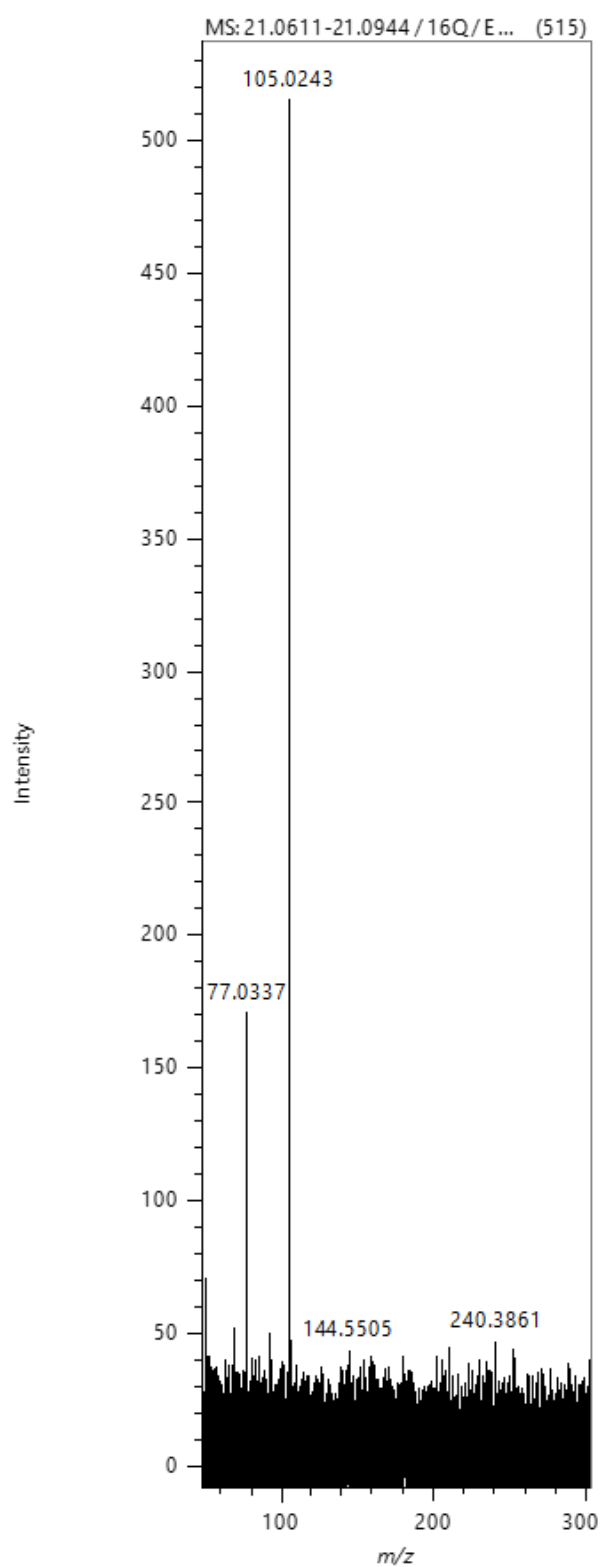
S99- GC-MS m/z of PET degraded with ethylene glycol impregnated with a 1:1 mass ratio with microwaves at an input power of 1.6 kW (powder fraction) $t=10.11$ minutes.



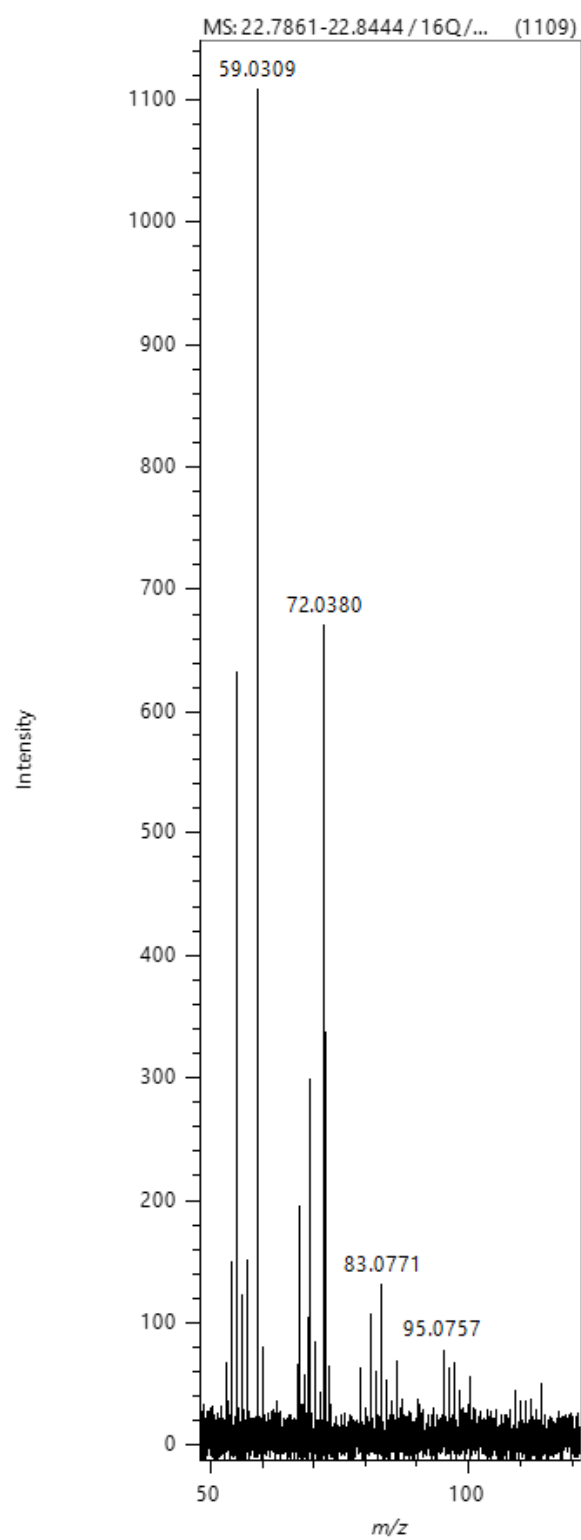
S100- GC-MS m/z of PET degraded with ethylene glycol impregnated with a 1:1 mass ratio with microwaves at an input power of 1.6 kW (powder fraction) $t=14.98$ minutes.



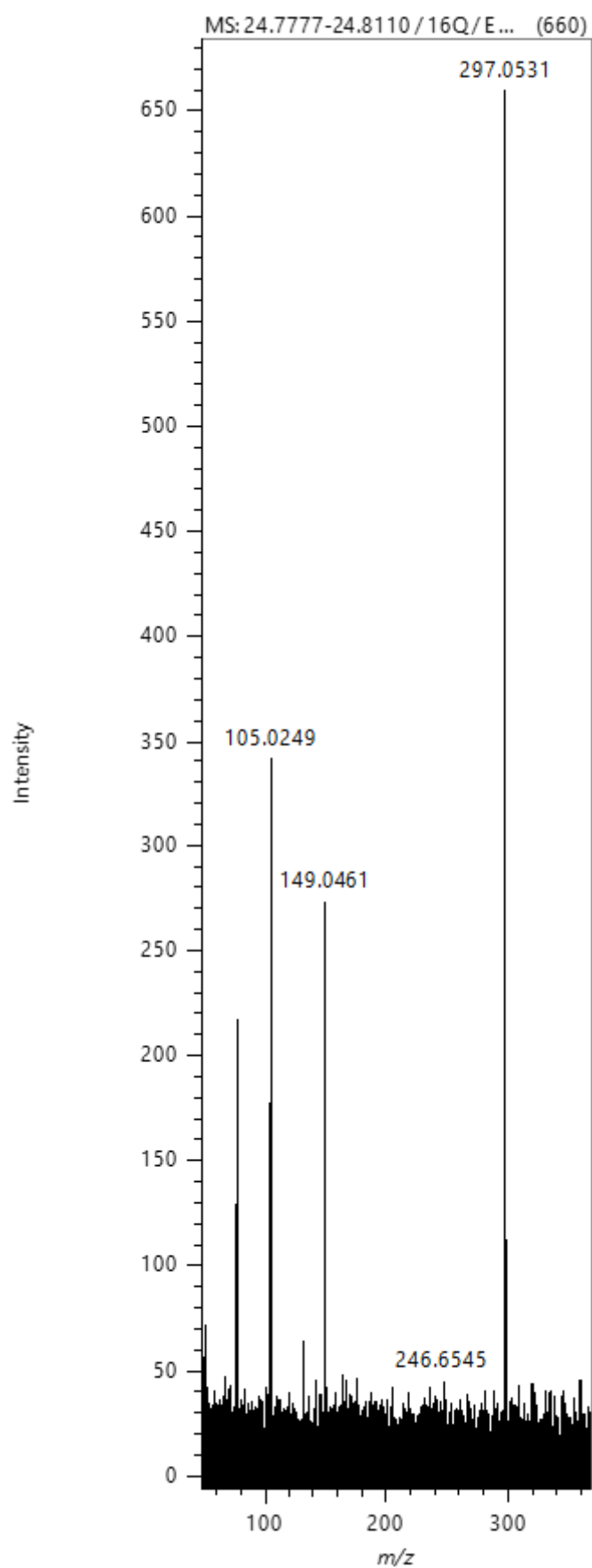
S101- GC-MS m/z of PET degraded with ethylene glycol impregnated with a 1:1 mass ratio with microwaves at an input power of 1.6 kW (powder fraction) t=15.45 minutes.



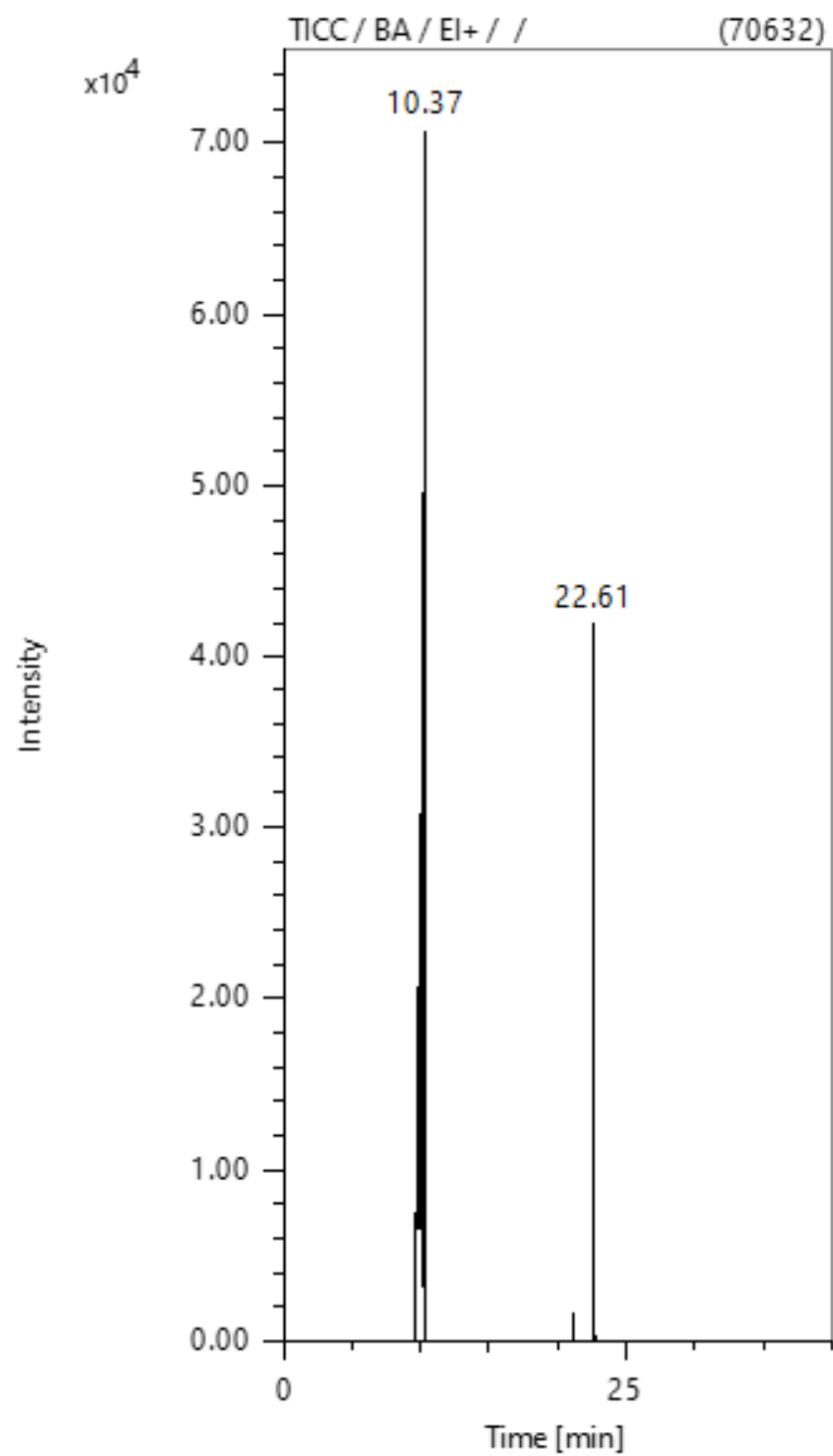
S102- GC-MS m/z of PET degraded with ethylene glycol impregnated with a 1:1 mass ratio with microwaves at an input power of 1.6 kW (powder fraction) t=21.07 minutes.



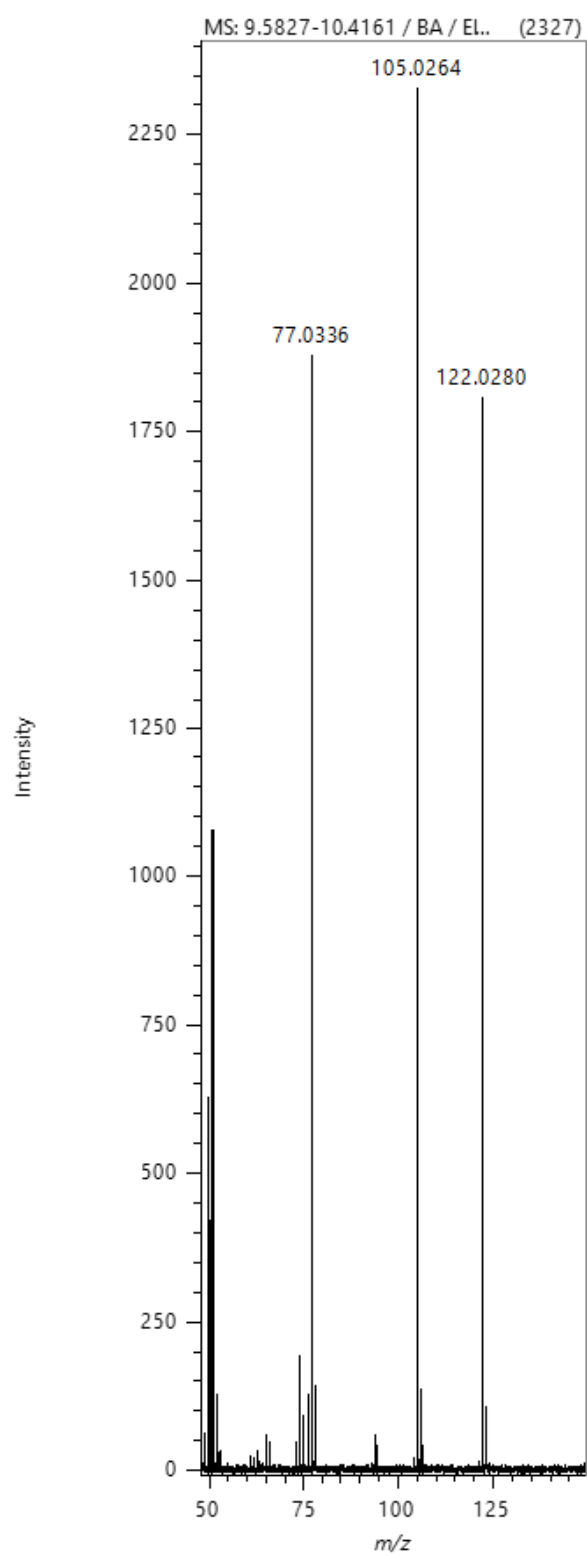
S103- GC-MS m/z of PET degraded with ethylene glycol impregnated with a 1:1 mass ratio with microwaves at an input power of 1.6 kW (powder fraction) t=22.81 minutes.



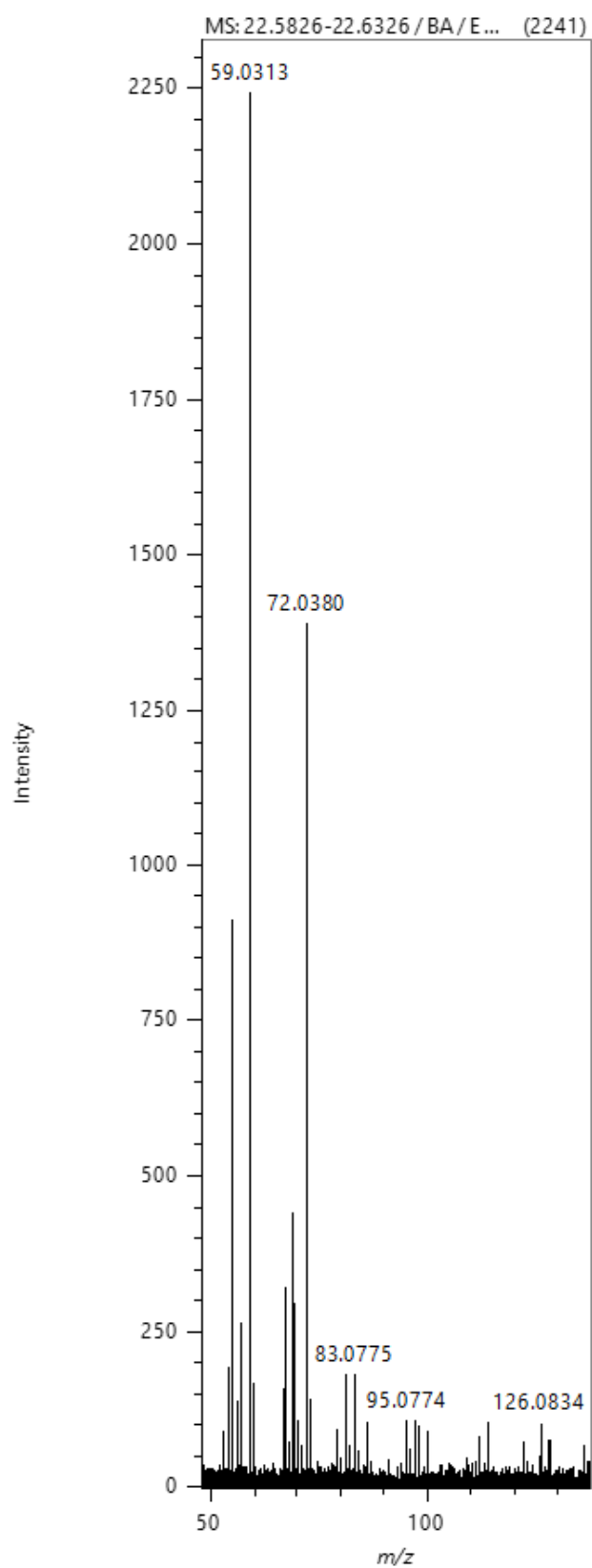
S104- GC-MS m/z of PET degraded with ethylene glycol impregnated with a 1:1 mass ratio with microwaves at an input power of 1.6 kW (powder fraction) $t=24.79$ minutes.



S105- GC-MS TICC of Benzoic Acid



S106- GC-MS mass spectrum of benzoic acid $t = 10.11$ minutes.



S107- GC-MS mass spectrum of benzoic acid $t = 22.61$ minutes.

S108 – Mass balance of all PET pyrolysis experiments undertaken

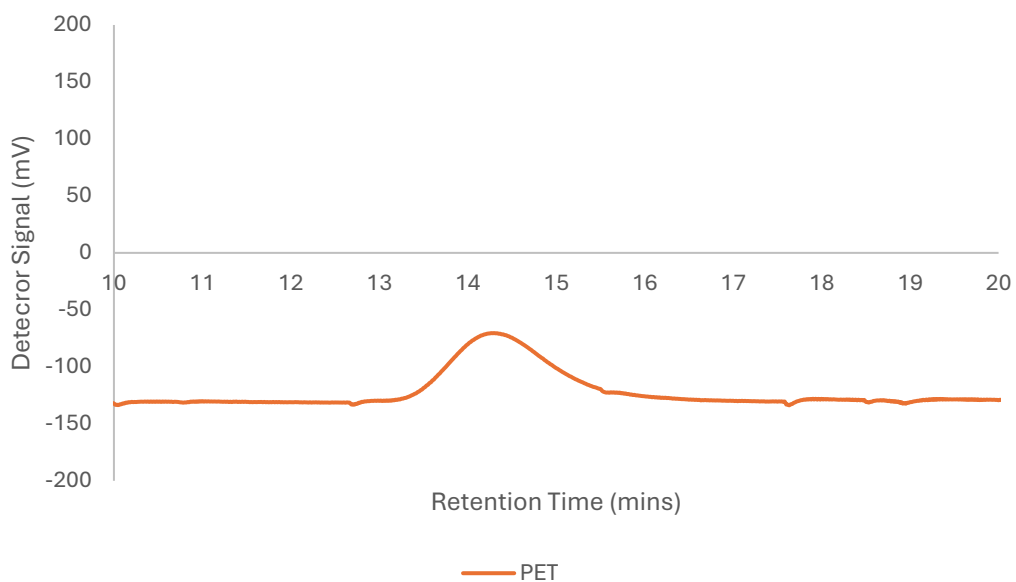
Input Power (kW)	PET: EG Mass Ratio	Endpoint	PET (g)	Char (g)	Wax (g)	Powder (g)	Limewater Precipitate (g)	Gas (g)
0.80	1:0	EOF	14.91	9.68	2.16	0.81	/	2.26
0.80	1:0	EOF + 1 min	14.83	8.45	2.88	0.78	/	2.72
0.80	1:1	EOF	14.33	7.16	1.44	2.31	0.0557	3.42
0.80	1:1	EOF + 1 min	15.08	7.80	1.60	3.11	0.0641	2.57
0.80	1:10	EOF	15.68	6.44	2.32	3.97	0.0468	2.95
0.80	1:10	EOF + 1 min	15.32	5.03	3.85	4.07	0.0359	2.37
1.20	1:0	EOF	15.41	6.44	4.11	1.31	/	3.55
1.20	1:0	EOF + 1 min	15.02	6.12	4.17	1.75	/	2.98
1.20	1:1	EOF	14.77	6.89	2.34	2.54	0.0360	3.00
1.20	1:1	EOF + 1 min	15.03	8.31	0.24	2.99	0.0303	3.49
1.20	1:10	EOF	14.93	6.62	2.09	4.86	0.0249	1.36
1.20	1:10	EOF + 1 min	14.42	5.53	2.46	2.95	0.0268	3.48
1.60	1:0	EOF	15.02	4.81	5.33	1.63	/	3.25
1.60	1:0	EOF + 1 min	15.10	3.69	5.85	1.81	/	3.75
1.60	1:1	EOF	14.71	5.97	2.24	4.56	0.0523	1.94
1.60	1:1	EOF + 1 min	10.79	4.64	0.51	2.09	0.0331	3.55
1.60	1:10	EOF	13.90	4.36	3.02	3.26	0.0296	3.26
1.60	1:10	EOF + 1 min	13.19	4.35	3.31	3.72	0.0256	1.81

S109 – Product fractions expressed as percentages of the original PET mass. An increase in solid % of total can be seen with increasing PET:EG mass ratio at an input power of 0.80 kW, but it is stationary regardless of PET:EG mass ratio at 1.20- and 1.60 kW input power.

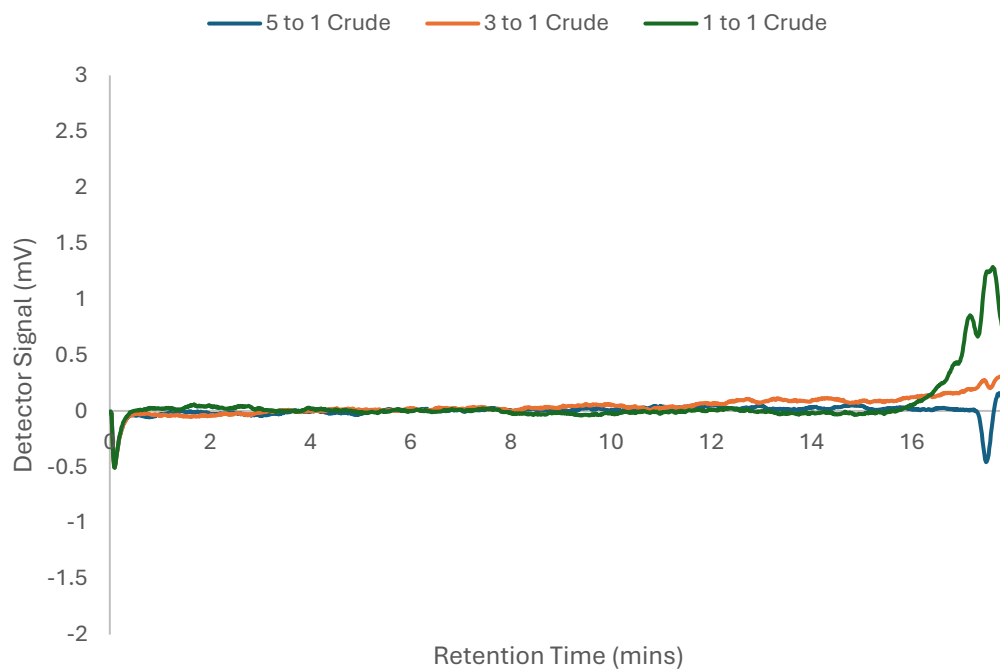
Input Power (kW)	PET: EG Mass Ratio	Endpoint	PET (g)	Char % of Total	Solid % of Total	Gas % of Total
0.80	1:0	EOF	14.91	64.9	19.9	15.2
0.80	1:0	EOF + 1 min	14.83	75.5	24.7	18.3
0.80	1:1	EOF	14.33	49.97	26.2	23.9
0.80	1:1	EOF + 1 min	15.08	51.7	31.2	17.0
0.80	1:10	EOF	15.68	41.1	40.1	18.8
0.80	1:10	EOF + 1 min	15.32	32.8	51.7	15.5
1.20	1:0	EOF	15.41	41.8	35.2	23.0
1.20	1:0	EOF + 1 min	15.02	40.7	39.4	19.8
1.20	1:1	EOF	14.77	46.6	33.0	20.3
1.20	1:1	EOF + 1 min	15.03	55.3	21.5	23.2
1.20	1:10	EOF	14.93	44.3	46.6	9.1
1.20	1:10	EOF + 1 min	14.42	38.3	37.5	24.1
1.60	1:0	EOF	15.02	32.0	46.3	21.6
1.60	1:0	EOF + 1 min	15.10	24.4	50.7	24.8
1.60	1:1	EOF	14.71	40.9	46.2	13.0
1.60	1:1	EOF + 1 min	10.79	43.0	24.1	32.9
1.60	1:10	EOF	13.90	31.4	45.2	23.5
1.60	1:10	EOF + 1 min	13.19	33.0	53.3	13.7

Chapter 5

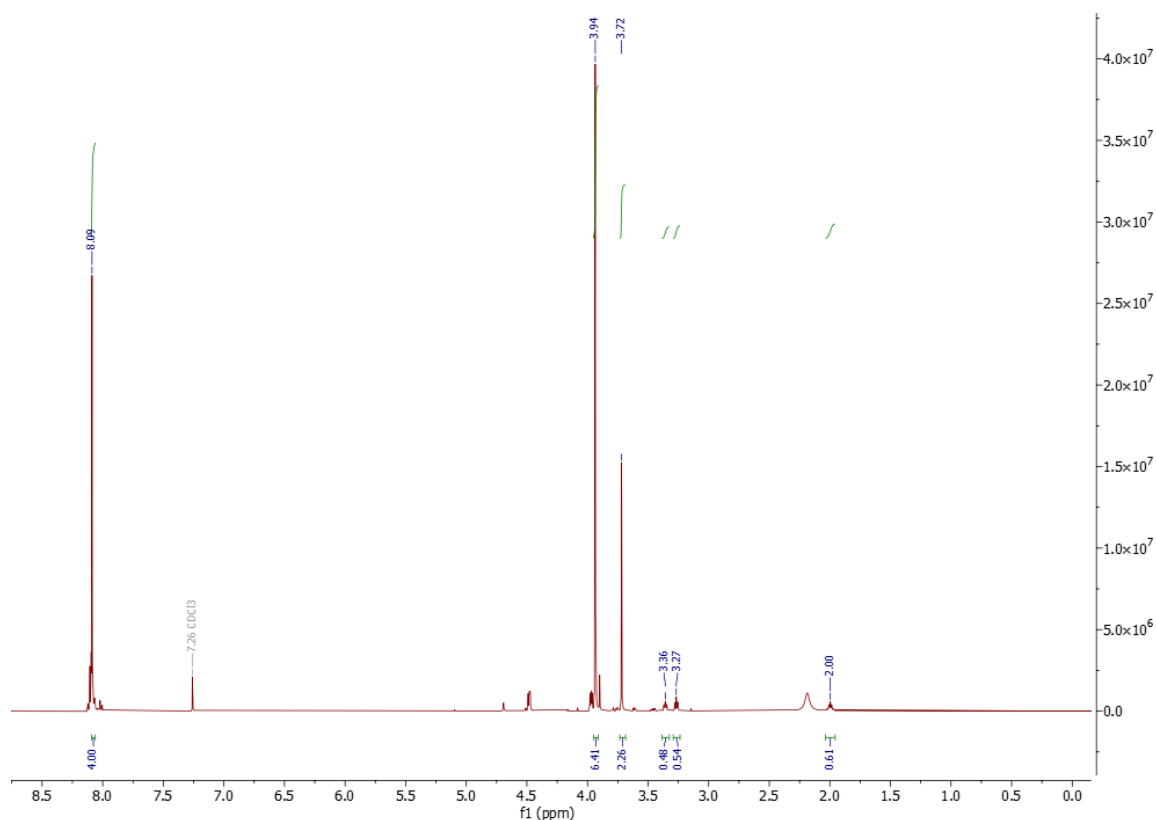
GPC results on PET (S108) were provided by the Research Technology Platform at the University of Warwick



S110- GPC chromatogram of unmodified PET. $M_w = 46.209$ g/mol measured by refractive index.

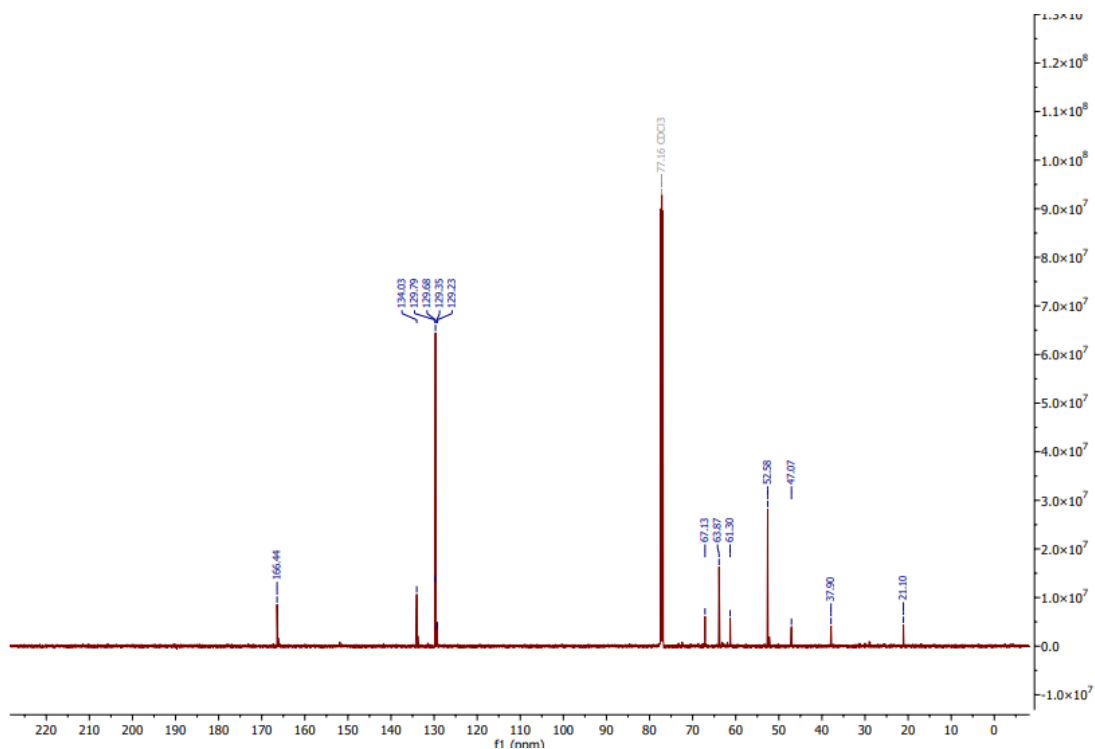


S111- GPC chromatogram of crude methanolysis product. PET. Molecular weight could not be determined due to total permeation. Refractive index was used to measure here.



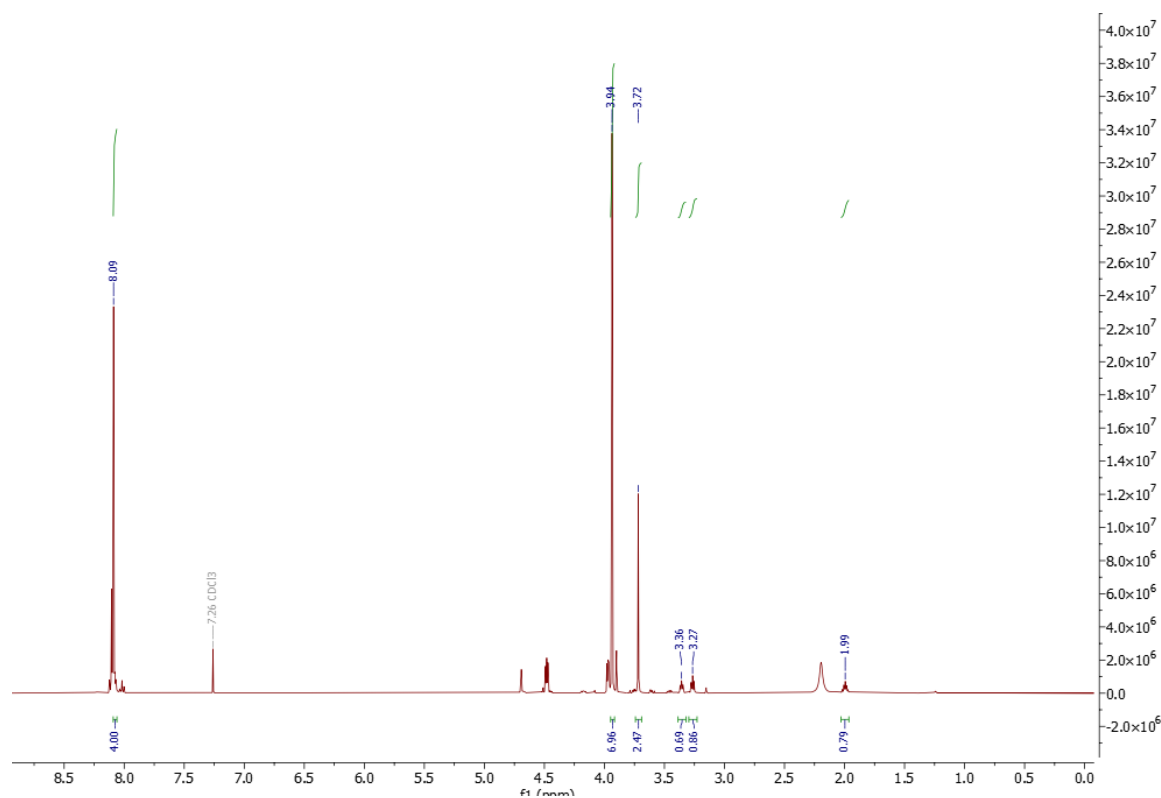
S112- ¹H NMR of crude methanolysis product where PET was degraded with a 5:1 molar excess of methanol. DMT, EG and TBD peaks assigned.

Temperature = 180 °C, time = 3 hours, pressure = 172 bar



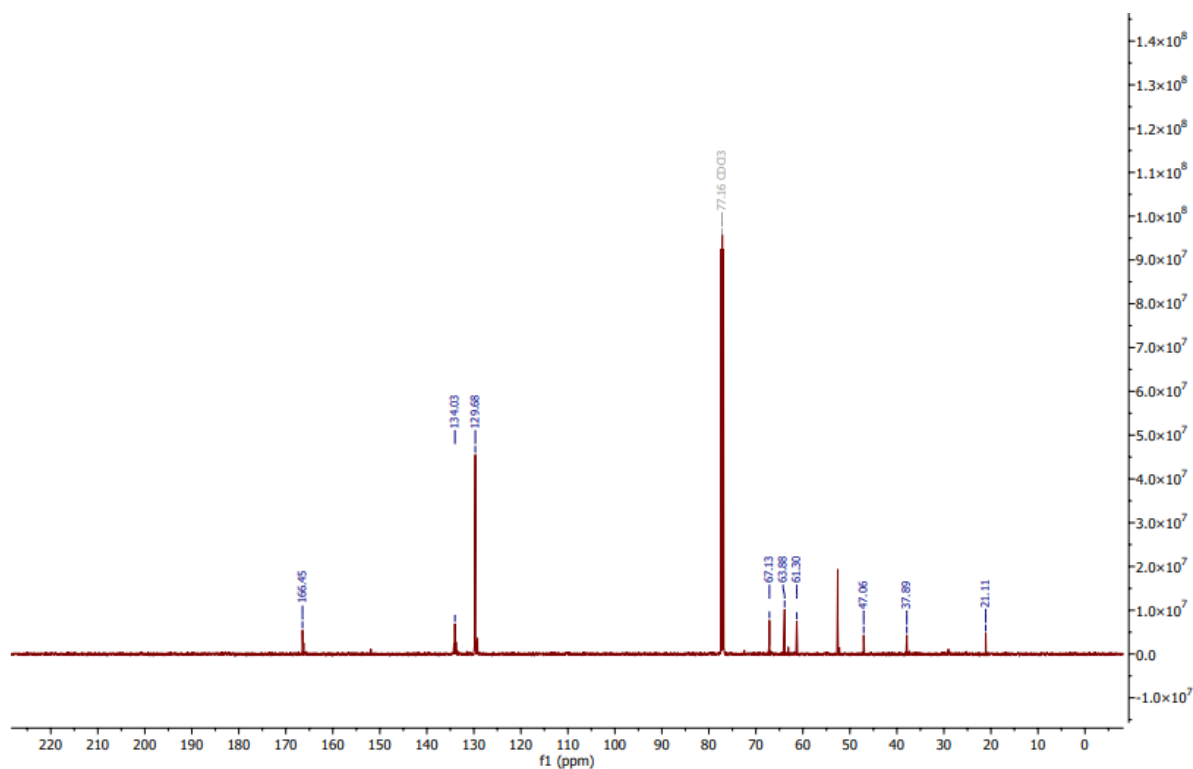
S113- ¹³C NMR of crude methanolysis product where PET was degraded with a 5:1 molar excess of methanol. DMT, EG and TBD peaks assigned.

Temperature = 180 °C, time = 3 hours, pressure = 172 bar



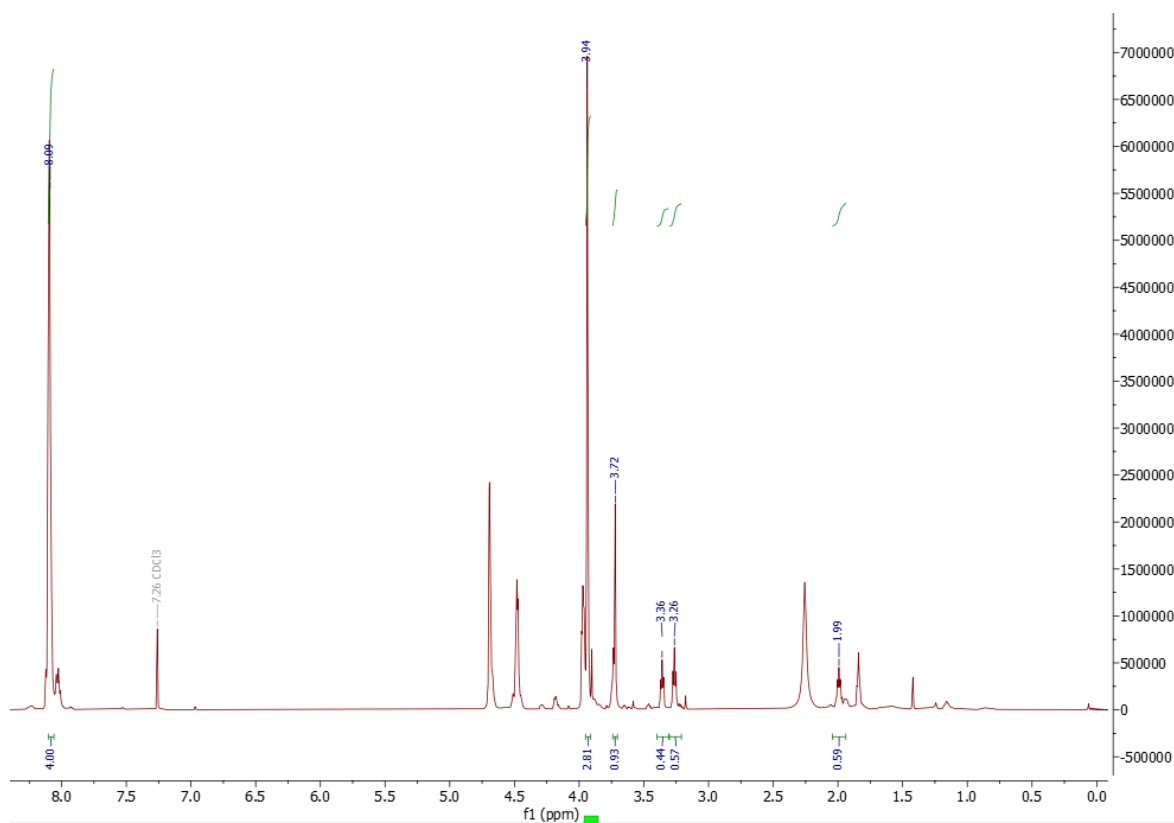
S114- ^1H NMR of crude methanolysis product where PET was degraded with a 3:1 molar excess of methanol. DMT, EG and TBD peaks assigned.

Temperature = 180 °C, time = 3 hours, pressure = 172 bar



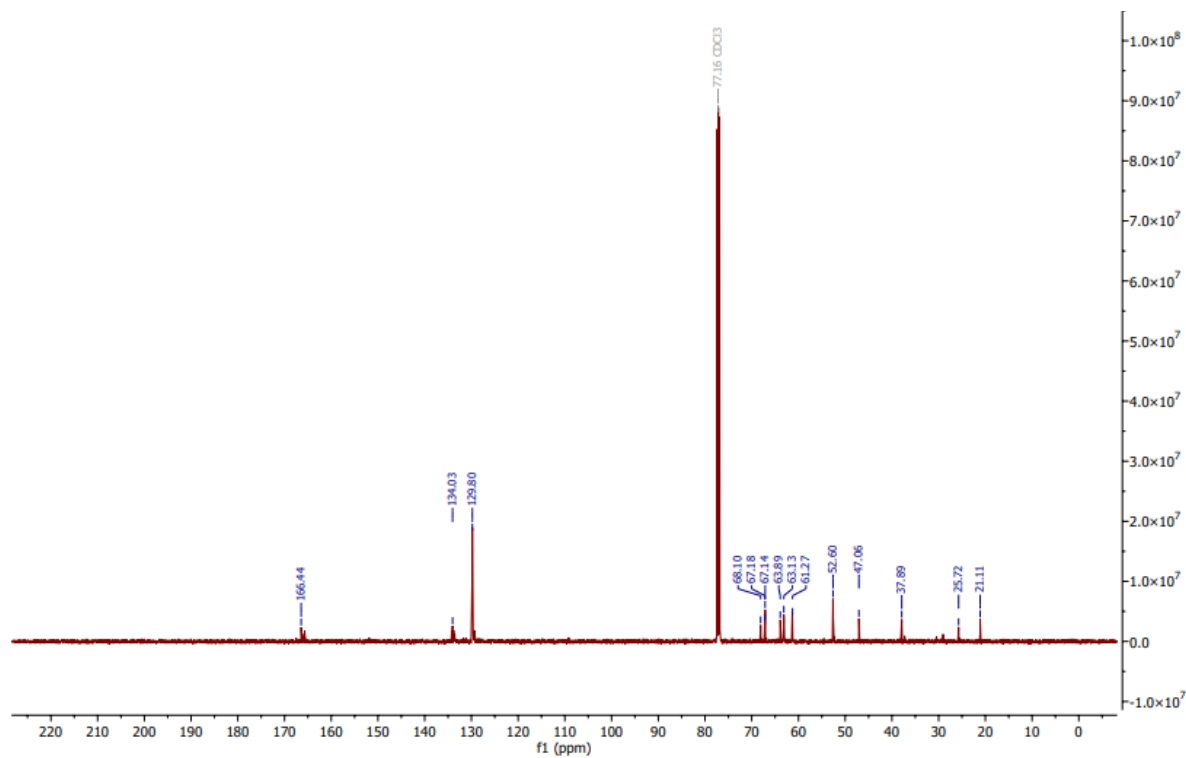
S115- ^{13}C NMR of crude methanolysis product where PET was degraded with a 3:1 molar excess of methanol. DMT, EG and TBD peaks assigned.

Temperature = 180 °C, time = 3 hours, pressure = 172 bar



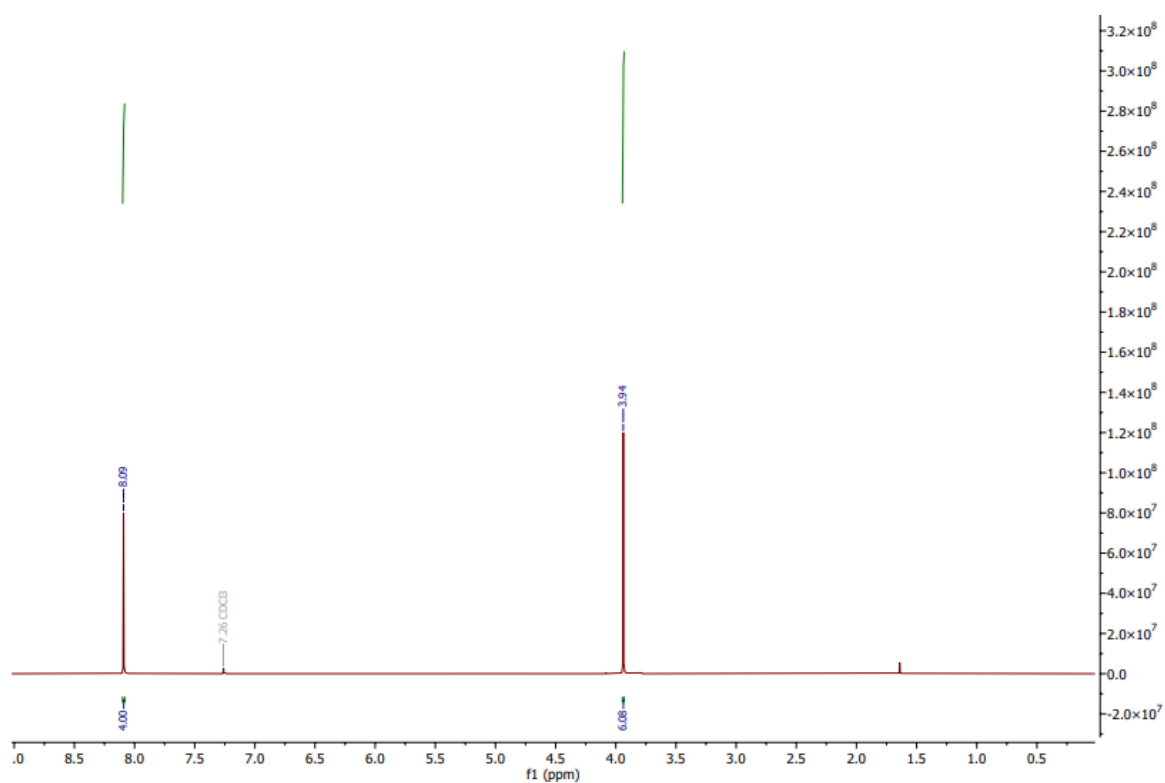
S116- ¹H NMR of crude methanolysis product where PET was degraded with a 1:1 molar excess of methanol. DMT, EG and TBD peaks assigned.

Temperature = 180 °C, time = 3 hours, pressure = 172 bar

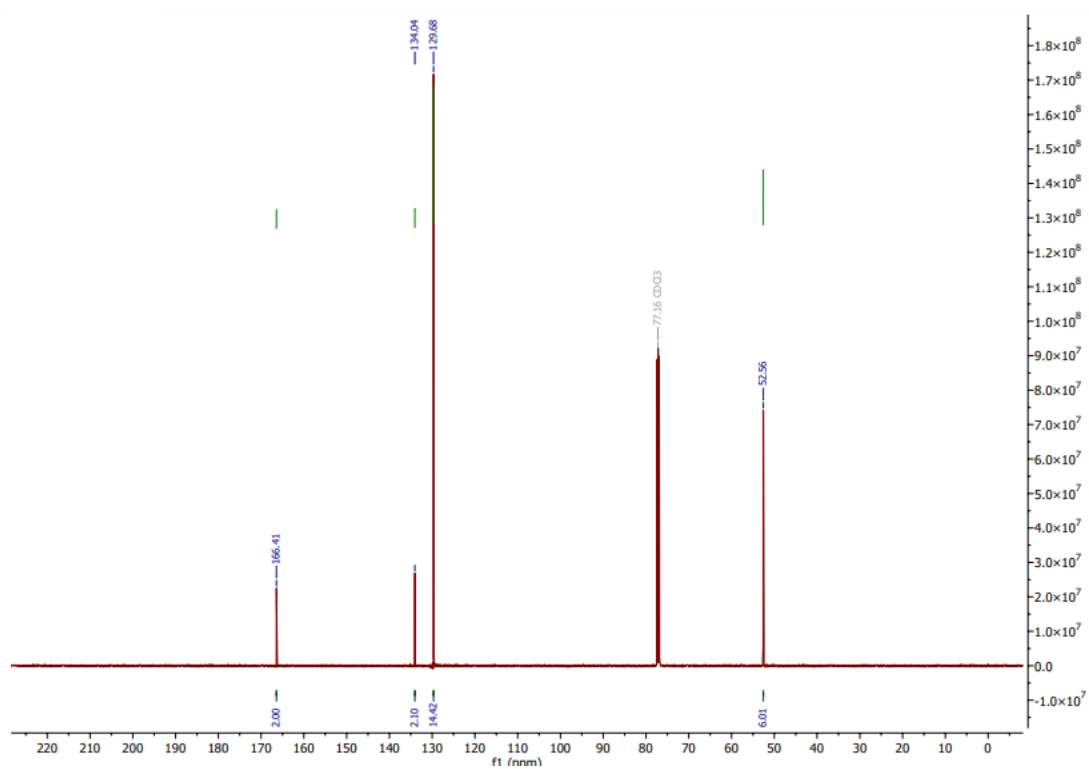


S117- ¹³C NMR of crude methanolysis product where PET was degraded with a 1:1 molar excess of methanol. DMT, EG and TBD peaks assigned.

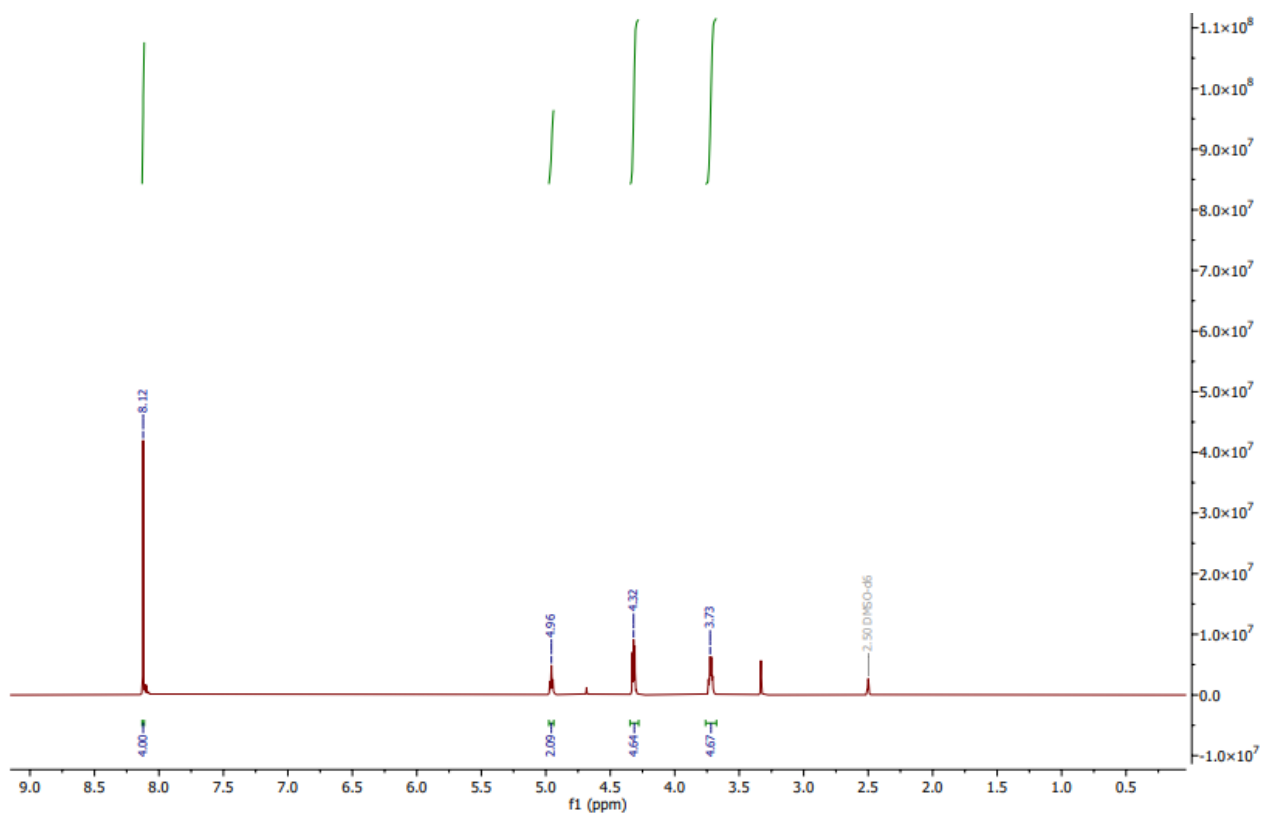
Temperature = 180 °C, time = 3 hours, pressure = 172 bar



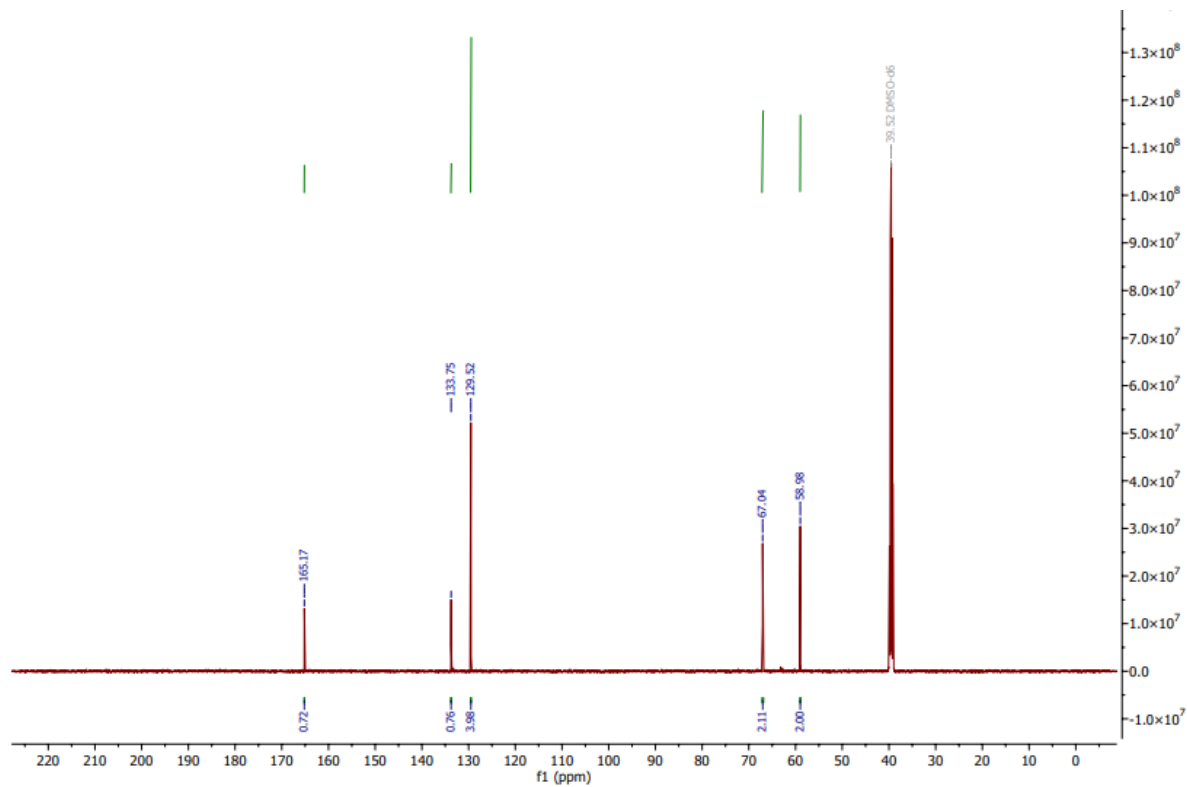
S118- ¹H NMR of dimethyl terephthalate (DMT).



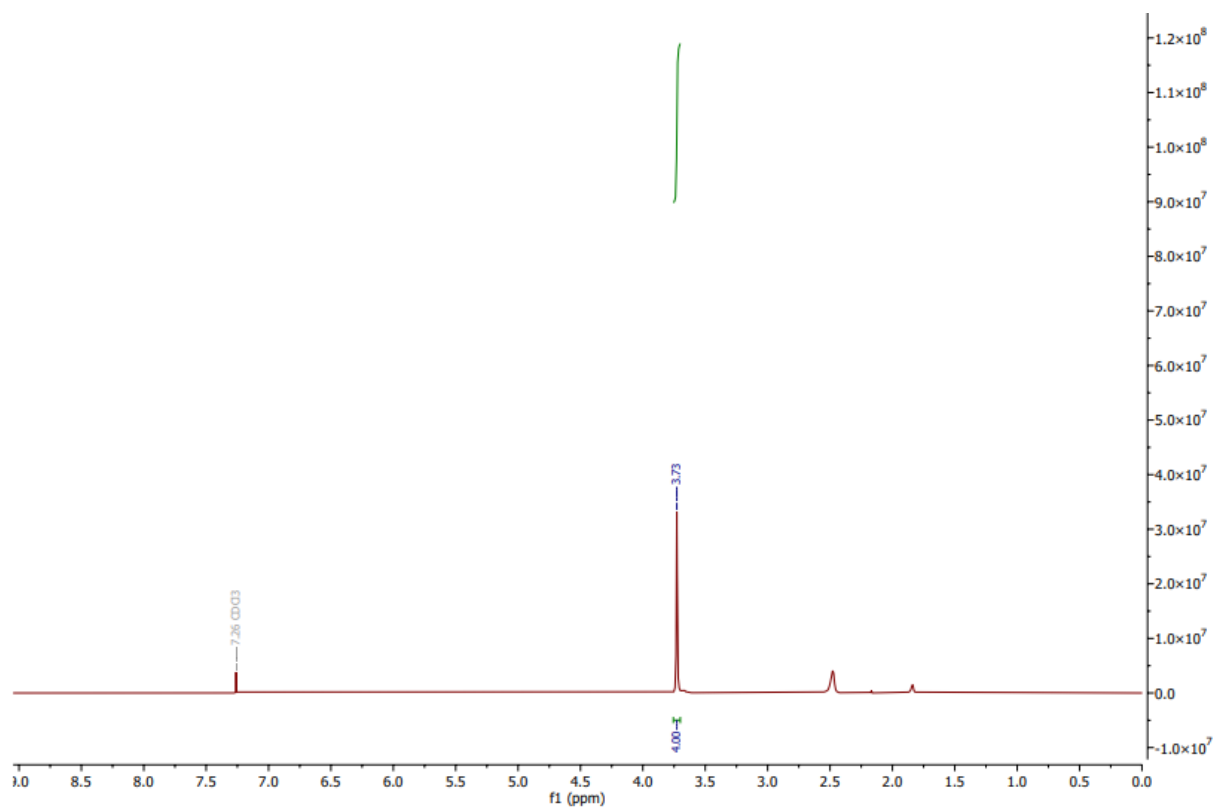
S119- ¹³C NMR of dimethyl terephthalate (DMT).



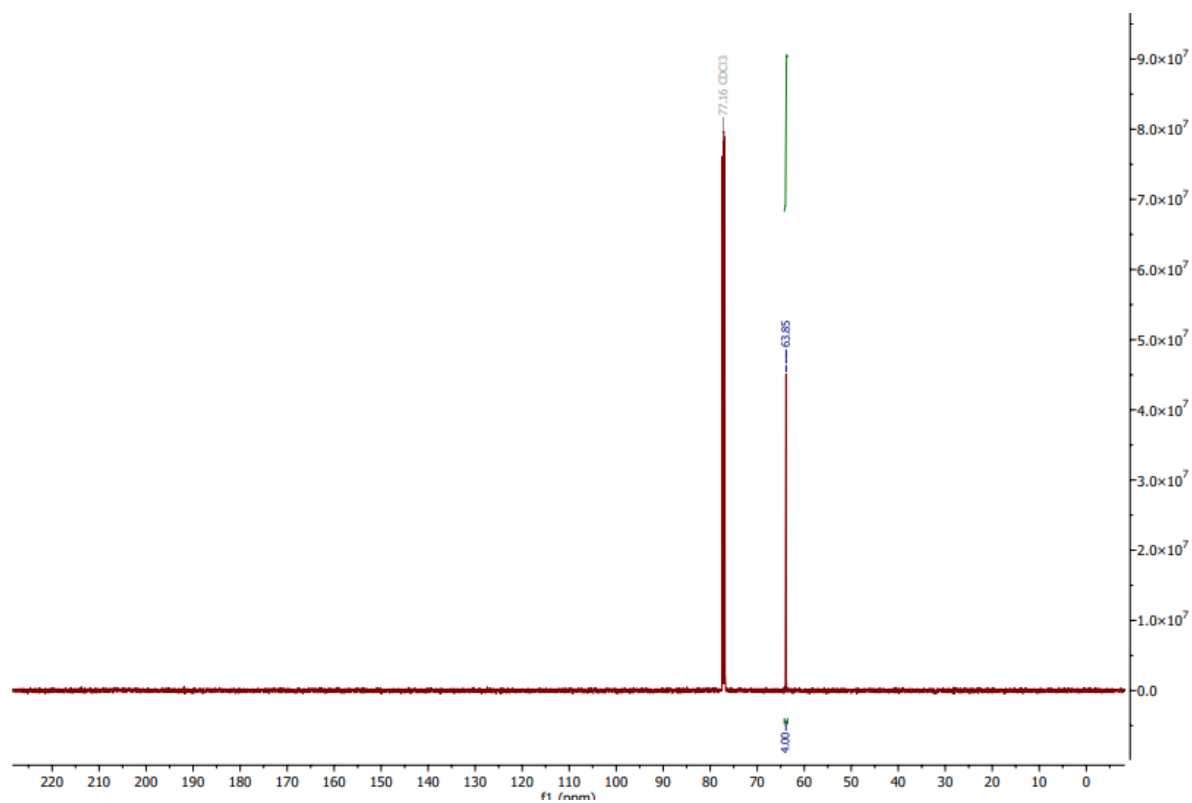
S120- ¹H NMR of bis(2-hydroxyethyl) terephthalate (BHET).



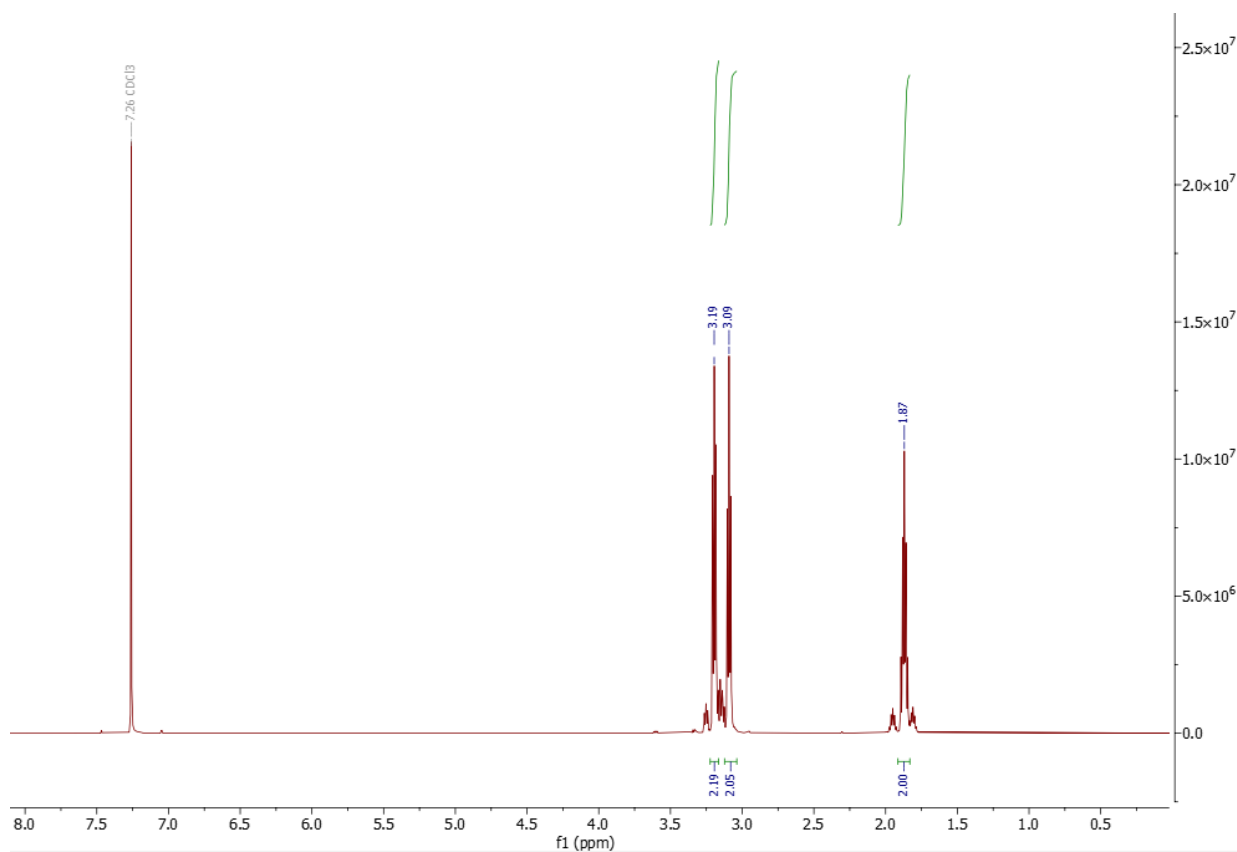
S121- ¹³C NMR of bis(2-hydroxyethyl) terephthalate (BHET).



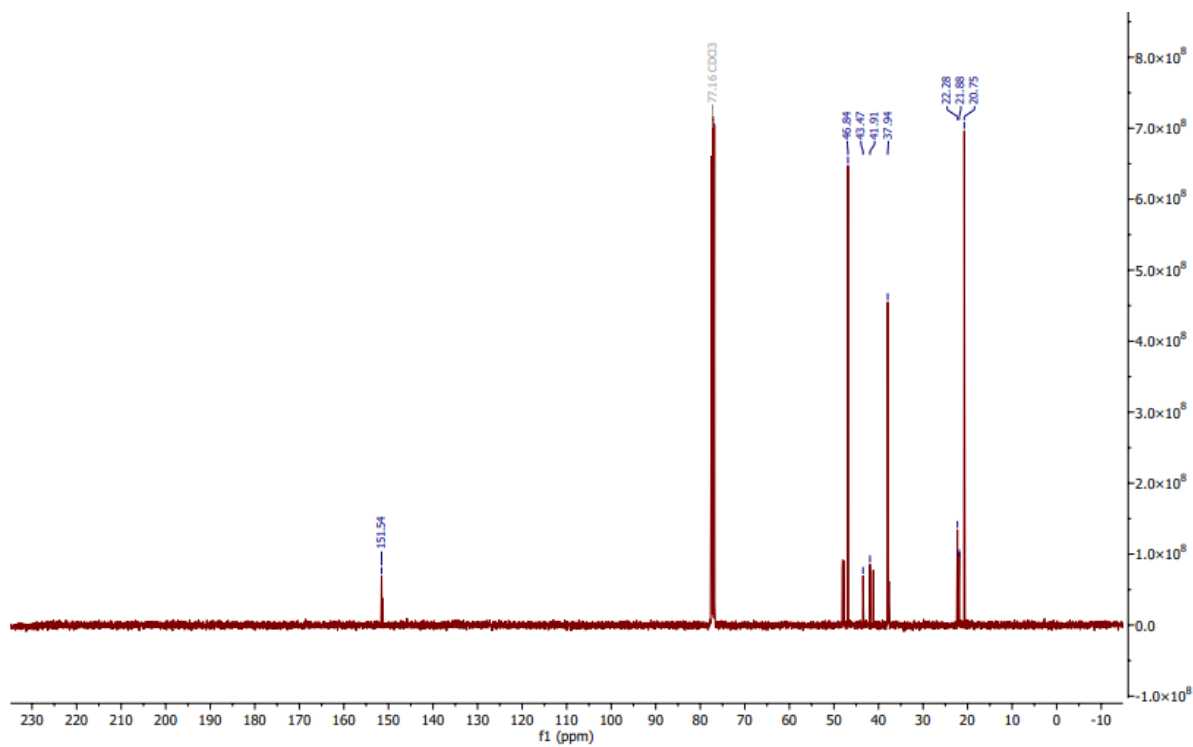
S122- ^1H NMR of ethylene glycol (EG).



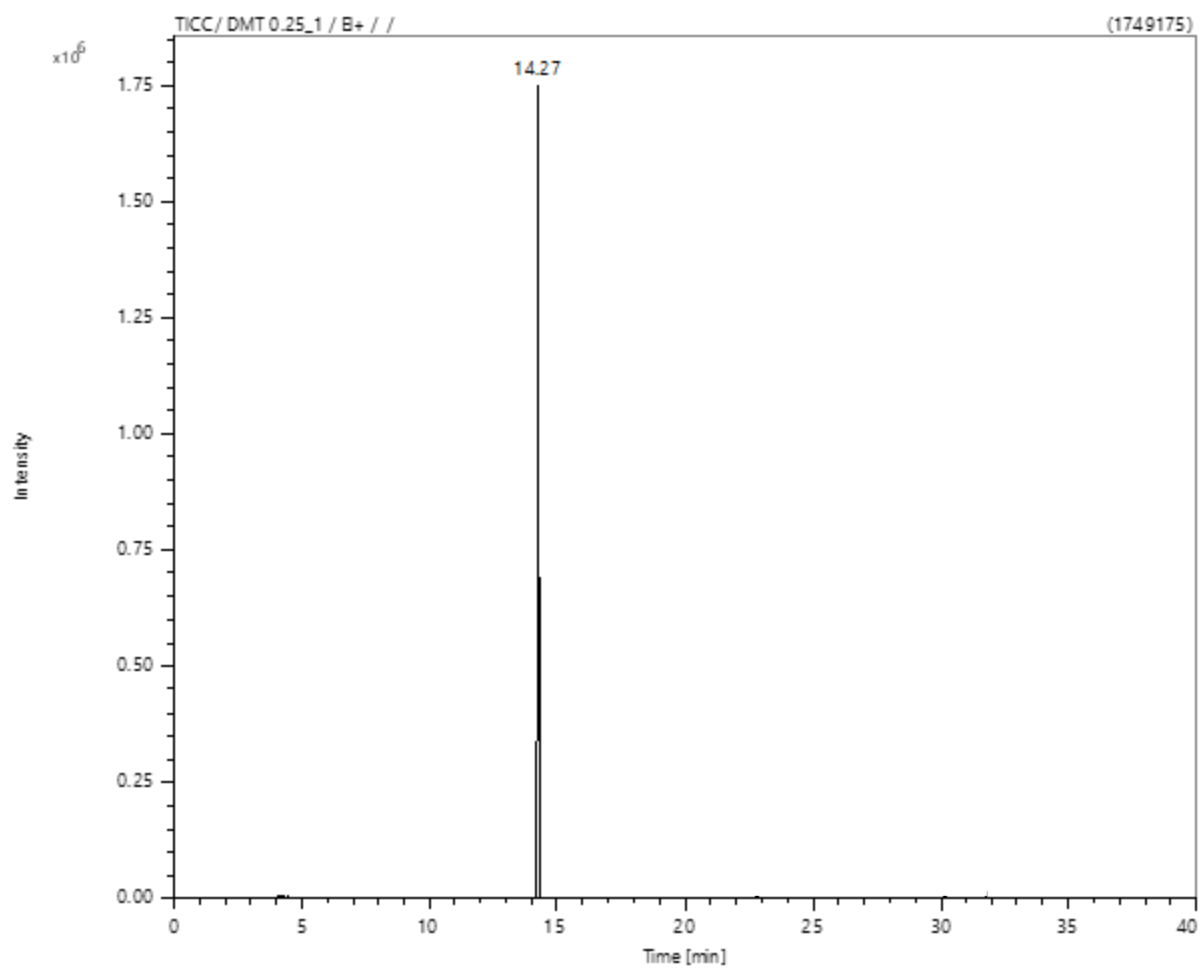
S123- ^{13}C NMR of ethylene glycol (EG).



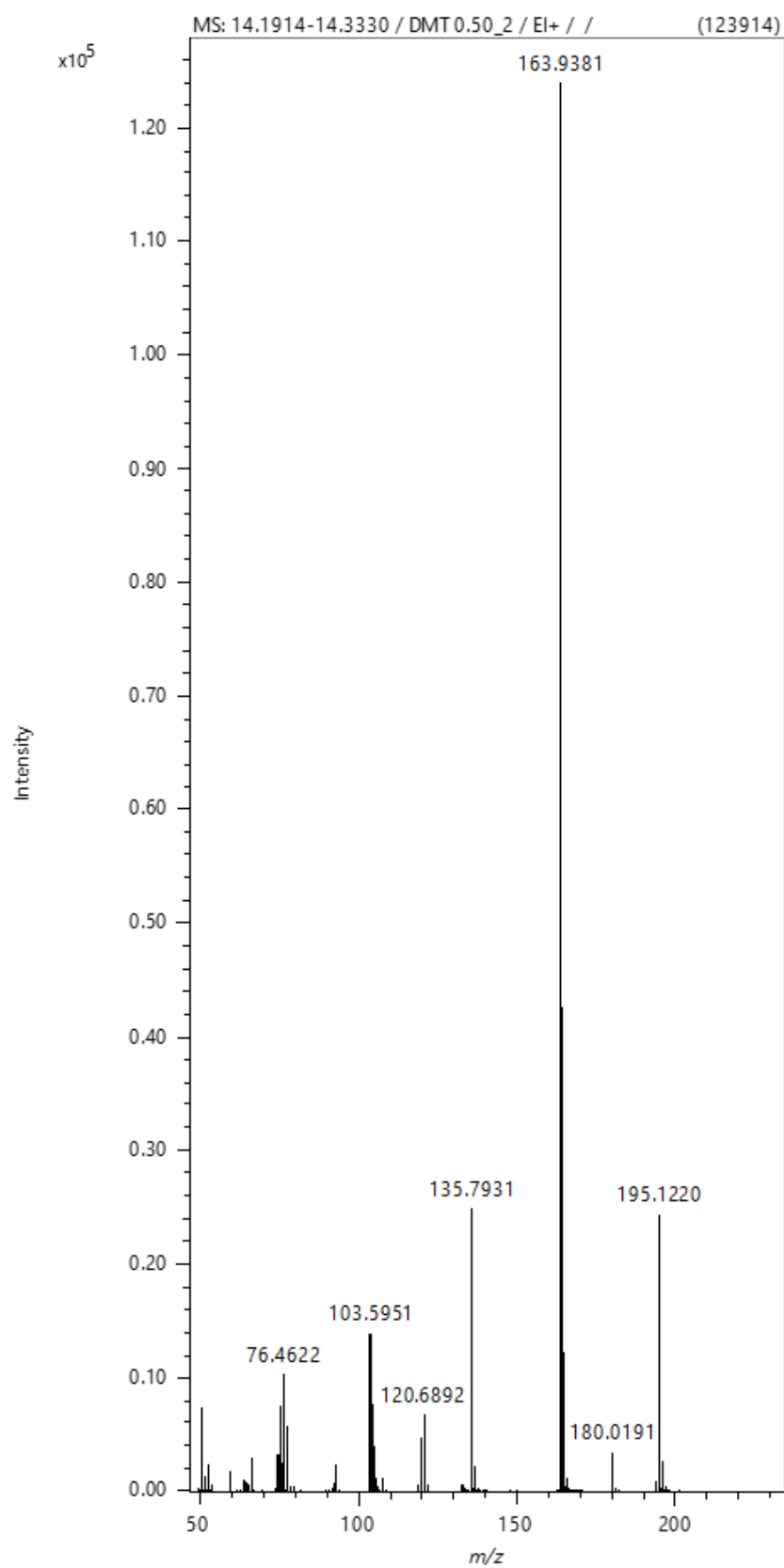
S124- ¹H NMR of 1,5,7-Triazabicyclo[4.4.0]dec-5-ene (TBD).



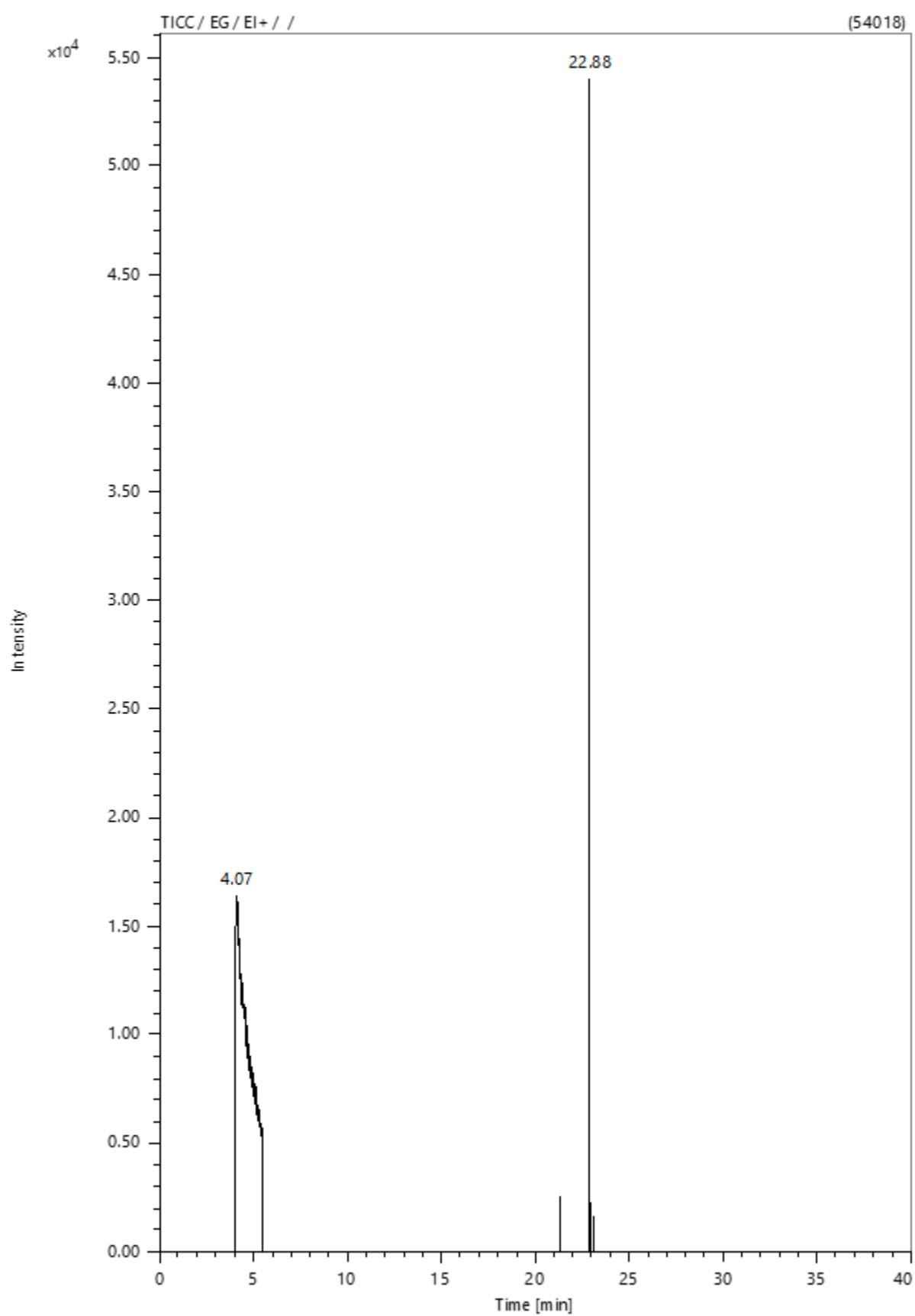
S125- ¹³C NMR of 1,5,7-Triazabicyclo[4.4.0]dec-5-ene (TBD).



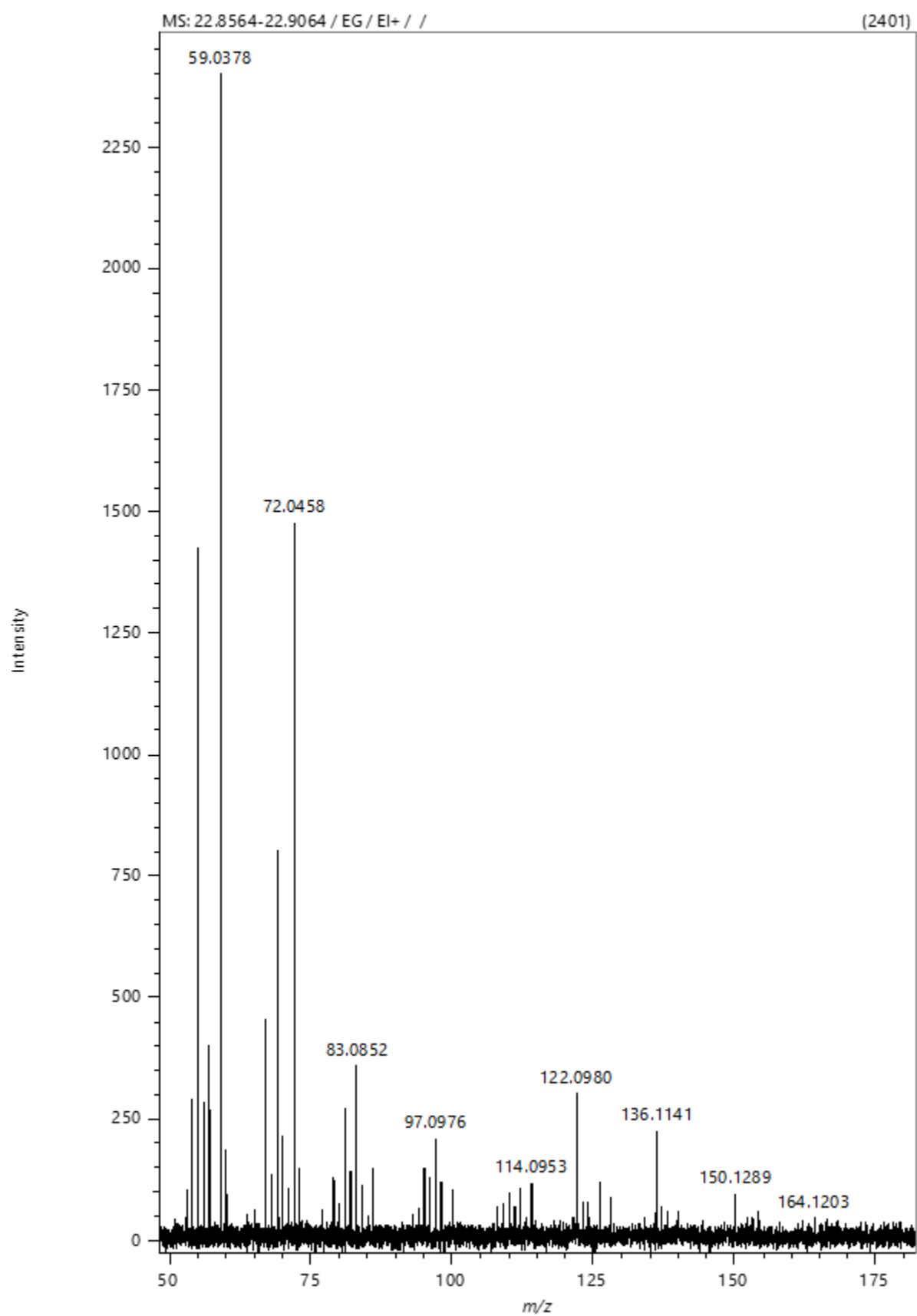
S126- GCMS TICC of dimethyl terephthalate (DMT).



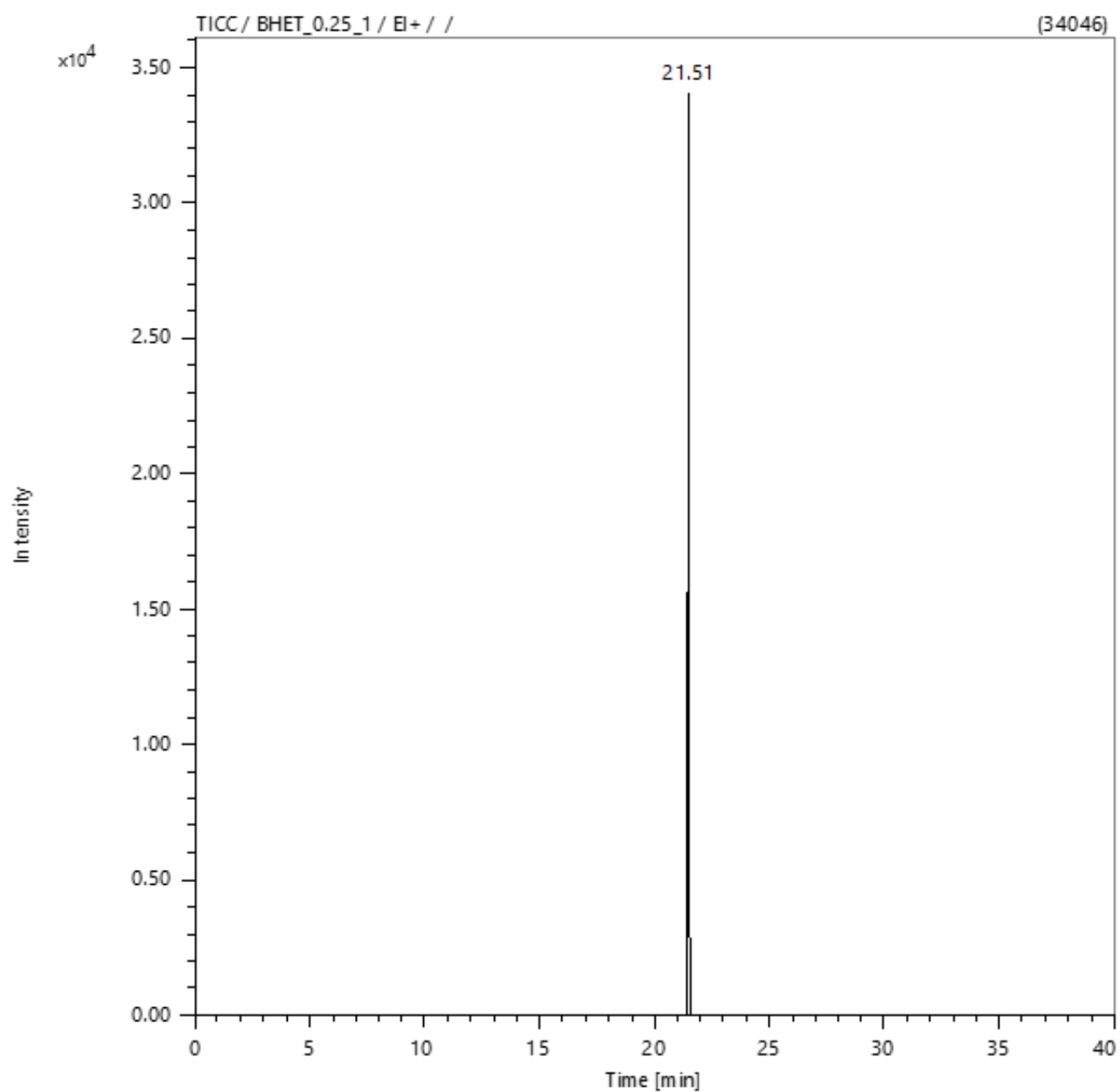
S127- GCMS mass spectrum of dimethyl terephthalate (DMT).



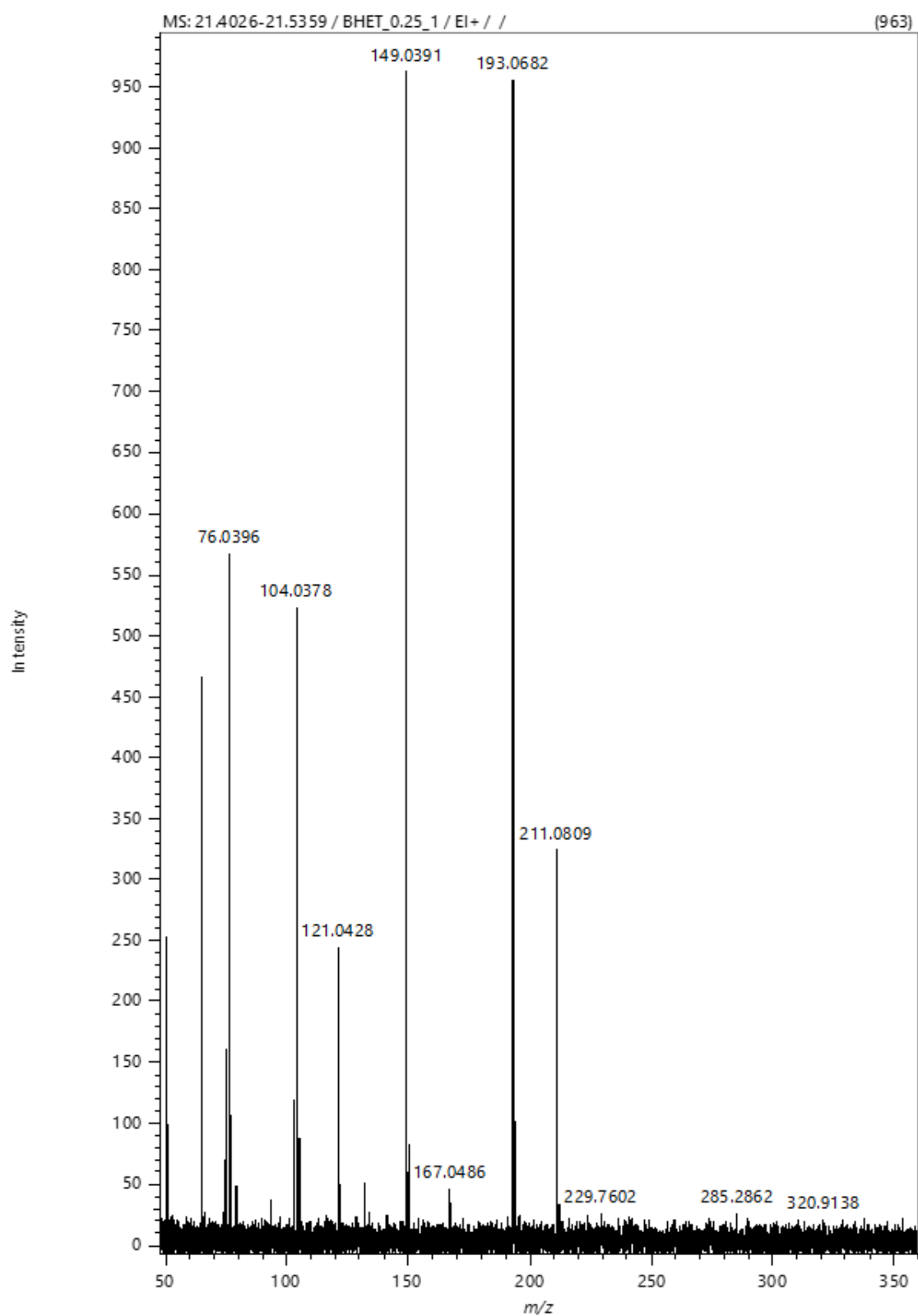
S128- GCMS TICC of ethylene glycol (EG).



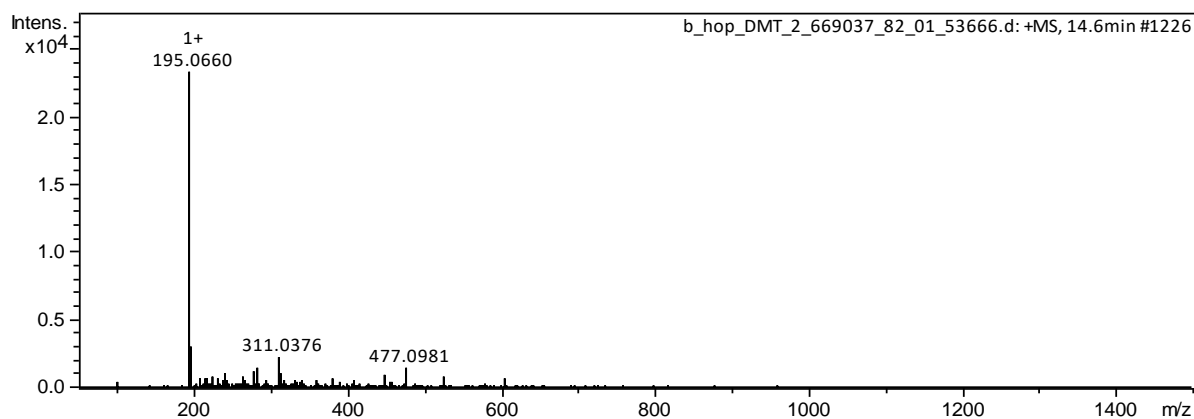
S129- GCMS mass spectrum of ethylene glycol (EG).



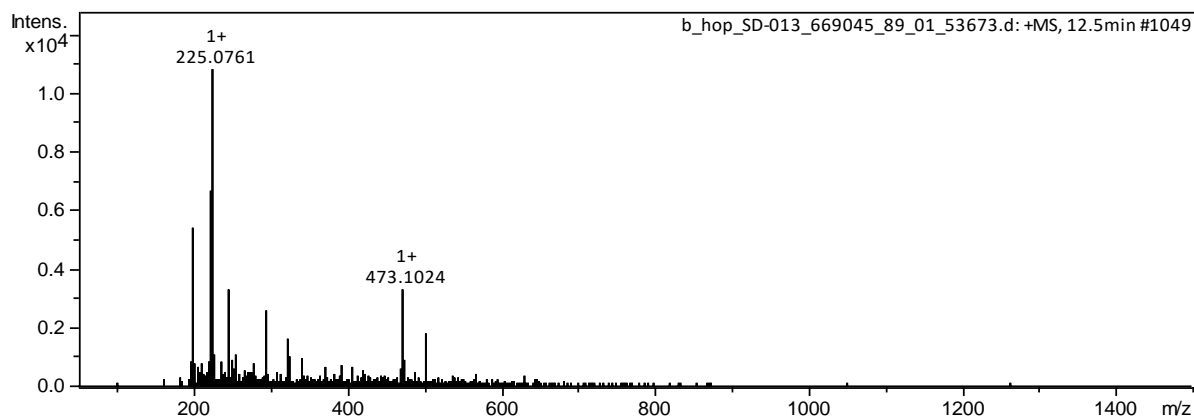
S130- GCMS TICC bis(2-hydroxyethyl) terephthalate (BHET).



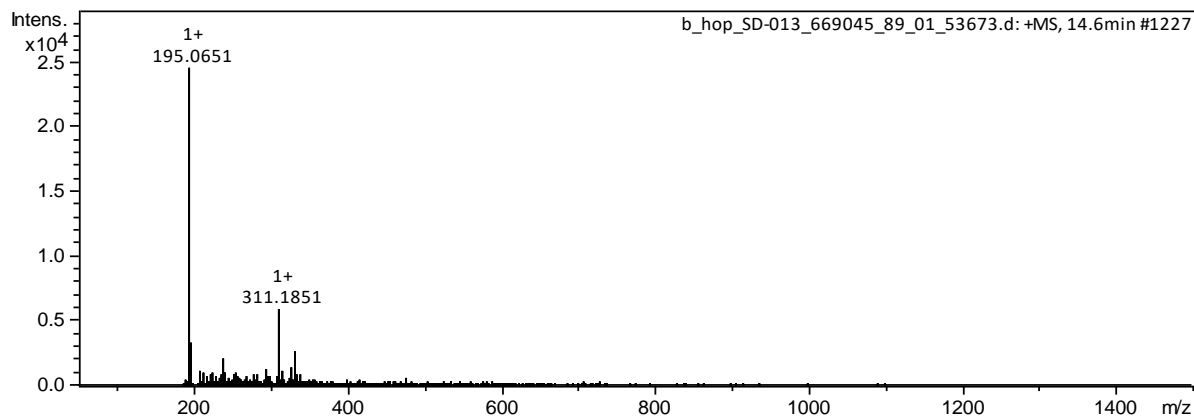
S131- GCMS mass spectrum bis(2-hydroxyethyl) terephthalate (BHET).



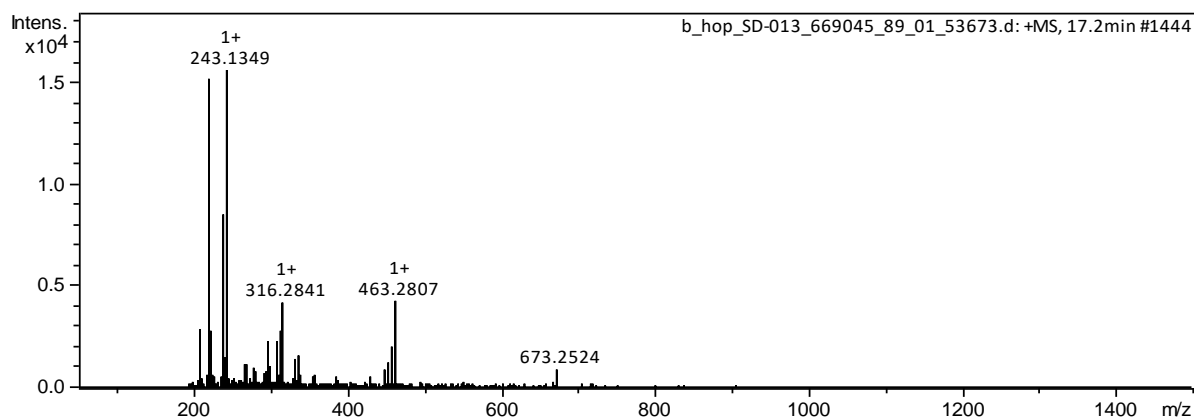
S132- ESI mass spectrum dimethyl terephthalate (DMT) obtained post-HPLC.



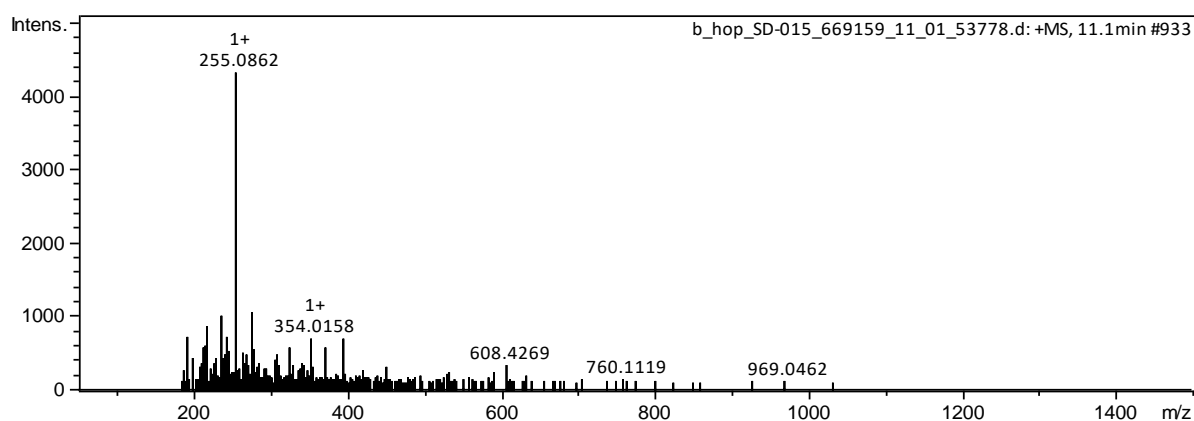
S133- ESI mass spectrum of crude methanolysis product degraded with a 5:1 molar excess of methanol to PET obtained post-HPLC separation, elution time = 12.5 minutes.



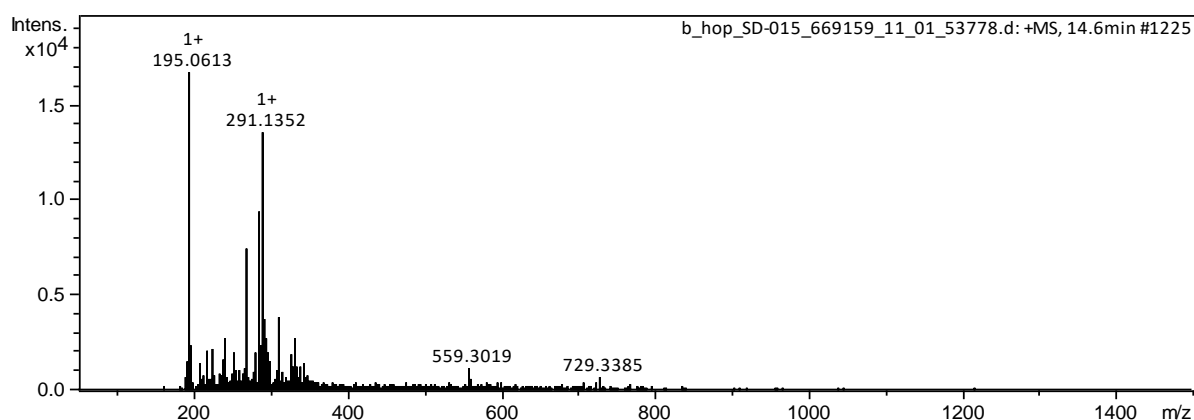
S134- ESI mass spectrum of crude methanolysis product degraded with a 5:1 molar excess of methanol to PET obtained post-HPLC separation, elution time = 14.6 minutes.



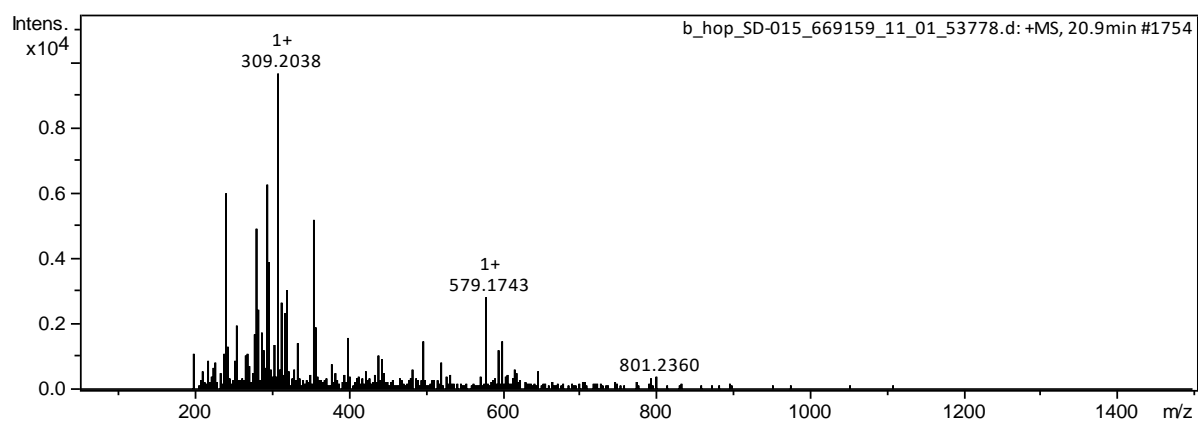
S135- ESI mass spectrum of crude methanolysis product degraded with a 5:1 molar excess of methanol to PET obtained post-HPLC separation, elution time = 17.2 minutes.



S136- ESI mass spectrum of crude methanolysis product degraded with a 3:1 molar excess of methanol to PET obtained post-HPLC separation, elution time = 11.1 minutes.



S137- ESI mass spectrum of crude methanolysis product degraded with a 3:1 molar excess of methanol to PET obtained post-HPLC separation, elution time = 14.6 minutes.



S138- ESI mass spectrum of crude methanolysis product degraded with a 3:1 molar excess of methanol to PET obtained post-HPLC separation, elution time =20.9 minutes.